GAUGE THEORIES AND LEPTONS

XIII th Rencontre de Moriond - Session II, Les Arcs (Savoie) France - March 18 - 24, 1978

GAUGE THEORIES AND LEPTONS

ISBN 2-86332-003-3

1978 Editions Frontières 7 avenue Kennedy
28100 DREUX - France

Printed in Korea

Proceedings of the

THIRTEENTH RENCONTRE DE MORIOND, 13 1978.

Les Arcs - Savoie (France), March 12 - March 24, 1978

VOL. II

GAUGE THEORIES AND LEPTONS

edited by

J. TRAN THANH VAN

SPONSORED BY

- INSTITUT NATIONAL DE PHYSIQUE NUCLEAIRE ET DE PHYSIQUE DES PARTICULES
- COMMISSARIAT A L'ENERGIE ATOMIQUE

The Second Session of the Thirteenth Rencontre de Moriond on
Gauge Theories and Leptons
was organized by

J. TRAN THANH VAN

with the active collaboration of

M. DAVIER
F. HAYOT
F.M. RENARD
and R. TURLAY

Permanent secretariat:

Rencontre de Moriond

Laboratoire de Physique Théorique et Particules Elémentaires
Bâtiment 211 - Université de Paris-Sud
91405 ORSAY (France)
Tel. 941.73.66

FOREWORD

The XIII th Rencontre de Moriond was held at Les Arcs - Savoie (France) from March 12 to March 24, 1978.

The first such meeting was at Moriond in the French Alps in 1966. There, experimental as well as theoretical physicists, not only shared their scientific preoccupations but also the household chores. The participants at the first meeting were mainly French physicists interested in electromagnetic interactions. In subsequent years, a session on high energy strong interactions was also added.

The main purpose of these meetings is to discuss recent developments in contemporary physics and to promote effective collaboration between experimentalists and theorists in the field of elementary particle physics. By bringing together a relatively small number of participants, the meeting helps to developp better human relations as well as a more thorough and detailed discussion of the contributions.

This concern for research and experimentation of new channels of communication and dialogue which from the start animated the Moriond Meetings, inspired us, starting eight years ago, to organize a simultaneous meeting of biologists on Cellular Differentiation. Common seminars are organized to study to what extent analytical methods used in physics could be applied to biological problems. This year, an introductory talk and a beautiful film "The Genetic Code" was presented by Professor J. TAVLITZKI (Institute of Molecular Biology, Paris), Professor DEDONDER (University of Paris) gave a comprehensive talk on "Genetic Engineering", and Dr D. FOURME (L.U.R.E., Orsay) described the Orsay storage ring facilities for biology experiments. These conferences and lively discussions make us hope that biological problems, at present so complex, may give birth in the future to new analytical methods or new mathematical languages.

The first session of the XIII th Rencontre de Moriond (March 12 - March 18, 1978) was devoted to high energy hadronic interactions. Special emphasis was put on the phenomenology of quantum chromodynamics especially on lepton pair production, gluon physics and multiquark states.

The second session (March 18 - March 24, 1978) was devoted to high energy leptonic interactions. Particular attention was given to e^+e^- physics and recent discoveries in neutrino interactions.

I thank CHAN HONG-MO, G. KANE, TAN CHUNG-I for the first session, M. DAVIER, F. HAYOT, F.M. RENARD and R. TURLAY for the second session and the conference secretaries L. NORRY and N. CORNIQUEL who have devoted much of their time and energy to the success of this Rencontre.

I am also grateful to Mr TOURAILLE, the hotel Director, Mr MONTEGU and Ms FERRANDON, who contributed through their hospitality and active cooperation to the well-being of the participants enabling them to work in a relaxed atmosphere.

P A R T I C I P A N T S

Second Session

ALTARELLI Guido	Istituto di Fisica "G. Marconi", Universita di Roma, Piazzale delle Science, 5 Roma 00185 (Italy)
BARBARINO Carlo G.	Frascati Laboratori Nazionali (University), Via A. Tari, 3, Napoli 80138 (Italy)
BERTHELOT André	DPhPE C.E.N. Saclay, B.P.2, 91190-Gif-sur-Yvette France)
BIGI Ikaros	Max Planck Institüt, Fähringer Ring, 6 München-40 D-8000 (Fed. Rep. of Germany)
BINETRUY Pierre	L.A.P.P. B.P. 909, 74019-Annecy-le-Vieux (France)
BJORKEN James	S.L.A.C. Stanford University, Stanford Ca. 94305 (U.S.A.)
BLOCH Philippe	DPhPE C.E.N. Saclay, B.P.2, 91190-Gif-sur-Yvette (France)
BOUCHEZ Jacques	DPhPE C.E.N. Saclay, B.P.2, 91190-Gif-sur-Yvette (France)
BRISSON Violette	L.P.T.H.E. Ecole Polytechnique, 91120-Palaiseau (France)
"	
BURGER Jochen	Dept. of Physics, Siegen University, Siegen D-5900 (Fed. Rep. of Germany), and D.E.S.Y. Notkestieg 85, Hamburg-52 D-2000 (Fed. Rep. of Germany)
BURNETT Toby H.	University of Washington, Physics Dept. FM 15, Seattle 98195 Wa. (U.S.A.)
CABIBBO Nicola	L.P.T.H.E. Université Paris VI, 4, Place Jussieu, Tour 16, 75230-Paris Cedex 05 (France)
CARNESECCHI Giorgio	Division EP, C.E.R.N. 1211-Geneva 23 (Switzerland)

CHEN K. Wendell	Fermi National Laboratory, P.O.Box 500, Batavia Ill. 60510 (U.S.A.)
COURAU André	Laboratoire de l'Accélérateur Linéaire, Bât. 200, Université Paris-Sud, 91405-Orsay (France)
DAVIER Michel	Laboratoire de l'Accélérateur Linéaire, Bât. 200, Université Paris-Sud, 91405-Orsay (France)
DIAMANT-BERGER Alain	DPhPE, S.E.E. C.E.N. Saclay, B.P.2, 91190-Gif-sur-Yvette (France) and S.L.A.C. P.O.Box 4349, Stanford Ca. 94305 (U.S.A.)
DETOEUF Jean-François	DPhPE C.E.N. Saclay, B.P.2, 91190-Gif-sur-Yvette (France)
ELLIS Stephen P.	Physics Dept. FM.15, University of Washington, Seattle Wa. 98195 (U.S.A.)
FOURME Daniel	Laboratoire de l'Accélérateur Linéaire, Bât. 200, Université Paris-Sud, 91405-Orsay (France)
FRANCOIS Thierry	L.P.N.H.E. Ecole Polytechnique, 91128-Palaiseau (France)
FRIES Dietrich	Institut für Exp. Kernphysik, P.O.Box 3640, Karlsruhe D-7500 (Fed. Rep. of Germany)
FRITZSCH Harald	Dept. of Physics, University of Wuppertal, Wuppertal(Fed. Rep. of Germany) and C.E.R.N. 1211-Geneva 23 (Switzerland)
FULDA Frédérique	Laboratoire de l'Accélérateur Linéaire, Bât. 200, Université Paris-Sud 91405-Orsay (France)
GOLDBERG Marcel	L.P.N.H.E. Université Paris VI, 11, Quai Saint Bernard, 75230-Paris Cedex 05 (France)
GOODMAN Stuart	L.P.N.H.E. Université Pierre et Marie Curie, 4, Place Jussieu, Tour 32, 75231-Paris (France)
GOULIANOS Dino	Rockfeller University, New York N.Y. 10021 (U.S.A.)

GRINDHAMMER Günter	Max Planck Institut für Physik und Astrophysik, München-40 D-8000 (Fed. Rep. of Germany) and D.E.S.Y. F.36, Notkestieg 1, Hamburg-52 D-2000 (Fed. Rep. of Germany)
GUNDERSON Bruce N.	Max Planck Institut für Physik und Astrophysik, München-40, D-8000 (Fed. Rep. of Germany)
GUNION Jack	Physics Dept. University of Davis, Davis Ca. 95616 (U.S.A.)
HANSL Traudl	Division EP, C.E.R.N., 1211-Geneva 23 (Switzerland)
HANSON Gail	S.L.A.C., Bin 61, P.O.Box 4349, Stanford Ca. 94305 (U.S.A.)
HAYOT Fernand	DPhT, C.E.N. Saclay, B.P.2, 91190-Gif-sur-Yvette (France)
HEINE Peter	Institut für Experimental Physik, University of Hamburg, Hamburg-52, D-2000 (Fed. Rep. of Germany)
JACQUET François	L.P.N.H.E. Ecole Polytechnique, 91128-Palaiseau (France)
JAUNEAU	Inst. Nat. de Phy. Nucl. et de Phys. Part. 11, rue Pierre et Marie Curie, 75231-Paris Cedex 05 (France)
KANE Gordon	Physcis Dept. University of Michigan, Ann Arbor Mi. 48104 (U.S.A.)
KANG Kyungsik	Dept. of Physics, Brown University, Providence R.I. 02912 (U.S.A.)
KIM Jae Kwan	Korea Advanced Institute of Science, P.O.Box 150 Chongyangni, Seoul (Korea)
KLUBERG-STERN Hannah	DPhT C.E.N. Saclay, B.P.2, 91190-Gif-sur-Yvette (France)
KLUBERG Louis	L.P.N.H.E. Ecole Polytechnique, 91120-Palaiseau
KLEINKNECHT Konrad	Inst. für Physik, Univ. Dortmund, Dortmund-50, D-46 (Fed. Rep. of Germany)
KOUNNAS Costas	Laboratoire de Physique Théorique, Ecole Normale Supérieure, 24, rue Lhomond, 75005-Paris (France)

KRAMMER Margarete	D.E.S.Y. Notkestieg 85, Hamburg-52 D-2000 (Fed. Rep. of Germany)
LAPLANCHE Francis	Laboratoire de l'Accélérateur Linéaire, Bât. 200, Université Paris-Sud, 91405-Orsay (France)
LEVEQUE Antoine	DPhPE/S.E.C.B., C.E.N. Saclay, B.P. 2, 91190-Gif-sur-Yvette (France)
LING Ta-Yung	Dept of Physics, Smith Laboratory, The Ohio State University, Colombus OH 43210 (U.S.A.)
LUBATTI Henry J.	Dept. of Physics, Visual Techniques Laboratory, University of Washington, Seattle Wa. 98195 (U.S.A.)
MAIANI Luciano	Laboratoire de Physique Théorique, Ecole Normale Supérieure, 24, rue Lhomond, 75231-Paris (France)
MOREL André	DPhT C.E.N. Saclay, B.P.2, 91190-Gif-sur-Yvette (France)
NEVEU Monique	DPhPE C.E.N. Saclay, B.P.2, 91190-Gif-sur-Yvette (France)
PALMER Robert B.	Physics Dept. Brookhaven National Lab. Upton N.Y. 11973 (U.S.A.)
PERL Martin L.	S.L.A.C. Stanford Ca. 94305 (U.S.A.)
PERROTET Michel	Centre de Physique Théorique, C.N.R.S., 31, Chemin J. Aiguier, 13274-Marseille Cedex 2 (France)
PESSARD Henri	L.A.P.P. B.P. 909, 74019-Annecy-le-Vieux (France)
PHILLIPS Roger J.N.	Rutherford Laboratory, Chilton, Didcot, Oxon, OX11, OQX (United Kingdom)
PISTILLI Pio	Istituto di Fisica "G. Marconi", Piazzale delle Science 5, 00185-Roma (Italy)
POVEL Hans Peter	Swiss Institute for Nuclear Research, 5234-Villingen (Switzerland)
QUIRK	Nuclear Physics Lab. University of Oxford, Keble Road, Oxford OX13RH (United Kingdom)

QUENZER Alain	Laboratoire de l'Accélérateur Linéaire, Bât. 200, Université Paris-Sud, 91405-Orsay (France)
RENARD Fernand	Laboratoire de Physique Mathématique U.S.T.L. 34060-Montpellier Cedex (France)
RICHARD François	Laboratoire de l'Accélérateur Linéaire, Bât. 200, Université Paris-Sud, 91405-Orsay (France)
RIESTER Jean-Louis	C.B.L.L. C.N.R.S. B.P.20 CRO, 67037-Strasbourg Cedex (France)
RITSON David M.	Stanford Linear Accelarator Center, Bin 94, Stanford University, P.O.Box 4349, Stanford Ca. 94305 (U.S.A.)
RUEGG Henri	Dept. de Physique Théorique, Université de Genève, 32, bd d'Yvoy, 1211-Geneva 4 (Switzerland)
SACQUIN Yves	DPhPE C.E.N. Saclay, B.P.2, 91190-Gif-sur-Yvette (France)
SAVOY-NAVARRO Aurore	DPhPE C.E.N. Saclay, B.P.2, 91190-Gif-sur-Yvette (France)
SCHILDKNECHT Dieter	Fak. für Physik, Univ. Bielefeld, 48-Bielefeld (Fed. Rep. of Germany)
SLEEMAN John	Laboratoire de l'Accélérateur Linéaire, Bât. 200, Université Paris-Sud, 91405-Orsay (France)
SMITH Jack	Institute for Theoretical Physics, State Univ. of New York, Stony Brook N.Y. 11794 (U.S.A.)
SPINETTI Marco	Laboratori Nazionali di Frascati, C.P. 13, 00044-Frascati (Italy)
STEIGMAN Gary	Astronomy Dept. Yale University, New Haven CT. 06520 (U.S.A.)
STODOLSKY Leo	Max Planck Inst. Postfach 40 12 12, München-40 D-8000 (Fed. Rep. of Germany)
SUKHATME Uday	L.P.T.P.E. Bât. 211, Université Paris-Sud, 91405-Orsay (France)
TALLINI Bruno	DPhPE C.E.N. Saclay, B.P.2, 91190-Gif-sur-Yvette (France)

TAN CHUNG I	Brown University, Providence R.I. (U.S.A.) and L.P.T.P.E. Bât. 211, Université Paris-Sud, 91405-Orsay (France)
THENARD Jean-Michel	L.A.P.P. B.P. 909, 74019-Annecy-le-Vieux (France)
TRAN THANH VÂN Jean	L.P.T.P.E., Bât. 211, Université Paris-Sud, 91405-Orsay (France)
TRUONG TRAN N.	Centre de Physique Théorique, Ecole Polytechnique, 91120-Palaiseau (France)
TURLAY René	DPhPE C.E.N. Saclay, B.P.2, 91190-Gif-sur-Yvette (France)
UDO Fred	EP Division, C.E.R.N. 1211-Geneva 23 (Switzerland)
VANDER VELDE-WILQUET C.	Service de Physique des Part. Elémentaires, Université Libre de Bruxelles, Bd du Triomphe, 1050-Brussels (Belgium)
VIDEAU Henri	L.P.N.H.E. Ecole Polytechnique, 91120-Palaiseau (France)
WEITSCH G. Andreas	Laboratoire de l'Accélérateur Linéaire, Bât. 200, Université Paris-Sud, 91405-Orsay (France)
WEILER Thomas	D.A.M.T.P. University of Liverpool, Liverpool L.69.3BX (United Kingdom)
WERNHARD Karl-Ludwid	EP Division, C.E.R.N. 1211-Geneva 23 (Switzerland)
WOLF Günter	D.E.S.Y Notkestieg 1, Hamburg-52 D-2000 (Fed. Rep. of Germany)
WOTSCHACK Jörg	EP. Division, C.E.R.N. 1211-Geneva 23 (Switzerland)

CONTENTS

I - PHOTON AND ELCTRON-POSITRON PHYSICS

II - NEUTRINO PHYSICS

JETS IN e^+e^- ANNIHILATION*

Gail G. Hanson
Stanford Linear Accelerator Center
Stanford University, Stanford, California 94305, U.S.A.

Abstract: The latest results on R, the ratio of the total cross section for production of multihadronic events to the muon pair production cross section, and inclusive distributions of hadrons from e^+e^- annihilation in the center-of-mass energy range from 2.6 to 7.8 GeV are presented. The evidence for jet structure is reviewed. Inclusive distributions of hadrons in Feynman x, rapidity, and transverse momentum relative to the jet direction are studied. Particular emphasis is placed on the method used to measure these inclusive distributions and the biases which might result from this method.

Résumé: Les résultats les plus récents concernant la mesure de R, rapport de la section efficace totale de production de hadrons à la section efficace de production de paires de muons, ainsi que la mesure des distributions inclusives des hadrons dans les annihilations e^+e^- sont presentés pour des energies dans le centre de masse comprises entre 2.6 et 7.8 GeV. L'evidence d'une structure en jet est passée en revue. Les distributions inclusives des hadrons sont étudiées en fonction de la variable de Feynman x, de la rapidité et du moment transverse par rapport à la direction du jet. L'accent est mis sur la méthode utilisée pour mesurer ces distributions inclusives et sur les biais qui peuvent en résulter.

*Work supported by the Department of Energy.

I. INTRODUCTION

Electron-positron annihilation has proved to be a very fruitful source of exciting new physics. The increase in the total cross section for hadron production was the first hint that a new quantum number - charm - existed.[1] The ψ and ψ' and their associated states were discovered.[2] A heavy lepton τ was found.[3] And finally charmed mesons themselves were isolated and found to be produced copiously in pairs at the ψ''.[4,5]

The reason that e^+e^- collisions are so useful is that the electron and positron predominantly annihilate to form a single virtual photon which subsequently produces a particle-antiparticle pair (e.g., $\tau^+\tau^-$) or a quark-antiquark pair which converts into hadrons. These general theoretical ideas have so far been substantiated by experimental data. One of the predictions of quark-parton constituent models is that at sufficiently high energy multihadronic events produced by e^+e^- annihilation should form two back-to-back jets due to the limiting of transverse momentum relative to the original quark direction.[6] Evidence for such jet structure is seen in e^+e^- annihilation data for center-of-mass energies ($E_{c.m.}$) of 4.8 GeV and greater.[7] If it is true that the jet structure is due to quark jets, then it is of interest to study the inclusive distributions of hadrons relative to the jet direction in order to obtain information about the fragmentation of quarks into hadrons. In this talk I will present hadron inclusive distributions in Feynman x, rapidity, and transverse momentum relative to the jet direction in multihadronic events from e^+e^- annihilation in the $E_{c.m.}$ range from 3.0 to 7.8 GeV.

II. DETECTOR AND EVENT SELECTION

The data for this analysis were taken by the SLAC/LBL magnetic detector collaboration[8] at SPEAR. The SPEAR Mark I magnetic detector is shown schematically in Fig. 1. The detector consisted of a 3-meter long, 3-meter diameter solenoid magnet with a 4 kG magnetic field parallel to the beam direction and wire spark chambers and scintillation counters for triggering and measuring events. The detector axis was centered on the beam direction at one of two interaction regions at SPEAR. Particles entering the detector from the interaction region could pass through, in order: a 150 μm steel vacuum chamber, inner cylindrical scintillation counters used in the trigger to reduce background from cosmic rays, inner multiwire proportional chambers, a system of 4 sets of cylindrical wire spark chambers, an array of trigger time-of-flight scintillation counters, the magnet coil, an array of lead-scintillator shower counters, the iron return yoke of the magnet, and finally wire spark chambers used for muon-hadron separation. The detector extended over 65% of 4π sr solid angle with full acceptance in azimuthal angle and acceptance in polar angle from 50° to 130°. The apparatus was triggered by two or more charged particles which produced

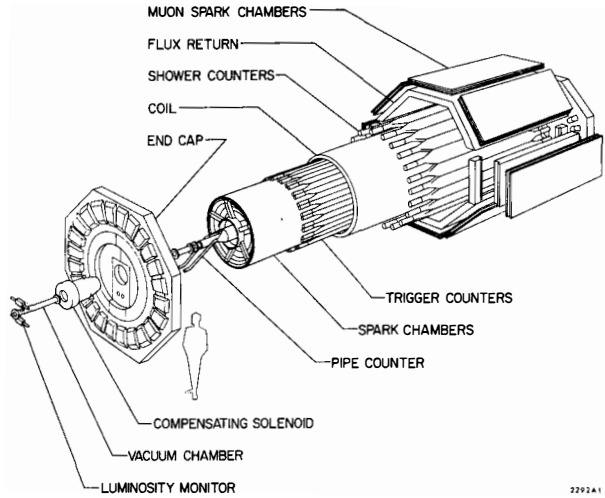

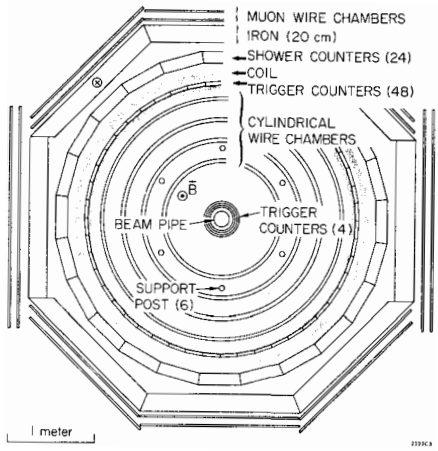

Fig. 1. Schematic diagrams of the SLAC/LBL magnetic detector.

signals in the inner scintillation counters and in at least two outer trigger counters and their associated shower counters. This trigger requirement could be satisfied only by events with two or more charged particles within the detector acceptance and having momenta greater than 200 MeV/c and is mainly responsible for the uncertainties in efficiency calculations.

Events from the QED reactions

$$e^+e^- \rightarrow e^+e^- \text{ (Bhabha scattering)} \quad (1)$$

and

$$e^+e^- \rightarrow \mu^+\mu^- \quad (2)$$

were recorded simultaneously with the multihadronic events and provided a convenient normalization. Of those events originating from the interaction-region fiducial volume, those with two oppositely-charged prongs collinear within 10° were candidates for the QED reactions. Those events in which there were two prongs acoplanar with the incident beam direction by at least 20° and in which both prongs had momenta greater than 300 MeV/c and those with three or more prongs were classified as hadronic. Additional cuts were applied to remove non-collinear two-prong and multiprong events originating from QED processes.

III. TOTAL CROSS SECTION AND INCLUSIVE MOMENTUM DISTRIBUTIONS

The total hadronic cross section was calculated from the total number of multihadronic events detected at each energy $E_{c.m.}$ from 2.6 to 7.8 GeV, corrected for losses due to geometric acceptance, triggering efficiency, cuts, and contamination from other sources. The cross section was normalized to the integrated luminosity obtained from Bhabha scattering events observed in the magnetic detector. Losses due to geometric acceptance, triggering efficiency, and data analysis cuts were estimated using a Monte Carlo simulation, described in more detail in Section IV, in which hadronic events were produced according to a jet model. The Monte Carlo calculation resulted in a matrix of efficiencies for detecting a particular number of charged particles for each charged particle multiplicity in the produced state. Radiative corrections were applied separately for each produced multiplicity. At each energy a produced multiplicity distribution was obtained as the maximum-likelihood solution to an overdetermined set of linear equations. The average detection efficiency, given by the number of detected events divided by the number of produced events, increased monotonically from about 33% at the lowest energy to about 65% at the highest energy. The data were corrected for background from beam-gas scattering (<8% for $E_{c.m.}$ less than 5 GeV and <5% for $E_{c.m.}$ above 5 GeV) and from two-photon processes (<2%) and for losses due to vertex reconstruction outside the interaction-region fiducial volume (5%).

The ratio R of the total hadronic cross section to the theoretical total cross section for production of muon pairs is presented in Fig. 2. Heavy lepton

production, which contributes primarily to the two-prong cross section, has not been subtracted. The errors shown are statistical only. The overall normalization uncertainty is ±10% and a further smooth variation as large as 10% from the lowest energy to the highest energy could arise from systematic errors in the estimation of the detection efficiency. The ψ and ψ' peaks are not shown and the binning of the data between 3.9 and 4.5 GeV is not optimized to show the structure in this region. R is approximately constant at about 2.6 for $E_{c.m.}$ less than 3.5 GeV. Above 4.8 GeV R is again approximately constant at a value of about 5.3. Although the data have been reanalyzed using more sophisticated techniques and more data have been taken, the results for R are very similar to those presented at the 1975 Lepton and Photon Symposium.[9] The values for R presented here are in good agreement with those presented by the DASP collaboration at DORIS, except for the detailed structure in the 4 GeV region, for the energy range between 3.6 and 5.2 GeV which they have measured.[10] The R values from the Pluto collaboration are somewhat lower but are probably consistent within the systematic errors of the two experiments.[11] The mean charged particle multiplicity $\langle n_{ch} \rangle$, obtained as part of the procedure for determining the total cross section, plotted versus the logarithm of $E_{c.m.}$ is presented in Fig. 3. $\langle n_{ch} \rangle$ rises from about 3.5 at the lowest energies to about 5 at

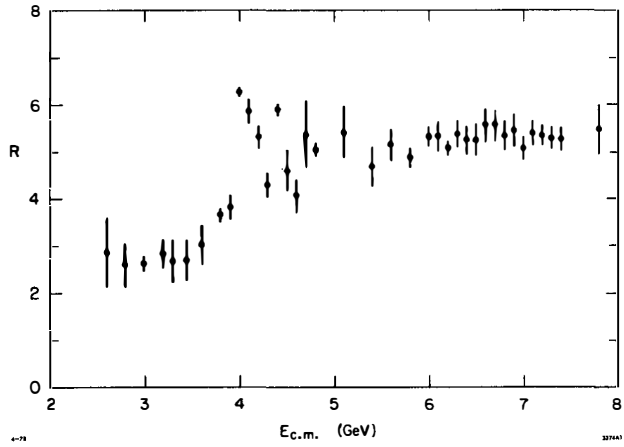

Fig. 2. R vs. $E_{c.m.}$ (heavy lepton production not subtracted).

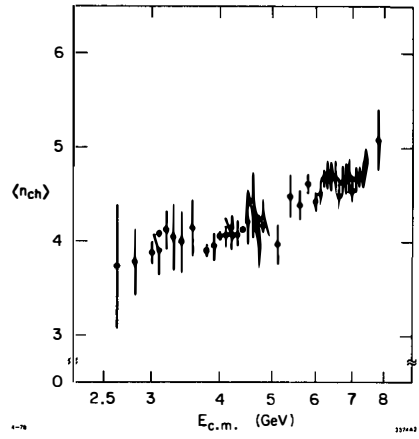

Fig. 3. Mean charged particle multiplicity $\langle n_{ch} \rangle$ vs. $E_{c.m.}$ (heavy lepton production not subtracted).

the highest energies. Heavy lepton production has not been subtracted.

Single particle inclusive momentum distributions have been measured at $E_{c.m.}$ values of 3.0 and 4.8 GeV and in three energy ranges from 5.6 to 7.8 GeV. The momentum distributions are presented in terms of the "experimental" scaling variable x, where

$$x = 2p/E_{c.m.}, \tag{3}$$

and p is the particle momentum. The momentum is used instead of the energy because π's, K's, and p's can be separated unambiguously by our time-of-flight system only for momenta less than 1.1 GeV/c. Only multihadronic events with three or more detected charged particles were used in this analysis and for the analyses in the remainder of this presentation. The two-prong events were not used because they are more subject to background contamination due to beam-gas and two-photon interactions. Because the two-prong events were not used, the inclusive distributions presented here contain little contribution from heavy lepton production.

The detected single particle momentum distributions were corrected for trigger bias, geometric acceptance, and data analysis cuts using the jet model Monte Carlo simulation. The distributions were corrected so as to include multihadronic events with all produced multiplicities, including events with two charged particles. In addition, the Monte Carlo efficiencies contain a momentum-dependent correction for initial-state radiation so that the distributions are radiatively corrected. The effects of this radiative correction are an overall decrease in efficiency because nonradiative events have higher multiplicities than those in which there was significant radiation and an additional decrease in efficiency for large x because events with significant radiation cannot have particles with large x.

The single particle inclusive x distributions are presented in Fig. 4. The quantity plotted is $s\,d\sigma/dx$ ($s = E_{c.m.}^2$) which is expected to scale at very high energies. The area under each curve is equal to $s\sigma_T\langle n_{ch}\rangle \propto R\langle n_{ch}\rangle$ (σ_T is the total hadronic cross section), so the area under the curve must increase as the energy increases, even for constant R, since $\langle n_{ch}\rangle$ increases. We see that most of this increase occurs for $x<0.3$. $s\,d\sigma/dx$ roughly scales for $x\geq 0.3$ for the entire energy range. The 3.0 GeV data seem to be systematically high for $x\geq 0.6$; however, systematic errors due to the Monte Carlo corrections at the highest and lowest values of x could be as large as 20%. In addition, the detected two-prong events, which we do not use but correct for, form the largest fraction of the total number of events (25%) at 3.0 GeV. The data for $E_{c.m.} \geq 4.8$ GeV scale rather well for $x \geq 0.2$, although there is a spread of about 20 % from the lowest energy to the highest energies for x between 0.3 and 0.5. More will be said about scaling in Section V when inclusive distributions in Feynman x are discussed.

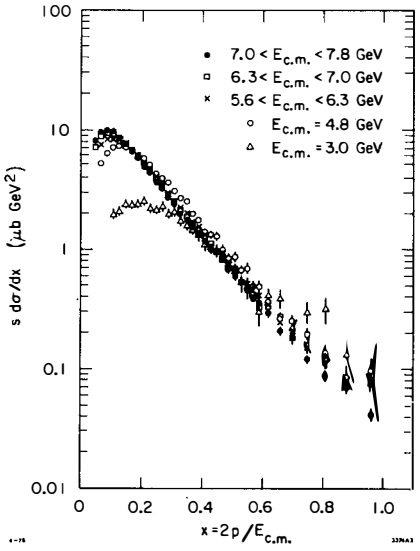

Fig. 4. Single particle inclusive x distributions s dσ/dx vs. x for various $E_{c.m.}$.

Our measurements of s dσ/dx are consistently higher for all x than are those presented by the DASP and PLUTO collaborations.[12] The reason for this difference is not understood. However, the areas under our s dσ/dx curves agree with the independently calculated $\langle n_{ch} \rangle$ from the total cross section determinations.

IV. JET STRUCTURE AND DESCRIPTION OF MONTE CARLO SIMULATION

In quark-parton constituent models for hadron production by e^+e^- annihilation, the e^+ and e^- annihilate to form a virtual photon which subsequently produces a quark-parton pair, each of which decays into hadrons, as shown in Fig. 5. At sufficiently high energy a two-jet structure is expected to arise due to the limited transverse momentum of the hadrons with respect to the original parton direction.[6]

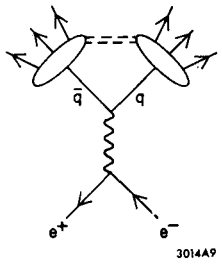

Fig. 5. Quark-parton model picture of production of hadrons in e^+e^- annihilation.

The spins of the constituents can, in principle, be determined from the angular distribution of the jets. A review of the jet structure observed in e^+e^- annihilation will be presented in this section.

In order to search for jet structure, we find the direction which minimizes the sum of squares of transverse momenta for each event. This direction will be referred to as the observed jet axis. To determine how jet-like an event is, we calculate a quantity which we call the sphericity S:

$$S = \frac{3\left(\sum_i p_{ii}^2\right)_{min}}{2\sum_i \vec{p}_i^{\,2}} , \qquad (4)$$

where the numerator is the minimum sum of squares of transverse momenta found in the determination of the observed jet axis. S approaches 0 for events with limited transverse momentum (jet-like events) and approaches 1 for events with large multiplicity and isotropic particle distributions.

Since the magnetic detector covered only part of the total solid angle and neutral particles were not detected, we needed to use a Monte Carlo simulation to

determine how jet-like and isotropic hadronic events would differ in the detector. Events were generated according to either Lorentz-invariant phase space or a jet model in which phase space was modified by a matrix element squared of the form

$$M^2 = e^{-\left(\sum_i p_{\perp i}^2\right)/2b^2} , \qquad (5)$$

where $p_{\perp i}$ is the momentum perpendicular to the jet axis for the i^{th} particle. The sum is over all produced particles. The jet axis angular distribution was of the form

$$\frac{d\sigma}{d\Omega} \propto 1 + \alpha \cos^2\theta , \qquad (6)$$

where θ is the polar angle relative to the e^+ beam. In both models only charged and neutral pions were produced, although some checks were performed using models which included etas, kaons, and nucleons. The charged-pion and neutral-pion multiplicities were given by separate Poisson distributions. The simulation included the geometric acceptance, trigger efficiency, momentum resolution ($\sigma_p/p = .013p$ (GeV/c)), conversion probability for photons from π^0 decay, and all other known characteristics of the detector. Radiation of the initial e^+ and e^- was included. At each energy $E_{c.m.}$ the total multiplicity and ratio of charged pions to neutral pions for both models were obtained by fitting to the observed charged particle mean momentum and mean multiplicity. The parameter b in the jet model was chosen by fitting to the observed mean $p_\perp$ with respect to the observed jet axis. We used $\alpha = 1$ for the jet axis angular distribution in agreement with the measurement which will be described.

We found evidence for jet structure in the agreement of the observed S distributions with the jet model predictions as opposed to the phase-space model predictions for $E_{c.m.} \geq 4.8$ GeV.[7,13] The data peak toward low S in disagreement with the phase-space model. At 3.0 GeV the data agree with either model; the predictions of the two models are the same. In addition, the jet model momentum and $p_\perp$ distributions are in much better agreement with the data than are the phase-space model distributions.[13]

We were able to measure the jet axis angular distribution directly for a subset of the data at $E_{c.m.} \approx 7.4$ GeV. For this data the e^+ and e^- beams were transversely polarized due to synchrotron radiation and absence of depolarizing resonances. The beam polarization was useful because it induced an azimuthal asymmetry through the following general angular distribution for production through a single virtual photon:[14]

$$\frac{d\sigma}{d\Omega} \propto 1 + \alpha \cos^2\theta + P^2\alpha \sin^2\theta \cos 2\phi , \qquad (7)$$

where ϕ is the azimuthal angle with respect to the plane of the storage ring, P is the transverse polarization of each beam, and α is given by

$$\alpha = \frac{\sigma_T - \sigma_L}{\sigma_T + \sigma_L} \quad . \tag{8}$$

σ_T and σ_L are the transverse and longitudinal production cross sections, respectively. Since the detector had a small range of acceptance in $\cos^2\theta$ but full acceptance in ϕ, the polarization was necessary to determine α for the jet axis. P^2 was determined from the QED reaction (2). After correction for incorrect jet axis determination using the Monte Carlo simulation, we measured $\alpha = 0.97 \pm 0.14$ for the produced jet axis angular distribution.[7,13] In terms of σ_L and σ_T this value of α corresponds to $\sigma_L/\sigma_T = 0.02 \pm 0.07$. The jet axis angular distribution is consistent with that for a pair of spin-1/2 particles. With $\alpha = 1$ the jet model correctly predicts the inclusive hadron $\cos^2\theta$ dependence as a function of hadron momentum.[7,13]

The jet model Monte Carlo simulation has been found to give a good, although not perfect, representation of the multihadronic data. It reproduces the sphericity distributions for whole events and the single particle inclusive momentum and angular distributions. Its most important use beyond the observation of jet structure itself is in the calculation of various efficiency corrections for the measurements of the total cross section and single particle inclusive distributions.

V. INCLUSIVE DISTRIBUTIONS IN VARIABLES RELATIVE TO THE JET DIRECTION

The limiting of transverse momentum relative to an axis for e^+e^- hadron production is evidence for jet structure. If this jet structure is due to quark-parton jets, inclusive distributions in variables relative to the quark direction, which is expected to be the jet direction, may give us information about the fragmentation of quarks into hadrons. The inclusive hadronic cross section might be expected to be factorizable into a function of momentum parallel to the jet axis and a function of momentum perpendicular to that axis. In addition, these inclusive distributions can be compared with similar distributions from other processes, such as leptoproduction and hadron-hadron interactions.

In order to investigate such questions we have measured inclusive distributions in Feynman x, rapidity, and transverse momentum relative to the jet axis. A preliminary attempt to measure these distributions was reported previously,[13] but these measurements, although correct as stated, suffered from a bias introduced in order to obtain a good determination of the jet axis. The measurements presented here are better representations of the "true" inclusive distributions, and the biases which may be introduced by the method of determining them are studied.

For each hadronic event with three or more detected charged particles we construct an observed jet axis as described in Section IV. The components of each particle momentum parallel to ($p_{||}$) and perpendicular to ($p_\perp$) the jet axis

are then calculated, as shown in Fig. 6.

We can then produce observed inclusive distributions in $p_{||}$, $p_{\perp}$, and rapidity. The problem then is to correct these distributions for geometric acceptance, trigger bias, data analysis cuts, and incorrect determination of the jet axis. Studies were made using the jet model Monte Carlo simulation described in Section IV in which we knew the true jet axis for every event. It was found that the observed distributions in $p_{||}$ for all events were similar enough to the produced distributions that they could be corrected to give the true distributions. The reason for this was that in cases where the true jet direction was very different from the observed jet axis the detected particles had relatively low momenta and were nearly isotropic. The rapidity and $p_{\perp}$ distributions, however, were more sensitive to the correct determination of the jet axis and could not be reasonably corrected for all events. The method used for these distributions will be described later.

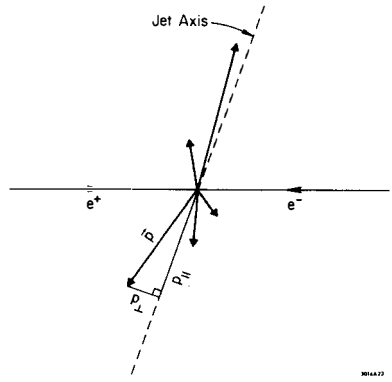

Figure 6. Illustration of a hadronic event from e^+e^- annihilation showing the jet axis and the components of the momentum $\vec{p}$ of a particle parallel to ($p_{||}$) and perpendicular to ($p_{\perp}$) the jet axis.

Since the inclusive quantity $s\, d\sigma/dx$, which was shown in Fig. 4, nearly scales, we are led to examine the inclusive distributions for $s\, d\sigma/dx_{||}$, where $x_{||}$, or Feynman x, is defined by

$$x_{||} = 2p_{||} / E_{c.m.} \tag{9}$$

In quark-parton models $x_{||}$ is the fraction of parton momentum carried by the hadron in the direction of the parton. The distributions $s\, d\sigma/dx_{||}$, corrected for acceptance, trigger bias, data analysis cuts, incorrect jet axis determination, and initial-state radiation are shown in Fig. 7 for the $E_{c.m.}$ values considered in Section III.

If we compare the distributions in $s\, d\sigma/dx_{||}$ with those in $s\, d\sigma/dx$, we see that as $E_{c.m.}$ increases the two distributions become more alike because $p_{\perp}$ is a decreasing fraction of p. At the lower energies the two distributions have quite different shapes. When e^+e^- inclusive momentum distributions are compared, for example, with leptoproduction, they should be compared in terms of the variable $x_{||}$. Except for the $E_{c.m.} = 3.0$ GeV data, the $s\, d\sigma/dx_{||}$ distributions scale for $0.1 < x_{||} < 0.8$ to within 10% which is at the level of our normalization and systematic uncertainties. For $E_{c.m.} \geq 4.8$ GeV scaling in $s\, d\sigma/dx_{||}$ appears to work better than scaling in $s\, d\sigma/dx$.

In order to measure the inclusive distributions in $p_\perp$ and rapidity we need to require that a fairly high momentum particle be detected in order to be able to find an observed jet axis which is close enough to the true jet direction that we can use the jet model Monte Carlo simulation to calculate corrections. However, requiring that a high momentum particle be detected biases the inclusive distributions. A method which can be used to remove the bias is the following:

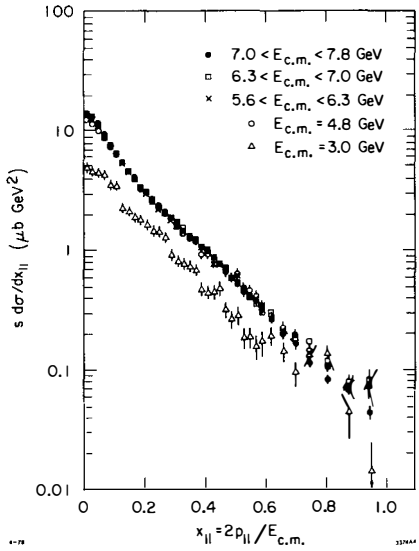

Fig. 7. Single particle inclusive $x_{||}$ distributions $s\,d\sigma/dx_{||}$ vs. $x_{||}$ for various $E_{c.m.}$. $x_{||} = 2p_{||}/E_{c.m.}$, where $p_{||}$ is the component of particle momentum parallel to the jet direction.

1. Find the observed jet axis in the usual way.
2. Divide the event into two jets with a plane through the interaction vertex and perpendicular to the jet axis.
3. If the highest-momentum particle on one side of the plane (x_{max}) has x greater than some minimum value, orient the jet axis to have a direction within 90^0 of this highest-momentum particle and measure the inclusive distributions in $x_{||}$, $p_\perp$, and rapidity for all the particles on the other side of the plane.
4. Repeat this procedure for the other side of the plane. This means that an event may be counted twice in the inclusive distributions, but no particle is counted more than once. The inclusive distributions are normalized to the total number of jets contributing.

Corrections are calculated by applying this procedure to both the produced and detected events in the jet model Monte Carlo simulation. For the produced events we know the true jet direction, so we can calculate corrections for finding the wrong jet axis in the detected events. The corrections, of course, are somewhat model dependent. We have some confidence in this correction procedure, however, because the jet model distributions agree rather well with the data.

As a test of the effectiveness of this method for removing biases due to requiring a high momentum particle, we apply it to the $x_{||}$ distributions which we have already measured for all events. We used the highest energy data sample, $7.0 < E_{c.m.} < 7.8$ GeV, because it has the best statistics (and also because it

should have the best-defined jet structure). In Fig. 8 are shown the distributions $(1/\sigma)d\sigma/dx_{||}$ versus $x_{||}$ for various cuts on x_{max} (which is at positive $x_{||}$ and is not plotted) for $7.0 < E_{c.m.} < 7.8$ GeV. σ is the cross section for jets with x_{max} within the specified range and the distributions $(1/\sigma)d\sigma/dx_{||}$ are thus distributions of particle density in $x_{||}$. The distributions are corrected for acceptance, trigger bias, data analysis cuts, incorrect jet axis determination, and initial-state radiation using the jet model Monte Carlo simulation and are therefore our best estimates of the true distributions. We see

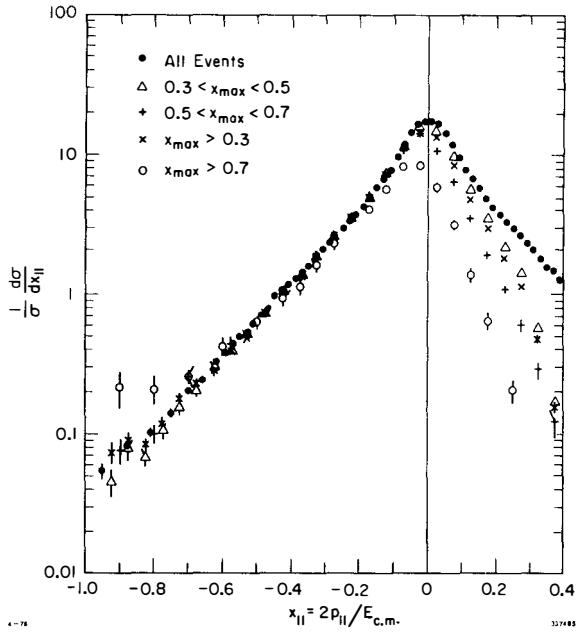

Fig. 8. Particle density distributions $(1/\sigma)d\sigma/dx_{||}$ vs. $x_{||}$ for various x_{max} cuts for $7.0 < E_{c.m.} < 7.8$ Gev. x_{max} is the highest-x particle on one side of the event and is not plotted. The jet direction is oriented so that x_{max} is at positive $x_{||}$. The distributions are normalized to the cross sections for jets with x_{max} within the specified range.

that these distributions are nearly independent of the x_{max} cut and agree with the distribution for all events for negative $x_{||}$. Only for $x_{max} > 0.7$ do we see a significant effect in the $x_{||}$ distribution on the opposite side: requiring a particle with $x_{max} > 0.7$ reduces the multiplicity for small $|x_{||}|$ and increases the multiplicity for large $|x_{||}|$. On the same side as the x_{max} particle we do see a correlation: the multiplicity decreases as x_{max} increases. We conclude that this method produces a relatively bias-free $x_{||}$ distribution for negative $x_{||}$; the $x_{||}$ distribution opposite a jet with $x_{max} > 0.3$ looks like the $x_{||}$ distribution for all events. We choose to use $x_{max} > 0.3$ for our analysis because the statistics are best. Of those observed jets with $x_{max} > 0.3$, only 4.7% have $x_{max} > 0.7$, so the difference in distributions for $x_{max} > 0.7$ has little effect. In fact, we have made a physical observation: we have shown that the $x_{||}$ distribution in one jet is independent of the x_{max} cut in the other jet. There is no particular reason why this has to be so. In Fig. 9 we show the $(1/\sigma)d\sigma/x_{||}$ distributions produced by

the jet model Monte Carlo calculation. The Monte Carlo shows a dependence of the negative $x_{||}$ distribution on the x_{max} cut used on the opposite side. For the Monte Carlo the multiplicity for small $|x_{||}|$ decreases and that for large $|x_{||}|$ increases as x_{max} increases. The $x_{||}$ distribution opposite a jet with $x_{max} > 0.3$ is significantly different from the distribution for all events.

The corrected $(1/\sigma)\, d\sigma/dx_{||}$ distributions for $x_{max} > 0.3$ for various $E_{c.m.}$ values are shown in Fig. 10. $(1/\sigma)d\sigma/dx_{||}$ distributions for all events at the same energies are shown in Fig. 11.

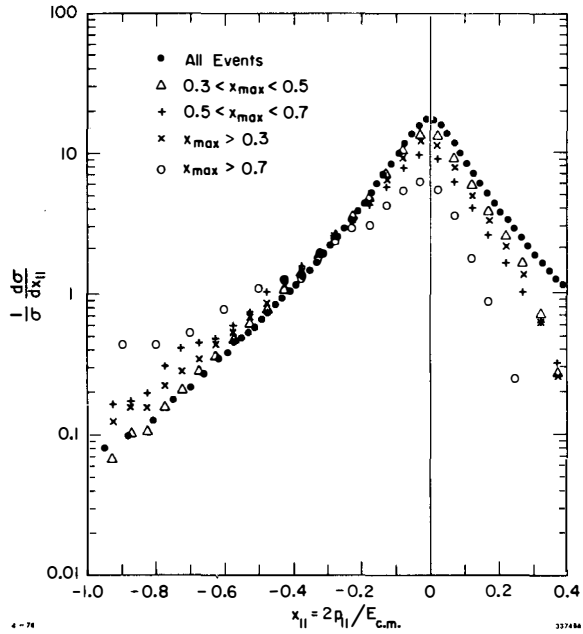

Fig. 9. Particle density distributions $(1/\sigma)d\sigma/dx_{||}$ vs. $x_{||}$ for various x_{max} cuts for jet model Monte Carlo at $E_{c.m.} = 7.276$ GeV.

Here σ is the event cross section. The distributions in Fig. 10 for negative $x_{||}$ agree quite well with those in Fig. 11 for all $x_{||}$ considered to be positive if those in Fig. 11 are divided by two (because the distributions in Fig. 11 are for both jets). We see that the method works well for all energies; the $x_{||}$ distributions opposite a jet with $x_{max} > 0.3$ look like those for all events. To obtain $(1/\sigma)d\sigma/dx_{||}$ for all events from $(1/\sigma)d\sigma/dx_{||}$ for particles opposite a jet with $x_{max} > 0.3$, assume that the distribution for positive $x_{||}$ is the reflection of that for negative $x_{||}$ about $x_{||} = 0$. Then, since the distribution is symmetric about $x_{||} = 0$, it can be folded over at $x_{||} = 0$ so all particles are at positive $x_{||}$. One observation that can be made about the distributions $(1/\sigma)d\sigma/dx_{||}$ for various energies is that they scale rather well for all energies, including 3.0 GeV, for $x_{||} \geq 0.2$. That $(1/\sigma)d\sigma/dx_{||}$ scales for $E_{c.m.} \geq 4.8$ GeV is not surprising since s $d\sigma/dx_{||}$ scales and R is approximately constant. However, R at 3.0 GeV is a factor of two smaller than R at the higher energies. Evidently, normalizing the inclusive distributions in $x_{||}$ to the total cross section rather than the luminosity makes up for this difference.

Inclusive distributions in rapidity and $p_{\perp}$ relative to the jet direction can

then be measured using the method just described. The rapidity y is defined by

$$y = \frac{1}{2} \ln\left(\frac{E+p_{||}}{E-p_{||}}\right), \quad (10)$$

where E is the energy of the particle assuming a pion mass and $p_{||}$ is the component of particle momentum parallel to the jet axis. In Fig. 12 are shown the corrected particle density distributions $(1/\sigma)d\sigma/dy$ versus y for various x_{max} cuts for $7.0 < E_{c.m.} < 7.8$ GeV. As was the case for $(1/\sigma)d\sigma/dx_{||}$ for negative $x_{||}$, we see that the distributions for negative y are nearly independent of the x_{max} cut.

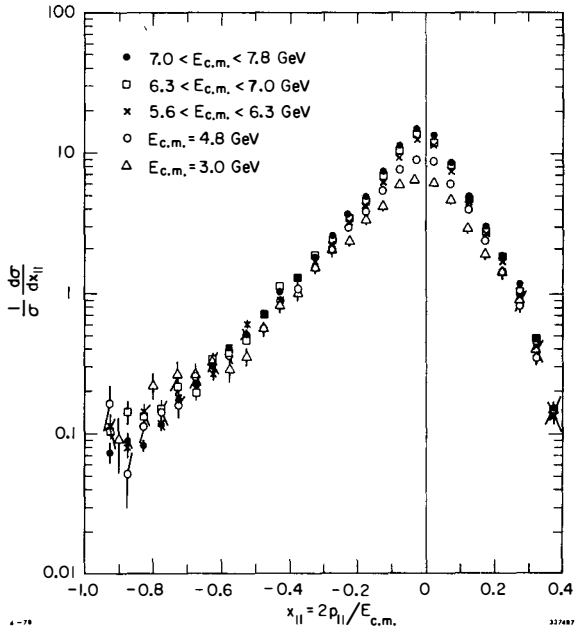

Fig. 10. Particle density distributions $(1/\sigma)d\sigma/dx_{||}$ vs. $x_{||}$ for $x_{max} > 0.3$ for various $E_{c.m.}$. x_{max} is at positive $x_{||}$ and is not plotted. The distributions are normalized to the cross sections for jets with $x_{max} > 0.3$.

For $x_{max} > 0.7$ there is a decrease in particle density for y between -1.5 and 0. For positive y, of course, we see a decrease in multiplicity as the x_{max} cut increases, as was shown previously for the $x_{||}$ distributions. We then used the cut $x_{max} > 0.3$ to produce corrected distributions in rapidity density at the other energies, as shown in Fig. 13. The distributions for negative y are our best estimates of the true rapidity distributions; those for positive y are distorted by the x_{max} cut. The real distributions of particles in rapidity relative to the jet direction would look like Fig. 13 with the distributions for positive y given by a reflection of those for negative y about y = 0. The distributions $(1/\sigma)d\sigma/dy$ increase in width as $E_{c.m.}$ increases. The distributions for the three highest energy ranges are quite similar in shape and appear to level off to a kind of plateau for y between -1.0 and 0. The value of $(1/\sigma)d\sigma/dy$ at the plateau is about 1.45 and is somewhat energy-dependent. A dip in $(1/\sigma)d\sigma/dy$ for y between -0.2 and 0 may be due to systematic errors in our data analysis. Because of tracking problems, we do not use particles with transverse momentum relative to the beam direction less than 150 MeV/c and must rely on the Monte Carlo simulation to

correct for this cut.

Distributions in $p_\perp$ relative to the jet direction are of some interest because they are the basis of the definition of jet structure. Jets occur because $p_\perp$ is limited as $E_{c.m.}$ increases. Figure 14 shows the corrected distributions $(1/\sigma)\,d\sigma/dp_\perp^2$ versus $p_\perp^2$ for particles opposite (negative $x_{||}$) jets with various x_{max} cuts for $7.0<E_{c.m.}<7.8$ GeV. The distributions are independent of the x_{max} cut, except for $x_{max}>0.7$ which shows a decrease in particle density for $p_\perp^2<0.6\,(GeV/c)^2$. The corrected distributions $(1/\sigma)\,d\sigma/dp_\perp^2$ versus $p_\perp^2$ for the various $E_{c.m.}$ values measured for particles opposite jets with $x_{max}>0.3$ are presented in Fig. 15. The $p_\perp^2$ distributions are very similar in shape for $E_{c.m.}\geq 4.8$ GeV. The area under each curve increases as $E_{c.m.}$ increases because of the increasing multiplicity. For $E_{c.m.}=3.0$ GeV the $p_\perp^2$ distribution falls off slightly faster as $p_\perp^2$ increases and there are no particles with $p_\perp^2>0.6$ $(GeV/c)^2$. For events, these distributions should

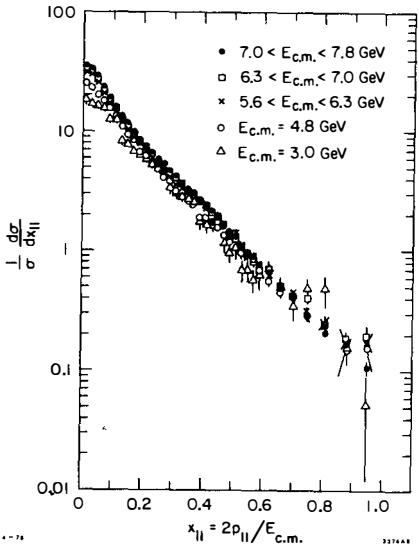

Fig. 11. Particle density distributions $(1/\sigma)\,d\sigma/dx_{||}$ vs. $x_{||}$ for all events for various $E_{c.m.}$. The distributions are normalized to the total cross sections for multihadronic events.

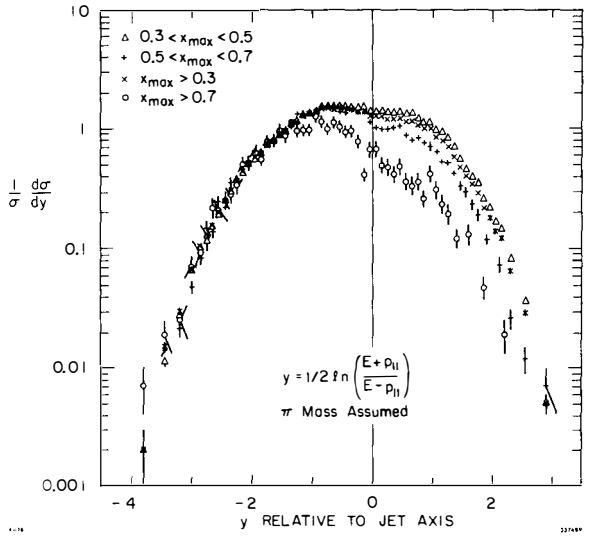

Fig. 12. Particle density distributions $(1/\sigma)\,d\sigma/dy$ vs. y for various x_{max} cuts for $7.0<E_{c.m.}<7.8$ GeV. x_{max} is the highest-x particle on one side of the event and is not plotted. The jet direction is oriented so that x_{max} is at positive y. The distributions are normalized to the cross sections for jets with x_{max} within the specified range.

be multiplied by two since they represent only one of the two jets.

The distributions shown in Fig. 15 have been corrected using the Monte Carlo jet model to calculate losses due to acceptance, trigger bias, and data analysis cuts and to calculate corrections due to finding the jet axis incorrectly. In order to show how these corrections might affect the $p_\perp^2$ distributions we present in Fig. 16 the uncorrected observed distributions $(1/N_{ev})dN/dp_\perp^2$ for particles opposite jets with $x_{max}>0.3$, where N_{ev} is the number of observed jets with $x_{max}>0.3$ and $dN/dp_\perp^2$ is the number of particles observed per $(GeV/c)^2$ in each $p_\perp^2$ bin. By comparing Figs. 15 and 16 one can see that the effect of the Monte Carlo corrections is to increase the particle density at high $p_\perp^2$ relative to that at low $p_\perp^2$. This is a reasonable efficiency correction because the detector acceptance makes it more difficult to detect both a jet and a particle at high $p_\perp$ to it. In any case, the Monte Carlo corrections do not change appreciably the similarity in shapes of the distributions for $E_{c.m.}\geq 4.8$ GeV nor do they change the observation that the slopes decrease as $p_\perp^2$ increases.

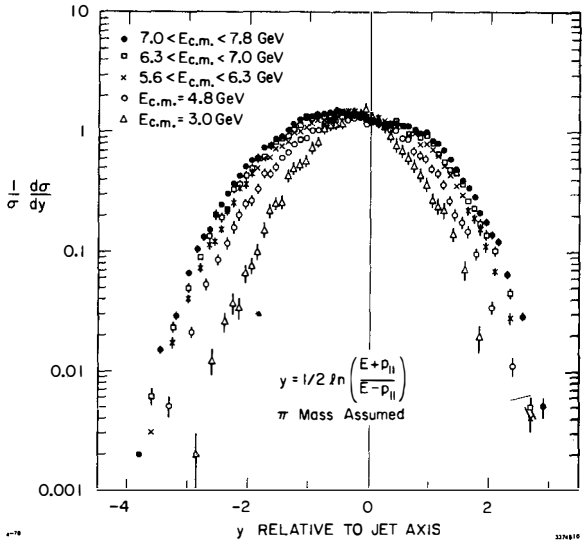

Fig. 13. Particle density distributions $(1/\sigma)d\sigma/dy$ vs. y for $x_{max}>0.3$ for various $E_{c.m.}$. y is the rapidity of the particle relative to the jet direction assuming a pion mass. x_{max} is at positive y and is not plotted. The distributions are normalized to the cross sections for jets with $x_{max}>0.3$.

Figure 17 shows the same distributions as in Fig. 15 plotted versus $p_\perp$ rather than $p_\perp^2$. These distributions are used to calculate the average transverse momentum relative to the jet direction $\langle p_\perp \rangle$ for each of the $E_{c.m.}$. Figure 18 shows $\langle p_\perp \rangle$ opposite jets with $x_{max}>0.3$ versus $E_{c.m.}$. The dependence of $\langle p_\perp \rangle$ on $E_{c.m.}$ is simple evidence for jet structure since $\langle p_\perp \rangle$ levels off as $E_{c.m.}$ increases. The value of $\langle p_\perp \rangle$ for $7.0<E_{c.m.}<7.8$ GeV is 364±2 MeV/c where the error is statistical only. To estimate the systematic error we calculated $\langle p_\perp \rangle$ for various x_{max} cuts for $7.0<E_{c.m.}<7.8$ GeV (see Fig. 14 for $p_\perp^2$ distributions for these x_{max} cuts). The range of $\langle p_\perp \rangle$ for different x_{max} cuts was within ±10 MeV/c of $\langle p_\perp \rangle$ for $x_{max}>0.3$,

Fig. 14. $(1/\sigma)d\sigma/dp_\perp^2$ vs. $p_\perp^2$ for particles opposite jets with various x_{max} cuts for $7.0<E_{c.m.}<7.8$ GeV. $p_\perp$ is the component of particle momentum perpendicular to the jet direction. The distributions are normalized to the cross sections for jets with x_{max} within the specified range.

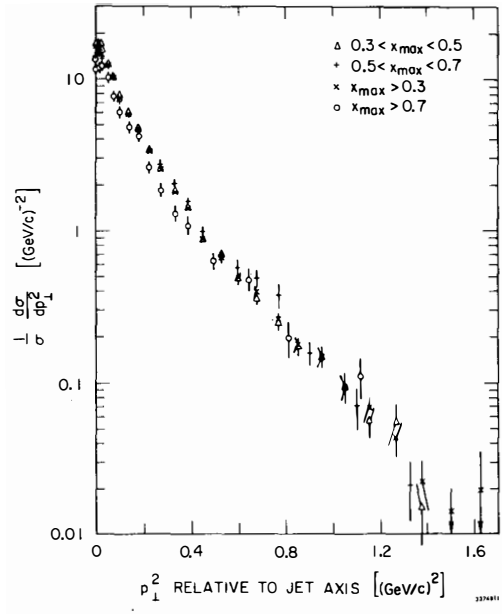

Fig. 15. $(1/\sigma)d\sigma/dp_\perp^2$ vs. $p_\perp^2$ for particles opposite (negative $x_{||}$) jets with $x_{max}>0.3$ for various $E_{c.m.}$. $p_\perp$ is the component of particle momentum perpendicular to the jet direction. The distributions are normalized to the cross sections for jets with $x_{max}>0.3$. The solid lines represent the fits, discussed in the text, to the distributions for $E_{c.m.}$ = 3.0 GeV and $7.0<E_{c.m.}<7.8$ GeV.

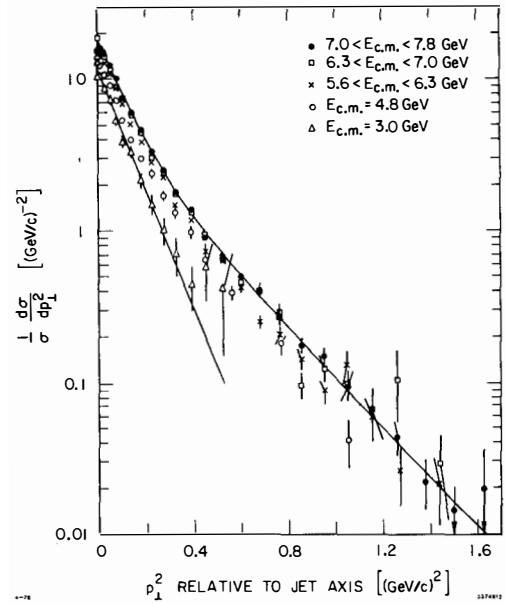

Fig. 16. Observed $(1/N_{ev})dN/dp_\perp^2$ for particles opposite jets with $x_{max}>0.3$ in events with 3 or more charged particles. N_{ev} is the number of observed jets with $x_{max}>0.3$ and $dN/dp_\perp^2$ is the number of particles observed per $(GeV/c)^2$ in each $p_\perp^2$ bin.

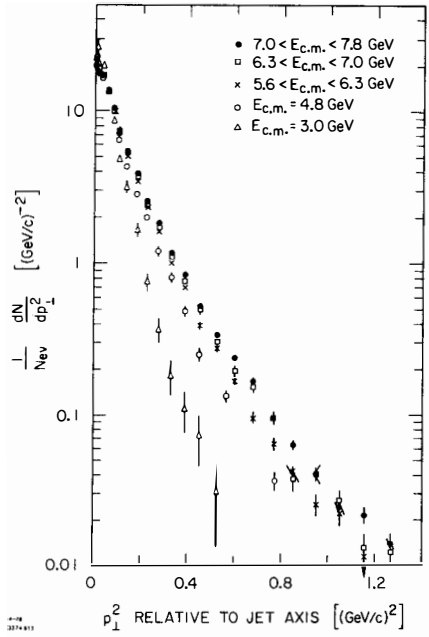

Fig. 17. $(1/\sigma)d\sigma/dp_\perp$ vs. $p_\perp$ for particles opposite jets with $x_{max}>0.3$ for various $E_{c.m.}$. $p_\perp$ is the component of particle momentum perpendicular to the jet direction. The distributions are normalized to the cross sections for jets with $x_{max}>0.3$.

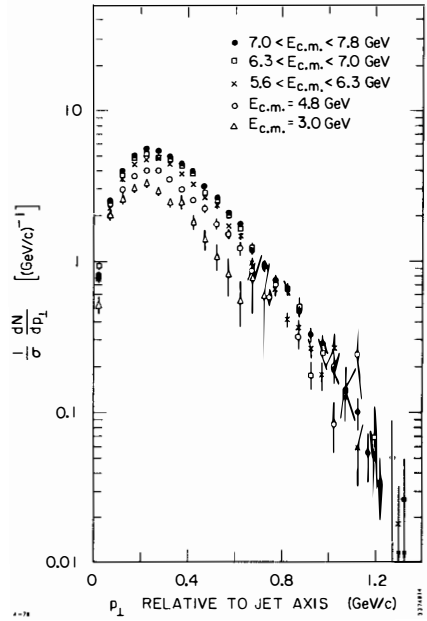

so we estimate the systematic error for $\langle p_\perp \rangle$ to be ±10 MeV/c.

The distributions $(1/\sigma)d\sigma/dp_\perp^2$ versus $p_\perp^2$, shown in Fig. 15, do not fit single exponentials in $p_\perp^2$, except for $E_{c.m.}$=3.0 GeV. The parameters for such attempted fits are listed in Table I. The χ^2/(degree of freedom) are very large for $E_{c.m.} \geq 4.8$ GeV. That a single exponential in $p_\perp^2$ is a poor fit for these energies is obvious from Fig. 15 since the slopes vary with $p_\perp^2$. For $E_{c.m.} \geq 4.8$ GeV the $p_\perp^2$ distributions fit reasonably well to a sum of two exponentials in $p_\perp^2$: $(1/\sigma)d\sigma/dp_\perp^2 = c_1 e^{-b_1 p_\perp^2} + c_2 e^{-b_2 p_\perp^2}$; the parameters for such fits are given in Table II. Only statistical errors were used to determine χ^2. The distributions given by the single exponential fit for $E_{c.m.}$=3.0 GeV and by the sum-of-two-exponentials fit for $7.0 < E_{c.m.} < 7.8$ GeV are represented by the solid lines in Fig. 15. The coefficients of $p_\perp^2$, b_1 and b_2, are plotted versus $E_{c.m.}$ in Figs. 19a and 19b. The larger coefficient b_1 is consistent with about 10 $(GeV/c)^{-2}$ for the three highest energy ranges; it is a little larger at $E_{c.m.}$ =4.8 GeV and a little smaller at $E_{c.m.}$ = 3.0 GeV. The smaller coefficient b_2 is consistent with about 4 $(GeV/c)^{-2}$ for all energies $E_{c.m.} \geq 4.8$ GeV. We have shown quantitatively that the shapes of the $p_\perp^2$ distributions are quite similar for $E_{c.m.} \geq 4.8$ GeV.

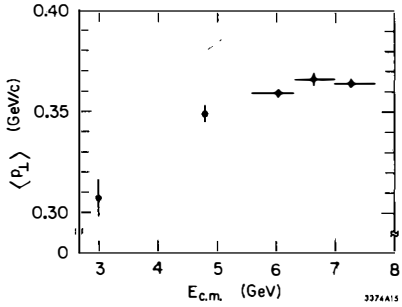

Fig. 18. Average transverse momentum relative to the jet direction $\langle p_\perp \rangle$ for particles opposite jets with $x_{max}>0.3$ vs. $E_{c.m.}$

In Fig. 20 we compare the $p_\perp^2$ distribution for $7.0 < E_{c.m.} < 7.8$ GeV with that for the jet model Monte Carlo. We see that for $p_\perp^2 > 0.6$ $(GeV/c)^2$ the Monte Carlo distribution is lower than the data. $\langle p_\perp \rangle$ for the Monte Carlo distribution is 343 MeV/c, about 20 MeV/c lower than for the data. We also note that the Monte

TABLE I

Fits to $\frac{1}{\sigma}\frac{d\sigma}{dp_\perp^2} = c\, e^{-bp_\perp^2}$ for particles opposite jets with $x_{max}>0.3$ for various $E_{c.m.}$ for $p_\perp^2 > 0.01$ $(GeV/c)^2$.

$E_{c.m.}$ (GeV)	c $[(GeV/c)^{-2}]$	b $[(GeV/c)^{-2}]$	χ^2	degrees of freedom
3.0	11.08±0.45	8.95±0.42	10.40	11
4.8	12.03±0.24	6.96±0.14	92.19	13
5.6-6.3	14.18±0.17	6.64±0.07	240.25	21
6.3-7.0	14.99±0.21	6.40±0.08	182.23	20
7.0-7.8	16.03±0.14	6.43±0.05	472.34	23

TABLE II

Fits to $\frac{1}{\sigma}\frac{d\sigma}{dp_\perp^2} = c_1 e^{-b_1 p_\perp^2} + c_2 e^{-b_2 p_\perp^2}$ for particles opposite jets with $x_{max}>0.3$ for various $E_{c.m.}$ for $p_\perp^2>0.01$ (GeV/c)^2.

$E_{c.m.}$ (GeV)	c_1 [(GeV/c)$^{-2}$]	b_1 [(GeV/c)$^{-2}$]	c_2 [(GeV/c)$^{-2}$]	b_2 [(GeV/c)$^{-2}$]	χ^2	degrees of freedom
3.0	11.08 ±0.45	8.95 ±0.42	--	--	10.40	11
4.8	9.37 ±0.86	13.18 ±1.56	4.93 ±0.98	4.43 ±0.36	4.86	11
5.6-6.3	12.15 ±0.69	10.41 ±0.68	4.13 ±0.80	3.93 ±0.27	23.75	19
6.3-7.0	11.53 ±1.01	11.07 ±1.08	5.87 ±1.17	4.25 ±0.30	36.70	18
7.0-7.8	13.97 ±0.49	10.23 ±0.44	4.62 ±0.56	3.77 ±0.17	29.86	21

Carlo distribution is not a single exponential in $p_\perp^2$. What is the reason for the excess of high $p_\perp$ particles? After testing several hypotheses, we finally found an answer. In Figs. 21a and 21b are shown the $K^{\pm}\pi^{\mp}$ invariant mass distributions for $7.0<E_{c.m.}<7.8$ GeV for both particles with $p_\perp<0.8$ GeV/c and for one or both particles with $p_\perp \geq 0.8$ GeV/c. For the first case we see no signal, but for the second case we see a peak near the D^0 mass of 1863 MeV/c^2.[5] (The only other way that has been found to isolate a D^0 signal in the high-energy data is to require the $K\pi$ momentum to be greater than 1.5 GeV/c.[15]) We therefore have conclusive evidence that some of the high $p_\perp$ particles are the result of D^0 production and decay into $K^-\pi^+$. Other D decays have been studied by Monte Carlo, but of these the decay of a heavy particle into two charged particles is the primary source of particles with $p_\perp>0.8$ GeV/c. In fact, it is possible to produce a quite adequate representation of the observed $p_\perp^2$ distribution by adding to the jet model Monte Carlo a contribution from $D^{0*}\bar{D}^{0*}\pi^+\pi^-$, where $D^{0*}\to D^0\gamma$ or $D^0\pi^0$ and D^0 decays only to $K^-\pi^+$, as shown in Fig. 22. One should note that all high $p_\perp$ particles do not necessarily come from charmed particle decays, and we cannot show that the second exponential in $p_\perp^2$ is completely due to charm. Some high $p_\perp$ particles can

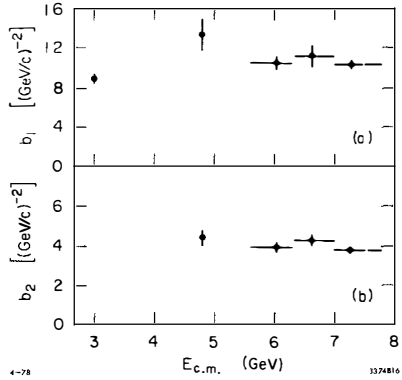

Fig. 19. Coefficients of $p_\perp^2$, (a) b_1 and (b) b_2, for fits of the form $(1/\sigma)d\sigma/dp_\perp^2 = c_1 e^{-b_1 p_\perp^2} + c_2 e^{-b_2 p_\perp^2}$ for particles opposite jets with $x_{max}>0.3$ vs. $E_{c.m.}$.

result from two-jet production, and the jet model $p_\perp^2$ distribution is not a single exponential in $p_\perp^2$.

We have measured the dependence of the $p_\perp$ distributions on $x_\parallel$, or Feynman x, for $7.0<E_{c.m.}<7.8$ GeV. Figure 23 shows the corrected distributions $(1/\sigma)d\sigma/dp_\perp^2$ versus $p_\perp^2$ for several $x_\parallel$ ranges for particles opposite jets with $x_{max}>0.3$. The distributions are normalized to the cross section for jets with $x_{max}>0.3$. From these distributions we see that particles with $x_\parallel$ between 0.1 and 0.3 are the major contributors to the high $p_\perp^2$ region. Particles with $x_\parallel$ less than 0.1 and between 0.3 and 0.5 contribute about equally to the high $p_\perp^2$ region. We were able to calculate $\langle p_\perp \rangle$ for the $x_\parallel$ ranges with $x_\parallel$ less than 0.5; the $p_\perp$ distributions for $x_\parallel$ greater than 0.5 are too poorly defined because of the limited statistics to allow a calculation of $\langle p_\perp \rangle$. In Fig. 24 we present $\langle p_\perp \rangle$ versus $x_\parallel$ for three $x_\parallel$ ranges. $\langle p_\perp \rangle$ increases with increasing $x_\parallel$ in a manner quite like the "seagull" effect seen in leptoproduction.[16]

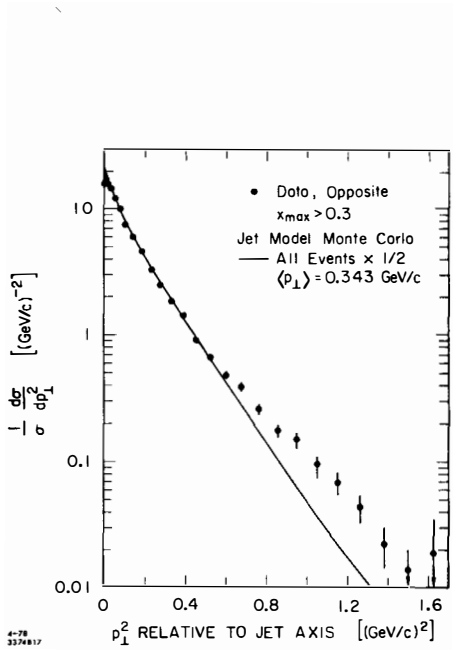

Fig. 20. Comparison of $(1/\sigma)d\sigma/dp_\perp^2$ vs. $p_\perp^2$ for particles opposite jets with $x_{max}>0.3$ for $7.0<E_{c.m.}<7.8$. GeV with the jet model Monte Carlo distribution for all events at $E_{c.m.}= 7.276$ GeV.

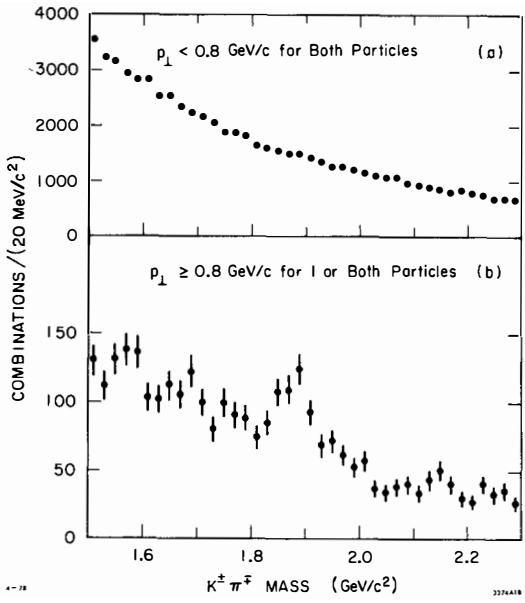

Fig. 21. $K^\pm\pi^\mp$ invariant mass distributions for $7.0<E_{c.m.}<7.8$ GeV for (a) both particles with $p_\perp<0.8$ GeV/c and (b) one or both particles with $p_\perp \geq 0.8$ GeV/c. $p_\perp$ is the component of particle momentum perpendicular to the observed jet axis. No time-of-flight information was used; each combination was plotted twice - once for each mass assignment.

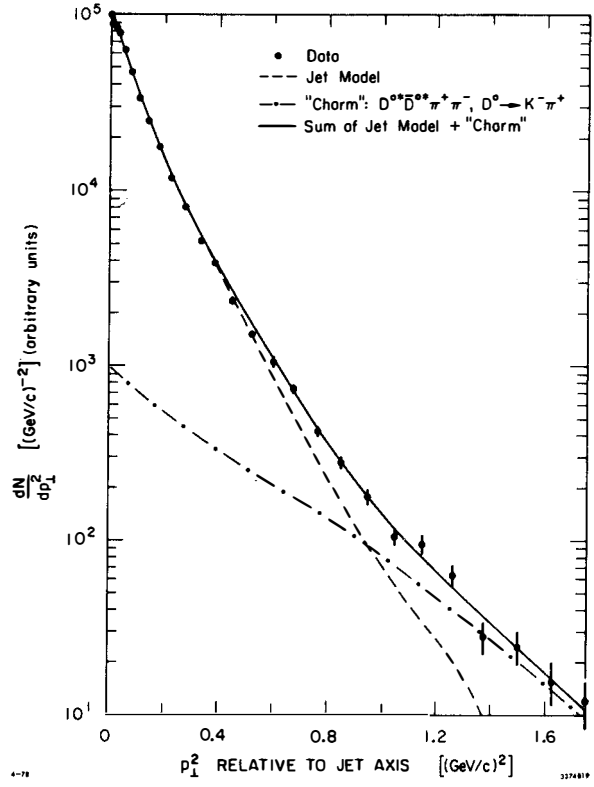

Fig. 22. Observed $p_\perp^2$ distribution for particles opposite jets with $x_{max}>0.3$ in events with 3 or more prongs for $7.0<E_{c.m.}<7.8$ GeV. $p_\perp$ is the component of particle momentum perpendicular to the observed jet axis. The data is compared with the sum of the Monte Carlo predictions of the jet model and a charmed meson production model. The Monte Carlo distribution is normalized to the total number of particles in the data. The relative normalization of the two models was chosen by requiring that the number of high $p_\perp^2$ particles agree with the data.

The p_i^2 distributions for $x_{||}<0.1$ and $0.1<x_{||}<0.3$ can be fitted to sums of two exponentials in p_i^2, and the distribution for $0.3<x_{||}<0.5$ requires only a single exponential. The parameters of the fits to $(1/\sigma)d\sigma/dp_i^2 = c_1e^{-b_1p_\perp^2} + c_2e^{-b_2p_\perp^2}$ are listed in Table III. The minimum p_i^2 used in the fits was varied somewhat to obtain reasonable fits. The fitted distributions are represented by the solid lines in Fig. 23. The values of the coefficients of p_i^2, b_1 and b_2, are plotted versus $x_{||}$ in Figs. 25a and 25b. Since the single coefficient for $0.3<x_{||}<0.5$ was

TABLE III

Fits to $\frac{1}{\sigma}\frac{d\sigma}{dp_\perp^2} = c_1 e^{-b_1 p_\perp^2} + c_2 e^{-b_2 p_\perp^2}$ for particles in various $x_\parallel$ ranges opposite jets with $x_{max}>0.3$ for $7.0<E_{c.m.}<7.8$ GeV.

$x_\parallel$ range	c_1 $[(GeV/c)^{-2}]$	b_1 $[(GeV/c)^{-2}]$	c_2 $[(GeV/c)^{-2}]$	b_2 $[(GeV/c)^{-2}]$	χ^2	degrees of freedom
<0.1 $p_\perp^2>0.09(GeV/c)^2$	8.98 ±0.47	10.37 ±0.72	0.96 ±0.33	3.79 ±0.41	19.17	15
0.1 - 0.3 $p_\perp^2>0.04(GeV/c)^2$	3.09 ±0.47	8.82 ±1.12	2.50 ±0.52	4.17 ±0.24	21.44	17
0.3 - 0.5 $p_\perp^2>0.16(GeV/c)^2$	1.24 ±0.09	3.88 ±0.21	--	--	15.69	11

in agreement with the smaller coefficient for the other two $x_\parallel$ ranges, it was plotted in Fig. 25b. The larger coefficients for $x_\parallel<0.1$ and $0.1<x_\parallel<0.3$ are both consistent with 10 $(GeV/c)^{-2}$, the same value that was found for the $p_\perp^2$ distribution integrated over $x_\parallel$. The smaller coefficients and the single coefficient for $0.3<x_\parallel<0.5$ are consistent with 4 $(GeV/c)^{-2}$, again in agreement with the smaller coefficient for the $p_\perp^2$ distribution integrated over $x_\parallel$. If we were to assume that the exponential with the smaller slope is due to charmed particle production, then we would be forced to conclude that all particles with $0.3<x_\parallel<0.5$ are the result of charmed particle decay, which is unlikely. Unfortunately, we have been able to study only the decay $D^0 \to K^- \pi^+$ which has a branching ratio of only (2.2±0.6)%.[5] We are otherwise unable to separate the charm production component in this analysis.

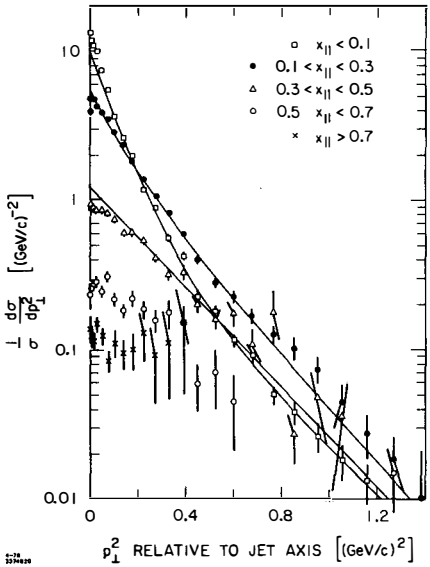

Fig. 23. $(1/\sigma)d\sigma/dp_\perp^2$ vs. $p_\perp^2$ for particles in various $x_\parallel$ ranges opposite jets with $x_{max}>0.3$ for $7.0<E_{c.m.}<7.8$ GeV. The distributions are normalized to the cross section for jets with $x_{max}>0.3$.

We have looked for charge correlations between the leading particle in one jet and all other observed particles in events with three or more charged prongs. The data sample used was the highest energy range $7.0<E_{c.m.}<7.8$ GeV. We plotted $x_\parallel$ distributions using the same method as was described in connection with Fig. 8, except that two distributions were produced - one for those particles with the same charge as x_{max} and another for those particles with the opposite charge to

the x_{max} particle. In Fig. 26 we present the observed ratio $\frac{\text{opposite charge}}{\text{same charge}}$ of these two distributions in $x_{||}$ for two different x_{max} cuts: $x_{max}>0.5$ and $x_{max}>0.7$. x_{max} is at positive $x_{||}$, and, of course, is not included. For this distribution we have used only events in which the total charge was 0 if an even number of particles was observed or ±1 if an odd number was observed. In general, since the detector did not have complete acceptance, one or more particles were not detected, so we do not expect to conserve charge. We also plotted the charged particle multiplicity distribution for each $x_{||}$ bin so that we could calculate the statistical expectation for the charge ratio. For example, for an event with 3 charged particles and total charge ±1 the probability that any 2 particles have opposite charge is 2/3 and the probability that any 2 particles have the same charge is 1/3, so the ratio of opposite charge to same charge is expected to be 2. The expected ratio decreases as the multiplicity increases. The statistical expectation versus $x_{||}$ is represented by the dashed line in Fig. 26. We see that for positive $x_{||}$ the ratio of opposite charge to same charge is much larger than the statistical expectation. This means that there are same-side correlations: particles in the same jet as the x_{max} particle tend to have the opposite charge to the x_{max} particle. Such an effect can be caused by neutral resonances and is expected for various other models. For negative $x_{||}$ there is no evidence for charge correlations. For $x_{max}>0.7$ the point at $x_{||}=-0.85$ is high compared with the statistical expectation, but the difference is not statistically significant. There were only

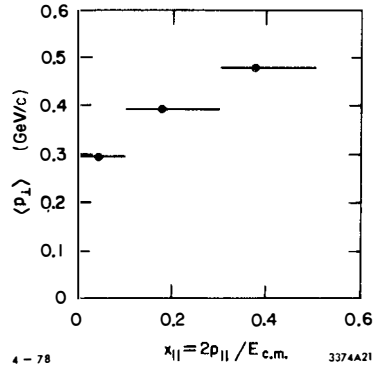

Fig. 24. Average transverse momentum relative to the jet direction $\langle p_\perp \rangle$ vs. $x_{||}$ for particles opposite jets with $x_{max}>0.3$ for $7.0<E_{c.m.}<7.8$ GeV.

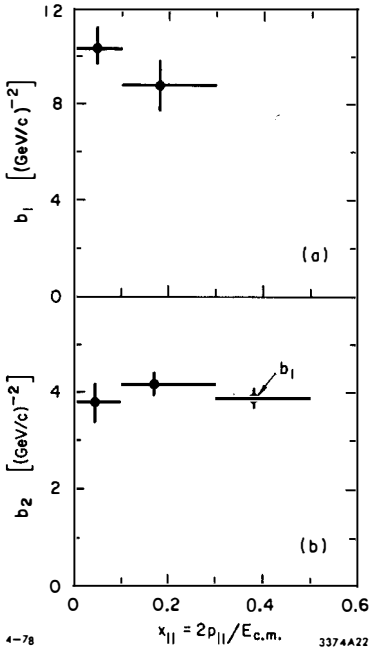

Fig. 25. Coefficients (a) b_1 and (b) b_2 for fits of the form $(1/\sigma)\, i\sigma/dp_\perp^2 = c_1 e^{-b_1 p_\perp^2} + c_2 e^{-b_2 p_\perp^2}$ vs. $x_{||}$ for particles opposite jets with $x_{max}>0.3$ for $7.0<E_{c.m.}<7.8$ GeV.

18 events contributing to this point. Of these 3 had the same charge as x_{max} and 15 had the opposite charge, whereas we would have expected 6 and 12. The probability of observing a charge ratio of 5 or more is about 10%. The statistical expectation is generally a little larger than the measured charge ratio for negative $x_{||}$. In principle, when calculating the statistical expectation for negative $x_{||}$ we should have taken into account the observed charge correlation at positive $x_{||}$. This would have had the effect of lowering the statistical expectation slightly for negative $x_{||}$. The effect would be small because the number of particles at positive $x_{||}$ is small for such large x_{max} cuts (see Fig. 8). Some quark-parton models predict a charge correlation between leading particles in opposite jets due to their production from a quark-antiquark pair. Particles at $x_{||}<-0.5$ are certainly the leading particles in the jet opposite the jet with x_{max}, yet we see no such effect. It may be that to see these leading-particle charge correlations, both particles must have x very near 1; unfortunately, the statistics of our data sample are not sufficient for such a measurement.

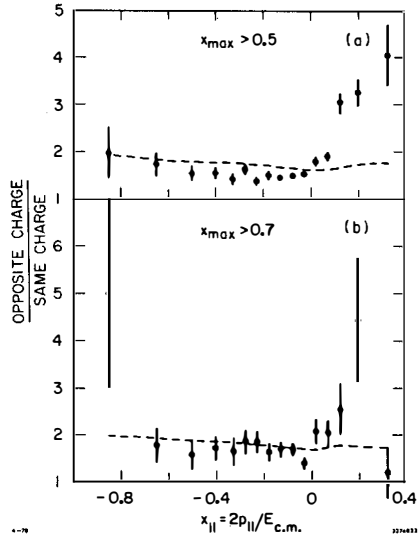

Fig. 26. Observed ratio of the number of particles with opposite charge to the x_{max} particle to the number of particles with the same charge as x_{max} for (a) $x_{max}>0.5$ and (b) $x_{max}>0.7$ vs. $x_{||}$ for $7.0<E_{c.m.}<7.8$ GeV. x_{max} is at positive $x_{||}$. The statistical expectations, calculated from the charged particle multiplicity distributions for each $x_{||}$ bin, are represented by the dashed lines.

VI. CONCLUSIONS

Studies of hadron production by e^+e^- annihilation have yielded very exciting results. The data discussed here were taken by the SLAC/LBL magnetic detector collaboration at SPEAR at center-of-mass energies between 2.6 and 7.8 GeV away from the resonance regions. The major results presented in this talk may be summarized as follows:

1. R, the ratio of the total hadronic cross section to the muon pair production cross section, shows the following behavior, apart from the ψ, ψ', and ψ'' peaks: below 3.5 GeV, R is approximately constant at a value of about 2.6; between 3.5 and 4.5 GeV, R shows a complex structure associated with charm production; above 4.8 GeV, R is again approximately constant

at a value of about 5.3 without subtracting heavy lepton production.

2. The single particle inclusive distributions $s\,d\sigma/dx$ roughly scale for $x \geq 0.3$ for the entire $E_{c.m.}$ range 3.0 to 7.8 GeV.
3. There is strong evidence for jet structure in hadronic events for $E_{c.m.} \geq 4.8$ GeV. At 7.4 GeV the jet axis angular distribution was measured to be proportional to $1 + (0.97 \pm 0.14)\cos^2\theta$, consistent with that for a pair of spin-1/2 particles. A jet model Monte Carlo simulation is able to reproduce the sphericity distributions and the single particle inclusive momentum and angular distributions for events with three or more charged particles.
4. Inclusive distributions in $s\,d\sigma/dx_{\parallel}$, where $x_{\parallel}$ (Feynman x) $= 2p_{\parallel}/E_{c.m.}$ and $p_{\parallel}$ is the component of particle momentum parallel to the jet direction, scale to within 10% for $0.1 < x_{\parallel} < 0.8$ for $E_{c.m.} \geq 4.8$ GeV. Inclusive distributions in $(1/\sigma)d\sigma/dx_{\parallel}$, where σ is the total hadronic cross section, scale rather well for $x_{\parallel} \geq 0.2$ for all energies.
5. The $x_{\parallel}$ distribution for one jet is nearly independent of the magnitude of the momentum of the leading particle in the other jet.
6. Distributions in rapidity with respect to the jet direction have been measured and show the development of a plateau for the three highest energy regions measured, from 5.6 to 7.8 GeV.
7. Distributions in $p_{\perp}^2$ relative to the jet direction have been measured. The average $p_{\perp}$ has been measured as a function of $E_{c.m.}$ and levels off at a constant value for the three highest energy regions measured, giving direct evidence for jet structure. The distributions in $p_{\perp}^2$ can be fitted to the sum of two exponentials in $p_{\perp}^2$. A contribution from charmed meson production needs to be added to the jet model in order to account for all of the high $p_{\perp}$ particles observed.
8. Distributions in $p_{\perp}^2$ as a function of $x_{\parallel}$ have been measured for $7.0 < E_{c.m.} < 7.8$ GeV. The average $p_{\perp}$ increases with increasing $x_{\parallel}$ for $x_{\parallel} \leq 0.5$.
9. Evidence for same-side charge correlations has been found: particles in the same jet as a large-x leading particle tend to have charge opposite to that of the leading particle. There is no evidence for opposite-side charge correlations.

The data seem to be in general agreement with the predictions of quark-parton constituent models. The production of charmed particles complicates the picture somewhat. It should be quite interesting to see what happens at the next higher-energy storage rings PEP and PETRA.

REFERENCES

1. See Gary J. Feldman and Martin L. Perl, Phys. Reports 33C, 285 (1977) and references therein.
2. See G.J. Feldman in Proceedings of Summer Institute on Particle Physics, SLAC-198 (Stanford Linear Accelerator Center, Stanford University, Stanford, California, 1976), p. 81, and references therein; W. Tanenbaum et al., SLAC-PUB-1987, to be published in Phys. Rev.
3. M.L. Perl et al., Phys. Lett. 70B, 487 (1977) and references therein.
4. See G.J. Feldman in Proceedings of Summer Institute on Particle Physics, SLAC-204 (Stanford Linear Accelerator Center, Stanford University, Stanford, California, 1977), p. 241, and references therein.
5. I. Peruzzi et al., Phys. Rev. Lett. 39, 1301 (1977).
6. S.D. Drell, D.J. Levy, and T.M. Yan, Phys. Rev. 187, 2159 (1969), and Phys. Rev. D 1, 1617 (1970); N. Cabibbo, G. Parisi, and M. Testa, Lett. Nuovo Cimento 4, 35 (1970); J.D. Bjorken and S.J. Brodsky, Phys. Rev. D 1, 1416 (1970); R.P. Feynman, Photon-Hadron Interactions (W.A. Benjamin, Inc., 1972), p. 166.
7. G. Hanson et al., Phys. Rev. Lett. 35, 1609 (1975).
8. Members of the SLAC/LBL Mark I magnetic detector collaboration were: G.S. Abrams, M.S. Alam, J.-E. Augustin, A.M. Boyarski, M. Breidenbach, D. Briggs, F. Bulos, W.C. Carithers, W. Chinowsky, J.T. Dakin, R.G. DeVoe, J.M. Dorfan, G.J. Feldman, G.E. Fischer, C.E. Friedberg, D. Fryberger, G. Goldhaber, G. Hanson, R.J. Hollebeek, J.A. Jaros, B. Jean-Marie, D.L. Hartill, A.D. Johnson, J.A. Kadyk, R.R. Larsen, A.M. Litke, D. Lüke, B.A. Lulu, V. Lüth, H.L. Lynch, D. Lyon, R.J. Madaras, C.C. Morehouse, H.K. Nguyen, J.M. Paterson, M.L. Perl, I. Peruzzi, M. Piccolo, F.M. Pierre, T.P. Pun, P. Rapidis, B. Richter, B. Sadoulet, R.H. Schindler, R.F. Schwitters, J. Siegrist, W. Tanenbaum, G.H. Trilling, F. Vannucci, J.S. Whitaker, F.C. Winkelmann, J.E. Wiss, and J.E. Zipse.
9. R.F. Schwitters in Proceedings of the International Symposium on Lepton and Photon Interactions at High Energies (Stanford University, Stanford, California, 1975), p. 5.
10. G. Grindhammer, talk presented at this conference.
11. J. Bürger, talk presented at this conference.
12. G. Wolf, talk presented at this conference.
13. Gail G. Hanson, Proceedings of the VIIth International Colloquium on Multiparticle Reactions (Tutzing, Germany, 1976), p. 313, and Proceedings of the XVIIIth International Conference on High Energy Physics (Tbilisi, U.S.S.R., 1976), p. B1.
14. Yung Su Tsai, Phys. Rev, D 12, 3533 (1975).

15. G.J. Feldman et al., Phys. Rev. Lett. 38, 1313 (1977).
16. See, for example, W.A. Loomis, et al., "Hadron Production in Muon-Proton and Muon-Deuteron Collisions," Harvard University preprint, submitted to Phys. Rev.

RECENT RESULTS FROM DELCO*

Alain-Michel Diamant-Berger
Physics Department, Stanford University
Stanford, California 94305 USA
and
DPhPE/SEE, CEN Saclay
BP n° 2, 91190 Gif sur Yvette FRANCE

Abstract: The new data from the DELCO experiment give conclusive evidence for the existence of the heavy lepton. Preliminary results on the τ branching ratio and an analysis of the electron spectrum are presented. A preliminary look at D beta decay in terms of K and K*(890) is also discussed.

Résumé: Les données récentes accumulées par l'expérience DELCO apportent une preuve convaincante de l'existence du lepton lourd τ. Cet exposé présente des résultats préliminaires sur les modes de desintégration du lepton τ ainsi qu'une analyse du spectre d'impulsion des électrons secondaires. La situation actuelle de notre analyse des desintégrations semileptoniques du méson D est aussi présentée.

* Work supported by the U.S. National Science Foundation and Department of Energy.

1. Introduction

The DELCO[1] experiment has been located at SPEAR, in the east pit, since the beginning of 1977. It was designed to study the production and decays of new particles, tagged by direct electrons emitted in weak decays. Two kinds of particles are now known to provide such a signal: the charmed particles[2] and the heavy lepton τ,[3] and DELCO is particularly well suited to study their properties. In this talk, I will briefly describe the detector and review older results, as they stood at the end of 1977, before presenting the latest data which are, of course, preliminary.

2. The Detector

The detector[4] is shown in Fig. 1. The interaction region sits in a 3.5 kG near axial field provided by two coils wrapped on steel pole pieces 85 cm apart. The beam passes through the poles of the magnet and the return yoke is extended far up and down to avoid interfering with the rest of the detector. A set of six cylindrical multiwire proportional chambers extend from the beam pipe to a radius of 30 cm. The inner four cylinders subtend 80% of 4π steradians. Four of the cylindrical high voltage foils are divided into 2 cm strips inclined at 45° to the beam axis, to provide a crude depth measurement. Scintillation counters on the pole tips increase the solid angle for detection of charged particles.

The MWPC are surrounded by a segmented Cerenkov counter filled with ethane at atmospheric pressure. In each of the 12 cells a double bounce optics focuses the Cerenkov light onto a 5 inch phototube coated with PTP wave-shifter yielding, on the average, 10 photoelectrons for a $\beta=1$ particle, and a hadron rejection better than 10^{-3}. Next in the sextants are located two planes of magnetostrictive spark chambers providing two ψ and z measurements per track. Together with the MWPC information they give the following accuracies: $\sigma p/p \simeq 10\ p\ (\text{Gev/c})\%$, $\sigma_{\phi} \simeq \sigma_{\theta} \simeq 5$ mrad. Finally, behind the spark chambers, an array of shower counters consisting of three layers of lead and scintillator covers roughly 60% of 4π steradians, the inner layer strips being timed at both ends. Over the last summer, we added two lead walls followed by spark chambers and scintillation counters to obtain a muon identification over 20% of 4π, for particles with a momentum above 700 MeV/c. We do not have results to report yet involving this new piece of equipment.

The trigger for the experiment relies heavily on the shower counters: the coincidence of at least two out of three layers of a shower module, called an S signal, is satisfied by charged particles, as well as by relatively soft photons. The basic trigger requires a track in the inner two MWPC in coincicence with two S signals from different sextants within 20 ns of the beam

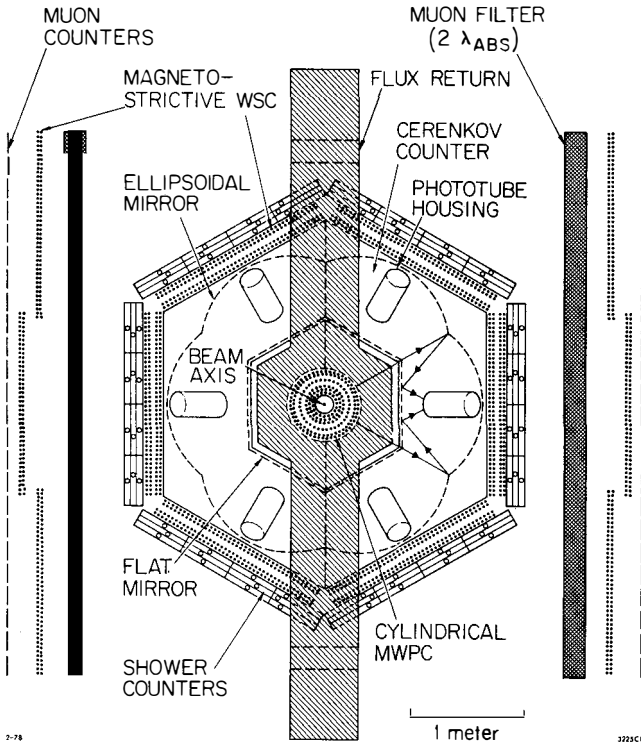

Fig. 1: The DELCO detector.

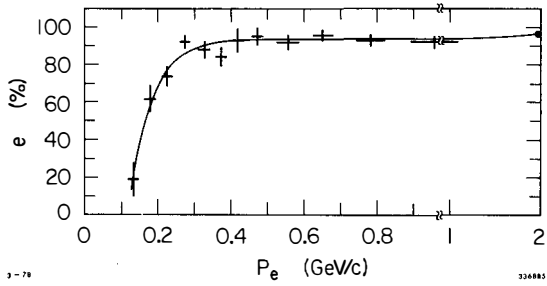

Fig. 2: Cerenkov efficiency as a function of the electron momentum. The curve was obtained by a Monte Carlo simulation of our optics.

crossover time. It is mixed with two other triggers which allow all neutral final states: three S from three different sextants, or two S with a minimum total pulse height rejecting cosmics. The combined trigger rate is 0.7 Hz.

After track finding, cosmic ray events and beam gas interactions are removed on the basis of timing and vertex cuts. The remaining 15% of the triggers are real e^+e^- interactions and are classified into two main categories:

- QED processes including the final states e^+e^-, $\mu^+\mu^-$, $\gamma\gamma$, $e^+e^-\gamma$, etc. These events represent roughly two thirds of the interactions and we use them very extensively for calibration and normalization purposes. In particular, the eeγ events gave us a way to measure the efficiency of our Cerenkov as a function of the electron momentum, as shown in Fig. 2.

- hadronic events including multiprong events (with three tracks or more emerging from the interaction region), and two-prong events (if they are acoplanar with the beam by more than 5^o, and one track is not an electron). Particular attention is given to the subset of events having one electron candidate, that is a track giving an in-time pulse in both a Cerenkov cell and a shower module.

The determination of our hadronic detection efficiency somewhat depends on the "true" multiplicity distributions which we tried to unfold from our observed events. Thanks to our neutral triggers, it is well above 90% for events with at least 4 prongs, and around 50% for two-prong events. An averaged detection efficiency at $E_{c.m.}$ of 3.8 GeV is 0.85±0.1.

3. Old Results[4]

The measured value of $R \equiv \frac{\sigma(e^+e^- \to \text{hadrons})}{\sigma(e^+e^- \to \mu^+\mu^-)}$ in the range 3.6 GeV < E_{CM} < 4.8 GeV is displayed on Fig. 3. The errors shown are statistical and the vertical scale may possess an overall systematic error of 20%. The general features of this plot are in reasonable agreement with those already measured at SPEAR[5] and DORIS.[6] We very carefully investigated the dip around 4.25 GeV and the new resonance ψ'' whose parameter we determine to be:

$$M = (3770 \pm 6)\ \text{MeV}/c^2$$
$$\Gamma = (24 \pm 5)\ \text{MeV}/c^2$$
$$\Gamma_{ee} = (180 \pm 60)\ \text{eV}$$

This resonance has been identified as the first $^3D_1$ state of charmonium predicted in 1975 by Eichten et al.[7] Since it sits above the expected $D\bar{D}$ threshold,[8] but below any $D\bar{D}^*$ threshold, it decays only into $D\bar{D}$ states, and thus provides a very clean laboratory to study the D meson.[9]

It is very interesting to compare the behavior of R with the variation of $R_e = \frac{\sigma(e^+e^- \to e^+ + XX)}{\sigma(e^+e^- \to \mu^+\mu^-)}$ in the same energy range, shown in Fig. 4. All the

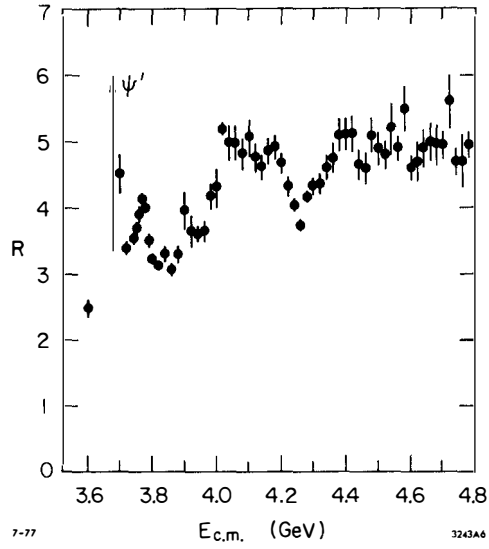

Fig. 3: The hadronic cross-section R as a function of the center of mass energy.

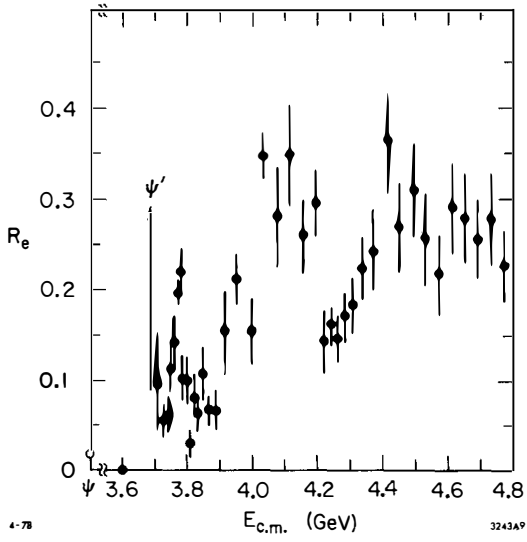

Fig. 4: Variation of R_e as a function of $E_{c.m.}$

structures observable in R are also visible in R_e, but with a much smaller background. In particular, the ψ'' resonance is clearly visible, and this provides unambiguous evidence for the semileptonic decay of D mesons. The comparison of the relative size of the ψ'' peaks in both plots, after correction for losses into two and fewer observed prongs gives a measurement of the semileptonic branching ratio:

$$\frac{BR\ (D \to e\nu X)}{BR\ (D \to all)} = 11 \pm 2\%$$

This is consistent with other measurements at SPEAR and DESY.[10]

Finally, the smooth excitation curve we obtained for the two-prong electron events contrasted sharply with the R_e curve and gave support to the hypothesis of a heavy lepton as a possible origin for those events.

4. New Results

Since last summer, in order to investigate further the heavy lepton hypothesis, we first took a lot of new data at energies below charm threshold (3.5 GeV, 3.625 GeV, 3.684 GeV, 3.72 GeV) and we performed a new analysis of our older data, in order to gain some statistics. The steps in our new procedure invole selecting events with only 2 charged prongs and any number of photons. One of the tracks, the electron cadidate, must have a momentum greater than 200 MeV/c and trigger the Cerenkov cell it traverses. The other track must have a momentum greater than 300 MeV/c and not trigger its Cerenkov cell. The relative azimuthal angle between the two tracks has to be less than 160°. Events with a topology compatible with $ee\gamma$ (15) are then rejected, leaving a sample of 660 events. The shower pulse height for both tracks in these events is shown in Fig. 5, together with the distribution expected for a non-electron track. To further eliminate electrons which have not been tagged by the Cerenkov, the X prong is required to have a shower counter pulse less than 3.3 times a minimum ionizing pulse. This leaves 540 events with an estimated background of 15 events, consistant with the rate of events seen at the $\psi(3095)$ and at 3.5 GeV. The contribution from two photon processes ($e^+e^- \to e^+e^-\mu^+\mu^-$) where only two particles are detected is estimated to be less than 2% by comparing the number of events witn like sign and opposite sign particles.

The number of events for different values of the center of mass energy is given in Table I, and the corresponding rate normalized to muon pairs, r_e, is shown in Fig. 6. It is already clear from the table that there is a threshold between 3.5 and 3.6 GeV for the production of eX events, and that this threshold is definitively different from the charm threshold, since we observe 35 events without photons at energies between 3.6 and 3.72, with an expected background of at most 2 events.[11] The data at the ψ'' are estimated to contain a 20% background from charm and will be eliminated from all the subsequent analysis.

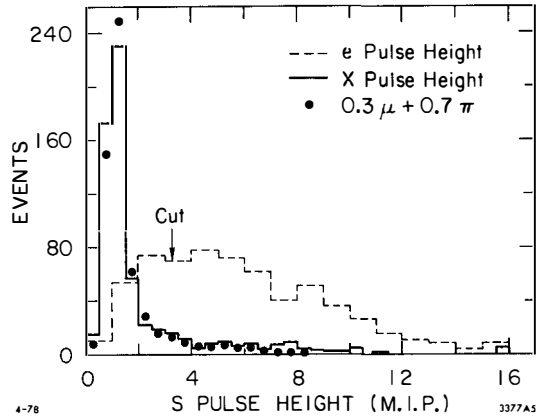

Fig. 5: Shower counter pulse height for both tracks in eX events, normalized to minimum ionizing particles.

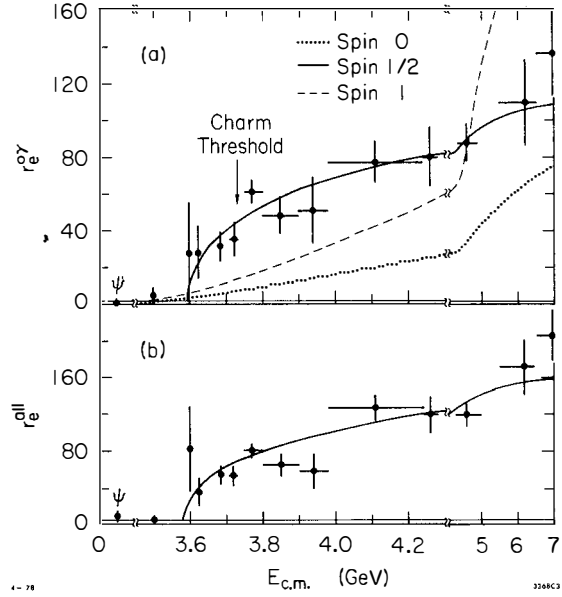

Fig. 6: Rate of eX production, normalized to muon pairs for a) events without photons, b) all events.

Table I: Measurement of the eX production rate as a function of energy.

$E_{c.m.}$	$N_{\mu\mu}^{4\pi}$	eX(noγ)	$r_e^{o\gamma}(\times 10^{-3})$	eX(all)	$r_e(\times 10^{-3})$
ψ	2456	0	0 + 2.3	4	9±5
3.5	1253	1	4.5±4.5	1	4.5±4.5
3.6	207	1	27.5±27.5	3	82.6±47.7
3.625	817	4	27.9±14	5	34.9±15.6
'ψ'(3.689)	2724	15	31.4±8.1	26	54.4±10.7
3.725	2434	15	35.1±9	23	54±11
ψ"(3770)	8329	89	60.9±6	118	81±7
3.80-3.90	2615	22	48±10	30	65±12
3.90-3.98	889	8	51.3±18	9	68±19
3.98-4.24	3841	52	77.1±11	86	128±14
4.24-4.28	1856	26	79.8±16	39	120±19
4.28-4.99	4899	76	88.4±10	104	121±12
4.99-6.5	1187	23	110.4±23	36	173±29
6.5-7.4	1535	37	137.4±23	56	208±28

Charm background at higher energies is expected to be less than our statistical errors and has therefore been neglected. Also shown on Fig. 6 are the fitted excitation curves for a pointlike spin 1/2 particle, letting the mass and the branching ratios vary. The results of the fits are summarized in Table II.[12] It is not possible to get a good fit to the data, either with a spin 0 pointlike particle because of the high yield of eX events, or with a spin 1 particle because of the very slow rise with the center-of-mass energy.

Table II: Results of the fits to the excitation curve (see ref.12)

		eX,noγ	eX,all
M_τ (GeV/c^2)	:	$1.795\ ^{+.005}_{-.011}$	$1.792\ ^{+.006}_{-.011}$
$2b_e b_x$	:	0.118 ± .008	0.170 ± 0.10
χ^2/NDF	:	7.6/11	17.0/11

In order to extract some branching ratio information from the asymptotic values of r_e, we use the results of the theoretical computation by Gilman and Miller[13] and assume that the relative decay rates for τ giving one charged prong are well known. This yields a branching ratio to electrons of (16±1)% and a branching ratio to multiprongs of (32±3)%, where the errors are

statistical only.

We can now use our two-prong electron events to study the electron momentum distribution which, in complete analogy to muon decay, yields information about the helicity of the τ neutrino and thus about the V-A or V+A coupling responsible for the decay. In the same spirit, it is very convenient to parametrize this momentum spectrum in terms of the Michel parameter ρ whose values are 0 for V+A, and 0.75 for V-A. We first compare in Fig. 7 the mean value of the electron energy divided by the beam energy, for different energy bins, with the predicted values:[14] 0.35 for V-A and 0.30 for V+A. Next, we fit the electron spectrum integrated over all energies (Fig. 8) with spectra obtained by Monte Carlo, for different values of ρ. The results of the fits are summarized in Table III. We conclude from those two tests that the agreement with V-A is excellent, and that if V+A is not completely ruled out, it is at least very unlikely (<1% probability). We also investigated the effect of a finite neutrino mass[15] on the electron spectrum and found an upper limit of 250 MeV/c^2 at the 90% confidence level.

Table III: Results of fits to the electron spectrum

Hypothesis	ρ	χ^2/NDF
V+A	0	38/18
V-A	0.75	17.6/18
	0.73±0.15	17.5/17

We also tried to extract some information on the τ from our multiprong electron events. The problem there is to take care of the very important contribution of the charmed particles to those events. We used two different methods. First we selected the multiprong electron events in the charm depleted regions at $E_{c.m.}$ of 3.72, 3.85 and 4.25 GeV, and we rejected the remaining charm contribution by requiring the electron momentum to be greater than one third of the beam momentum. This gives us 78 multiprong events to be compared with 29 eX events with the same cuts. After correction for the relative detection efficiencies and assuming our measured value for the branching ratio into electrons, we obtain a multiprong branching ratio of (34±6)%. The other method relies on the assumption that charm events do not contribute to the highest part of the electron momentum spectrum: as we cut progressively higher on the electron momentum, the ratio of multiprong to two-prong electron events should become constant, when the charm limit has been reached. This is shown on Fig.9. The ratio of 1.8±.3 gives, after correction for detection efficiencies, a multiprong branching ratio of (35±6)%.

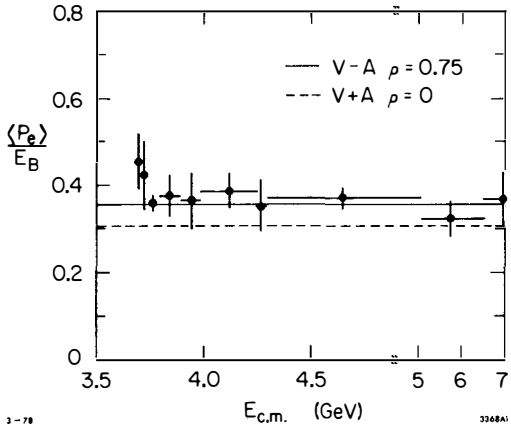

Fig. 7: Averaged electron momentum divided by the beam energy, for eX events.

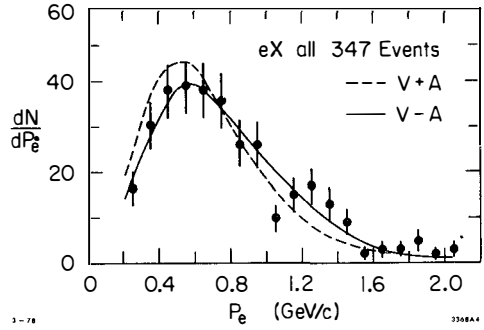

Fig. 8: Electron momentum spectrum for eX events, Ψ" excluded. The curves are Monte Carlo generated simulations.

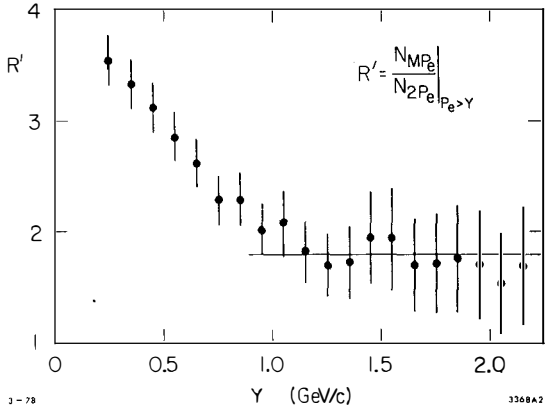

Fig. 9: Ratio of the number of multiprong electron events to the number of two-prong electron events, as a function of the lower cut on the electron momentum.

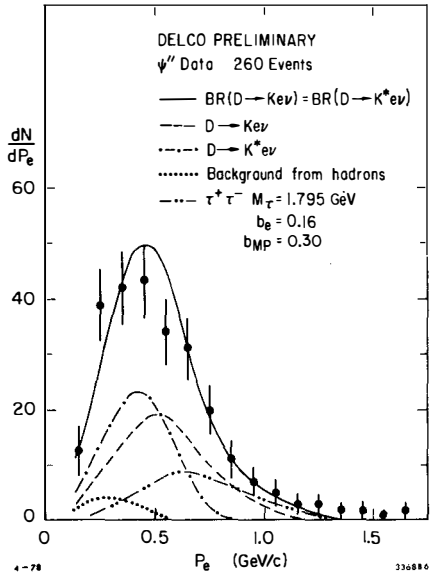

Fig. 10: Electron momentum spectrum for multiprong events at the Ψ''(3370). The full line represents the sum of all the other contributions.

It is worth pointing out that our three independant determinations of the multiprong branching ratio are in very good agreement with each other and with earlier estimates by the PLUTO and DASP collaborations at DESY.[16] Such a high multiprong branching ratio implies a very important contribution of the τ in the multiprong events all over the charm region, and in particular a 20% background at the ψ"(3770)!!

Let us finally turn to the D meson semileptonic decays and assume we understand reasonably well the τ background under the ψ". The multiprong electron spectrum at this resonance is shown on Fig. 10 together with our best estimates for the background from misidentified hadrons and heavy lepton events. The remaining part has been fitted with $D \to Ke\nu$ and $D \to K^*(890)e\nu$ in variable amounts. The best agreement has been obtained for equal amounts of those two decay modes and the resulting curve is also drawn on Fig. 10. It should be noted that this result is still very preliminary, and that it is very sensitive to the τ background subtraction which we are still investigating.

5. Conclusion

In the present status of our experiment, I have tried to convince you that the heavy lepton τ exists and in particular that the charm is completely ruled as a single source for the two-prong electron events. All the properties we could investigate so far are perfectly compatible with a spin 1/2 pointlike particle decaying through V-A into a massless neutrino and other particles, with branching ratios accurately predicted by different models.

The second conclusion is that the complete study of the 4 GeV energy region will be very delicate, with a sizeable contribution from charm into the two-prong class (at least at the ψ"), and a contribution of the same order of magnitude from the heavy lepton in the multiprong class.

We are now trying to pursue our analysis using our new muon detector, and we are still taking data which will, maybe, bring still other unexpected developments.

Acknowledgments

The results presented here are the work of the physicists presently involved with DELCO: W. Bacino, A. Diamant-Berger, T. Ferguson, A. Hall, G. Irwin, J. Kirz, F. Merritt, L. Nodulman, M. Schwartz, W. Slater, H. Ticho and S. Wojcicki, under the efficient leadership of our spokesman, J. Kirkby.

I wish to thank M. Schwartz and S. Wojcicki for their warm hospitality during my stay at Stanford, and Tran Thanh Van for giving me an opportunity to present these results during the XIII Rencontre de Moriond at Les Arcs.

References

1. The DELCO experiment (an acronym for Direct Electron Counter) was built as a collaboration of three universities: Stanford, U.C. Irvine and U.C. Los Angeles.

2. S.L. Glashow, Illiopoulos and Maiani, Phys. Rev. D2, 1285 (1970).
G. Goldhaber et al., Phys. Rev. Lett. 37, 1755 (1976).
H.K. Nguyen, Proceedings of the XII Rencontre de Moriond, Tran Thanh Van editor p 39.

3. M.L. Perl et al., Phys. Rev. Lett. 35, 1489 (1975).
M.L. Perl, Proceedings of the XII Rencontre de Moriond, Tran Thanh Van editor p. 75.

4. W. Bacino et al., Phys. Rev. Lett. 40, 671 (1978).
J. Kirkby, Proceedings of the 1977 Symposium on Lepton and Photon Interaction, Hamburg, p 3.

5. J. Siegrist et al., Phys. Rev. Lett. 36, 700 (1976).
P. Rapidis et al., Phys. Rev. Lett. 39, 526 (1977).

6. See the contributions by Dr. Burger and Grindhammer in these proceedings.

7. E. Eichten et al., Phys. Rev. Lett. 34, 369 (1975).
K. Lane and E. Eichten Phys. Rev. Lett. 37, 477 (1976).

8. G. Goldhaber et al., Phys. Lett. 69B, 503 (1977).

9. I. Peruzzi et al., Phys. Rev. Lett. 39, 1301 (1977).

10. R. Brandelik et al., Phys. Lett. 70B, 387 (1977).
J.M. Feller et al., Phys. Rev. Lett. 40, 274 (1978).

11. Two-prong electron events below charm threshold have been previously reported by R. Brandelik et al., Phys. Lett. 73B, 109 (1978).

12. Since the time of the Conference, new data have been taken and analyzed at center-of-mass energies of 3.52 GeV and 3.57 GeV. One event for 1060 $\mu\mu$ and 6 events for 2670 $\mu\mu$ have been found respectively. This gives a possible range for the τ mass: $1.760\ \text{GeV} < M_\tau < 1.785\ \text{GeV}$. A fit including the new points yields: $M_\tau = 1.777 \pm \begin{smallmatrix}0.05\\0.09\end{smallmatrix}\ \text{GeV}/c^2$.

13. F. Gilman and D.H. Miller SLAC-PUB-2046 (1977) to be published in Phys.Rev.

14. O. Nachtmann and A. Pais, Phys. Rev. D16, 630 (1977).

15. We thank Yung-Su Tsai for providing us with the formulas including a massive τ neutrino.

16. J. Burmeister et al., Phys. Lett. 68B, 297 (1977).
R. Brandelik et al., Phys. Lett. 73B, 109 (1978).

NEW RESULTS ON e^+e^- ANNIHILATION FROM DASP[1)] (I)

Günter Grindhammer

Max-Planck-Institut für Physik und Astrophysik, München

ABSTRACT

This report focuses on the following topics:

- a measurement of the total hadronic cross section in e^+e^- annihilation between 3.6 and 5.2 GeV,
- new data on the cascade decay from the $\psi'(3.7)$,
- a search for the decay $\psi' \to J/\psi\ \pi^o$, and
- measurements of J/ψ radiative decays mediated by two gluon exchange.

RESUME

Le rapport comporte les sujets suivants:

- la mesure de la section efficace hadronique totale de l'annihilation e^+e^- dans l'intervalle d'énergie de 3.6 à 5.2 GeV
- résultats récents sur la désintégration en cascade de la résonance $\psi'(3.7)$
- la recherche de la désintégration $\psi' \to J/\psi\ \pi^o$ et
- les mesures des désintégrations radiatives de la résonance J/ψ par l'échange de deux gluons.

I. INTRODUCTION

In this talk on recent results by the Double Arm Spectrometer (DASP) collaboration[1] at the e^+e^- storage ring DORIS, the following topics will be covered:

1. Measurement of $R = \frac{\sigma(e^+e^- \to \text{hadrons})}{\sigma(e^+e^- \to \mu^+\mu^-)}$ between 3.6 and 5.2 GeV and the observation of three resonance like structures above charm threshold.
2. New high statistic measurement of the cascade decay $\psi' \to P_c/\chi$, $P_c/\chi \to \gamma J/\psi$, $J/\psi \to \mu^+\mu^-$ and a review of all experimental data concerning the status of the $\chi(3.45)$ state, plus a search for the decay $\psi' \to J/\psi\pi^0$.
3. Measurement of two gluon exchange in J/ψ radiative decays

For other results obtained recently by DASP the reader is referred to the talk by G. Wolf at this meeting.

II. THE DETECTOR

The DASP detector (see Figs. 1 and 2) consists of two identical magnetic spectrometer arms and a nonmagnetic inner detector located between the two magnets.

The magnetic spectrometer arms cover a solid angle of $\simeq 2 \cdot .04 \cdot 4\pi$ and have a maximum bending power of 1.8 Tm. The momentum resolution σ_p/p^2 (p in GeV/c) varies typically between 0.8 % and 2.5 % depending on the magnet excitation. A particle entering a magnetic arm traverses the following counters and chambers: a total of three scintillation counters, two proportional chambers, a threshold Cerenkov counter for electrons, and one spark chamber in front of the magnet, and five spark chambers, time of flight, shower, and range counters behind the magnet. Muons are identified by the range counters. Electrons are detected through the Cerenkov and shower counters. Using the momentum and time of flight information, it is possible to separate pions and kaons up to momenta of 1.5 GeV/c and to identify protons up to momenta of 3 GeV/c.

The nonmagnetic inner detector covers a solid angle of $0.7 \cdot 4\pi$. It is azimuthally divided into 6 segments, each consisting of four modules and lead scintillator shower counters at the end. Each module is made up of a scintillation counter hodoscope, a sheet of lead 5 mm thick, and a propor-

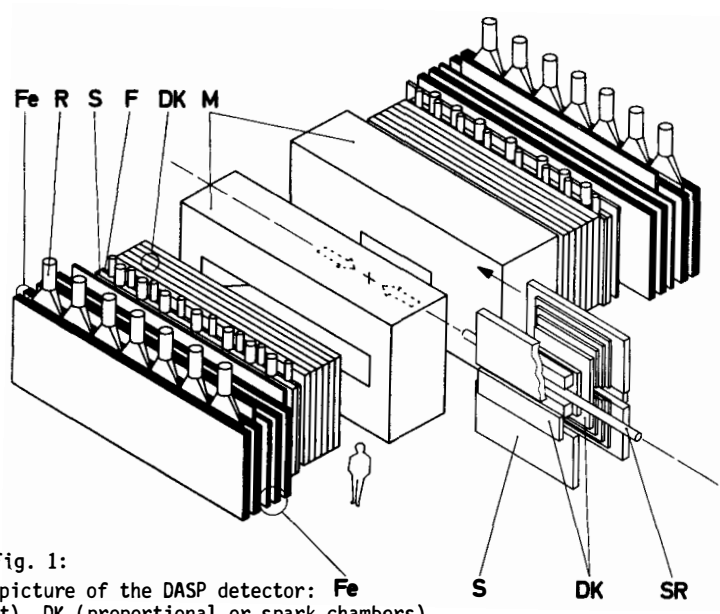

Fig. 1:
Blow up picture of the DASP detector: M (Magnet), DK (proportional or spark chambers), F (time of flight counters), S (shower counters), R (range counters), Fe (iron), SR (beam pipe)

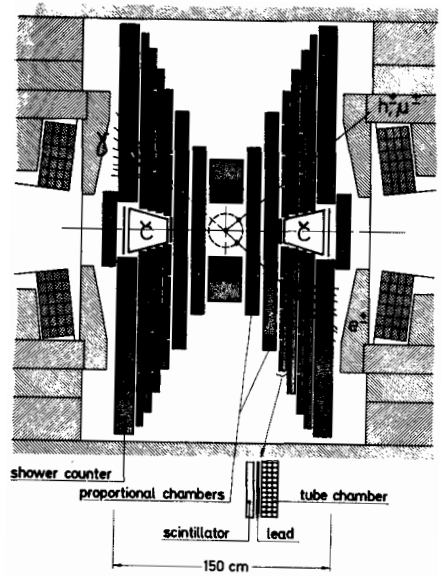

Fig. 2: Nonmagnetic Inner Detector

tional chamber. Each of the 6 segments is split perpendicular to the beam line at the interaction point into two segments leading to a total of 12 inner detector segments. For a 50 MeV photon the detection efficiency is about 50 % and rises to 90 % at 100 MeV and to 95 % above 200 MeV. The rms energy resolution for photons is about 14 % for a 1 GeV photon.

The inclusive trigger[2] of DASP demands that at least one charged particle traverses one of the spectrometer arms. The requirements of the multi-hadronic trigger[3] are that at least 3 of the 12 inner detector segements and at least one of the 22 beam pipe counters fire.

III. THE TOTAL HADRONIC CROSS SECTION

The total hadronic cross section including contributions from $\tau\bar{\tau}$ production has been previously measured by SLAC-LBL[4] and PLUTO[5] using solenoidal detectors. While these two experiments agree on the general shape of the cross section, they show differences in detail.

In contrast to the previous experiments, the DASP experiment[2] has in particular two features which help improve our knowledge of the total cross section and which give different systematic uncertainties. First, we used a nonmagnetic detector with similar trigger and detection efficiency for both, charged particles and photons. Second, in first approximation, the detection efficiency was determined experimentally and not by a Monte Carlo computation.

We have collected data for center of mass energies between 3.6 and 5.2 GeV. The total integrated luminosity excluding the ψ' was about 7500 nb^{-1}. The multihadron trigger requirements as described in section II led to about 10^7 events consisting mainly of beam gas and cosmic ray background and of only about 1 % good events. Several stringent software cuts were applied removing 25 % to 30 % of the good events but eliminating almost all of the background. Using the time of flight between the outermost scintillation counters of the inner detector, the remaining background due to cosmic rays was found to be less than 2 %. A remaining background of 3 to 5 % due to beam gas, as estimated from the distribution of the reconstructed vertex points along the beam axis, was subtracted from the data. The background in the remaining data due to higher order QED-processes ($e^+e^- \to L^+L^-\gamma$, $e^+e^- \to e^+e^-L^+L^-$ with L = e ,μ) and due to $e^+e^- \to e^+e^-$ + hadrons was found to be negligible.

To determine the detection efficiency for hadronic events, we took advantage of the fact that the inclusive trigger (see section II) operates independently and parallel to the multihadronic trigger. Therefore the hadronic detection efficiency to first approximation is given by:

$$\varepsilon^{EXP} = N^{MH}_{INC}/N_{INC} \qquad (1)$$

where N^{MH}_{INC} is the number of inclusive events which in addition satisfy the multihadron trigger and software requirements and N_{INC} is the total number of inclusive events. Numerically ε^{EXP} is about 40 %. This experimental determination of the efficiency is not free of bias (for example, only a charged particle can lead to an inclusive trigger) and has to be corrected for by Monte Carlo. For this purpose a program was used which simulated in detail the DASP-detector. The production of pions, kaons and nucleons was taken into account, reproducing the momentum spectra as measured by DASP[2]. The production and decay of charmed mesons and $\tau\bar{\tau}$ was also included. The computations showed that the efficiency for the detection of heavy lepton events is only 1/3 the efficiency for real hadronic events. Since the heavy lepton production should not be counted in the total hadronic cross section, we subtracted the small heavy lepton contribution (~ 10 %) from the data. The total hadronic cross section is then given by

$$\sigma(e^+e^- \to \text{hadrons}) = \frac{N \cdot \varepsilon^{EXP} \cdot (\text{correction factor})}{L} \qquad (2)$$

where N is the number of hadronic events and L is the integrated luminosity which was determined from small angle Bhabha scattering. ε^{EXP} is the experimentally determined efficiency as described above. The correction factor is about 1.07 and turns out to be rather insensitive to the specific parameters of hadron production such as jet versus phase-space production or charged and neutral multiplicities. The overall efficiency (ε^{EXP} · correction factor) is shown in Fig. 3 as a function of the center of mass energy. The final efficiency corrections which were applied were taken from the straight line interpolation of the data.

The radiatively corrected hadronic annihilation cross section normalized to the $\mu^+\mu^-$ cross section is shown in Fig. 4. The systematic normalization uncertainty is estimated to be 15 % and is not indicated in Fig. 4. The data show three peaks centered around 4.04, 4.16 and 4.42 GeV. The fit shown in the figure was made under the simplifying assumptions that

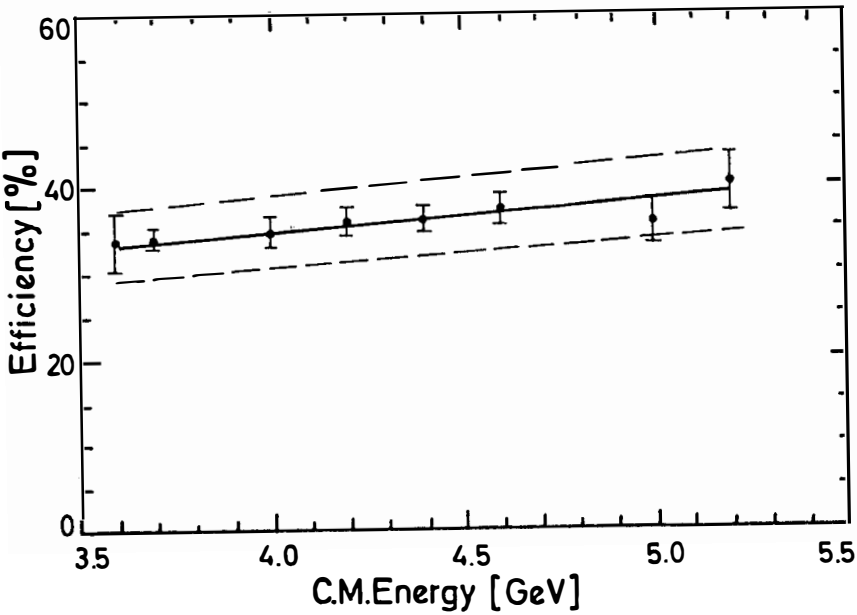

Fig. 3 Detection efficiency versus energy. The straight line interpolation of the data points is indicated together with the estimated error band of ± 12 %.

the cross section can be described by three Breit-Wigner resonances

$$\sigma_R^i = \frac{3\pi}{s} \frac{\Gamma_{ee}^i \Gamma_{tot}^i}{(\sqrt{s} - M_R^i)^2 + (\Gamma_{tot}^i/2)^2} \tag{3}$$

and by a nonresonant background term of the form

$$\sigma_B = \sigma_{3.6} \frac{3.6^2}{s} + \sum_{k=1}^{6} A_K \beta_K^3 \frac{F^2}{s} \tag{4}$$

where the sum is over the $D\bar{D}$, $D\bar{D}^*$, $D^*\bar{D}^*$, $F\bar{F}$, $F\bar{F}^*$, and $F^*\bar{F}^*$ channels. A_K is a free parameter, β_K is the velocity and F is a form factor chosen as $F = (1-s/(3.1)^2)^{-1}$. The resonance parameters of the fit are given in Table 1.

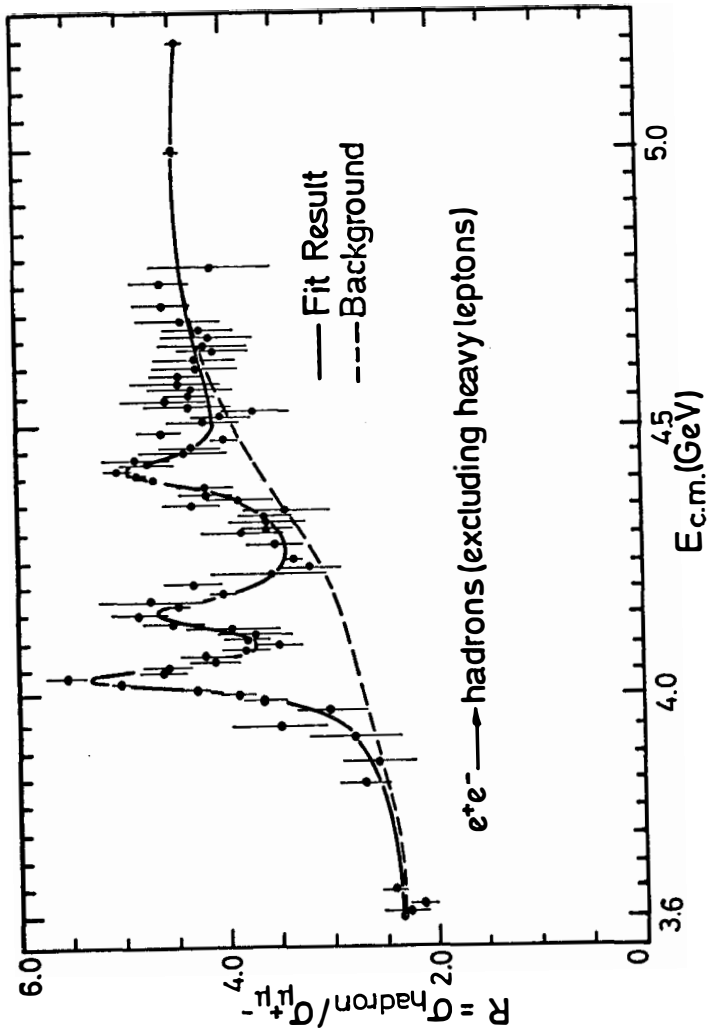

Fig. 4 The ratio R without heavy lepton production versus energy. Only statistical errors are indicated. The fit to the data described in the text and separately the nonresonant background term are shown.

Table 1

Mass (MeV)	Γ_{tot} (MeV)	$\Gamma_{e^+e^-}$ (keV)	Experiment
4040 ± 10	52 ± 10	0.75 ± 0.15	DASP
4159 ± 20	78 ± 20	0.77 ± 0.23	DASP
4417 ± 10	66 ± 15	0.49 ± 0.13	DASP
4414 ± 7	33 ± 10	0.44 ± 0.14	SLAC-LBL

Resonance parameters of the best fit to the DASP data as described in the text and shown in Fig. 4. The errors include statistical and detection efficiency uncertainties, and some coarse estimate of interference between the resonance amplitudes.

The structure at 4.4 GeV was first seen by SLAC-LBL[4]. From the table we can see that despite the increasing mass and therefore increasing phase space, the total hadronic widths of these resonance-like structures are the same within errors.

In the naive four quark model, we would expect a difference in R between its value above and below charm threshold of $R = \frac{4}{3}$. Experimentally we find

$$\Delta R = R(s=27\ \text{GeV}^2) - R(s=13\ \text{GeV}^2) \simeq 2.1 \pm 0.3.$$

In asymptotically free gauge theories the simple quark model result is modified by gluon corrections. Taking the measured value for $R(s=27\ \text{GeV}^2) = 4.5$ at face value, we obtain for the quark gluon coupling constant

$$\alpha_s(s=27\ \text{GeV}^2) = \frac{g^2}{4\pi} = 0.6 \pm 0.3$$

and for the scale parameter

$$\Lambda = 1.6 \pm 0.9\ \text{GeV}.$$

(Formulae 19 and 20 for α_s and R(s) from ref. 6 were used.). The large error

on α_s and Λ is due to the 15 % normalization uncertainty in R. The value of Λ is not inconsistent with $\Lambda \simeq 0.6$ GeV[7] obtained from electron and muon deep inelastic scattering.

In Fig. 5 a comparison between our R-values and the results from SLAC-LBL and PLUTO is made. Since these groups did not separate the heavy lepton contribution, we added it to our data for the purpose of comparison. Our data agree with those of PLUTO as far as the shape and in particular the three structures are concerned. However, above 4 GeV the DASP values of R are about 0.5 units higher than those of PLUTO. As far as the magnitude is concerned our data are in better agreement with the data from SLAC-LBL. The structure we see at 4.16 GeV, however, is not resolved in their data. Below 4 GeV our statistics are insufficient to observe the structure near 3.95 GeV seen in the SLAC-LBL data. All three experiments agree on the position of a minimum in the cross section at about 4.25 GeV. Note, however, that the differences observed between the three experiments are of the order of their systematic uncertainties.

IV. THE CASCADE DECAYS: $\psi' \to \gamma P_c/\chi$, $P_c/\chi \to \gamma J/\psi$

New high statistics data from DASP on the cascade decays have become available which I want to use together with older data from DASP[8,9] SLAC-LBL[10,11], MPPSSSD[12], PLUTO[13] and preliminary new data from DESY-Heidelberg[14] to focus on the question of the existence of the $\chi(3.45)$ state. Three intermediate states $\chi(3.4)$, $P_c(3.51)$ and $\chi(3.55)$ have been clearly established. An additional state lying in mass between ψ' and J/ψ is predicted by the charmonium model whose level scheme is indicated in Fig. 6.

The total DASP cascade data correspond to about 7.5×10^5 produced ψ' states. The final states selected contain two photons and a $\mu^+\mu^-$ pair coming from J/ψ decay. A 3(2) C-fit was made depending on whether the momentum of both (or only one) muon was measured. The background due to $\psi' \to J/\psi\,\eta$ was eliminated by taking only events with $M_{\gamma\gamma} < 520$ MeV.

In Fig. 7 the $J/\psi\,\gamma$ high mass projection is shown, clearly exhibiting peaks at 3.5 and 3.55 GeV and indications of structure at 3.41 and 3.45 GeV. Note one of the events at 3.45 GeV is also possibly due to the decay $\psi' \to J/\psi\pi^0$, as seen in Fig. 10. A summary of the DASP, PLUTO and SLAC-LBL data is given in Fig. 8. This figure also contains some background from the decay $\psi' \to J/\psi\,\pi^0\pi^0$, with two photons escaping detection.

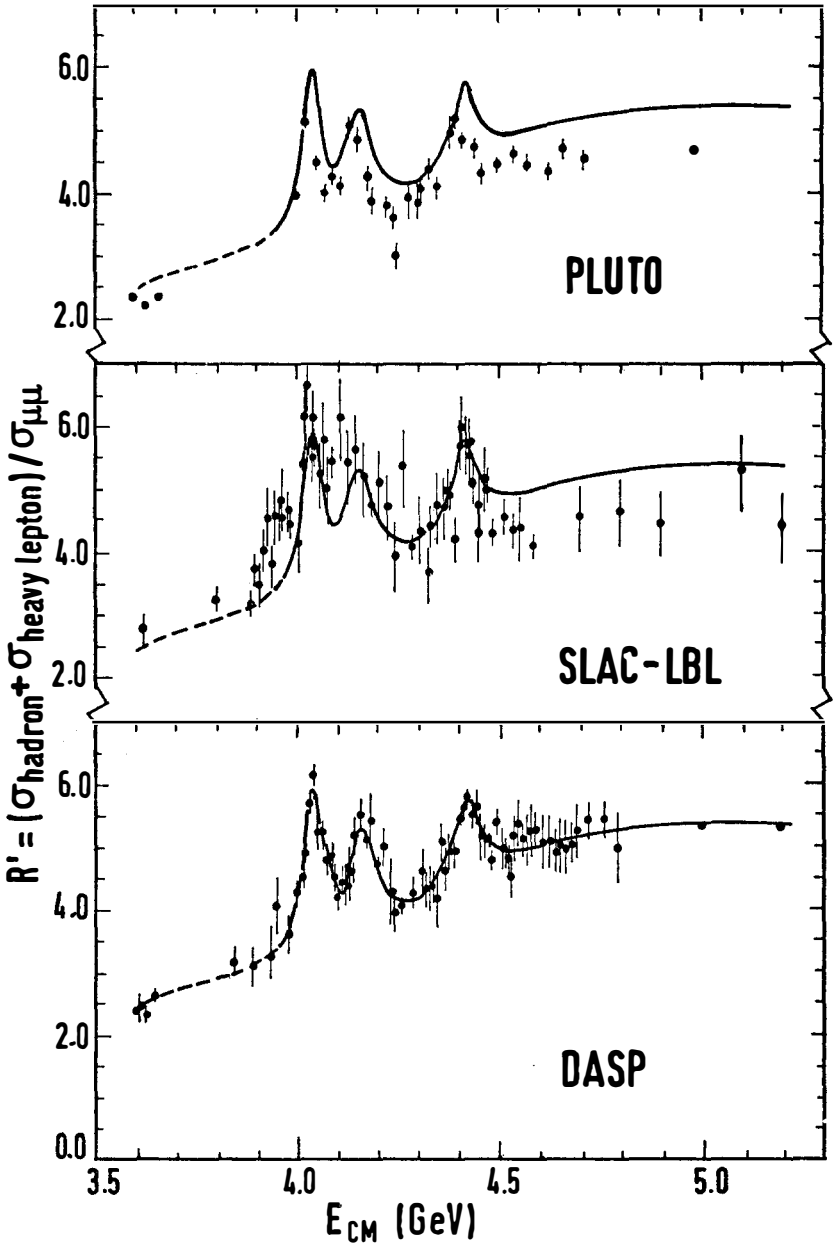

Fig. 5 The ratio R' including heavy lepton production versus energy is shown. The heavy lepton contribution plus the fitted curve of Fig. 4 is drawn in each data set for comparison.

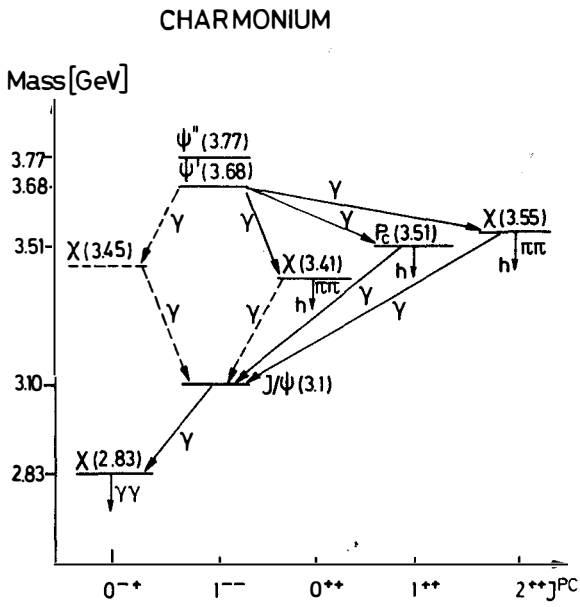

Fig. 6

The clustering of the events from three different experiments is rather suggestive of the existence of a state at a mass of 3.45 GeV. Naively adding up the events and estimated background from the three experiments gives a ratio of 11 to about 4 events. New preliminary data from the DESY-Heidelberg group[14] shown in Fig. 9 also exhibit an excess of events at 3.45 GeV.

The $\chi(3.41)$ state has been clearly seen in the inclusive photon spectrum[10] from the decay $\psi' \to \gamma\ \chi(3.41)$ and in hadronic decay channels[15] of the $\chi(3.41)$. In Fig. 8 there is also evidence for the cascade decay $\psi' \to \gamma\ \chi(3.41)$, $\chi(3.41) \to J/\psi\gamma$; however, more statistics would be clearly desirable.

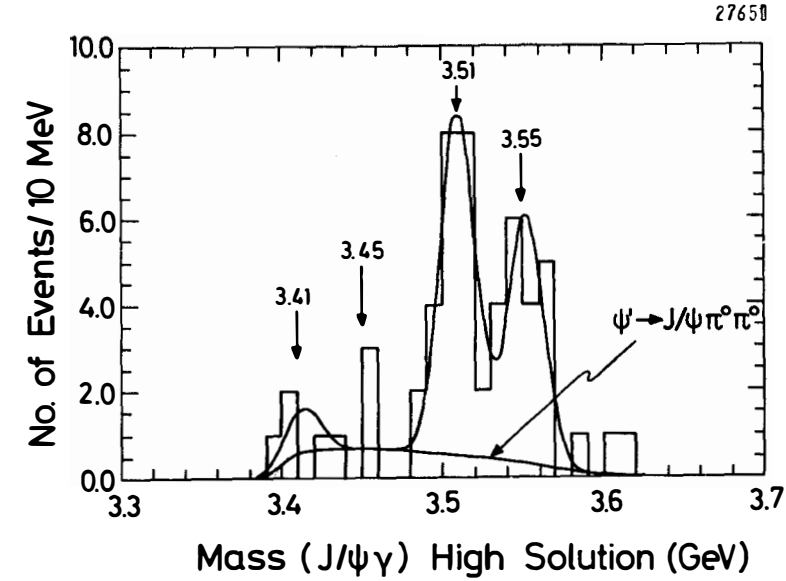

Fig. 7 Mass distribution of the P_c/χ states observed in $\psi' \to P_c/\chi\ \gamma$, $P_c/\chi \to \gamma\ J/\psi$. The curves are Gaussians for the masses 3.41, 3.51, and 3.55 GeV. Also shown is the background due to $\psi' \to J/\psi\pi^o\pi^o$.

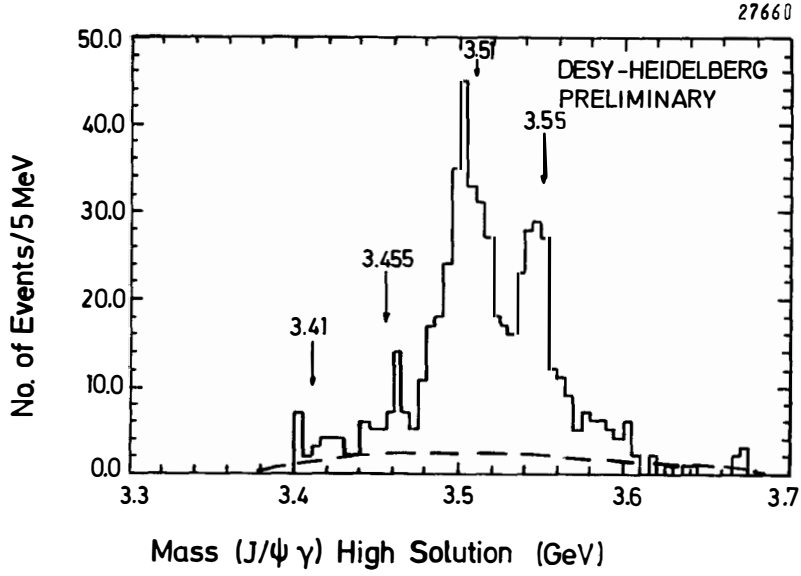

Fig. 9

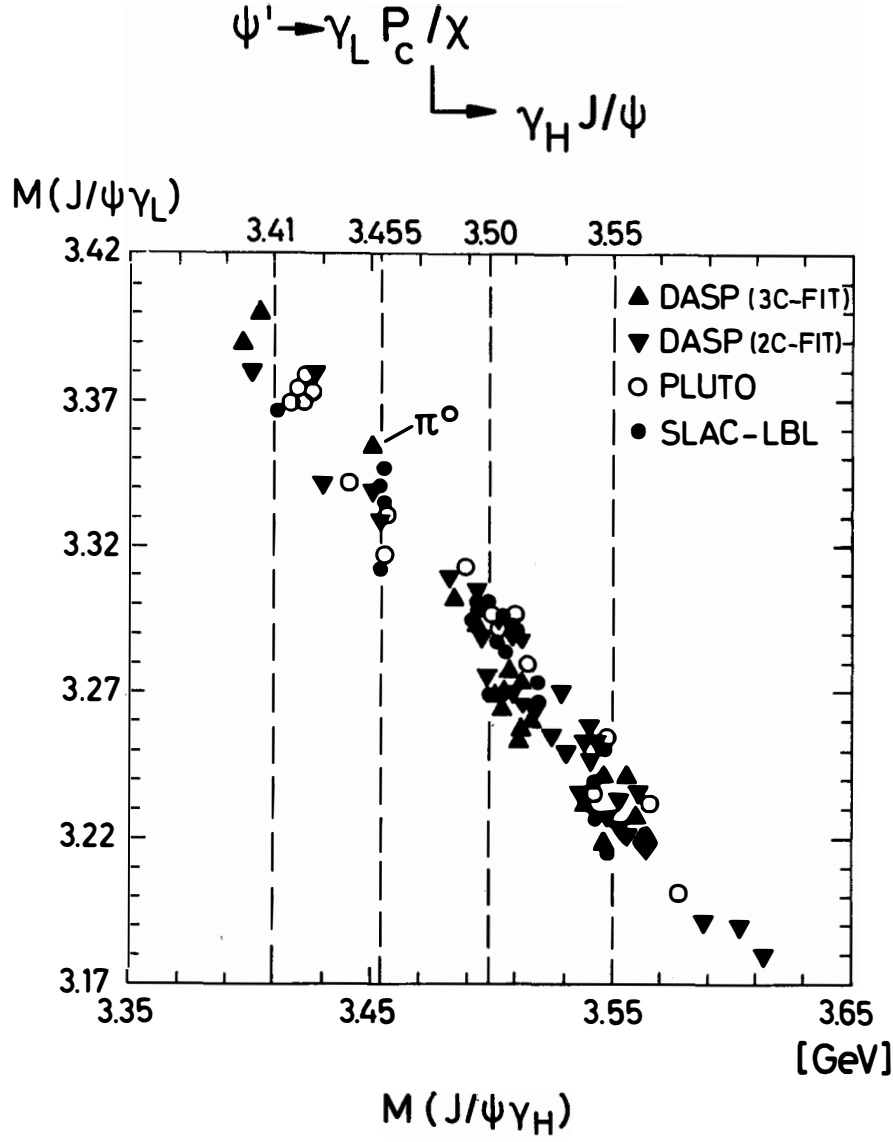

Fig. 8 Cascade decay events obtained by DASP, SLAC-LBL and PLUTO are plotted as a function of the low mass solution versus the high mass solution

Table 2 contains a list of the combined branching ratios for the cascade decays indicating good agreement within errors among the five different experiments.

Table 2

$B(\psi' \to \gamma P_c/\psi) \cdot B(P_c/\chi \to \gamma J/\psi)$ in %

	DASP	DESY-Heidelberg*[14]	MPPSSSD[12]	PLUTO[13]	SLAC-LBL[11]
$\chi(3550)$	1.6 ± 0.4	1.1 ± 0.4	2.2 ± 1.0	0.9 ± 0.8	1.0 ± 0.6
$P_c/\chi(3510)$	2.1 ± 0.4	2.1 ± 0.5	5.0 ± 1.5	1.2 ± 0.8	2.4 ± 0.8
$\chi(3415)$	0.3 ± 0.2	0.1 ± 0.1	3.3 ± 1.7	1.2 ± 0.8	0.2 ± 0.2
$\chi(3455)$	$\leq$ 0.5**	0.4 ± 0.2	< 2.5	0.7 ± 0.7	0.8 ± 0.4

* preliminary

** assuming isotropic production and decay

Assuming the existence of the $\chi(3.45)$ state, one would naively identify it with the $2^1S_0 \equiv \eta_c'$ state predicted by the charmonium model. From the photon angular distribution of $P_c(3.5o)$ as measured by SLAC-LBL and the $\pi^+\pi^-$ (K^+K^-) decay of $\chi(3.41)$ and $\chi(3.55)$ as observed by SLAC-LBL and DASP, it is likely that none of these three states has the quantum numbers of the η_c'. Identifying the $\chi(3.45)$ with the η_c' however, leads to a serious disagreement with QCD. The η_c' can decay to lowest order via two gluon emission into hadrons, whereas the ψ' must emit at least three gluons. Therefore one expects

$$\Gamma(\eta_c' = \chi(3.45) \to \text{all}) \gg \Gamma(\psi' \to \text{all}). \qquad (5)$$

From the measured product of branching ratios $B(\psi' \to \gamma\chi(3.45)) \cdot B(\chi(3.45) \to \gamma J/\psi)$ and the upper limit for $B(\psi' \to \gamma\chi(3.45)) < 0.025$ as measured by MPPSSSD, we get $B(\chi(3.45) \to \gamma J/\psi) > 0.24$. Making the assumption $\Gamma(\eta_c' \to \gamma J/\psi) \leq \Gamma(\psi' \to \gamma\eta_c)$ and using the upper limit for $B(\psi' \to \gamma\eta_c(=X)) < 0.01$ from MPPSSSD, we obtain

$$\Gamma(\chi(3.45) \to \text{all}) \leq 10 \text{ KeV}$$

as compared to the usual expectation of about 2 MeV for the η_c'. If this

QCD result is correct, then the identification of the η_c' of the charmonium model with the $\chi(3.45)$ is not possible.

Looking at Fig. 10 we observe a few events with the invariant two photon mass around the π^0 mass, some of them possibly due to the decay $\psi' \to J/\psi\pi^0$. This decay can only occur electromagnetically since G-parity is not conserved. However, the ψ' could first decay strongly into a J/ψ and a virtual η which then turns into a π^0. This $\eta - \pi^0$ transition could be anomalously large due to a nonelectromagnetic isospin violating term in the interaction Hamiltonian (like in the $\eta \to 3\pi$ decay). Segre and Weyers[16] have estimated $0.05\ \% \lesssim B(\psi' \to J/\psi\ \pi^0) \lesssim 0.3\ \%$; a possible η'-contribution could increase this value.

To extract the $\psi' \to J/\psi\ \pi^{0'}$ events from the cascade decay background, we can take advantage of the differences in the spread of the two photon opening angles for π^0 J/ψ and $\gamma P_c/\chi$ events. The opening angles for the photons coming from π^0 decay are strongly peaked within less than 10 degrees, whereas the distribution for photons from the cascade decay is essentially flat. This is indicated by the Monte Carlo generated curves in Fig. 11b. The measured opening angles for those events which give a good kinematic fit to the hypothesis $\psi' \to J/\psi\ \pi^0$ are also plotted. The χ^2 for these events is plotted in Fig. 11a. No clear signal for the decay $\psi' \to J/\psi\ \pi^0$ is seen in Fig. 11b. We can extract a 90 % confidence upper limit of

$$B(\psi' \to J/\psi\ \pi^0) < 0.5\ \%.$$

A preliminary 90 % confidence upper limit of 0.1 % was found by DESY-Heidelberg[14]. These results lie within the range estimated by Segre and Weyers.

V. J/ψ RADIATIVE DECAYS

Before discussing new and old results on J/ψ radiative decays mediated primarily by two gluon exchange, I would like to remind you of the status of the $\chi(2.82)$ state[17,18]. In e^+e^- interactions the only evidence for such a state is seen by DASP in the 3 photon decay of the J/ψ. Of the two independent two photon pair mass combinations the highest photon pair mass distribution is shown in Fig. 12. We observe a 5 standard deviation signal at a mass

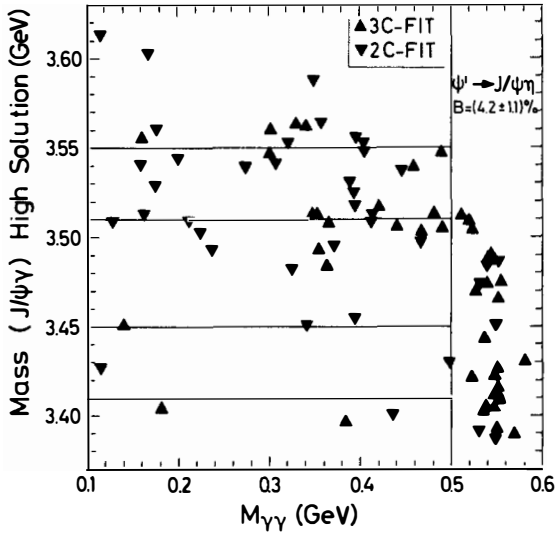

Fig. 10 Cascade decay events obtained by DASP are plotted as a function of the high mass solution versus the two photon mass

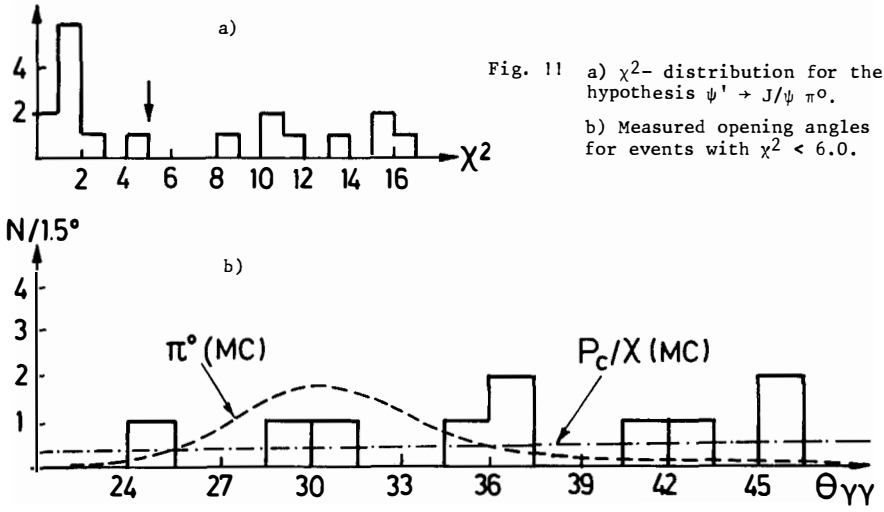

Fig. 11 a) χ^2- distribution for the hypothesis $\psi' \rightarrow J/\psi\ \pi^o$.

b) Measured opening angles for events with $\chi^2 < 6.0$.

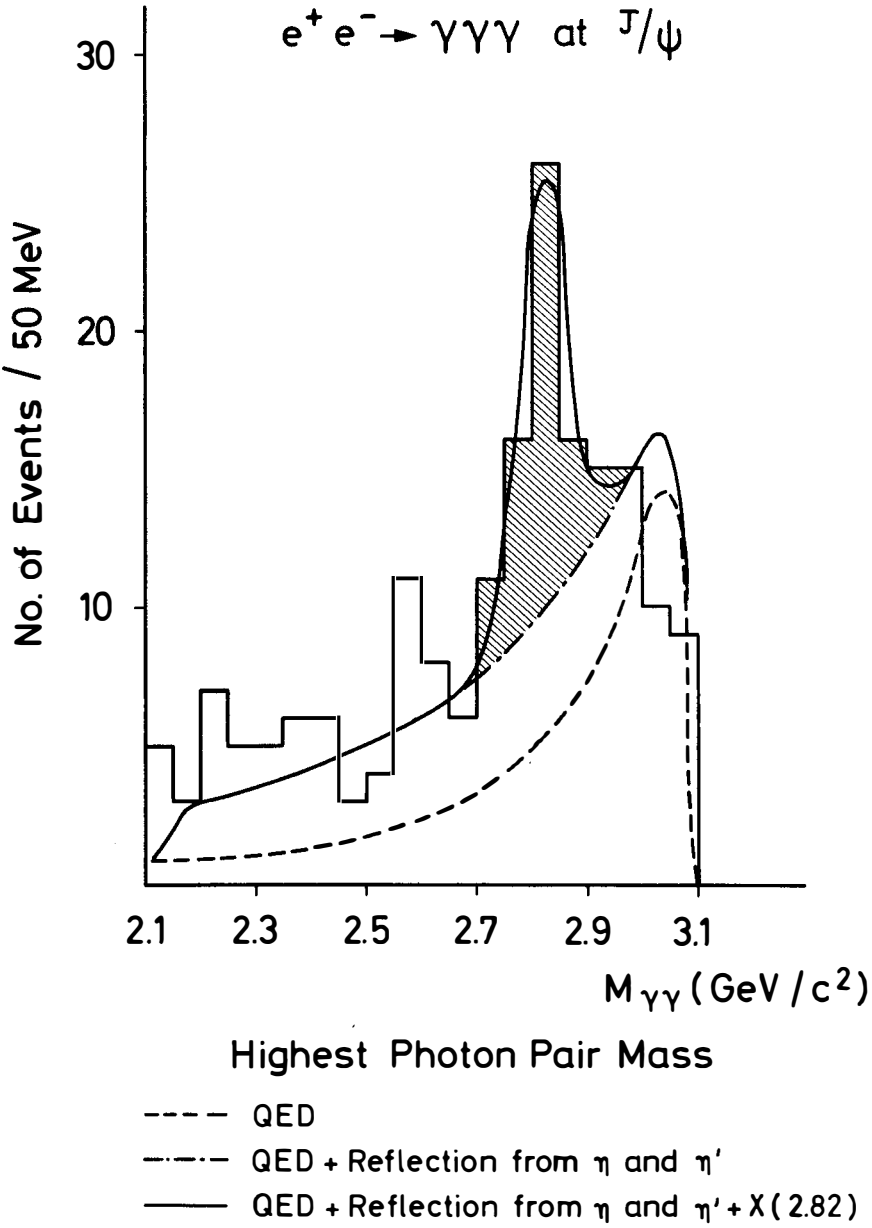
$e^+ e^- \to \gamma\gamma\gamma$ at J/ψ
No. of Events / 50 MeV
30
20
10
2.1
2.3
2.5
2.7
2.9
3.1
$M_{\gamma\gamma}$ (GeV / c^2)
Highest Photon Pair Mass
QED
QED + Reflection from η and η'
QED + Reflection from η and η' + X(2.82)

Fig. 12

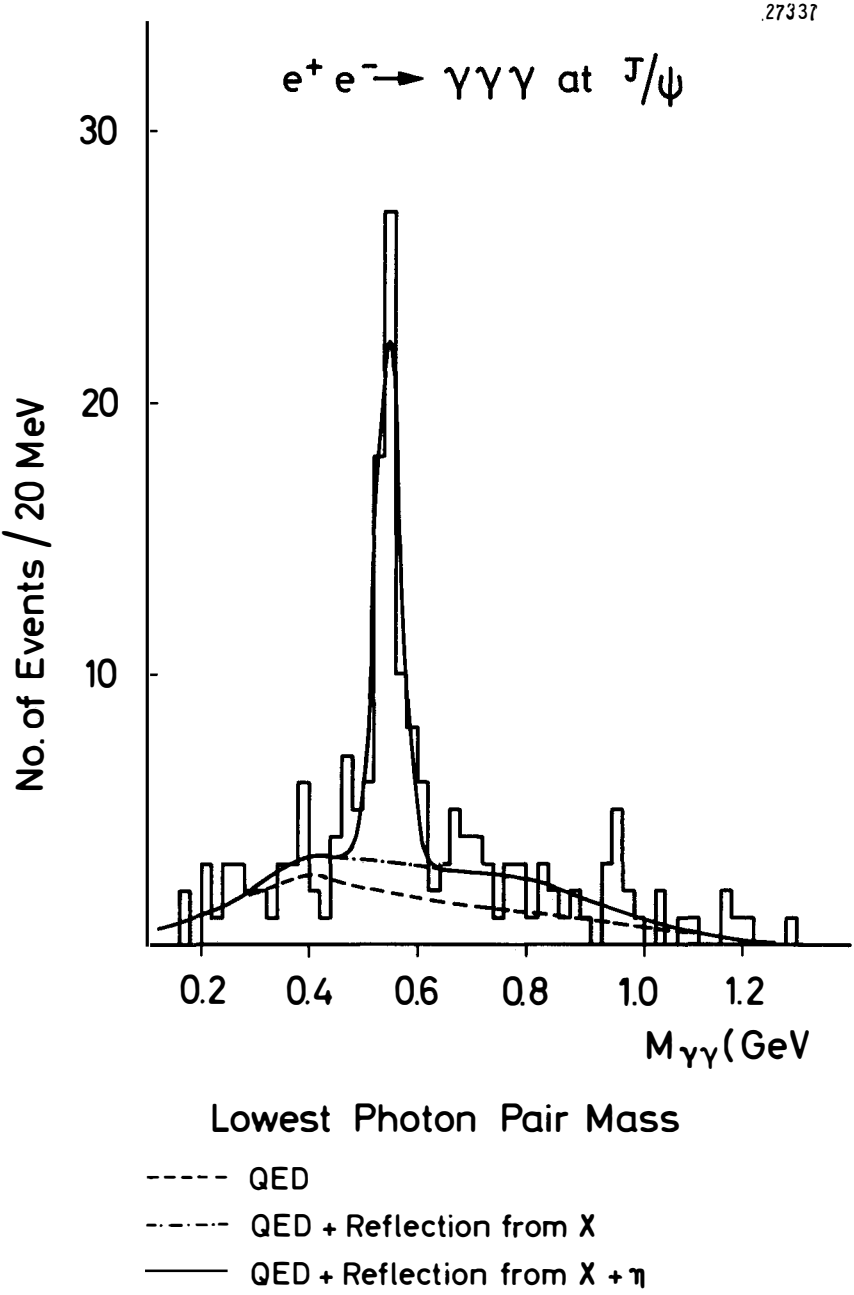
$e^+ e^- \rightarrow \gamma\gamma\gamma$ at J/ψ
30
20
10
No. of Events / 20 MeV
0.2
0.4
0.6
0.8
1.0
1.2
$M_{\gamma\gamma}$ (GeV
Lowest Photon Pair Mass
----- QED
-·-·-·- QED + Reflection from X
——— QED + Reflection from X + η

Fig. 13

$M(X) = (2.82 \pm 0.014)$ GeV and with a width $\Gamma(X) = (40 \pm 14)$ MeV.

For the combined branching ratios we find

$$B(J/\psi \to \gamma X) \cdot B(X \to \gamma\gamma) = (1.4 \pm 0.4)\ 10^{-4}.$$

The two photon decay mode shows that the X has even charge conjugation and spin different from one. Further evidence for this state has been found in the reaction $\pi^- p \to M^0 n$ ($M^0 \to \gamma\gamma$) by a CERN-Serpukhov collaboration[19].

Fig. 13 shows that our analysis of the three photon final state really works. Here we plotted the lowest photon pair mass distribution which shows two peaks due to η and η'. The fitted η mass of (547.1 ± 4.2) MeV agrees well with the known mass value. The fitted width (24 ± 4) MeV of the η peak is in agreement with the expected mass resolution of 20 MeV. The small η' peak is observed at the correct mass value. The branching ratios[16] for the radiative J/ψ decays into η and η' are in good agreement with measurements performed by the DESY-Heidelberg group[20].

Table 3 contains a list of the branching ratios for these radiative decays together with new results of γf, $\gamma f'$, $\gamma\pi^+\pi^-$ and γK^+K^- from DASP[21]. For comparison the strength of some related strong decays measured at DORIS and SPEAR are also shown. One notices that the J/ψ decays into $\gamma\eta$, $\gamma\eta'$ and γf are of about the same order of magnitude or larger than the OZI-suppressed strong decays into $\phi\eta$, $\phi\eta'$, ϕf and ωf. Their radiative decay widths can therefore not be explained by $\phi(\omega)$ vector dominance. The J/ψ decay rate into $\gamma\pi^0$ however, is an order of magnitude smaller. This can be understood by considering the three graphs in Fig. 14 which can contribute to radiative decays.

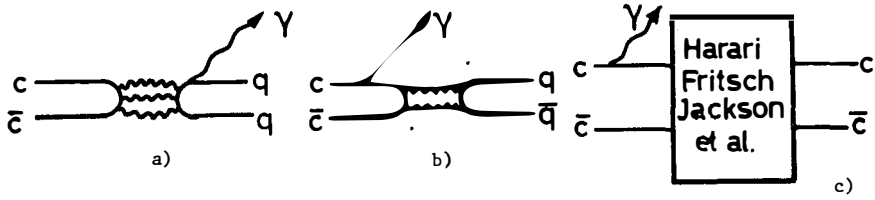

Fig. 14 Feynman graphs for the radiative decays of the J/ψ into a meson.

Table 3: J/ψ Radiative Decays: Branching Ratio $B = \Gamma_f/\Gamma_{tot}$

Decay Mode	B	Experiment
$\gamma\pi^0$	$(0.73 \pm 0.47)\ 10^{-4}$	DASP
$\gamma\eta$	$(0.82 \pm 0.10)\ 10^{-3}$	DASP
	$(1.3 \pm 0.4)\ 10^{-3}$	DESY-Heidelberg
$\gamma\eta'$	$(2.9 \pm 1.1)\ 10^{-3}$	DASP
	$(2.4 \pm 0.7)\ 10^{-3}$	DESY-Heidelberg
$\gamma f(1250)$	$(2.0 \pm 0.7)\ 10^{-3}$	PLUTO
	$(1.1 \pm 0.3)\ 10^{-3}$	DASP
$\gamma\pi^+\pi^-(M_{\pi\pi} < 1\ \text{GeV})$	$\leq(0.7 \pm 0.2)\ 10^{-3}$	DASP
$\gamma\varepsilon\ \ (M_{\pi\pi} < 1\ \text{GeV})$	$< 1.1 \cdot 10^{-3}$	DASP
$\gamma\ \pi^+\pi^-(M_{\pi\pi} > 1.6\ \text{GeV})$	$(1.7 \pm 1.1)\ 10^{-4}$	DASP
$\gamma\ f'(1516)$	$\leq 3.4 \cdot 10^{-4}$	DASP
$\gamma\ K^+K^-\ (M_{KK} > 1.6\ \text{GeV})$	$\leq 2.5 \cdot 10^{-4}$	DASP
some related strong decays (DORIS,SPEAR)		
$\rho^0\pi^0$	$(4.5 \pm 0.3)\ 10^{-3}$	
$\phi\eta$	$(1.0 \pm 0.6)\ 10^{-3}$	
$\phi\eta'$	$< 1.3 \cdot 10^{-3}$	
ϕf	$< 3.7 \cdot 10^{-4}$	
ωf	$(2.8 \pm 1.1)\ 10^{-3}$	
$\omega f'$	$< 1.6 \cdot 10^{-4}$	

In graph a of Fig. 14 the J/ψ decay proceeds via three gluon exchange, in graph b via two gluon exchange. Graph c assumes the produced meson to have a small $c\bar{c}$ component in its wave function. The π^0 can only be produced via graph a where the photon is radiated by an old quark (u,d,s), whereas for example the η, η' and f can also be produced via graphs b and c where the photon is radiated by the initial charmed quark (c). In QCD the suppression of $\gamma\pi^0$ is due to the fact that three gluon exchange is weaker than two gluon exchange.

Computing graph a via the measured OZI-suppressed strong $J/\psi \to \pi^0\rho^0$ decay and ρ^0 vector dominance, one obtains

$$\Gamma(J/\psi \to \gamma\pi^0) \simeq \frac{\alpha}{f_\rho^2/4\pi}\,\Gamma(J/\psi \to \pi^0\rho^0) \simeq 4 \text{ eV} \qquad (6)$$

which is in good agreement with our experimental value of (5 ± 3) eV. Assuming SU(3) invariance and neglecting phase space, we obtain:

$$\Gamma_{\pi^0} : \Gamma_\eta : \Gamma_{\eta'} = 3 : \cos^2\Theta : \sin^2\Theta \qquad (7)$$

Experimentally we find $\Gamma_{\pi^0} << \Gamma_\eta \simeq \Gamma_{\eta'}$.
Therefore the three gluon exchange contribution to η, η' (and also f and f') is expected to be negligible.

The two gluon exchange diagram b, where the photon is radiated by the initial charmed quark, is then expected to provide the dominant contribution for the measured radiative decays $J/\psi \to \gamma\eta$, $\gamma\eta'$, γf, $\gamma f'$, and $\gamma\varepsilon$. Assuming SU(3) invariance for the $q\bar{q}$-state and neglecting phase space, we find:

$$\Gamma_{\pi^0} : \Gamma_\eta : \Gamma_{\eta'} = 0 : \sin^2\Theta : \cos^2\Theta$$
$$\frac{\Gamma_{\eta'}}{\Gamma_\eta} = \cot^2\Theta = 26 \text{ (for a mixing angle of } 11^0) \qquad (8)$$

The experiment gives a value of 2.9 ± 0.9. For f' and f assuming ideal mixing, one obtains

$$\Gamma_{f'}/\Gamma_f = 0.5$$

as compared to the experimental upper limit of 0.3. These data indicate that SU(3) symmetry breaking is important. A QCD prediction on the helicity of the f in the γf decay of the J/ψ, and the comparison with experiment can be found in the contributions to this conference by M. Krammer and J. Bürger.

We have also obtained branching ratios for the J/ψ decays into $\pi^+\pi^-\gamma$ and $K^+K^-\gamma$ with dimeson masses outside the mass region of the f and f' resonances. They are listed in Table 3. With the extremely cautious assumption that all $\pi^+\pi^-$ pairs with $M_{\pi\pi} < 1$ GeV are due to genuine radiative decays, we

obtain:

$$B(J/\psi \to \gamma\pi^+\pi^-,\ M_{\pi\pi} < 1\ \text{GeV}) \lesssim (0.7 \pm 0.2)\ 10^{-3}.$$

Correcting for isospin, we find:

$$B(J/\psi \to \gamma\varepsilon) < 1 \cdot 10^{-3}.$$

This value is an order of magnitude smaller than a prediction[22] using vector dominance and the measured width for the decay $\psi' \to J/\psi\ \pi^+\pi^-$. The branching ratios for radiative decays into $\pi^+\pi^-$ and K^+K^- pairs with dimeson masses above 1.6 GeV are found to be

$$\frac{\Gamma(J/\psi \to \gamma\pi^+\pi^-(M_{\pi\pi} > 1.6\ \text{GeV}))}{\Gamma(J/\psi \to f\gamma)} \approx \frac{\Gamma(J/\psi \to \gamma K^+K^-\ (M_{KK} > 1.6\ \text{GeV}))}{\Gamma(J/\psi \to f\gamma)} \lesssim \frac{1}{10}.$$

Fritzsch and Jackson[23] and many others have investigated the possibility of a $c\bar{c}$ admixture in the wave function of the meson, as represented by diagram c. Assuming $\eta_c = c\bar{c} + \varepsilon\eta + \varepsilon'\eta'$ and taking the SU(3) symmetry breaking into account, they find via QCD $\varepsilon \simeq 1.0 \cdot 10^{-2}$ and $\varepsilon' \simeq 2.2 \cdot 10^{-2}$. Using the quark model formula for computing the radiative decay width and assuming for the overlap integral $\Omega^2 \lesssim 0.1$ (as compared to $\Omega^2 \simeq 1.0$ for $J/\psi \to \gamma\eta_c$), they find

$\Gamma(J/\psi \to \gamma\eta) \simeq 60$ eV (exp.: 57 ± 7 eV DASP)

$\Gamma(J/\psi \to \gamma\eta') \simeq 220$ eV (exp.: 166 ± 50 eV DESY-Heidelberg)

in good agreement with experiment.

VI. CONCLUSIONS

a) There are three resonance like structures between $4 \lesssim \sqrt{s} \lesssim 5$ GeV with masses: 4.04, 4.16, 4.42 GeV and with similar hadronic widths and similar leptonic widths.

b) The measured difference in R between 3.6 GeV and 5.2 GeV is $\Delta R = 2.1 \pm 0.3$.

c) Four different experiments including two new high statistics experiments from DASP and DESY-Heidelberg have observed an excess of events at a mass of 3.45 GeV in the ψ' cascade decay. However, to be firmly convinced of the existence of $\chi(3.45)$ more data are still needed.

d) Many J/ψ radiative decay widths have been measured and can be used to test QCD calculations on two gluon exchange.

REFERENCES

1. DASP collaboration
   R. Brandelik, W.Braunschweig, H.-U. Martyn, H.G. Sander, D. Schmitz, W. Sturm, and W. Wallraff, I. Phys. Inst. RWTH Aachen,
   D. Cords, R. Felst, R. Fries, E. Gadermann, H. Hultschig, P. Joos, W. Koch, U. Kötz, H. Krehbiel, D. Kreinick, H.L. Lynch, W.A. McNeely, G. Mikenberg, K.C. Moffeit, D. Notz, R. Rüsch, M. Schliwa, A. Shapira, B.H. Wiik, and G. Wolf, DESY, Hamburg,
   J. Ludwig, K.H. Mess, A. Petersen, G. Poelz, J. Ringel, O. Römer, K. Sauerberg, and P. Schmüser, II. Inst. f. Exp.-Phys., Univ. Hamburg,
   W. de Boer, G. Buschhorn, W. Fues, Ch. von Gagern, G. Grindhammer, B. Gunderson, R. Kotthaus, H. Lierl, and H. Oberlack, MPI f. Phys. and Astrophys., München
   S. Orito, T. Suda, Y. Totsuka, and S. Yamada, Lab. of Int. Coll. on Elementary Particle Phys. and Dept. of Phys., Univ. of Tokyo
2. DASP collaboration: R. Brandelik et al., Phys. Lett. 67 B(1977)358
3. DASP collaboration: R. Brandelik et al., DESY 78/18 (1978), to be published
4. J. Siegrist et al., Phys. Rev. Lett. 36 (1976) 700, and G. Hanson, these proceedings
5. PLUTO collaboration: J. Burmester et al., Phys. Lett. 66B(1977) 395, and J. Bürger, these proceedings
6. E.C. Poggio, H.R. Quinn, and S. Weinberg, Phys. Rev. D13 (1976),1958
7. H.L. Anderson, H.S. Matis, and L.C. Myrianthopoulos, Phys. Rev. Lett. 40(1978) 1061
8. DASP collaboration: W. Braunschweig et al., Phys. Lett. 57 B(1975) 407
9. DASP collaboration: B.H. Wiik, in "Proceedings of the XVIII Intern. Conference on High Energy Phys. in Tbilisi 1976 (Dubna, 1977)
10. J.S. Whitaker et al., Phys. Rev. Lett 37 (1976) 1596
11. W. Tannenbaum et al., SLAC-PUB-1987, LBL-6720, July 1977, to be published

12. Maryland-Pavia-Princeton-SLAC-Stanford-San Diego, C. Biddick et al., Phys. Rev. Lett. 38 (1977) 1324

13. PLUTO collaboration: V. Blobel, in "Proceedings of the Twelfth Rencontre de Moriond", Flaine-Haute-Savoie, March 1977, and J. Bürger, private communication

14. D. Pandoulas: Talk given at the DPG meeting in Heidelberg, March 1978

15. G.J. Feldman et al., Phys. Rev. Lett. 35 (1975) 821

16. G. Segre and J. Weyers, Phys. Lett. 62B (1976) 91

17. DASP collaboration: W. Braunschweig et al., Phys. Lett. 67B (1977) 243

18. DASP collaboration: S. Yamada, in "Proceedings 1977 International Symposium on Lepton and Photon Interactions at High Energies, Hamburg, August 1977

19. W.D. Apel et al., Phys. Lett. 72B (1978) 5oo

2o. W. Bartel et al., Phys. Lett. 66B (1977) 489

21. DASP collaboration: R. Brandelik et al., Phys. Lett. 74B (1978) 292

22. H. Primakoff et al., University of Hawaii, Report UH-5111-191-75 (1975)

23. H. Fritzsch and J.D. Jackson, Phys. Lett. 66B (1977) 365

ACKNOWLEDGEMENTS

I would like to thank all my colleagues, in particular R. Felst, E. Gadermann, A. Petersen, and G. Wolf, who helped me in preparing this talk.

RECENT RESULTS FROM DASP ON e^+e^- ANNIHILATION (II)

Günter Wolf*
Deutsches Elektronen-Synchrotron DESY,
Hamburg

Abstract:

Inclusive production of $\pi^{\pm}$, $K^{\pm}$ and $\bar{p}$ by e^+e^- annihilation has been analyzed for cm energies W between 3.6 and 5.2 GeV. The experimental information on the F and F* mesons is reviewed including new data on $F\bar{F}$ production at 4.16 GeV. Data are presented on semileptonic decays of charmed particles. Electron-two-prong data have revealed τ production at the ψ' which is below charm threshold. With these data a precise value for the τ mass has been obtained, $m_{\tau} = 1.807 \pm 0.020$ GeV. Leptonic and semileptonic decay modes of the τ are discussed.

The members of the DASP collaboration are
R. Brandelik, W. Braunschweig, H.-U. Martyn, H.G. Sander, D. Schmitz, W.Sturm, and W. Wallraff, I. Physikalisches Institut der RWTH Aachen,
D. Cords, R. Felst, R. Fries, E. Gadermann, H. Hultschig, P. Joos, W. Koch, U. Kötz, H. Krehbiel, D. Kreinick, H.L. Lynch, W.A. McNeely, G. Mikenberg, K.C. Moffeit, D. Notz, R. Rüsch, A. Shapira, M. Schliwa, B.H. Wiik, and G. Wolf, Deutsches Elektronen-Synchrotron DESY, Hamburg,
J. Ludwig, K.H. Mess, A. Petersen, G. Poelz, J. Ringel, O. Römer, K. Sauerberg, and P. Schmüser, II. Institut für Experimentalphysik der Universität Hamburg,
W. De Boer, G. Buschhorn, W. Fues, Ch. v. Gagern, G. Grindhammer, B. Gunderson, R. Kotthaus, H. Lierl, and H. Oberlack, Max-Planck-Institut für Physik und Astrophysik, München,
S. Orito, T. Suda, Y. Totsuka, and S. Yamada, Lab. of Int. Coll. on Elementary Particle Physics and Department of Physics, University of Tokyo.

1. INTRODUCTION

New results from DASP on the total hadronic cross section, on the p_c/χ states and on the radiative J/ψ decays are discussed by G. Grindhammer[1] at this meeting. This lecture concentrates on inclusive particle production, the evidence for F and F^*, the semileptonic decays of charmed particles, and the properties of the τ. Most of the information presented here was obtained after the 1977 Hamburg conference[2].

2. INCLUSIVE HADRON PRODUCTION AND A TEST FOR SCALING

One of the basic properties of electron hadron scattering is the almost perfect scale invariance exhibited by the structure functions in the deep inelastic region. Inclusive hadron production in e^+e^- annihilation is expected to possess similar properties. First measurements on this subject were carried out by the SLAC-LBL collaboration who observed approximate scaling of the sum over all charged hardons produced[3]. In the DASP experiment[4] the $\pi^\pm$, $K^\pm$ and $\bar{p}$ spectra were determined separately, which allowed to test scaling for each particle species.

2.1 Kinematics

We start with a brief description of the formalism[5] for inclusive hadron production

$$e^+e^- \to h^\pm X \qquad (2.1)$$

depicted in the following figure:

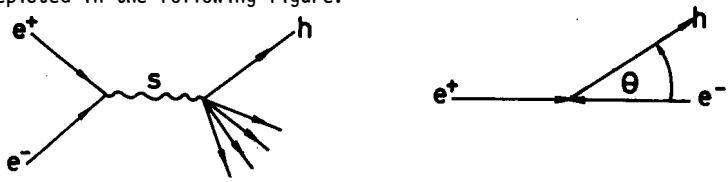

Define:

q	=	$p_+ + p_-$	four momentum vector of the virtual photon
q^2	=	s	square of the cm energy
p	=	$(\vec{p},E)$	four momentum vector of the hadron h
Θ	=	production angle of h with respect to the e^+ direction	
x	=	$\frac{2q \cdot p}{s} = \frac{2E}{\sqrt{s}}$	fractional energy of h
ν	=	$\frac{q \cdot p}{m} = \frac{E}{m}\sqrt{s}$	energy of γ in h rest system

Note that $\frac{2m\nu}{s} = x$.

The virtual photon, as seen in the rest system of h, has transverse (T) and longitudinal (L) components. As a consequence the process (2.1) is described by two independent structure functions, e.g. $\bar{W}_T$ (s,ν) and $\bar{W}_L$ (s,ν). The differential cross section has the form

$$\frac{d^2\sigma}{dx\, d\Omega} = \frac{\alpha^2}{s} \frac{|\vec{p}|}{\sqrt{s}} m \{\bar{W}_T (1 + \cos^2\Theta) + \bar{W}_L (1 - \cos^2\Theta)\} \tag{2.2}$$

Special cases of (2.2) are pair production of fermions (e.g. $e^+e^- \to \mu^+\mu^-$) where $\bar{W}_L = 0$ and of scalar or pseudoscalar mesons (e.g. $e^+e^- \to \pi^+\pi^-$), where $\bar{W}_T = 0$. It is customary to use instead of $\bar{W}_L$, $\bar{W}_T$ the structure fucntions $\bar{W}_1$ and $\bar{W}_2$ which are defined as:

$$\bar{W}_1 (s,\nu) = \bar{W}_T (s,\nu) \tag{2.3}$$

$$\bar{W}_2 (s,\nu) = \frac{m^2}{|\vec{p}|^2} (\bar{W}_L (s,\nu) - \bar{W}_T (s,\nu) \tag{2.4}$$

Note that in the pure transverse case ($\bar{W}_L = 0$) the equivalent of the Callan-Gross relation reads

$$\nu\bar{W}_2 = - \frac{2m}{x\beta^2} \bar{W}_1 \tag{2.5}$$

From (2.2) and (2.4) we find

$$\frac{d^2\sigma}{dx\, d\Omega} = \frac{\alpha^2}{s} \beta x \{m \bar{W}_1 + \frac{1}{4} \beta^2 x \nu\bar{W}_2 \sin^2\Theta)\} \tag{2.6}$$

where $\beta = |\vec{p}| / E$. Note that $m\bar{W}_1 \geq 0$ since the cross section has to be a positive quantity. After integrating over the angles and replacing $4\pi\alpha^2/3s$ by $\sigma_{\mu\mu}$ one has

$$\frac{d\sigma}{dx} = 3\sigma_{\mu\mu} \beta x \{m \bar{W}_1 + \frac{1}{6} \beta^2 x \nu\bar{W}_2\} \tag{2.7}$$

For E >> m this simplifies to

$$\frac{d\sigma}{dx} = 3\sigma_{\mu\mu} x \{m \bar{W}_1 + \frac{1}{6} x \nu\bar{W}_2\} \tag{2.8}$$

If the structure functions $\bar{W}_1$ and $\bar{W}_2$ obey scaling they become functions of the ratio ν/s alone. Using $x = \frac{2m\nu}{s}$ as the scaling variable and substituting

$$\begin{aligned} - m\bar{W}_1 (s,\nu) &\equiv \bar{F}_1 (x,s) \\ \nu\bar{W}_2 (s,\nu) &\equiv \bar{F}_2 (x,s) \end{aligned} \tag{2.9}$$

scale invariance is defined as

$$\lim_{\substack{\nu \to \infty \\ x = \text{const}}} m\bar{W}_1(s,\nu) = \lim_{\substack{s \to \infty \\ x = \text{const}}} \bar{F}_1(x,s) \equiv \bar{F}_1(x) \tag{2.10}$$

and similarly

$$\lim \nu\bar{W}_2(s,\nu) = \bar{F}_2(x).$$

Scale invariance leads to the following expression for the inclusive cross section:

$$\frac{d\sigma}{dx} = 3\sigma_{\mu\mu} x \{-\bar{F}_1(x) + \frac{1}{6} x \bar{F}_2(x)\} \tag{2.11}$$

If scale invariance is valid the shape of the particle energy spectra, $d\sigma/dx$, is independent of s. Furthermore, the magnitude of the inclusive cross section behaves like s^{-1}.

2.2 Experimental Procedure

The inclusive spectra measured by DASP[4] were obtained employing a genuine inclusive trigger: besides a charged particle in one of the spectrometer arms no other requirement was imposed on the final state. A detailed description of the particle identification can be found in Ref. 4. Basically, particles penetrating the iron filter were identified as muons; electrons were recognized by shower, cerenkov and time-of-flight counters; pions, kaons and protons (antiprotons) were identified by time-of-flight. The momentum range was for pions 0.14-1.5 GeV/c, for kaons 0.28-1.6 GeV and for protons (antiprotons) 0.45-3 GeV/c.

Data were taken at cm energies between 3.6 and 5.2 GeV for a total luminosity of ~ 8100 nb^{-1}. They were grouped into eight different energy intervals. A total of ~10^4 $\pi^{\pm}$, ~10^3 $K^{\pm}$ and 130 $\bar{p}$ were used for the analysis. Since the majority of the protons were due to beam gas interactions only antiprotons were considered. The proton yield was assumed to be the same as for antiprotons.

The differential cross section for inclusive production in general depends on the polar angle Θ (see e.g. eq. (2.6)). In the present analysis the polar angular acceptance was $|\cos\Theta| < 0.55$. Within this range no statistically significant $\cos\Theta$ dependence was observed and a constant angular

distribution was assumed in order to integrate the cross section over $\cos\Theta$.

To estimate the possible error introduced by this procedure we consider the limit that only transverse photons contribute, $W_L = 0$. In this case the cross sections given below would have to be increased by at most 24 %. With the angular dependence observed by SLAC-LBL[3] the estimated increase is less than 5 % for $x \lesssim 0.5$ and ≈13 % above.

2.3 General Behaviour of Inclusive Particle Production

Fig. 2.1 gives an impression of the relative frequency of pions, kaons and nucleons. It shows the cross sections $d\sigma/dp$ as a function of momentum for the individual types of particles averaged over cm energies between 4 and 5.2 GeV. (Here $d\sigma/dp$, e.g. for $\pi^\pm$ means the sum for π^+ and π^- production.) The dashed curves were obtained from an extrapolation of the invariant cross sections $E/4\pi p^2\, d\sigma/dp$ (see below). They indicate the expected momentum dependence at low momenta, where the particles are swept out of the spectrometer due to the magnetic field (pions), are lost by decay (kaons) or suffer too big an energy loss in the material in front of the magnet (antiprotons). Below 0.5 GeV/c the $\pi^\pm : K^\pm : 2\bar{p}$ yields are roughly in the ratio 100 : 10 : 1. With increasing momenta the differences become smaller.

Fig. 2.2 shows the same data plotted in terms of the invariant cross section $E\, d^3\sigma/d^3p \equiv E/4\pi\, p^2\, d\sigma/dp$. To within 20 or 30 % accuracy the $\pi^\pm$, $K^\pm$ and $2\bar{p}$ fall on the same curve which is well approximated by an exponential,

$$E/4\pi p^2 \quad d\sigma/dp \quad \sim \exp(-bE)$$

The exponent b has the value 5.4 GeV^{-1}. A similar behaviour was observed for the inclusive spectra from J/ψ decay (see Fig. 2.3)[6]. Inclusive spectra in hadronic collisions behave in the same way if the data are plotted as a function of the transvers energy $E_T = \sqrt{m^2 + p_\perp^2}$. This is demonstrated in Fig. 2.3 where the curves represent the inclusive spectra from pp collisions in the central region at $\sqrt{s} = 53$ GeV. It is surprising to see that inclusive spectra that come from such different initial states as e^+e^- collisions, J/ψ decay and pp collisions are very similar.

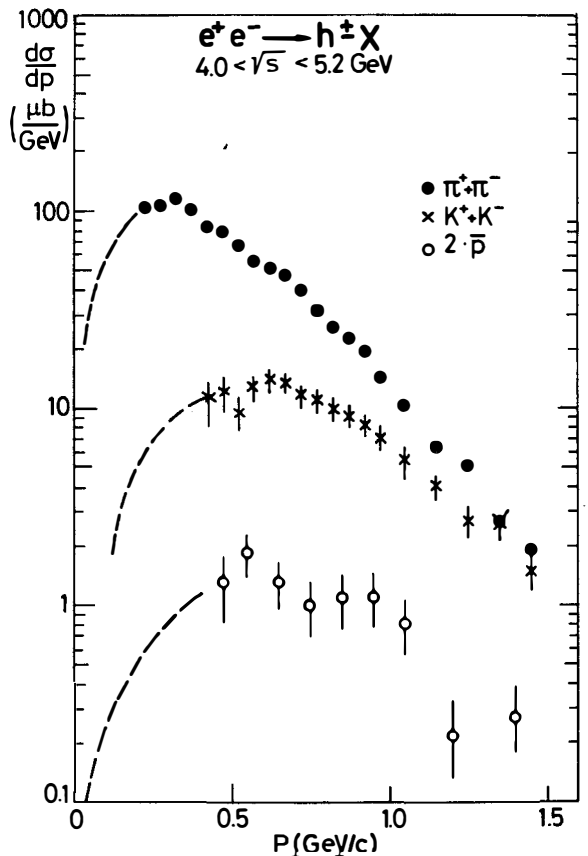

2.1 Momentum spectra of $\pi^\pm$, $K^\pm$ and $\bar{p}$ as measured by DASP

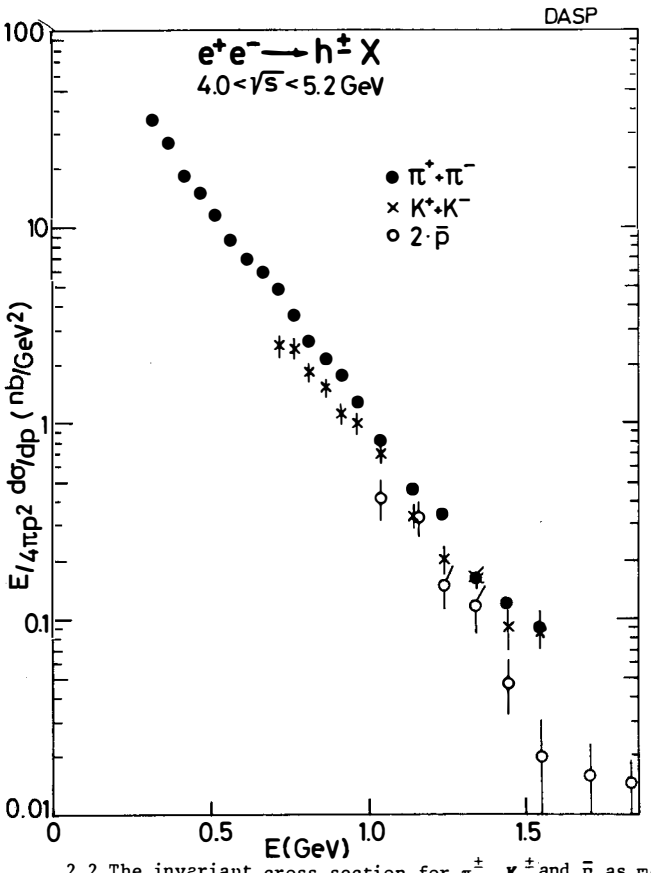

2.2 The invariant cross section for $\pi^\pm$, $K^\pm$ and $\bar{p}$ as measured by DASP

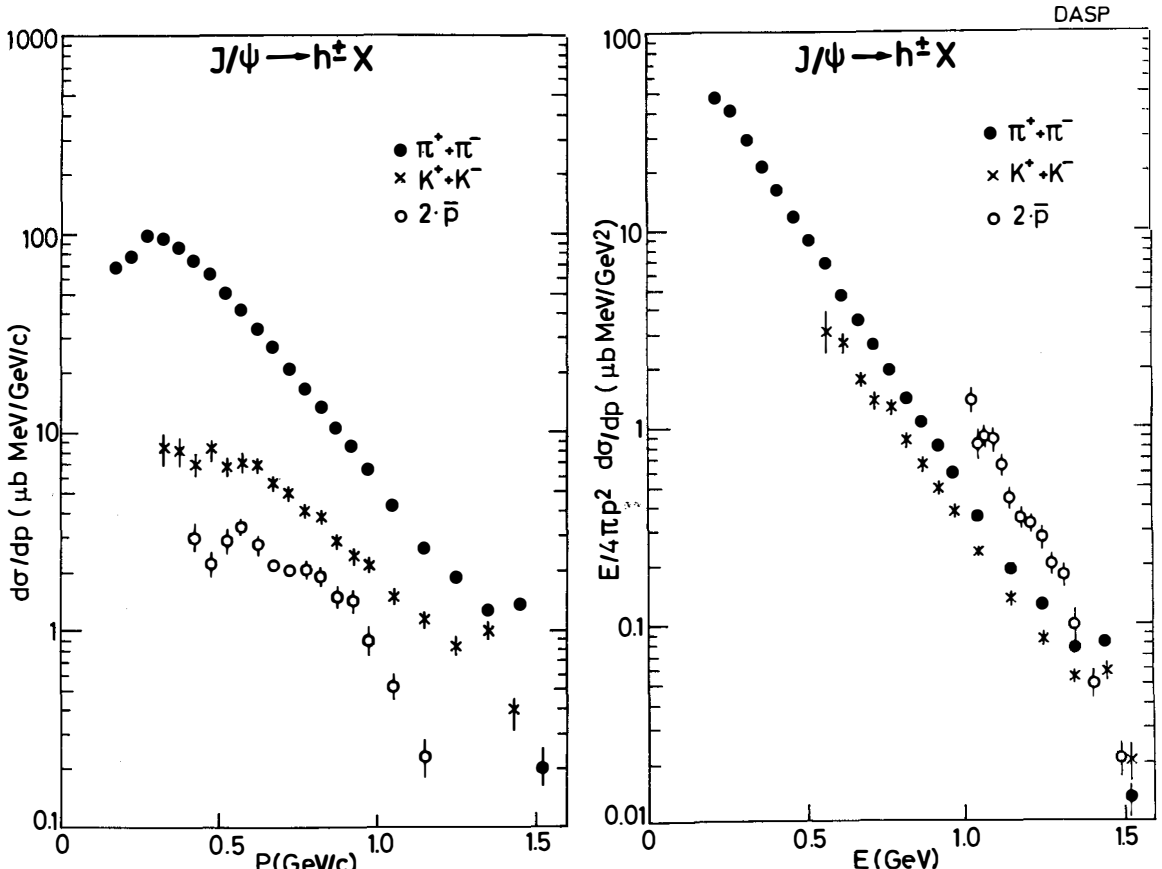

2.3 The momentum spectra and invariant cross sections for the sum of $\pi^{\pm} + \pi^{\pm}$, $K^{+} + K^{-}$ and $2.\bar{p}$ from J/ψ decay (Ref. 6).

2.4 Test for Scaling

Since the angular distribution was found to be consistent with isotropy we neglect the second term in eq. (2.6) and obtain

$$\frac{d\sigma}{dx} \simeq \frac{4\pi\alpha^2}{s} \beta x \bar{W}_1 (s,\nu) \qquad (2.12)$$

The quantity $\frac{s}{\beta}\frac{d\sigma}{dx}$ is then proportional to the structure function $\bar{W}_1$. For the purpose of orientation Fig. 2.4 shows first the ratio $R = \sigma_{tot}/\sigma_{\mu\mu}$ in the energy region analyzed here[1]. Note that the heavy lepton contribution has been excluded. At 3.6 GeV which is the first energy analyzed and which is below charm threshold, R is of the order of 2.3. Above charm threshold three resonance-like structures show up at 4.04, 4.16 and 4.41 GeV. Beyond 4.5 GeV R seems to have reached its post charm level with a value of 4.5.

Fig. 2.5 shows the x dependence of $\frac{s}{\beta}\frac{d\sigma}{dx}$ for $\pi^{\pm}$(i.e. sum of π^+ and π^-), $K^{\pm}$ and twice the $\bar{p}$ production as measured in the eight energy intervals. The π, K and $\bar{p}$ cross sections for $x \gtrsim 0.2$ decrease nearly exponentially. Moreover, with increasing energy $\sqrt{s}$, and increasing x the cross sections for the three particle species become more and more alike. The $\bar{p}$ data, within large errors, do not show any significant change with s, i.e. they appear to scale.

In order to test the pion data for scaling we compare in Fig. 2.6 the cross sections at the "nonresonant" energies s = 13 and 25 GeV^2. Below $x \simeq 0.3$ the cross section rises by a factor of 1.5 to 2 between s = 13 and 25 GeV^2. At higher x values the two cross section sets agree within errors. In other words, the rise of R from a value of 2.3 at s = 13 GeV^2 to ~ 4.5 at 5.0 GeV is associated with low x pions only.

In Fig. 2.7 $(s/\beta)\, d\sigma/dx$ is plotted for $\pi^{\pm}$ and $K^{\pm}$ as a function of s for fixed x. A large increase in the π cross section at s = 16 GeV^2 is most prominent for $x < 0.4$. The cross sections at s = 13 and 27 GeV^2 for $x \gtrsim 0.4$ are equal within errors. The K cross sections increase by a factor of two or three from s = 13 to s = 16 GeV^2. For $x > 0.4$ the K cross section above the 4 GeV resonance region falls back to its pre-charm level. This suggests that at high energies ($s > 30$ GeV^2) charm contributions to K production are confined to x values below 0.4. Note also that for $s \gtrsim 25$ GeV^2 and $x \geq 0.3$ π and K cross sections tend to be the same.

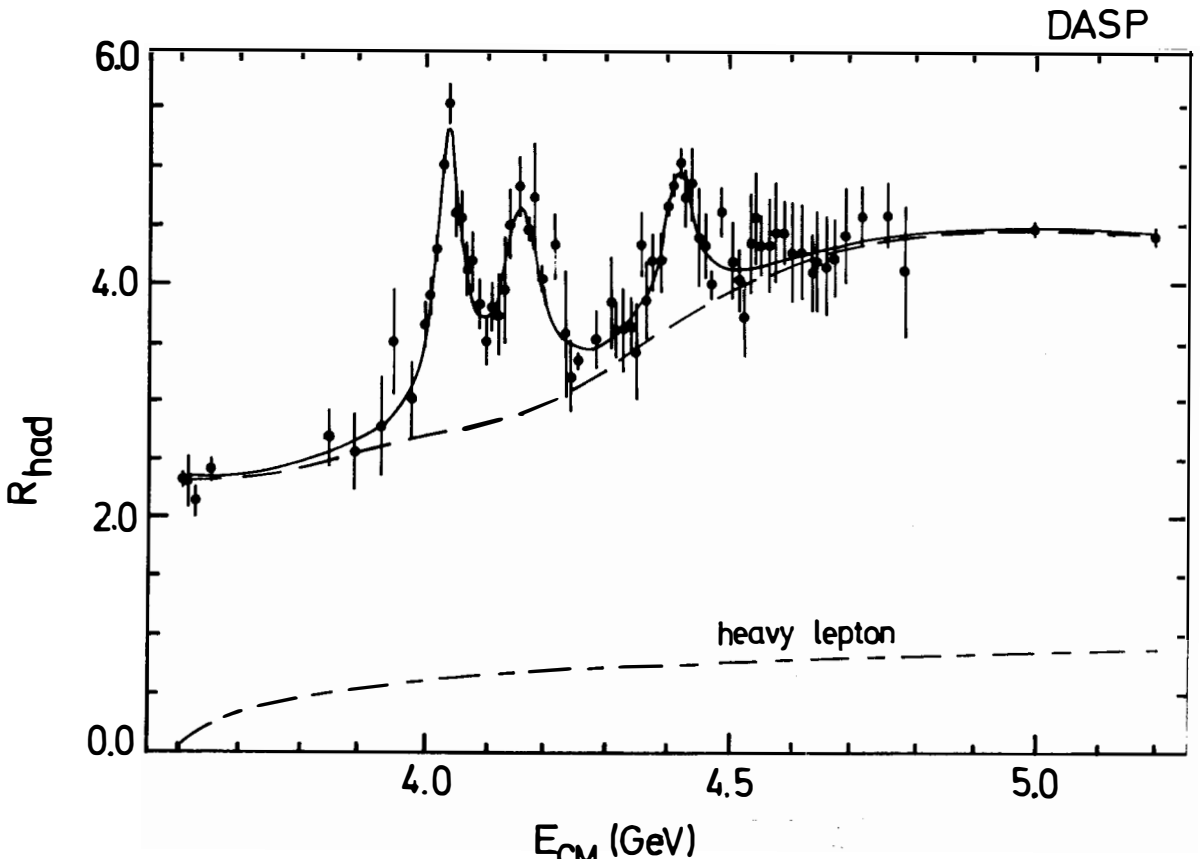

2.4 $R = \sigma^{tot}/\sigma_{\mu\mu}$ without the heavy lepton contribution as measured by DASP (Ref. 4)

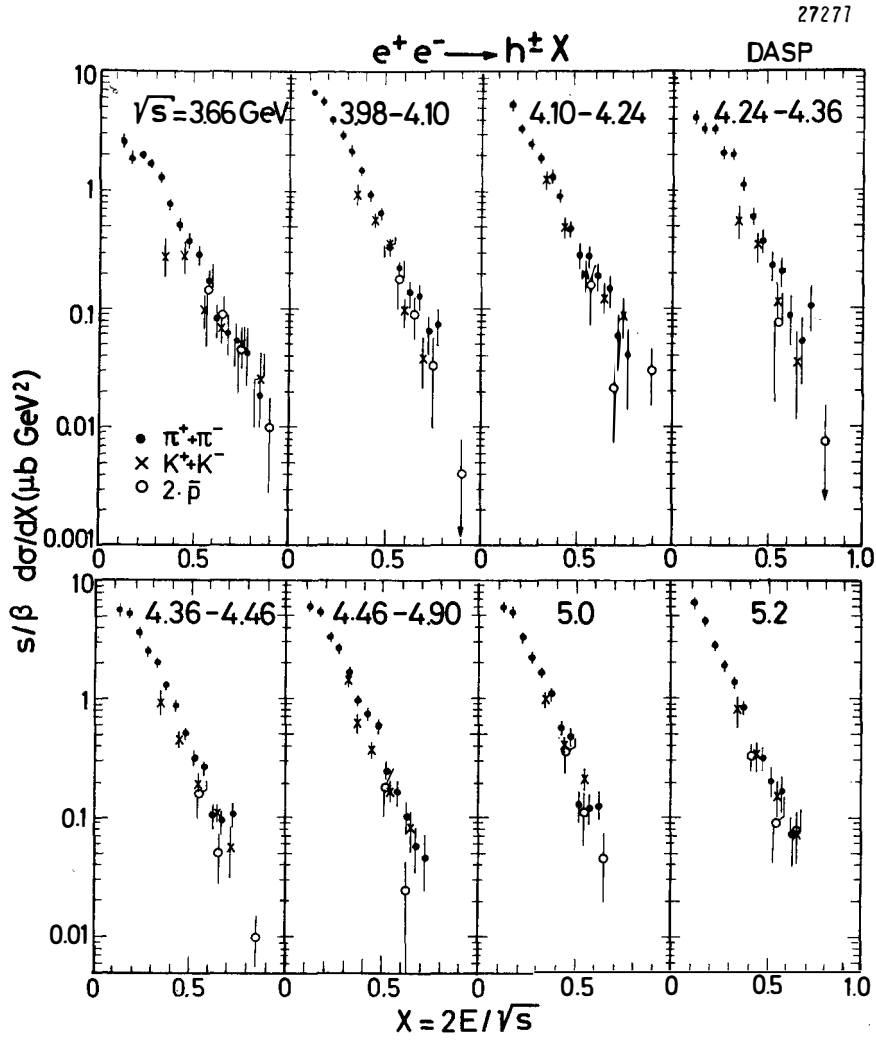

2.5 The cross section $(s/\beta)d\sigma/dx$, $x \equiv 2E/\sqrt{s}$, versus x for the sum of π^+ and π^-, K^+ and K^-, and twice the $\bar{p}$ yield, as measured by DASP (Ref.4).

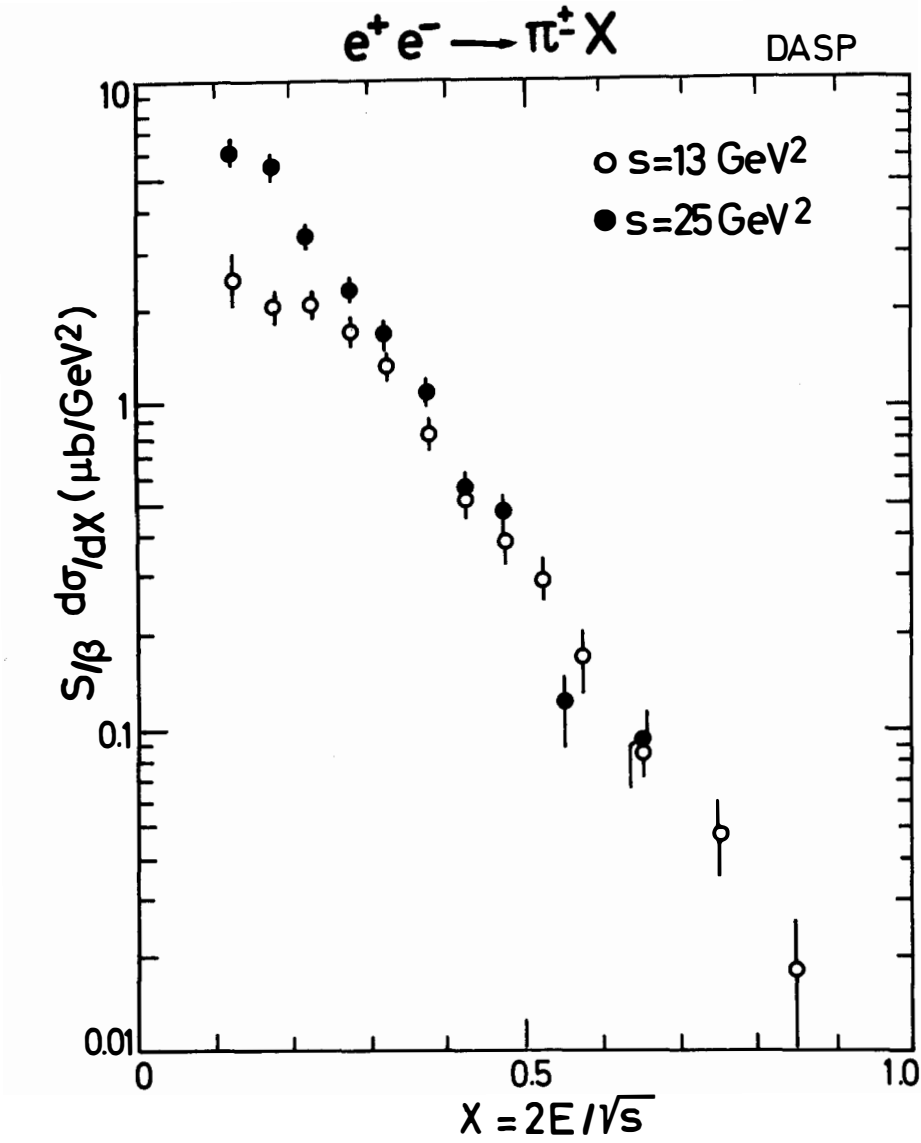

2.6 Comparison of the crsoss section $s/\beta \; d\sigma/dx$ for $\pi^\pm$ production at $s = 13$ and 25 GeV^2 (Ref. 4).

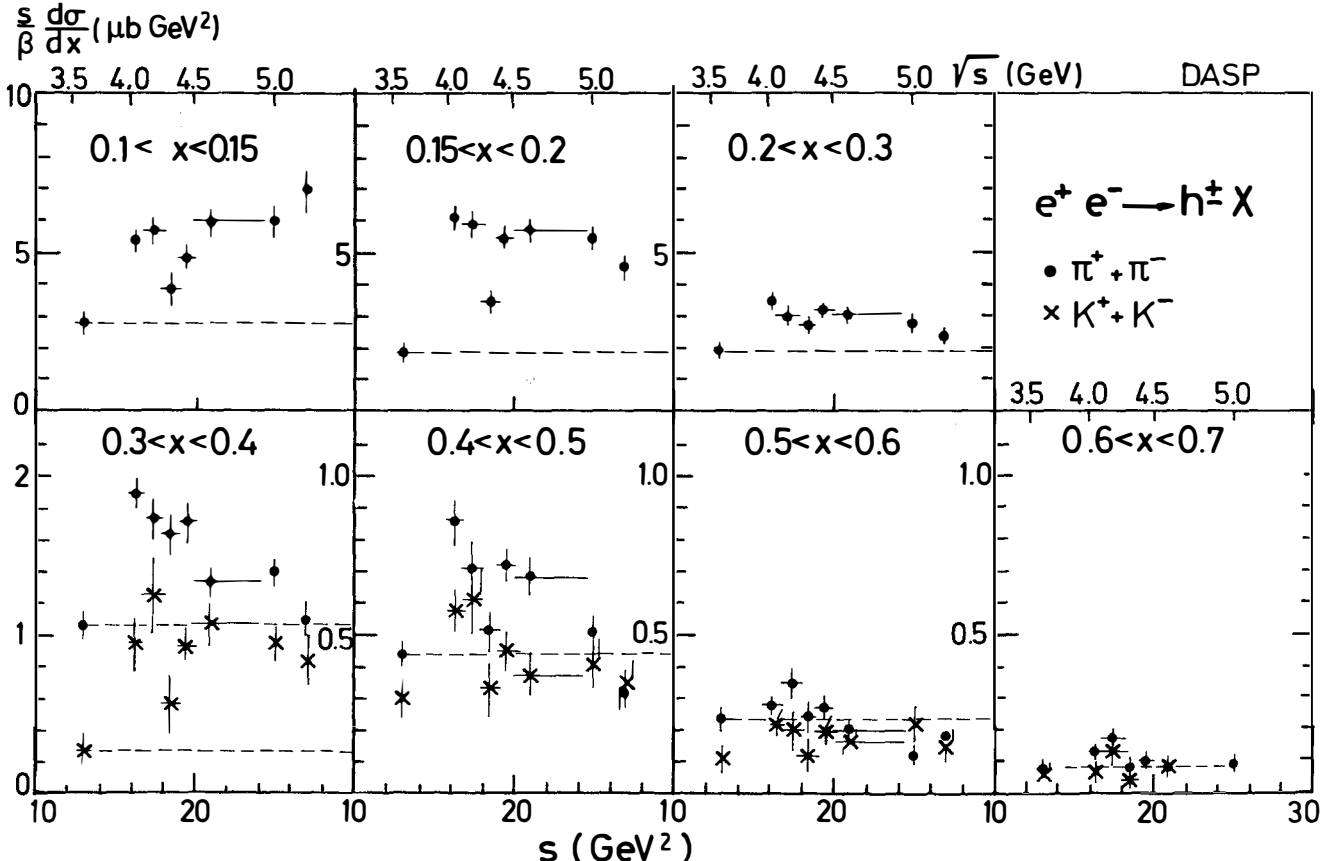

2.7 The cross section $(s/\beta)\, d\sigma/dx$ versus s for fixed x for $\pi^\pm$ and $K^\pm$ production as measured by DASP (Ref. 4).

2.5 $e^+e^- \to \bar{p}X$ and $e\,p \to e'X$

Inclusive production of a particle h by e^+e^- annihilation and inelastic electron scattering on particle h are related by crossing (see diagrams below). At the special point x = 1 (where for inelastic electron scattering x is defined as $2\,p \cdot q\,/(-q^2)$, q, p four momenta of the virtual photon and the target particle h) the structure functions for one process can be calculated from those of the other one if scaling holds. Consider $e^+e^- \to \bar{p}X$ and $e\,p \to e'X$. In this case[5]

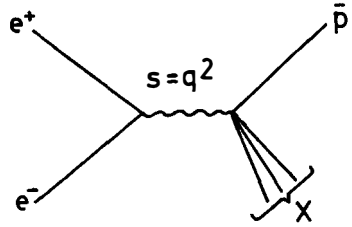

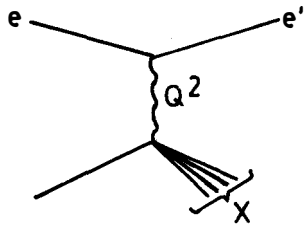

$e^+e^- \to pX$

$$\bar{F}_1\,(x = 1) = -\,F_1(x = 1)$$
$$\bar{F}_2\,(x = 1) = \;\;F_2(x = 1) \qquad (2.13)$$

$e\,p \to e'X$

However, an analytic continuation which would connect points at $x \neq 1$ is in general not possible[7].

Gribov and Lipatov[8], studying both processes in a field theoretical model predicted the following relations:

$$\bar{F}_1(x) = \frac{-1}{x}\;F_1\left(\frac{1}{x}\right)$$
$$\bar{F}_2(x) = \frac{1}{x^3}\;F_2\left(\frac{1}{x}\right) \qquad (2.14)$$

A preliminary analysis of the DASP data for $F_2(x)$ is shown in Fig. 29. The experimental points were obtained by summing over cm energies from 4 to 5.2 GeV. The structure function $\bar{F}_2(x)$ was determined from the data assuming the Callan-Gross relation

$$x\bar{F}_2(x) = -\bar{F}_1(x) \qquad (2.15)$$

which leads to

$$\frac{d\sigma}{dx} = \frac{3}{2}\;\sigma_{\mu\mu}\beta(1 - \beta^2/3)\;x\;\;\bar{F}_2(x) \qquad (2.16)$$

The Gribov-Lipatov prediction calculated from deep inelastic ep scattering data is shown by the curve in Fig. 2.8. It fails to describe the data: the

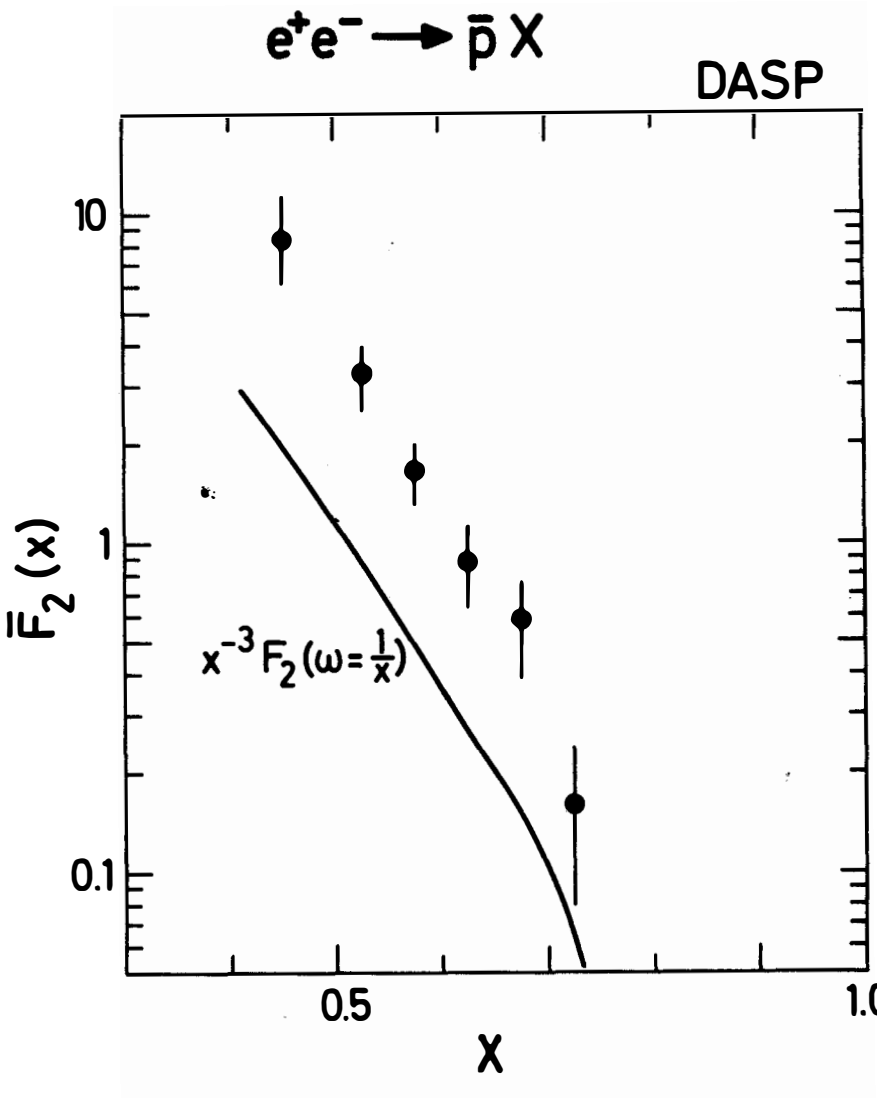

2.8 The structure function $\bar{F_2}(x)$ for $e^+e^- \to \bar{p}X$ as obtained from a preliminary analysis of DASP. The curve shows the prediction of Gribov-Lipatov.

theoretical curve is always below the measured points. The discrepancy is a factor of ~2 at x = 0.8 rising to ~4 at x = 0.4. Part of this failure - if not all - may have to be attributed to contributions from processes of the type

$e^+e^- \rightarrow h\,X,\ h\ \bar{p} + \ldots$ where $h = \Lambda_{\bar{p}\ldots}, \Sigma_{\bar{p}\ldots}, N_{\bar{p}\ldots}$, etc.

which should be excluded from the e^+e^- data before the comparison is being made. It is this type of contributions which prevent in general an analytic continuation from the scattering to the annihilation case[7].

3. THREE GLUON VERSUS $q\bar{q}$ ANNIHILATION

Approximately 70 % of the J/ψ decays are direct decays into hadrons which are believed to proceed via three gluon annihilation. Electron-positron annihilation into hadrons on the other hand at high energies appears to proceed via a primary quark-antiquark pair. For this reason one might expect the J/ψ to yield more low energy particles than nonresonant hadron production. DASP[6] has analyzed the inclusive spectra for $\pi^\pm$, $K^\pm$ and $\bar{p}$ from J/ψ decay and for a cm energy $\sqrt{s}$ of 3.6 GeV (i.e. below charm threshold). In Fig. 3.1 the cross section $\frac{1}{\sigma_{tot}} \frac{1}{\beta} \frac{d\sigma}{dx}$ is shown as a function of the fractional particle energy $x \equiv 2E/\sqrt{s}$. The data points represent the values at 3.6 GeV, the curves the result at the J/ψ. The J/ψ curves were normalized such that the integrated π cross section from J/ψ agrees with that at 3.6 GeV for x = 0.3. Within errors no difference is observed in the shape of the π and K spectra at the two energies. Most likely the energy of ~3 GeV is too low for the two mechanisms to produce a noticecable difference. Remember that at 3 GeV the sphericity distributions for the two extreme cases of phase space and jet formation are the same[9].

The only difference between on and off resonance data in Fig. 3.1 is seen to occur for antiprotons. The J/ψ decay relative to the π and K yields produces more antiprotons by a factor of 2-3. No explanation has been offered for this fact.

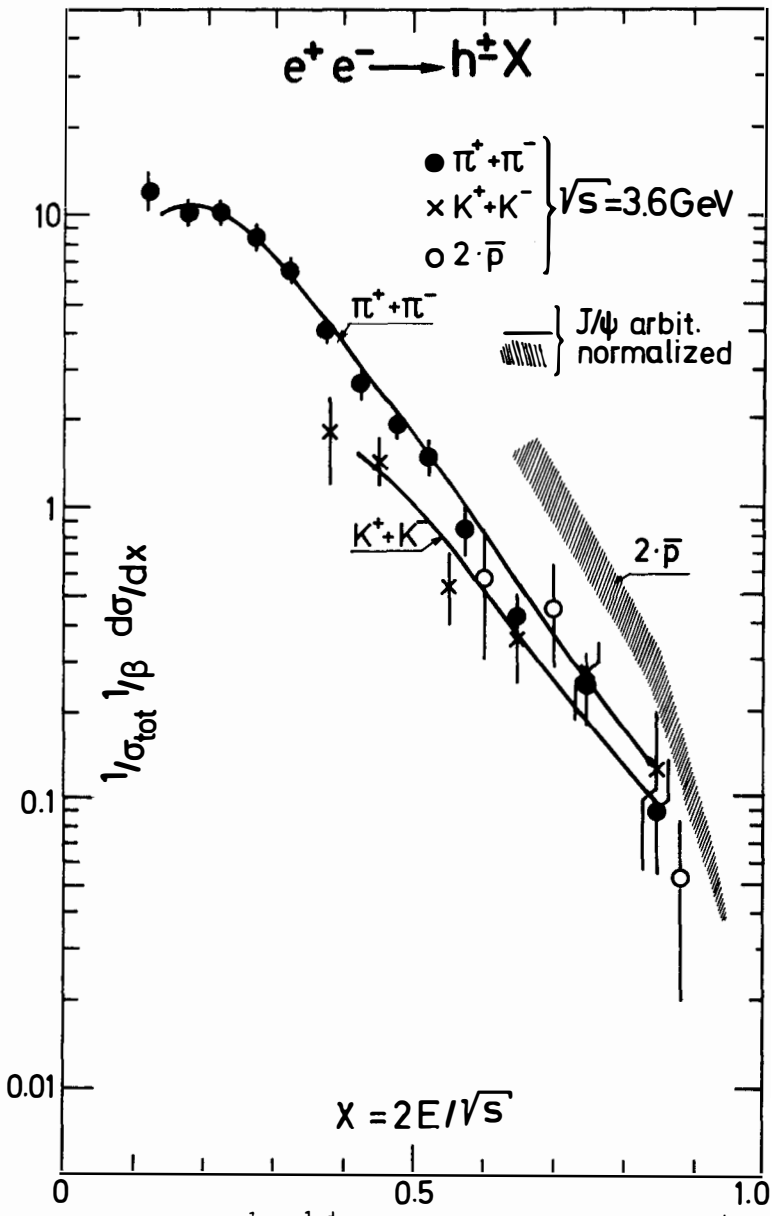

3.1 The cross section $\frac{1}{\sigma_{tot}} \frac{1}{\beta} \frac{d\sigma}{dx}$ versus $X = 2E/\sqrt{s}$ for the sum of $\pi^+ + \pi^-$, $K^+ + K^-$ and twice the $\bar{p}$ yield at 3.6 GeV (data points) and from J/ψ decay (curves) measured by DASP[6]. The J/ψ data have been normalized by a common normalization factor.

4.1 The F mesons

The charm model predicts mesons carrying both charm and strangeness. The ground state is F^+. The GIM favored decay of the F is into an $s\bar{s}$ system leading to final states containing $K\bar{K}, \Phi$, η or η'.

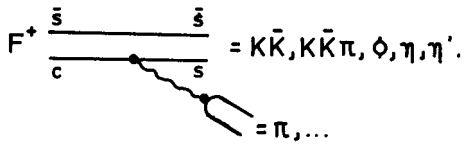

Sizeable η production is therefore a hint for F production. The production characteristics for F mesons can be expected to be similar to that for D's. Copious D production was found near the D^+ threshold at 4.028 GeV proceeding mainly via DD^* and D^*D^* formation. Assuming a similar behaviour for the F meson one expects large FF^* and F^*F^* cross sections near threshold. Since both, F and F^* are isospin singlets the favored decay of the F^+ is the radiative transition $F^* \to F\gamma$ provided the F^* - F mass difference is less than 2 m_π[10]. The signal for F production can therefore be enhanced by requiring a low energy photon in addition to the η signal.

DASP[11] searched for the F meson by studying events of the type

$$e^+e^- \to \eta\gamma_{low} + \geq 2 \text{ charged tracks} + X$$

The η was identified by its decay into two photons. A search of this type is hampered by the $\gamma\gamma$ mass resolution which in the DASP experiment was 80 MeV, and by the large $\gamma_i\gamma_j$ combinatorial background: on the average there are 2-3 π^0's produced near 4 GeV leading to 4-6 photons or 6-15 two-photon mass combinations. The event selection was done as follows: The photons were detected in the inner detector and their angles and energies measured. The detection efficiency was 50 % at 0.05 GeV rising to 80 % at 0.1 GeV and 95 % above 0.3 GeV. Events accepted were required to have at least two charged tracks coming from the interaction region and at least two photons with energies exceeding 0.1 GeV. The vector sum of the momenta of these two photons was required to be between 0.3 and 1.2 GeV. Events containing a photon of less than 0.14 GeV (γ_{low}) in addition to the two used for forming $m_{\gamma\gamma}$ were called low energy photon events.

Fig. 4.1 shows the $m_{\gamma\gamma}$ distribution for events containing a low energy photon for five energy intervals between 4.0 and 5.2 GeV excluding energies around 4.4 GeV; the 4.4 GeV region (4.36 - 4.48 GeV) is presented in Fig. 4.2. There is a clear η signal at 4.4 GeV not observed at the other energies.

The occurence of η production in association with low energy photons at 4.4 GeV is strongly suggestive of FF^* (F^*F^* production). A search was made for the two body decay of the $F^{\pm}$ into $\eta\pi^{\pm}$ detecting the pion in one of the spectrometer arms. A total of 35 events were found with a pion momentum above 0.6 GeV/c, a $\gamma\gamma$ combination in the η region (0.35 - 0.65) and a low energy photon (this time E_γ < 0.2 GeV). These events were fitted to the reactions

$$e^+e^- \to F^{\pm}F^{*\mp} \to (\pi^{\pm}\eta)\ (F^{\mp}\gamma_{low}) \to (\pi^{\pm}\gamma\gamma)\ (F^{\mp}\gamma_{low}) \qquad (4.1)$$

and

$$e^+e^- \to F^{+*}\ F^{-*} \to (\pi^{\pm}\eta\gamma_{low})\ F^{*\mp} \to (\pi^{\pm}\gamma\gamma\gamma_{low})\ F^{*\mp} \qquad (4.2)$$

These are two constraints fits because of the mass constraint on $m_{\gamma\gamma}$ and the requirement that for (4.1) $\pi\eta$ and the missing vector must have the same mass m_F; for (4.2) the $\pi\eta\gamma_{low}$ system and the missing vector must have the same mass m_{F*}.

A total of 25 events gave a fit to (4.1) with a χ^2 < 8. These events are plotted in Fig. 4.3a as a function of Δ, the difference between the measured and the fitted $\pi\eta$ mass. The distribution peaks at Δ = 0. Cutting at $|\Delta|$ = 0.25 GeV 21 events with $|\Delta|$ < 0.25 GeV are retained. These events are shown in scatter plots (Fig. 4.3b,c) of the mass difference between the recoil mass and the $\pi\eta$ mass versus the $\pi\eta$ mass. The data taken at 4.4 GeV have a cluster of 6 events with a well defined $\pi\eta$ mass and a recoil mass some 100 MeV higher. The background is found to be negligible from the event distribution outside the 4.4 region (Fig. 4.3c). In the latter data no event with a $\pi\eta$ mass compatible with the signal at 4.4 GeV was found for an integrated luminosity five times larger than that at 4.4 GeV. Fig. 4.4 shows a scatter plot of the fitted $\pi\eta$ mass versus the mass of the recoil system and Fig. 4.5 gives the projection onto the $\pi\eta$ mass axis. There are six events which give the same ($m_{\pi\eta}$, m_{recoil}) mass values within errors: $m_{\pi\eta}$ = 2.04 GeV, m_{recoil} = 2.17 GeV, m_{F*} = 2.11 GeV. Allowing for possible systematic uncertainties the best estimates are

$$m_F = 2.03 \pm 0.06 \text{ GeV}$$
$$m_{F*} = 2.14 \pm 0.06 \text{ GeV}$$

The mass difference between F^* and F can be directly determined from the energies of the low energy photon:

$$m_{F*} - m_F = 0.12 \pm 0.04 \text{ GeV}.$$

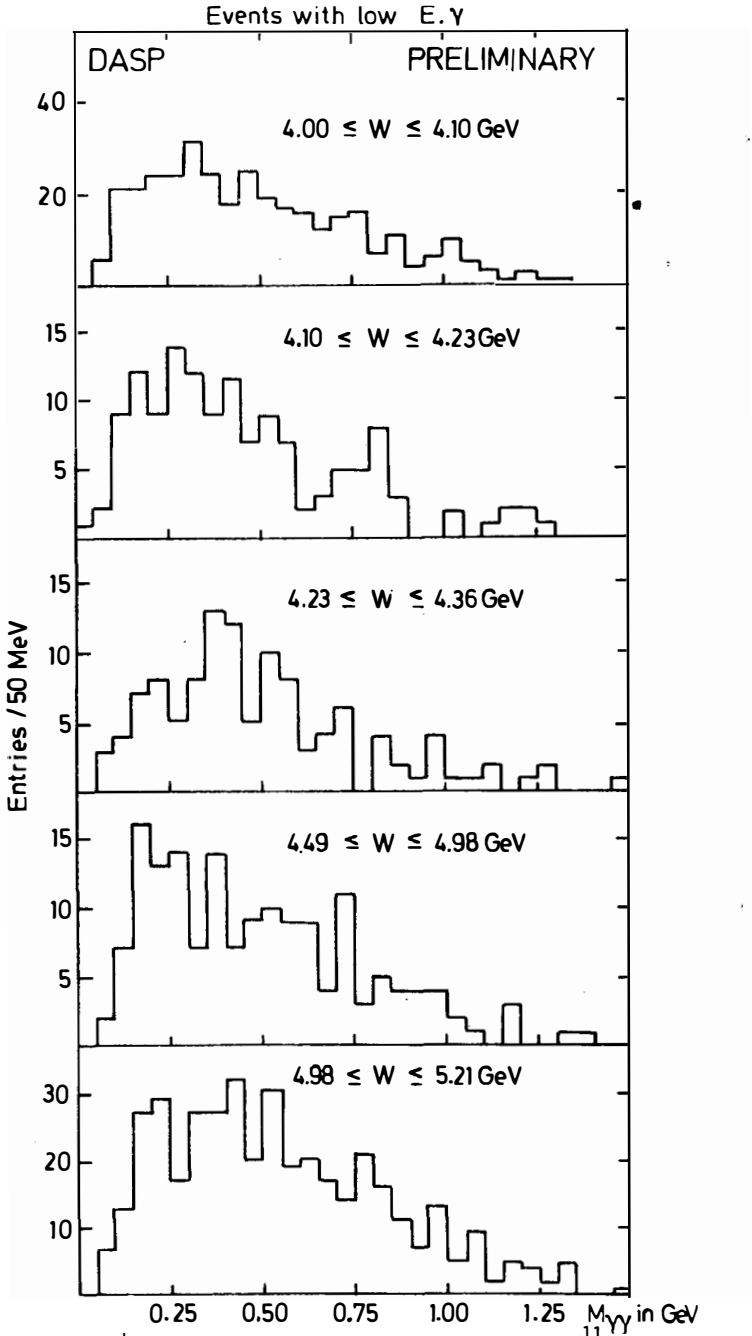

4.1 Reaction $e^+e^- \to \gamma\gamma\gamma + \geq 2$ charged as measured by DASP[11]. The $\gamma\gamma$ low mass distribution for different cm energy intervals.

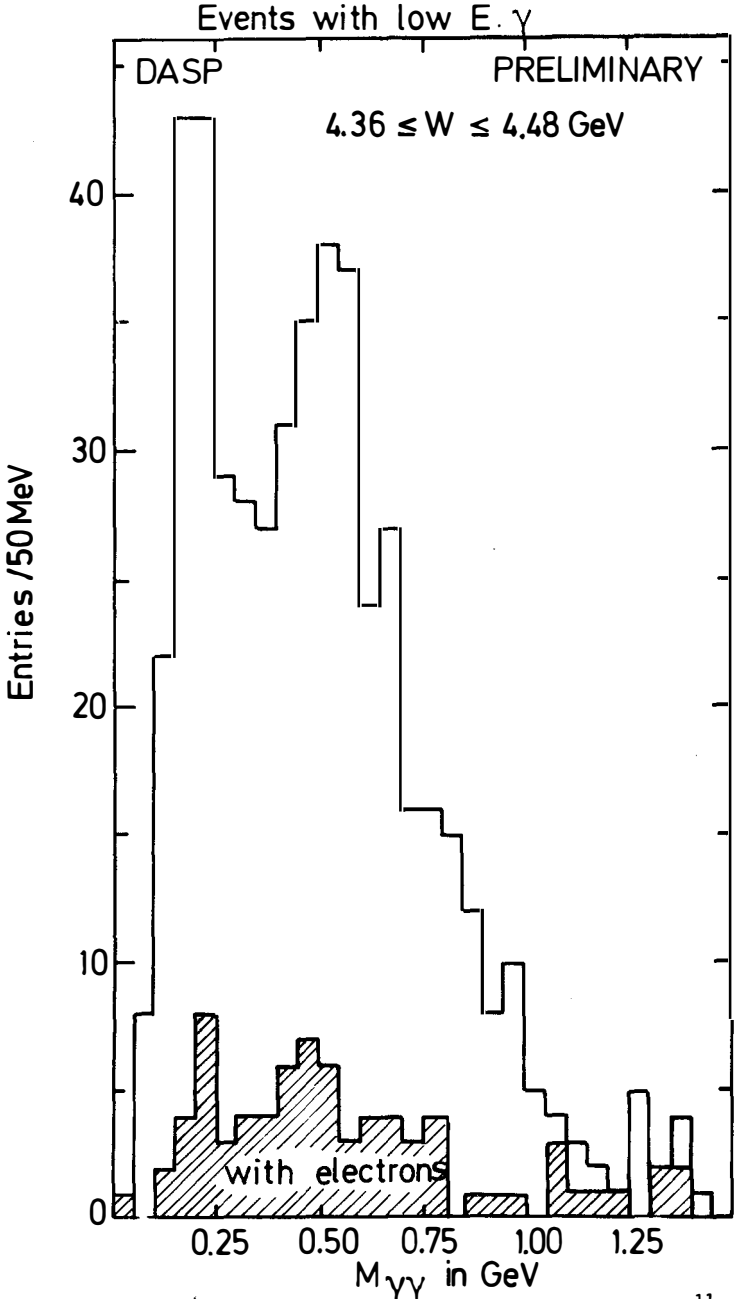

4.2 Réaction $e^+e^- \to \gamma\gamma\gamma_{low} + \geq 2$ charged as measured by DASP[11]. The $\gamma\gamma$ distribution for cm energies between 4.36 and 4.48 GeV.

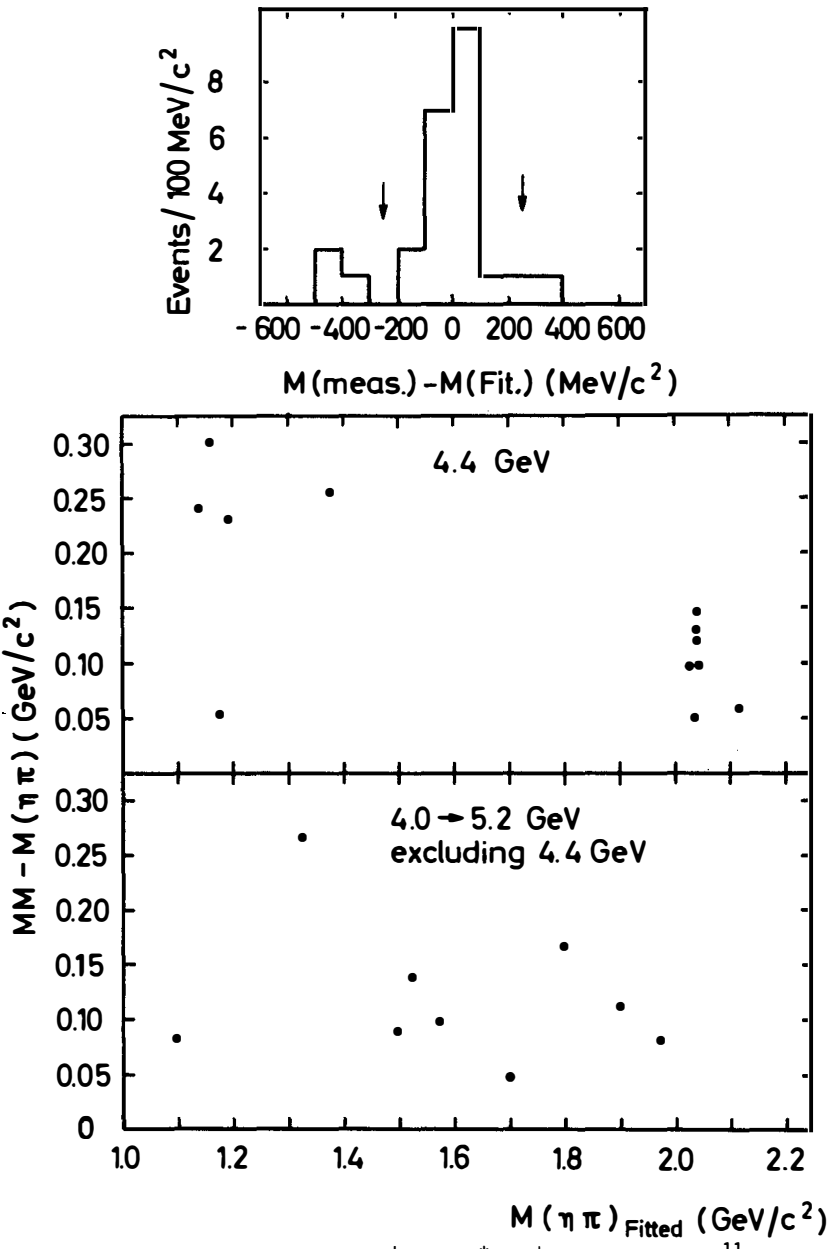

4.3 Results for the fit $e^+e^- \to FF^* \to \pi^\pm \eta \gamma_{low} F$ from DASP[11].
a) difference between measured and fitted $\pi\eta$ mass
b) and c) difference between $\pi\eta$ mass and recoil mass.

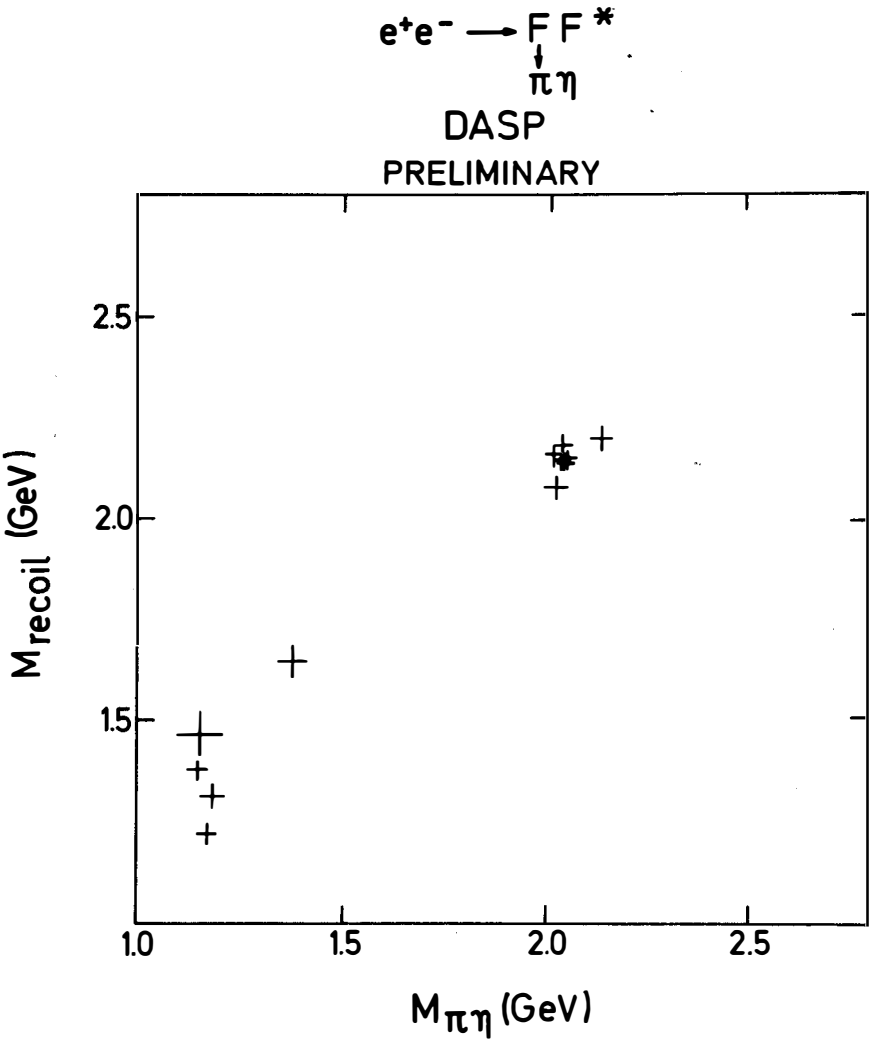

4.4 Results for the fit $e^+e^- \to FF^* \to \pi^\pm \eta \gamma_{low} F$ at 4.4 GeV from DASP[11]. Scatterplot of the fitted F mass versus the F* mass.

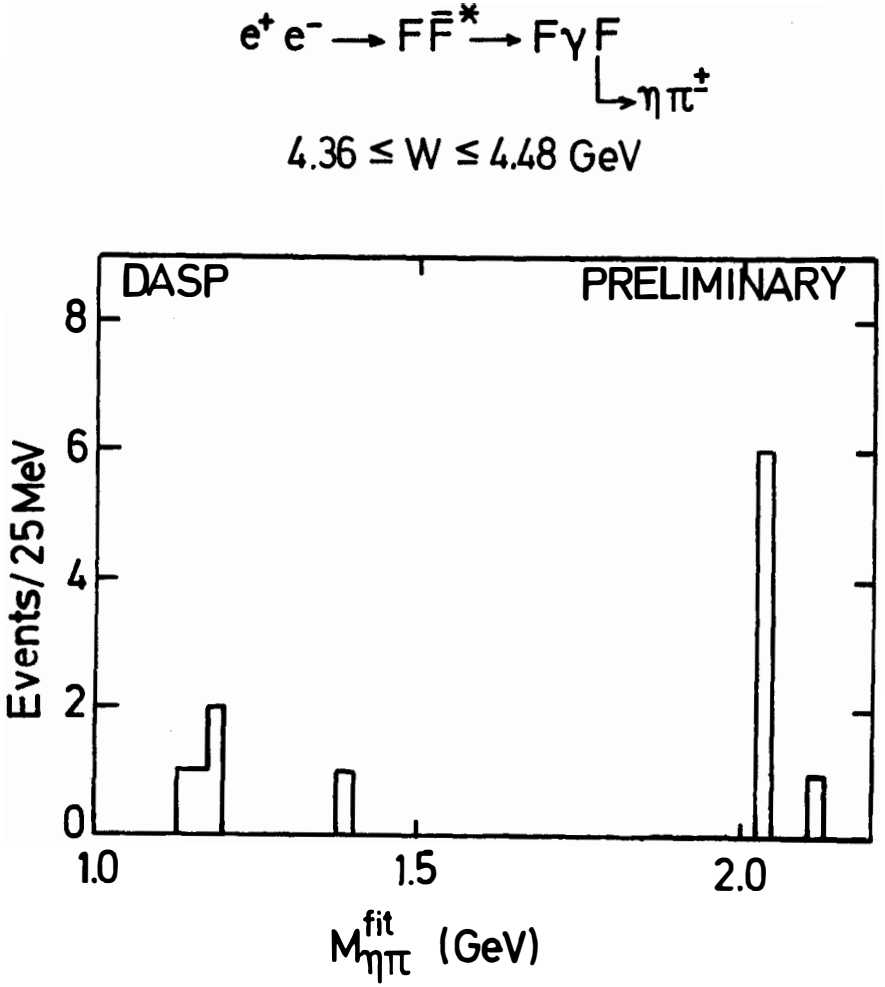

4.5 Results for the fit $e^+e^- \to FF^* \to \pi^\pm\eta\gamma_{low}F$ at 4.4 GeV from DASP[11]. Distribution of the fitted $\pi^\pm\eta$ mass.

By comparison with $D\bar{D}$ production one might expect to find a strong $F\bar{F}$ signal close to the $F\bar{F}$ threshold (~4.06 GeV). In this case no correlation between production of F and a low energy photon will exist. Using the same selection criteria as before but not demanding a low energy photon the $m_{\gamma\gamma}$ mass distribution shown in Fig. 4.6 (cm energy 4.0 - 4.10 GeV) and Fig. 4.7 (4.10 - 4.22 GeV) were obtained. The first energy bin shows a π^0 peak but no η signal. The second energy bin, besides the π^0 exhibits a clear η peak. Since no η signal is observed at 4.0-4.10 GeV the η mesons do not come from D decay and $D\bar{D}\eta$ production is excluded by kinematics.

The observed features strongly suggest to associate the η signal with $F\bar{F}$ production. A search for events with $F^{\pm} \to \pi^{\pm}\eta$ revealed one event. From the fit a value of 2.03 ± 0.01 GeV was found for the F mass.

5. SEMILEPTONIC DECAYS OF CHARMED PARTICLES

5.1 Electron inclusive events

The semileptonic decays of charmed particles were studied with inclusive electron events,

$$e^+e^- \to eX \qquad (5.1)$$

Events of this type can come from charmed particle decays but also from a variety of other sources, trivial ones like QED processes, Dalitz pairs, hadrons faking electrons, or from other new particles such as heavy leptons.
The analysis was done for cm energies between 3.6 and 5.2 GeV and for electron momenta p_e above 0.2 GeV/c.[12,13] The total integrated luminosity amounted to 6300 nb^{-1}. The electron was identified in the magnetic spectrometer by a Cerenkov counter together with either time-of-flight (for $p_e < 0.35$ GeV/c) or shower counters ($p_e > 0.35$ GeV/c). The probability for a pion to fake an electron was measured to be $4 \cdot 10^{-4}$. Electron pairs from Dalitz decay or pair conversion were rejected by pulse height cuts on the scintillation counters mounted before the magnet. Background from QED processes was suppressed by requiring the system X to contain at least one nonshowering track $T^{\pm}$ (e.g. $\mu^{\pm}$, $\pi^{\pm}$, $K^{\pm}$ but not e).
As a result of the selection criteria the trivial background to the events selected turned out to be small (see table 5.1).

In a second step the charged multiplicity distribution and the electron momentum spectra were analysed[12]. It was found that by a simple cut on the multiplicity (shown in Fig. 5.1) a clear separation between events from charmed particle and from heavy lepton decay is possible. Electron events with a single charged track (they will be called electron two prongs) are due basically to heavy leptons; electron events with two or more charged tracks (electron multiprong events) originate from charmed particles. The relevant numbers are

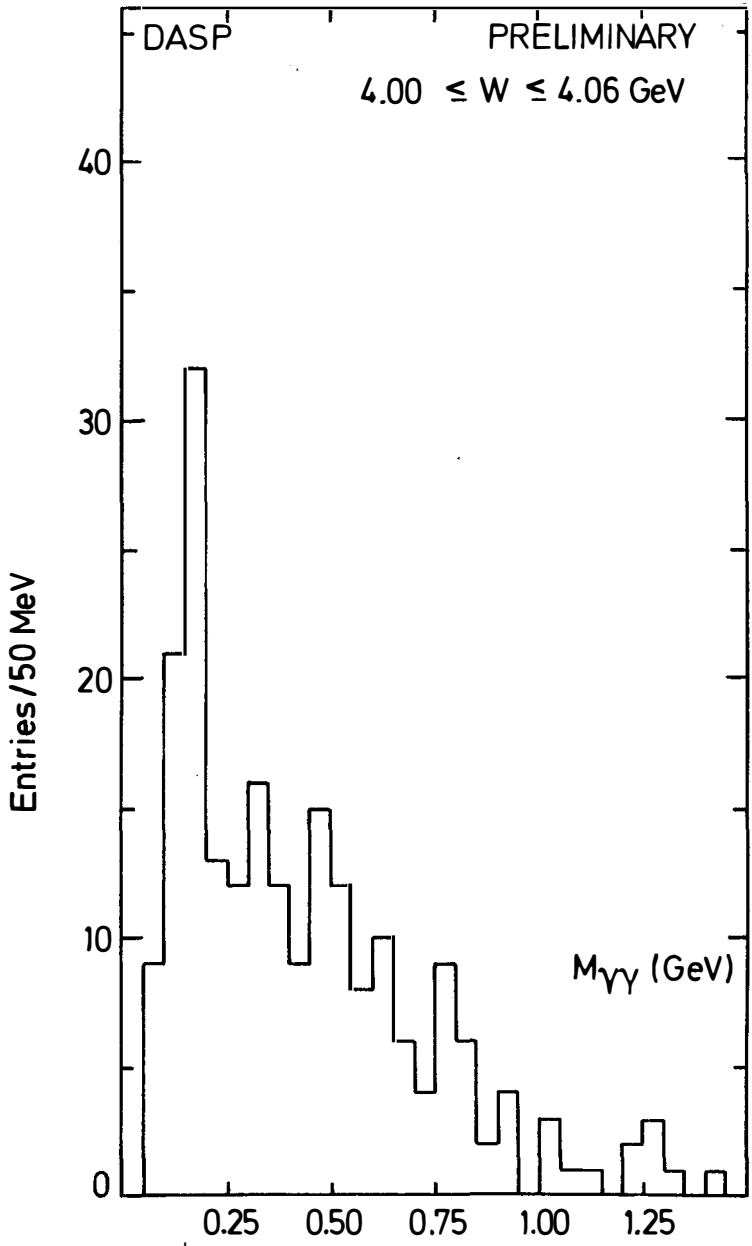

4.6 Reaction $e^+e^- \to \gamma\gamma + \geq 2$ charged for cm energies between 4.0 and 4.1 GeV as measured by DASP[11]

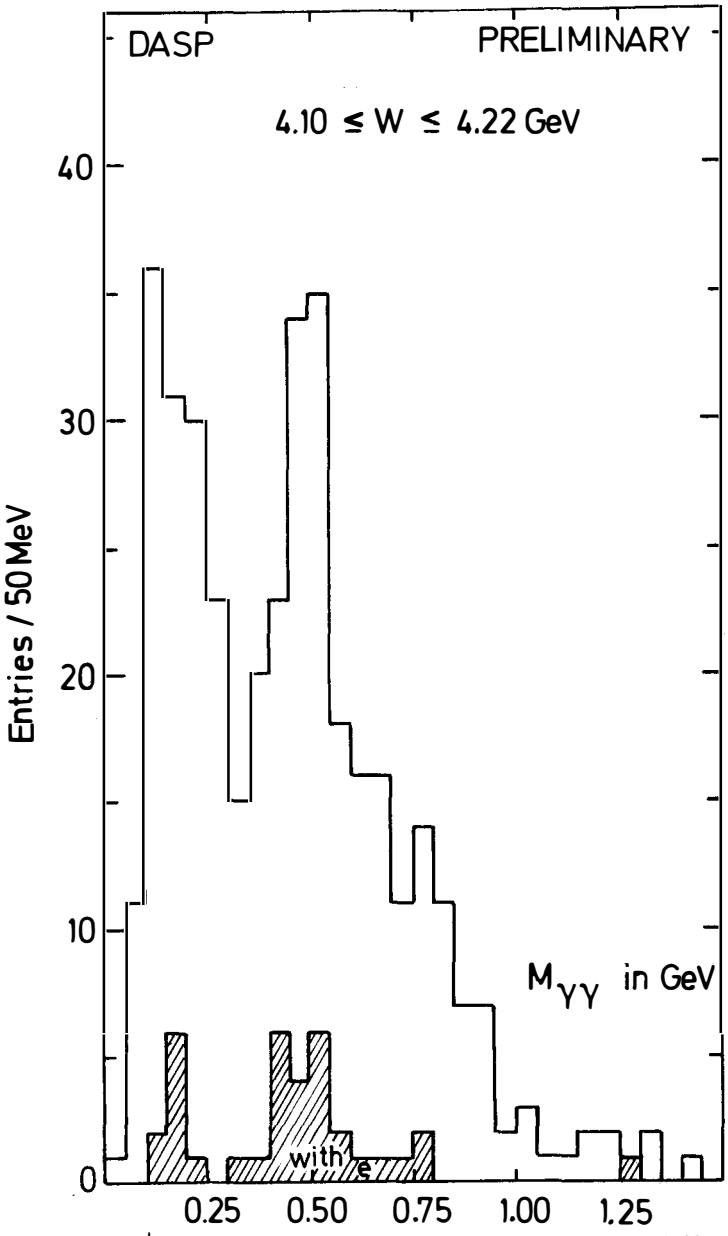

4.7 Reaction $e^+e^- \to \gamma\gamma + \geq 2$ charged for cm energies between 4.10 and 4.22 GeV as measured by DASP[11].

listed in table 5.1. The difference in multiplicity (and electron spectrum as shown below) can be understood (and was expected) in terms of the production and decay characteristics of charmed particles and heavy leptons. This is explained by table 5.2.

Table 5.1 Event statistics for inclusive electron events[12-14]

	Number of events	
	$e^+e^- \to eT^{\pm} n\gamma$, $n \geq 0$	$e^+e^- \to eT^{\pm}$ + charged + $n\gamma$, $n \geq 0$
satisfying selection criteria	60	182
trivial background	7 ± 2	28 ± 9
background from charmed particles	5 ± 2	
background from τ production		<22

Table 5.2 Properties of heavy sequential leptons and new hadrons (taken from Ref. 15)

	L	H
Production	$e^+e^- \to L^+L^-$ (point cross section)	$e^+e^- \to H\bar{H}$ (damped by form factors)
	$e^+e^- \to L^+L^-$ + hadrons (negligible small, less than α^2 of elastic production near threshold)	$e^+e^- \to H\bar{H}$ + hadrons or $H^*\bar{H}^*$ (dominant at higher energies, cross section will have structure)
Decay Modes	$L \to \ell \bar{\nu}_\ell \nu_L$	$H \to \ell \bar{\nu}_\ell$
	$\to \nu_L$ · hadrons	(suppressed if the lowest flavour state has spin 0)
		$\to \ell \bar{\nu}_\ell$ · hadrons
		$\to$ hadrons
Final States:		
$e\mu$ + neutrinos	important, clear signature ($e(\mu)$ from three body decay	negligible ($e(\mu)$ from a multibody decay)
$\ell\ell$ + neutrinos + hadrons	negligible, order α^2 at threshold	large ($e(\mu)$ from a multibody decay)
$e(\mu)$ + neutrino + hadrons	large, lepton spectrum computable and hard, hadrons have low multiplicity	large, lepton spectrum soft, hadrons have high multiplicity

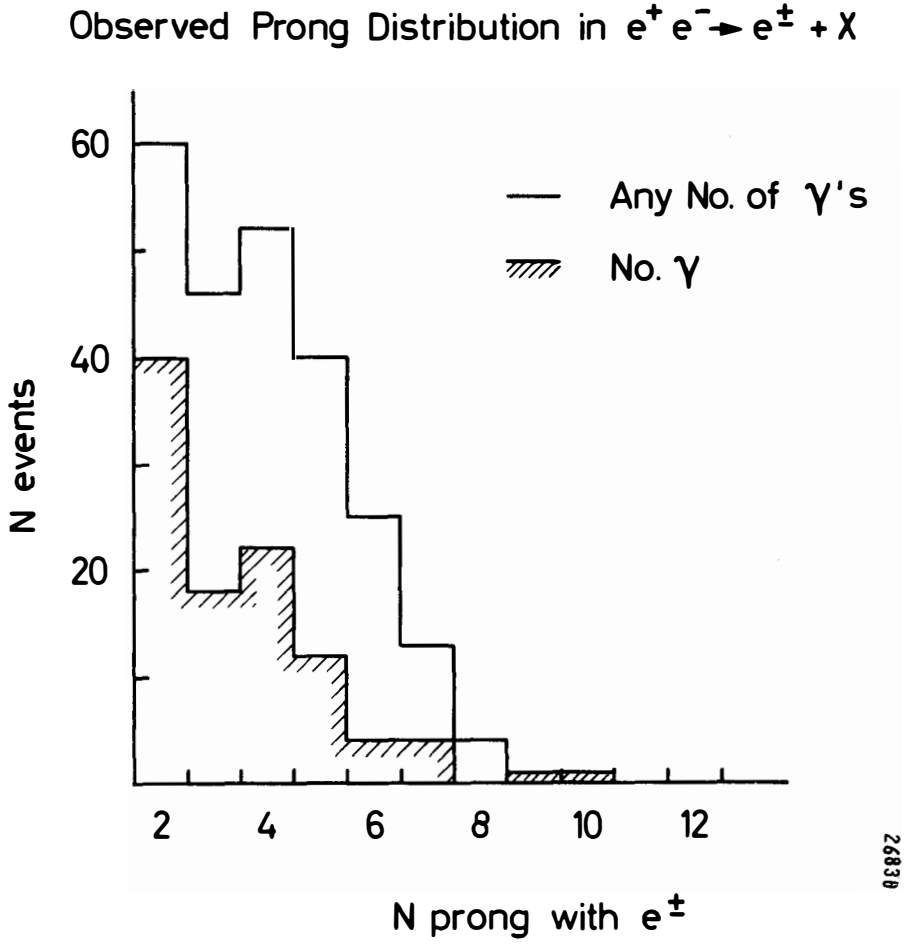

5.1 The charged track distribution observed by DASP[12,13] for inclusive electron events. The electron is included in the prong number. The shaded distribution is for events without photons.

5.2 Electron multiprong events and semileptonic decays of charmed particles

The properties of semileptonic decays of charmed particles were deduced from the electron multiprong events. The lepton spectrum associated with the multiprong sample is shown in Fig. 5.2. The estimated background due to hadron misidentification or heavy lepton production is also plotted. The background was scaled from measurements below threshold. The heavy lepton contribution was estimated assuming a τ branching ratio of 30 % to decay into final states with three or more charged particles. It was found that less than 12 % of the events with $n_{ch} \geq 3$ can be explained as heavy lepton production. The simple cut on hadron multiplicity therefore yields a rather clean sample of charm decays.

The electron spectrum contains information on the semileptonic and the leptonic decay modes of the lowest mass charmed hadrons. Fig. 5.2 demonstrates that semileptonic decays are much more important than leptonic decays because the latter, being two body decays, would produce a peak in the electron spectrum around 1 GeV/c. This is in gross disagreement with the data which peak around an electron momentum of 0.5 GeV/c with only few events above 0.7 GeV/c. To study the observed momentum spectrum in more detail we consider the spectrum obtained for cm energies between 3.99 GeV and 4.08 GeV. The charm cross section in this energy region is dominated by $D\bar{D}^*$ and $D^*\bar{D}^*$ production and is below the threshold for F production. The spectrum, corrected for the background and the heavy lepton contribution, is shown in Fig. 5.3.

The spectrum in Fig. 5.3 was fitted to three possible channels: $D \to e\bar{\nu}_e\pi$, $D \to e\bar{\nu}_e K$ and $D \to e\bar{\nu}_e K^*(892)$. A V-A current was assumed and the form of the spectra was taken from a paper by Ali and Yang[16]. Note that the theoretical spectra are model dependent. These fits gave a χ^2 value for 10 degrees of freedom of: 29.6 for $D \to e\bar{\nu}_e\pi$, 6.3 for $D \to e\bar{\nu}_e K$ and 2.8 for $D \to e\bar{\nu}_e K^*(892)$. The decay $D \to e\bar{\nu}_e\pi$ can therefore be excluded as the sole semileptonic decay mode of the D. The data can be fitted with either $D \to e\bar{\nu}_e K$ or $D \to e\bar{\nu}_e K^*(892)$.

The absolute cross section for inclusive electron production $e^+e^- \to e^\pm + X$, where X contains at least two charged tracks and any number of photons, is plotted in Fig. 5.4a as a function of energy. The data have been corrected for radiative effects. The background from hadron misidentification and the contribution from heavy leptonic production have been subtracted.

The inclusive cross section due to charmed particle production can be written as:

$$\sigma(e^+e^- \to e^\pm X) = \Sigma_{i,j}\, \sigma(e^+e^- \to C_i\bar{C}_j) \cdot \{B(C_i \to e\bar{\nu}_e X) + B(\bar{C}_j \to e\bar{\nu}_e X)\}$$

Here $(e^+e^- \to C_i\bar{C}_j)$ denotes the effective cross section for producing the

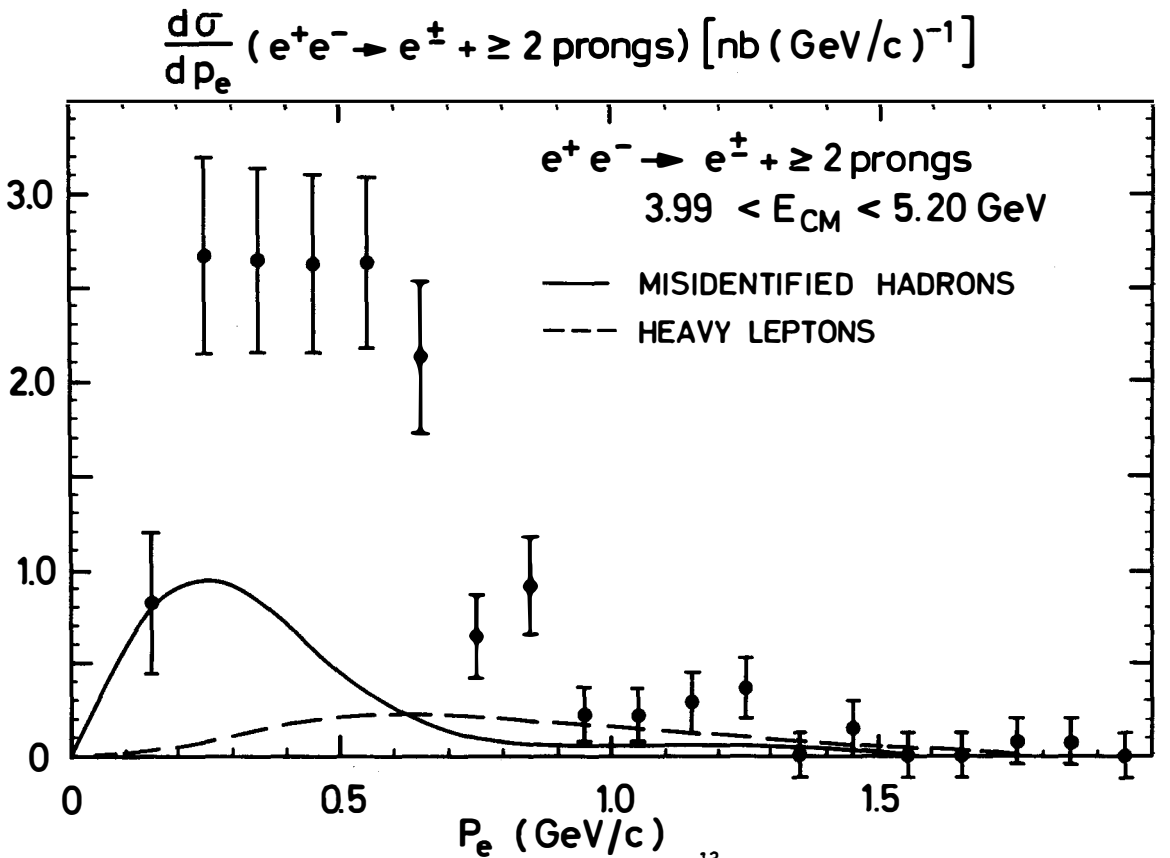

5.2 The inclusive electron momentum spectrum measured by DASP[13] between 3.99 GeV and 5.2 GeV for multi-prong events.

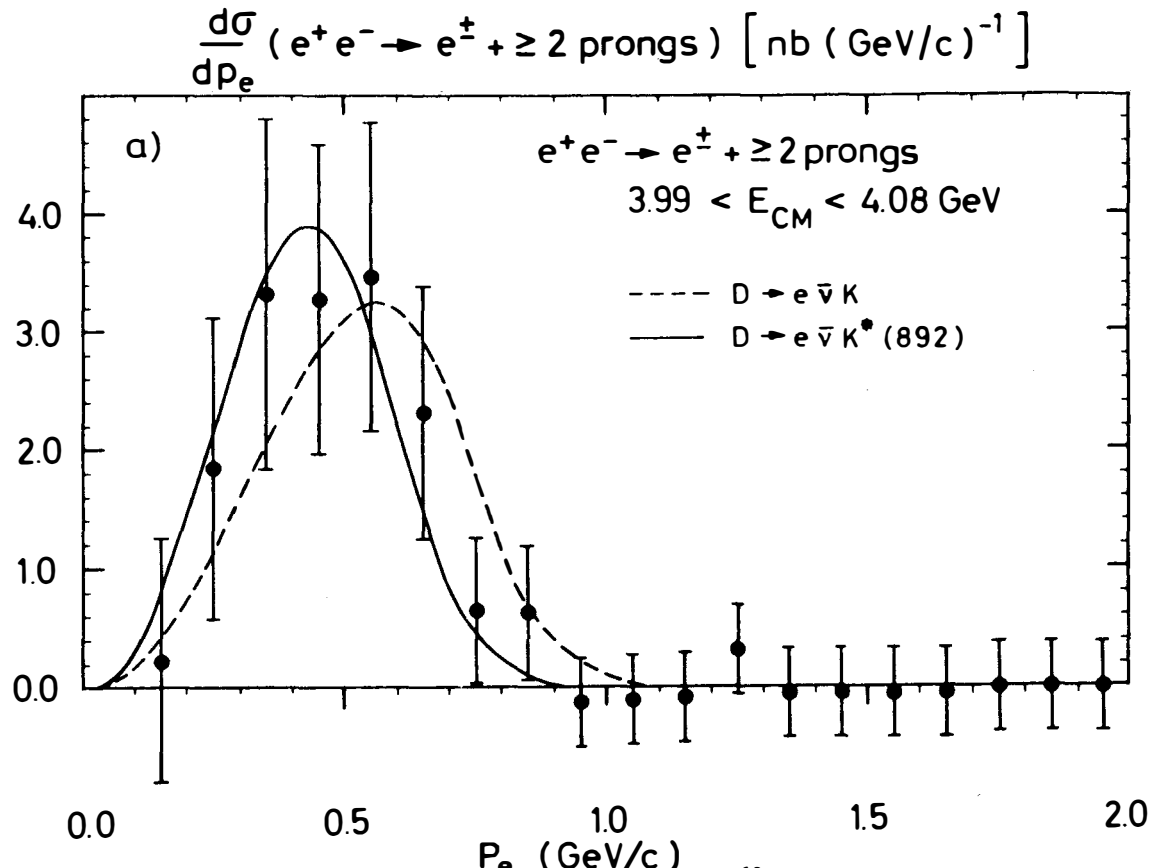

5.3 The electron momentum spectrum for $D \to e\nu X$ as measured by DASP[13]. The momentum distribution expected for $D \to e\bar{\nu}_e K$ and $D \to e\bar{\nu}_e K^*(892)$ are shown by the dashed and the solid curves.

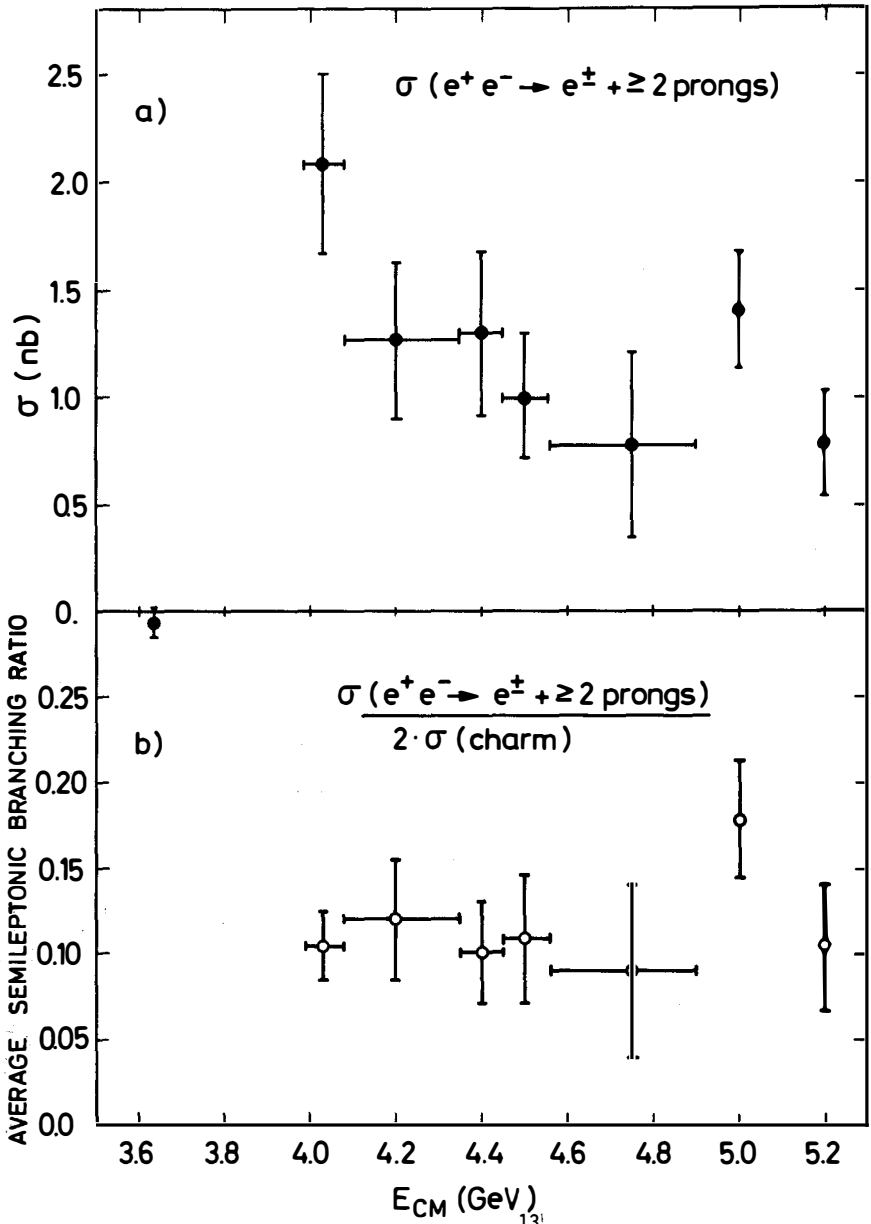

5.4 a) The cross section measured by DASP[13] for the inclusive production of electrons plus nonshowering track plus additional charged tracks as a function of cm energy.
b) The average semileptonic branching ratio for charmed hadrons as a function of energy. The error bars are statistical only.

lightest charmed hadron stable against strong and electromagnetic decays. These particles might either be produced directly or result from the cascade decay of excited charmed hadrons. The cross section $\sigma(e^+e^- \to C_i\bar{C}_j)$ was obtained by subtracting the cross sections for "old" hadron production from the total hadronic cross section.

Near threshold, where only neutral and charged D production can contribute DASP finds:

$$B(D \to e + X) = 0.08 \pm 0.02$$

This should be compared to the value

$$B(C \to e + X) = 0.072 \pm 0.02$$

obtained by avering over all energies between 3.9 GeV and 5.2 GeV (see Fig.5.4b). These values were extracted using the DASP[1] data for the total cross section and the error quoted is mainly systematic. Evaluating the branching ratio using the SPEAR data[17] on the total cross section as input led to an average semileptonic branching ratio of 0.08 ± 0.03, compared to 0.11 ± 0.03 obtained using the PLUTO[18] total cross section.

The semileptonic branching ratio can also be determined from the fraction of inclusive electron events containing a second electron. Using this method the DASP group finds $B(C \to e^-X) = 0.16 \pm 0.06$. Note that this value is independent of the charm cross section.

The semileptonic branching ratio of D's as measured by DASP is in accord with the results by LBL-SLAC[19] and the preliminary analysis of DELCO[20] (see Table 5.3).

Table 5.3 Semileptonic branching ratio of D mesons

Experiment	$B(D \to eX)$
DASP[13]	8 ± 2 %
DELCO[20]	11 ± 3 %
LBL-SLAC[19]	7.2 ± 2.8 %

The semileptonic branching ratio is larger than the value of 4 % predicted[21] from the weak decays of strange particles. This indicates that the mechanism responsible for enhancing the nonleptonic channels in strange particle decays are less effective[22] for charmed particle decays. In fact if none of the available channels are selectively enhanced one expects a semileptonic branching ratio of 0.20. This number is obtained by simple counting: the W decay can proceed in five different ways, $W \to e\nu$, $\mu\nu$ and $q\bar{q}'$ times three because of three

different colours: Assuming the same coupling strength, each channel has the probability 1 : 5 = 20 %.

One event was found by DASP with 3 electrons plus hadrons[13]. This number is consistent with the expected background leading to an upper limit of

$$(e^+e^- \to 3e + X) < 0.1 \text{ nb},$$

with 90 % confidence. Events of that type could arise from a charm changing neutral current, which allows a charmed hadron to decay into two electrons plus hadrons[23]. A neutral lepton paired with the electron in a right handed doublet would also yield events with three electrons and hadrons[22].

DASP[12] has determined the number of charged kaons emitted in electron multihadron events. This provides an independent consistency check on the nature of the weak current responsible for charm decay. If it is the GIM current then almost every electron event will have a $K\bar{K}$ pair. The measurement was done with events that had an identified charged hadron (π, K or $\bar{p}$) in the magnetic spectrometer, an electron in the inner detector and possibly other charged particles or photons. No $e\bar{p}X$ events were seen. From the observed K to π ratio and the measured charged multiplicity it was found that each multiprong event contained on the average 0.90 ± 0.18 charged kaons per event in agreement with the GIM prediction.

6. τ production

Measurements on lepton events of the type

$$e^+e^- \to e\mu + \text{nothing} \qquad (6.1)$$

and $e^+e^- \to e(\mu)$ + nonshowering charged particle + any number of photons (6.2)

provided convincing evidence that besides charmed particles a new type of weakly decaying particle, τ, is being produced above 4 GeV [24]. Conclusive proof for its existence was recently given by the DASP collaboration who observed τ production below charm threshold at the ψ'.

6.1 τ production below charm threshold

τ production at the ψ' was studied with electron twoprong events (6.2). The selection criteria for this sample were discussed in the previous section. A total of 17 events were found at the ψ' and 1 event at a cm energy of 3.6 GeV.

The electron momentum spectrum measured at the ψ' and plotted in Fig. 6.1 shows two clear clusters of events, one centered around 1.5 GeV/c and

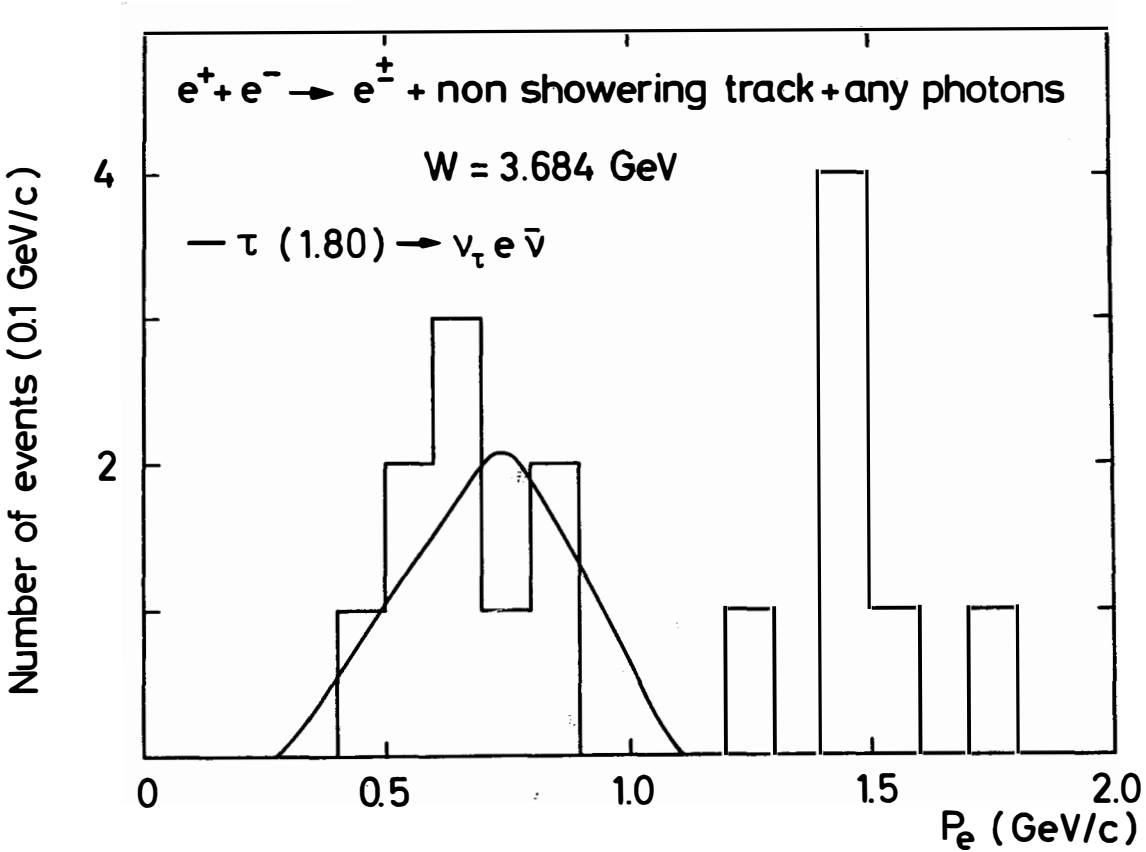

6.1 Raw electron momentum distributions observed by DASP[14] at 3.684 GeV. The events here are identified as electron, one nonshowering particle and any number of photons.

the other with momenta between 0.4 GeV/c and 0.9 GeV/c. The first cluster can be associated with the cascade decay $\psi' \to J/\psi\ X \to e^+e^-X$.

The electrons in the second cluster have a relatively flat momentum distribution. The background from the reaction $e^+e^- \to e^+e^-\mu^+\mu^-$ has been estimated to contribute (0.6 ± 0.2) events. An estimate using data at other energies shows that we expect less than 0.1 event from beam-gas interactions. Indeed, all the events originate within the nominal interaction volume. A twobody hadron final state can fake events of type (1) if the charged hadron traversing the magnet is misidentified as an electron. For hadrons with momenta above 0.35 GeV/c the measured probability P_{he} for this to happen is 4×10^{-4}. At the ψ' resonance 2113 events were observed of the type $e^+e^- \to h^\pm$ + nonshowering track + $\geq$ 0 photons where h is either a kaon or a pion traversing the magnet and the nonshowering track is observed in the inner or outer detector. This class of events therefore contributes a background of (0.84 ± 0.02) events. Dalitz decays of π^0 and η and photons converting in the beam pipe were estimated using the two prong sample above. A total of (0.2 ± 0.1) events were estimated compared to 9 events observed. The computation of background associated with multihadron events was checked by searching for inclusive electron events at the J/ψ resonance. One event of the type $e^+e^- \to e^\pm$ + nonshowering track + $\geq$ 0 photon was found which is to be compared with an estimated background of 1.3 events.

Further evidence that the electron events observed at the ψ' are not true hadron events comes from an inspection of the photon multiplicity. Table 6.1 shows a comparison of the photon multiplicities for twoprong electrons (0.4 GeV/c < p_e < 0.9 GeV/c) and twoprong hadron events (p_h > 0.4 GeV/c) from ψ' decay.

Table 6.1 Photon multiplicity distributions

Number of photons	0	1	2	3	4	5	6	7
$e^\pm$ + nonshowering track at the ψ'(0.4 < p_e < 0.9 GeV/c)	4	3	1	1	0	0	0	0
$h^\pm$ + nonshowering track at the ψ'(p_h > 0.4 GeV/c)	207	370	440	428	312	199	99	32
$e^\pm$ + nonshowering track $\sqrt{s}$: 4-5.2 GeV (p_e > 0.2 GeV/c)	49	17	10	1	2	0	1	0

The distributions are strikingly different. The electron events are accompanied by a few events as expected for τ decay whereas the hadron events have a large multiplicity.

We conclude therefore that an anomalous electron signal is observed at a cm energy of 3.684 GeV which is below charm threshold. This signal is then assumed to come from $\tau\bar{\tau}$ production. The electron spectrum predicted for a τ of mass 1.80 GeV and a zero mass neutrino fits the data well (see curve in Fig. 6.1).

6.2 τ production above 4 GeV

We turn now to the electron twoprong data at higher energies. A total of 80 events were found at cm energies between 4.0 and 5.2 GeV. A fraction of the twoprong electron events observed above 3.9 GeV might result from associated production and semileptonic decays of charmed particles. An upper limit can be obtained by assuming that all inclusive electron events with more than two prongs are due to charm production. From the measured multiplicity distribution of these events (Fig. 5.1) and the known detection efficiency a total of (5 ± 2) events has been estimated from this source. The direct decay of a pair of charmed hadrons into a final state with one electron and one non-showering track is expected to contribute less than one event. The background from all other sources has been estimated to (9 ± 3) events, in agreement with (7 ± 7) events extrapolated from the 3.6 GeV data.

6.2.1 τ mass and spin

The quantity $2\sigma_{\tau\bar{\tau}}\, B_e \cdot B_{ns}$ is plotted in Fig. 6.2 as a function of cm energy. Radiative corrections were applied and the data were corrected for the enhancement at the ψ' due to vacuum polarization. Note the rapid rise near threshold which is characteristic for s-wave production. The data shown in Fig. 6.2 were used to determine the mass of the τ and its spin[14]. The cross section for $\tau\bar{\tau}$ production for a τ spin of 0, 1/2 and 1 reads as follows:

spin 0:

$$\sigma_{\tau\bar{\tau}} = 1/4\ \sigma_{\mu\mu}\ \beta_\tau^3\ |F|^2\ B_e \cdot B_{ns} \qquad (6.3)$$

where $\sigma_{\mu\mu} = \frac{4\pi\alpha}{3s}$ and F is the τ formfactor.

spin 1/2:

$$\sigma_{\tau\bar{\tau}} = \sigma_{\mu\mu}\ \beta_\tau \left\{1 + 1/2\ (1-\beta_\tau^2)\right\}\ B_e \cdot B_{ns} \qquad (6.4)$$

The τ is assumed to be pointlike.

Spin 1 :

$$\sigma_{\tau\bar{\tau}} = \sigma_{\mu\mu}\ \beta_\tau \left\{\left(\frac{s}{4M_\tau^2}\right)^2 + 5\ \frac{s}{4M_\tau^2} + 3/4\right\} \cdot B_e \cdot B_{ns} \qquad (6.5)$$

The τ is assumed to have the same electromagnetic properties as the W boson[25].

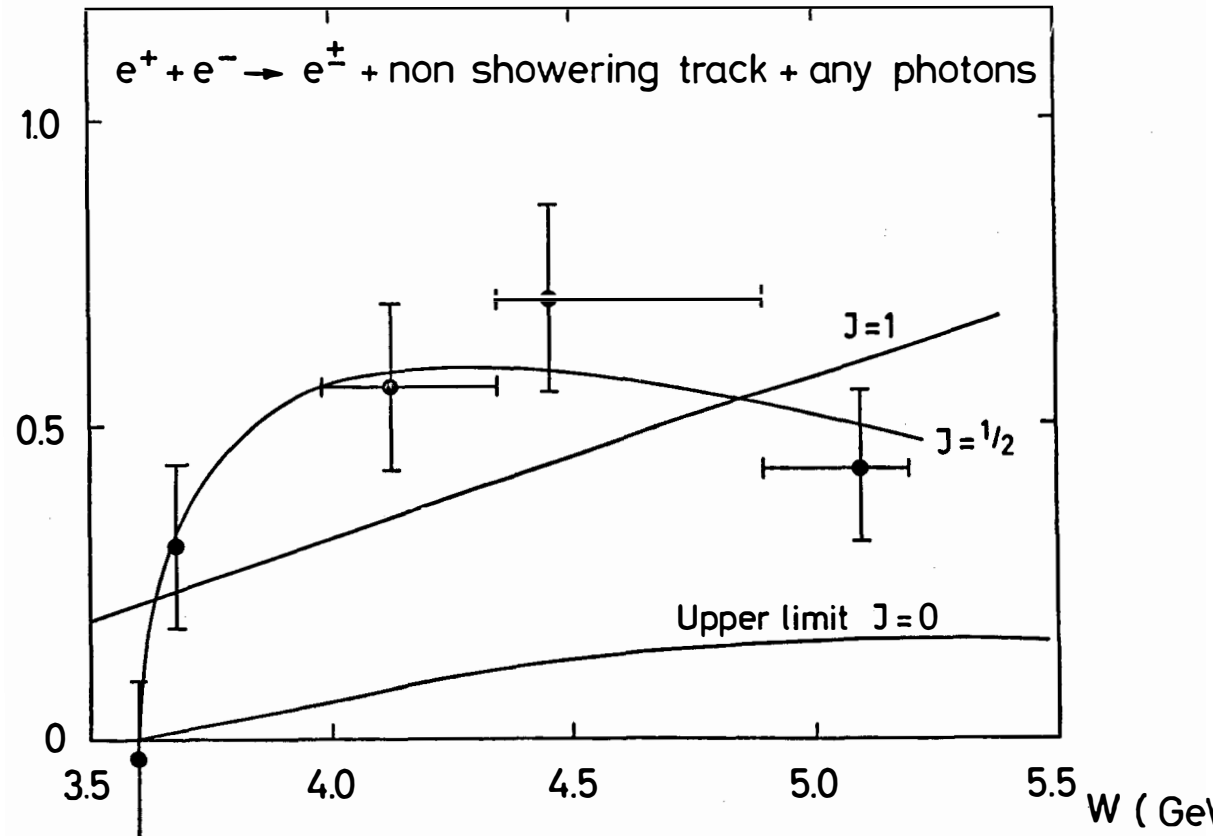

6.2 Integrated inclusive cross section for events having an identified electron, a nonshowering particle, and any number of photons as a function of cm energy. The data are from DASP[14]. The solid curves show fits to the data assuming pairproduction of point particles with spin 0, 1/2 and 1.

For spin 0 the upper limit on $2\sigma_{\tau\tau} B_e B_{ns}$ was calculated with F = 1 and the conservative assumption that the τ has only leptonic decays and $B_e = B_\mu$. This upper limit is plotted in Fig. 6.2 und is seen to be lower than the data by an order of magnitude. For spin 1/2 and 1 a fit was made treating the τ mass and the products of the branching ratios $B_e \cdot B_{ns}$ as free parameters. The spin 1 curve (see Fig. 6.2) does not describe the data; including the data obtained at higher energies at SPEAR excludes spin 1. The data are well described by a pointlike fermion of spin 1/2. The fit yielded for the τ mass

$$m_\tau = 1.807 \pm 0.02 \text{ GeV}.$$

6.2.2 The lepton momentum spectrum

Besides electron inclusive events the DASP group studied also μ inclusive events[14]. Candidates for muon inclusive events had to have one muon track in the spectrometer, a second nonshowering track and any number of photons observed either in the inner detector or in the spectrometer arms. A charged particle was called a muon if it had a momentum greater than 1.0 GeV/c, gave no signal in the threshold Cerenkov counter, suffered an energy loss consistent with that of a minimum ionizing particle in the shower counter and penetrated at least 60 cm of iron. A total of 25 events with a background of 3.8 events was found.

After all corrections (21 ± 5) muon inclusive events and (18.5 ± 4.6) electron inclusive events were observed with momenta above 1.0 GeV/c. The ratio of the leptonic widths evaluated directly from these data are independent of the form of the coupling. This yields $B_\mu/B_e = 0.92 \pm 0.32$ with a systematic uncertainty of 0.07. The result is consistent with $e\mu$ universality.

The lepton momentum spectrum, obtained by combining the electron and the muon data, is plotted in Fig. 6.3 for cm energies between 4.0 GeV and 5.2 GeV. This spectrum extends to much higher momenta than the electron spectrum observed in the semileptonic decays of the charmed hadrons, reflecting the pointlike structure of the τ and the low mass of its neutrino.

The solid line shows a fit to the data assuming $m_\tau = 1.80$ GeV, a massless neutrino and a (V-A) structure of the current. The dotted line is a fit keeping the masses constant but changing the left handed V-A current into a right handed V+A current. Both fits are clearly acceptable.

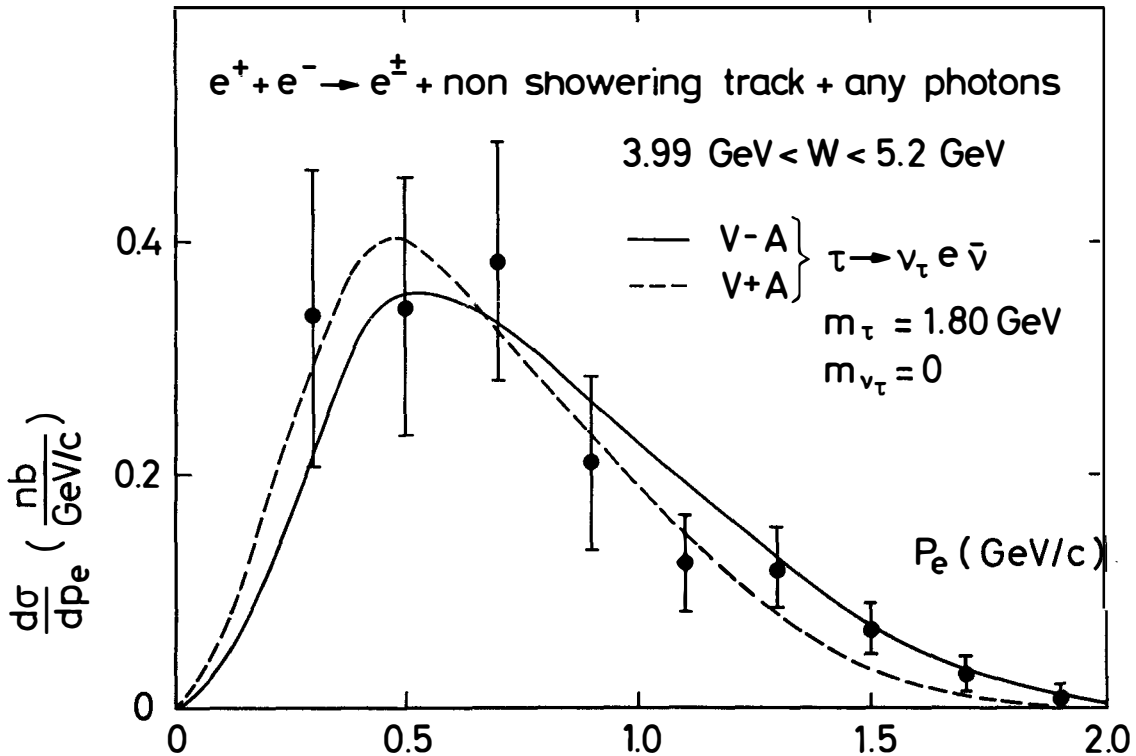

6.3 Corrected electron momentum distribution measured by DASP[14] for events having an identified electron, a nonshowering particle, and any number of photons. (Above 1 GeV/c data having a muon instead of an electron are combined with the electron data to form a weighted mean.)

6.3 Leptonic and topological τ decay branching ratios

The DASP group measured[14] $e^+e^- \to e\mu$ + missing energy in the cm range of 0.4 GeV to 5.2 GeV. Muons of momenta greater than 0.7 GeV/c were identified in the outer detector ($P_{h\mu} = 4.2 \pm 0.8$ %) by range, electrons with momenta above 0.2 GeV/c either in the inner detector ($P_{he} = 2 \pm 0.9$ %) or the outer ($P_{he} = 4 \times 10^{-4}$). A total of 13 $e\mu$ events with an estimated background of 1.2 ± 0.4 events were found. Using the known production cross section and assuming $e\mu$ universality yield:

$B_e = B_\mu = 0.182 \pm 0.028 \pm 0.014$ for a V-A current and

$B_e = B_\mu = 0.206 \pm 0.033 \pm 0.015$ for a V+A current. The first error is the statistical one.

The fit used to evaluate the τ mass from the electron inclusive events yields $B_e \cdot B_{ns} = 0.086 \pm 0.012$. Using $B_e = 0.182 \pm 0.028$ the DASP group derived the branching ratio for $\tau \to \nu_\tau$ + nonshowering particle + ≥ 0 photons, $B_{ns} = 0.47 \pm 0.10$. The branching ratio B_{1h} for $\tau \to \nu_\tau$ + hadron + ≥ 0 photons is given by $B_{1h} = B_{ns} - B = (0.29 \pm 0.11)$. The systematic errors are small compared to the statistical error. The average number of photons associated with $\tau \to \nu_\tau$ + hadron + ≥ 0 photons can be obtained from table 6.1 after making background corrections. Averaging the observed photon multiplicity over all two prong events in the higher energy data and correcting for the photon detection efficiency the decay of the type $\tau \to \nu_\tau$ + charged hadron + any number of photons was found to yield on the average 2.8 ± 0.7 photons.

The branching ratio B_{3h} for the τ to decay into final states with at least three charged particles can be obtained from $B_{3h} = 1 - B_e - B_{ns}$. (The number of electron events with $p_e > 1$ GeV/c and 5 or more charged tracks were found to be small.) The result is $B_{3h} = 0.35 \pm 0.11$ in agreement with the Pluto[26] measurement, B(≥ 3 prong) = 0.30 ± 0.10.

Fits were also made varying the mass of the τ neutrino. The 90 % confidence upper limits on the neutrino mass are $m_{\nu_\tau} < 0.74$ GeV for V-A and $m_{\nu_\tau} < 0.54$ GeV for V+A.

6.4 Semihadronic decays of the τ

A characteristic feature of the standard weak interaction is that decays involving strange particles are suppressed relativ to decays involving nonstrange final states by $tg^2\theta_c \approx 0.05$. The DASP group determined[12] the ratio of strange to nonstrange particles in semihadronic τ-decays from a measurement of

$$\frac{\sigma(e^+e^- \to e^{\mp} + K^{\pm} + \geq 0 \text{ photons})}{\sigma(e^+e^- \pm e^{\mp} + \pi^{\pm} + \geq 0 \text{ photons})}$$

It was shown that the two prong cross section including one electron predominately results from $e^+e^- \to \tau\bar{\tau} \to (\nu_\tau e\bar{\nu}_e)(\nu_\tau + \text{hadrons} + \geq 0 \text{ photons})$ with only a small contamination from charm decays. The hadrons were identified and measured using one of the spectrometer arms. The electron was identified in either the inner or the outer detector.

The results was

$$\frac{\sigma(e^{\mp} + K^{\pm} + \geq 0 \text{ photons})}{\sigma(e^{\mp} + \pi^{\pm} + \geq 0 \text{ photons})} = 0.07 \pm 0.06$$

Therefore on the average only 7 % of all semihadronic τ-decays yield a strange particle in accordance with theory. This should be compared to multiprong events where DASP found[12]:

$$\frac{\sigma(e^{\mp} + K^{\pm} + \geq 1 \text{ prong} + \geq 0 \text{ photons})}{\sigma(e^{\mp} + \pi^{\pm} + \geq 1 \text{ prong} + \geq 0 \text{ photons})} = 0.24 \pm 0.05.$$

Since the charged multiplicity is on the order of 4 this is equivalent to (0.9 ± 0.18) charged kaons per multiprong event. (See discussion in section 5.)

6.4.1 $\tau \to \pi\nu$

We have searched[27] for the $\tau \to \pi\nu$ decay by studying the process

$$e^+e^- \to \tau\bar{\tau} \to (e\nu\nu)(\pi\nu)$$

leading to the final state $e\pi^{\pm}\,0\gamma$. In order to reduce background from charm production only cm energies W > 4.48 GeV were considered. The electron was detected in the inner detector or in the magnetic spectrometer, the $\pi^{\pm}$ was identified in the magnetic spectrometer. To enhance the $\tau \to \pi\nu$ signal only $\pi^{\pm}$ with momenta above 1.1 GeV/c were considered. Two events satisfying these selection criteria were observed.

From $\tau\bar{\tau}$ production 6.7 events were expected plus 1 event from background (e.g. $\tau \to \rho\nu$ where the π^0 from τ decay escaped detection). The difference between expected and observed number of events corresponds to a 2 s.d. effect. The observed number of events lead to

$$B_e \cdot B_\pi = 0.004 \,{}^{+\,0.005}_{-\,0.004}$$

or

$$B_\pi = 0.02 \,{}^{+\,0.03}_{-\,0.02}$$

which can be compared to the theoretical value of $B_\pi = 0.10$. The data from SLAC-LBL presented at this meeting[28] suggest, however, that the $\pi\nu$ decay exists with the expected strength.

The DASP group has also searched for events of the type

$$e^+e^- \to \tau\bar{\tau} \to \{(K\nu)\ (e\nu\nu) + (\mu\nu\nu) + (\pi\nu)\}$$

$$= K^\pm + \text{charged track} + \text{missing energy}.$$

Only one event with $p_K > 1.0$ GeV/c was found[27]. This yields a 90 % confidence upper limit of $B_K < 0.016$.

6.4.2 $\tau \to \rho\nu$

DASP measured[27] the decay $\tau \to \rho\nu_\tau$ by selecting final states with $\pi^\pm$ + charged track + two photons. Events in which the two photons are compatible with resulting from a π^0 decay are retained provided that both computed photon energies are above 50 MeV. The remaining events are plotted versus $M(\pi^\pm\pi^0)$ in Fig. 6.4a. Events with an identified electron are hatched. Events within the ρ-band (0.5 GeV < $M(\pi^\pm\pi^0)$ < 1.0 GeV) are plotted versus the momenta of the $\pi^\pm\pi^0$-system in Fig. 6.5. The momentum distribution expected from the decay $\tau \to \rho\nu_\tau$ is shown as the dotted line. Note the flat distribution above 0.9 GeV/c which is characteristic for a two body decay of a moving object. The enhancement at low momenta is presumably due to multihadron events. To reduce the background, only events with a $(\pi^\pm\pi^0)$-momentum above 1.0 GeV/c are considered. The $\pi^\pm\pi^0$ mass distribution for these events are plotted in Fig. 6.4b. These events yield as a preliminary value

$$B_\rho = 0.24 \pm 0.09$$

in good agreement with the theoretical prediction, $B_\rho = 0.22$.[29]

6.5 Summary of the τ properties

Table 6.2 summarizes the information on mass, leptonic and semi-hadronic decay modes of the τ from this and other experiments.

The observation of the τ at the ψ' below charm threshold conclusively demonstrates that the τ signal has nothing to do with charm. The shape and magnitude of the $\tau\bar{\tau}$ production cross section exclude spin 0 and 1 for the τ: they strongly favor the assignment as a pointlike, spin 1/2 fermion. The best value for the τ mass at present is 1.807 ± 0.02 GeV. The analysis of the decay spectra puts a limit of 0.54 GeV on the mass of the τ neutrino. The lifetime of the τ is less than $3.5 \cdot 10^{-12}$ sec.

The lepton momentum spectra can be described by a V-A as well as a V+A coupling of the weak current to the $\tau\bar{\nu}_\tau$ system although the first possibility is

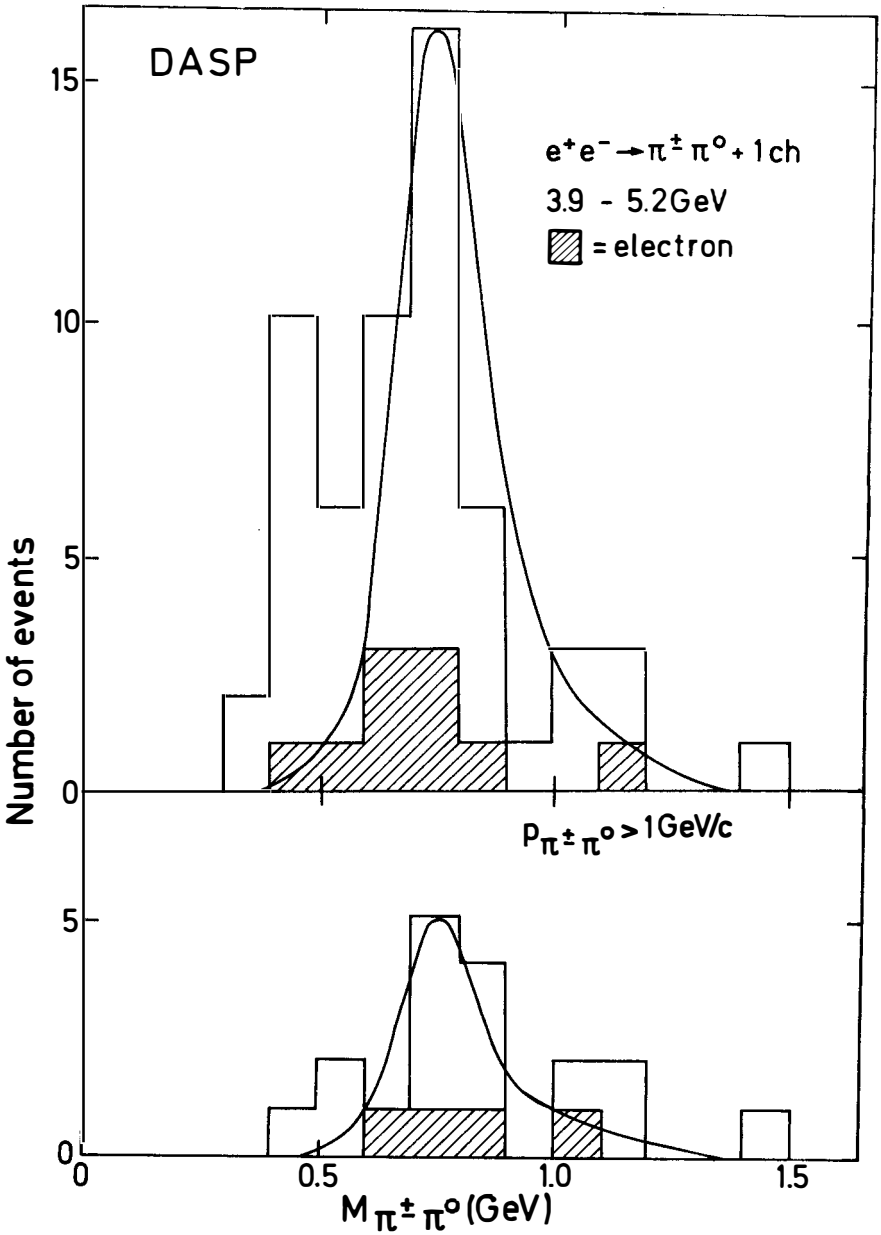

6.4 a) The distribution of $M(\pi^\pm\pi^o)$ observed by DASP[27] for events with the topology $e^+e^- \rightarrow \pi^\pm\pi^o$ + charged track.
b) The $M(\pi^\pm\pi^o)$ distribution for events of the same topology as above but with $p_{\pi^\pm\pi^o} > 1$ GeV/c.

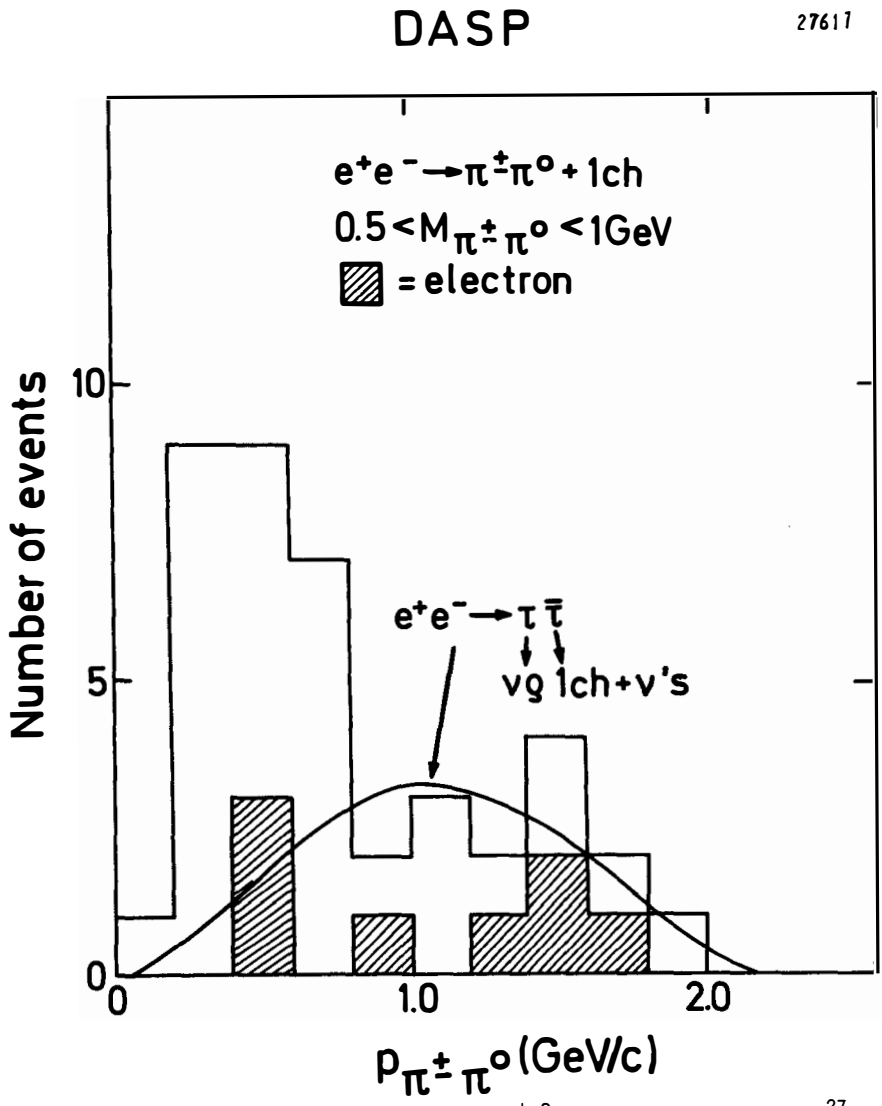

6.5 The momentum distribution of the $(\pi^{\pm}\pi^{0})$ system observed by DASP[27] in $e^{+}e^{-} \rightarrow \pi^{\pm}\pi^{0}T$. The mass of the $\pi^{\pm}\pi^{0}$ system was between 0.5 GeV and 1.0 GeV.

Table 6.5 Properties of the

	experimental results	predicted by theory	experiment	comments
mass (GeV)	1.807 ± 0.020		DASP[14]	
Spin	1/2			
lifetime (sec)	$<3.5\cdot10^{-12}$	$2.8\cdot10^{-13}$	PLUTO[30]	
m_{ν_τ} (GeV)	<0.54		SLAC-LBL[31], PLUTO[30]	
$\tau\nu_\tau$ coupling to weak current	V-A favored		SLAC-LBL[31], PLUTO[26]	
B_μ / B_e	0.92 ± 0.32	1 (seq.lept.)	DASP[14]	
B_e	0.186 ± 0.010 ± 0.028	0.18	SLAC-LBL[32]	from $e\mu$; assume B_e = B and V-A
	0.16 ± 0.06		PLUTO[30]	from $e\mu,\mu X$; assume V-A
	0.224 ± 0.032 ± 0.044		LBL-SLAC[33]	from $e\mu$; assume B_e = B
	0.182 ± 0.028 ± 0.014		DASP[14]	from $e\mu$; assume B_e - B and V-A
	0.15		DELCO[20]	from eX; preliminary
B_μ	0.175 ± 0.072 ± 0.030	0.18	SLAC-LBL	from μX; assume B_{18} = 0.85 and V-A
	0.14 ± 0.034		PLUTO[26]	from μX; assume V-A
	$0.22\ ^{+\ 0.07}_{-\ 0.08}$		Iron ball[35]	from $\mu\mu$
	0.20 ± 0.10		Maryland-Princeton -Pavia	from μX
$B(\tau \to e\gamma)$	<0.026		LBL-SLAC[31]	
$B(\tau \to \mu\gamma)$	<0.013		LBL-SLAC[31]	
B(τ → 3 charged leptons)	<0.006		SLAC-LBL[31]	
	<0.01		PLUTO[36]	

Table 6.5 continued

	experimental results	predicted by theory	experiment	comments
$B(\tau \to 1$ charged + any photons)	0.70 ± 0.10		PLUTO[26]	
	0.90 ± 0.10		LBL-SLAC[33]	
	0.65 ± 0.12		DASP[14]	
$B(\tau \to 1$ charged hadron + any photons)	0.40 ± 0.15		PLUTO[26]	
	0.45 ± 0.19		LBL-SLAC[33]	
	0.29 ± 0.11		DASP[14]	
$B(\tau \to 3$ charged hadrons + any photons)	0.35 ± 0.11		DASP[14]	
$B(\tau \to \pi\nu)$	0.02 ± 0.03	0.10	DASP[27]	
$B(\tau \to k\nu)$	<0.016	0.005	DASP[12]	
$B(\tau \to \rho\nu)$	0.24 ± 0.09	0.22	DASP[27]	
$B(\tau \to \rho^0\pi^\pm\nu)$	0.050 ± 0.015	~0.1	PLUTO[30]	$\rho\pi$ sepctrum consistent with A_1 decay. Including neutral decay modes would give $B(\tau \to A_1\nu) = 0.10 \pm 0.03$

slightly favored by the data. The measured leptonic decay rates are consistent with e/μ universality. The leptonic and semihadronic branching ratios agree with those expected from theory for a heavy lepton of mass 1.8 GeV, except perhaps for the decay $\tau \to \pi\nu$ which needs further study.

The consistency with e/μ universality classifies the τ as either a ortholepton or a sequential lepton. In the first case the τ has the same lepton number as e or μ. In the second case the τ carries a new lepton number. Recent neutrino experiments rule out that the τ is μ-like[37] and strongly indicate that it is not e-like[38] either. The τ is therefore most probably a sequential heavy lepton with a new lepton quantum number and with its own neutrino.

ACKNOWLEDGEMENTS

I want to thank Profs. Tran Thanh Van and M. Davier for the invitation to give these lectures. In preparing them I have profitted from a close collaboration with Björn Wiik.

References:

The following shorthand notations shall be used: 1971 Cornell Conference for the Proceedings of the 1971 Symposium on Electron and Photon Interactions at High Energies, Cornell, ed. by N. Mistry.

1975 Stanford Conference for the Proceedings of the 1975 Symposium on Lepton and Photon Interactions at High Energies, Stanford, ed. by W.T. Kirk.

1976 Tbilisi Conference for the XVIIIth International Conference on High Energy Physics, Tbilisi, USSR (1976).

1977 Hamburg Conference for the Proceedings of the 1+77 International Symposium on Lepton and Photon Interactions at High Energies, Hamburgs, ed. by F. Gutbrod.

1) G. Grindhammer, Lecture given at this meeting.

2) The DASP results were summarized bv S. Yamada, 1977 Hamburg Conference, p.69.

3) R.F. Schwitters, rapporteur talk, 1975 Stanford Conference, p.5;
G. Hanson, rapporteur talk, 1976 Tbilisi Conference, and SLAC-PUB-1814 (1976).

4) DASP Collaboration, R. Brandelik et al., Phys. Lett. 67B (1977) 358 and paper to be published.

5) See e.g. S.D. Drell, D. Levy and T.M. Yan, Phys. Rev. 187 (1969) 2159;
ibid D1 (1970) 1035, 1616, 2402;
see also B.H. Wiik and G. Wolf, Electron-Positron Interactions in Les Houches, Session XXIX, 1976,
Interaction électromagnétiques et faibles à haute énergie/ Weak and electromagnetic interactions at high energy, ed. by R. Balian and C.H. Llewellyn Smith, Course 5, p. 407,

6) DASP Collaboration, W. Braunschweig et al., Phys. Lett. 63B (1976) 115.

7) R. Gatto, P. Menotti and I. Vendramin, Lettre Nuovo Cimento 5 (1972) 754;
R. Gatto and G. Preparata, Nucl. Phys. B47 (1972) 313.

8) V.N. Gribov and L.N. Lipatov, Yadernaya Fisika 15 (1972) 1218.

9) G. Hanson et al., Phys. Rev. Lett. 35 (1975) 609.

10) D. Fakirov and B. Stech, Heidelberg preprint HD-THEP-77-8 (1977) and Nucl. Phys.
H. Fritzsch, Phys. Lett. 71B (1977) 429.

11) DASP Collaboration, R. Brandelik et al., Phys. Lett. 70B (1977) 132 and
G. Mikenberg, Proceedings of the Triangle Seminar, 1977.

12) DASP Collaboration, R. Brandelik et al., Phys. Lett. 70B (1977) 125.

13) DASP Collaboration, R. Brandelik et al., Phys. Lett. 70B (1977) 387.

14) DASP Collaboration, R. Brandelik et al., Phys. Lett. 73B (1978) 109.

15) see e.g. B.H. Wiik, rapporteur talk, 1976 Tbilisi Conference.

16) a) I. Hinchliffe and C.H. Llewellyn Smith, Nucl. Phys. B114 (1976) 45
b) A. Ali and T.C. Yang, Phys. Lett. 65B (1976) 275
c) F. Bletzacker, H.T. Nieh and A. Soni, Phys. Rev. D16 (1977) 732
d) R. Nabari, X.Y. Pham and W. Cottingham, J. Phys. G: Nuclear Physics 3 (1971) 1485
e) G.L. Kane, Phys. Lett. 70B (1977) 272
f) X.Y. Pham and J.M. Richard, Preprint PARIS/LPTHE 77.20.

17) A.M. Boyarski et al., Phys. Rev. Lett. 34 (1975) 764;
R.F. Schwitters, 1975 Stanford Conference, p.5.

18) J. Burmester et al., Phys. Lett. 66B (1977) 395; and
G. Knies, rapporteur talk, 1977 Hamburg Conference, p. 93.

19) J.M. Feller et al., Phys. Rev. Lett. 40 (1978) 274 and
A. Barbaro-Galtieri, rapporteur talk, 1977 Hamburg Conference, p. 21.

20) DELCO Collaboration, J. Kirkby, rapporteur talk, 1977 Hamburg Conference, p.3.

21) M.K. Gaillard, B.W. Lee and J.L. Rosner, Rev. Mod. Phys. 47 (1975) 277.

22) J. Ellis, M.K. Gaillard and D.V. Nanopoulos, Nucl. Phys. B100 (1975) 313.

23) P. Fayet, Nucl. Phys. B78 (1974) 14;
T.D. Cheng and L.F. Li, Phys. Rev. Lett. 38 (1977) 381.

24) see e.g.M.L. Perl, review talk, 1977 Hamburg Conference, p. 145.

25) W. Alles, Ch. Boyer and A.J. Buras, CERN-TH 220 (1977).

26) PLUTO Collaboration, J. Burmester et al., Phys. Lett. 68B (1977) 297.

27) see S. Yamada, rapporteur talk, 1977 Hamburg Conference, p. 69.

28) G. Hanson and M.L. Perl, data of the SLAC-LBL Collaboration presented at this meeting.

29) H.B. Thacker and J.J. Sakurai, Phys. Lett. 36B (1971) 103;
Y.S. Tsai, Phys. Rev. D4 (1971) 2821;
J.D. Bjorken and C.H. Llewellyn Smith, Phys. Rev. D7 (1973) 887;
K. Fujikawa and N. Kawamoto, Phys. Rev. D14 (1976) 59;

Y.I. Azimov, L.L. Frankfurt and V.A. Khoze, Leningrad Nuclear Physics Institute, Preprint 245, June 1976;
N. Kawamoto and A.I. Sanda, DESY 78/14;
Similar results are reported also by:
F.J. Gilman and D.H. Miller, SLAC-PUB-2046, 1977 and
Y.S. Tsai, private communication.

30) PLUTO Collaboration, G. Alexander et al., Phys. Lett. 73B (1978) 99 and G. Knies, rapporteur talk, 1977 Hamburg Conference, p. 93.

31) M.L. Perl, rapporteur talk, 1977 Hamburg Conference, p. 145.

32) M.L. Perl et al., Phys. Lett. 70B (1977) 487;
M.L. Perl et al., Phys. Lett. 63B (1976) 466.

33) A. Barbaro-Galtieri, Phys. Rev. Lett. 39 (1977) 1058).

34) G.J. Feldman et al., Phys. Rev. Lett. 38 (1977) 117.

35) Contribution to the Hamburg Conference
see H. Sadrozinski, rapporteur talk, 1977 Hamburg Conference, p. 47.

36) See the recent review talks by
M.L. Perl, Proceedings of the XII Rencontre de Moriond, Flaine, 1977, to be published, and SLAC-PUB-1923;
and 1977 Hamburg Conference, p. 145;
G. Flügge, Invited talk at the Vth International Conference on Experimental Meson Spectroscopy, Northeastern University, Boston, MA, 1977, DESY-Report 77/35 (1975.

37) see e.g. K. Kleinknecht, rapporteur talk, 1977 Hanburg Conference, p. 271.

38) R. Palmer, results reported at this meeting.

Recent Results of the PLUTO-Collaboration

Jochen Bürger

Siegen University, Department of Physics
D 5900 Siegen 21, Fed.Rep. of Germany
and
Deutsches Elektronen Synchrotron DESY
D 2000 Hamburg 52, Fed.Rep. of Germany

Abstract: New results obtained in e^+e^--annihilation are presented, concerning the total hadronic cross section, the ρ-inclusive production, the radiative decay $J/\psi \to f^0\gamma$ and properties of the heavy lepton τ.

Résumé: On a présenté des nouveaux résultats qui ont été obtenus dans l'annihilation e^+e^- et qui concernent la section efficace hadronique, la production inclusive des mesons ρ, la désintégration radiative $J/\psi \to f^0\gamma$ et des propriétés du lepton lourd τ.

1. Introduction

The results of the PLUTO-collaboration* presented in this talk are based on data taken in the runperiod of 1976. In 1977 the PLUTO detector was upgraded with several new components. In the same year the DORIS-storage ring has also been upgraded to higher energies.

Thus the set of data discussed in the following is the same as described in the talk of V.Blobel held at the XII. Rencontre de Morion[1] one year ago, where he gave details on the energies we run and the integrated luminosities.

My talk is organized as follows:
In chapter 2 I shall give a brief description of the PLUTO detector, chapters 3 to 5 are dealing with the total hadronic cross section, with the ρ-inclusive production and with the radiative decay $J/\psi \to f^0\gamma$, which may be compared with theoretical predictions especially from quantumchromodynamics (QCD), chapter 6 discusses new results on the heavy lepton τ. In a concluding chapter 7 a short review on the present and future programs of the PLUTO detector is given.

---

*at present the PLUTO-Collaboration consists of the following physicists:

Ch.Berger, W.Lackas, F.Raupach, W.Wagner, I.Physikalisches Institut der RWTH Aachen;

G.Alexander[1], L.Criegee, H.C.Dehne, K.Derikum, R.Devenish, G.Flügge, G.Franke, Ch.Gerke, E.Hackmack, P.Harms, G.Horlitz, Th.Kahl[2], G.Knies, E.Lehmann, B.Neumann, R.L.Thompson[3], U.Timm, P.Waloschek, G.G.Winter, S.Wolff, W.Zimmermann, Deutsches Elektronen-Synchrotron DESY, Hamburg;

O.Achterberg, V.Blobel, L.Boesten, H.Daumann, A.F.Garfinkel[4], H.Kapitza, B.Koppitz, W.Lührsen, R.Maschuw, H.Spitzer, R.van Staa, G.Wetjen, II. Institut für Experimentalphysik der Universität Hamburg;

A.Bäcker, J.Bürger, C.Grupen, H.J.Meyer, G.Zech, Siegen University;

H.J.Daum, H.Meyer, O.Meyer, M.Rössler, K.Wacker, Wuppertal University.

([1]On leave from Tel-Aviv University, Israel; [2]Now at Max-Planck-Institut für Physik und Astrophysik, München; [3]On leave from Humboldt University, Arcata, California, USA; [4]On leave from Purdue University, W.Lafayette In.,USA.)

2. Brief Description of the Detector

PLUTO is a magnetic 4π detector at the DORIS e^+e^- storage ring at DESY in Hamburg. The details of this detector are described in several publications[2,3], thus I shall only mention the most important features of this apparatus.

A schematic view of the PLUTO detector as used in 1976 is given in fig.1. The detector consists of a superconducting solenoid providing a magnetic field of 2 Tesla in its inner volume (1.4 m diameter and 1.1 m length), which is filled with 14 cylindrical proportional wire chambers and two cylindrical lead converters all concentric to the beam. Thus track recognition and momentum measurement for charged tracks is possible. The flux return yoke which is used simultanously as hadron absorber, is covered with a muon detector consisting of plane proportional tube chambers. On the average a particle coming from the interaction point has to penetrate 68 cm of iron equivalent to reach the muon chambers.

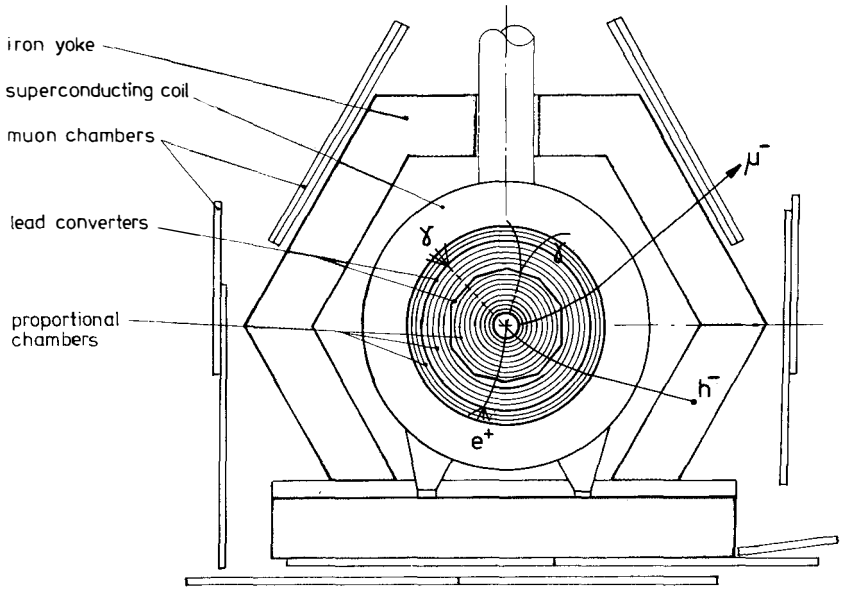

Fig.1 Schematic view of the PLUTO detector (1976) with typical particle signatures (view along the beamline)

The geometrical acceptances of the different detector components are listed in the table below.

Table 1. Solid angle coverage of detector components

Detector component	Solid angle in % of 4π
Proportional wire chambers	
- purely geometric	92
- with trigger	87
Inner lead converter (r = 37.5 cm) (0.44 radiation lengths thick)	78
Outer lead converter (r = 59.5 cm) (1.71 radiation lengths thick)	60
Muon chambers	51
- with $\|\cos\theta\| < .55$	45

Particle identification is possible to a certain extent with this apparatus, the signatures of particles used in the context of this talk are the following:

Electrons are charged tracks giving showers behind one of the two lead converters.

Muons are non showering charged tracks which can be extrapolated from the inner detector to a muon chamber having a set wire within a certain region around the extrapolated track. Charged hadrons (mostly assumed to be pions) are all charged tracks coming from the interaction point not showering behind both lead converters. A special class of these hadrons are the "identified" ones, having sufficient energy to penetrate the iron if they were muons, and pointing towards a muon chamber which has no set wire within the appropriate region around the extrapolated track. If a photon has been converted in the second layer of lead, if can be identified by a shower in the two proportional chambers behind the lead, if this shower is not correlated with a track. In this case only the determination of the direction of the photon is possible. If the photon produces an electron-positron pair already in the first converter, also its energy can be measured.

3. Total Hadronic Cross Section

Our measurements of the total hadronic cross section have been published in an updated version at the Hamburg-Conference last summer[4]. Here I shall discuss these results only in a brief manner comparing them with other results.

The data used to gain our cross section include all events with $\geq$ 2tracks, having at least one track with an angle against the beam axis $\theta > 30^0$ and a momentum $p > 240$ MeV/c. For two-prongs a coplanarity angle $15^0 < \Delta\phi < 165^0$ is required. Radiative corrections have been applied to the measured cross section. To determine all acceptances a Monte Carlo procedure was used, which simulates as exact as possible all details of the detector. The data are best described, if the physical model fed into this Monte Carlo procedure is of the "jet"type, with a jet-axis distribution proportional to $(1+\cos^2\theta)$ and an average transverse momentum with respect to the jet-axis of $\langle p_t \rangle = 350$ MeV/c[5].

The overall efficiency and acceptance is for two-prongs $\sim$ 40% and for >2-prongs $\sim$ 95% giving a total efficiency of $\sim$75% for all events. Due to these high efficiencies the Monte Carlo corrections applied to our data are relatively small compared to other detectors.

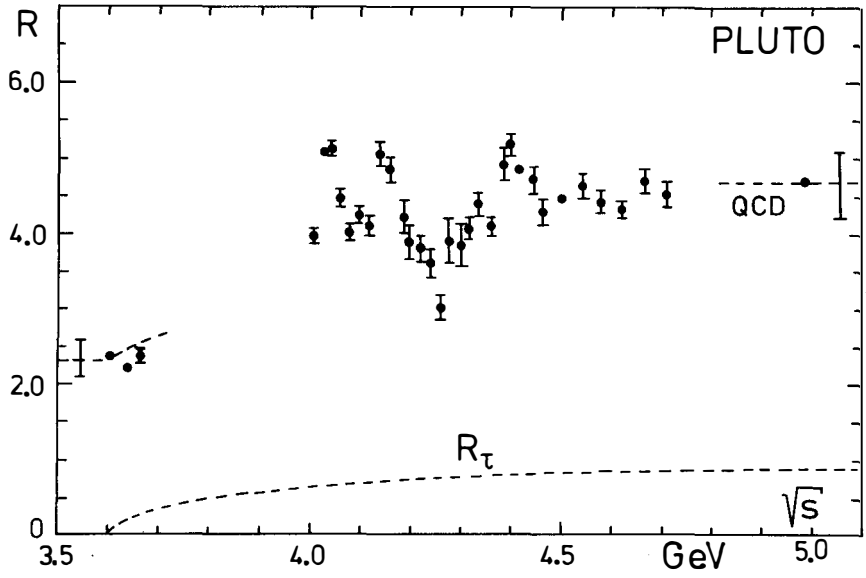

Fig.2 Total hadronic cross section $R_{tot} = \sigma_{had}/\sigma_{\mu\mu}$ (contribution from the heavy lepton τ included)

In fig.2 the ratio

$$R_{tot} = \sigma(e^+e^- \to \text{hadrons}) \; / \; \sigma(e^+e^- \to \mu^+\mu^-)$$

is plotted as a function of the center of mass energy $\sqrt{s}$.

In the framework of quantumchromodynamics (QCD) the total hadronic cross section (without the contribution from the heavy lepton τ) including the first order gluonic corrections is given by

$$R_{had} = 3 \sum_i Q_i^2 \cdot (1 + \alpha_s/\pi)$$

where Q_i are the quark charges (i = u, d, s for $\sqrt{s} < 3.6$ GeV and i = u, d, c, s for $\sqrt{s} >> 3.6$ GeV) and α_s the running coupling constant of the strong interactions:

$$\alpha_s = \frac{12\pi}{(33-2n)\ln(s/\Lambda^2)}$$

(n = number of quark flavours)

The only free parameter is Λ. A fit to deep inelastic lepton-nucleon scattering data yields a value of $\Lambda \sim 0.5$ GeV, which will be used in this estimation. For $\sqrt{s}$ = 3.6 GeV this leads to a value of $R_{had} = R_{tot} = 2.2$ and for $\sqrt{s}$ = 5.0 GeV to $R_{had} = 3.7$. But these corrections are far too small to be measured with existing detectors. To obtain at the latter energy the value of R_{tot} one must add the contribution of the threshold factor of the heavy lepton τ

$$R_\tau = (3\beta - \beta^3)/2 \qquad (\beta = \text{velocity of the } \tau)$$

At $\sqrt{s}$ = 5 GeV one has $R_\tau = .98$ yielding for $R_{tot} = 4.7$, because all $\tau^+\tau^-$-events contribute to the hadronic events selected. For both values at 3.6 GeV below and at 5.0 GeV above charm - and heavy lepton - thresholds the measured R_{tot} is in good agreement with theoretical expectations, but one must always keep in mind that an overall systematic uncertainty of about 10% must be taken into account, which is on top of the gluonic corrections.

The topology of the cross section shows three distinct peaks. The results of separate fits to each of these resonance like regions are given in table 2. An overall fit of the complete energy interval between 3.6 and 5.0 GeV seems unreasonable since the exact charm threshold behavior is not really known.

Table 2. Resonance parameters of the resonancelike regions between 4.0 GeV < $\sqrt{s}$ < 5.0 GeV

Mass (GeV/c^2)	Width (MeV/c^2)
4.04 ± 0.02	55 ± 10
4.15 ± 0.04	47 ± 11
4.40 ± 0.03	33 ± 9

Although within the systematic uncertainties our measurements are in overall agreement with other results, there are some differences. The PLUTO cross section is somewhat lower than that of the DASP[6]- and the SLAC-LBL[7]-detectors while it is in agreement with the preliminary cross section of the DELCO-detector[8]. The peaks at 4.04 GeV and at 4.15 GeV are well separated in the PLUTO and DASP results, but this is not so for DELCO and SLAC-LBL results.

4. ρ-inclusive Production

The quarks are assumed to be pointlike spin half constituents of hadrons. A meson h is built up by a quark-antiquark pair. So it is obvious from simple spin state counting that the vector mesons (spin J = 1) should be produced three times more frequent than the pseudoscalar-mesons (J = 0) in the inclusive reaction

$$e^+e^- \to h + \text{anything}.$$

(In this estimate more sophisticated items of the theory, like quark mass differences, are neglected). We compared our measurements of the inclusive reaction

$$e^+e^- \to \rho^0 \;(\to \pi^+\pi^-) + \text{anything} \qquad (1a)$$

with

$$e^+e^- \to \pi^\pm + \text{anything}, \qquad (1b)$$

taking ρ(J = 1) and π(J = 0) as the mesons with the smallest mass of each type to test this prediction. Reaction (1b) has been measured by the DASP-collaboration[9]. To look for events of the

reaction (1a) we assigned pion mass to all tracks and plotted the invariant mass of two tracks with opposite charge (fig.3a,upper histogram). The background was determined using pairs of tracks, each track coming from a different event (fig.3a,lower histogram).

The invariant masses of the remaining events have been plotted in fig.3b.The mass distribution has been fitted to the ρ^0-resonance (giving mass and width of 767±7MeV and 160±40 MeV respectively from a Breit-Wigner-fit), a smooth polynomial background and a possible kinematic reflection of K*(890) which contributes to the left tail of the ρ^0-signal when the $K\bar{K}$ is interpreted as two pions.

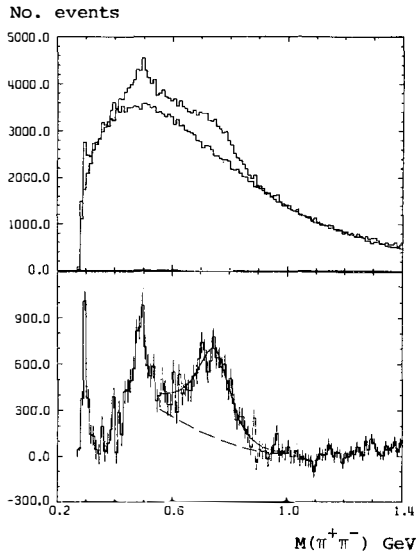

Fig.3 a) Invariant mass of $\pi^+\pi^-$-system (upper histogram) and uncorrelated pairs (lower histogram)
b) Difference between correlated and uncorrelated $\pi^+\pi^-$-pairs

The cross section of the reaction (1a) as a function of the center of mass energy $\sqrt{s}$ is shown in fig.4 in terms of

$$R_\rho = \sigma(e^+e^- \to \rho^0 + X)/\sigma_{\mu\mu} .$$

Like the total hadronic cross section the ρ^0-inclusive cross section shows also a threshold behavior between 3.6 GeV $\leq \sqrt{s} \leq$ 4.1 GeV. Above $\sqrt{s}$ = 4.1 GeV a value of $R_\rho \sim 1$ is obtained.

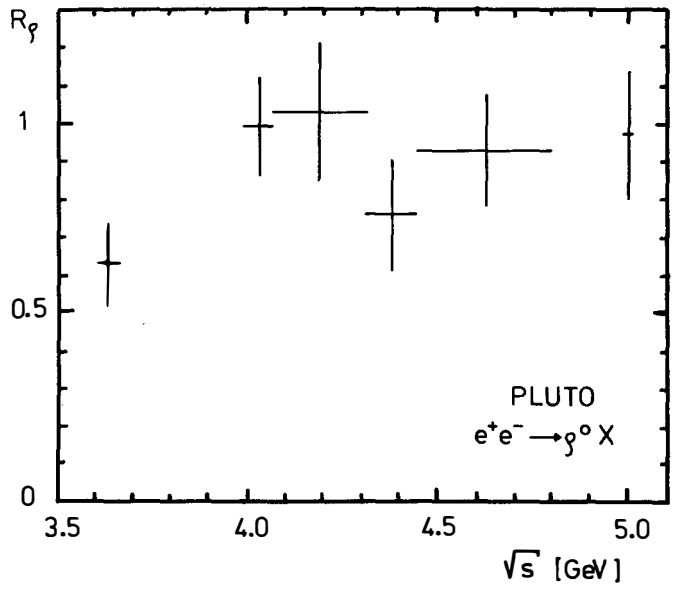

Fig.4. ρ^o inclusive cross section normalised to the μ-pair cross section as a function of the center of mass energy $\sqrt{s}$

The energy distribution of the ρ can be written as

$$\frac{s}{\beta} \frac{d\sigma}{dx_E} = f(x_E, s)$$

with $x_E = 2 E\rho/\sqrt{s}$, $E\rho$ = energy of the ρ, and β = velocity of the ρ. For high center of mass energies scaling predicts f to become only a function of x_E

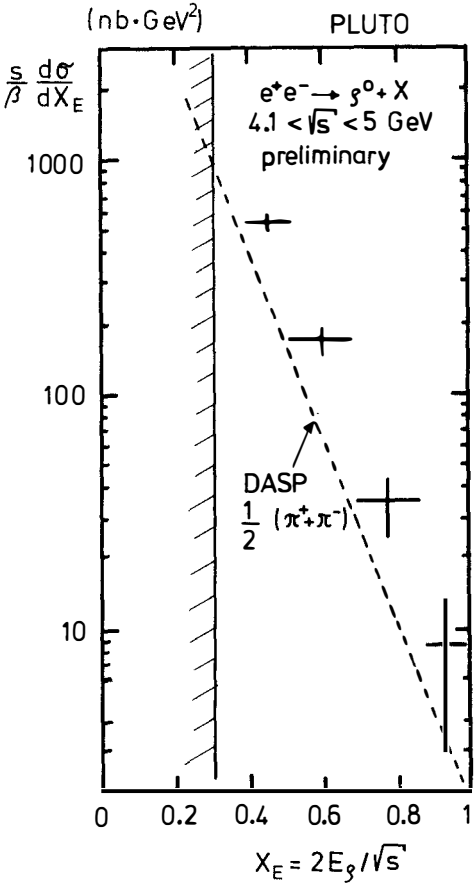

Fig.5. ρ^0 inclusive energy distribution. The broken line represents the DASP result for the charged pion inclusive reaction (1b). The full line is the kinematic limit at $x_E = 2m_\rho/\sqrt{s}$

The obtained spectrum is shown in fig.5. Due to the limited center of mass energy interval from 3.6 GeV to 5.0 GeV, in which data have been taken, there is a lower kinematical limit for x_E at $\sim .3$. Events from the reaction

$$e^+e^- \rightarrow \rho^0\gamma \quad \rho^0 \rightarrow \pi^+\pi^-$$

have been detected experimentally and removed as a background which contributs to the events in the $x_E \sim 1$ region. This reaction can be calculated from QED. The measured contribution is in agreement with this calculations.
The slope of the curve can be parameterized as

$$f_\rho(x_E) \propto \exp(-b \cdot x_E)$$

with $b = 8.4 \pm 0.8$ or as

$$f_\rho(x_E) \propto \frac{1}{x_E} \cdot (1-x_E)^n$$

with $n = 2.4 \pm 0.4$.

The broken line in fig.5 represents the inclusive π production as measured by DASP. To compare the ρ-inclusive production, one must take into account that a certain number of observed pions are coming from the ρ-decay. Assuming the cross section for all ρ to be

$$\sigma(\rho^+ + \rho^- + \rho^0) = 3 \cdot \sigma(\rho^0)$$

one can calculate the fraction of pions from a ρ decay and can subtract them from the π-inclusive spectrum, obtaining a direct π spectrum.

Comparing this spectrum with the measured ρ-inclusive spectrum one obtains for $x_E \geq 0.4$

$$\frac{\left(\frac{s}{\beta}\frac{d\sigma}{dx_E}\right)_\rho}{\left(\frac{s}{\beta}\frac{d\sigma}{dx_E}\right)_\pi \text{ direct}} = 3.1 \pm 0.6$$

in good agreement with expectation. However, this is an upper limit since there are also contributions to the π-direct-spectrum from other resonance decays.

5. The Radiative Decay $J/\psi \to f^0\gamma$

Radiative decays of the J/ψ like

$$J/\psi \to \pi^0\gamma \qquad (2a)$$

$$J/\psi \to \eta\,\gamma \qquad (2b)$$

$$J/\psi \to \eta'\gamma \qquad (2c)$$

$$J/\psi \to f^0\gamma \qquad (2d)$$

are a useful tool to provide information on the mechanism of Zweig-rule violation. In the language of QCD radiative decays are described by two different types of graphs (fig.6)

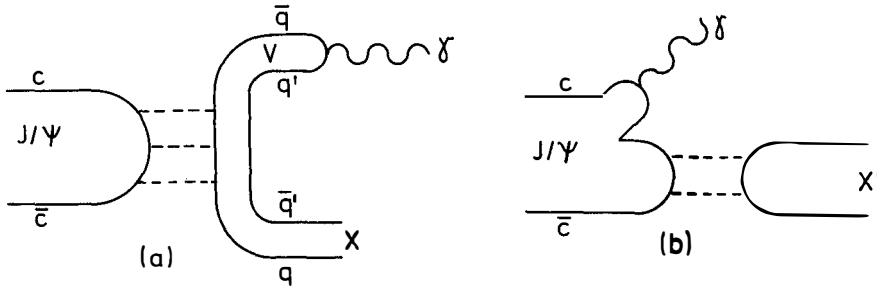

Fig.6 Diagrams for radiative decays via 3 gluon-(a) and 2 gluon-exchange (b)

In the first diagram (fig.6a) the decay is mediated by a three gluon coupling to an intermediate vectormeson V and a hadronic system X with a subsequent transition of V via vectordominance to a photon. The calculation of this decay scheme leads to relatively small branching ratios. This has been found to be true for the decay (2a), indeed, the DASP-collaboration found

$$BR(J/\psi \to \pi^0\gamma) = (7.3 \pm 4.7)\ 10^{-5} \qquad (10)\,.$$

But the branching ratios for decays (2b) and (2c) are considerably higher. The DASP- und DESY-Heidelberg-groups measured

$$BR(J/\psi \to \eta\gamma) = \begin{cases} (0.80 \pm 0.18)\ 10^{-3} & \text{DASP}\,(10) \\ (1.3 \pm 0.4)\ 10^{-3} & \text{DESY-HD}\,(11) \end{cases}$$

$$BR(J/\psi \to \eta'\gamma) = \begin{cases} (2.2 \pm 1.7)\ 10^{-3} & \text{DASP}\,(10) \\ (2.4 \pm 0.7)\ 10^{-3} & \text{DESY-HD}\,(11) \end{cases}$$

These branching ratios can be explained with the second graph (fig.6b), where the decay is mediated only by a two gluon exchange. The branching ratio into a photon and two gluons has been estimated to be

$$BR(J/\psi \to \gamma + 2\ \text{gluons}) \sim 10\%\,. \qquad (12)$$

This leads to predictions that decays like (2b) and (2c) should have considerably higher branching ratios than reaction (2a). The decay (2a) cannot proceed via this graph (fig.6b) due to isospin conservation.

To provide more information it is worthwhile to study the decay (2d). In doing so, the PLUTO collaboration - as recently reported[13] - selected from 84000 J/ψ events those with two prongs plus one photon. For the latter only the direction has been determined. 1650 events fit the hypothesis

$$J/\psi \to \pi^+\pi^-\gamma \qquad \text{(3-C-fit)}\,.$$

After QED-background rejection we obtain a sample of 852 events which are either $\pi^+\pi^-\gamma$ or $\pi^+\pi^-\pi^0$ (with only one γ of the π^0 detected or both γ are not resolved).

The invariant mass distribution of the neutral combination $\pi^+\pi^-$ of events not lying in the $\rho^\pm$-band (0.6 GeV/$c^2 \leq M(\pi^\pm\pi^0) \leq$ 1 GeV/c^2) shows two peaks (fig.7a). A fit gives two Breit-Wigner-resonances with masses of (0.78±0.02) GeV/c^2 and (1.23±0.04) GeV/c^2 and widths of (0.13±0.02) GeV/c^2 and (0.13±0.05) GeV/c^2 respectively, in agreement with the ρ^0 and the $f^0(1270)$ mesons. $\rho'(1250)$ could be excluded for the second peak, because the invariant mass distribution of the charged combination ($\pi^\pm$ + X, X = γ or π^0) shows no adequate peak in this region (fig.7b) which is expected for the isospin triplet $\rho'(1250)$.

Charge conjugation implies that the ρ^0 is accompanied by a π^0 and the f^0 by a γ. Using our Monte-Carlo-procedure to determine the overall efficiency we obtained the following branching ratios:

$$BR(J/\psi \to \rho^0\pi^0) = (1.6\pm0.4)\ \%$$
$$BR(J\ \psi \to f^0\gamma\ ) = (0.2\pm0.07)\%$$

The DASP-collaboration has obtained similar results [14]. Due to the fact that the branching ratio for the decay (2d) is of the same order of magnitude as for the decays (2b) and (2c), one is urged to study this decay in the terms of the two-gluon-exchange diagram (fig.6b).

If one calculates this diagram, as done by M.Krammer[15], one obtains predictions for the angular distributions of the final state.

The decay (2d) is described by three independent f^0-helicity amplitudes A_0, A_1 and A_2. The combined production- and decay-angular distribution for this reaction $W(\Theta_p, \Theta_M, \phi_M)$ is only a function of the ratios $A_1/A_0 = X$ and $A_2/A_0 = Y$, where Θ_p is the angle between the f^0 direction and the e^+-beam, Θ_M and ϕ_M are polar and azimuthal angles of the π^+ in the f^0 helicity frame. X and Y may have values between plus and minus infinity in principle.

For a given pair of values X and Y we have fitted our data (after a background subtraction) to the angular distribution $W(\Theta_p, \Theta_M, \phi_M)$ comparing by χ^2-values the distributions for different X and Y values. Details of this procedure will be published soon[16].

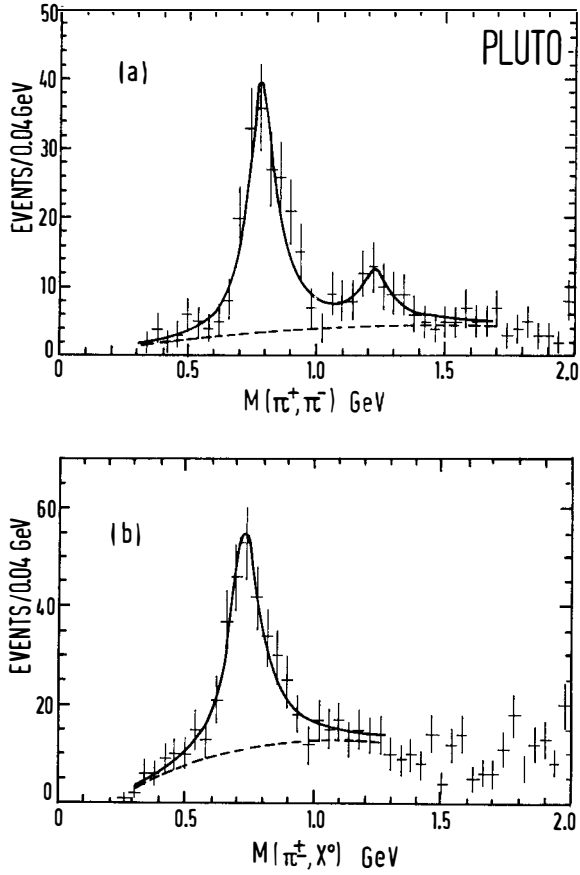

Fig.7. Invariant mass distributions
a) Neutral combination ($\pi^+\pi^-$), excluding events from the $\rho^{\pm}$-band
b) Charged combination ($\pi^{\pm}$+X, X = γ or π^0)

The full line gives the fit above an estimated polynomial background (dashed line)

The results of these fits are presented in fig.8 in form of equal χ^2 contours in the X-Y-plane. The χ^2-values assigned to the curves are measured from the minimum of χ^2 = 26 (25 degrees of freedom). The best values obtained in these fits are

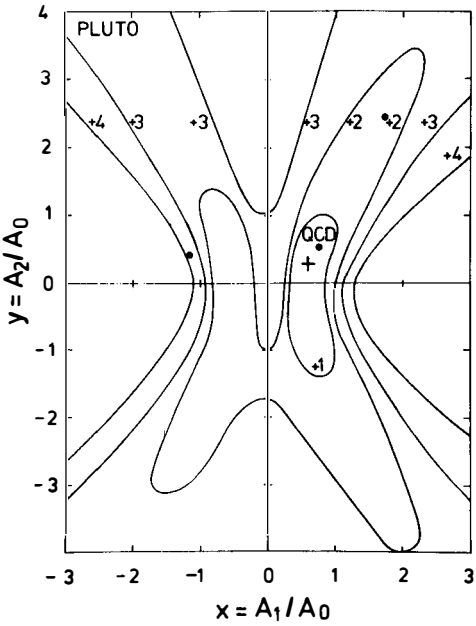

$$X = A_1/A_0 = 0.6 \pm 0.3$$

$$Y = A_2/A_0 = 0.3^{+0.6}_{-1.6}$$

(crossed point in fig.8). The values of X = 0.76 and Y = 0.54 as predicted by from the QCD-two-gluon-exchange[15] are in very good agreement with our results.

Fig.8
Fit of the f^0-decay distribution. Curves are representing equal χ^2-values, measured from the minimum of χ^2=26. QCD markes the prediction from the two gluon-exchange model

6. Heavy Lepton

6.1 Introduction

Just one year ago the existence of the heavy lepton, found in e^+e^--annihilation in 1975 by the SLAC-LBL-collaboration [17], has been confirmed by the PLUTO-Collaboration [18,19]. It should also be mentioned that M.Perl named this new particle τ [20] at the Rencontre de Moriond one year ago.

During the last year a very fruitful work on this particle has been performed by several groups, but there are still some questions open.

The PLUTO collaboration can contribute new results on two of such subjects: we measured the branching ratio of the hadronic decay mode $\tau \to \rho\pi\nu$ and we can give an new upper limit on the lifetime of the τ.

Before going into the details of our measurements let me repeat some main properties of the τ. As discussed above, in the total hadronic cross section there is need to explain at least one unit of R_{tot} above the threshold around 3.6 GeV, which is assigned to the heavy lepton τ. From very accurate measurements of DASP [21] and DESY-Heidelberg [22], we know that the mass of the τ is a few MeV less than 1.8 GeV, further we know that the τ behaves like a point-like spin half particle. In the decays of the τ a neutral particle is emitted, presumably a new neutrino ν_τ.

Therefore it is reasonable to discuss the properties of the τ in terms of a sequantial (heavy) lepton, having its own (conserved) lepton number and thus its own neutrino (mass assumed to be zero). Using conventional weak current-current-interactions (with at least an arbitrary mixture of V and A components in the τ-part of the current), one can calculate the branching ratio into its simplest decay modes, as done e.g. by Thacker and Sakurai [23]. Using their formulae and taking into account recent measurements of the total hadronic cross section in the region below the mass of the τ, one obtains the branching ratios of table 3 [24]. The measured branching ratios for the purely leptonic decay modes are in good agreement with theory: the world's average value, as presented at the Hamburg Conference last summer [25], is

$$BR(\tau \to e\nu\nu) = BR(\tau \to \mu\nu\nu) = (18\pm3)\ \%$$

Table 3 Branching ratios of the heavy lepton

Decay mode	Branching ratio in %
$\tau^- \to \nu_\tau e^- \bar{\nu}_e$	15.1
$\tau^- \to \nu_\tau \mu^- \bar{\nu}_\mu$	14.7
$\tau^- \to \nu_\tau \pi^-$	7.5
$\tau^- \to \nu_\tau \rho^-$	20.3
$\tau^- \to \nu_\tau$ + (strange particles)	1.9
$\tau^- \to \nu_\tau A_1^-$	7.8
$\tau^- \to \nu_\tau$ + (hadr. continuum)	32.7

But there are still some difficulties with some hadronic decay modes. The vector part of the weak hadronic current behaves as predicted. The branching ratio $\tau^- \to \nu_\tau \rho^-$ has been measured by the DASP-Collaboration to be in agreement with theory[26]. But the axialvector part of the weak hadronic current should couple to the A_1-meson as the lowest axialvector ($J^P = 1^+$) state and via the divergence of the current to the π as lowest pseudoscalar ($J^P = 0^-$) state. Especially the decay $\tau \to \nu\pi$ can be calculated, because it depends only on the pion coupling constant f_π, which is well known from the decay $\pi^- \to \mu^- \bar{\nu}_\mu$. The ratio should be

$$BR(\tau^- \to \nu_\tau \pi^-) \; / \; BR(\tau^- \to \nu_\tau e^- \bar{\nu}_e) \;\; = \;\; 0.5$$

but there is no positive evidence for this decay. The only measurement of the DASP[26,27] detector is somewhat lower than the predicted branching ratio.

On the other hand the decay to the A_1-meson is problematic because the A_1 is in the language of the Particle Data Group[28] a "not established resonance". But to test the axialvector part of the current it is sufficent to look for a $J^P = 1^+$ hadronic final state (e.g. $\tau \to \nu\rho\pi$) avoiding discussions on the existence of the A_1. If the branching ratio of this decay is of the order of magnitude as predicted it is a strong evidence for the normal behaviour of the axialvector current.

6.2 The Decay $\tau \to \nu\rho\pi$ *)

We looked for events with a final state containing an identified lepton $\ell^{\pm}$($e^{\pm}$ or $\mu^{\pm}$) and three prongs with missing energy and no photon in the detector according to the reaction

$$e^+e^- \to \tau^+\tau^- \quad \begin{cases} \to \ell^-\nu\nu \\ \to \pi^+\rho^0\nu \quad \to \pi^+\pi^- \end{cases} \qquad (3)$$

Our selection criteria have been:
For an electron we required a momentum $p_e > .4$ GeV/c and for a muon $p_\mu > 1$ GeV/c, a missing mass MM > .9 GeV/c^2 and the energy of the 3-pion-system not greater than the beam energy. A typical event is shown in fig.9. After these cuts our sample contained 66 events, 52 of them with an identified electron. Fig.10 shows the mass of the 3-pion-system versus the lepton momentum. There is no correlation between these two quantities as expected for reaction (3). The 3-pion-mass is distributed in a small band around 1.1 GeV/c . Both the electron and the muon momentum spectra are relatively hard. Several checks have been made to assure that the observed events are really in agreement with reaction (3) [30]. As an example I shall discuss here only the spectrum of electrons (fig.11, histogram). From the measured spectrum we subtracted the background from hadron - electron misidentification p(h → e)=1.2%, taking into account, that the electron detection efficiency is a function of the electron momentum,

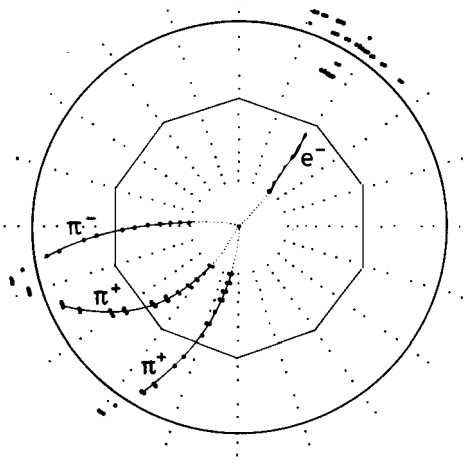

Fig.9.Typical event of reaction (3) (view along the beam-line)

*) Results of this channel have recently been published by the PLUTO group [29]. Meanwhile we doubled statistics lowering some cuts and taking also events with a muon instead of an electron.

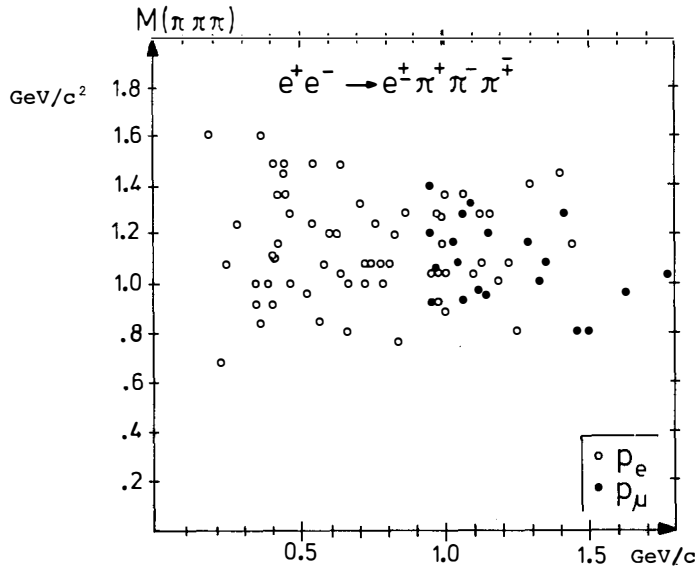

Fig.10. Mass of the 3-pion system versus lepton momentum. Muons with momenta less than ∿1 GeV/c are not recorded due to the cut-off of the iron yoke

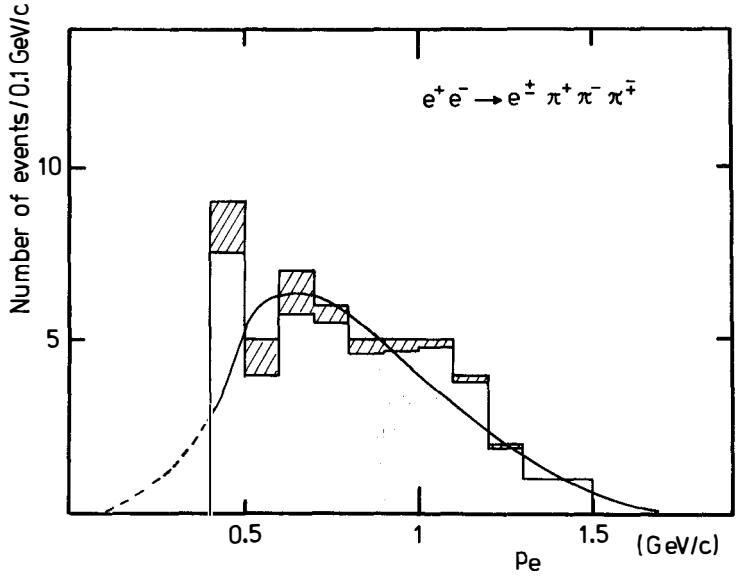

Fig.11 Measured spectrum of the electrons. The hatched area represents background from hadron-electron misidentification. The curve is the calculated electron spectrum of the τ decay folded with the electron detection efficiency and normalized to the data.

which raises from 30% at p_e = 0.4 GeV/c to 65% at p_e = 1.0 GeV/c. In fig.11 the hatched area represents this background. The ramaining electron spectrum is in good agreement with the theoretical electron spectrum from τ-decay (full line in fig.11).

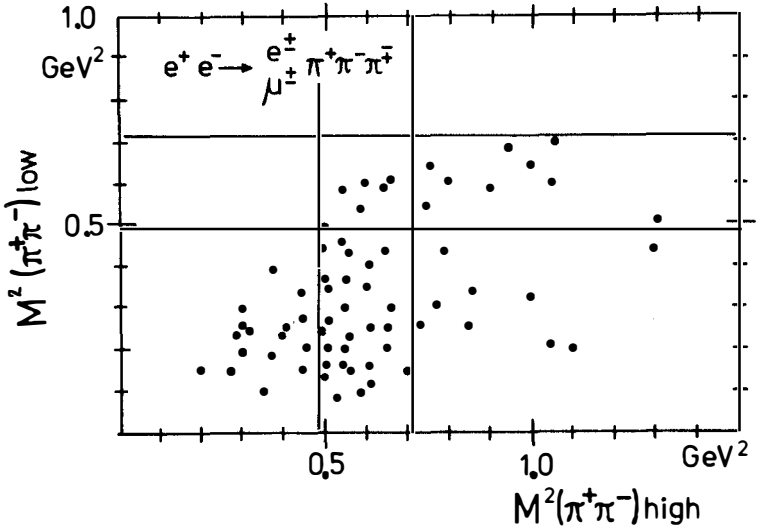

Fig.12. Low mass combination versus high mass combination of the 2-pion-system. The full lines at .49 GeV² and at .7 GeV² are representing the ρ^0-cut applied to the data in further use.

The Dalitz plot (fig.12) shows a well populated ρ^0-band. Thus we required for our further analysis at least one 2-pion-combination to have a mass in the ρ^0-band i.e. 0.7 GeV/c² $\leq M(\pi^+\pi^-) \leq$ 0.84 GeV/c². After this cut 42 events (35 with an electron) remained in our analysis.

The background shows no ρ^0-signal. Furthermore one can estimate the charm contribution to this channel to be less than 3 events. The momentum spectrum of the 3-pion-system is compatible with a two-body-decay of the τ which supports the interpretation of the (ρπ)-system to be the A_1 resonance. Using our Monte-Carlo-procedure to determine all acceptances and efficiencies we obtained a branching ratio

$$BR(\tau^- \to \rho^0\pi^-\nu) = (5 \pm 1.5)\ \%$$

or if one assumes an A_1-resonance

$$BR(\tau^- \to \nu A_1^-) = (10 \pm 3)\ \%.$$

From the 3-pion-mass-spectrum we derived further (under assumption of a two-body decay of the τ) an upper limit of the mass of the τ-neutrino $m_{\nu_\tau} < .4\ GeV/c^2$.

From the negative G-parity of the $(\rho\pi)$-system one can conclude assuming conventional weak hadronic currents with V and A parts that the only allowed states have a spin-parity $J^P = 0^-$ or 1^+. This is equivalent to the statement that the weak hadronic current must have an axialvector component.

If one admits non conventional weak interactions the lowest angular momentum states of the $(\rho\pi)$-system are listed in table 4.

Table 4. Spin-Parity assignments of $(\rho\pi)$-system
Assignments in brackets are only possible in non conventional weak interactions.

	ℓ =	S	P	D
		0	1	2
J =	0		0^-	
	1	1^+	(1^-)	(1^+)
	2		(2^-)	(2^+)

In fig.13a the 3-pion-mass-spectrum, corrected for background and acceptance is compared with the S, P and D-wave solutions. No pure state gives an acceptable fit. The data fit best, if one uses the S-wave plus a Breit-Wigner-resonance with a mass of 1 GeV/c^2 and a width of 400 MeV, parameters which are in agreement with the A_1 resonance (fig.13b). Thus we conclude that the A_1 - if existing would give a good description of our data.

6.3 Upper limit of the Lifetime

From the standard model of a sequential heavy lepton with V-A decay structure the lifetime of the τ, τ_o, is determined by

$$\tau_o = BR(\tau \to e\nu\nu) \cdot (M_\mu / M_\tau)^5 \cdot \tau_\mu$$

where τ_μ and M_μ are lifetime and mass of the muon. Using a branching ratio $BR(\tau \to e\nu\nu) = 18\ \%$ and a mass of the heavy lepton

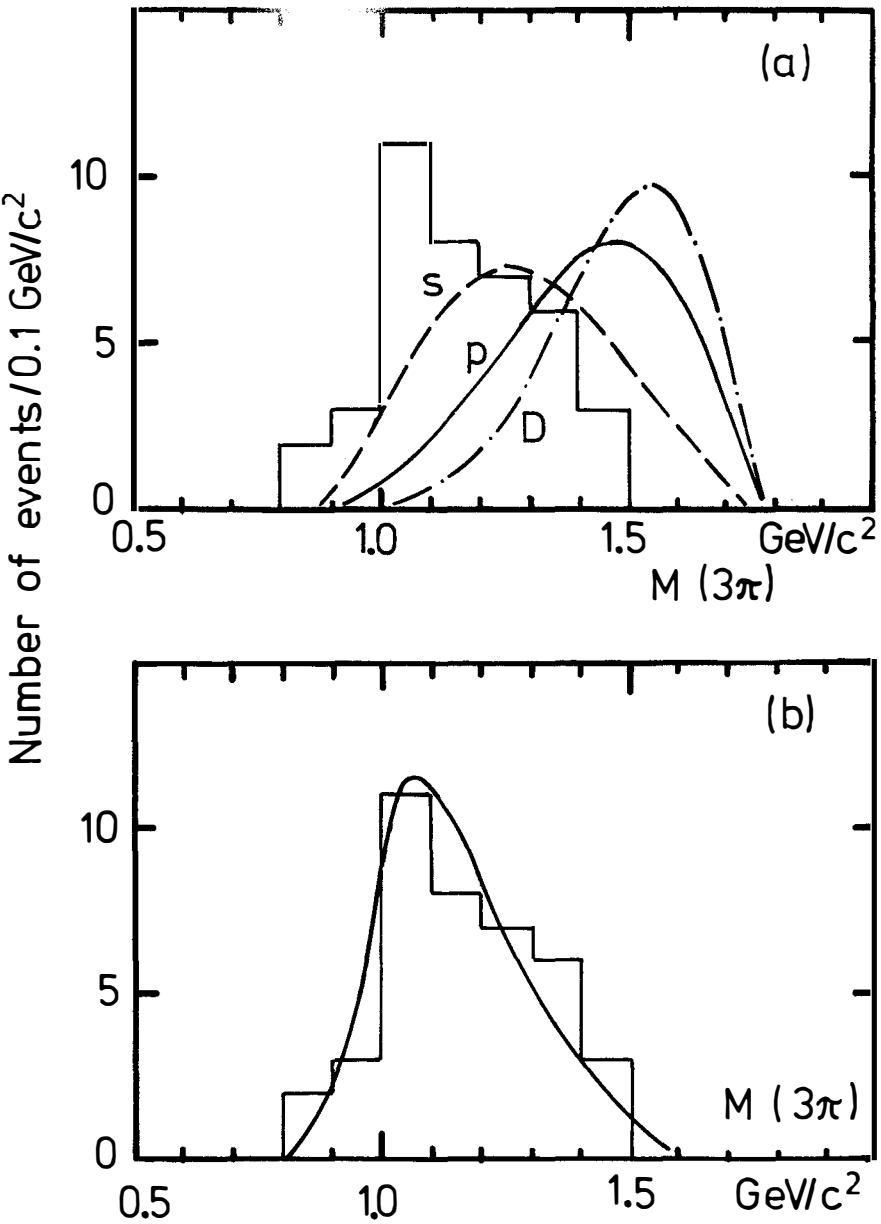

Fig.13 3-pion mass spectrum, corrected for background and acceptance (histogram) and
a) theoretical distributions for S, P and D wave solutions
b) theoreticel distribution for a S-wave plus a Breit-Wigner resonance (M= 1GeV/c^2, Γ= 400 MeV/c^2)

M_τ = 1795 MeV/c^2 one obtains

$$\tau_o = 2.8 \cdot 10^{-13} \text{ sec.}$$

The lifetime can be determined by measuring the average decay length d_o at a fixed momentum of the τ. But this length is far too small ($d_o \sim 0.05$ mm) to be determined by the PLUTO-detector.

For this analysis we used our ($e^+e^- \to \mu^\pm$ + 1 prong + no photon) event sample as used for our anomalous muon analysis [18] and applied some further cuts to get a sample of events which make a very accurate momentum measurement possible. Thus we required a missing mass $MM^2 > 0.4\ E^2_{beam}$, a coplanarity angle $15^o < \Delta\phi < 165^o$, $\geq$ 10 coordinates for each track and a momentum for the non-muon track $p_2 > 0.4$ GeV/c. In addition we used a special tracking procedure, taking into account the energy loss in the matter transversed by the particle.

Fig.14 shows the vertex-distribution from the remaining 65 events. For each track the minimal distance to the interaction point in the plane perpendicular to the beam (r_{min}) has been determined and entered into the plot. The accuracy of the position of the interaction point in this plane is Δx = 0.5 mm and Δy = 0.7 mm (FWHM). The vertex-distribution fits well by a Gaussian with a σ = 3.05±0.15 mm (broken line in fig.14). To examine the influence of a finite decay length on the width of the vertex distribution we used our Monte-Carlo-procedure and generated events with different decay lengths. The result of this calculations is presented in fig. 15, showing σ of the vertex-distributions as a function of the decay length.

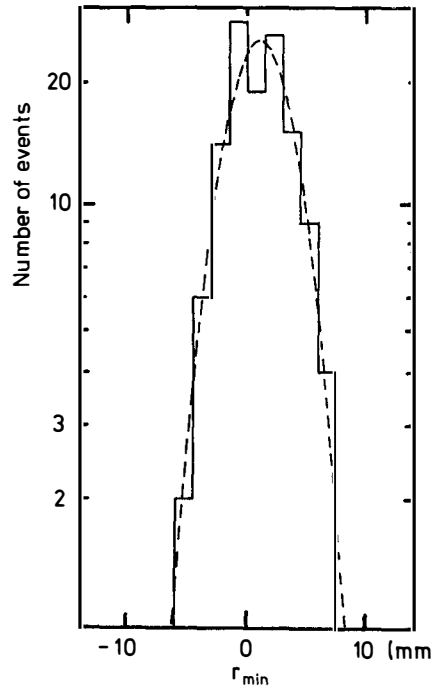

Fig.14 Vertex distribution in the plane perpendicular to the beam axis. The full linegives a fit to a Gaussian with σ = (3.05±0.15)mm

The Monte-Carlo calculations show that the decay length distribution is compatible with the experimental resolution and therefore with a zero lifetime of the τ. Further we obtain from the calculation a two standard-deviation (95% C.L.) upper limit for the τ decay length $d_o < 0.8$ mm, giving an upper limit on the lifetime of the

$$\tau_o < 3.4 \cdot 10^{-12} \text{ sec.} \quad (95\% \text{ C.L.})$$

This upper limit excludes models of the heavy lepton predicting relatively long lifetimes (e.g. models mixing lepton numbers (31), predicting a lifetime of about 10^{-11} sec).

Since the lifetime is a very important parameter for testing theories, and unfortunately none of the existing experiments is sensitive enough to measure τ_o, it might be worthwhile to design a detector specially for this purpose.

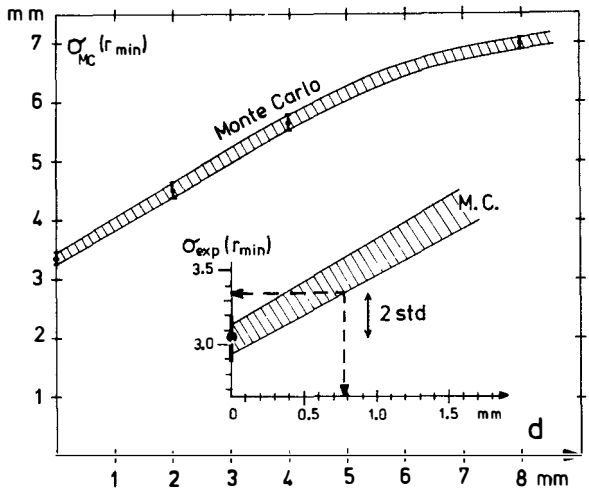

Fig.15. Width of the vertex distribution as a function of decay length obtained with a Monte-Carlo-procedure. In the insert the Monte-Carlo function is scaled down to the experimental value to derive the 2-σ- upper limit.

7. Present and Future Program of the PLUTO-detector

During the last year PLUTO was upgraded by installing a new system of shower counters of the lead-scintillator-sandwich type, covering a solid angle of 92% of 4π. The lead converters, shown in fig.1, have been removed. The new shower counters are equipped with proportional chambers to determine the position of the shower.

In addition, the muon detector has been enlarged and covers now 65% of the full solid angle.

During the same time the DORIS-storage ring has been upgraded to reach energies of more than 3.0 GeV per beam. It was operated from December 77 to February 78 at an energy of about 4 GeV per beam in single ring single bunch mode. During the time of this conference the energy will again be increased to reach a center of mass energy of 9.5 GeV to measure the Υ-resonance in e^+e^- annihilation. This resonance, recently found at Fermilab[32], is supposed to be a bound state of a new quark-antiquark pair. The resonance energy will be reached mid April. After a short runperiod of five weeks at the Υ-energy region PLUTO is scheduled to move to the new large e^+e^--storage ring PETRA at DESY which will come into operation next autumn.

Note added after the conference

The DORIS-storage ring reached the energy of 9.2 GeV in schedule. An energy scan between 9.35 and 9.5 GeV center of mass energy was performed. PLUTO found the Υ-resonance at a mass of $(9.46 \pm 0.01)\,\mathrm{GeV/c^2}$ (fig.16). The observed width of the resonance is compatible with the expected energy resolution of the storage ring. Thus we conclude, that the Υ is a narrow resonance being in agreement with the hypothesis of a bound state of a new quark-antiquark pair. From the value of the peak integral we further derive after applying radiative corrections an electronic width of the resonance of $(1.3 \pm 0.4)\,\mathrm{keV}$, which favours a $-1/3$ charge assignment of the new quark[33].

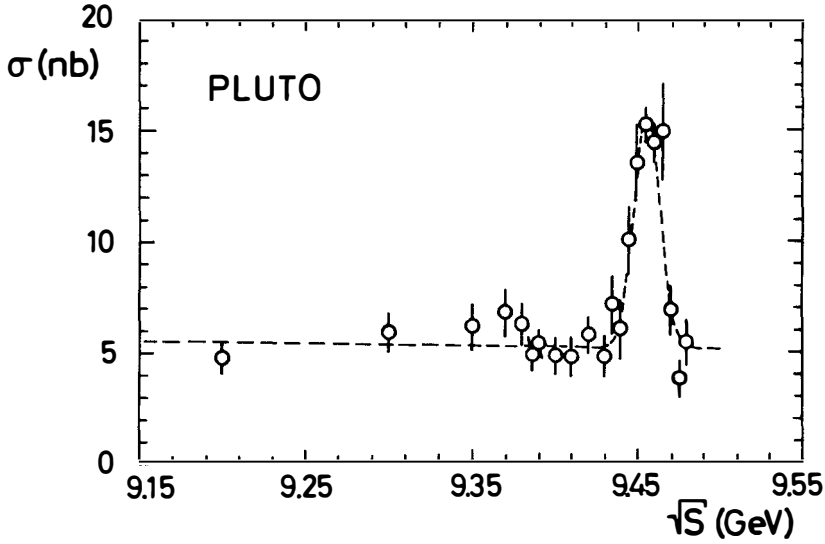

Fig.16. The total hadronic cross section in the Υ-resonance region in e^+e^--annihilation (without radiative corrections). Only statistical errors are shown. The broken line gives a gaussian fit to the resonance curve with a 1/s hadronic background.

Acknowledgements

I wish to thank all my colleagues from the PLUTO-collaboration for their active help in preparing this talk, namely Prof.C.Grupen, Dr.G.Flügge, Prof.H.Meyer and Prof.G.Zech for many useful discussions. Further I like to thank the DESY directorate for their kind hospitality.

This work was supported by the Bundesministerium für Forschung und Technologie.

References

1. V.Blobel, in Proceedings of the XII Rencontre de Moriond (J.Tran Thanh Van, ed.), Paris 1977, Vol.I, p.99
2. PLUTO-collaboration, J.Burmester et al.,Phys.Lett.64B(1976)369
3. PLUTO-collaboration, J.Burmester et al.,Phys.Lett.66B(1977)395
4. G.Knies, in Proceedings of the 1977 Intern.Symp.on Lepton and Photon Interactions (F.Gutbrod, ed.),Hamburg 1977, p.93
5. A.Bäcker, Ph.D. thesis, Siegen Univ.(1977), DESY-internal report F33-77/03 (unpublished)
6. DASP-collaboration, R.Brandelik et al.,DESY-report 78/18(1978)
7. G. Hanson, this conference
8. J.Kirkby, Proceedings of the 1977 Intern.Symp.on Lepton and Photon Interactions (F.Gutbrod, ed.) Hamburg 1977, p.3; A.Diamant-Berger, this conference
9. DASP collaboration, R.Brandelik et al.,Phys.Lett.67B(1977)358
10. DASP collaboration, W.Braunschweig et al., Phys.Lett.67B(1977) 243
11. DESY-Heidelberg-collaboration, W.Bartel et al.,Phys.Lett. 66B(1977) 489
12. T.Appelquist et al.,Phys.Rev.Lett.34(1975)365, M.Chanowitz, Phys.Rev.D12 (1975)918, L.Okun and M.Voloshin, Moscow 1976, IETF-95
13. PLUTO-collaboration, G.Alexander et al.,Phys.Lett.72B(1978)493
14. DASP-collaboration, R.Brandelik et al.,Phys.Lett.74B(1978)292
15. M.Krammer, DESY report 78/06 (1978) and this conference
16. PLUTO-collaboration, G.Alexander et al.,DESY report 78/20(1978) (to be published in Phys.Lett.B.)
17. M.Perl et al.,Phys.Rev.Lett.35(1975)1489
18. PLUTO-collaboration, J.Burmester et al.,Phys.Lett.68B(1977)297
19. PLUTO-collaboration, J.Burmester et al.,Phys.Lett.68B(1977)301
20. M.Perl, in Proceedings of the XII Rencontre de Moriond (J.Tran Thanh Van, ed.), Paris 1977, Vol.I, p.75
21. DASP-collaboration, R.Brandelik et al.,Phys.Lett.73B(1978) 109
22. DESY Heidelberg-collaboration., P.Steffen, talk at the "Frühjahrstagung der DPG" at Heidelberg (1978)
23. H.B.Thacker and J.J.Sakurai, Phys.Lett.36B(1971)103
24. M.Rößler, Ph.D.thesis,Hamburg Univ.1978,DESY internal report F14-78/01 (unpublished)
25. E.Lohrmann, in Proceedings of the 1977 Intern.Symp.on Lepton and Photon Interactions (F.Gutbrod, ed.),Hamburg 1977, p.641
26. S.Yamada, in Proceedings of the 1977 Intern.Symp.on Lepton and Photon Interactions (F.Gutbrod,ed.),Hamburg 1977, p.69
27. G.Wolf, this conference

28. Particle Data Group, N.Barash-Schmidt, Rev.Mod.Phys.48,No.2, Part II (1976)

29. PLUTO-collaboration, G.Alexander et al.,Phys.Lett.73B(1978)99

30. W.Wagner, Ph.D.thesis, Aachen Univ.(1978)(unpublished)

31. H.Fritsch, Phys.Lett.67B (1977) 451

32. W.Herb et al.,Phys.Rev.Lett. 39 (1977) 252; L.Lederman, this conference

33. PLUTO-collaboration, Ch.Berger et al.,DESY report 78/21 (1978)(to be published in Phys.Lett.B)

FUTURE PROJECTS IN FRASCATI:

1. ALA STORAGE RING.

2. MDA EXPERIMENT FOR ALA.

G.C. BARBARINO

Istituto Nazionale di Fisica Nucleare, Sezione di Napoli, and

Laboratori Nazionali dell'INFN, Frascati, Italia.

ABSTRACT

A proposal is given of the high luminosity e^+e^- storage ring and the experiment for it to investigate the physics in the C.M. energy interval between 1 and 2.4. GeV.

On présente une proposition d'anneau de collision e^+e^- a haute luminosité et de l'experimentation associeé qui permet d'étudier la phisique pour des valeurs de C.M. énergie comprises entre 1 et 2.4 GeV.

1.1 Why are we looking to the 1-2 GeV energy region?

In the last months there have been very interesting results from many laboratories. The principal contributions come from $e^+ e^-$ colliding beams[1] and photoproduction experiment[2]; there are evidences of structures also in $\bar{p}p$ states[3]. The following table summarizes the observed resonances in this energy region.

M (MeV)	Γ (MeV)	experiment
1097	31	Desy- Frascati γp
1266	110	Desy- Frascati γp
1470	10	Adone $e^+ e^-$
1498	4	Adone $e^+ e^-$
1462	190	DCI $e^+ e^-$
1662	25	DCI $e^+ e^-$
1676	170	DCI $e^+ e^-$
1769	53	DCI $e^+ e^-$
1792	79	Adone $e^+ e^-$
1812	34	Adone $e^+ e^-$
2130	30	Adone $e^+ e^-$
1930	9	
2020	24	in $\bar{p}p$
2204	16	

All these measurement show that there is a very rich field of physics in the 1-2 GeV mass region. According to Veneziano Mass formula, some of these resonances might be interpreted as radial excitation of ρ, ω, ϕ mesons. In this outline a tentative energy mass position assignement might be:

ϕ family (ϕ': 1498, 1470? ↑ K decays ?) (ϕ'': 1812 ↑ K decays ?) (ϕ''': 2130 ↑ K seen)

(narrow resonances)

ρ family (ρ': 1250) (ρ'': 1550)

(even number of π)

ω': 1350? ω'': 1769

ω family

(odd numbers of π)

However the experimental informations are generally poor and many questions at the moment are open:

- decay modes are not well known.
- $\phi(\lambda\bar{\lambda})$ spectroscopy might be like $\Psi(c\bar{c})$ spectroscopy
- nature of these structures: recurrences of ρ, ω, ϕ or $N\bar{N}$ bound states?

1.2 The luminosities of the colliding beams machines available between 1-2GeV C.M. energy is shown in fig.1.1.

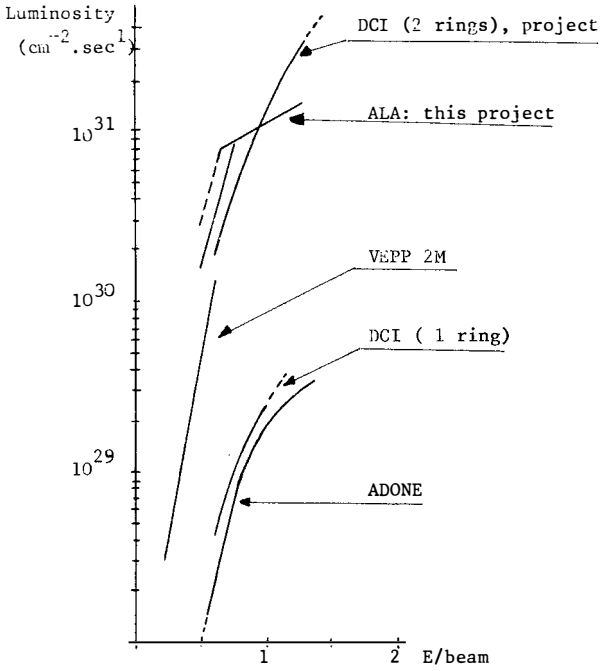

In the same picture and in the following are presented the main features of the proposed machine ALA. The new ring could have a luminosity from one to two orders of magnitude higher than that obteinable from machines presently operating in the same energy range.

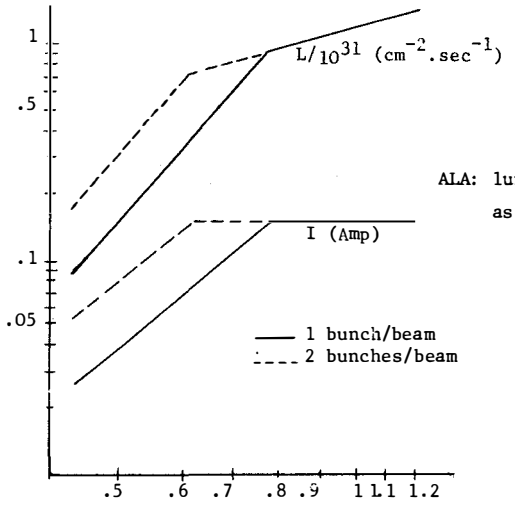

ALA: luminosity and total current as function of energy.

MACHINE CHARACTERISTICS					
Energy (GeV)	.5	.62	.78	1	1.2
Luminosity $x10^{31}$ ($cm^{-2}s^{-1}$) .. 1 bunch	.15	.36	.90	1.17	1.4
.. 2 bunch	.30	.72	.90	-	-
Total current (mA) .. 1 bunch/beam	40	75	150	150	150
.. 2 bunches/beam	80	150	150	-	-
Lifetime (hours)	16	14	12	11	10
C.M. energy resolution (FWHM, MeV)	.45	.69	1.10	1.80	2.59
r.m.s. bunch length (250 KV) (mm)	49	67	95	103	117
Experimental straight section length (m)			3		
Orbit length (m)			70		
Radiofrequency system MHz [a]			51,4		

INJECTION[b]	Direct from LIN.AC	Through ADONE
Positron injection rate (mA/min)	5	30
Electron injection rate (mA/min)	150	-

ALA: Parameter Summary

Supposing to work on ALA for 17 hours/day with a large solid angle apparatus the expected counting rates are:

multihadronic events $\sim$15.000 evs/day ; ϕ' (1500) $\sim$ 7500 evs/day; ϕ''(1800) $\sim$7500 evs/day; ρ'' (1550)$\sim$ 12000 evs/day.

2.1 MDA experiment for ALA (FRASCATI- NAPLES-PISA collaboration)

spokesman: G. Bellettini.

The general features of this apparatus are:

-large solid angle.

-longitudinal magnetic field.

-high efficiency for low energy photon (as low as 50 MeV)

-good π K separation.

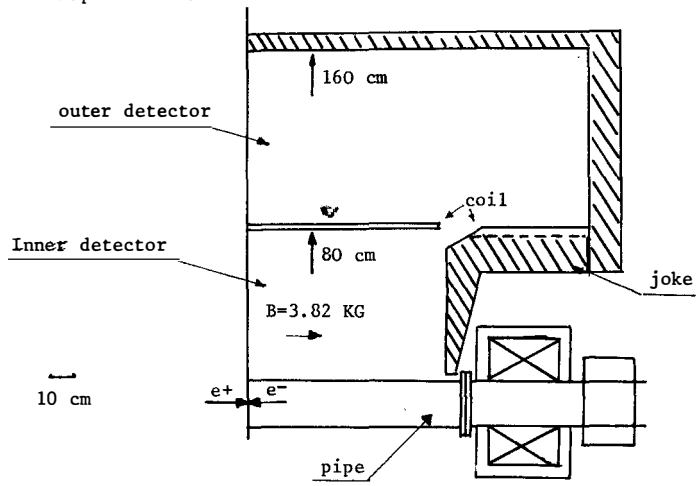

2.2 Inner detector: kinematical region.$\vec{B}$ and wires

-B: 3.82 KGauss (solenoid) - coil radius: 80cm

-Joke radius: 160 cm -max local disuniformity: 3-5%

Inside the coil:

-10 drift chambers, 96 sense wires/chamber along beam axis 0.8-5 cm. spacing; - 5 of them give information on second coordinate by current division. In total there are:

1000 drift time read out, 1000 charge read out

β measurement.

-time of flight between 2 hodoscopes of scintillation counters allowes identification of π and K on 80 cm. path inside the coil. In the worse condition ($p \sim 500$ MeV/c) the difference between the time of flight is $\sim$1nsec. The resolution required is $\pm$300psec.

Features of kinematical region

$\frac{\Delta p}{p^2} \lesssim 5\% \rightarrow \frac{\Delta p}{p} \sim 2\%$ at typical momentum emerging multihadrons.

$\frac{\Delta\Omega}{4\pi} \sim 90\%$ $\sigma_{Tof} \pm 300$ ps

2.3 Outer detector: particle identification region.

It can be made in two ways:

resistive tube calorimeter:

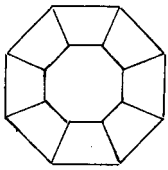

-8 telescopes arranged in quasi cylindrical geometry $\frac{\Delta\Omega}{4\pi} \sim 80\%$

- each is made of 20 resistive tubes layers in quasi-Geiger mode operation interlived the same numbers of Pb sheet plus Pb-scintillator sandwiches (total r.l.=8)

tubes array

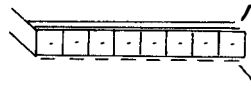

figures of this calorimeter are:

-High accuracy in shower vertex localization (1 cm) and photon direction measurement

-poor energy measurement (worse than 50%)

liquid argon calorimeter

4000 channels in the same geometry

-each is made of 32 wired- or strips

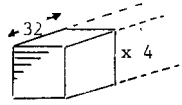

repeated in depth 4 times. The H.V. plates are divided into strips 2.5 cm wide and with a 3.2mm spacing (in total 4.r.l.)

Calculated resolution for γ's

E (MeV)	σ
50	10%
100	7%
500	3%

figures of this calorimeter are:

- high energy resolution
- good π k identification: in the worse condition, p=500 MeV/c the overlap is $\leq$ 8%
- poor γ direction measurement.

Both calorimeter will be tested. The apparatus will also be have a μ filter and a tagging system for $\gamma\gamma$ events.

2.4 Typical efficiencies of this apparatus

for $4\pi^{\pm}$ events: at least 3 prongs seen	90% (geometrical)
	80% (reconstructed event)
the worse case: $2\pi^{\pm}2\pi^{\circ}$ at least 3prongs	76% (geometrical)
seen of which 2 charged	60% (reconstructed event)

NOTES AND REFERENCES

1) C. Bemporad and F.Laplanche talks given at the 1977 Intern. Symposium on lepton and photon interaction at High Energies-Hamburg, August 1977.
2) S. Bartalucci et al; Desy report 77/59. An additional evidence for the presence of a resonance at M 2130 MeV in the Kπ Kπ mass spectrum, comes from the CORNELL LAME exp. The data were presented by L.Hand at the Hamburg Symposium, August 1977.
3) V. Chaloupka et al..; Phys. Letters 61B, 487 (1976)
W. Brückner et al.; Phys. Letters 67 B, 222 (1977)
P. Benkheiri et al.; Phys. Letters 68 B, 483 (1977)
For a review see Montanet, talk given at the 5° Intern. Conf. on Experimental Meson Spectroscopy, Boston, 1977, CERN preprint EP/Phys. 77-22 (1977).

a) Machine performance could be further improved by raising the R.F. frequency. At higher frequency would shorten the bunch leugth (which is itself an advantage for physics experiments) allowing also to increase the luminosity.
b) From the machine point of view, injection using ADONE as booster is preferable.

PHOTOPRODUCTION IN THE CERN Ω SPECTROMETER.

F. Richard

Introduction.

Since August 1977 a British-French-German collaboration has been taking data with a tagged photon beam ($20 < k < 72$ GeV/c) and with a large solid angle device, the Ω spectrometer. The results which I will present in this talk are still preliminary and are based on 15 % of our data. In the final experiment we will reach a sensitivity of 70 to 100 events per nanobarn.

I. Experimental set up.

a) The γ beam is obtained in two stages : we produce an electron beam ($p \rightarrow \pi^\circ \rightarrow \gamma \rightarrow e$) which is analyzed and transported to the Ω ; we then convert these electrons into a beam of photons. Electrons' momentum and direction are accurately measured before and after radiation giving the direction and momentum of the photon.

This method has the advantage of giving a pure and well defined photon beam at the expense of intensity. The main caracteristics of the beam are listed in table I.

Protons	210 GeV/c
Electrons	80 GeV/c
$\Delta p/p$	± 2 %
e/p	$3\ 10^{-6}$
Radiator	7.6 %
γ/e	6 %
Vert spot size at Ω	20 mm
Horiz. spot size at Ω	40 mm
Tagging accuracy (σ)	2 mm

TABLE I

We usually work with $2\ 10^5$ γ/spill.
Comparing the Ω measurement and the energy predicted we presently find $\sigma_E \simeq 400$ MeV. The best possible figure is like 200 to 300 MeV.

b) The Ω apparatus is a well known set up (fig. 1). The main improvements from the PS set up are :

- High precision chambers in the beam region.
- Two lever arm drift chambers at the exit of the magnet.
- A large lead glass detector covering a surface of about 7 m^2. Photons are converted in 3 Xo of lead glass. Their position is measured horizontally and vertically in two hodoscopes of 800 scintillators giving an accuracy of σ = 4 mm. The shower is then absorbed in an array of 340 blocs of 20 Xo of lead glass 14 x 14 cm^2 each. π° and η (fig. 2) are measured with this device. The electron signature is obtained by cut on the energy deposited in the first 3 Xo of lead glass and by comparing the total energy deposited to the momentum found in the spectrometer. The rejection factor against pions is already better than 1000. In order to increase the acceptance to electrons we have reduced the nominal value of the bending power to 3 Tesla-meter.

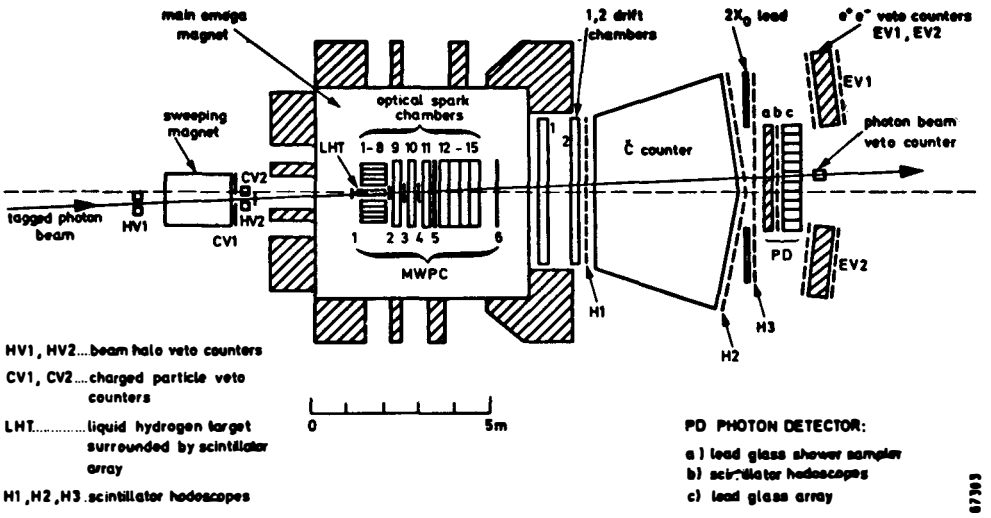

LAYOUT OF THE OMEGA SPECTROMETER FOR PHOTOPRODUCTION EXPERIMENTS

Fig. 1. Ω set up for this experiment.

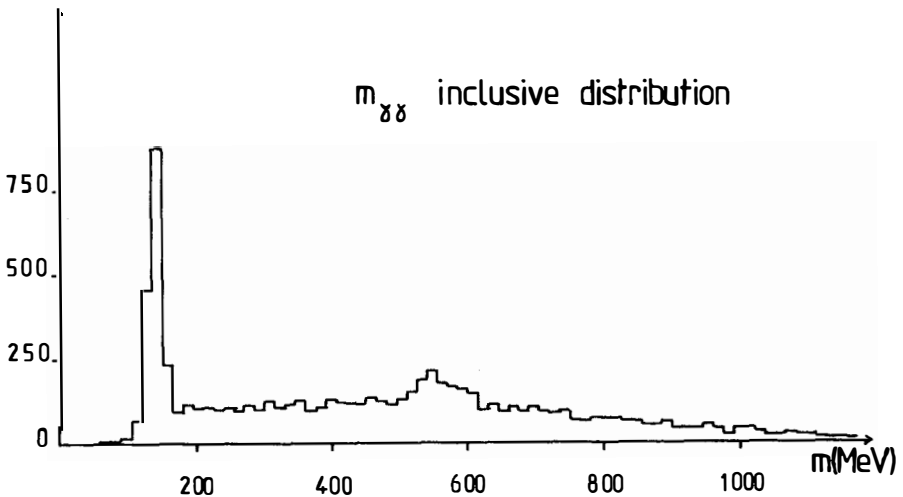

Fig. 2. $\gamma\gamma$ mass distribution. Both γ have more than 3 GeV and combinatorial background is eliminated (i.e. γ giving a π° with an other γ having less than 3 GeV is not used).

c) We trigger selectively on hadron interactions : the requirement is four charged particles at the target plus the same requirement 1.3 m downstream. Our trigger cross section is of 65 μb and 80 % of these triggers are hadronic

Other triggers :
- 3 prongs
- $p\bar{p}$, k^+k^-
- High $p_\perp\gamma$

II. Exclusive channels.

Elastic events are defined by energy balance within ± 1 GeV. The recoil proton is not required, due to limited detection efficiency around the target, so that no $p_\perp$ balance cut is added.

a) k^+k^- , $p\bar{p}$.

In both cases we ask for double identification, this means :

$$5.5 < p_k < 16 \text{ GeV/c}$$
$$20 < p_p < 33 \text{ GeV/c}$$

which puts a severe limitation on acceptances.

Mass distributions in k^+k^- are shown in fig. 3 and fig. 4 indicating a strong ϕ signal and two secondary bumps at 1270 MeV and 1500 MeV. In $p\bar{p}$, we see a clear threshold enhancement (fig. 5) with a cross section of 40 ± 15 nb.

A carefull study of Cerenkov inefficiencies, using the $\gamma p \to \rho p$ reaction, was performed. We concluded that ρ misidentified will reflect as a small bump at 1270 MeV in k^+k^- and at 2000 MeV in $p\bar{p}$ (see fig. 5).

b) $\pi^+\pi^-\pi^+\pi^-$, $\pi^+\pi^-\pi^+\pi^-\pi^+\pi^-$.

In four prongs a bump is seen at the ρ' mass (fig. 6) superimposed on a broad "background". The region of the bump (M < 1.7 GeV) is more peripheral with a t slope of 5 GeV^{-2} than the rest which has a slope of 3 GeV^{-2}. Since we expect $\rho' \to \rho^\circ\pi^+\pi^-$, we cut in the ρ region and use a substraction method with the result shown in fig. 7 . The $\rho\pi\pi$ channel above the ρ' region shows an indication of a $A_1\pi$ contribution (fig. 8) Renard and Layssac[1] using a VDM model have indeed predicted a large coupling of the photon to $A_1\pi$.

The 6π mass distribution is displayed in fig. 9 . A sphericity analysis has been performed on the 6π in their center of mass showing, at masses above 3 GeV, a clear non spherical behaviour. The effect is manifest in fig. 9 bis where $\langle p^*_\perp \rangle$ and $\langle p^{*2}_\perp \rangle$ variations versus $m6\pi$ are clearly different. Further investigations of this jet-like structure is underway and fits rather well with theoretical predictions à la Feynman and Field.

Such a behaviour could allow some elimination of the non resonant background.

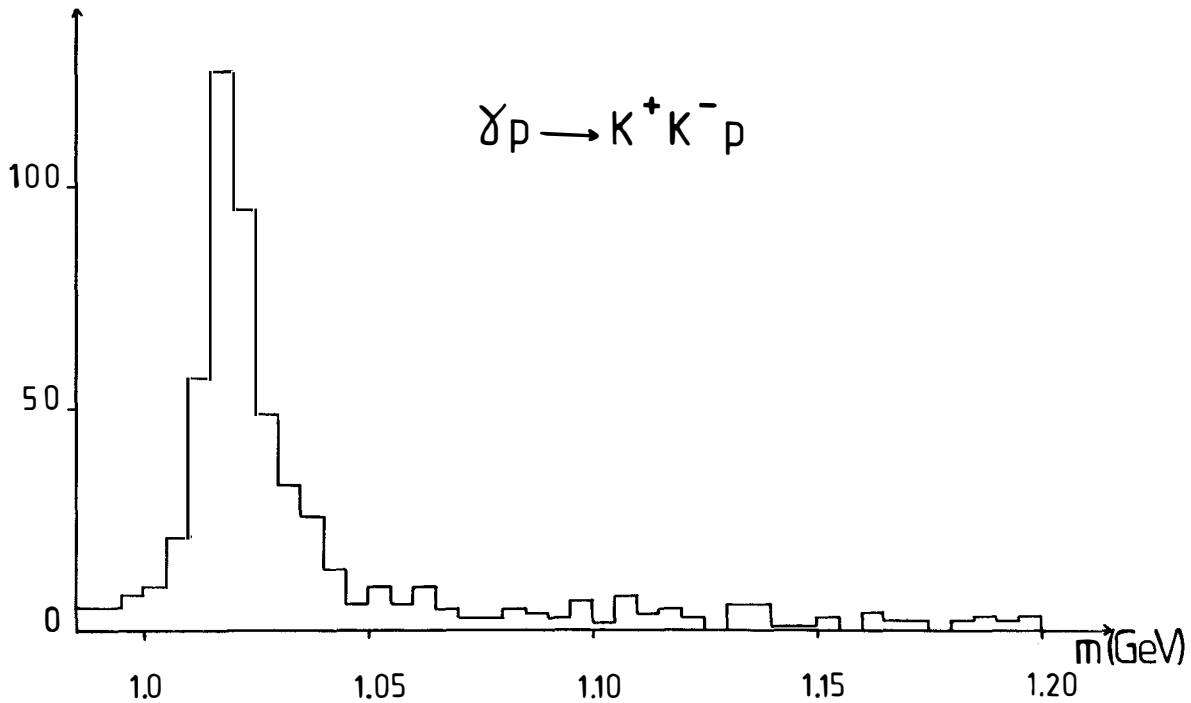

Fig. 3. k^+k^- mass distribution for elastic events in the region of the ϕ

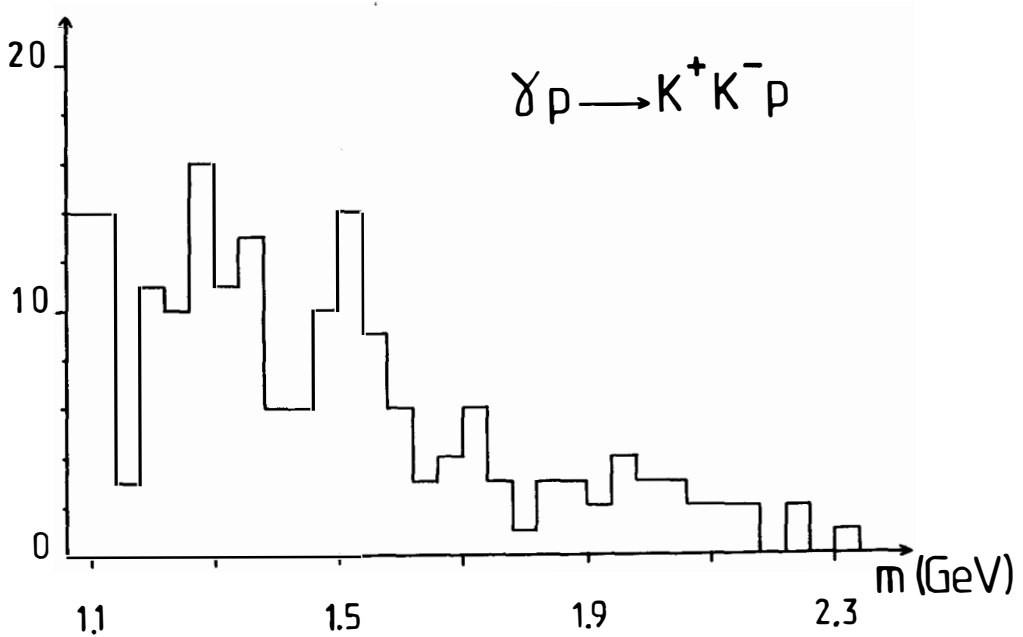

Fig. 4. k^+k^- mass distribution for elastic events with three prongs seen, above the ϕ. The enhancement seen at 1270 MeV could be due to a reflexion from misidentified ρ events.

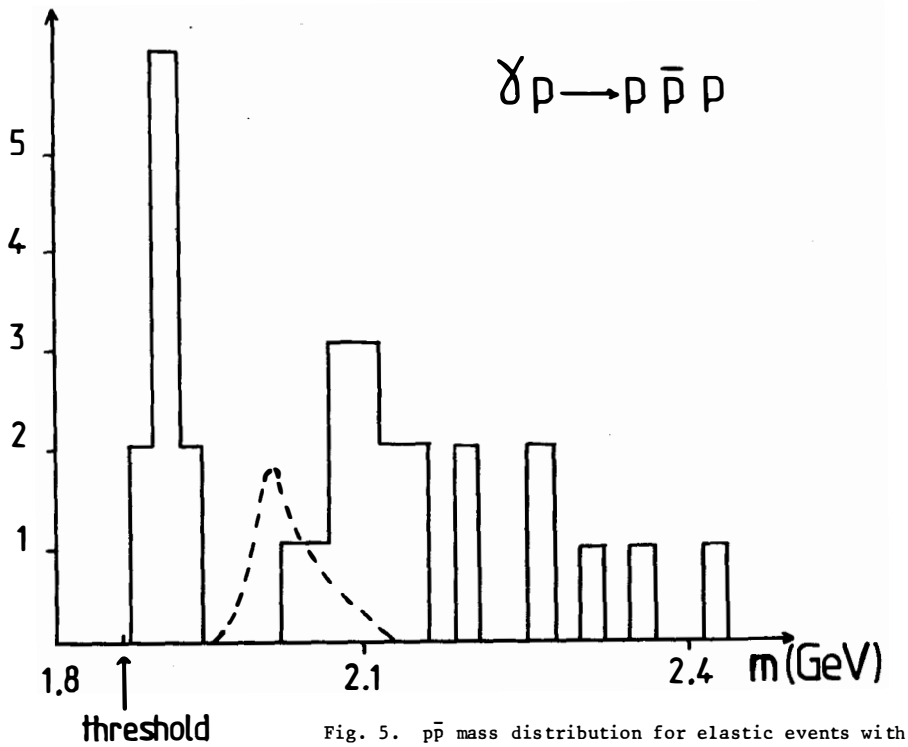

Fig. 5. $p\bar{p}$ mass distribution for elastic events with $20 \lesssim |\vec{P}_{p,\bar{p}}| \lesssim 33$ GeV/c. The dotted curve represents our estimate for the reflexion coming from misidentified ρ events.

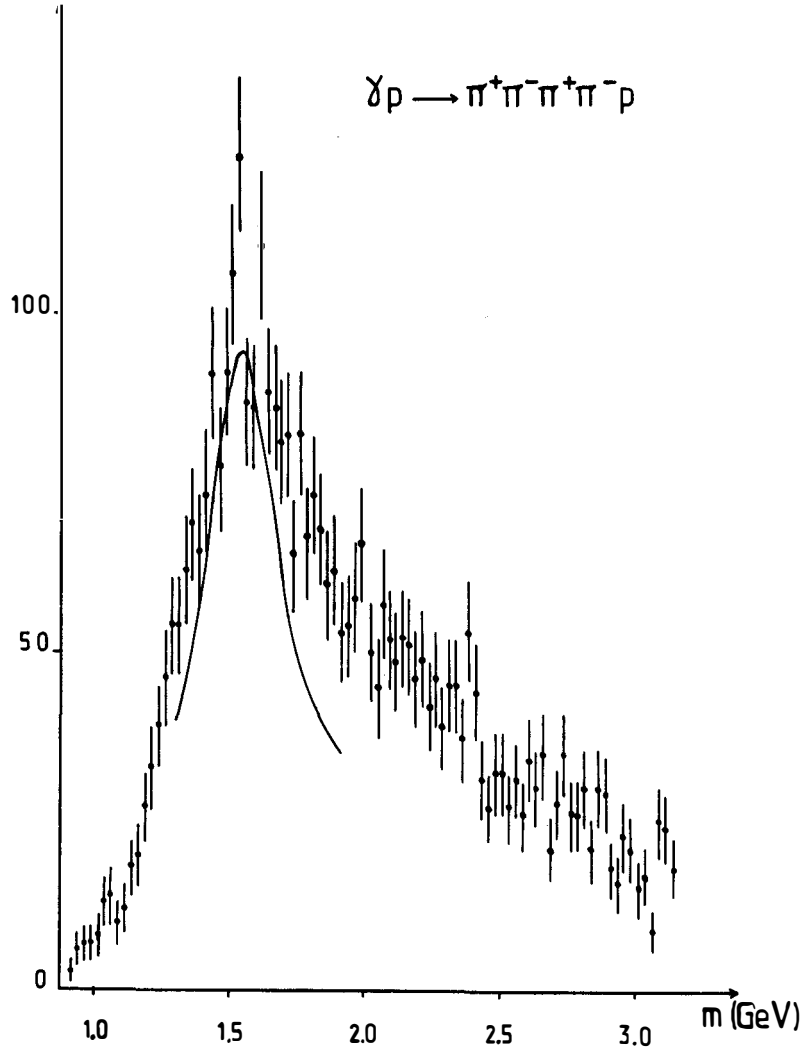

Fig. 6. $\pi^+\pi^-\pi^+\pi^-$ mass distribution for elastic events. The curve represents a one resonance fit to the e^+e^- data from DCI.

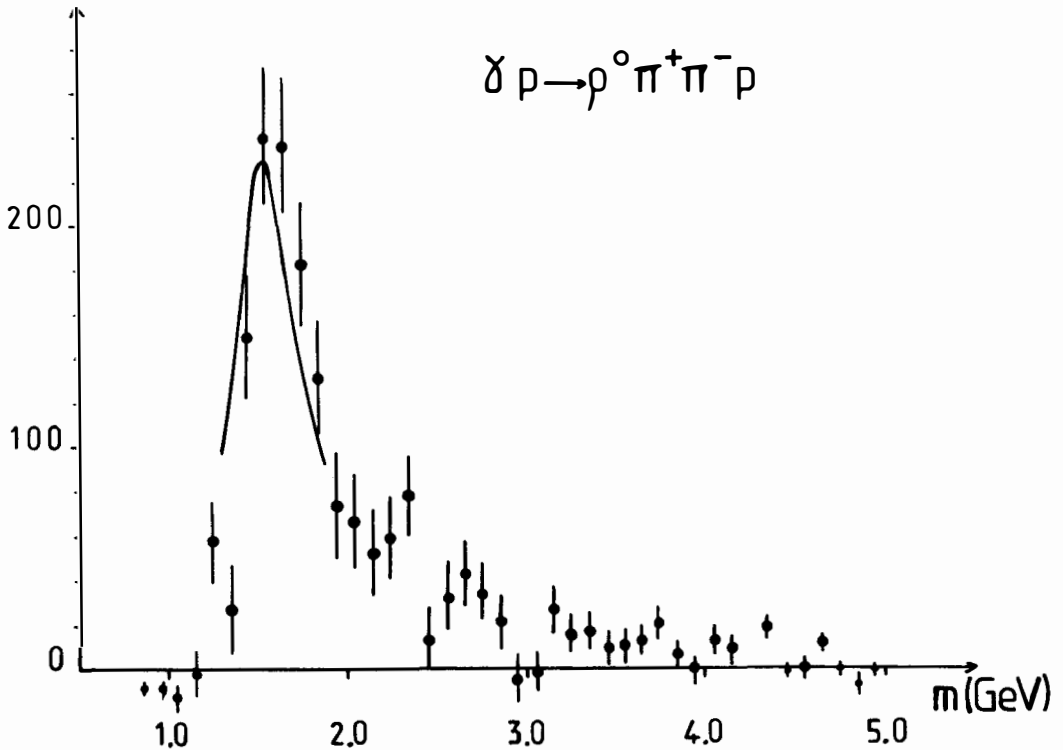

Fig. 7. $\pi^+\pi^-\pi^+\pi^-$ mass distribution for elastic events showing a ρ° combination. A background substraction is obtained by using events giving $\pi^+\pi^-$ masses in the vicinity of the ρ. The curve represents a one resonance fit to the e^+e^- data from DCI.

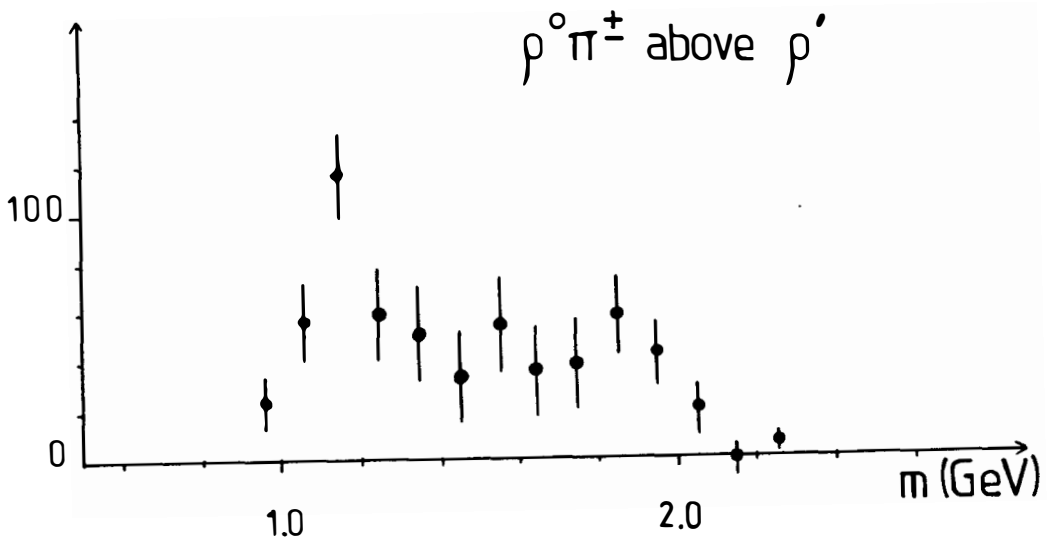

Fig. 8. $\rho^{\circ}\pi^{\pm}$ mass combinations corresponding to events falling outside the ρ' region : $2 < M_{4\pi} < 2.5$ GeV.

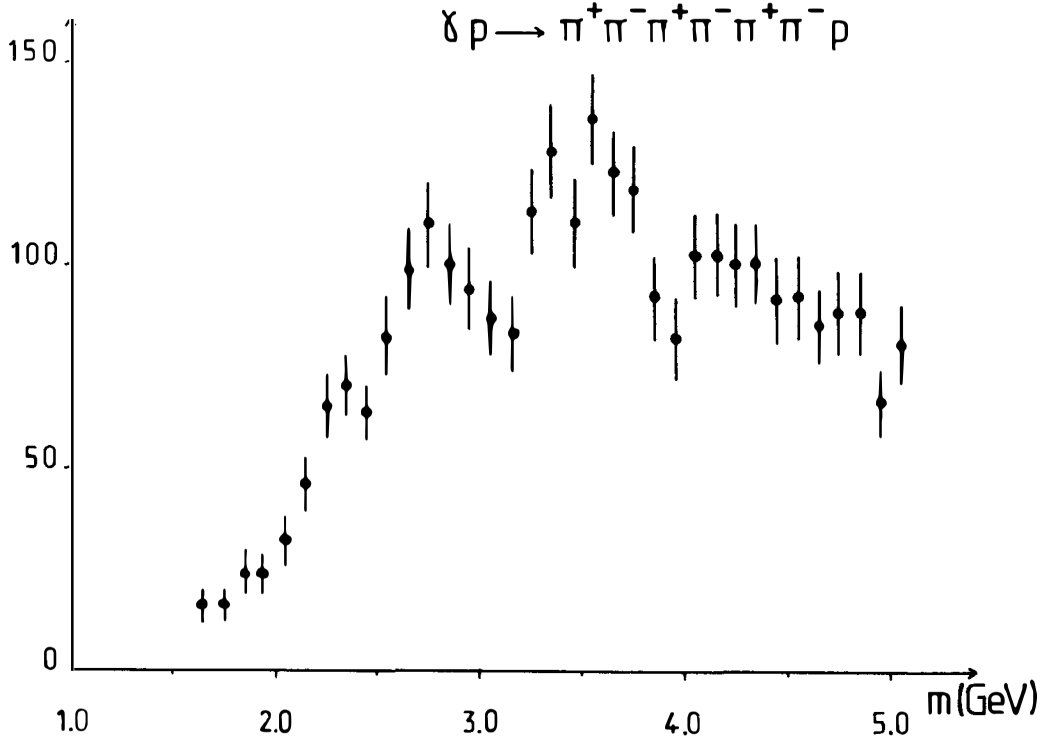

Fig. 9. $\pi^+\pi^-\pi^+\pi^-\pi^+\pi^-$ mass distribution for elastic events.

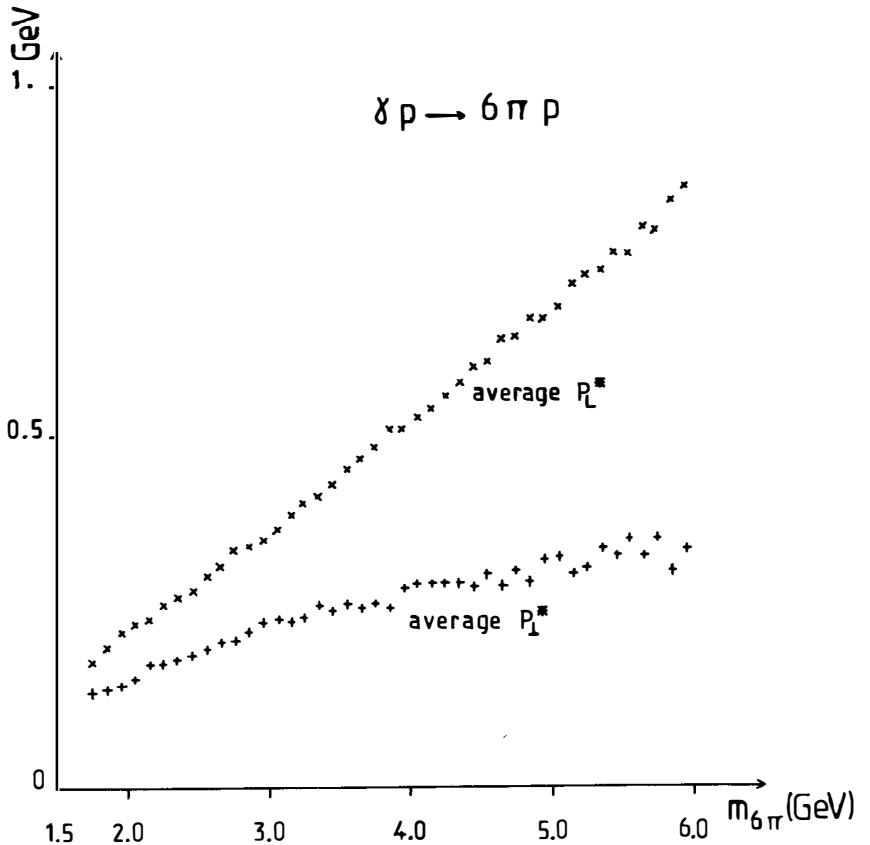

Fig. 9 bis. Average longitudinal p_L^* and transverse momenta $p_\perp^*$ with respect to the sphericity axis plotted versus the mass of the 6π system.

We indeed observe an increase in the average sphericity at the ρ' mass in 4π. In fig. 10 we show the 6π mass distribution at low momentum transfer with a cut on sphericity.

Spin parity analysis[12] using $\vec{p}\pi^+ + \vec{p}\pi^+$ as an analyzer in the s channel helicity frame confirms the 1^- nature of the observed bump (fig. 11). The background is not structureless and gives a negative contribution to $< Y_2^\circ >$. It is of interest to note a similarity between the structures observed in 6π, and those appearing in $< Y_2^\circ >$.

III. Charm.

Although we expect a relatively large charm total cross section of 1 μb, charm "visibility", that is to say the number of events we can identify, reconstruct and separate from the combinatorial background, is quite small.

To reduce the combinatorial background we look at $D^\circ \to k^-\pi^+$ channel. Very crudely, we expect :

$$\sigma_{charm} \times \frac{D}{all} \times BR\ (D \to k\pi) \times K\ detection \times Trigger \times Reconstruction = 1.4\ nb$$

800 nb .5 .02 .5 .6 .6

From this estimate we get a feeling for the visibility for a particular channel. In the data so far analyzed, we should see about 20 $k^-\pi^+$ from charm. Fig. 12 shows the raw data where we have already 40 events per 20 MeV bin in that region. We then demand a leading D with large x or equivalently small momentum transfer t between γ and D : $|t| < 1.5\ GeV^2$. This cut, which reduces considerably the background, assumes that charm quarks are photoproduced in some kind of Drell mechanism :

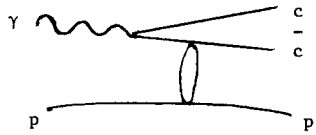

where we expect one of the c to be fast to minimize the propagator appearing in this process.

Furthermore we have eliminated events with slow π which experimentally dominate in the high mass $k\pi$ combinations. We do this by putting a cut on the center of mass decay angle of the D : $\cos\theta^* > -.30$. In fig. 13, we can see the result of these cuts on the background and notice an accumulation of eight events in a mass bin of 20 MeV centered at 1870 MeV. Since we do not know the production mechanism and thus the effect of our different cuts it is hard to make a good guess on the total cross section. It should not be, at least, much smaller than 1 μb.

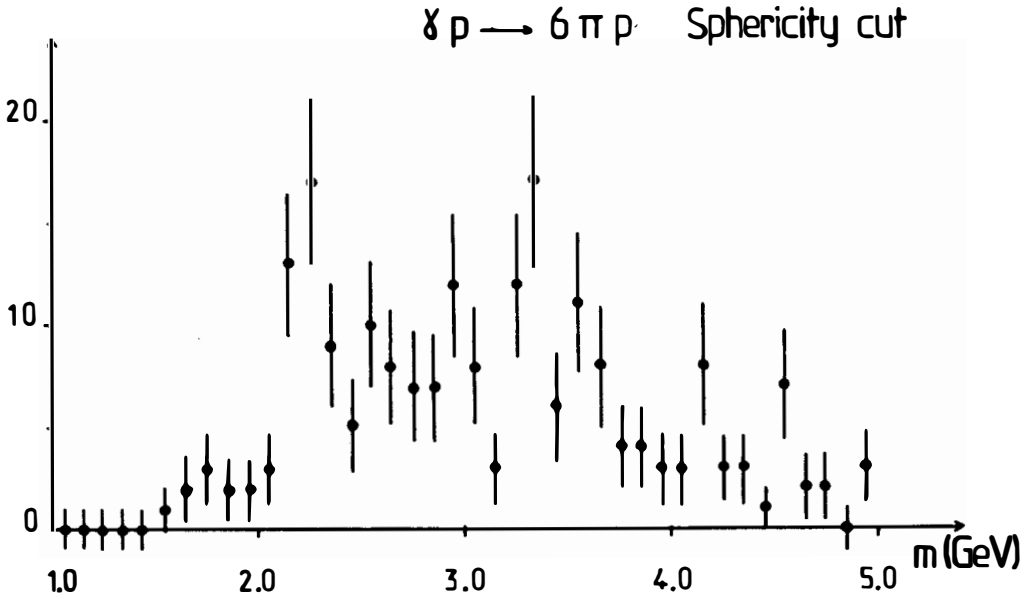

Fig. 10. $\pi^+\pi^-\pi^+\pi^-\pi^+\pi^-$ mass distribution for elastic events with sphericity between .5 and .7 .

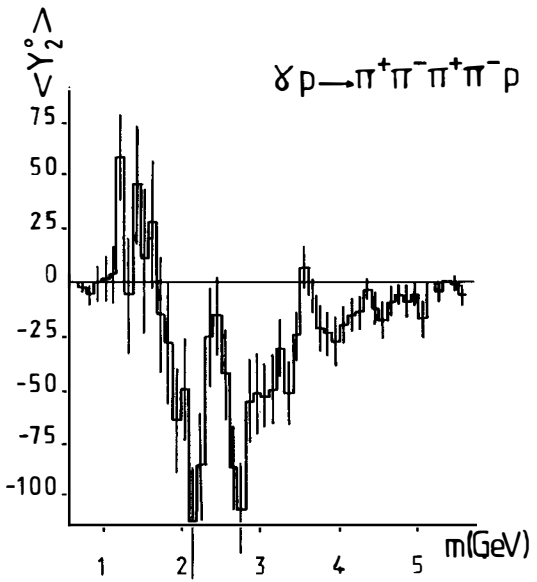

Fig. 11. $\langle Y_2^0 \rangle$, the p wave momentum , versus the 4π mass. We take $\vec{p}\pi_+ + \vec{p}'\pi_+$ as an analyser in the s channel helicity frame.

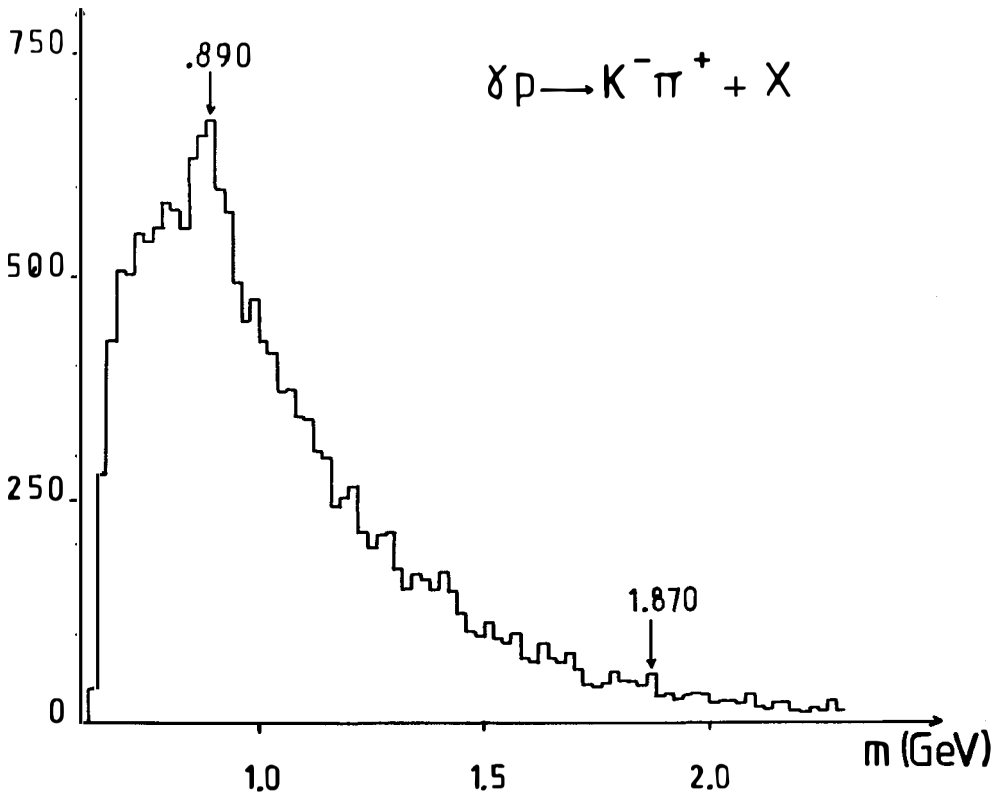

Fig. 12. Inclusive $k^{-}\pi^{+}$ mass distribution. The bin size is 20 MeV.

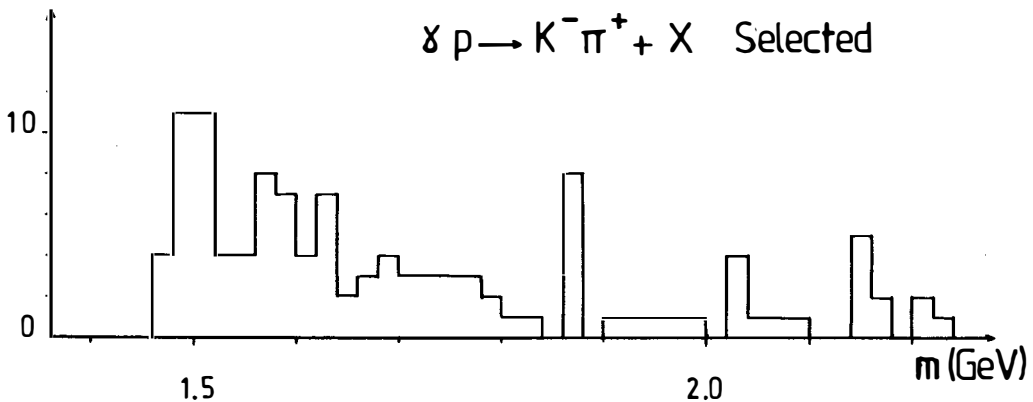

Fig. 13. Inclusive $k^-\pi^+$ mass distribution in the high mass region after the following cuts : $|t| < 1.5$ GeV^2 where $t = (k - p_D)^2$
$\cos \theta^* > -.3$ where θ^* is the π angle with respect to the direction of the D in the center of mass.

Summary and conclusion :

- The data suggest a resonance in k^+k^- at 1500 MeV.
- $p\bar{p}$ is photoproduced with $\sim$ 40 nb cross section mainly near threshold.
- 4π data show the $\rho' \rightarrow \rho\pi\pi$ resonance.
- 6π, and through spin parity analysis 4π, suggest a series of structures above 2 GeV.
- Charm, in $k^-\pi^+$, seems present at the expected level.
- π° detection is operating and will allow to increase the number of channels explored.
- With fives times more statistics and with significantly better analysis, we should explore rare resonances (ϕ') and a wider variety of charm channels.

References.

|1| Lettere al Nuovo Cimento 1, 197 (1971).

|2| G. Smadja et al. LBL report 991.

RESULTS OF A BEAM DUMP EXPERIMENT AT THE CERN SPS NEUTRINO FACILITY

T. HANSL, M. HOLDER, J. KNOBLOCH, J. MAY, H.P. PAAR, P. PALAZZI, F. RANJARD, D. SCHLATTER, J. STEINBERGER, H. SUTER, W. Von RUDEN, H. WAHL, S. WHITAKER, E.G.H. WILLIAMS,
CERN, Geneva

F. EISELE, K. KLEINKNECHT, H. LIERL, G. SPAHN, H.J. WILLUTZKI,
Institut für Physik der Universität, Dortmund

W. DORTH, F. DYDAK, C. GEWENIGER, V. HEPP, K. TITTEL, J. WOTSCHACK,
Institut für Hochenergiephysik der Universität, Heidelberg

P. BLOCH, B. DEVAUX, S. LOUCATOS, J. MAILLARD, B. PEYAUD, J. RANDER, A. SAVOY-NAVARRO, R. TURLAY,
DPhPE, CEN-Saclay

F.L. NAVARRIA,
Istituto di Fisica dell'Universita, Bologna.

SUMMARY

We report results from a beam dump experiment performed at the CERN SPS facility. An excess of electron- and muon-neutrinos has been observed. This new source of prompt neutrinos gives $2\ 10^{-7}$ ν_e or $\bar{\nu}_e$ per incident proton with $E_\nu > 20$ GeV and neutrino angle smaller than 1.85 mrad. A possible explanation would be the pair production of charmed meson $D\bar{D}$ with an inclusive cross section of the order of 40 μb.

RESUME

Dans une expérience de Beam Dump utilisant un des faisceaux du SPS au CERN, nous avons observé un excès de neutrinos-électron et de neutrinos-muon. La nouvelle source de neutrinos ainsi mise en évidence donne $2\ 10^{-7}$ ν_e par proton incident pour une énergie de neutrino supérieure à 20 GeV et un angle de production inférieur à 1,85 milliradians. L'explication la plus probable est la production en paire de mésons charmés $D\bar{D}$ avec une section efficace inclusive de l'ordre de 40 microbarns.

1. INTRODUCTION

The Beam Dump experiment [1,2,3] at the CERN SPS Neutrino facility was performed to search for long-lived neutral particles promptly produced at the target.

New types of penetrating particles could be produced either directly in the primary interaction in the target or in the decay of short-lived particles.

Such processes had been suggested recently by several experiments :

i) Part of the dimuon and trimuon events detected in high energy neutrino experiments [4] might be explained as due to the interaction of new neutrinos, coupled to new heavy leptons.

ii) The existence of the τ lepton [5] implies the existence of a τ neutrino. A large production of ν_τ in the Dump would give an abnormal ratio of muonless to charged current events.

Axion production [6] might also be detected in such an experiment.

To be sensitive to such a small source of prompt neutrinos, one has to suppress the conventional beam component of ν_μ induced by π and K decay.

This was obtained by using a large copper target where the secondary pions and kaons were absorbed so that the ν fluxes were reduced by $\sim$ 3000 [7].

The CDHS detector [8] recorded events provided the energy deposition was larger than $\sim$ 7 GeV.

Events were retained if they occured in a fiducial volume (9.3 m of iron, 1.6 m Ø) corresponding to a target mass of $\sim$ 580 tons. In the final sample a cut in visible energy was applied above 20 GeV. In these conditions and after double scan for event selection, we obtain the final event numbers summarized in Table I.

2. MULTIMUON EVENTS

We observed 6 dimuon events in the fiducial volume. The rate of dimuons relative to charged current interactions above 30 GeV is

Table I

Summary of event numbers

Number of protons E > 20 GeV		
Single muon events	μ^-	850
	μ^+	187
Dimuon events*		6
Trimuon events		0
Muonless events**		372

* E_{vis} > 30 GeV

** Fiducial cuts and selection criteria are different from single muon analysis.

The quoted numbers differ from those of a previous publication[15] because of some data overlooked in a first scan.

Table II

Summary of muonless event numbers

Observed muonless events	372 ± 30
Expected NC events from ν_μ (435 * 0.3)	130 ± 10
Expected muonless events from known ν_e in the beam	45 ± 15
New source	197 ± 35

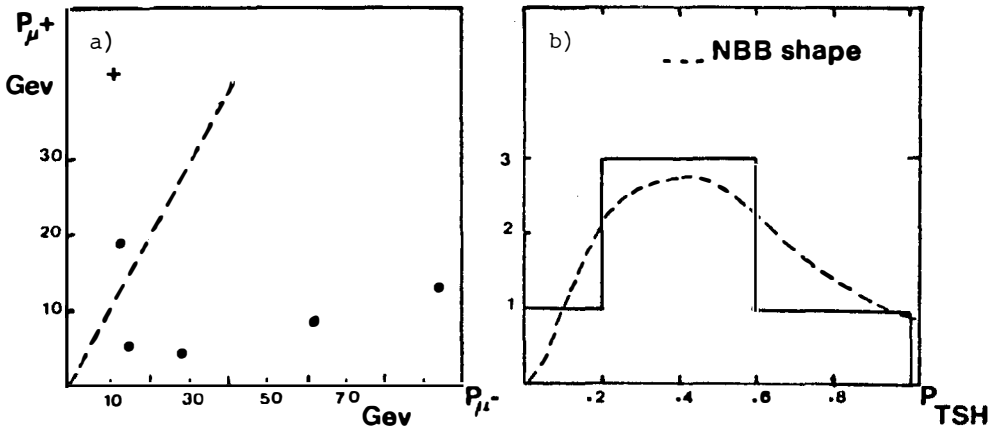

Figure 1 a) $P_{\mu-}$ versus $P_{\mu+}$ plot of the dimuon events.
b) Transverse momentum of the non-leading muon relative to the shower axis. The dashed line is the distribution observed in the narrow Band Beam data[4].

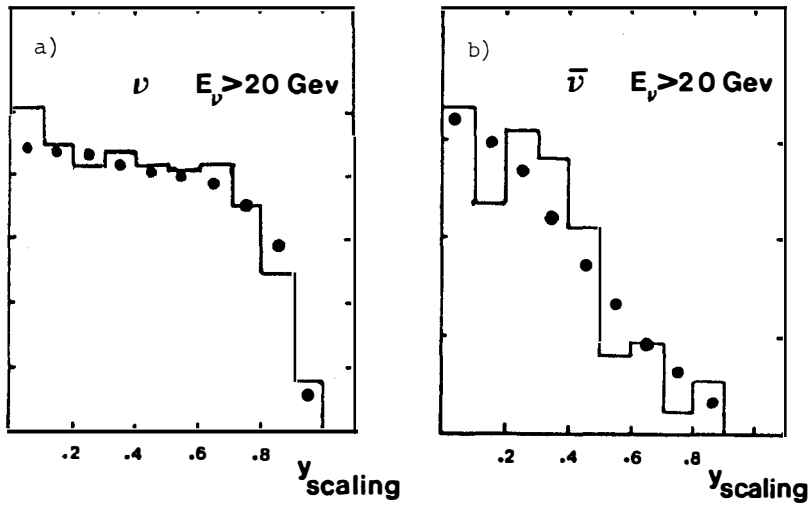

Figure 2 Y distribution of the neutrino (a) and antineutrino (b) single muon events. The dots show the prediction of a Monte-Carlo simulation including 16 % antiquarks.

$$\frac{N(\mu^+\mu^-)}{N(\mu)} = (0.7 \pm 0.3)\ \%$$

This ratio is not in disagreement with the measured rate in the Narrow Band Beam Data [9]. The kinematical distributions of the dimuon events are shown in Fig. 1.

We do not observe any trimuon event. In order to give upper limits on multimuon production by new neutrinos, we compare the rate of multimuons in the Beam Dump and in the Wide Band Beam running.

In the same detector, using the same trigger and the same energy of the primary protons (400 GeV), we have recorded :

$$\sim 1500 \text{ dimuons and } 12 \text{ trimuons}$$

corresponding to 2.10^{17} protons on the target [10].

We can conclude that, in the Wide Band Beam sample, less than 0.3 % of the dimuons and less than 10 % of the trimuons (90 % CL) are due to prompt neutrinos.

3. SINGLE MUON EVENTS

A total number of 850 μ^- charged current and 187 μ^+ charged current interactions with $P_\mu > 5$ GeV/c has been selected. The x and y scaling distributions are compatible with those observed in other neutrino beams (Figure 2).

The energy spectrum of the single muon events is drawn in Figure 3. The expected neutrino and antineutrino fluxes due to the remaining background of π and K decay[+] are also shown. Absolute flux is difficult to compute. However, we think that the relative flux of antineutrinos to neutrinos is estimated with a reasonable accuracy. The expected ratio (0.14 ± 0.015) is not compatible with the measured ratio (0.22 ± 0.02). This shows an excess of antineutrino interactions which has to be attributed to prompt antineutrinos. In the following we will see that there is a reason to believe that this new source gives as many neutrinos as antineutrinos. If this is assumed and if we use the experimental cross section ratio [11] $\sigma_{\bar{\nu}}/\sigma_\nu = 0.48$, we find of prompt signal of $210 \pm 86\ \nu_\mu$ and $91 \pm 40\ \bar{\nu}_\mu$.

+) We wish to thank Dr. H. Wachsmuth for making these calculations available to us.

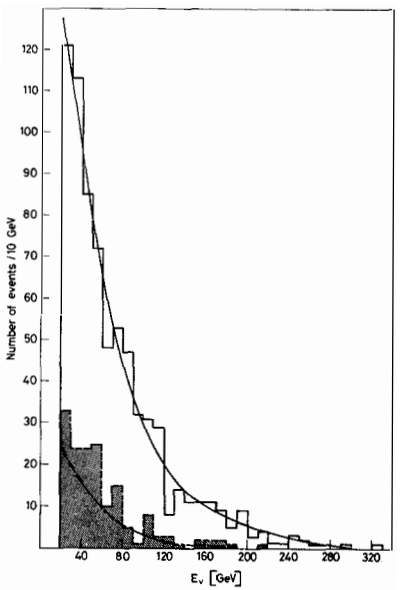

Figure 3 :

Total visible energy spectra for single μ^- (upper histogram) and single μ^+ events (shaded histogram) compared to the expectations from π- and K-decay neutrinos normalized to the total number of negative muons.

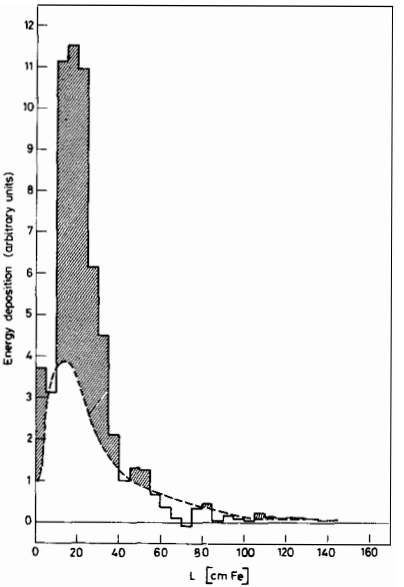

Figure 4 :

Longitudinal shower development in the iron calorimeter for excess muonless events compare to the shape of hadronic showers (dashed curve) as measured by single muon events.

4. MUONLESS EVENTS

Muonless events have been analysed using the standard technique already used in our detector [12] : without any requirement on muon reconstruction, all events with shower energy larger than 20 GeV are classified according to their penetration length in iron. The fiducial volume is $\sim$ 70 % of the one used in the single muon analysis.

We find 372 $\pm$ 30 muonless events and 435 $\pm$ 27 muon events giving a ratio

$$R = \frac{\text{muonless}}{\geq 1 \text{ muon}} = 0.86 \pm 0.08$$

This ratio has to be corrected for the interaction of $\nu_e/\bar{\nu}_e$ in the beam due to Ke_3 and hyperon decays. However this correction cannot account for the difference with respect to the ratio R = 0.30 $\pm$ 0.01 measured in ν_μ beam [12].

The known contributions to the signal are summarized in Table II. It can be seen that there remain 197 $\pm$ 35 muonless events which are not ν_μ or $\bar{\nu}_\mu$ neutral current events. These events could be interpreted as :

i) ν_e interactions due to a prompt source :
In our detector electrons induce electromagnetic showers which are seen as muonless events,

ii) ν_τ interactions :
Charged current interactions of ν_τ produce τ leptons which decay with emission of either hadrons, electrons or muons : [5]

$$\nu_\tau + N \rightarrow \tau + X$$
$$\rightarrow \text{hadrons} + \nu_\tau \sim 60\ \% \quad \Big\} \quad 80\ \% \text{ muonless events}$$
$$\rightarrow e + \nu_e + \nu_\tau \sim 20\ \% \quad \Big\}$$
$$\rightarrow \mu + \nu_\mu + \nu_\tau \sim 20\ \%$$

iii) If axions [13] exist, with properties similar to those of π^0's, their interaction in iron would produce hadrons much as neutral current events of neutrinos.

It is important to note that in the case i) a large fraction of the energy is transferred to the electromagnetic shower. On the contrary in hypotheses ii) and iii) most of the energy goes into the hadronic part.

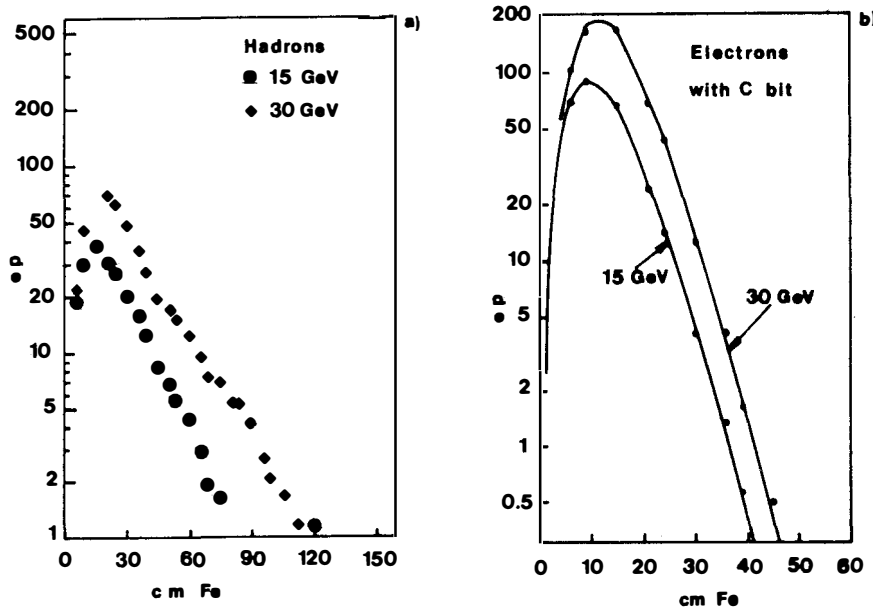

Fig. 5A

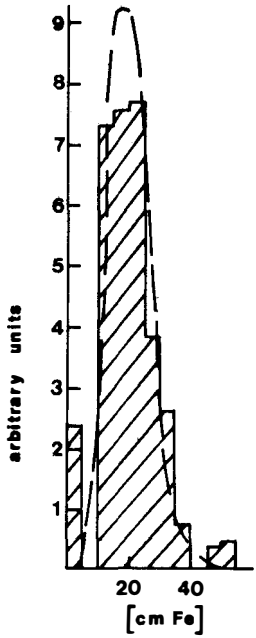

Fig. 5B

Figure 5A :

Longitudinal development of hadronic showers induced by π^-(a) and electromagnetic showers induced by electrons (b) at 15 and 30 GeV in the test calorimeter[10]

Figure 5B :

Comparison of the pulse height not due to hadronic showers with the shape of purely electromagnetic showers.

In iron, as the radiation length (1.7 cm) is substantially smaller than the interaction length (18 cm), the longitudinal shower development looks different for electromagnetic and hadronic showers. We have compared the shower development of the excess events (solid curve in Figure 4) to that observed in ν_μ charged current interactions (dashed curve). The early shower development is clearly different : normalizing the two plots for thicknesses above 40 cm, we find that only 57 % of the visible energy can be attributed to hadron showers (including π° component). The remaining 43 % (dashed area) can be attributed to electromagnetic showers. The shape of this excess is in agreement with the development observed for electron induced showers measured with a test calorimeter [14] in an electron beam (Figure 5).

This large fraction of electromagnetic energy is expected from ν_e ($\bar{\nu}_e$) interactions and in disagreement with the ν_τ and axion hypotheses.

Using the ratio R = 0.3 and taking into account the cut $E_{shower} > 20$ GeV, we conclude that we observe a prompt signal of 171 ± 31 charged current (e^+, e^-) events and 26 ± 5 neutral current (ν_e, $\bar{\nu}_e$) events.

5. SUMMARY

Adjusting the muonless sample to the same fiducial volume as for the single muon sample, we obtain :

$$N_{\nu_e} + N_{\bar{\nu}_e} = 236 \pm 40$$

$$N_{\nu_\mu} + N_{\bar{\nu}_\mu} = 301 \pm 126^{+)} \ .$$

The magnitudes of the two signals are compatible with equal fluxes of prompt muon and electron neutrinos. If we assume further an equal number of prompt ν_e and $\bar{\nu}_e$ in the beam, then taking into account the difference in the cross section

$$N_{\nu_e} = 158 \pm 27 \ , \qquad N_{\bar{\nu}_e} = 78 \pm 14 \ .$$

The absolute number of prompt ν_e within the angular acceptance of the detector (1.85 mrad) and with the cut $E_{shower} > 20$ GeV may be computed on the basis of this result, the neutrino cross-section

+) This number is obtained assuming equality of prompt ν_μ and $\bar{\nu}_\mu$ fluxes, see section 3.

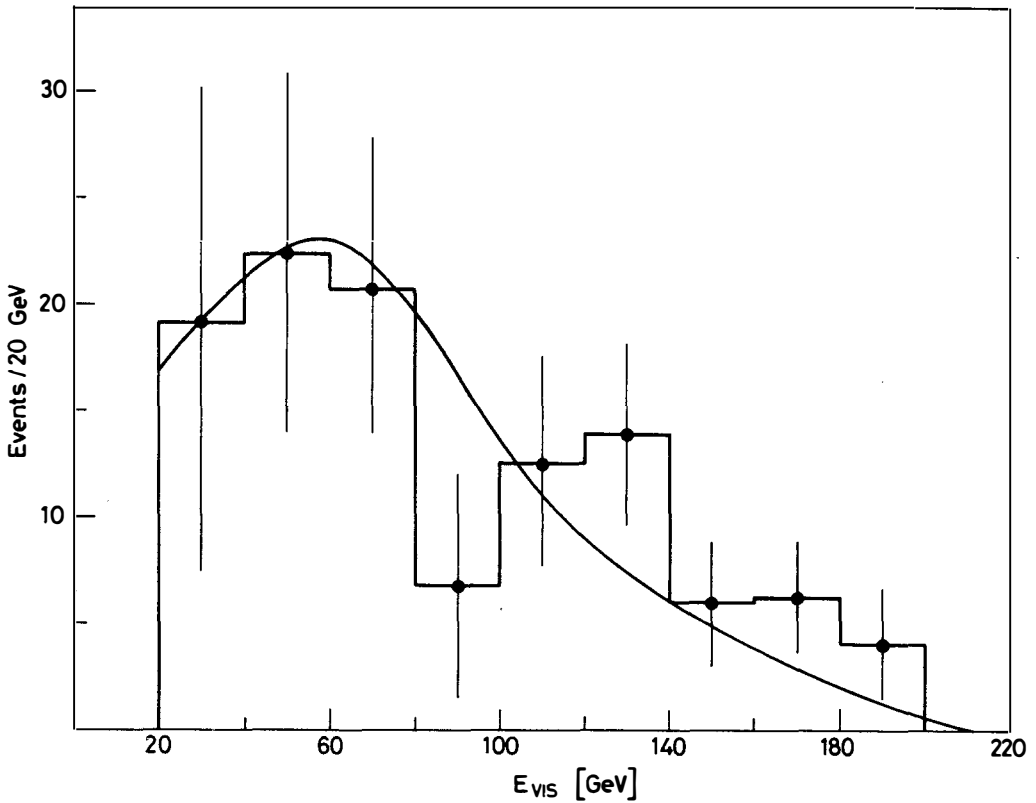

Figure 6 : Total visible energy distribution for the charged current events from prompt ν_e and $\bar{\nu}_e$. The line shows the prediction of our charm pair production model.

and the measured proton flux :

$$N_{\nu_e}/\text{incident proton} = (1.9 \pm 0.4)\ 10^{-7}$$

The prompt flux may also be compared to ν_μ flux from K decay. We attribute to $K_{\mu 2}$ decay 367 $\pm$ 39 events so that

$$N_{\nu_e}/N_{\nu_K} = 158/367 = 0.43 \pm 0.09$$

6. INTERPRETATION

The only known process, which might be the origin of this prompt neutrino flux, is the production of charmed particles. Approximately 20 % of charmed mesons decay semi-leptonically, giving equal fluxes of electron and muon neutrinos, as supported by the data.

In order to make cross-section estimates, we need additional assumptions on production mechanisms as our detector covers only a small fraction of the phase space in the forward direction.

We have used a simple model for $D\bar{D}$ pair production :

- invariant cross section [16]

$$\frac{d^2\sigma}{dx_F\ dp_T^2} \propto (1 - x_F)^3\ e^{-\alpha p_T^2}$$

  where x_F is the Feynman variable and $\langle p_T \rangle$ = 0.7 GeV/c

- equal branching ratio

  BR ($D \to K\mu\nu$) = BR ($D \to K^*\mu\nu$) = 10 %

  BR ($D \to Ke\nu$) = BR ($D \to K^*e\nu$) = 10 %

The computed energy spectrum of the neutrinos is in agreement with the visible energy distribution of the excess muonless events (Figure 6).

Then, using the observed ratio of ν_μ from K decay to prompt ν_e events, we can give an estimate of the inclusive cross section for $pp \to D\bar{D}$ relative to kaon production at 400 GeV :

$$\sigma(pp \to D\bar{D}) = \frac{N_{\nu_e}}{N_{\nu_K}} * \frac{\varepsilon(\nu_\mu K)}{\varepsilon(\nu_e D)} * \sigma(pp \to K) \qquad \text{where } \varepsilon \text{ is the acceptance of the detector}$$

$$\simeq 3.10^{-3} * \sigma(pp \to K)$$

Using $\sigma(pp \to K)$ = 13 mb we find that the charm production cross section is of the order of 40 µb per nucleon. If we assume different production mechanisms, this number may easily change by a factor two.

One should note that $\sigma(pp \rightarrow K)$ infers a $A^{2/3}$ dependence for the cross-section.

Finally, the data can be used to set upper limits on axion production. From geometric acceptance of our detector for π°, we obtain

$$\sigma(pN \rightarrow a^\circ) * \sigma(a^\circ N \rightarrow X) < 10^{-67} \text{ cm}^4 \quad (90 \text{ \% CL}).$$

The production rate of axions relative to π° would be

$$\left(\frac{n_{a^\circ}}{n_{\pi^\circ}}\right) < 0.5\ 10^{-8} \quad (90 \text{ \% CL}).$$

REFERENCES

1) B. Pontecorvo, IUPAP Conference, Balatonfüred, 1975.
2) M. Schwartz, Report on Progress in Physics, XXVII, 75 (1965).
3) D. FRYBERGER et al., Science News 100, 252 (1971).
4) A. Benvenutti et al., Phys. Rev. Letters 38 (1977) 1110.
5) M.L. Perl, Intern. Symposium on Lepton and Photon Interactions at High Energies, Hamburg, 1977.
6) S. Weinberg, Phys. Rev. Letters 40 (1978) 223.
7) Dr. Wernhart, this conference, Review of BEBC results from the CERN Beam Dump experiment.
8) M. Holder et al., Nuclear Instr. Met. 148 (1978) 235.
9) M. Holder et al., Phys. Letters 69B (1977) 377.
10) T. Hansl et al., Characteristics of trimuon events in neutrino interactions (to be published).
    See also J. Knobloch, in "Neutrinos-78" Intern. Conf. on Neutrino Physics and Neutrino Astrophysics, Purdue Univ., 1978 : "Trimuons in CDHS experiment".
11) Results of CDHS Charged Current analysis, see for example H. Wahl, "Neutrinos-78".
12) M. Holder et al., Phys. Letters 71B (1977) 222.
13) S. Weinberg, Phys. Rev. Letters 40 (1978) 223.
14) M. Holder et al., Nuclear Instr. Met. 151 (1978) 69.
15) T. Hansl et al., Phys. Letters 74B (1978) 139.
16) G.J. Feldman, SLAC PUB 2068/1977.

BEAM DUMP EXPERIMENT AT 400 GeV

GARGAMELLE COLLABORATION

(Aachen, Bari, Bergen, Brussels, CERN, Ecole Polytechnique Palaiseau, Milano, LAL Orsay, Strasbourg, UCL London) presented by

F. JACQUET

Ecole Polytechnique - Palaiseau

ABSTRACT

Results on the beam dump experiment using Gargamelle are presented. An excess of ν_e , $\bar{\nu}_e$ production is found corresponding to a production of $\frac{\delta N_{\nu_e}}{\delta \Omega} = 4.6\ 10^{-2}$ per proton and per steradian in the forward direction.

Some models for D $\bar{D}$ production are discussed and a comparison with other experiments is made.

RESUME

Les résultats sur l'expérience beam dump utilisant Gargamelle sont présentés. Un excès d'événements ν_e , $\bar{\nu}_e$ est mis en évidence, correspondant à une production de $\frac{\delta N_{\nu_e}}{\delta \Omega} = 4.6\ 10^{-2}$ vers l'avant par proton et par stéradian.

Des modèles de production de D $\bar{D}$ sont discutés et les résultats sont comparés à ceux d'autres expériences.

The beam dump experiment (ref.1) has been performed to look at the reaction

$$p\ p \rightarrow (\ ) \rightarrow \nu + \ldots$$

Gargamelle was filled with heavy freon C F_3 Br (radiation length = 11 cm). The fiducial volume was 7 m^3 corresponding to 10 tons of detector. Around 70 000 pictures have been taken corresponding to 3.5×10^{17} incoming protons. With this dump experiment the classical source of neutrino events is reduced by a factor $\sim$ 2 000 (compared to the usual wide band beam).

After the analysis the following number of events have been found (table 1) :

Table 1

	ν_μ	ν_μ or $\bar{\nu}_\mu$	$\bar{\nu}_\mu$	ν_e or $\bar{\nu}_e$	Neut.Curr.
$E_{vis} >$ 10 GeV	12	2	2	9	7
$E_{had} >$ 10 GeV	8	1	1		7
$E_{vis} >$ 10 GeV corrected	18			8.9	5.1

The main correction on the raw numbers are the following :

- 2 events have to be transferred from neutral to charged current because of the EMI efficiency (73% for E_ν = 10 GeV ; 99% for E_ν = 50 GeV)

- .1 event have to be transferred from ν_e , $\bar{\nu}_e$ to neutral current. This corresponds to the background of N C with a γ ray simulating an electron.

The expected number of ν_e , $\bar{\nu}_e$ events due to classical sources and using the ν_μ , $\bar{\nu}_\mu$ events for normalization is 1 event. So there appears a significant excess of ν_e , $\bar{\nu}_e$ events.

An origin of this excess of ν_e , $\bar{\nu}_e$ events can be the D $\bar{D}$ production in the dump. Monte-Carlo calculation using models (Bourquin-Gaillard compilation Ref.2) gives for $B = \frac{D \to \text{semi lept}}{D \to \text{all}} \approx 10\%$

$$\sigma \sim 300 \, {}^{+150}_{-100} \, \mu b \text{ (statistical error)}$$

In order to compare with D production on hydrogen and assuming that the D production cross section on a nucleus is $\sim A$, the corrected cross section on H is $\sigma \sim 300/A^{1/3} \sim 80 \, {}^{+40}_{-25} \, \mu b$.

This result appears higher than previous estimates but is model dependent.

In order to estimate the model dependence of this value a very simple formula can be used :

$$N_{\nu_{int}} = \frac{\sigma_D}{\sigma_{TOT}} B N_{p_{inc}} \frac{\theta^2}{\theta_o^2} K 2 \gamma p^{*} \qquad (1)$$

where σ_D is the D production cross section

σ_{TOT} is the pp total cross section — $\sigma_{TOT} \sim 40$ mb

B is the branching ratio $\frac{D \to \nu_e + \ldots}{D \to \text{all}}$ — $B \sim 10\%$

$N_{p_{inc}}$ is the number of incoming protons — $N_{p_{inc}} = 3.5 \, 10^{17}$

θ is the angle seenby the detector — $\theta = .75$ mrad

θ_o is the caracteristic angle of emission in the lab. for the D desintagration :

$$\theta_o^2 \sim \frac{1}{\gamma^2} (1 + \frac{p_\perp^2}{M^2})^2 \quad \text{where}$$

- $p_\perp$ is the transverse momentum of the D
- γ is the γ of the D in the lab.
- M is the mass of the D

K is a coefficient relating the number of produced ν to the number of detected ν in Gargamelle.

$$n_{\nu_{det}} = K E_\nu n_{\nu_{prod}}$$

p^{*} is the average momentum of the ν in the D frame .

Relation (1) can be expressed as follows

$$N_{\nu_{int}} = \frac{\sigma_D}{\sigma_{TOT}} \; B \; N_{p_{inc}} \; 2 \; K \; E_B^3 \; \frac{p^*}{M^3} \; x^3 \; \frac{1}{(1 + \frac{p_\perp^2}{M^2})^2} \qquad (2)$$

using $x = \frac{p_{\parallel D}}{E_B} = \frac{\gamma M}{E_B}$ (E_B is the incoming proton energy).

Fig. 1 and 2 show, using Monte-Carlo calculation, that these formulae are a very good approximation for the acceptance dependence on x and $p_\perp$. Its appears that the $p_\perp$ dependence is not very crucial (factor 30%) but the x dependence (x^3) has to be examined carrefully.

As an example an x distribution for the D like $(1 - x)^n$ gives a D cross section from 100 to 300 μb when n goes from 3 to 8. Furthermore the average observed ν energy ($< E_{\nu_{det}} >$ = 72 GeV) gives another constraint which favour n = 4 to 6.

In conclusion the model dependance for the D production can give a factor 2 to 3 in the D production cross section.

In order to compare these results with other experiments (Ref 2 and 3), the D $\bar{D}$ cross section is not used but only the ν production rate in the forward direction.

Using the following formula :

$$N_{\nu_{int}} = K \; N_{p_{inc}} \; E_\nu \; N_{\nu_{prod}} = K \; \delta\Omega \; N_{p_{inc}} \; \frac{\delta N_{\nu_{prod}}}{\delta\Omega}$$

where $N_{\nu_{prod}}$ is the number of producted ν per proton in the solid angle of the detector.

$\frac{\delta N_{\nu_{prod}}}{\delta\Omega}$ is the number of produced ν per proton and per steradian in the forward direction.

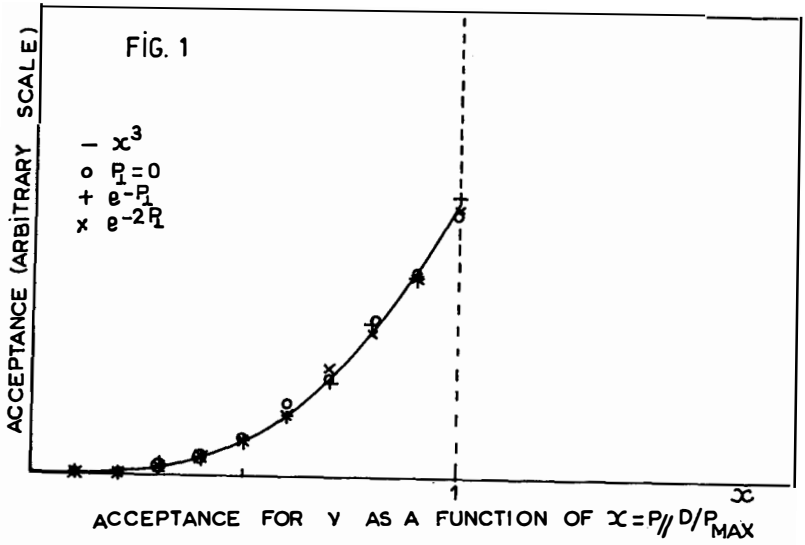
FIG. 1
— x^3
o $P_\perp = 0$
+ $e^{-P_\perp}$
× $e^{-2P_\perp}$
ACCEPTANCE (ARBITRARY SCALE)
1
x
ACCEPTANCE FOR ν AS A FUNCTION OF $x = P_{//} D/P_{MAX}$

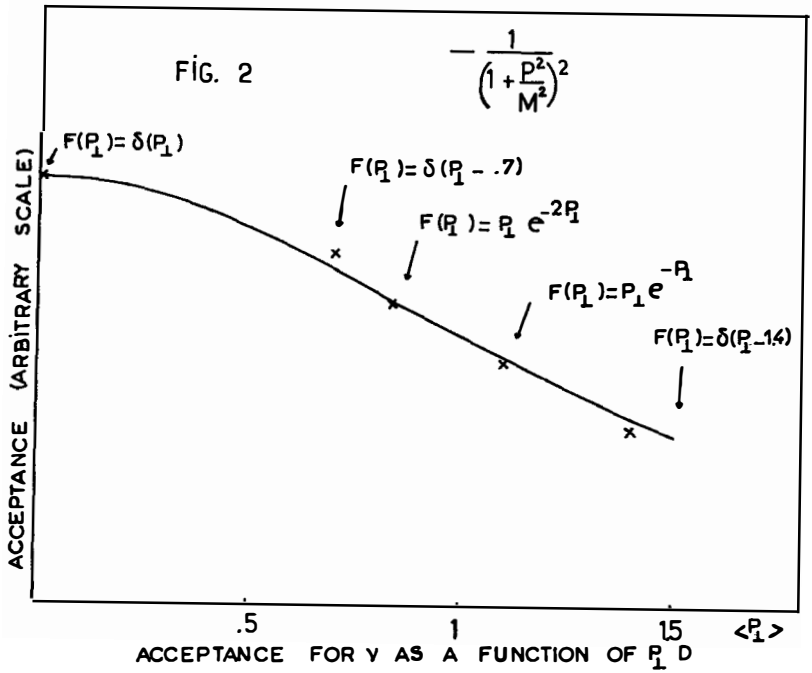
FIG. 2
$-\frac{1}{\left(1+\frac{P^2}{M^2}\right)^2}$
$F(P_\perp) = \delta(P_\perp)$
$F(P_\perp) = \delta(P_\perp - .7)$
$F(P_\perp) = P_\perp e^{-2P_\perp}$
$F(P_\perp) = P_\perp e^{-P_\perp}$
$F(P_\perp) = \delta(P_\perp - 1.4)$
ACCEPTANCE (ARBITRARY SCALE)
.5
1
1.5
$\langle P_\perp \rangle$
ACCEPTANCE FOR ν AS A FUNCTION OF $P_\perp D$

The table 2 summarizes the results of the 3 beam dump experiments

Table 2 (1)

	$\delta\Omega$ 10^{-6}	K 10^{-12}	M (TON)	$N_{p_{inc}}$ 10^{17}	$N_{\nu_e, \bar{\nu}_e}$ int	N_{ν_e} prod 10^{-7}	$\frac{\delta N_e}{\delta\Omega}$ 10^{-2}
GGM	1.71	2.45	10.5	3.5	7.3	.8	4.6
BEBC	11.2	.62	13	3.5	12	5.1	4.6
CDHS1	10.8	26.4	626	4.3			
CDHS2	10.2	20.1	450	4.3	112	1.2	1.2

A discrepancy on the number of produced in the forward direction can be observed between BEBC-GARGAMELLE and CDHS to be of the order of 3.8 ± 1.4 .

To conclude, the beam dump experiment shows that :

- there is a signicant excess of ν_e , $\bar{\nu}_e$ events
- there is no signficant excess of neutral current events
- if this excess of ν_e , $\bar{\nu}_e$ is due to D $\bar{D}$ production, the D $\bar{D}$ production cross section seems higher than previous results.

(1) The number of events $N_{\nu_e \text{ int}}$ quoted in table 2 are determined assuming the cut-off $E_{vis} > 20$ GeV. Further more we assume $N_{\nu_e \text{ prod}} = N_{\bar{\nu}_e \text{ prod}}$ and $\sigma_{\nu_e} = 2\,\sigma_{\bar{\nu}_e}$

FIGURE CAPTION

Fig. 1 Relative acceptance of Gargamelle for ν's produced by D desintegration as a function of $x = \frac{p_{\nu D}}{p_{Max}}$

Fig. 2 Relative acceptance of Gargamelle for ν's produced by D desintegration as a function of $p_{\perp}$ of the D

REFERENCES

1 ALIBRAN et al., Phys. Lett. 74B (1978) 134

2 M. BOURQUIN, J.M. GAILLARD, Phys. Lett. 59B (1975), 191
M. BOURQUIN, J.M. GAILLARD, Nucl. Phys. B114 (1976), 334

3 HANSE et al., Phys. Lett. 74B (1978), 139

4 BOSETTI et al., Phys. Lett. 74B (1978), 143.

A STUDY OF THE INTERACTIONS OF PROMPT NEUTRAL PARTICLES EMITTED FROM A BEAM DUMP AND DETECTED IN BEBC

K.L. WERNHARD
CERN, Geneva, Switzerland
Aachen-Bonn-CERN-London(I.C.)-Oxford-Saclay Collaboration

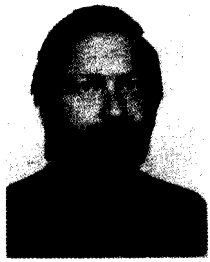

ABSTRACT

In the CERN beam dump experiment eleven e^- and four e^+ events induced by neutral primaries were observed in BEBC. This number of electron events cannot be due to electron neutrinos from conventional sources (K, Λ, Σ^- decays). The flux of the addtional (prompt) neutrinos is evaluated. Possible origins are discussed in terms of charmed particles, τ's, and as yet undiscovered particles.

RESUME

Onze événements avec un e^- et quatre événements avec un e^+ ont été trouvés dans BEBC pendant l'expérience beam dump au CERN. Ce nombre d'événements ne peut pas être expliqué par des sources conventionnelles (désintégrations de K, Λ, Σ^-). Le flux des neutrinos additionnels est évalué. L'origine est analysée en termes de particules charmées, de τ leptons et de particules pas encore découvertes.

1. INTRODUCTION

Recently a proton beam dump experiment has been performed using the CERN SPS neutrino facility. The aim of this experiment was to search for new penetrating neutral particles or neutrinos other than from π, K and hyperon decays. The flux of neutrinos from these sources was strongly reduced ($\sim$ 1/2000) by absorbing secondary particles in the large dense target (dump). Prompt neutrinos produced either directly or in the decay of particles with lifetime < 10^{-11} s are not affected by this procedure.

2. EXPERIMENTAL LAYOUT AND DETECTOR

Fig. 1 shows the experimental layout. The 400 GeV/c extracted proton beam of the CERN SPS was directed onto a copper target (27 cm in diameter and 2 m long) at zero degrees. A 1 m and a 3 m long block of iron both placed downstream of the target made sure that any flux of π and K mesons escaping from the dump did not enter the 300 m long decay tunnel. The muon shield consisted of 180 m iron and 170 m rock and earth. During the run the muon fluxes were continuously monitored at depths of 10, 30 and 50 m in the iron shield.

The bubble chamber BEBC was filled with a 72% neon-hydrogen mixture (density 0.66 g/cm^3, radiation length 44 cm). The distance between the target and the chamber was 820 m. Muons originating from interactions in the chamber were identified by the External Muon Identifier (EMI)[1] consisting of two planes of proportional wire chambers.

3. CHARACTERISTICS OF THE OBSERVED EVENTS

A total of 70 000 photographs were taken corresponding to $3.5 \cdot 10^{17}$ protons on target. The background from cosmic rays was investigated by taking 14 000 pictures without beam. The film was scanned twice for any interaction induced by a neutral primary with at least one forward-going secondary of more than 1 GeV/c. The scanning efficiency was calculated to > 98%. The relatively short radiation length made it possible to identify electrons with an efficiency > 90%. Seventy events with visible energy > 10 GeV were observed in a fiducial volume of 19 m^3 corresponding to a target mass of 13 t. Events were classified as charged currents $\mu^{\pm}$ if they contained a $\mu^{\pm}$ of momentum

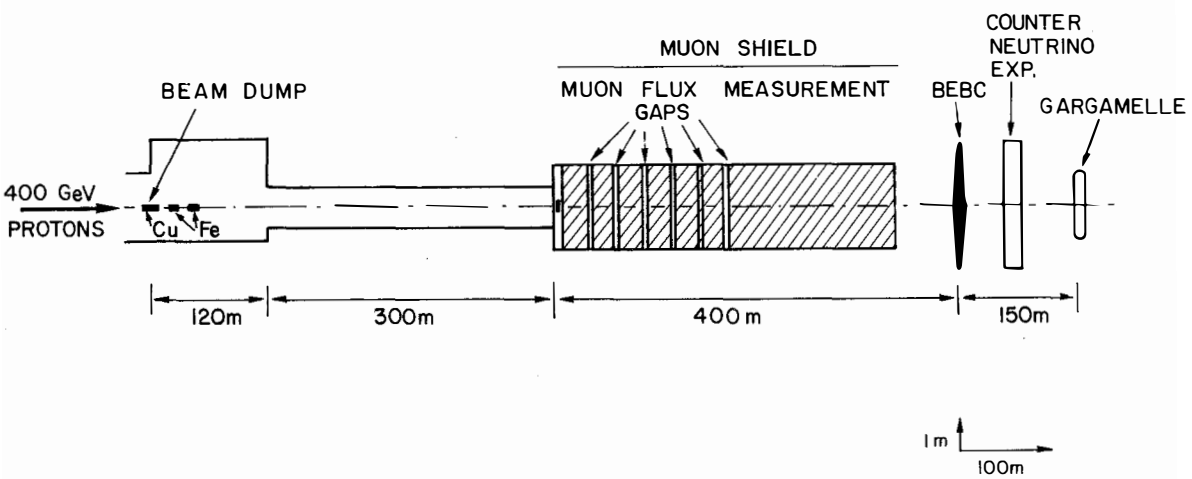

Fig. 1

Layout of the CERN SPS proton beam dump experiments

greater than 5 GeV/c identified in both EMI planes. If the secondary lepton was an electron or positron, the event was classified as $e^{\pm}$ and events with neither muon nor electron were called neutral currents (NC). The energy distributions for the five event categories is shown in fig. 2. The composition of the 70 events is given in table 1.

Table 1

NC	μ^-	μ^+	e^-	e^+
21	29	5	11	4

No abnormal V^o rate was observed. The y distributions are compatible with what one expects from (V - A) theory (flat for ν interactions and $\sim (1 - y)^2$ for $\bar{\nu}$ interactions). The ratio of neutral current over charged current events for $E_{hadron} > 15$ GeV is NC/CC = 0.42 ± 0.17. This is in agreement with the results recently published by this collaboration: $(NC/CC)_{\nu} = 0.32 \pm 0.03$ and $(NC/CC)_{\bar{\nu}} = 0.34 \pm 0.07$[2].

However, the striking feature is the large number of e^- and e^+ events relative to the number of μ^- events.

4. EXCESS OF $e^{\pm}$ EVENTS

The expected ratio of e^-/μ^- events from π and K decay neutrinos can be accurately predicted independent of absolute flux calculations. It is given by the K/π production ratio, relative Q-values, absorption lengths and branching ratios. Assuming the same production spectra for K^o and K^+ a ratio of $e^-/\mu^- = 0.06$ is obtained. To calculate the ratio e^+/μ^+ one has in addition to take into account the neutrinos from Λ and Σ^- decays. A similar calculation gives $e^+/\mu^+ = 0.1$. These ratios have errors of $\sim$ 10% due to uncertainties in the K/π production ratio and relative absorption lengths. From those ratios and the observed μ events 1.8 ± 0.4 e^- and 0.5 ± 0.25 e^+ events with $E_{vis} > 10$ GeV are expected, to be compared with eleven e^- and four e^+ events observed.

Absolute event rates have been calculated replacing the nuclear cascade in the beam dump by a decay path of one absorption length and using particle production spectra from the thermodynamical model[3] corrected in order to fit available data[4]. The predicted spectra are the curves shown in fig. 2. The

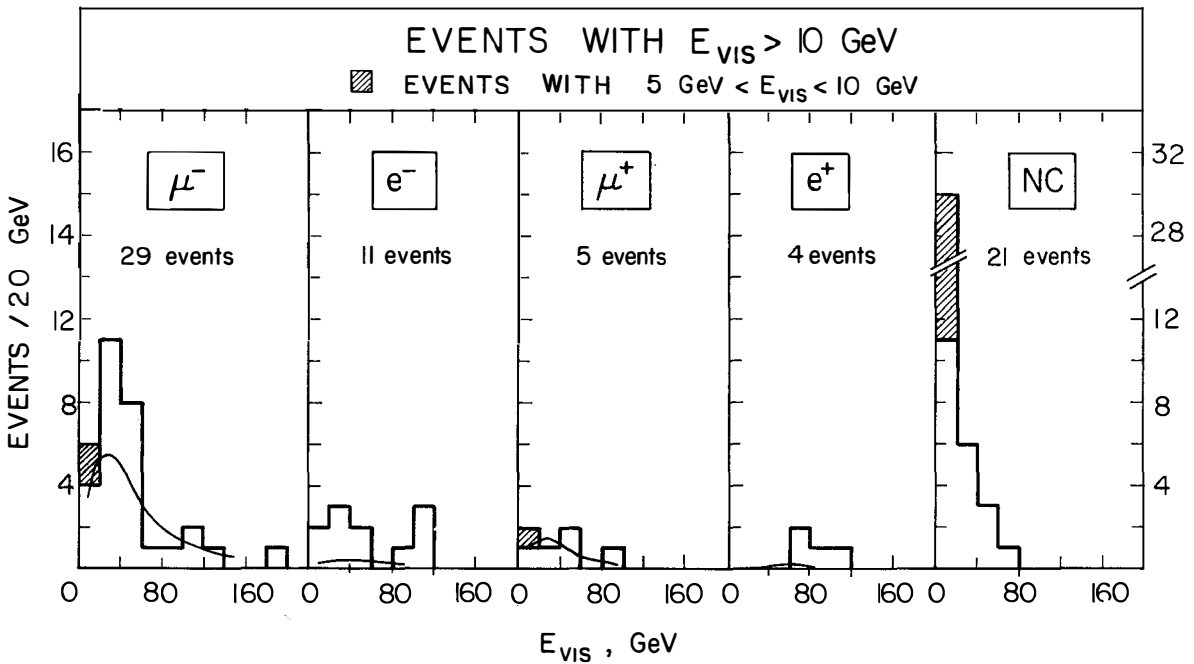

Fig. 2

Energy distribution of events. The curves are predictions from conventional sources

Narrow band beam

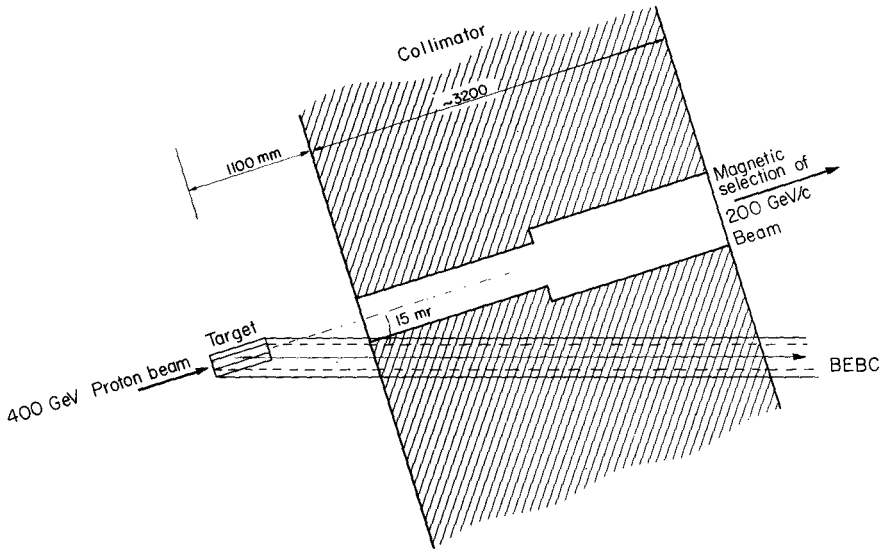

Fig. 3

Layout of narrow-band beam target and collimator

observed event rates are consistent with the assumption of equal amounts of prompt ν_μ, $\bar{\nu}_\mu$, ν_e and $\bar{\nu}_e$ fluxes.

The flux of prompt neutrinos necessary to account for the excess of e^- and e^+ events is calculated using the energy of the events and the charged current cross sections[5], $\sigma_{\nu_e} = \sigma_{\nu_\mu} = 0.6\ E\ 10^{-38}\ cm^2 = 2.1\ \sigma_{\bar{\nu}_e}$, where E is in GeV. From the known pion flux the ratios ν_e/π^+ are obtained. The results are shown in table 2.

Table 2

Fluxes of prompt neutrinos ν_e and ν_e/π^+ ratios

($\langle\nu_e\rangle = \frac{\nu_e + \bar{\nu}_e}{2}$ after subtraction of background)

E, GeV	10-50	50-90	90-130
$10^{-11} \cdot \langle\nu_e\rangle$	1.33 ± 0.6	0.83 ± 0.4	0.53 ± 0.2
$10^{4} \cdot \langle\nu_e\rangle/\pi^+$	0.34 ± 0.15	0.17 ± 0.08	0.11 ± 0.5

5. THE SKEW BEAM DUMP EXPERIMENT

Additional information on the production of these prompt neutrinos is given by the wide-band beam background (neutrinos from π and K decays before the momentum selection) in the narrow-band beam antineutrino experiment. In the narrow-band beam the neutrino parents are sign and momentum selected and wide-band background is largely reduced. The relatively large number of e^- events and μ^- events observed in the antineutrino narrow-band run could not be explained by normal wide-band background but can now be interpreted in terms of a skew beam dump experiment.

In this experiment the 400 GeV/c proton beam was directed on to the target at 15.6 mr with respect to the direction towards BEBC in order to reduce the wide-band beam background. The layout of the target and the first collimator is shown in fig. 3. This set-up represents a dump for $\sim$ 2/3 of the incident protons with an average decay path of $\sim$ 1.3 m for long lived particles produced in the target. However, prompt neutrinos will reach BEBC if they are produced within 13.8 to 17.4 mr with respect to the proton beam direction.

Fig. 4 shows the energy spectra for the observed e^- and μ^- events. It can be seen that the spectrum for the e^- events is softer than the one observed in the beam dump experiment at 0 mr. However, the calculation gives approximately equal fluxes of prompt ν_e in both experiments.

6. INTERPRETATION AND POSSIBLE SOURCES

6.1 $D\bar{D}$ production

The observed prompt neutrinos could be due to the production and semileptonic decay of charmed mesons produced in the dump. Several models for production (thermodynamical[3] and phenomenological[6,7]) have been assumed to estimate the order of magnitude of the cross section for D production. Different decay modes ($Ke\nu$, $K^*e\nu$, $K\pi\pi e\nu$) have also been considered. As a result production rates of (3 to 12) . 10^{-3} D's per incident proton are required to account for the observed $e^{\pm}$ events. This corresponds to a cross section for $pp \to D\bar{D} + X$ of 100 to 400 μb based on a total inelastic proton-proton cross section of 33 mb and neglecting cascade effects. Such large values seem to be hardly consistent with published upper limits on charm production in strong interactions[8,9].

6.2 Charmed baryons

Another possible source of prompt neutrinos could be the reaction $pp \to Y_c\bar{D}$ + anything, where Y_c is a charmed baryon. If one assumes charmed baryon production to be peaked at large x ($x = p^*_L/p^*_{L_{max}}$) then a production cross section as low as 20 μb would be enough to explain the number of e events observed. However, the observed number of events at 15 mr in the narrow-band beam experiment is inconsistent with what is expected from such a production spectrum ($N_{obs} \approx 20 \cdot N_{exp}$). It is therefore concluded that the production of charmed baryons cannot be the dominant source.

6.3 Heavy leptons

Prompt neutrinos from the decay of heavy leptons could also account for the characteristics of the observed events, but the production cross section required is of the same order as for charmed particles and this seems unlikely. In the particular case of τ's the high branching ratio for $\tau \to \nu_\tau$ + hadrons (∼ 50%[10]) would lead to an anomalously large NC/CC ratio (> 1) which is not observed.

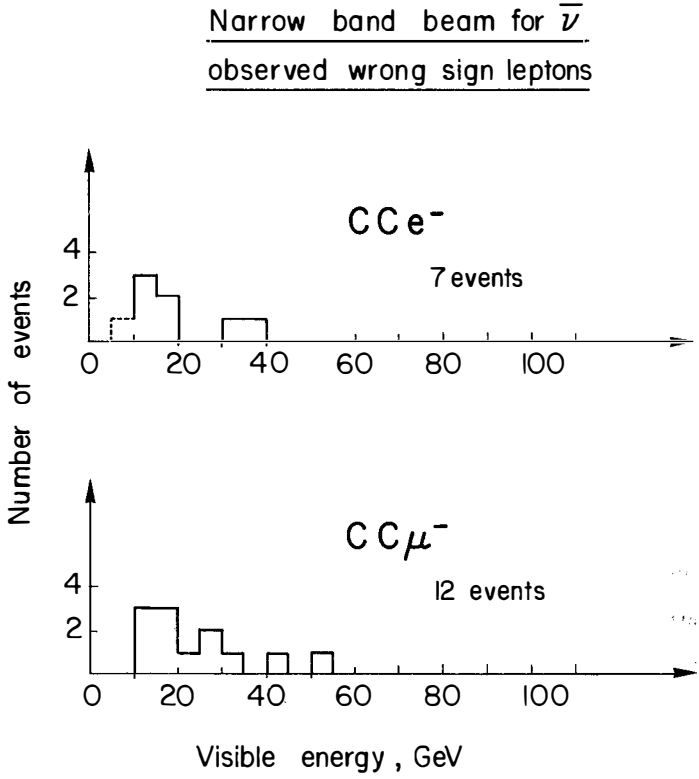

Fig. 4

Energy distribution of "wrong sign" events observed in the narrow-band beam antineutrino run

6.4 Other sources

Light particles (of less than the kaon mass) short-lived and as yet unknown, cannot be excluded as a source for the prompt neutrinos by the data. In this case the production cross section could be much smaller than in the case of D, depending on the mass, production mechanism and decay modes of these hypothetical particles.

7. CONCLUSIONS

The production of prompt neutrinos in proton-nucleus interactions has been observed both in the beam dump and in the antineutrino narrow-band beam experiment. The data are not inconsistent with equal fluxes of prompt ν_μ, $\bar{\nu}_\mu$, ν_e and $\bar{\nu}_e$. The production and subsequent decay of charmed particle pairs as the source of these neutrinos would require cross sections in the range of 100-400 μb. Tau leptons as the source are incompatible with the data. The decay of short-lived light particles of a new type could account for the prompt neutrino flux with much smaller cross sections.

REFERENCES

1. C. Brand et al., Nucl. Instr. and Methods 136 (1976) 485.
2. K. Schultze, International Symposium on Lepton and Photon Interactions, Hamburg (1977).
3. J. Ranft, Leipzig University Report KMU-HEP 75-03 (1975).
4. W.F. Baker et al., NAL-PUB 74/13 EXP.
   A.S. Carroll et al., Phys. Rev. Lett. 33 (1974) 928.
5. P.C. Bosetti et al., Phys. Lett. 70B (1977) 273.
   T. Eichten et al., Phys. Lett. 46B (1973) 281.
6. M. Bourquin and J.M. Gaillard, Nucl. Phys. B114 (1976) 334.
7. J.G. Branson et al., Phys. Rev. Lett. 38 (1977) 1331.
8. W.R. Ditzler et al., Phys. Lett. 71B (1977) 451. Using $\sigma_T \approx 2\, d\sigma/dy$ and 2.2% branching ratio $D \to K\pi$, $\sigma(D\bar{D}) < 26$ μb.
   J.C. Alder et al., Phys. Lett. 66B (1977) 480.
9. G. Coremans-Bertrand et al., Phys. Lett. 65B (1976) 480.
10. A. Barbaro-Galtieri et al., Phys. Rev. Lett. 39 (1977) 1058.

NEW RESULTS ON DIMUON PRODUCTION BY HIGH ENERGY NEUTRINOS AND ANTINEUTRINOS

T.Y. Ling
Department of Physics
The Ohio State University
Columbus, Ohio 43210
USA

I. Introduction

The subject of multimuon production by high energy neutrinos and anti-neutrinos began more than three years ago with the observation of dimuons by the HPWF collaboration at Fermilab.[1] The opposite sign dimuon events were interpreted as evidence for a new hadronic quantum number - charm.[2,3] Much has been learned since then. Recent experiments[4] not only confirmed the earlier observation but also supported the 'charm' interpretation. The origin of the like-sign dimuons ($\mu^-\mu^-$) remain, however, unknown. Because of the smaller observed rate for these events, decays of pions and kaons from ordinary deep inelastic neutrino interactions might account for a large fraction, if not all, of the observed events. It is important to determine whether 'prompt' like-sign dimuons exist, for the rate and nature of the prompt $\mu^-\mu^-$ events would provide important clues to the overall understanding of another facet of multimuon phenomena, in particular, the recently discovered trimuon events.[5]

In this talk I would like to report on recent dimuon data from the FHOPRW collaboration (E-310) at Fermilab. The issues I will concentrate on are: Is there a prompt like-sign dimuon signal? What are the nature of these like-sign events as compared to the opposite sign events? How consistent are the rates and properties of the opposite sign events with charm particle production and their semi-leptonic decay? The trimuon events observed during the same runs from which the present dimuon samples were obtained have already been published and reported at various other conferences and therefore will not be discussed here.

II. Beams

The data samples reported here were acquired at Fermilab in three runs, using a quadrupole triplet (QT) and sign-selected bare target (SSBT) beams. In the QT beam the secondary hadrons produced in the proton-target collision were focussed by a quadrupole triplet and left to decay without charge selection.[6] The resultant neutrino flux contains a mixture of ν_μ and $\bar{\nu}_\mu$. The SSBT beams employed no focussing elements but did charge selection of the secondary hadrons by means of a "dog-leg" arrangement of bending magnets.[7] Hence the resultant beams contain only ν_μ or $\bar{\nu}_\mu$ depending on the selected sign of the parent hadrons. These will be referred to as the SSBTν and SSBT$\bar{\nu}$ beams. The calculated spectra of ν_μ and $\bar{\nu}_\mu$ from these beams are shown in Fig. 1. The QT and SSBTν runs yielded 199 $\mu^-\mu^+$ events and 46 $\mu^-\mu^-$ events. The SSBT$\bar{\nu}$ run yielded 49 $\mu^+\mu^-$ events and 2 $\mu^+\mu^+$ events.

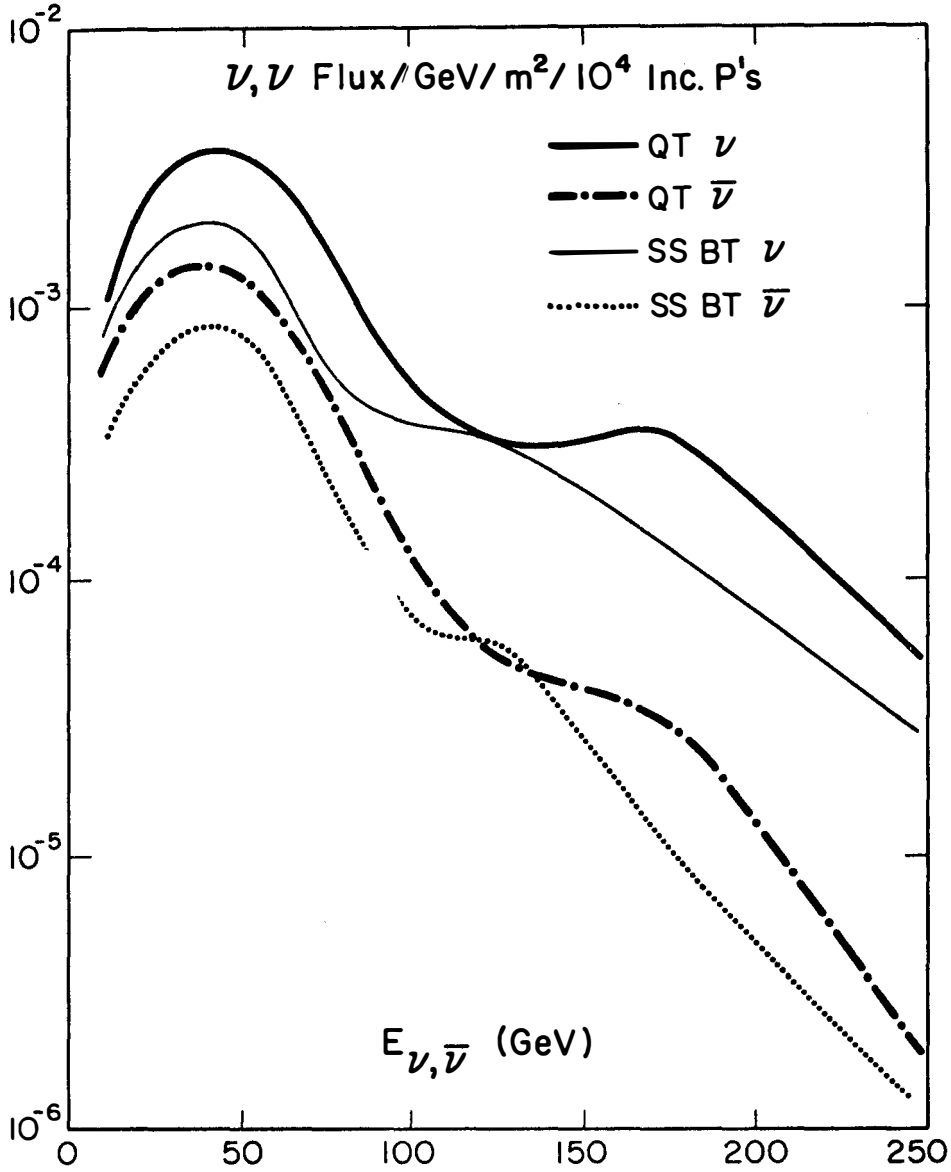

Fig. 1 Calculated neutrino and antineutrino spectra for the Quadrupole Triplet and Bare Target Selected Beams.

III. Detector

The detector of E-310 is shown in Fig. 2. It is an enlarged version of the earlier detector of E-1A with important modifications. i) A target-detector of three parts, an iron target (FeT), a liquid scintillator calorimeter (LiqC), and an iron-plate (4" thick plates) calorimeter (FeC), each part of different density. This makes possible an empirical determination of the pion and kaon decay background in the multimuon data. Table I shows the hadronic absorption length and fiducial masses of the three target-detectors. ii) A large solid angle muon spectrometer consists of three large area toroidal magnets (24' diameter) in addition to the existing 12' diameter toroids. Muons of angles up to 500 mrad relative to the ν_μ beam direction can be detected, compared with the limited angle of 225 mrad of E1A.

IV. Like-Sign Dimuons

1. Existence of a Prompt Signal?

The issue of foremost importance is to determine whether the like-sign dimuons are indeed all due to pion and kaon decays. This can in principle be inferred from the observed $\mu^-\mu^-$ rate produced in each target. The relative rates $R(\mu^-\mu^-)/R(\mu^-)$ are difficult to determine because of differences in acceptance, trigger requirements, etc between the targets. The ratio $N(\mu^-\mu^-)/N(\mu^-\mu^+)$ is, however, insensitive to these target dependent systematic effects, for to a good approximation these are the same for both the $\mu^-\mu^+$ and $\mu^-\mu^-$ events. The numbers of observed $\mu^-\mu^+$ and $\mu^-\mu^-$ events are shown in columns 3 and 5 of Table I for muon momentum cuts p>5 and 10 Gev/c respectively. The ratios $N^{obs}(\mu^-\mu^+)/N^{obs}(\mu^-\mu^+)$ are plotted against absorption length in Figs. 3a and 3b. To simplify the interpretation, we subtract from $N^{obs}(\mu^-\mu^+)$ the calculated numbers of the $\mu^-\mu^+$ events resulting from π and K decays[8], also listed in Table 1. The numbers of prompt $\mu^-\mu^+$ events are then given by $N^{obs}(\mu^-\mu^+)-N^{decay}(\mu^-\mu^+)$. In Figs. 3c and 3d, we show the ratios $N^{obs}(\mu^-\mu^-)/N^{prompt}(\mu^-\mu^+)$, again for the muon momentum cuts p>5 and 10 Gev/c. Linear fits to the data with both the slope and intercept as free parameters, are also shown. We observe that i) the decay of pions and kaons account for a significant fraction of the $\mu^-\mu^-$ events for the case $p_\mu > 5$ Gev/c; ii) the fitted slope decreases as the minimum momentum cut of the muon is raised from 5 to 10 Gev/c, resulting from the reduction of pion and kaon decay backgrounds as expected, and iii) the intercept of the fits at zero absorption length (infinite density) are different from zero in both cases.

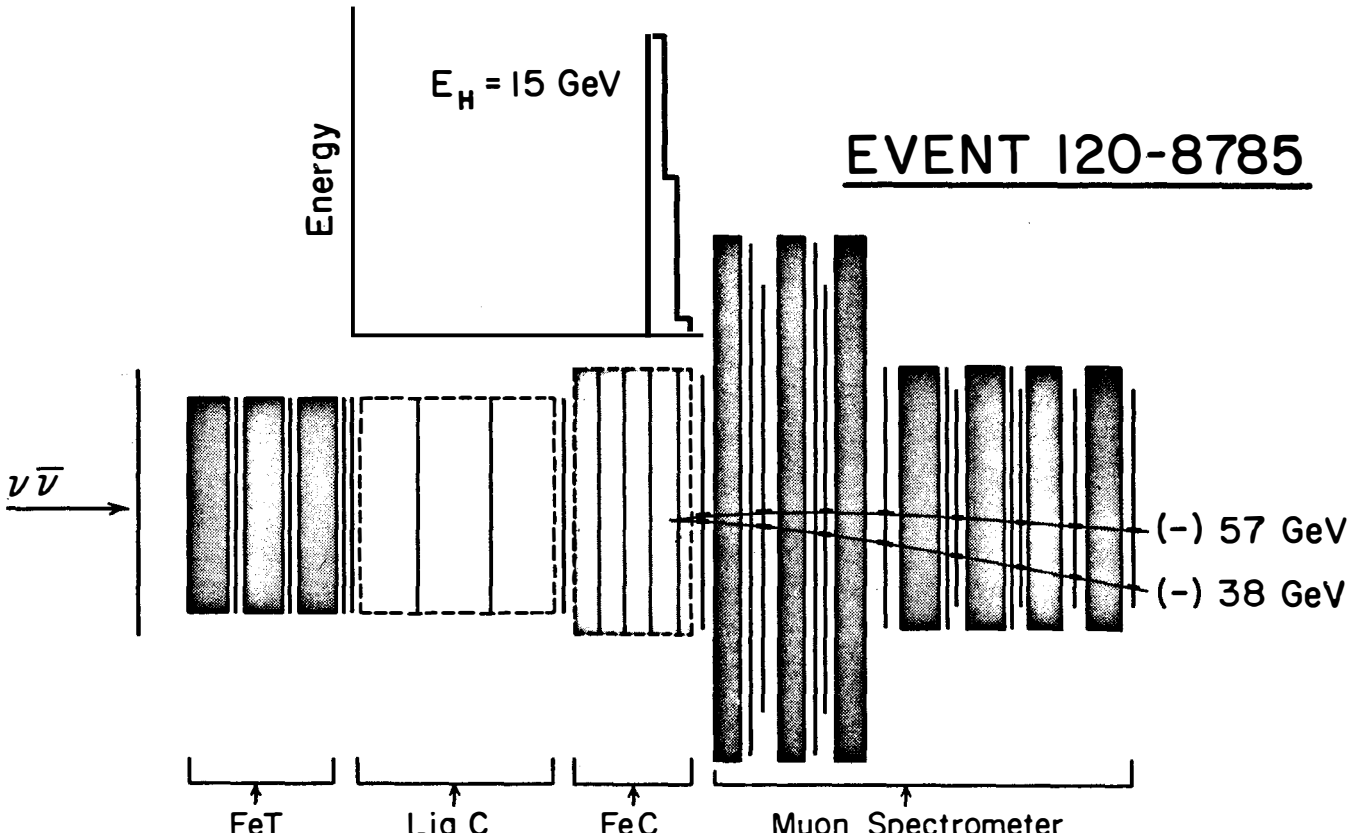

Fig. 2 Schematic layout of the E-310 Neutrino Detector. The tracing of an observed $\mu^-\mu^-$ event is superimposed on the apparatus.

TARGET	FIDUCIAL MASS (Tons)	ABS. LENGTH (cm)	$N^{obs}(\mu^-\mu^+)$		$N^{decay}(\mu^-\mu^+)$		$N^{obs}(\mu^-\mu^-)$		$N^{decay}(\mu^-\mu^-)$	
			$p_\mu>5$ GeV	$p_\mu>10$ GeV	$p_\mu>5$ GeV	$p_\mu>10$ GeV	$p_\mu>5$ GeV	$p_\mu>10$ GeV	$p_\mu>5$ GeV	$p_\mu>10$ GeV
IRON (FeT)	198	31	75	50	11	3.5	12	8	6.1	1.6
IRON CAL. (FeC)	42	61	42	23	10.5	2.6	10	4	5.9	1.5
LIQ. CAL. (LiqC)	36	120	56	32	22.2	7.7	16	6	12.0	3.2
TOTAL			173	105	43.7	13.8	38	18	24.0	6.3

TABLE 1. Fiducial masses, absorption lengths and numbers of observed dimuon events in the three targets. Also shown are the calculated numbers of dimuon events from pion and kaon decays.

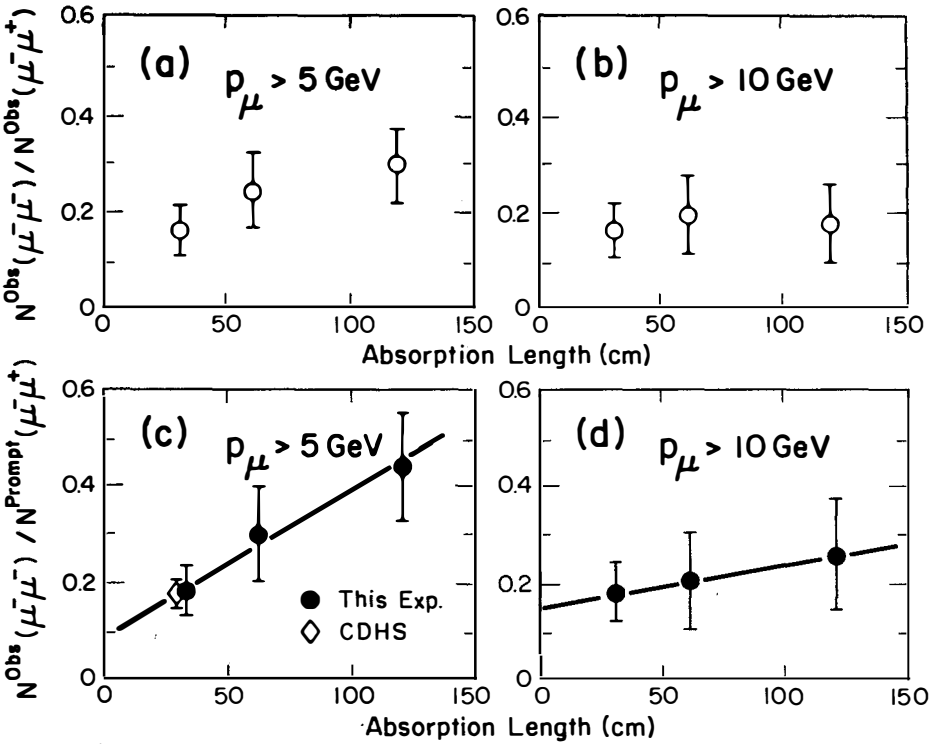

Fig. 3 Ratios of observed numbers of $\mu^-\mu^-$ events to that of the $\mu^-\mu^+$ events against hadronic absorption length for (a) p_μ > 5 Gev and (b) p_μ > 10 Gev. Ratios of observed numbers of $\mu^-\mu^-$ events to the $\frac{\text{prompt}}{p_\mu > 5}$ $\mu^-\mu^+$ events against hadronic absorption length for (c) Gev and (d) p_μ > 10 Gev.

It should be noted that although the analysis described above depend to some extent on the correction to subtract π, K decay contribution from $N^{obs}(\mu^-\mu^+)$, the value of the intercept from the extrapolation is relatively insensitive to this correction. The reason for this is that π and K decay contributions are relatively much smaller fraction of the $\mu^-\mu^+$ events. This is true especially for the FeT point which carries a lot of weight in determining the value of the intercept. Nonetheless, we have checked the reliability of the π, K decay calculation by comparing the density dependence of $N^{obs}(\mu^-\mu^+)/N(\mu^-)$. This comparision is shown in Fig. 4. The calculated slope is found to be very consistent with the data as shown. We further note that the fitted slope for the $p_\mu > 5$ Gev/c data in Fig. 3c is $(3.0 \pm 1.0)\times10^{-3}cm^{-1}$, also in good agreement with the value $(2.7 \pm 0.7)\times10^{-3}cm^{-1}$ obtained from the calculated numbers $N^{decay}(\mu^-\mu^-)$ shown in Table 1. These agreements check the validity of the decay calculation and gives us confidence in using the calculated numbers $N^{decay}(\mu^-\mu^-)$ to determine the magnitude of the prompt $\mu^-\mu^-$ signal in each target. The result is shown in Fig. 5. The ratios $N^{prompt}(\mu^-\mu^-)/N^{prompt}(\mu^-\mu^+)$ are seen to be systematically non-zero and independent of absorption length. Averaging over all three targets we obtain $N^{prompt}(\mu^-\mu^-)/N^{prompt}(\mu^-\mu^+) = 0.10 \pm 0.05$ for $p_\mu > 5$ Gev/c, and 0.13 ± 0.05 for $p_\mu > 10$ Gev/c.

In a run using the dichromatic beam at CERN, the CDHS collaboration reported the observation of 257 $\mu^-\mu^+$ events and 47 $\mu^-\mu^-$ events which satisfy the muon momentum cutoff of 4.5 Gev/c.[9] The ratio $N^{obs}(\mu^-\mu^-)/N^{prompt}(\mu^-\mu^+)$ for $p_\mu > 5$ Gev, obtained using the reported[9] π, K decay contributions and the slow muon momentum spectra, is 0.17 ± 0.03. The target detector of the CDHS experiment is primarily iron with an average hadronic absorption length of 30 cm. The CDHS result is plotted on Fig. 3c for comparison with this experiment. The good agreement between the two experiments supports our measurement in the iron target.

The two $\mu^+\mu^+$ events observed in the SSBT($\bar{\nu}$) run have very low energy muons ($\approx$5 Gev/c). Pion and kaon decays are estimated to yield 4 ± 2 events. Hence the two observed events are consistent with being backgrounds. If a prompt $\mu^+\mu^+$ signal were to exist at the same rate relative to the $\mu^+\mu^-$ event as the $\mu^-\mu^-$ signal, we would expect to observe 5 events in addition. So from this sample there is as yet no clear evidence of a prompt $\mu^+\mu^+$ signal.

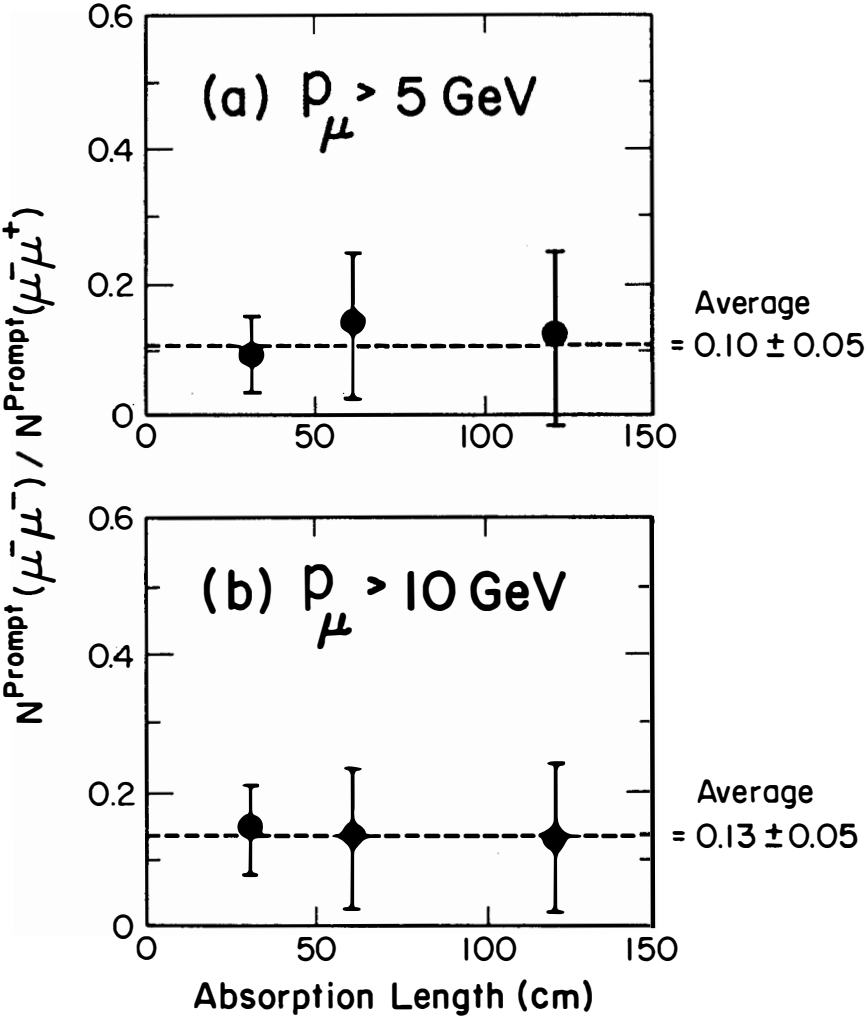

Fig. 4 Number of prompt $\mu^-\mu^-$events in each of the three targets for (a) $p_\mu > 5$ Gev and (b) $p_\mu > 10$ Gev.

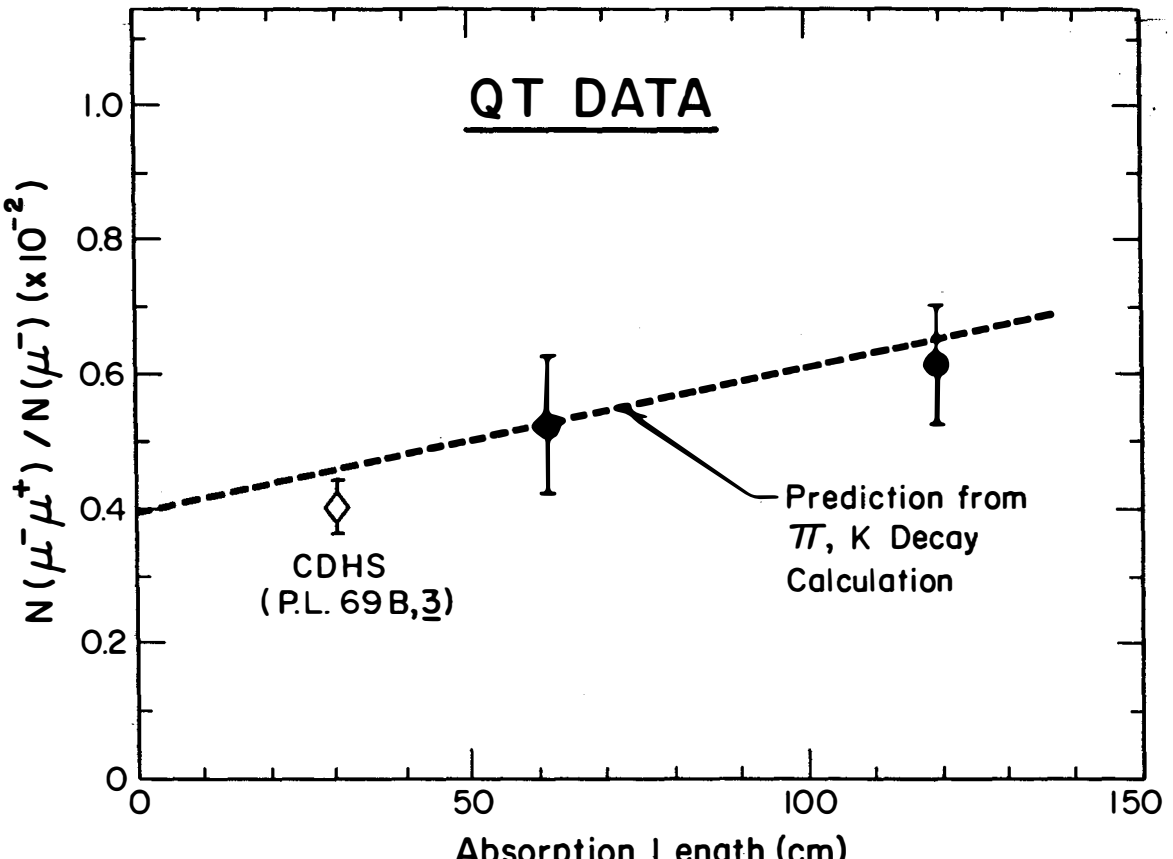

Fig. 5 Numbers of opposite sign dimuon events relative to that of the single muon events vs of hadronic absorption length.

2. Properties of the $\mu^-\mu^-$ events

The important properties of the $\mu^-\mu^-$ events are shown in Figures 6 - 10. Figure 6 shows the scatter plot of the momentum of the fast μ^- against the slow μ^-. A rather large momentum asymmetry between the two muons is observed, similar to that observed in the $\mu^-\mu^+$ data as shown in Fig. 7. The distribution in the azimuthal angle between the two muons is shown in Fig. 8a and 8b for the $\mu^-\mu^-$ and $\mu^-\mu^+$ events. Both distributions tend to peak at $\Delta\Phi = 180^\circ$, suggestive of a hadronic origin for the second muon. Fig. 9a shows the distribution in $p^s_{\perp W}$, the transverse momentum of the slow μ^- with respect to the direction of the W-boson which is defined by the directions of the incident neutrino and the fast μ^-. Again for comparison we show in Fig. 9 the distribution in $p^+_{\perp W}$ of the μ^+ for the $\mu^-\mu^+$ events. No distinctive differences can be seen. The distribution in the E_{vis} distributions are also similar between the $\mu^-\mu^-$ and $\mu^-\mu^+$ events as shown in Fig. 10a and 10b.

It could be argued that since a significant fraction of the $\mu^-\mu^-$ events are in fact from π or K decays, the properties of the prompt events could be largely masked. For this reason, the $\mu^-\mu^-$ events which satisfy the 10 Gev momentum cut are shaded for comparison. Contamination of pion and kaon decays are much smaller in this case. We note that although the statistics is very limited, the distribution exhibit the same general features. Properties of energetic $\mu^-\mu^-$ events where both muons have $p_\mu > 15$ Gev are shown in Table 2.

V. Opposite-Sign Dimuons

We now turn to the measurements of the rates of opposite-sign dimuons. The observed E_{vis} ($\equiv E_h + E_{\mu^-} + E_{\mu^+}$) distribution for the $\mu^-\mu^+$ events from the QT run is shown in Fig. 11a. The energy spectrum of the single muon events from the same run is shown in Fig. 11b. Figure 11 shows the relative rate $R(\mu^-\mu^+)/R(\mu^-)$ as a function of $E_{\ }$. Two things were further taken into account to obtain the data points shown in Fig. 13. First, the dimuon events were individually weighted by a factor which corrected for the geometric acceptance and triggering biases. This weighting factor was calculated for each of the observed events by azimuthally rotating the event in the detector. Secondly, the contribution from π and K decays had been subtracted from the data. Figs. 12 and 14 show the corresponding data for $\bar{\nu}$ induced $\mu^+\mu^-$ events from the SSBT($\bar{\nu}$) run. We note that the apparent rise in the dimuon rate relative to single muon rate with energy for both the ν and $\bar{\nu}$ samples are predominantly the result of the 5 Gev/c momentum cut.

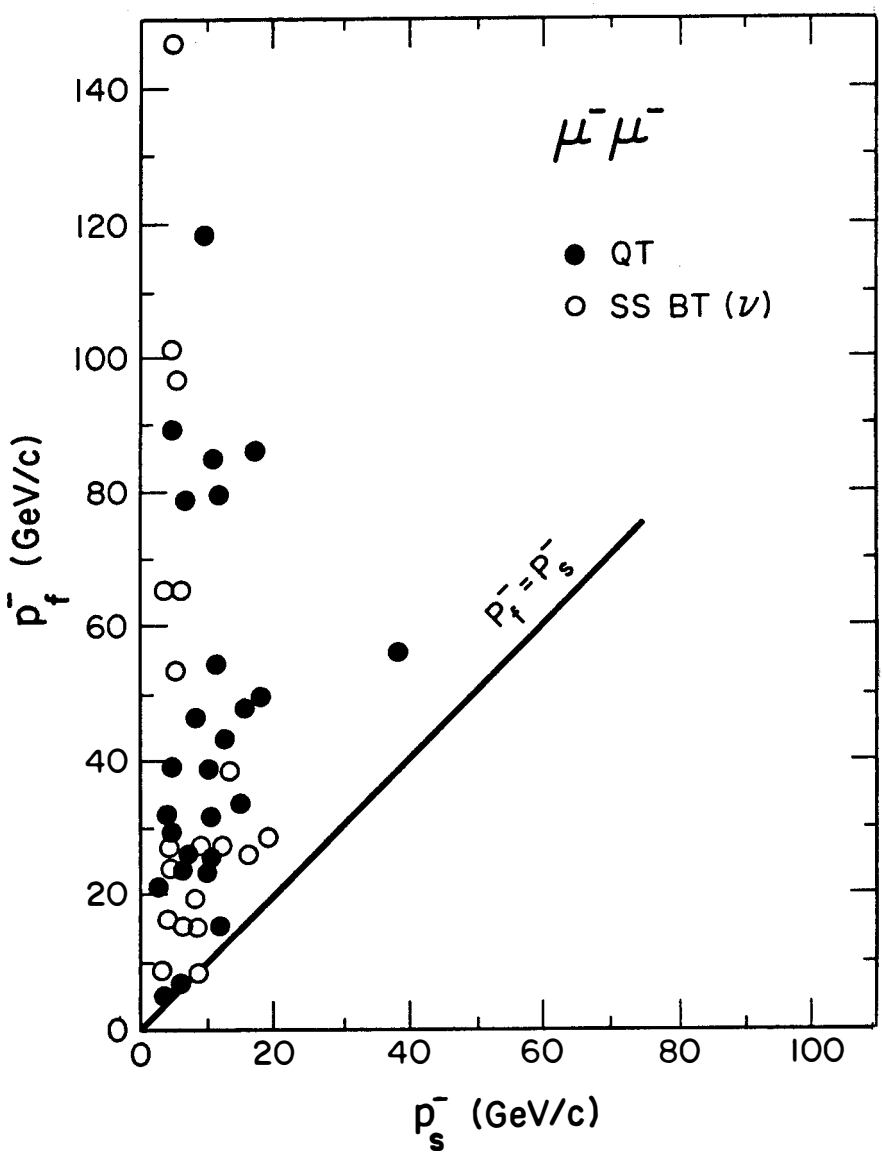

Fig. 6 Scatter plot of the muon momenta for the like-sign dimuon events.

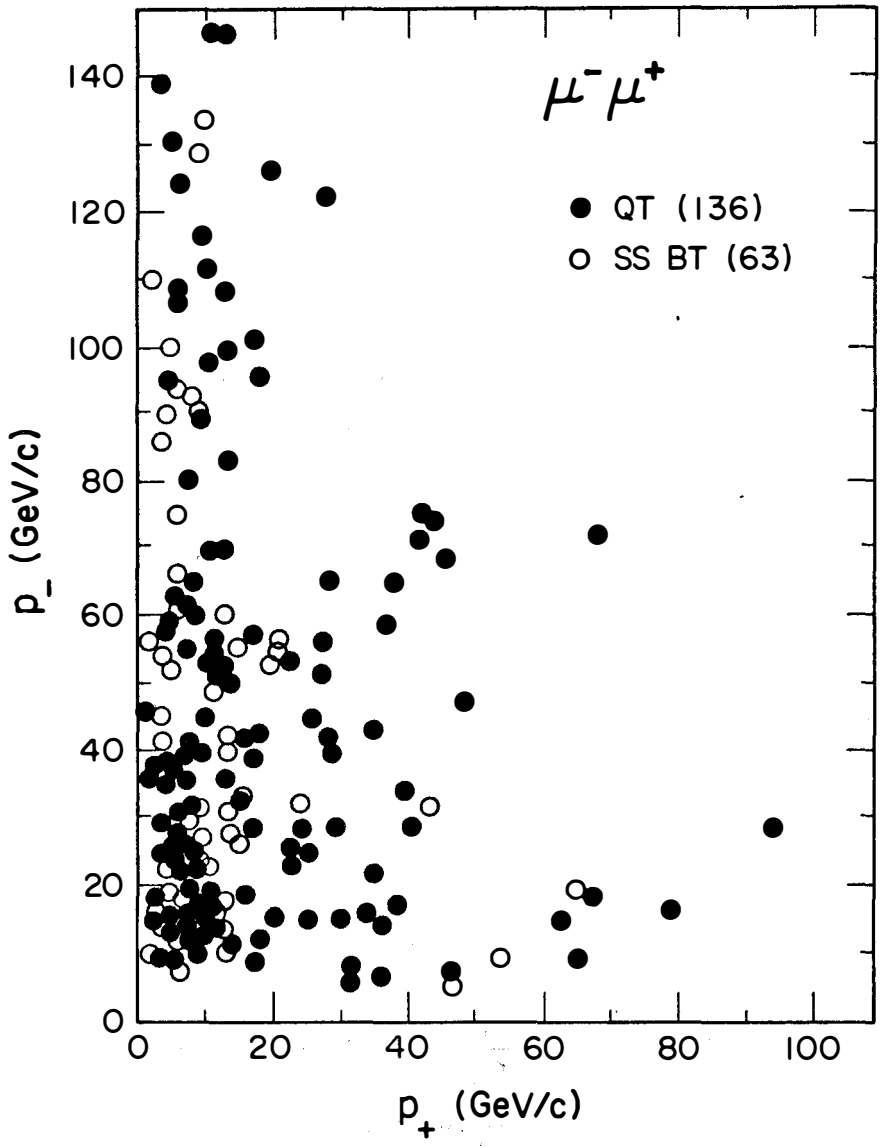

Fig. 7 Scatter plot of the muon momenta for the opposite sign dimuon events.

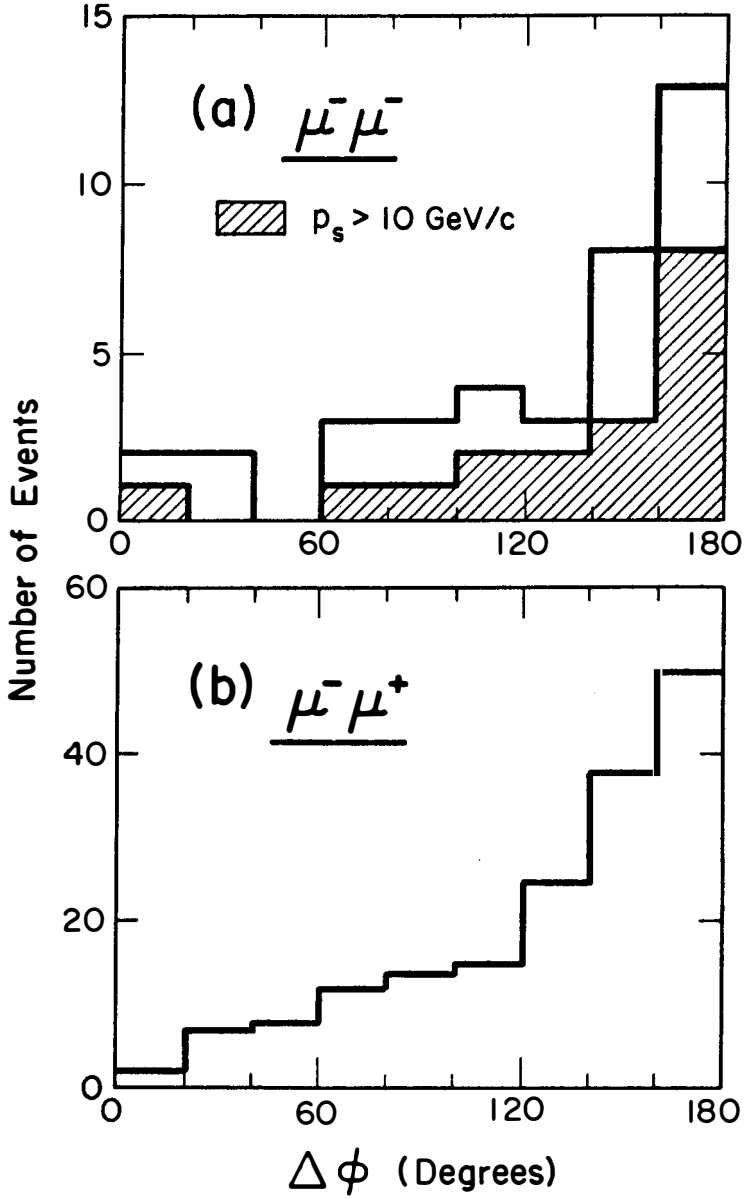

Fig. 8 Distributions in the relative azimutha angle, $\Delta\phi$ between the two muons for (a) the like-sign dimuons and (b) the opposite-sign dimuons.

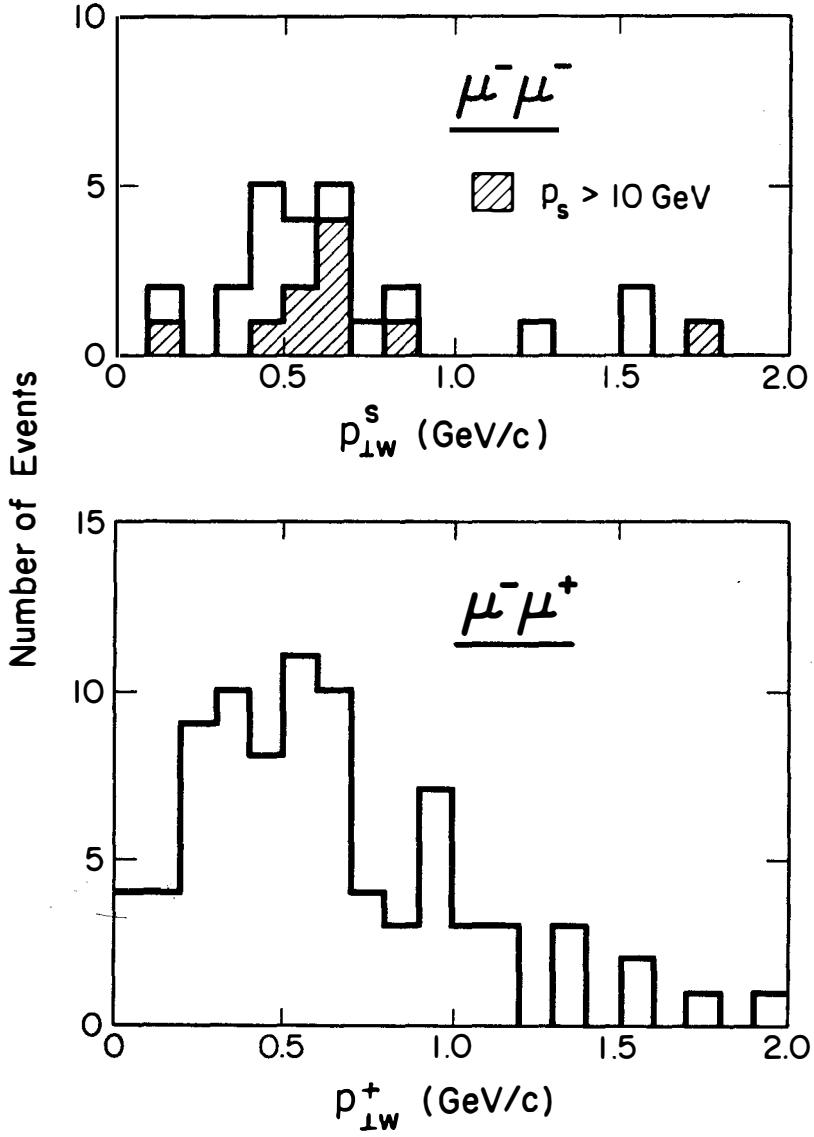

Fig. 9 Distributions in the transverse momentum relative to the W-direction for the (a) like-sign dimuons and (b) opposite-sign dimuons.

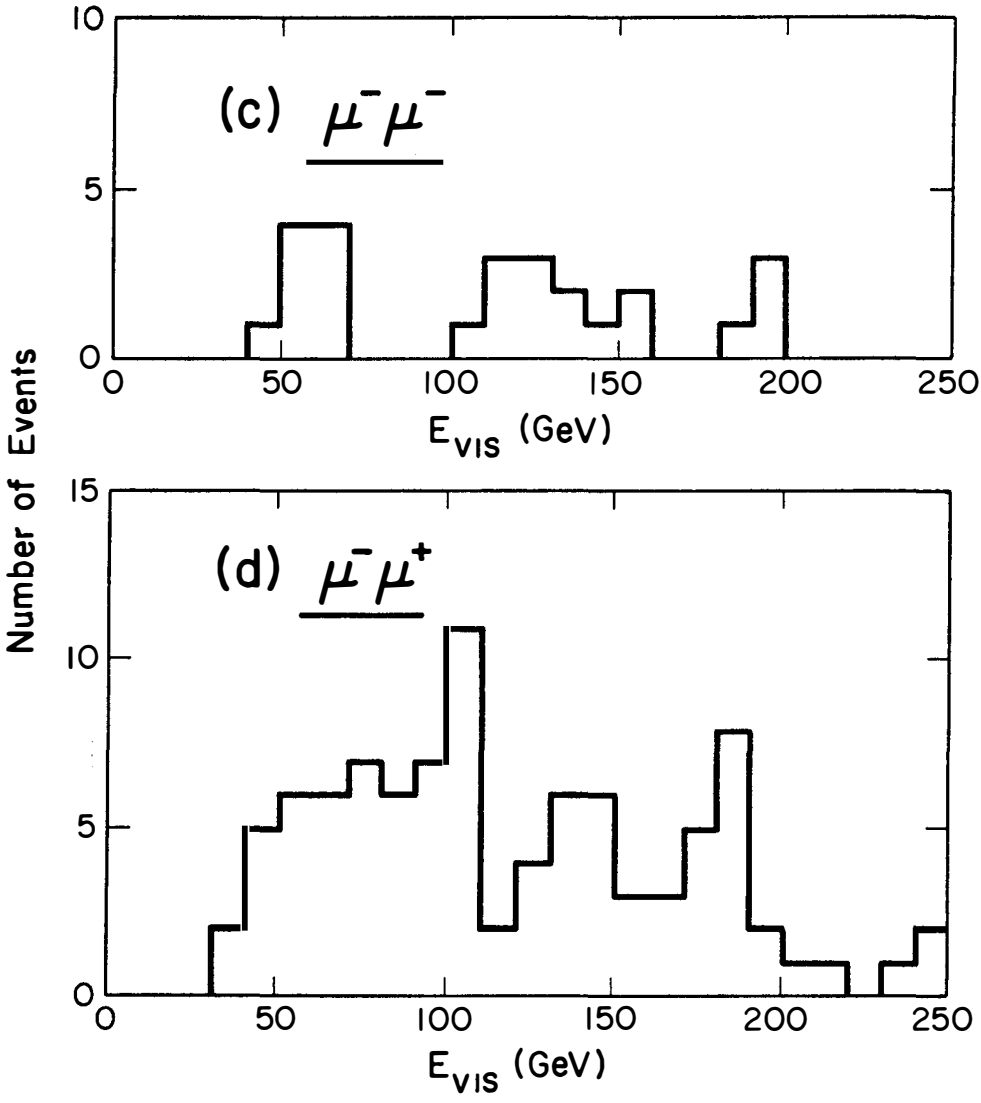

Fig.10 Distributions of total visibleenergy for (a) like-sign dimuons and (b) opposite-sign dimuons.

RUN FRAME	TGT MOD	ENERGY (GeV)		TRACK 1			TRACK 2		
		E_{vis}	E_h	QP	Px	Py	QP	Px	Py
117 15365	Liq 13	127	24	-86 ±7.3	1.87 ±.13	.21 ±.04	-17 ±.7	-1.42 ±.06	.07 ±.05
120 18783	FeC 21	114	19	-57 ±5.7	.27 ±.13	-1.22 ±.23	-38 ±4.4	.52 ±.17	1.21 ±.11
137 31940	FeT 2	>110	>46	-48 ±3.2	.50 ±.04	1.05 ±.11	-16 ±1.2	-.23 ±.08	.27 ±.09
141 35757	FeT 1	> 48	-	-33 ±12.8	.87 ±.23	-2.02 ±.65	-15 ±1.2	-.35 ±.14	.71 .05
146 39767	FeT 2	> 67	-	-49 ±3.8	1.94 ±.11	-.09 ±.06	-18 ±1.5	-.82 ±.06	.15 ±.06
279 145416	FeC 20	12	83	-26 ±2.2	-.69 ±.12	1.34 ±.13	-16 ±1.3	.52 ±.05	-.59 ±.05
282 149196	FeT 3	>58	>11	-28 ±1.4	.96 ±.05	-1.33 ±.04	-19 ±1.1	-.83 ±.04	.15 ±.04

TABLE 2. Properties of the energetic $\mu^-\mu^-$ events ($p_\mu > 15$ GeV).

Units of all momenta are in GeV.

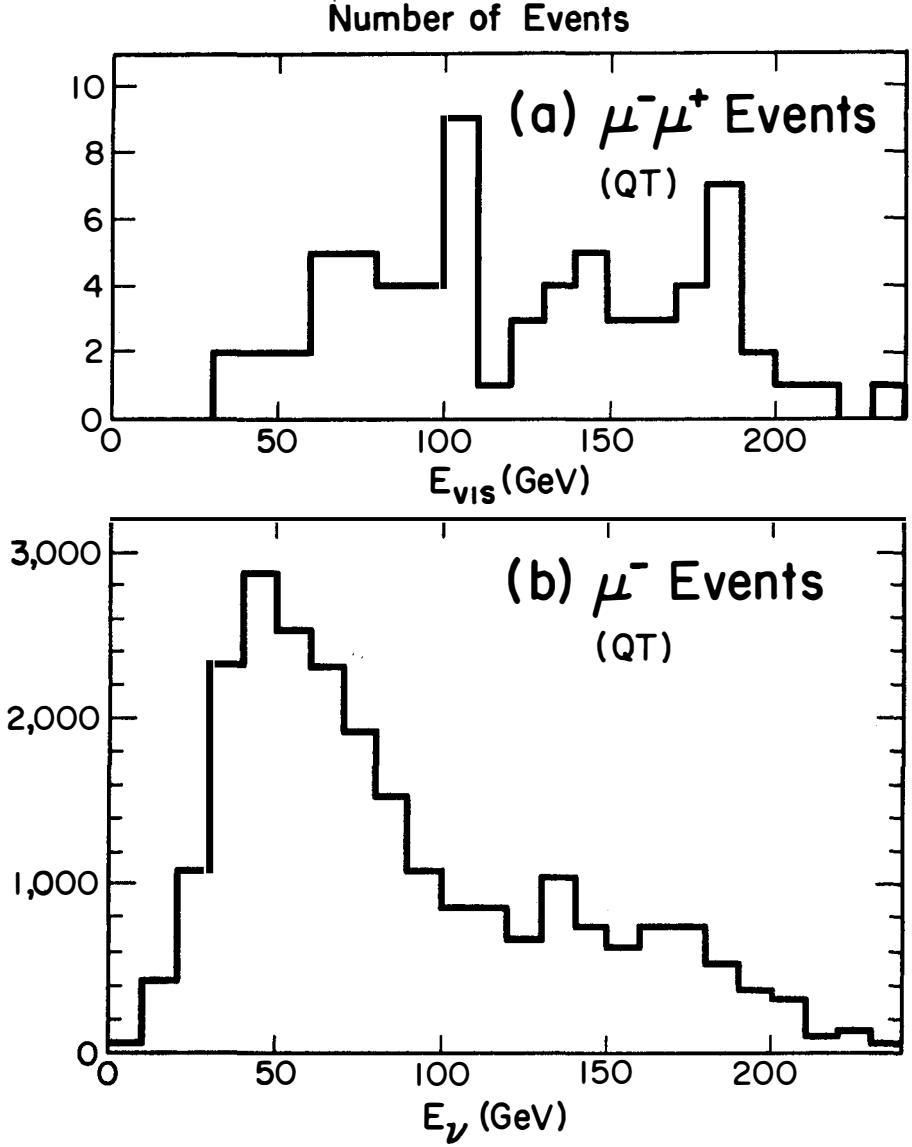

Fig.11 (a) Distributions of total visible energy for the ν-induced opposite-sign dimuons, (b) Distributions of neutrino energy for the ν-induced single muon events.

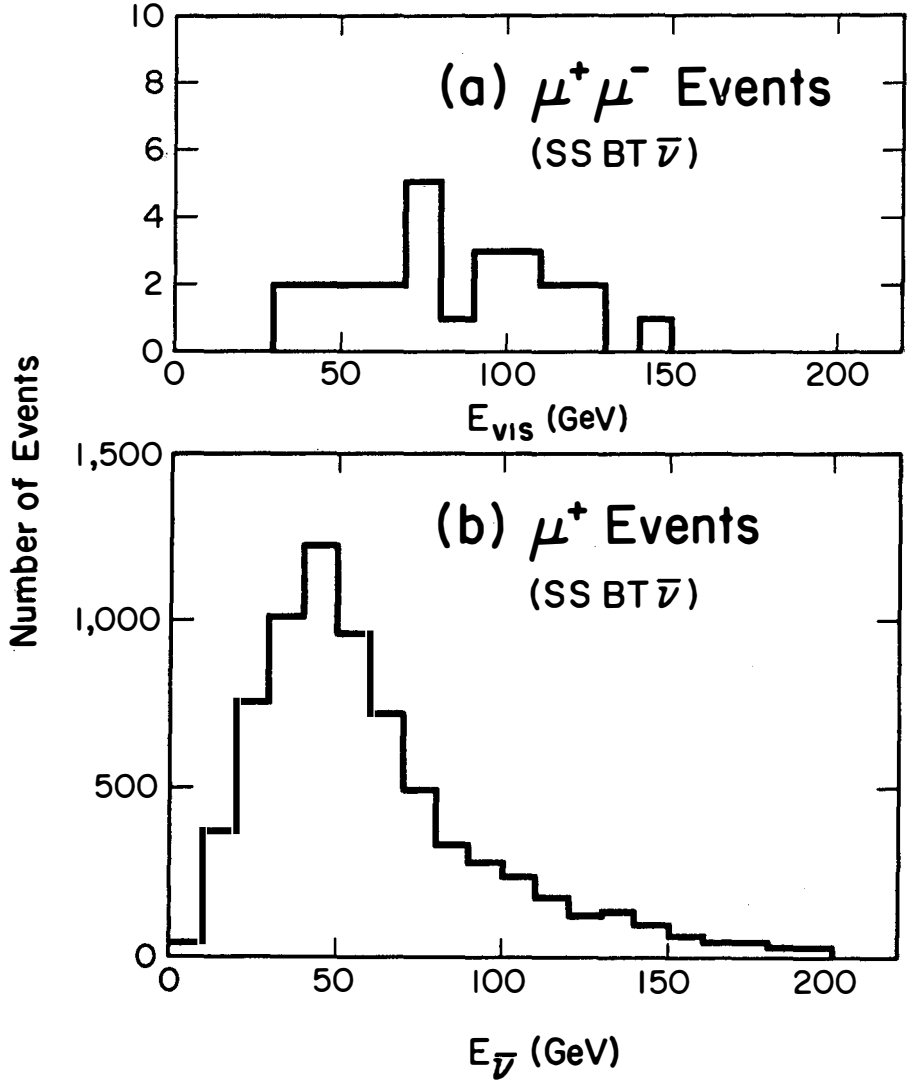

Fig.12 (a) Distributions of total visible energy for the $\bar{\nu}$-induced opposite-sign dimuons events, and (b) distributions of antineutrino energy for the $\bar{\nu}$-induced single muon events.

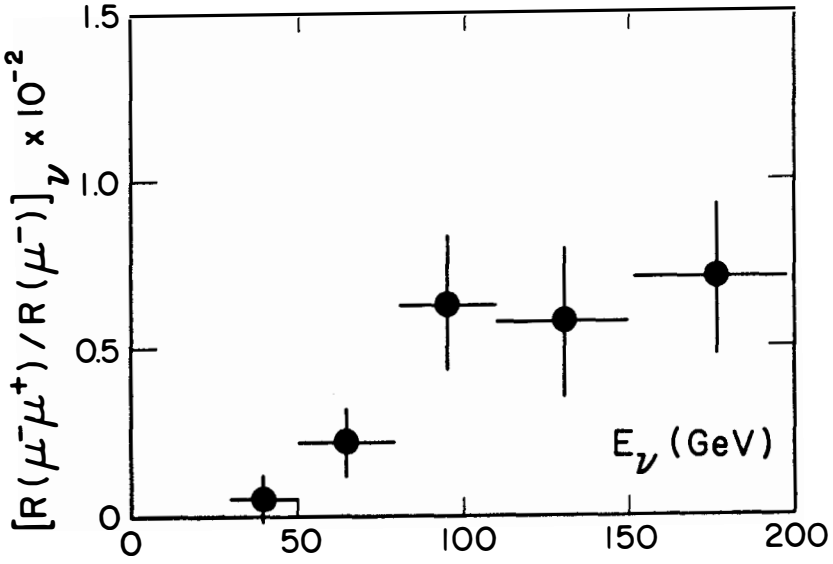

Fig.13 Rate of $\mu^-\mu^+$ events relative to rate of single muon events as a function of energy for neutrinos.

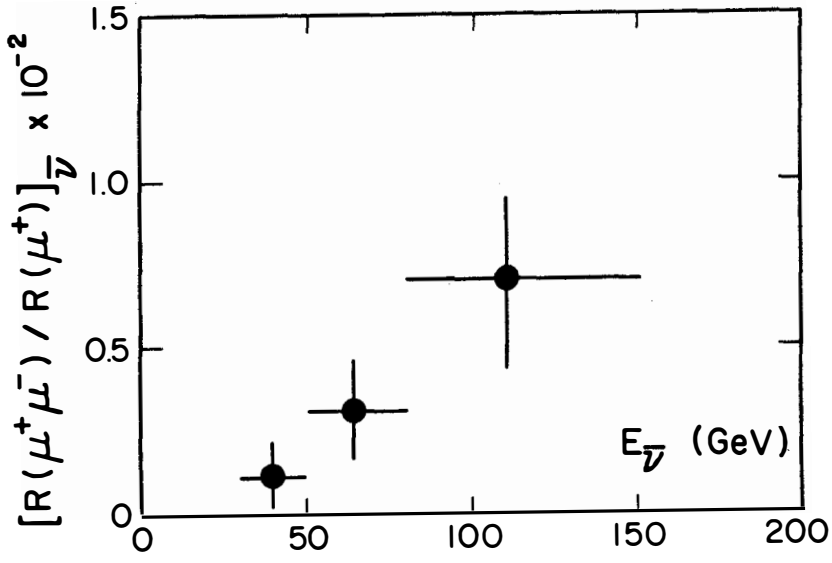

Fig.14 Rate of $\mu^-\mu^+$ events relative to rate of single muon events as a function of energy for antineutrinos.

The relative rates averaged over the corresponding beam energy spectra are

$$\{R(\mu^-\mu^+)/R(\mu^-)\}\quad \nu(30\text{-}200\ \text{Gev}) = (0.4 \pm 0.08) \times 10^{-2}$$

and

$$\{R(\mu^-\mu^+)/R(\mu^+)\}\quad \bar{\nu}(30\text{-}200\ \text{Gev}) = (0.27 \pm 0.09) \times 10^{-2}$$

The average $\bar{\nu}$ dimuon rate is lower because the SSBT($\bar{\nu}$) spectrum is substantially softer than the QT neutrino spectrum. For a given energy bin, we observe that the $\mu^-\mu^+$ rate relative to single μ rate is approximately the same for the ν and $\bar{\nu}$ data. At high energy, say $E_{vis} > 80$ Gev, where acceptance due to kinematic cutoff is less limited we have

$$\{R(\mu^-\mu^+)/R(\mu^-)\}\quad \nu(>80\ \text{Gev}) = (0.65 \pm 0.13) \times 10^{-2}$$

and

$$\{R(\mu^-\mu^+)/R(\mu^+)\}\quad \bar{\nu}(>80\ \text{Gev}) = (0.70 \pm 0.25) \times 10^{-2}$$

If we assume $\sigma^{\bar{\nu}}/\sigma^{\nu} \simeq 0.5$, it then follows from the data that

$$R^{\nu}(\mu^-\mu^+)/R^{\bar{\nu}}(\mu^+\mu^-) \simeq 2.$$

To compare this with the prediction of the GIM model, we note that in that model, charm quarks are produced by neutrino through their interaction either with the d(valence) or with the s(sea) quarks, namely,

$$\nu + d \to \mu^- + c\ ;\ (\sigma \propto \sin^2\theta_c)$$

$$\nu + s \to \mu^- + c\ ;\ (\sigma \propto f_s \cos^2\theta_c),$$

where θ_c is the Cabbibo angle and f_s is the fraction of momentum carried by the s(or $\bar{s}$) quarks relative to that carried by the d quarks in the nucleon. In antineutrino interactions, however, the charm quark can only be produced by the process

$$\bar{\nu} + \bar{s} \to \mu^+ + \bar{c};\ (\sigma \propto f_s \cos^2\theta_c).$$

Therefore $\sigma^{\nu}(\mu^-\mu^+)/\sigma^{\bar{\nu}}(\mu^+\mu^-) \simeq 2$ provided that $f_s \simeq \tan^2\theta_c = 0.05$.

The X_{vis} and Y_{vis} distributions of the ν and $\bar{\nu}$ induced $\mu^-\mu^+$ events are shown in Figs. 15 and 16. The Y_{vis} distributions are similar for ν and $\bar{\nu}$ and are consistent with kinematic and acceptance cut-off in the low and high-y regions. The $\bar{\nu}$ induced dimuons, however, have a sharper X_{vis}

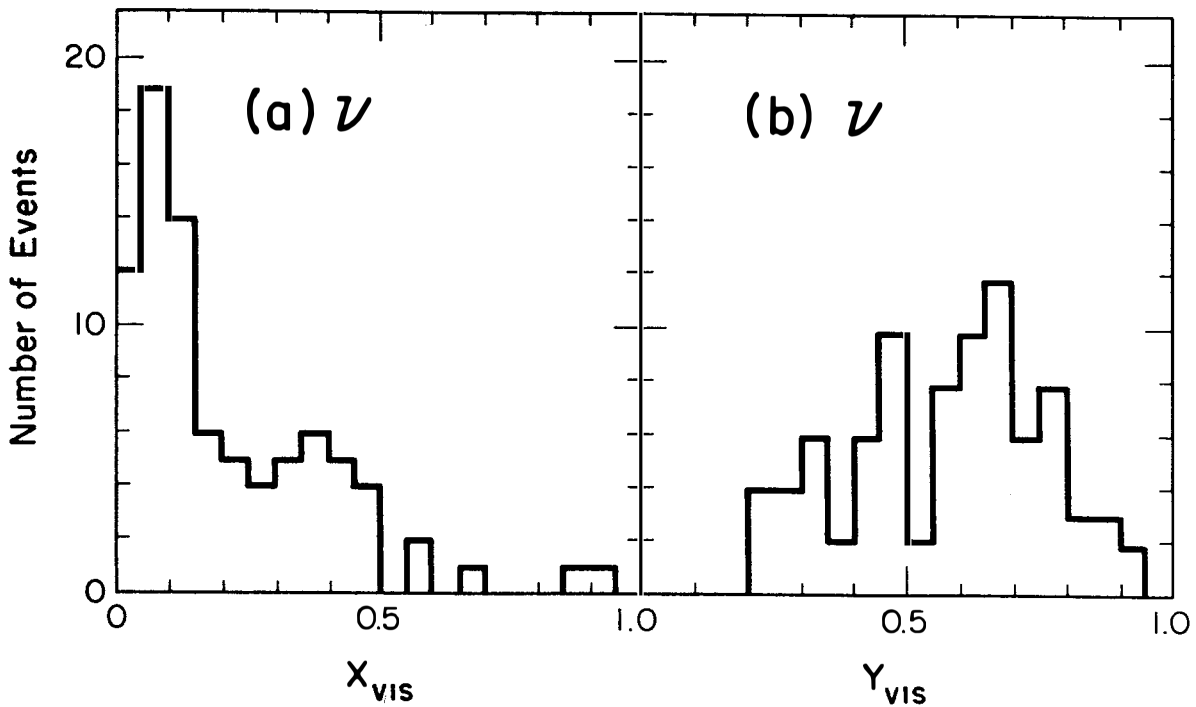

Fig.15 Distributions of X_{vis} and Y_{vis} for ν-induced $\mu^-\mu^+$ events.

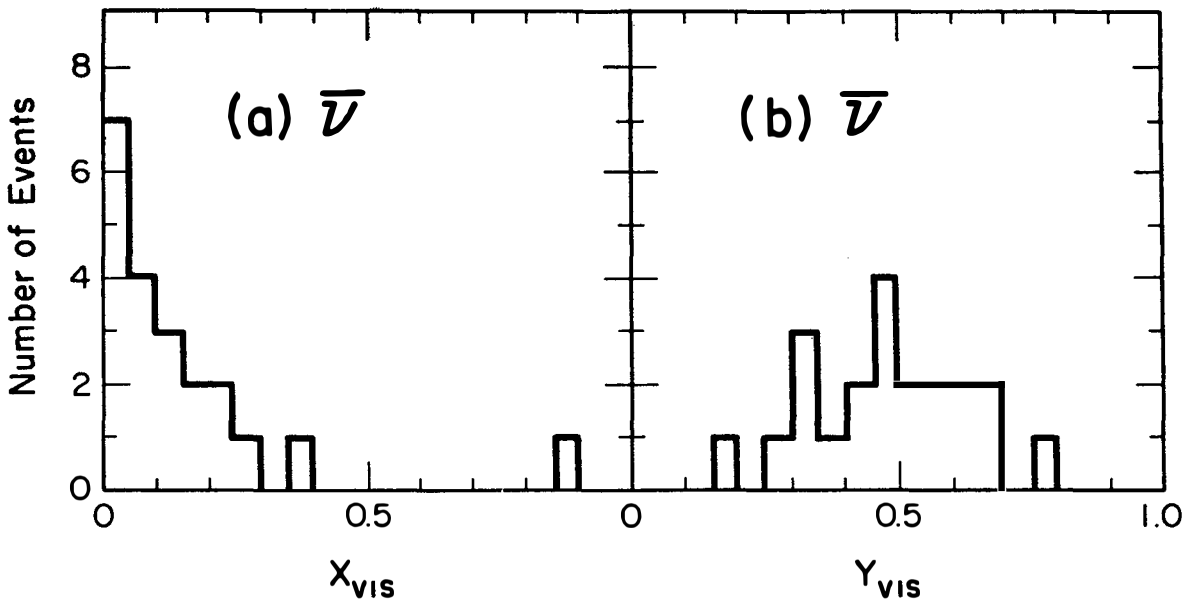

Fig.16 Distributions of X_{vis} and Y_{vis} for $\overline{\nu}$-induced $\mu^-\mu^+$ events.

distribution when compared to that of the ν data. This is also consistent with the GIM model since only the sea quark ($\bar{s}$) play the role for charm production by antineutrinos.

To give an overall perspective of the multimuon physics, we present in Table 3 the rates for neutrino induced $\mu^-\mu^+$, $\mu^-\mu^-$ and $\mu^-\mu^-\mu^+$, all relative to the charge-current interaction rate.

VI. Summary and Concluding Remarks

In summary, we have presented evidence for the production of prompt $\mu^-\mu^-$ events by neutrinos. The rate of the prompt $\mu^-\mu^-$ events relative to the prompt $\mu^-\mu^+$ rate is measured to be 0.10 ± 0.05 for $p_\mu > 5$ Gev/c, and 0.13 ± 0.05 for $p_\mu > 10$ Gev/c. The properties of the $\mu^-\mu^-$ events are similar to that of the $\mu^-\mu^+$ events. No clear evidence has as yet been established for prompt $\mu^+\mu^+$ events from $\bar{\nu}$ interactions.

What are the origins of the prompt $\mu^-\mu^-$ events? We remark that only $\mu^-\mu^+$ events are expected if charm particles are singly produced by neutrinos. Mechanisms to explain the $\mu^-\mu^-$ events which invokes new physics beyond charm must be measured against the following alternatives: (a) radiative or direct muon pair production in deep inelastic charged-current interactions;[10] (b) associated production of charmed particles.[11] Only trimuons can in principle be produced by mechanism (a). However, $\mu^-\mu^-$ events could result from this source if the μ^+ escapes experimental detection. Then one would expect $R(\mu^-\mu^-)/R(\mu^-\mu^-\mu^+) < 1$, contrary to the experimental observation (see Table 3). Therefore mechanism (a) is unlikely to be the dominant source for the $\mu^-\mu^-$ events. In associated charm production, both $\mu^-\mu^-$ and $\mu^-\mu^-\mu^+$ are expected. The ratio $R(\mu^-\mu^-)/R(\mu^-\mu^-\mu^+)$ should be about $\{BR(c \to \mu + x)\}^{-1} \sim 10$. The properties of the $\mu^-\mu^-$ events shown earlier are qualitatively compatible with the mechanism. The problem may lie in the absolute $\mu^-\mu^-$ rate.[11] If the measured $\mu^-\mu^-$ rate are confirmed with more data, then a large fraction, if not all, of the trimuons have to be attributed to associated charm production. More trimuon data is required to check consistency.

We have shown that both the rates and properties of the opposite-sign dimuon events are consistent with the GIM model. Based on this model, we may use the $\mu^-\mu^+$ data to determine f_s, the amount of strange quark relative to valence d-quark in the nucleon. The data gives approximately $f_s \sim \tan^2\theta_c = 0.05$.

	No E_ν cut††	E_ν > 100 GeV
$R(\mu^-\mu^+)/R(\mu^-)$	$(4.0 \pm 0.8) \times 10^{-3}$	$(6.5 \pm 1.3) \times 10^{-3}$
$R(\mu^-\mu^-)/R(\mu^-)$ †	$(4 \pm 2) \times 10^{-4}$	$(6.5 \pm 3.5) \times 10^{-4}$
$R(\mu^-\mu^-\mu^+)/R(\mu^-)$	$(9 \pm 5) \times 10^{-5}$	$(2.6 \pm 1.5) \times 10^{-4}$

TABLE 3. Multimuon rates relative to the rate of deep inelastic single muon events.

† Obtained using $R(\mu^-\mu^-)/R(\mu^-\mu^+) = 0.10 \pm 0.05$

††Averaged over the Quadrupole Triplet Spectrum

The data shown in this talk is the result of a collaboration of physicists from Fermilab, Harvard, Ohio State, Pennsylvania, Rutgers and Wisconsin. Individual members of the collaboration are A. Benvenuti, F. Bobisut, D. Cline, P. Cooper, M.G.D. Dilchriese, M. Heagy, R. Imlay, M. Johnson, T.Y. Ling, R. Lundy, A.K. Mann, P. McIntyre, S. Mori, D.D. Reeder, J. Rich, R. Stefanski and D. Winn.

References and Footnotes

*Work supported in part by the Dept. of Energy.

1. A Benvenuti et al., Phys. Rev. Lett. 34, 419 (1975).
2. J.D. Bjorken and S.L. Glashow, Phys. Lett. 11, 255 (1964); S.L. Glashow, J. Iliopoulous and L. Maiani, Phys. Rev. D2, 1285 (1970).
3. A. Benvenuti et al., Phys. Rev. Lett. 35, 1199 (1975), ibid 35, 1203 (1975).
4. B.C. Barish et al., Phys. Rev. Lett., 36, 939 (1976). M. Holder et al., Phys. Lett. 69B, 377 (1977).
5. B.C. Barish et al., Phys. Rev. Lett. 38, 577 (1977); A. Benvenuti et al., Phys. Rev. Lett 38, 1110 (1977) and 40,488 (1978).
6. A. Skuja, R. Stefanski and A. Windelbon, FNAL Technical Note TM469 (1974).
7. R. Stefanski and H.B. White, FNAL Technical Note TM26A (1976).
8. R. Imlay, Calculations of background from pion and kaon decays in neutrino interactions. (unpulbished)
9. M. Holder et al., Phys. Lett. 70B, 396 (1977).
10. J. Smith and J.A.M. Vermaseren, Stony Brook Report ITP-SB-77-66; R.M. Barnett et al., SLAC-PUB-2063 (1977); V. Barger, T. Gottschalk and R.J.N. Phillips, Wisconsin Report COO-881-9.
11. H. Goldberg, Phys. Rev. Lett. 39, 1598 (1977).

NEUTRINO-INDUCED TRIMUON AND TETRAMUON EVENTS FROM THE CDHS EXPERIMENT

K. Kleinknecht
Institut für Physik der Universität Dortmund
4600 Dortmund 50, Germany

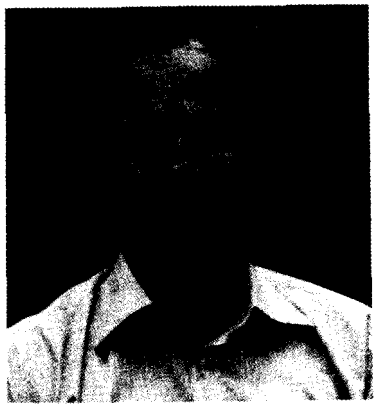

ABSTRACT

Experimental results on multimuon production by neutrinos from the CERN- Dortmund - Heidelberg - Saclay Neutrino experiment are presented: a) 76 trimuon ($\mu^-\mu^-\mu^+$) events are compared to different models assuming an electromagnetic, hadronic or purely leptonic origin of the events. The data are consistent with being due to hadronic and electromagnetic μ-pair production in a charged-current neutrino reaction b) a first tetramuon event $\nu + N \rightarrow \mu^-\mu^+\mu^-\mu^+ X$ has been observed.

RESUME

Nous présentons des resultats de la collaboration CERN - Dortmund - Heidelberg - Saclay concernant la production des evènements avec trois ou quatre muons par des neutrinos: a) 76 evènements à trois muons ($\mu^-\mu^-\mu^+$) sont comparés à des modèles supposant un origine electromagnetique, hadronique ou leptonique. Les données peuvent être expliquées par la production hadronique ou electromagnétique d'une paire de muons dans une reaction du type courant chargé; b) un premier evènement tetramuon $\nu + N \rightarrow \mu^-\mu^+\mu^-\mu^+ X$ a été observé.

1. INTRODUCTION

The neutrino detector[1] of the CDHS Collaboration[x)] has now been in operation for one year at CERN, and results on neutral currents[2,3], charged currents[4], opposite-sign dimuons[5], like-sign dimuons[6], trimuons[7], and a tetramuon event [8] have been published.
This report will be devoted to the multimuon events, i.e. events with three or four muons in the final state.

2. BEAMS AND DETECTOR

There are two neutrino beams at CERN (fig.1). In the narrow-band beam, π and K mesons produced by 400 GeV protons impinging on a Be target are entering a beam line of 120 m length which selects particles of given electric charge in a narrow momentum band around $p = (200 \pm 10)$ GeV/c. These mesons are then allowed to decay in an evacuated beam pipe of 300 m length and 1.5 m diameter. Behind this tube hadrons and nearly all muons are absorbed in 350 m of shielding material consisting mainly of iron.

On the other hand, in the wide-band-beam (WBB) there is no momentum selection of secondary mesons behind the proton target. Instead, a magnetic horn and a reflector are used for focussing of positive (neutrino beam) or negative (antineutrino beam) mesons. Decay pipe and shielding remain the same as in the narrow band beam.

x) The members of this group are: M. Holder, J. Knobloch, J. May, H.P. Paar, P. Palazzi, D. Schlatter, J. Steinberger, H. Suter, H. Wahl, E.G.H. Williams (CERN), F. Eisele, C. Geweniger, K. Kleinknecht, G. Spahn, H.-J. Willutzki (Universität Dortmund), W. Dorth, F. Dydak, V. Hepp, K. Tittel, J. Wotschak (Universität Heidelberg), P. Bloch, B. Devaux, M. Grimm, J. Maillard, B. Peyaud, J.Rander, A. Savoy-Navarro, R. Turlay (CEN-Saclay), F.L. Navarria (Universitá Bologna)

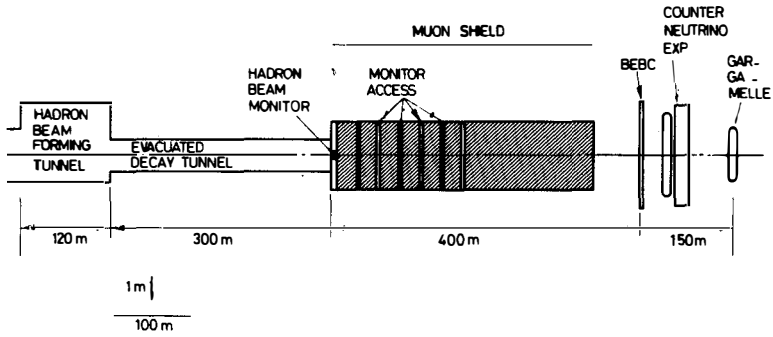

Fig. 1 Layout of neutrino beam area at the CERN SPS. The CDHS detector is labeled "counter neutrino experiment".

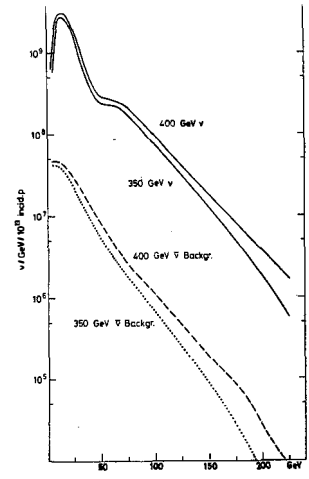

Fig.2 Neutrino beam flux as function of neutrino energy for the neutrino wide-band beam

The neutrino and antineutrino energy spectra for the WBB focussing positive secondaries are shown in fig.2.

The neutrino beams impinge on several detectors, as indicated in fig.1. The one labeled "counter neutrino experiment" is the detector of the CDHS collaboration.

In this detector (figs. 3,4) the functions of neutrino target, hadron calorimeter, muon identifier and muon magnetic spectrometer are integrated. It consists of 19 toroidal modules of magnetized iron plates interspaced with 19 triple plane drift chambers. The diameter of the toroids, 3.75 m is matched to the 90^{o} c.m. decay angle of neutrinos from $\pi \rightarrow \mu\nu$ decay such that nearly all π decay neutrinos hit the detector, while about half of the neutrinos from K decay miss the apparatus. The thickness of these magnets is 75 cm, composed of 15 plates of 5 cm thickness for the first seven modules and of 15 cm plates for the other twelfe. In each gap between two plates is inserted a plane of eight 6 mm plastic scintillators viewed by two phototubes at each end. The sum of right and left pulseheights is used for calorimetry, while their ratio serves for determining the shower position along the counter. Pulseheight calibration and measurement of light attenuation in the counters is done using cosmic muons continously between machine bursts.

The iron weight of the detector is 1240 t, of which 800 t are used as a fiducial target. The average magnetic field in the toroids amounts to 16.5 kG. An average density of 5.3 g/cm^3 is obtained, which is important for the suppression of $\pi \rightarrow \mu$ and $K \rightarrow \mu$ decays of π and K mesons from the hadron shower.

The drift chambers are hexagonal and consist of three independent gaps with wires in the vertical direction and at $\pm 60^{o}$ relative to the vertical. The wire spacing is 6 cm, the measurement accuracy 1 mm and the efficiency typically 99.5 % per gap.

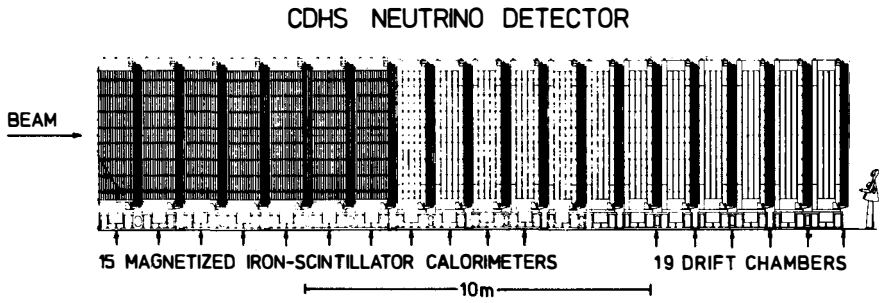

Fig. 3 Side view of the CDHS detector

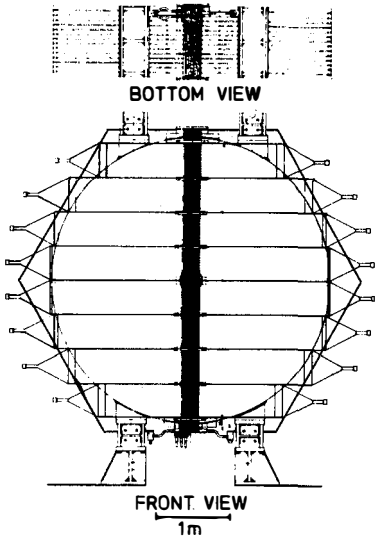

Fig. 4 Front view of one module of the CDHS detector

We study the inclusive processes $\nu + Fe \rightarrow n\,(\mu^{\pm}) + X$ ($n = 3,4$), where X is any hadronic final state. The hadron energy E_h of X is measured in the Fe-scintillator calorimeter. The response of this calorimeter to incident hadrons (and electrons) has been determined in a test calorimeter of smaller dimensions (150 cm long, 60 x 80 cm transverse size) exposed to hadron beams of energy between 15 and 140 GeV. The resolution is $\Delta E_h/E_h = 0.9/\sqrt{E_h(\mathrm{GeV})}$ for 5 cm sampling and $\sqrt{3}$ times larger for 15 cm sampling.

The resolution in muon momentum as measured in the magnetic spectrometer is determined mainly by the multiple scattering in the iron and is depending on the length L of the muon track. Using the measured value of the magnetic field, one obtains $\Delta p/p \simeq 0.2/\sqrt{L(m)}$.

The angular acceptance of the spectrometer is large due to the integration of target and spectrometer. Since we require an event to be detected in at least 5 consecutive drift chambers, this corresponds to an effective cut in muon laboratory angle around 400 mrad and to a cut in muon momentum at about 4.5 GeV/c.

3. TRIMUONS

Trimuons were observed in the CITF[9], HPWF[10] and CDHS[7] experiments. We report here on 76 $\mu^-\mu^-\mu^+$ events and 5 $\mu^-\mu^+\mu^+$ events obtained in a wide-band neutrino beam run at the CERN SPS. Apart from the trivial case of dimuons with an additional muon from a pion or Kaon decaying in the shower, trimuons may originate in several kinds of processes:

a) a charged-current interaction with electromagnetic production of a muon pair, either from the outgoing muon or from the incoming or outgoing quark[12,13,14]

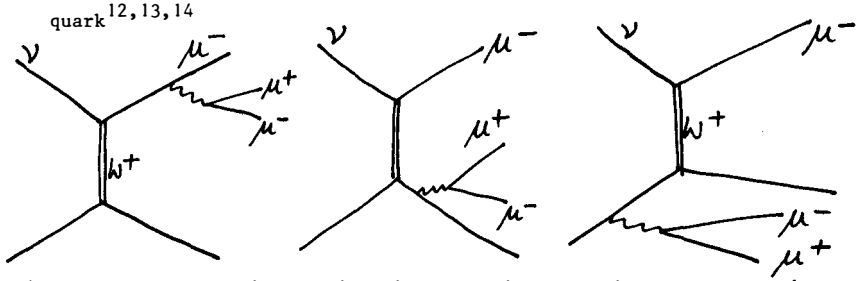

b) a charged-current interaction with hadronic production of a muon pair, e.g. by the decay of a vector meson

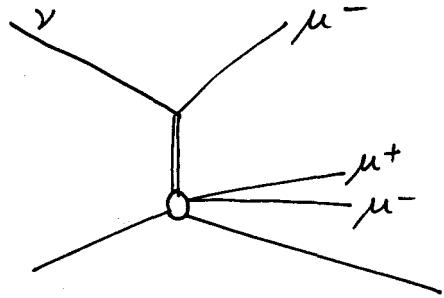

c) a charged-current interaction with charm-anticharm production at the hadron vertex and subsequent decay of both c and $\bar{c}$ to muons[15]

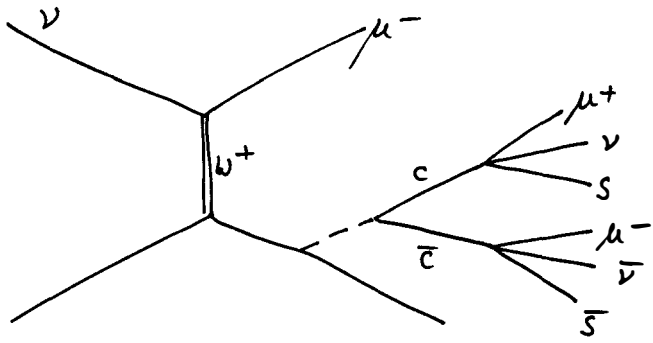

d) more exotic possibilities involving i) a heavy lepton cascade[16,17] ii) a quark cascade and iii) lepton-hadron models[18]

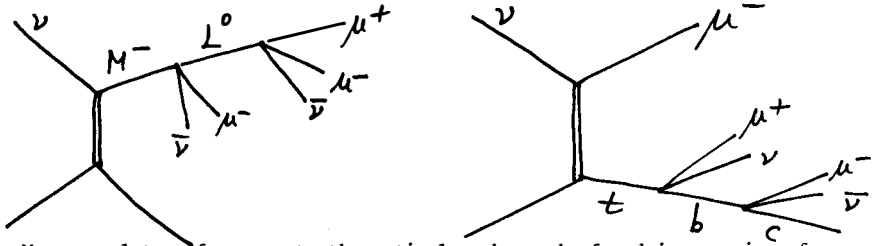

More complete references to theoretical work can be found in a review of Barger[19].

We then turn to experimental data. One example of a trimuon event ν Fe $\rightarrow \mu^-\mu^-\mu^+X$ in the CDHS detector exposed to the wide-band beam is shown in fig. 5 in three 120° views. From the measured vector momenta of all three muons, the hadron energy E_h and the neutrino direction we can reconstruct the kinematics of the event. In particular the total visible energy is $E = E_{\mu 1} + E_{\mu 2} + E_{\mu 3} + E_h$. A plot of trimuon event numbers vs. E is shown in fig. 6 for two different exposures together with the corresponding dimuon- and charged-current rates. The measured ratio R ($3\mu/1\mu$) ranges between $(1.2 \pm 0.3) \times 10^{-5}$ at 50 GeV and $(9 \pm 2) \times 10^{-5}$ at 120 GeV neutrino energy, which seems lower than in figure 5×10^{-4} quoted earlier in Refs. 10 and 20.* The energy dependence of the ratio R corrected for background from π/K decay is shown in fig.7. The background in the trimuon sample due to dimuons with a π or K meson of the hadronic cascade decaying into ($\mu\nu$) was obtained by measuring the π/K decay rate of hadronic showers produced by pion beams in our detector. We expect $6\mu^-\mu^-\mu^+$ events and 6.6 $\mu^-\mu^+\mu^+$ from this background in our sample. The 5 observed $\mu^-\mu^+\mu^+$ events are compatible with this number, while for the $\mu^-\mu^-\mu^+$ events this amounts to a background of 8%. The calculated rates for electromagnetic processes[12,13,14] are around (1 to 2) $\times 10^{-5}$ including experimental cuts, and the charm-anticharm production is estimated[15] to be less than 10^{-6}. A simple model on hadronic μ pair production was made using experimental data[21] on dimuon production in π N reactions and assuming a resemblence between the interaction of the virtual W boson and this π - N interaction. The resulting trimuon rate is 2×10^{-5}.

* A revised number $R = (9 \pm 5) \times 10^{-5}$ averaged over the neutrino spectrum in the quadrupole focussed beam was given at this conference by Dr.T.Ling.

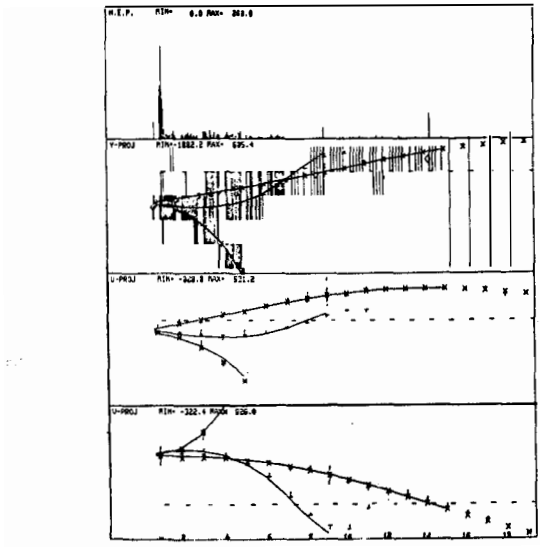

Fig. 5 Trimuon event display. On top, pulseheights. Next lower, horizontal drift chamber wires and scintillator hits. Bottom, drift chambers at ± 60 ^{o} to horizontal.

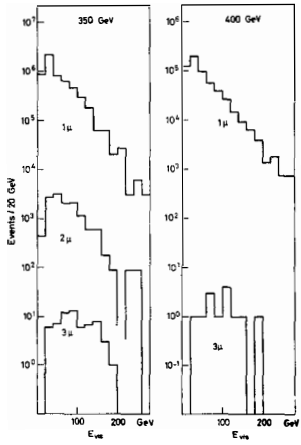

Fig.6 Rate of 1μ, 2μ, and 3μ events versus neutrino energy for 350 GeV and 400 GeV wide-band beam exposures

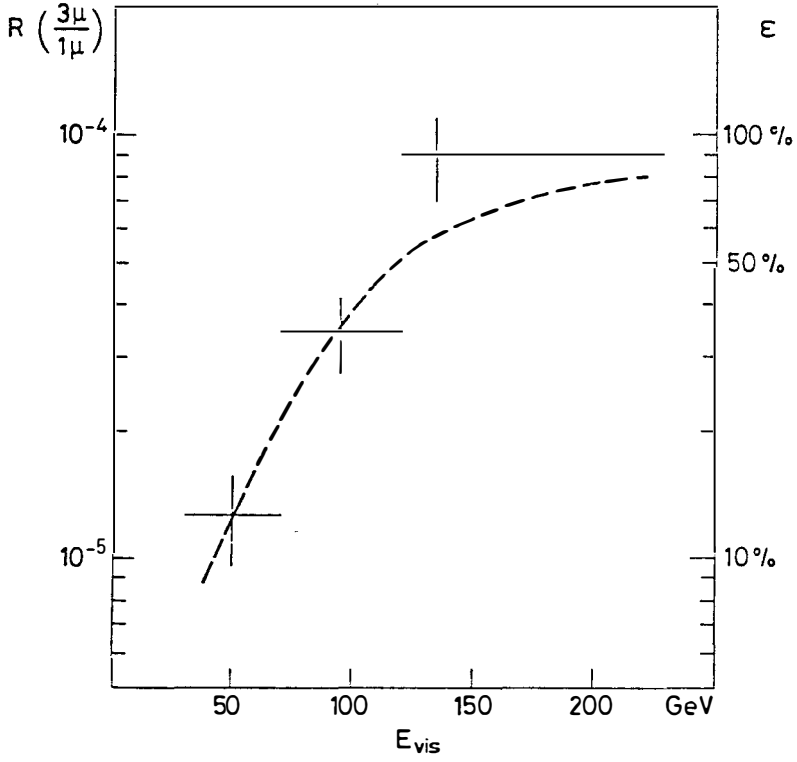

Fig. 7 Ratio of event rates R (3μ/1μ) corrected for background from π/K decay. The line shows the 3μ detection efficiency assuming a model for hadronic μ pair production (r.h. scale).

We see that from the rate alone a reliable choice between different production mechanisms is difficult to make. We therefore turn to kinematical properties of the trimuon events. Since there are two μ^- and one μ^+ in these events, we have to choose the leading μ^- amongst the two. In analogy to the dimuon events, we define here as leading muon (μ_1^-) the one for which the sum of the absolute values of the transverse momenta of the other negative muon (μ_2^-) and the positive muon (μ_3^+) relative to the direction of the virtual W-boson, $\vec{W} = \vec{\nu} - \mu_1$ is minimal. Fig. 8 then illustrates a difference between the leading and non-leading μ^-. Here the invariant dimuon masses M_{--} and M_{-+} are plotted against the trimuon invariant mass M_{--+}. For M_{-+} there are two possible combinations; the one indicated by a cross is the one between μ^+ and μ_1^-, the one given by a dot is the combination of μ^+ with the non-leading μ_2^-. It appears from the data that there is little correlation between the leading μ_1^- and both μ_2^- and μ^+, while the invariant mass of μ^+ with μ_2^- is bounded below 1.5 GeV, indicating a possible common origin of those two muons.

A similar conclusion can be drawn from the momentum asymmetries $\alpha_{ik} = (p_i - p_k)/(p_i + p_k)$ of pairs (i,k) of muons shown in figs. 9 and 10. While the combinations (μ_1^- μ^+) and (μ_1^- μ_2^-) are asymmetrical as the one from dimuons (top), the combination (μ_2^- μ^+) is symmetrical within the experimental error. The invariant masses corresponding to these combinations are displayed in fig. 11. They again show the striking difference between the (μ_2^- μ^+) pairing and the other combinations.

The low values of m (μ_2^- μ^+) are of course reproduced well by the electromagnetic μpair production models[12,13,14] and by the experimental data on hadronic μ pair production[21] which are dominated by ρ production. The leptonic cascade models[16,17] can only reproduce the data if the mass of the neutral heavy lepton L_o is around 1.5 GeV, which means a severe restriction on these models. Also the heavy quark cascade models with a b-quark mass m_b = 4.5 GeV predict a higher average invariant mass of this pair. We conclude from this that less than 10% of the events are due to a heavy quark cascade, with 90% confidence. A more decisive test can, as in the case of dimuons, be done on the basis of the projections of the muon momenta on the plane perpendicular to the neutrino direction. If we then compute the angle $\Delta\varphi_{1,23}$ in this plane between the leading

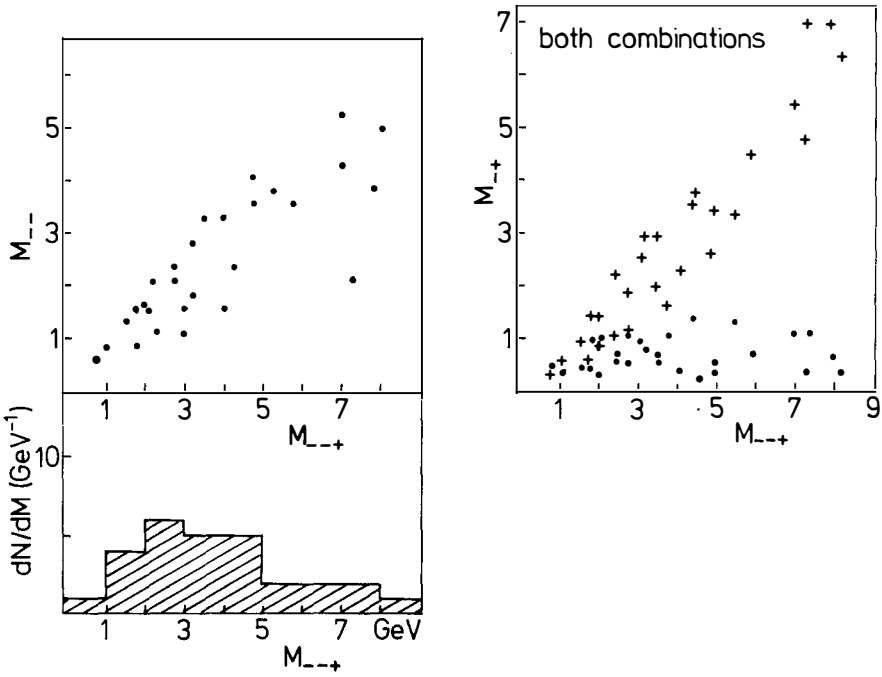

Fig. 8 Scatter plot of invariant 2μ and 3μ masses for trimuon events (subsample of 28 events).

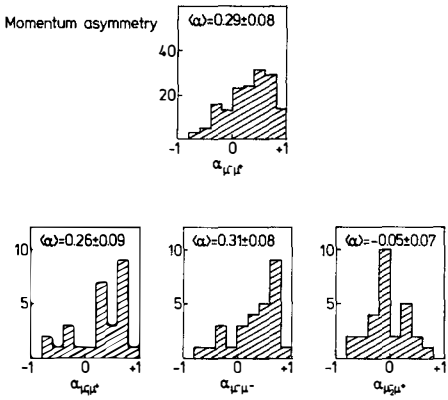

Fig. 9 Muon momentum asymmetries α_{ik} for dimuon events and for the three two-muon combinations of trimuons (subsample of 28 trimuon events).

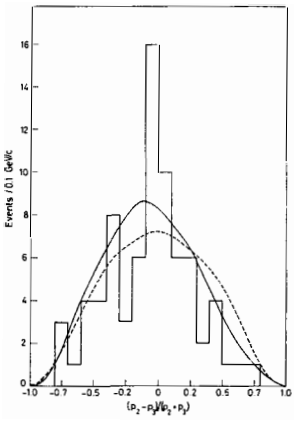

Fig.10 Momentum asymmetry α_{23} for all 76 trimuon events. Full line: Lepton cascade model; dashed line: hadronic μ pair production model.

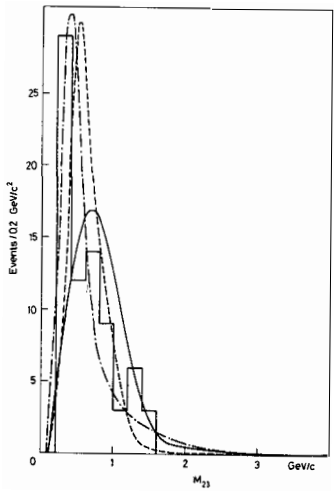

Fig.11a M_{23}

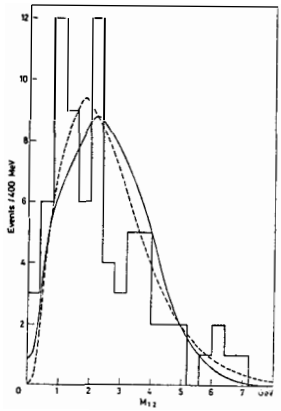

Fig.11b M_{12}

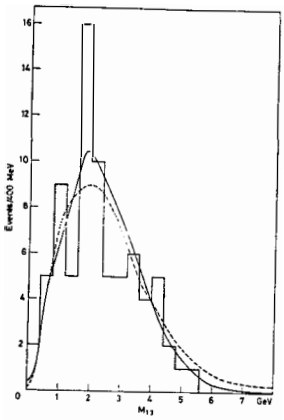

Fig.11c M_{13}

Fig.11 Invariant two-muon masses M_{ik} for the three two-muon combinations (i,k) in trimuon events (μ_1 = leading muon).

μ_1^- and the vector sum of μ_2^- and μ_3^+, we expect quite different distributions for the models in question: the electromagnetic models yield a distribution in $\Delta\varphi_{1,23}$ which has enhancements at 0^o and 180^o and a minimum around 90^o due to the interference of amplitudes from the radiation of the leading μ_1 and the in - and outgoing quarks. The relative strengths of forward and backward radiation differ slightly between the models[12,13,14]. Lepton cascade models[16,17] yield a rather flat distribution in $\Delta\varphi$, while the hadronic production will occur predominantly around $\Delta\varphi = 180^o$. Fig. 12 shows distributions according to several models and the data. Here we require that all muons have a transverse momentum of at least 200 MeV/c relative to the neutrino direction in order to improve on the resolution in $\Delta\varphi$. 60 events survive this cut. The curves are normalized to the same event number. It appears that the large peak of events around 180^o is well reproduced by the hadronic μ pair production model, while the component of events around below 60^o could be due to electromagnetic production. If we fit this distribution by a sum of hadronic and electromagnetic production mechanisms, we obtain a rate $R(3\mu/1\mu) = (0.8 \pm 0.5)\ 10^{-5}$ for trimuons of electromagnetic origin and $R(3\mu/1\mu) = (2.2 \pm 0.5)\ 10^{-5}$ for trimuons of hadronic origin.

The distributions in the azimuthal angles between μ_1 and μ_2 (fig. 13) and between μ_1 and μ_3 (fig. 14) show the same qualitative behavior as the one discussed above.

Additional information is obtained from the distribution of events in p_t^s 23, the transverse momentum of the pair (μ_2; μ_3) relative to the shower axis (fig. 15). This transverse momentum is, for all but two events, below 2.2 GeV/c, which is difficult to reconcile with a lepton cascade origin of the events, as indicated by the full line (for masses $m(M^-) = 9$ GeV and $m(L_o) = 1.5$ GeV). This leads to an upper limit on heavy lepton production: with 90 % CL less then 17 % of the trimuons are due to such a heavy lepton origin.

Summing up the results on trimuons ($\mu^-\mu^-\mu^+$), we conclude

i) The experimental $R(3\mu/1\mu)$ rises from $(1.2 \pm 0.3)\ 10^{-5}$ at 50 GeV to $(9.0 \pm 2.0)\ 10^{-5}$ at 120 GeV neutrino energy, where the variation is mostly due to the experimental cut of 4.5 GeV on muon energies.

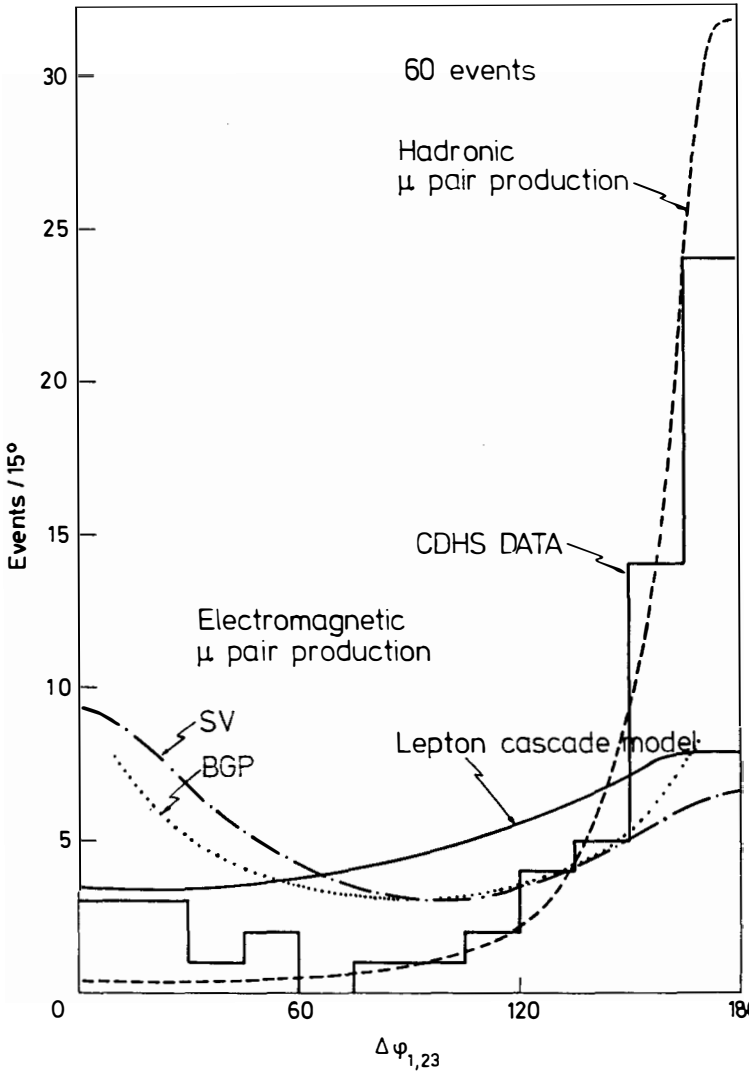

Fig. 12 Distribution in $\Delta\varphi_{1,23}$ the azimuthal angle in the plane transverse to the neutrino direction between the leading μ_1^- and the vector sum of μ_2^- and μ_3. SV (Ref.13) and BGP (Ref.12) are model calculations.

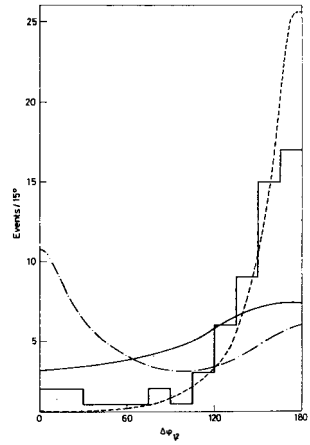

Fig. 13 Distribution of trimuon events in $\Delta\varphi_{1,2}$ the azimuthal angle in the plane transverse to the neutrino direction between the leading μ_1^- and the non-leading μ_2^-. The meaning of the curves is the same as in fig. 12.

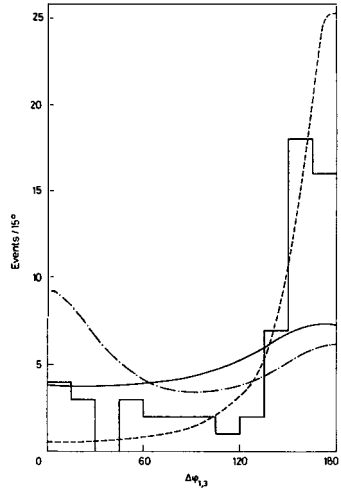

Fig. 14 Distribution of trimuon events in the azimuthal angle $\Delta\varphi_{1,3}$ between μ_1^- and μ_3^+. Curves as in Fig. 12.

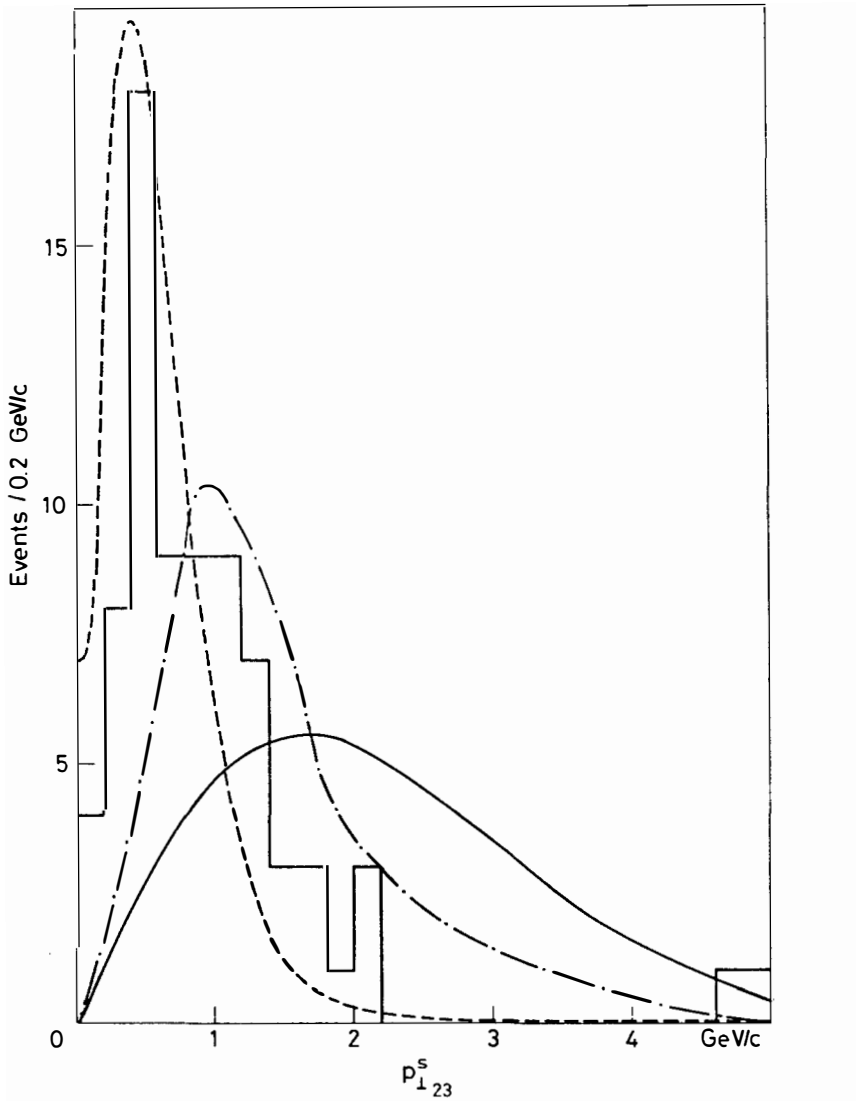

Fig. 15 Transverse momentum of the vector sum of the momenta of μ_2^- and μ_3^+ relative to the hadron shower axis as defined by the momenta of neutrino and leading μ_1^-. The calculations are from hadronic (dashed), electromagnetic (dot-dashed), and lepton cascade (full line) models.

ii) The 76 events can be explained by a sum of two mechanisms: internal pair bremsstrahlung with R $(3\mu/1\mu) = (0.8 \pm 0.5)\ 10^{-5}$ and hadronic pair production with R $(3\mu/1\mu) = (2.2 \pm 0.5)\ 10^{-5}$

iii) Upper limits for other mechanisms are: - less than 17 % of the events (90 % CL) are due to a heavy lepton cascade (M^-/L_o)
- less than 10% of the events (90 % CL) are due to a heavy quark cascade with $m_b = 4.5$ GeV.

4. THE TETRAMUON EVENT

In the wide-band neutrino beam exposure a first example of an event with four muons in the final state[8] has been found. The computer reconstruction of the event is shown in fig. 16. Since the number of charged-current events in the same exposure is estimated (on the basis of a sample) to be 3×10^6 events and the dimuon number $\sim 7 \times 10^3$, this tetramuon event corresponds to a rate of 1.4×10^{-4} relative to dimuons. The measured parameters of the event are contained in table I.

The largest background contribution comes from trimuons with a $\pi \to \mu$ or $K \to \mu$ decay in the dadron shower. For an average[11] $E_h = 28$ GeV we expect $(1.2 \pm 0.4) \times 10^{-2}$ background tetramuon events from this source.

If we now consider possible origins of the event, three conventional processes can be invoked (fig.17): 1) charm production together with electromagnetic μ pair production from the leading μ; 2) charm production together with μ pair production in the hadron shower; 3) charm-anticharm production by a charmed quark produced at the weak vertex. For the total contribution of processes 1) - 3) we estimate a rate of 0.2 events. Additional processes involving new particles could include a quark cascade with new flavours

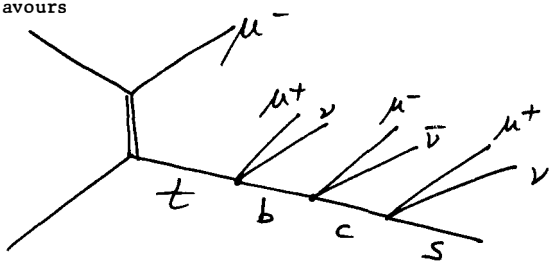

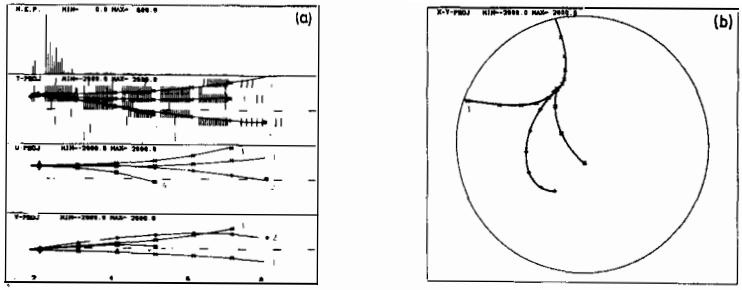

Fig. 16 Tetramuon event display a) On top, pulseheights; next lower, horizontal drift chamber hits and scintillator hits. Bottom, drift chamber hits in ± 60 ^{o} views to horizontal b) Drift chamber hits projected into the plane perpendicular to the neutrino direction.

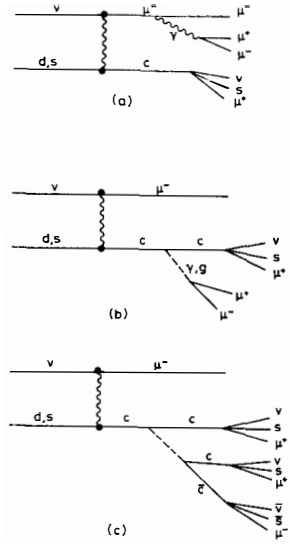

Fig. 17 Conventional sources of tetramuon events.

or a heavy lepton cascade together with charm production:

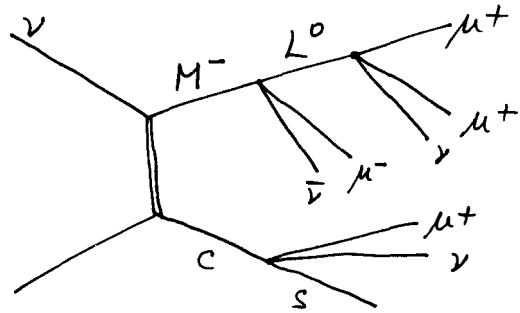

For the processes 2) and 3) and the quark cascade only one μ^- is associated with the lepton vertex, while the other three are produced in the hadron shower. For those processes we would then expect small transverse momenta of the three non-leading muons relative to the hadron shower axis. For the two possible choices of leading muon, these transverse momenta are given in table I. At least one of them is rather large in both cases. This gives slight preference to the other mechanisms listed, though it is premature to make a definite statement on the basis of this one event.

TABLE I

Measured quantities of the four muon event.

1.	Total observed energy			91.4 ± 7.3 GeV
2.	Hadron shower energy			58 ± 7 GeV
3.	Momenta of the muons (GeV/c)*)	P_x	P_y	P_z
	Muon 1 (+)	0.50	0.20	11.1
	Muon 2 (−)	−1.52	−1.69	8.4
	Muon 3 (+)	−0.93	−1.12	9.0
	Muon 4 (−)	−0.24	−0.63	4.45
4.	Muon masses, pair-wise*)			
	Muons 1 and 2			3.0 GeV
	Muons 1 and 3			2.1 GeV
	Muons 1 and 4			1.3 GeV
	Muons 2 and 3			0.95 GeV
	Muons 2 and 4			0.87 GeV
	Muons 3 and 4			0.40 GeV
5.	Three muon masses*)			
	Muons 1, 2 and 3			3.8 GeV
	Muons 1, 2 and 4			3.4 GeV
	Muons 2, 3 and 4			1.3 GeV
	Muons 1, 3 and 4			2.5 GeV
6.	Four muon invariant mass			4.1 GeV

*) The momenta and the masses have the following errors due to multiple scattering and measurement: $\Delta p/p = 0.12$; $\Delta M_{\mu\mu}/M_{\mu\mu} = 0.12$; $\Delta M_{\mu\mu\mu}/M_{\mu\mu\mu} = 0.16$; $\Delta M_{4\mu}/M_{4\mu} = 0.20$.

Transverse momenta with respect to the hadron shower direction for the three non-leading muons.

Leading Muon	$P_{TSH,1}$	$P_{TSH,2}$	$P_{TSH,3}$	$P_{TSH,4}$
2	0.29	--	1.71	0.80
4	0.48	2.33	1.52	--

REFERENCES

1) M. Holder et al., Nucl. Instr. Methods 148 (1978) 235
2) M. Holder et al., Phys. Lett. 71 B (1977) 222
3) M. Holder et al., Phys. Lett. 72 B (1977) 254
4) M. Holder et al., Phys. Rev. Lett. 39 (1977) 433
5) M. Holder et al., Phys. Lett. 69 B (1977) 377
6) M. Holder et al., Phys. Lett. 70 B (1977) 396
7) M. Holder et al., Phys. Lett. 70 B (1977) 393
8) M. Holder et al., Phys. Lett. 73 B (1978) 105
9) B.C. Barish et al., Phys. Rev. Lett. 38 (1977) 577
10) A. Benvenuti et al., Phys. Rev. Lett. 38 (1977) 1110
11) M. Holder et al., Characteristics of trimuon events in neutrino interactions, Nucl. Phys. B., to be published
12) V. Barger, T. Gottschalk and R.J. N. Phillips, Electromagnetic muon pair contributions in neutrino trimuon production, preprint COO-881-9, Nov. 1977
13) J. Smith and J.A.M. Vermaseren, Electromagnetic Backgrounds in Neutrino Produced Trimuon Events, preprint ITP-SB-77-66, and J. Smith, priv. comm.
14) R.M. Barnett, L.N. Chang and N. Weiss, SLAC-PUB-2063
15) B.L. Young, T.F. Walsh and T.C. Yang, Trimuons from Charm, preprint DESY 77/8/, Dec. 1977
16) C.H. Albright et al., Phys. Rev. Lett. 38 (1977) 1187
17) V. Barger et al., Phys. Rev. Lett. 38 (1977) 1190
18) D. Horn and G. Ross, Phys. Lett. 69 B (1977) 364
19) V. Barger, Phenomenology of heavy quark and heavy lepton production by neutrinos, Ben Lee memorial Conf., Oct. 1977, Wisconsin preprint COO-881-7
20) A. Benvenuti et al., Phys. Rev. Lett. 40 (1978) 488
21) K.F. Anderson et al., Phys. Rev. Lett. 37 (1976) 799

OBSERVATION OF TETRALEPTON ($\mu^+e^+e^-e^-$) PRODUCTION

Berkeley-Hawaii-Fermilab-Seattle-Wisconsin Collaboration†

Presented by H.J. Lubatti

Visual Techniques Laboratory, Department of Physics
University of Washington, Seattle, Washington 98195

Abstract: The observation of the production of two electrons, one positron, one positively-charged muon, a neutral K meson, and seven gammas in neutrino interactions in the Fermilab 15-foot bubble chamber is reported.

Résumé: Nous discutons un évènement avec deux électrons, un protons, un mu plus, un meson K et sept gammas produits dans une interaction de neutrino dans la chambre à bulles (15-foot) de Fermilab.

† The members of the collaboration are: H.C. Ballagh, H.H. Bingham, W.B. Fretter, T. Lawry, G.R. Lynch, J. Lys, J.P. Marriner, J. Orthel, M.L. Stevenson, M.D. Sokoloff, G.P. Yost, Department of Physics and Lawrence Berkeley Laboratory, University of California, Berkeley, California 94720; B. Chrisman, D. Gee, A. Greene, G. Harigel, F.R. Huson, T. Murphy, E. Schmidt, W. Smart, J. Wolfson, Fermilab, P.O. Box 500, Batavia, Illinois 60510; R.J. Cence, F.A. Harris, M.D. Jones, S.I. Parker, M.W. Peters, V.Z. Peterson, N. Wyatt, Department of Physics, University of Hawaii, Honolulu, Hawaii 96822; T.H. Burnett, D. Holmgren, H.J. Lubatti, K. Moriyasu, H. Rudnicka, G.M. Swider, E. Wolin, B.S. Yuldashev, Visual Techniques Laboratory, Department of Physics, University of Washington, Seattle, Washington 98195; R. Benada, U. Camerini, M. Duffy, W. Fry, R.J. Loveless, P. McCabe, D. Minette, M. Ngai, D.D. Reeser, Department of Physics, University of Wisconsin, Madison, Wisconsin 53706.

In a partial scan of events produced by neutrinos and antineutrinos, we have found an event with two electrons, one positron, one positively-charged energetic muon, one neutral K meson and seven gammas.[1] One four-muon event has been observed in a previous experiment.[2] This is the first reported example of tri-electron production by neutrinos and the first multi-lepton event in which the details of the accompanying hadron shower can be identified.

The event was observed in the Fermilab 15-foot bubble chamber which was exposed to a beam of neutrinos and antineutrinos. The chamber was filled with a 47% atomic mixture of neon in hydrogen for which the radiation length is 54 cm and the pion absorption length is 1.9 m. The target mass within the fiducial volume was approximately 9 metric tons. A two-plane External Muon Identifier (EMI)[3] was used to select events with muons.

The neutrinos were produced by a 400 GeV proton beam incident on a beryllium oxide target. The resultant mesons were focused using the FNAL quadrupole triplet beam, which enhances the fraction of neutrino flux at high energy.[4] The average ratio of the flux of antineutrinos to that of neutrinos is 0.30.[5]

The event is shown in Fig. 1 together with a magnified view of the vertex region showing the $K^0_s \to \pi^+\pi^-$ decay, which occurs 1.7 cm from the vertex. The electromagnetic processes which signify the electron identification are as follows: (1) trident production (TR); (2) non-visible change in curvature due to bremsstrahlung with an electron pair which points tangent to a track but not to a vertex (NVB + EP); and (3) visible change of curvature due to bremsstrahlung which may or may not have an accompanying electron pair (VB + EP). In addition to these electron signatures, each electron spirals at the end of its track. The measured momenta and energies of the tracks and the identifying signatures and some of the invariant mass combinations are given in Table I.

Except for three short stubs, presumably protons from fragmentation of the neon nucleus, there are no charged tracks leaving the vertex other than the four leptons. Each electron originates at the vertex. Seven gammas from the vertex convert within the fiducial volume; other gamma conversions are bremsstrahlung from the direct electrons. Some of these gammas can be interpreted as resulting from the decay of π^0's produced at the vertex (see Table I).

Fig. 1. The neutrino-induced event with two electrons, one positron, one muon, a $K_s \rightarrow \pi^+\pi^-$ decay, and multiple gammas. The insert provides a magnified view of the vertex showing the leptons originating at the vertex and the K^o_s decay.

TABLE I

Momenta of tracks from the vertex, electron identification signatures, and invariant mass combinations. The neutrino is incident along the x-axis. Bremsstrahlung corrections are included for the electron tracks.

Track	P_x	P_y (GeV/c)	P_z	E (GeV)	Signatures
1. μ^+	21.68±.43	1.54±.06	.65 ±.02	21.74±.44	EMI (2 planes)
2. e^+	1.95±.18	.32±.03	-.46 ±.05	2.03±.18	TR, NVB + EP, VB VB + EP, VB + EP
3. e^-	.74±.06	-.48±.05	-.24 ±.03	.91±.08	TR, NVB + EP, VB
4. e^-	2.27±.20	-.26±.03	.08 ±.01	2.29±.21	NVB + EP, VB + EP
5. K^o_s	1.95±.04	-.35±.02	.31 ±.02	2.06±.04	3C Kinematic fit $\chi^2 = 1.6$
6. γ_1	.04±.004	-.23±.02	.12 ±.01	.26±.03	
7. γ_2	.10±.01	.07±.01	.004±.001	.12±.01	
8. γ_3	.54±.05	-.03±.005	.01 ±.002	.54±.05	
9. γ_4	.16±.01	-.17±.02	.08 ±.01	.25±.02	
10. γ_5	.08±.01	-.02±.003	-.04 ±.004	.09±.01	
11. γ_6	1.60±.14	-.20±.02	-.20 ±.02	1.62±.15	
12. γ_7	.005±.001	.04±.005	-.06 ±.01	.07±.01	
13. p	.33±.07	.02±.01	.32 ±.07	1.05±.04	
14. p	.21±.05	-.17±.05	-.12 ±.13	.98±.003	
15. p	-.09±.01	.12±.01	.08 ±.01	.95±.001	

Invariant Masses
(GeV/c^2)

m_{234} =	1.15 ± .08	m_{2345} =	2.19 ± .10	$m(\gamma_5\gamma_6)$ =	.13 ± .02
m_{23} =	.96 ± .07	m_{25} =	1.24 ± .05	$m(\gamma_3\gamma_6)$ =	.15 ± .02
m_{24} =	.82 ± .05	m_{35} =	.98 ± .05	$m(\gamma_4\gamma_5)$ =	.13 ± .02
m_{34} =	.79 ± .08	m_{45} =	.78 ± .05	$m(\gamma_1\gamma_4)$ =	.14 ± .02
m_{15} =	2.49 ± .05	m_{1234} =	4.09 ± .10	$m(K^o\gamma_5\gamma_6)$ =	.89 ± .03
		m_{all} =	7.46 ± .06[a]		

a) Excluding proton stubs.

The muon track was extrapolated through 9 absorption lengths and was recorded in the two-plane EMI. One chamber in each plane has a good match to the extrapolated track. There are no other hits in either chamber within 1 μsec. of the muon signal. The probability that this muon comes from pion decay is 0.004.

Among the background processes which can simulate direct electron production are Compton scattering, internal conversion of photons and decay of charged K mesons by the K_{e3} mode. Since the invariant masses of the e^+e^- pairs exceed 0.8 GeV,[6] the Dalitz decay of a π^o or η^o meson can be ruled out. The probability that there is a Dalitz decay followed by a large angle electron scattering is $< 10^{-8}$ per event. The probability that any one electron originates as: (i) compton electron within one cm is $\lesssim 10^{-4}$ per event; (ii) an asymmetric Dalitz pair whose partner is undetected ($E \lesssim 3$ MeV) is $\lesssim 0.4 \times 10^{-4}$ per event. The probability that any one electron is produced by K_{e3} decay is $\lesssim 3.3 \times 10^{-4}$ per kaon. Therefore, the interpretation of the event as an ordinary interaction or a dilepton interaction with the additional electrons produced by these background processes is very unlikely. The estimated probabilities of various specific examples of this interpretation are $< 10^{-9}$ per $\nu(\bar{\nu})$ interaction.

The event can be interpreted as a charged current antineutrino interaction. The μ^+ has the largest momentum of all the tracks and has a characteristically large momentum transverse to the ν direction, $p_\perp(\mu^+) = 1.67 \pm .06$ GeV/c (see Fig. 2). The missing momentum transverse to the neutrino direction is 0.34 ± .11 GeV/c. The scaling variables and other kinematic quantities (assuming an inelastic $\bar{\nu}$ interaction) are presented in Table II.

A few possible interpretations of the event and the estimated rate per antineutrino charged current interaction are listed below.

(1) Charm production with inclusive vector meson production

$$\bar{\nu}_\mu + N \to \mu^+ + D \quad V + \chi$$
$$\qquad\qquad\quad \llcorner\!\to Ke\nu \quad \llcorner\!\to e^+e^-$$

Assuming the rate of inclusive vector meson production is 5%, we estimate the rate to be 10^{-7}.

(2) Trilepton production with associated $K\bar{K}$ production.

$$\bar{\nu}_\mu + N \to \mu^+e^+e^- + K\bar{K} + \chi$$
$$\qquad\qquad\qquad\qquad\quad \llcorner\!\to e^-\pi^o\nu$$

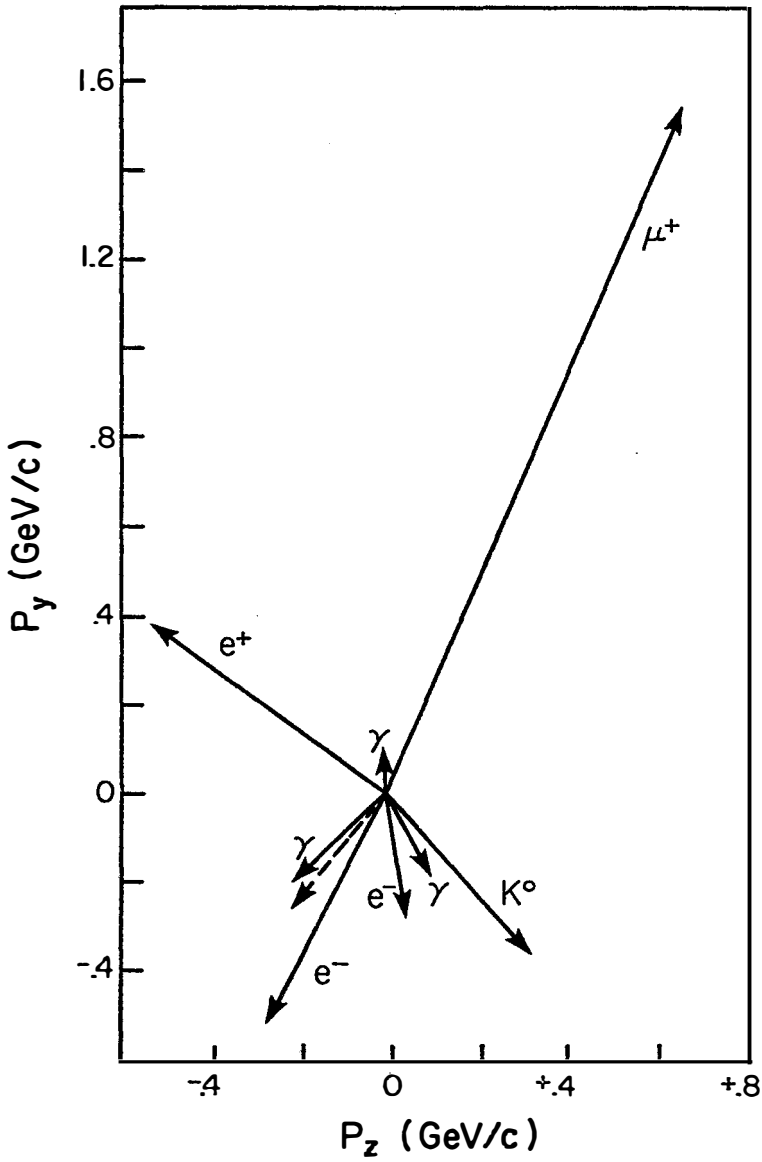

ig. 2. Momenta transverse to neutrino direction. The dotted line shows the missing transverse momentum excluding proton stubs.

Assuming the rate of trilepton production above 30 GeV is 10^{-4} and that the electron comes from K decay, Compton scattering or asymmetric Dalitz decay, we estimate the rate to be 10^{-7}.

(3) Production of the charmed F meson with $K\bar{K}$.[7]

$$\bar{\nu}_\mu + N \to \mu^+ + F^- \quad \bar{K}K + \chi$$
$$\qquad\qquad\quad \big|_{\to \phi e^- \nu}$$
$$\qquad\qquad\quad \big|_{\to e^+ e^-}$$

Assuming a 1% rate of F production, a branching ratio into $\phi e \nu$ of 15%, and the rate of associated production of 20%, we estimate the rate to be 10^{-7}.

(4) Charm production with a radiative e^+e^- pair. The large invariant mass of the pair makes this interpretation improbable. The estimated rate is 10^{-8}.

Other possible production mechanisms for tetralepton production are discussed by Roger Phillips in these proceedings.[8]

TABLE II

Summary of scaling variables assuming an inelastic antineutrino interaction.

E_{vis} = 32.0 GeV	
y_{vis} = 0.32	
x_{vis} 0.21	
v = 0.068 ± 0.004	
$W^2_o = (\Sigma_{vis} E_h)^2 - (\Sigma_{vis} p_h)^2$	= 14.3 ± 1.1 GeV^2
$W^2_{vis} = 2mE_{vis}y(1-x_{vis}) + m^2$	= 16.0 GeV^2
Q^2_{vis} = 4.11 GeV^2	
Missing transverse momentum	= 0.34 ± 0.11 GeV/c

We note that Experiments E-172 and E-180 at Fermilab have observed approximately 8×10^3 $\bar{\nu}$ interactions of which $\gtrsim 1/2$ are above 30 GeV. Thus, using the estimates given above, $\gtrsim 5 \times 10^{-4}$ is a "back-of-the envelope" estimate of how likely it is that such an event might have been observed in experiments to date.

In conclusion, we have observed one example of neutrino-induced four lepton production in an incomplete analysis of an exposure obtained using a neon-hydrogen bubble chamber.

Acknowledgments

We thank the FNAL 15-foot bubble chamber crew and the staffs of our respective laboratories for their assistance in constructing EMI chambers and scanning and measuring the data. H.J. Lubatti thanks the organizers of this years Conference for their hospitality.

This work has been supported in part by the U.S. Department of Energy and the National Science Foundation.

References

1. The event was found by R.J. Loveless of the University of Wisconsin.
2. M. Holder et al., Phys. Letters 73B, 105 (1978).
3. R. Cence et al., Nucl. Inst. and Meth. 138, 245 (1976). S. Parker, J. Orthel, and J. Marriner, IEEE Transactions on Nuclear Science, Vol. NS-25, No. 1, February 1978 (page 134).
4. A. Benvenuti et al., International Colloquium of the CNRS, Ecole Polytechnique, Paris, France, March 1975.
5. Stefanski and White, Fermilab Note FN-292, 1976 (unpublished).
6. If no bremsstrahlung corrections are made to the electrons, the minimum invariant mass of any e^+e^- pair is $0.66 \pm .04$ GeV.
7. The invariant masses reported in Ref. 1 for the four muon event are also consistent with this interpretation.
8. R.J.N. Phillips in these proceedings.

RESULTS ON CHARGED CURRENT DATA FROM C.D.H.S.

(reported by Aurore SAVOY-NAVARRO)
DPhPE, Centre d'Etudes Nucléaires de Saclay,
BP 2, 91190 Gif-sur-Yvette, France.

SUMMARY

We present results on the study of the reaction $\nu(\bar{\nu}) + Fe \rightarrow \mu^-(\mu^+) + X$ by the C.D.H.S. collaboration at the CERN-SPS with a narrow-band beam of 200 GeV. The X- and Y-distributions integrated over all ν-energies are in good agreement with the parton model ; they give a maximum value of 5 % for Callan-Gross violation and they confirm the results on the sea, obtained by this group, from the study of dimuon events. The Y-distribution, $\langle Y \rangle$, $\langle Q^2/E \rangle$ and σ/E do not show any clear dependence on the ν energy, while the X-distribution clearly shrinks as the ν-energy increases. This is a first evidence of scaling violation.

RESUME

On présente des résultats sur l'étude de la réaction $\nu(\bar{\nu}) + Fe \rightarrow \mu^-(\mu^+) + X$ obtenus par la collaboration C.D.H.S. au SPS-CERN avec un faisceau à bande étroite de 200 GeV. Les distribution X et Y intégrées en énergie, sont en bon accord avec les prédictions du modèle à parton ; elles donnent une valeur limite supérieure de 5 % pour la violation de la règle de Callan-Gross ainsi qu'une confirmation des résultats sur la mer obtenus par ce même groupe dans l'étude des événements dimuons. La distribution en Y, $\langle Y \rangle$, $\langle Q^2/E \rangle$, σ/E ne laissent apparaître aucune claire dépendence en énergie, la distribution en X par contre, présente un net effet de rétrécissement quand l'énergie augmente. Ceci est une première indication de violation de l'invariance d'échelle.

The results reported here on charged currents are obtained from data taken last year in the 200 GeV ν and $\bar{\nu}$ narrow-band beam (NBB) at CERN by the CERN - DORTMUND - HEIDELBERG - SACLAY Collaboration (CDHS).

First, we briefly recall the main characteristics of our data. Then we present the results on the data integrated over all energies, on their energy dependence and we end with very few remarks about scaling violations.

I - CHARACTERISTICS OF OUR DATA

The reaction we are interested in is : $\nu + \mathcal{N} \rightarrow \mu^- + X$

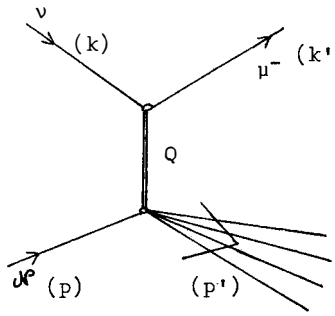

Let me first tell you what we can measure with our apparatus.

I-1 : Characteristics of our apparatus.

Our apparatus (Fig.1) is made of 19 modules, each one composed of iron plates with layers of 8 scintillators (5 or 15 cm) inserted in and a triple-plane drift chamber at the end of each module.

So, its main and powerful characteristic is to be a big ν-target, a μ-spectrometer and a hadron shower calorimeter at the same time.

Each module (Fig.2) is composed of iron plates of 3.75 meters in diameter, with an iron thickness of 75 cm corresponding to a target weight of 65 tons.

From the pulse-height (sum of right scintillators + sum of left scintillators) we measure the hadron shower energy (E_h).

The digitized information of the drift chamber and the magnetized iron (a toroïdal field of 16.5 kG on average) allow us to determine the angle of the muon (θ_μ) and its impulsion ($\vec{P}_\mu$).

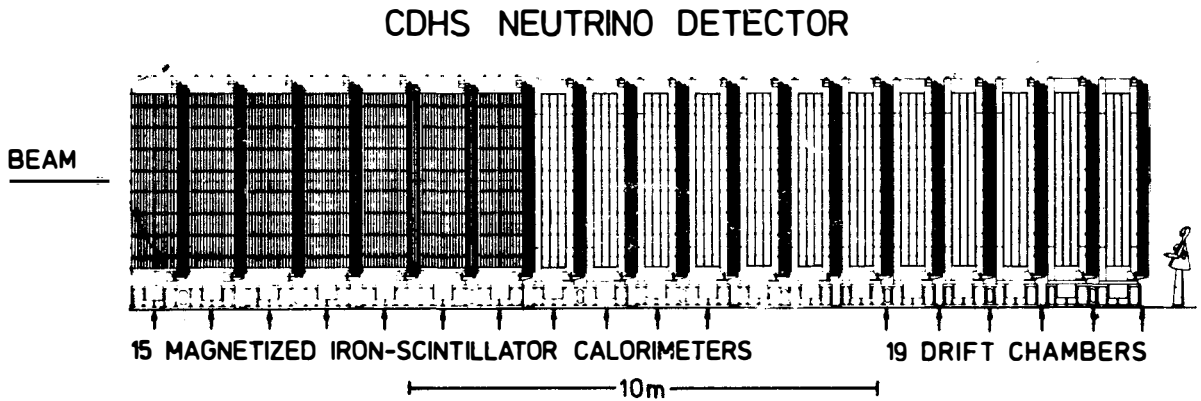

FIG. 1. Experimental Set-up.

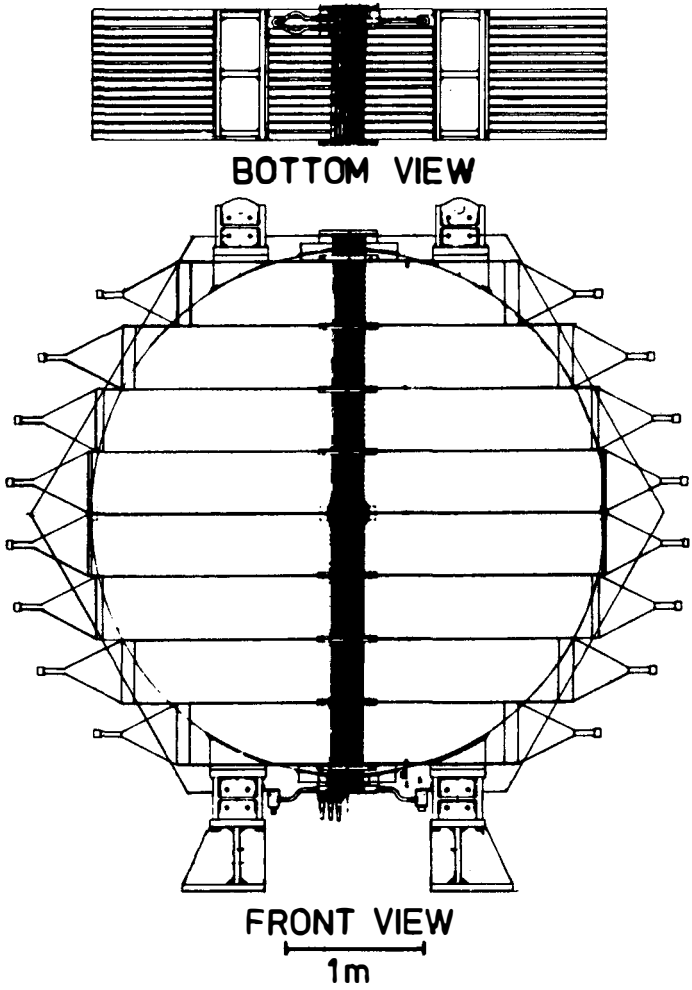

FIG. 2. Front view of the apparatus.

So, for each event we measure the following set of quantities : E_h, P_μ, θ_μ , with our apparatus.

I-2 : The narrow-band beam.

This apparatus is traversed by a dichromatic ν or $\bar{\nu}$ beam, the main features of which are quoted in Table 1.

Some kinematical properties of the NBB provide us with useful information ; the main sources of ν_μ are $\pi_{\mu 2}$ and $K_{\mu 2}$ decays. Because of the two body kinematics, the ν-energy spectrum from $\pi_{\mu 2}$ and $K_{\mu 2}$ decays is flat between zero and $E_{max} = E_{\pi,K} (1 - m_\mu^2 / m_{\pi,K}^2)$ (Fig.3).

The ν - energy is related to the ν emission angle by $E_\nu = E_{max} (1 + \gamma^2 \theta_\nu^2)^{-1}$; from this relation, and provided that the parent beam divergence is small and the decay region small enough, we can determine the ν energy (E_ν) event by event. But since we have another way of determining E_ν, namely by adding P_μ and E_h that are also measured for each event, we have a possibility with these two methods of cross-checking our determination of $E\nu$. The correlation indicated in Fig.4 between E_ν determined as the sum of E_h and P_μ , and the radius (i.e., the distance of the vertex of the event to the beam axis) shows a good agreement between these two methods.

I-3 : Resolution.

I shall now discuss the resolution in the three quantities we measure.

The resolution in the hadronic energy has been measured experimentally by a calibration of some of our heavily equipped modules in an hadronic beam. The results quoted in Fig. 5 give the following parametrization (hereafter in the formulas, energies and momenta are taken in GeV units) :

$$\frac{\Delta E_h}{E_h} = \frac{1}{\sqrt{E_h}} \quad \text{for the 5 cm sampling and,}$$

$$\frac{\Delta E_h}{E_h} = \sqrt{\frac{3}{E_h}} \quad \text{for the 15 cm sampling.}$$

Table I
Main features of the NBB

PROTON ENERGY	400 GeV
AVERAGE PROTON INTENSITY	2×10^{12} ppp
PARENT ENERGY	200 GeV
$\Delta p / p$ (r m s)	5 %
ANGULAR DIVERGENCE	0.2 mrad
DECAY TUNNEL	300 m
LENGTH FROM PROTON TARGET	$\simeq$ 900 m
SPILL LENGTH	23 μsec

Table II
Statistics on the data

	ν	$\bar{\nu}$
TOTAL NUMBER OF PROTONS ON THE TARGET	3×10^{17}	6×10^{17}
TOTAL NUMBER OF $\nu(\bar{\nu})$	36000	12000
NUMBER OF ν WITH $E_\nu > 100$ GeV	16000	3000
NUMBER OF ν AFTER CUTS	22500	6000

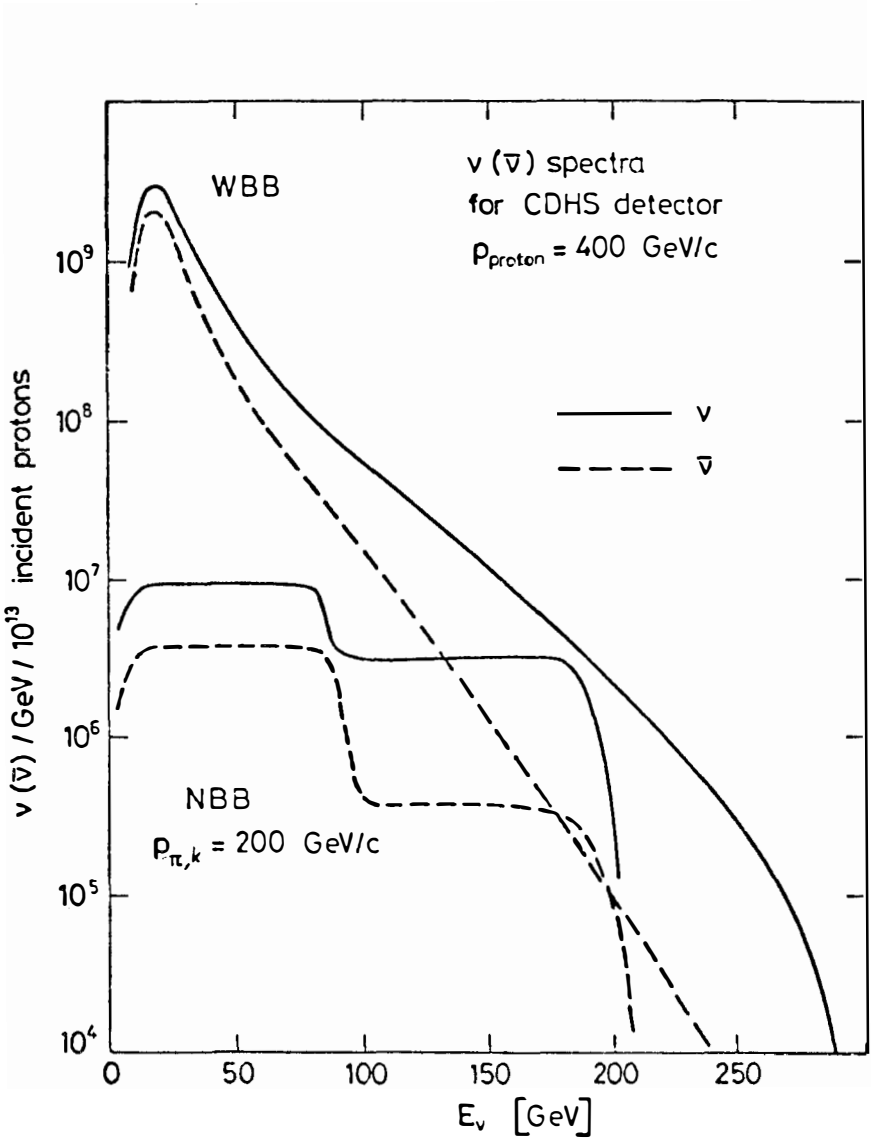

FIG. 3. $\nu(\bar{\nu})$ SPECTRA

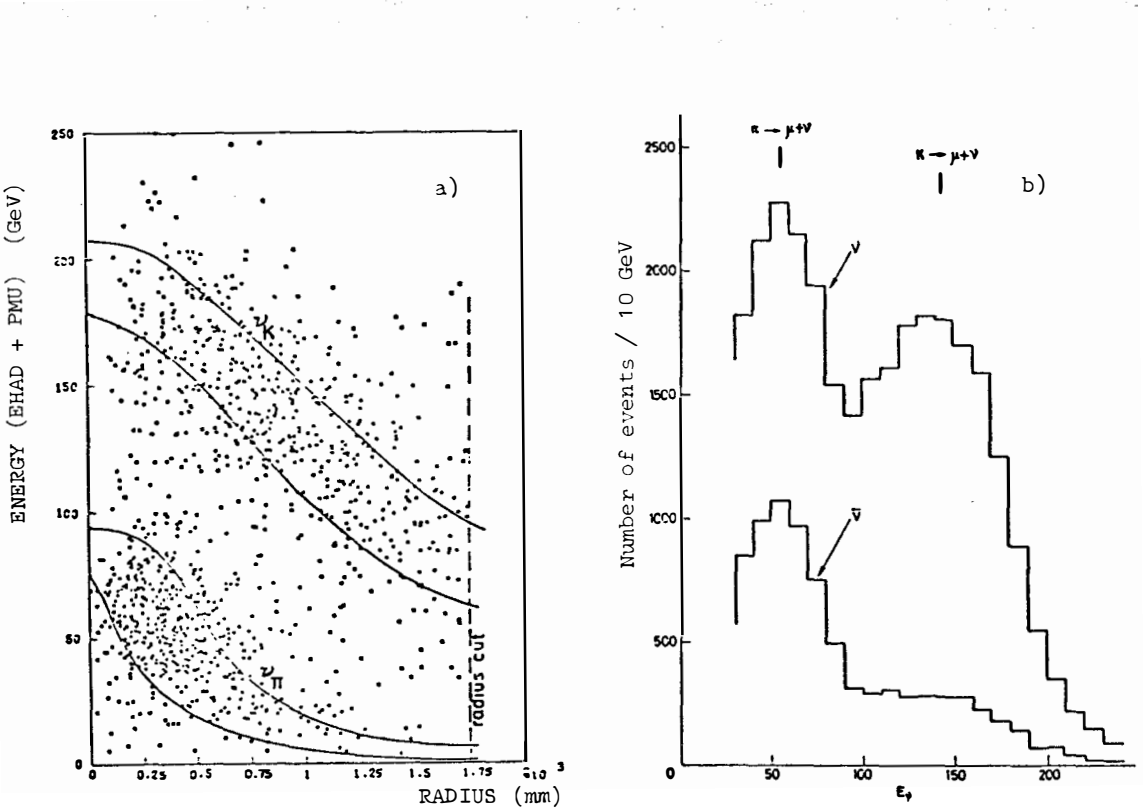

FIG. 4. a) Total energy versus radius and energy spectrum of ν and $\bar{\nu}$ events.
b) Energy spectrum of the events.

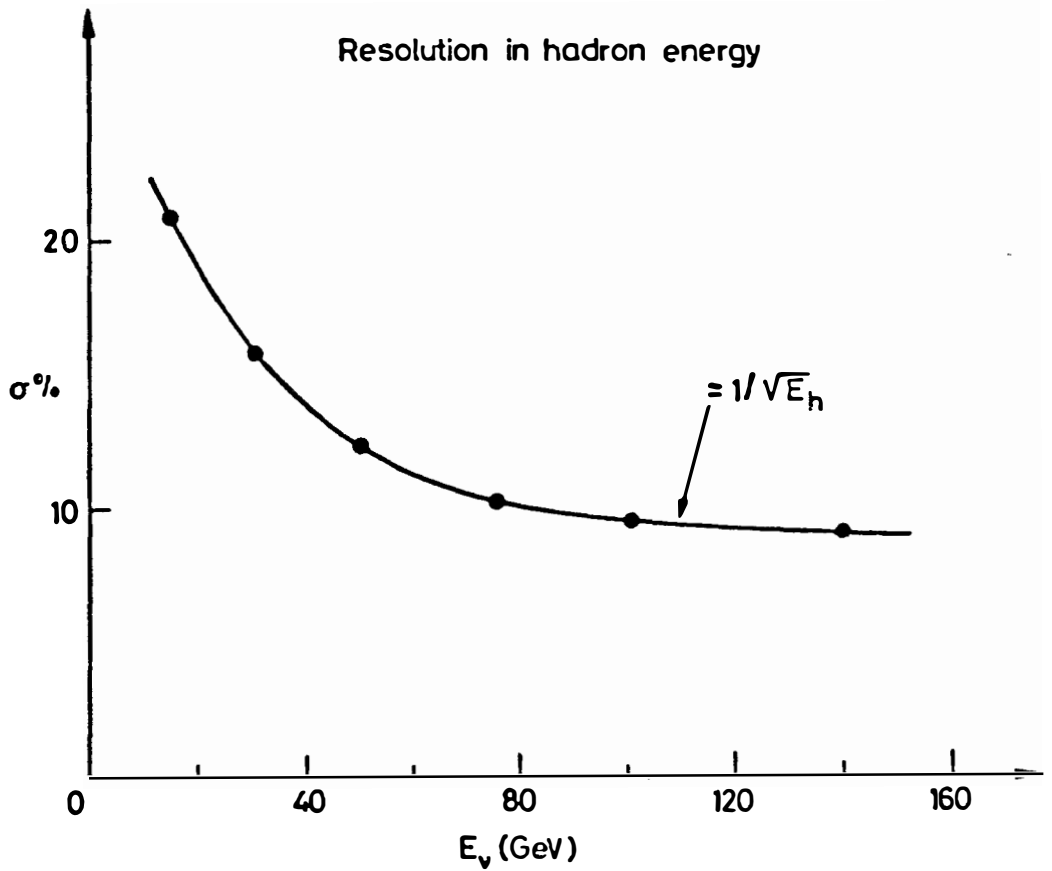

FIG. 5. Resolution in hadron energy (5 cm sampling)

The resolution in P_μ and θ_μ depend essentially on the multiple scattering, and they have been estimated to be :

$$\frac{\Delta P_\mu}{P_\mu} \simeq \left[\frac{0.1}{n} + \left(\frac{0.03 \times P_\mu}{n^2}\right)^2\right]^{1/2} ,$$

(where n is the number of modules taken into account in the fit routine). Typically, $\Delta P_\mu / P_\mu$ is of the order of 10%.

The resolution in the x-and y-projection of the θ_μ angle is well reproduced by :

$$(\Delta\theta_\mu)^{x,y} = 0.0035 \times (430 + 270 \ln E_h)^{1/2} .$$

(So it essentially depends on the hadron shower length.) This gives a typical $\Delta\theta_\mu$ of $0.2/P_\mu$.

From these resolutions, one derives the formulas for the errors in the determination of the X and Y scaling variables by :

$$(\Delta X)^2 = X^2 \left[4 \left(\frac{\Delta\theta_\mu}{\theta_\mu}\right)^2 + (2-Y)^2 \left(\frac{\Delta E_\mu}{E_\mu}\right)^2 + (1-Y)^2 \left(\frac{\Delta E_h}{E_h}\right)^2\right]$$

$$(\Delta Y)^2 = Y^2(1-Y)^2 \left[\left(\frac{\Delta E_h}{E_h}\right)^2 + \left(\frac{\Delta E_\mu}{E_\mu}\right)^2\right]$$

The graphs of Fig.6 show that the error in Y is always small with respect to the average of the Y-distribution in ν and $\bar{\nu}$, while the resolution in X is worse at small Y.

I-4 : Cuts

In order to select really clean data, we have applied the following cuts :

i) the vertex of the event is required to have a distance from the beam axis smaller than 1.6 m (in order to avoid side leakage of the hadronic shower).

ii) The interaction must take place in the first 11 modules so that we remain with about 700 fiducial tons.

iii) The muon must hit at least five drift chambers in order to be measurable, so that we restrict P_μ to be > 6 GeV/c and θ_μ to be < 400 mrad.

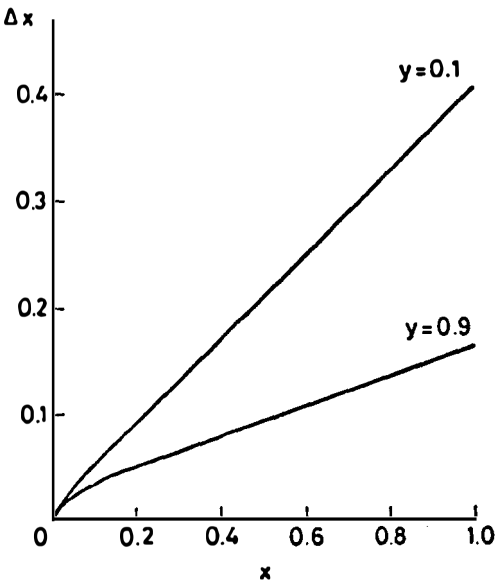

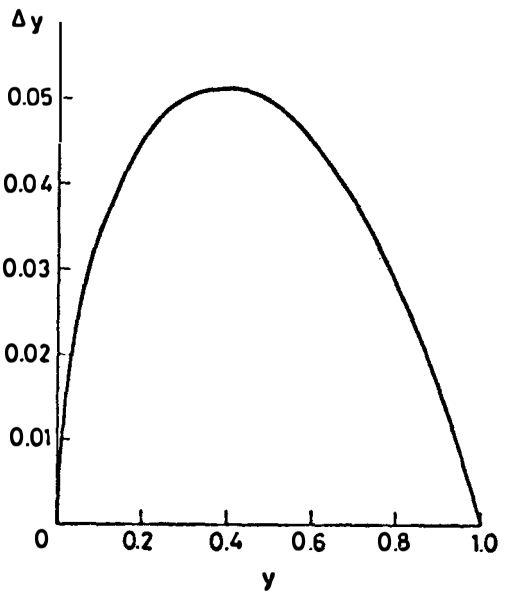

FIG. 6. Resolution in X and Y scaling variables.

iv) A hole cut derived from experimental study is done in order to avoid the surroundings of the central region where the hole creates a poor resolution region.

v) The two first planes of our apparatus are excluded (in order to avoid SPS muons).

In addition to these cuts, we also require 20-30 GeV < E_ν < 250 GeV and that the scaling variable Y is less than $(1 - 7/E_\nu)$ (to avoid poor acceptance region) ; in addition, for some special studies (for instance, a Y-distribution study) we require a cut at low Q^2 (i.E., $Q^2 > 1 GeV^2$).

I-5 : Statistics

The statistics obtained in our ν and $\bar{\nu}$ runs are quoted in Table 2.

We have described how, and how well, we measure the three quantities E_h, P_μ, θ_μ which allow us to determine the following kinematical set of variables, for each event.

$$S = (k+p)^2 \simeq 2 ME_\nu$$

$$Q^2 = -(k-k') \simeq 4E_\mu E_\nu \sin^2 \frac{\theta}{2}$$

$$\nu = pq \simeq ME_h$$

$$E_\nu = E_h + P_\mu$$

$$Y = \frac{2\nu}{s} \simeq \frac{E_h}{E_\nu}$$

$$X = \frac{Q^2}{2\nu} = \frac{2E_\nu E_\mu}{ME_h} \sin^2 \frac{\theta_\mu}{2}$$

and therefore to study the reaction $\nu + \mathcal{N} \rightarrow \mu^- + X$.

Below I report the results we have obtained from these data.

II - RESULTS

Let me first recall :

II-1 : The rules of the game :

The theory of weak interactions tells us that, if Q^2 is much smaller than M_W^2, reaction (1) is decribed by :

$$\frac{d^2\sigma^{\nu,\bar{\nu}}}{dQ^2 d\nu} = \frac{G^2}{2\pi M}\frac{E_\ell}{E_\nu}\left[\cos^2\frac{\theta}{2}\,W_2^{\nu,\bar{\nu}}(Q^2,\nu) + 2\sin^2\frac{\theta}{2}\,W_1^{\nu,\bar{\nu}}(Q^2,\nu) \mp \frac{E_\nu + E_\ell}{M}\sin^2\frac{\theta}{2}\,W_3^{\nu,\bar{\nu}}(Q^2,\nu)\right] \qquad (I)$$

Testing this formula is not such an easy task for the experimentalist; but a simpler formulation of equation (I) can be obtained with the help of further hypotheses.

i) Assume scale invariance, so that the differential cross-section can be expressed with a very simple Y-dependence and with structure functions depending on the X-variable only :

$$\frac{d^2\sigma^{\nu,\bar{\nu}}}{dX\,dY} = \frac{G^2 M E_\nu}{\pi}\left[(1-Y)\,F_2^{\nu,\bar{\nu}}(X) + X\,Y^2\,F_1^{\nu,\bar{\nu}}(X) \mp X\left(Y-\frac{Y^2}{2}\right)F_3^{\nu,\bar{\nu}}(X)\right] \qquad (II)$$

ii) Assume charge symmetry, then for an isoscalar nucleus :

$$F_j^{\nu N} = F_i^{\bar{\nu} N} \qquad i = 1, 2, 3$$

iii) Assume the parton model, with nucleons being composed of valence quark, a sea of $q\bar{q}$ pairs and gluons. Quarks being spin-half objects, one has the Callan-Gross relation : $2XF_1 = F_2$, and :

$$\frac{d^2\sigma^{\nu}}{dX\,dY} = \frac{G^2 M E_\nu}{\pi}\left[(1-Y)^2\,\bar{Q}(X) + Q(X)\right]$$

$$\frac{d^2\sigma^{\bar{\nu}}}{dx\,dY} = \frac{G^2 M E_\nu}{\pi}\left[\bar{Q}(X) + (1-Y)^2\,Q(X)\right] \qquad (III)$$

with : $F_2(X) = Q(X) + \bar{Q}(X)$

$$xF_3(X) = Q(X) - \bar{Q}(X)$$

and : $Q(X) = X\left[d(X) + u(X) + s(X) + c(X)\right]$

$$\bar{Q}(X) = X\left[\bar{d}(X) + \bar{u}(X) + \bar{s}(X) + \bar{c}(X)\right] \quad ,$$

[where d(X), u(X), s(X) and c(X) are the X-distribution of d, u, s and c quarks, respectively, discribing the way nucleon energy is shared amongst the partons] .

In this way, the theory provides the experimentalist with a very simple method (namely equation III) of extracting the structure function from $\frac{d^2\sigma^{\nu,\bar{\nu}}}{dX\,dY}$.

Then, the experimentalist's routine consists in :

1) check each one of these hypotheses, step by step ;

2) if all the hypotheses are true, determine the structure function F_i ;

If any hypothesis is not true, try another one and go to 1.

This is what we shall do in the following sections, by first looking at :

II-2: The Y-distribution integrated over all energies

We can rewrite equation II in the following way :

$$\frac{d\sigma^{\nu}}{dY} = \frac{G^2 M E_{\nu}}{\pi}\left[Q + \bar{Q}(1-Y)^2 + K(1-Y)\right]$$

$$\frac{d\sigma^{\bar{\nu}}}{dY} = \frac{G^2 M E_{\nu}}{\pi}\left[\bar{Q} + Q(1-Y)^2 + K(1-Y)\right] \quad , \qquad \text{(II')}$$

where :

$$Q = \int_0^1 Q(X)\,dX = \frac{1}{2}\int_0^1 (2\,X\,F_1(X) + X\,F_3(X))\,dX$$

$$\bar{Q} = \int_0^1 \bar{Q}(X)\,dX = \frac{1}{2}\int_0^1 (2\,X\,F_1(X) - X\,F_3(X))\,dX$$

$$K = \int_0^1 K(X)\,dX = \int_0^1 (F_2(X) - 2\,X\,F_1(X))\,dX$$

The first question we can ask ourselves is : Do the data verify this Y-dependence? From a first look at the data (Fig.7) we notice that in we have a very important flat component, while the contrary is observed in the $\bar{\nu}$ -data.

By fitting our $\bar{\nu}$ data according to equation (II'), we can check this parametrization and determine the amount of each one of these components. We obtain,

$$\frac{K}{Q+\bar{Q}} = \frac{\int F_2 - 2\,x\,F_1}{\int F_2} = \frac{2\,\sigma_L}{\sigma_L + \sigma_R} < 5\ \%$$

$$\frac{\bar{Q}}{Q+\bar{Q}} = 0.16 \pm 0.02$$

Now we go a little bit further, and look at the Y-distribution in ν and $\bar{\nu}$ separately, in the framework of the parton model. Neglecting Cabibbo 's angle (error of about 5%) and charmed partons inside the nucleus, and making the isoscalar approximation for Fe (error of about 5%) ; one has :

$$\frac{d\sigma}{dY}(\nu p) \propto \left(\frac{u+d}{2} + s\right) + \frac{\bar{u}+\bar{d}}{2}(1-Y)^2$$

$$\frac{d\sigma}{dY}(\bar{\nu} p) \propto \left(\frac{u+d}{2}\right)(1-Y)^2 + \left(s + \frac{\bar{u}+\bar{d}}{2}\right)$$

where

	ν	$\bar{\nu}$
Q	$\frac{u+d}{2} + s$	$\frac{u+d}{2}$
$\bar{Q}$	$\frac{\bar{u}+\bar{d}}{2}$	$\frac{\bar{u}+\bar{d}}{2} + s$

A fit to our data gives :

	ν	$\bar{\nu}$
$\frac{\bar{Q}}{Q+\bar{Q}}$	0.08 ± 0.04	0.16 ± 0.02

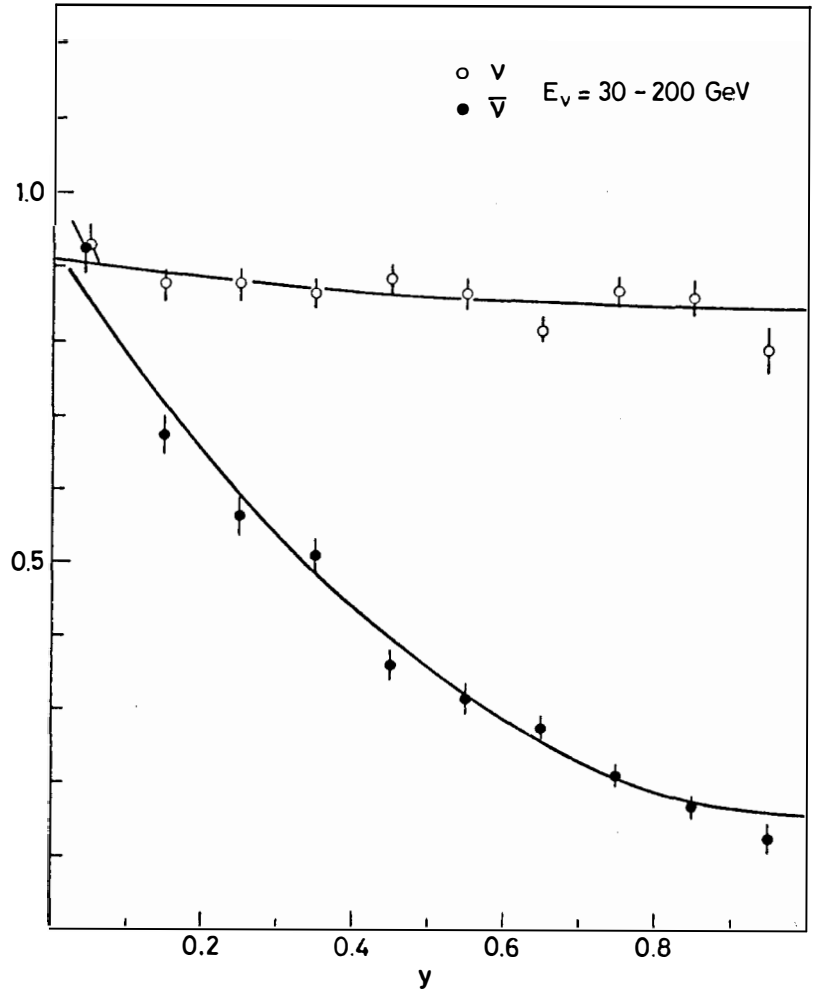

FIG. 7. Y - distribution integrated over all energies.

from which we determine :

$\frac{\bar{u}+\bar{d}}{u+d}$	0.10 ± 0.05
$\frac{s}{u+d}$	0.05 ± 0.025

At this point, we remember some of the results we obtained in the NBB from our study of dimuon opposite sign events. It was desmonstrated[1]) that the main origin of this type of events is charm production according to the GIM mechanism ; they can be explained by the following graphs :

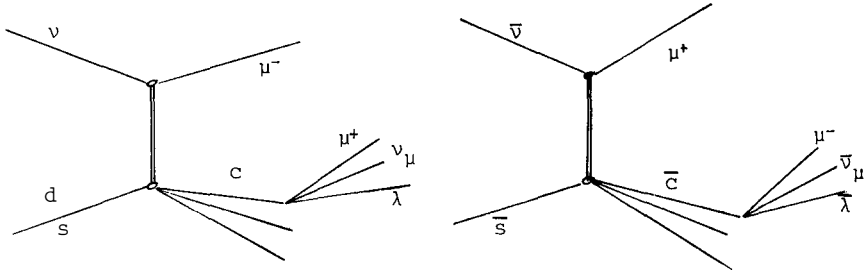

and the elementary cross-section for each of the processes are :

Process	$d\sigma/dx \quad \propto$
$\sigma(\nu+d \rightarrow \mu^-+c)$	$\sin^2 \theta_c \; d(x)$
$\sigma(\nu+s \rightarrow \mu^-+c)$	$\cos^2 \theta_c \; s(x)$
$\sigma(\bar{\nu}+\bar{s} \rightarrow \mu^+ +c)$	$\cos^2 \theta_c \; s(x)$
$\sigma(\bar{\nu}+\bar{d} \rightarrow \mu^+ +c)$	$\sin^2 \theta_c \; \bar{d}(x)$

(The last process is negligible). From this we get :

$$\frac{s}{u+d} = R \; tg^2 \; \theta_c \left[\frac{R_{21}}{\bar{R}_{21}} - 1 \right]$$

where $R = \sigma^{\bar{\nu}} / \sigma^{\nu}$ for the charged current

$$\frac{R_{21}}{\bar{R}_{21}} = \left(\frac{\sigma_{2\mu}}{\sigma_{1\mu}}\right)^{\nu} \Big/ \left(\frac{\sigma_{2\mu}}{\sigma_{1\mu}}\right)^{\bar{\nu}}$$

From our dimuon events we get :

$$\frac{s}{u+d} = 0.04 \pm 0.01$$

which is in good agreement with what we have derived from the Y-distribution of charged currents.

This small violation of charge symmetry due to the s - contribution (different for ν and $\bar{\nu}$) is consistent with our previous results for the test of the charge symmetry [2] (verified within $\pm$10% error).

II-3 : The X-distribution integrated over all energies

By fitting the X-distribution according to equation III (Fig.8), we get :

i) $\bar{Q}(X)$ is compatible with $(1-X)^{6.5\pm0.5}$. A restriction can be made here concerning the validity of such a fit in the very low X region (namely $X < 0.05$) ; the data seem to flatten.

ii) $Q(X) - \bar{Q}(X)$ is compatible with $\sqrt{X}\,(1-X)^{3.5\pm0.5}$

iii) We observe a shrinkage of about 15 % when we compare our data with ed data (Fig. 9). If now we look at the variation of the X-distribution for different Y-bins, equation (III), if true, would imply that at low Y, the X-distribution for ν is essentially $Q+\bar{Q}$ as well as the one for $\bar{\nu}$; for high Y, the X-distribution for $\bar{\nu}$ is essentially Q while the X-distribution for $\bar{\nu}$ is essentially $\bar{Q}$. By looking to our data (Fig.10) we see that this is nicely verified ; the $\bar{\nu}$ X-distribution is shrunk from $\langle X \rangle \simeq 0.22$ at low Y to $\langle X \rangle \simeq 0.13$ at high Y, while the ν X-distribution does not show such a big variation.

So by looking at "high" Y events (say $Y > 0.8$) in $\bar{\nu}$, we get EXPERIMENTALLY, a X-distribution of the sea and $\langle X \rangle_{sea} \simeq 0.13 \pm 0.02$ (Fig.11).

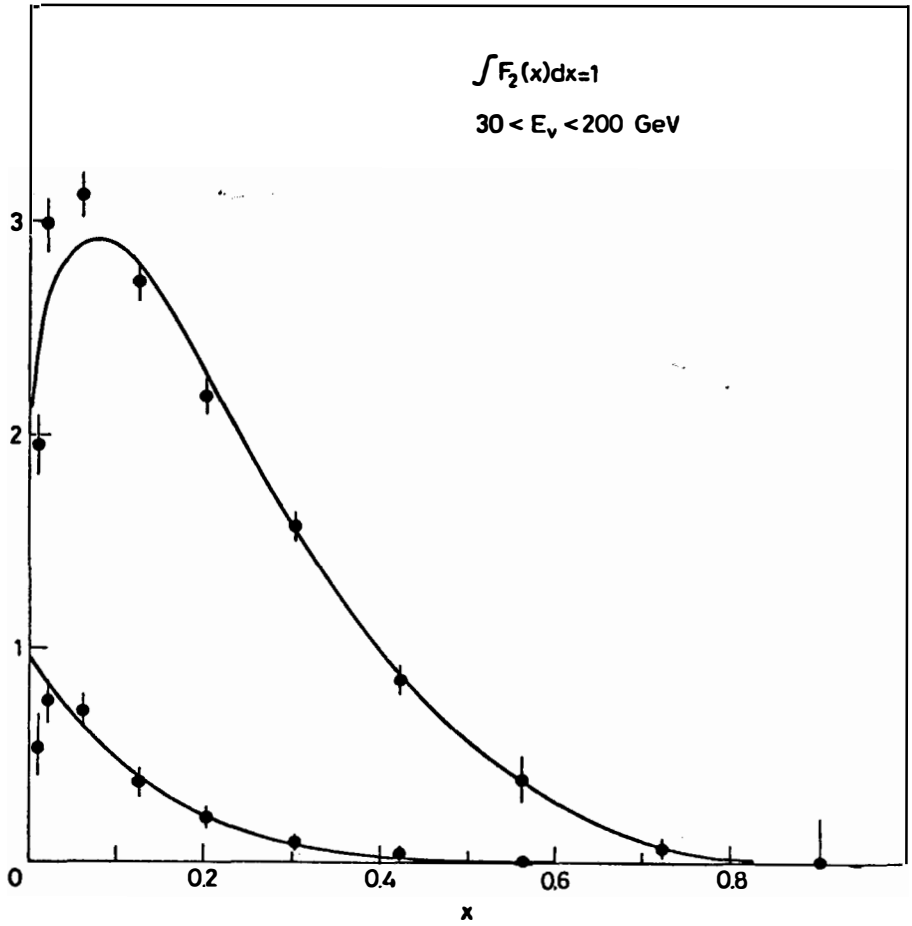

FIG. 8. $Q+\bar{Q}$ as a function of X
$\bar{Q}$ as a function of X.

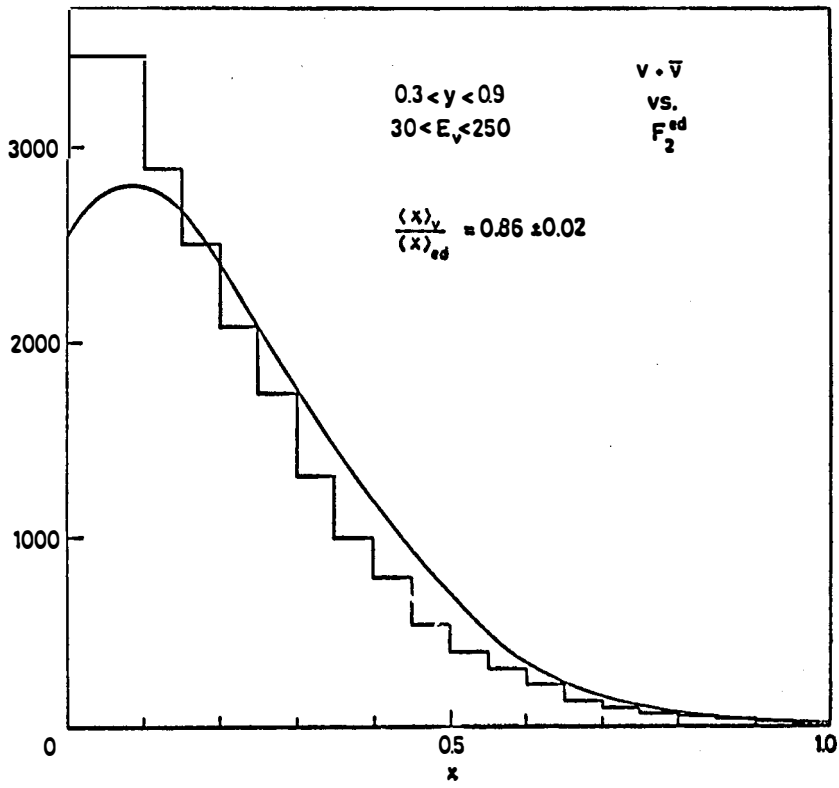

FIG. 9. Comparison between $F_2^{\nu N}$ and F_2^{ed}.

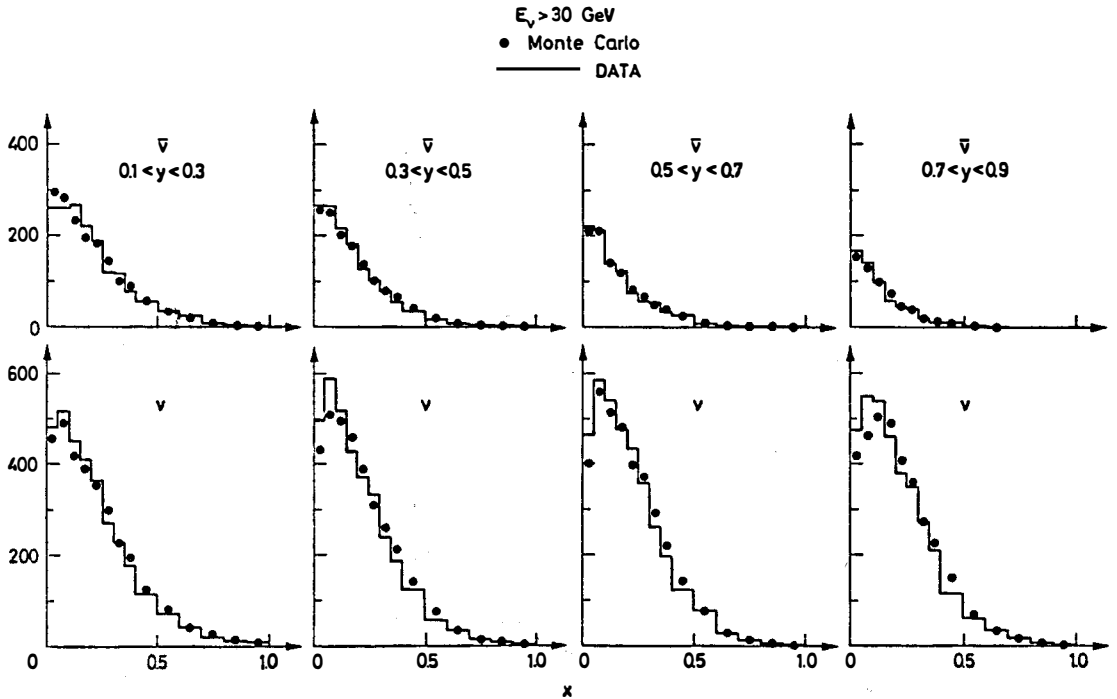

FIG. 10. X versus Y both for ν and $\bar{\nu}$

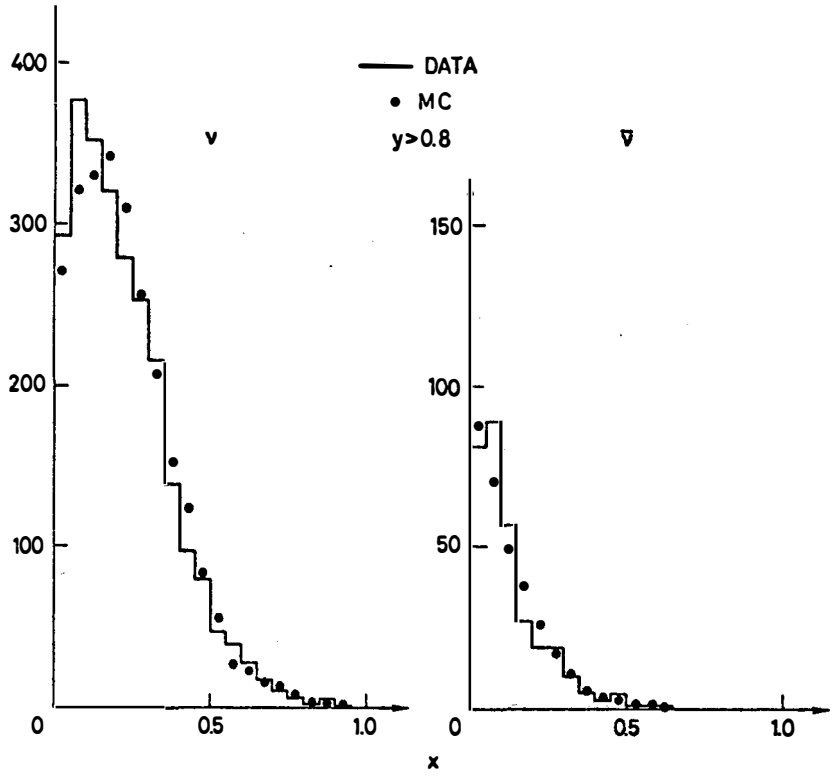

FIG. 11. X distribution for Y > 0.8 both for ν and $\bar{\nu}$.

Here again, we can compare with another interesting way we have, in our experiment, to get that distribution. As the $\bar{\nu}$ dimuon events[1] are essentially produced by the processus $\bar{\nu} + \bar{s} \rightarrow \mu^+ + \bar{c} + X$ (and $\bar{c} \rightarrow \mu^- \bar{\nu}_\mu \bar{\lambda}$), the X-distribution of these events is essentially the X-distribution of the strange sea (Fig.12). Taking into account the π and K decay background, estimated to be 13 % $\pm$ 4 %, we get $\langle X \rangle_{sea} \simeq 0.13 \pm 0.02$ (consistent with the result of our previous method).

We can now make some concluding remarks on what we have learnt from X-and Y-distribution integrated over all energies.

i) From the Y-distribution

Callan - Gross violation is less than 5%

$$\frac{\bar{Q}}{Q+\bar{Q}} \simeq 0.16 \pm 0.02 \quad \text{for } \bar{\nu}$$

$$\frac{\bar{Q}}{Q+\bar{Q}} \simeq 0.08 \pm 0.04 \quad \text{for } \nu$$

$$\frac{s}{\bar{u}+\bar{d}} \simeq 0.05 \pm 0.025$$

$$\frac{\bar{u}+\bar{d}}{u+d} \simeq 0.10 \pm 0.05$$

ii) From the X-distribution

$\bar{Q}(X)$ is compatible with $(1-X)^7$

$Q(X) - \bar{Q}(X)$ is compatible with $\sqrt{X}(1-X)^3$

F_2^ν shrinks about 15% compared with F_2^{ed}

$\langle X \rangle \simeq 0.13 \pm 0.02$ for $\bar{Q}$ and

$\langle X \rangle \simeq 0.22 \pm 0.01$ for $\bar{Q}$

In addition we can note :

iii) A nice consistency between the predictions of the parton model and the experimental X- and Y-distribution.

A nice consistency between the results from dimuon events and those from one - muon concerning the strange quark sea, as well as the mean X-value of the sea.

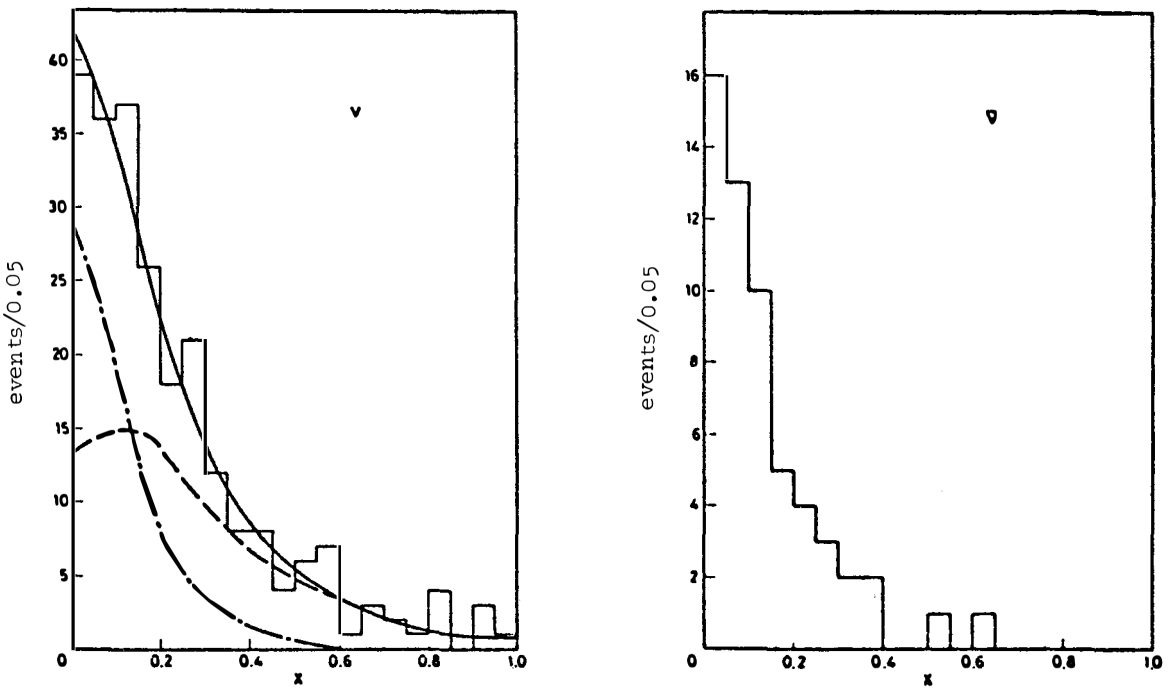

FIG. 12. X distribution from dimuon opposite sign events both for ν and $\bar{\nu}$

By pushing our analysis a little bit further, we now look at the

II-4 : Energy dependence

If we first compare the fit of the Y-distribution in two energy bin regions (namely ν_π region and ν_K region) we get (Fig.13 -a-b), and

E_ν (GeV)	$\frac{\bar{Q}}{Q+\bar{Q}}$ for $\bar{\nu}$
30 → 90	0.15 ± 0.02
90 → 200	0.18 ± 0.02

In addition, the $\langle Y \rangle$ is almost flat (Fig.13,c). If then we look at the X-distribution, we notice that $F_2(X)$ clearly shrinks as energy increases (Fig.14) and :

E_ν (GeV	$\int F_2$
30 → 90	0.44 ± 0.03
90 → 200	0.47 ± 0.05

$\bar{Q}(X)$ seems to become steeper when energy increases. Another interesting quantity to look at, as a function of the energy, is : $\langle Q^2/E_\nu \rangle \propto \langle XY \rangle$. Our data are consistent with a flat behaviour (Fig.15).

Finally plotting our total cross-sections versus energy, we notice again the same kind of shape : σ/E_ν for ν and $\bar{\nu}$ (Fig.16) as well as $\sigma^{\bar{\nu}}/\sigma^{\nu}$ (Fig.17) are almost flat.

Therefore our data show a shrinkage in the X-distributions for increasing ν-energies, while the Y-distributions, $\langle X \rangle$, $\langle XY \rangle$, cross-sections seem to be almost insensitive to E_ν .

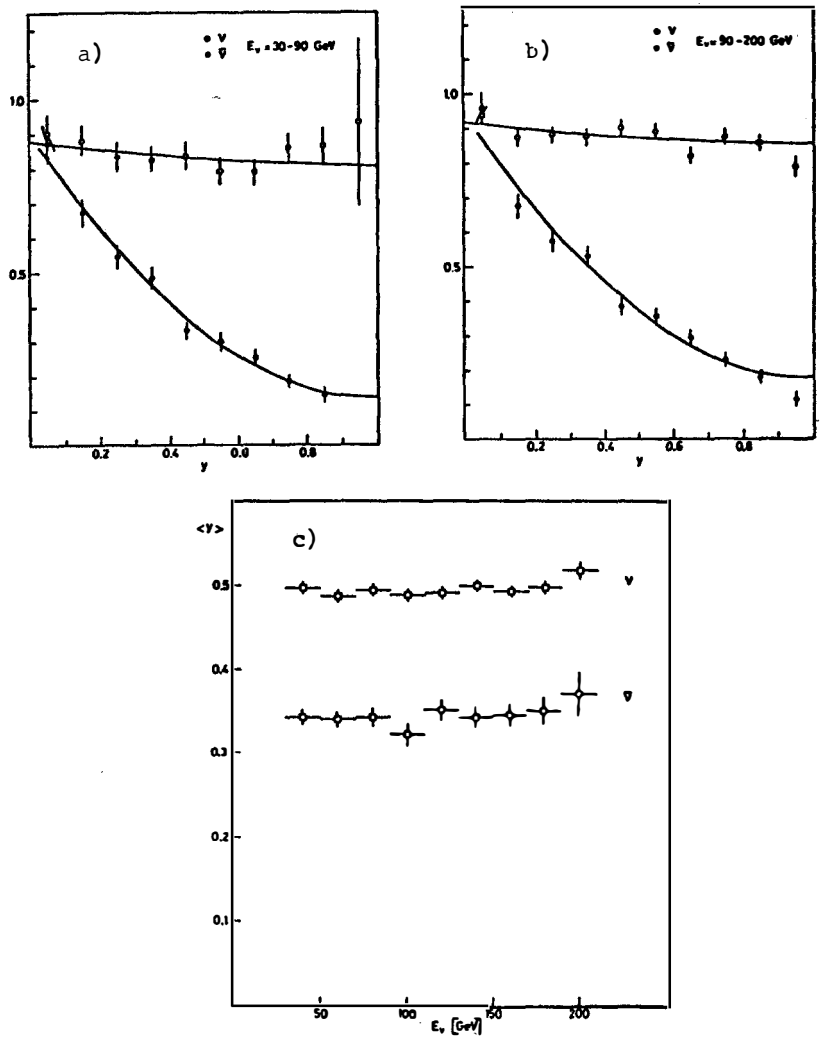

FIG. 13. a) Y - distribution both for ν and $\bar{\nu}$ and for $30 < E_\nu(\text{GeV}) < 90$.
b) Y - distribution both for ν and $\bar{\nu}$ and for $90 < E_\nu(\text{GeV}) < 200$.
c) $\langle Y \rangle$ versus $\nu(\bar{\nu})$ energy both for ν and $\bar{\nu}$.

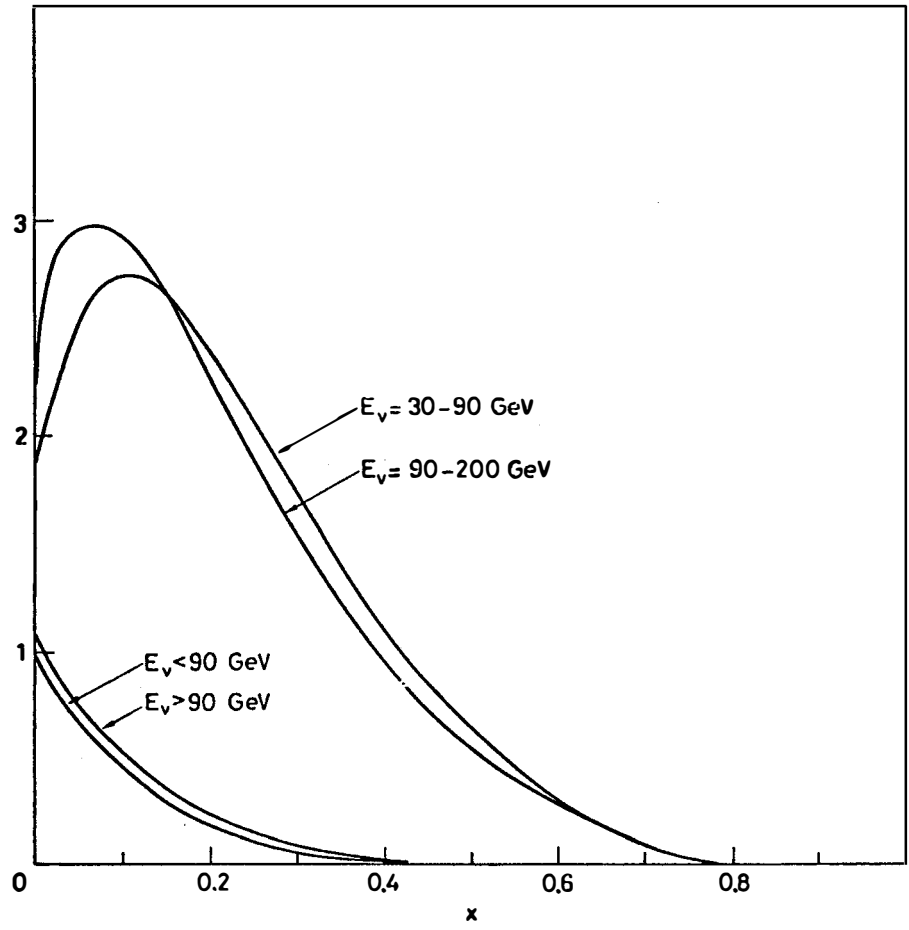

FIG. 14. $F_2(x)$ for $30< E_\nu(\text{GeV})<90$ and $90< E_\nu(\text{GeV})< 200$
$\bar{Q}(x)$ for $30< E_\nu(\text{GeV})<90$ and $90< E_\nu(\text{GeV})< 200$

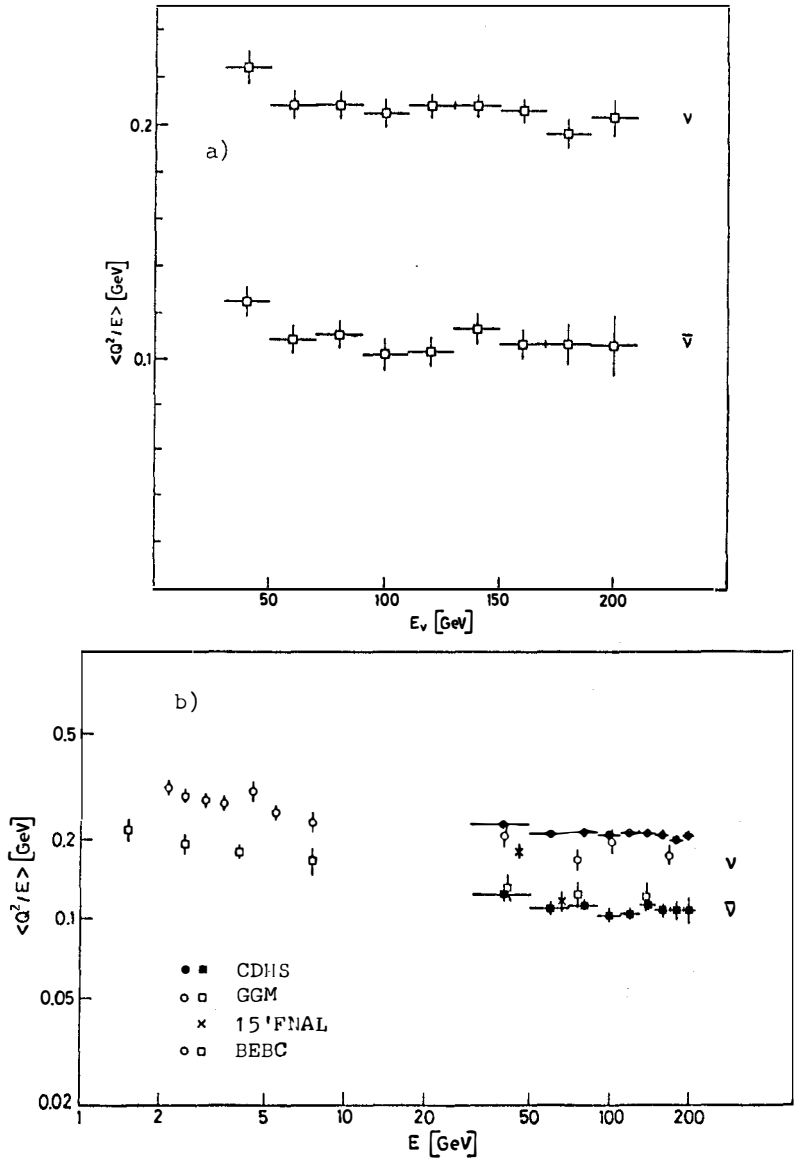

FIG. 15. -a) : $\langle Q^2/E_{\nu,\bar{\nu}} \rangle$ as a function of ν ($\bar{\nu}$) energy : our results
-b) : $\langle Q^2/E_{\nu,\bar{\nu}} \rangle$ as a function of ν ($\bar{\nu}$) energy : comparison between our results and these of BEBC/GGM and Caltech.

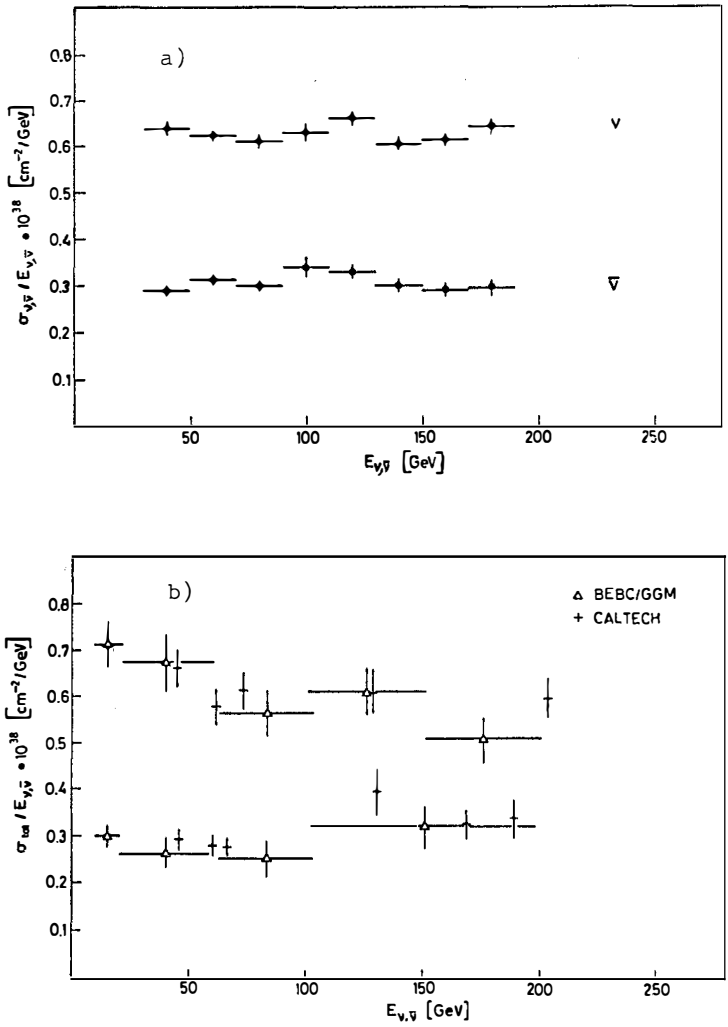

FIG. 16. -a) $\sigma/E_{\nu,\bar{\nu}}$ as a function of ν ($\bar{\nu}$) energy : our results
-b) $\sigma/E_{\nu,\bar{\nu}}$ as a function of ν ($\bar{\nu}$) energy : results of BEBC/GGM and Caltech.

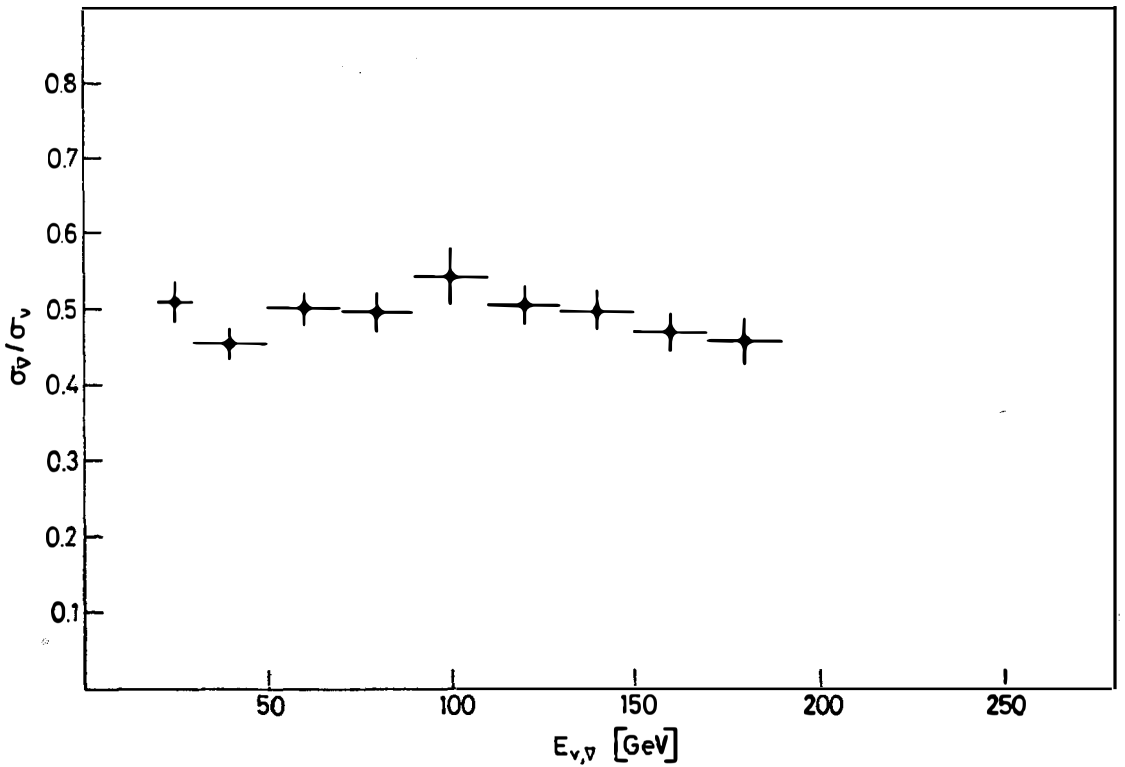

FIG. 17. $\sigma^{\bar{\nu}}/\sigma^{\nu}$ as a function of the ν ($\bar{\nu}$) energy.

Some concluding remarks :

At this level we can ask ourselves what the pattern of the eventual scaling violation is in our data. At the time this report was written, our group had not finished yet this part of the analysis ; but, at a preliminary stage, there is some indication of scaling violation in the variation of the X-distribution with the neutrino energy. It seems to fit well with what is found in ed and our study of the energy dependence suggests that it should not be very strong. We must notice here, that some theoreticians[3] expect the Y-distribution and $\langle Y \rangle$ to show a very weak energy-dependence while X-distribution and $\langle X \rangle$ would show stronger energy dependence. This is just how our data look like.

Our high statistics, our large Q^2 range (2 to 200 GeV^2) will certainly allow us to answer this question in the very near future.

These results were obtained by the collaboration of :
T. HANSL, M. HOLDER, J. KNOBLOCH, J. MAY, H.P. PAAR, P. PALAZZI, A. PARA, F. RANJARD, W. VON RÜDEN, D. SCHLATTER, J. STEINBERGER, H. SUTER, H. WAHL, S. WHITAKER, E.G.H. WILLIAMS (CERN),
F. EISELE, K. KLEINKNECHT, H. LIERL, G. SPAHN, H.J. WILLUTZKI (Dortmund),
W. DORTH, F. DYDAK, C. GEWENIGER, V. HEPP, K. TITTEL, J. WOTSCHACK (Heidelberg),
P. BLOCH, B. DEVAUX, S. LOUCATOS, J. MAILLARD, B. PEYAUD, J. RANDER, A. SAVOY-NAVARRO, R. TURLAY (Saclay),
F.L. NAVARRIA (Bologna).

References

1) M. HOLDER et al., Physics Letters 69B (1977) 377.
2) M. HOLDER et al., Physical Review Letters 39 (1977) 433.
3) A.J. BURAS, K.J.F. GAEMERS, TH-2322-CERN.

SINGLE PION PRODUCTION IN CHARGED CURRENT NEUTRINO INTERACTIONS

Presented by C. VANDER VELDE-WILQUET
Inter-University Institute for High Energies-Brussels.

Neutrino Propane Gargamelle Collaboration

Abstract.

Results are presented on all three neutrino induced, charged current reactions with a single pion in the final state. These reactions are observed in the Gargamelle bubble chamber, filled with a light propane-freon mixture, and exposed to the wide band ν beam at the CERN PS. The relative rates on free nucleons are calculated, taking into account nuclear reinteractions. Implications of these results on the isospin structure of the charged current are investigated.

Résumé.

Des résultats sont présentés concernant les trois réactions de neutrino de type courant chargé, avec un seul pion dans l'état final. Elles ont été observées dans la chambre à bulles Gargamelle remplie d'un mélange léger de fréon et de propane et exposée au faisceau à large spectre du PS au CERN. Leurs sections efficaces relatives sur nucléon libre sont calculées en tenant compte des réinteractions nucléaires. Les implications de ces résultats sur la structure en isospin des courants chargés sont envisagées.

Single pion production in neutrino interactions is one of the simplest reactions to study, in order to investigate the isospin structure of the weak current. Results are presented on all three neutrino induced, charged current reactions producing a pion in the final state :

$$\nu + p \rightarrow \mu^- + p + \pi^+$$

$$\nu + n \rightarrow \mu^- + p + \pi^\circ$$

$$\nu + n \rightarrow \mu^- + n + \pi^+$$

Examples of these three reactions were observed in the Gargamelle bubble chamber filled with a light propane (C_3H_8)-freon (CF_3Br) mixture of about 10 molar % freon. This mixture leads to a 60 cm radiation length. The liquid was exposed to the horn-focused wide band ν beam at the CERN PS. The neutrino energy ranges from 0 to 10 GeV with a maximum around 2 GeV.

The relative cross sections on free nucleons of the above channels are estimated taking into account, by means of a Monte Carlo calculation, the secondary interactions of hadrons created in a complex nucleus. For this analysis 100.000 pictures were used. They are double scanned and completely measured for all kinds of interactions. Candidates of the 1 π-charged current processes are then selected using very restrictive rules. The most important criteria are the following:

1) a μ^- candidate is a non interacting negative particle.

2) a π^+ meson is a positive particle identified either by its decay at rest, or by a mass dependent fit along its trajectory, or by the characteristic interaction features in the liquid, or by δ ray emission.

3) a proton is any positive particle that is not identified as a π^+.

4) a π° meson is detected by the observation of one or two materialized γ rays of more than 25 MeV pointing to the vertex. Whenever two γ rays were observed, they were required to have an invariant mass between the limits 80 and 180 MeV/c^2.

5) events with an additional proton emitted after a nuclear reinteraction are rejected in order to reduce the channel

mixing due to secondary interactions.
6) the total visible momentum of the event along the beam direction, p_x, must be greater than 600 MeV/c in order to eliminate background due to incident charged particles.

The numbers of candidates selected for each reaction are shown in table I.

Table I : Results.

	$\mu^- p \pi^+$	$\mu^- p \pi^\circ$	$\mu^- n \pi^+$
selected	332	109	89
2 π background :			
μ^-/π^-	-(17±4)	-(8±3)	-(3±2)
p/π^+	-(28±9)	-(21±8)	-
missing π°	-(21±2)	-(16±4)	-(5±1)
π absorption	-(8±1)	-(4±.6)	-(.5±.1)
remaining	258±21	60±14	80±10
corrected for p_x cut	258±21	61±14	92±11
corrected for particle detection	386±38	82±19	162±25
corrected for nuclear effects	485±55	156±41	346±56

The contamination of the ν beam by $\bar{\nu}$ was estimated to be less than .5 % and can be neglected in the present analysis. The selected sample of candidates is mainly contaminated by two sources of background : neutron and neutrino interactions producing two pions in the final state. Such interactions can simulate one of the selected topologies either if a π^- meson does not interact and is taken as a μ^- candidate, or if a π^+ meson is not identified and is taken as a proton, or if a π° escapes detection, or again if a pion is ab-

sorbed in the nucleus. All these backgrounds have been estimated by selecting neutral interactions with two identified pions in the final state. The contribution of each of these background configurations to the selected sample (see table I) has been calculated using measured pion detection efficiencies (see next paragraph) and pion absorption probabilities calculated using the same Monte Carlo program as the one used for other nuclear corrections.

The numbers of events remaining after background subtraction (see table I) must still be corrected for signal loss. A first correction is made to account for the different effects of the cut on the total visible momentum along the beam axis p_x, since for the $\mu^- p \pi^\circ$ and $\mu^- n \pi^+$ final states the momentum of the neutral particle is not known. A further correction is made for pion detection efficiencies. These have been measured[1] for the π° using the numbers of events with 1,2,3 and 4 converted γ rays, neglecting the contribution of events with more than two π°. For the π^+ detection correction, we used a sample of π^+ tracks from events satisfying a kinematical fit to the reaction $\nu + p \rightarrow \mu^- + p + \pi^+$ on a free proton. For the π^- detection efficiency, a sample of π^- tracks obtained by the antineutrino propane Gargamelle collaboration has been used.

A Monte Carlo simulation has been performed in order to study nuclear interactions[1]. It is based on a classical cascade model where the nucleus is described as a totally degenerate Fermi gas in a square well potential. Fermi motion and the Pauli exclusion principle are taken into account. The parameters of the model have been calibrated by comparing the Monte Carlo prediction to measurements of the hadron-nucleus inelastic cross sections. The model has then been successfully tested by comparing its predictions with several other data[1].

Applying the Monte Carlo program to the conditions of the present experiment, the transition probabilities for a given hadronic state $(N\pi)$ into another hadronic state $(N\pi)'$ are obtained. The numbers of events in each channel, taking

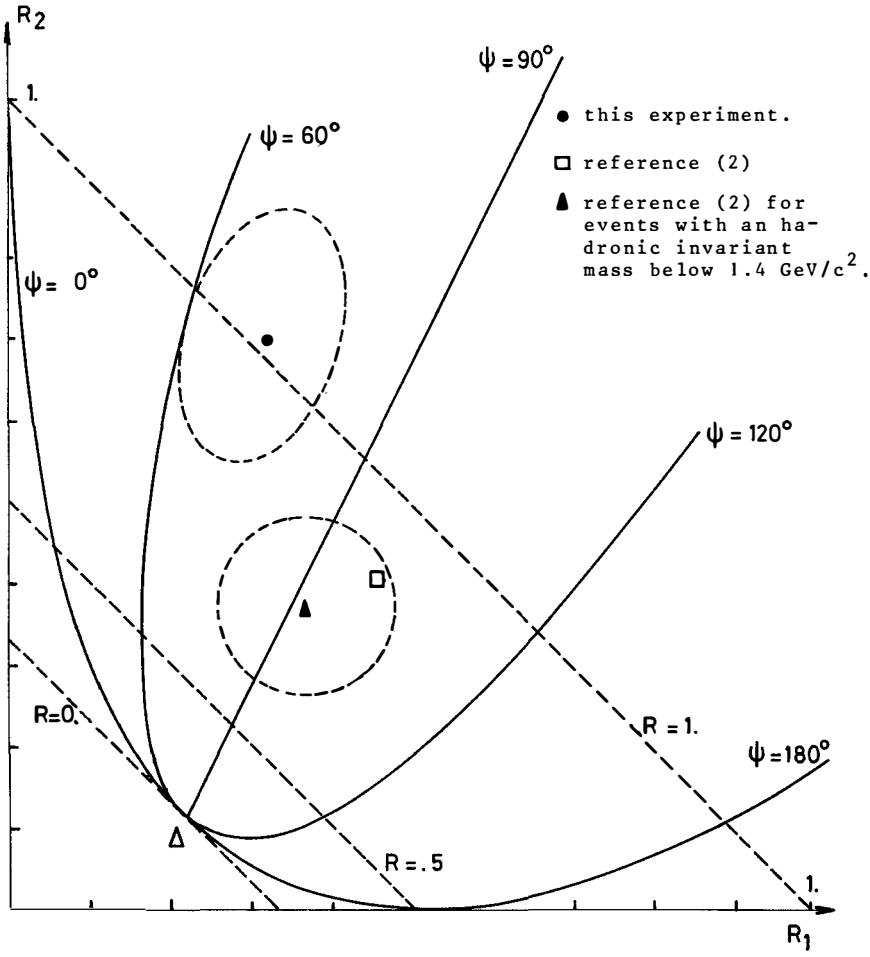

Fig. 1. : Plot of the two cross section ratios $R_1 = \sigma(\mu^- p \pi^0)/\sigma(\mu^- p \pi^+)$ and $R_2 = \sigma(\mu^- n \pi^+)/\sigma(\mu^- p \pi^+)$. Dashed straight lines correspond to points of equal values of $R = |A_{1/2}|/|A_{3/2}|$. The curves and the full straight line correspond to given values of the phase angle ψ. The dashed contours around the experimental points correspond to one standard deviation.

into account the nuclear corrections and also the ratio of neutrons to protons in the liquid, are shown on the last line of table I. They are proportional to the cross sections on free nucleons and allow one to calculate two independent ratios of cross sections; for example :

$R_1 = \sigma(\mu^- p \pi^\circ)/\sigma(\mu^- p \pi^+)$ and $R_2 = \sigma(\mu^- n \pi^+)/\sigma(\mu^- p \pi^+)$.

The values of the ratios R_1 and R_2 were found to be .32±.09 and .71±.14 respectively. Note that these ratio values are not statistically independent. There are correlations. Furthermore, the errors quoted do not include the possible systematic error due to the nuclear correction. This error is expected to be at most a few percents.

If no isotensor exchange is assumed the amplitudes of single pion producing charged current processes can be written as a function of two isovector amplitudes, $A_{3/2}$ and $A_{1/2}$, where the subscripts refer to the isospin of the final state :

$$A(\mu^- p \pi^+) = \sqrt{2}\, A_{3/2}$$

$$A(\mu^- p \pi^\circ) = \frac{2}{3}(A_{3/2} - A_{1/2})$$

$$A(\mu^- n \pi^+) = \frac{\sqrt{2}}{3}(A_{3/2} + 2A_{1/2})$$

The relative abundance of both amplitudes expressed by the ratio $R = |A_{1/2}|/|A_{3/2}|$ and the phase angle ψ between them can be easily calculated from the cross sections ratios R_1 and R_2 The values $R = 1.03 \pm .15$ and $\psi = 73^\circ {}^{+12^\circ}_{-10^\circ}$ were found. This result is reported on Fig. 1, showing the variation of R and ψ with R_1 and R_2, together with the result obtained by the ANL experiment[2]. The curves for $\psi = 0^\circ$ and $\psi = 180^\circ$ correspond to the triangular inequalities resulting from the assumption that there is no isotensor contribution. Both results do not contradict this hypothesis. A more important contribution of the $A_{1/2}$ amplitude is observed for the present experiment. This can be explained by the contribution of the spin 1/2 N resonance as our experiment is performed at higher neutrino energy.

References.

(1) W. Krenz et al, Nucl. Phys., to be published.
(2) S.J. Barish et al, Phys. Rev. Letters 36, 179 (1976).

MEASUREMENT OF (ν + n) TO (ν + p) CROSS-SECTION RATIO FOR CHARGED CURRENT PROCESSES IN THE GARGAMELLE PROPANE EXPERIMENT AT THE CERN-PS

GARGAMELLE neutrino-propane collaboration, presented by

T. FRANCOIS

LPNHE, Ecole Polytechnique, Palaiseau (France)

ABSTRACT :

The ratio of ν + n to ν + p total cross section for charged current processes in the energy range 1 - 10 GeV is determined by two independent methods in the Gargamelle propane experiment. The combined value is R = 2.08 ± 0.15 .

RESUME :

Nous déterminons le rapport des sections efficaces ν + n et ν + p pour les courants chargés par deux méthodes indépendantes. La valeur combinée est : R = 2.08 ± 0.15 .

I.- INTRODUCTION

Most of data in $\overset{(-)}{\nu}$ - physic concern interactions on nucleons -a neutron and proton average-. There are only few results for ν + p in charged current processes (CC) and nothing in neutral current processes (NC).

Here is a contribution to the determination of $R = \frac{\sigma(\nu+n \rightarrow \mu^- + \ldots)}{\sigma(\nu+p \rightarrow \mu^- + \ldots)}$ integrated over the CERN-PS neutrino energy spectrum (1-10 GeV). The experiment was done in the Gargamelle chamber filled with a light propane-freon mixture.

Contradictary results on R [1] were reported up to now, as can be seen in table 1.

	MYATT-PERKINS CERN-1.10 m 1 - 10 GeV	BNL 7' 2-10 GeV	ANL 12' 1.5 - 6 GeV
$R = \frac{\sigma(\nu+n)}{\sigma(\nu+p)}_{CC}$	1.5 ± 0.3	1.48 ± 0.17	2.02 ± 0.23

present determination of R

TABLE 1

II.- GENERAL OUTLINE OF THE METHODS

Two methods can be imagined to determine R.

The first one is based on a kinematical separation of events on free protons, allowed by the 33% ratio of free protons to bound protons in our mixture. The sample used, selected from 256 000 photographs, consists of 2082 "hydrogen-like" events, i.e. events for which the charge of the final state is 1 and with no more than one identified proton. The selected events are required to have an energy greater than 1 GeV.

The second method starts with the naïve idea that events with charge 0 occured on neutrons and those with charge 1 are on protons. This ideal conception is distorted by the nuclear reinteractions inside the target-nucleus. Correcting for nuclear effects in a purely experimental way, we can give the number of events on protons and neutrons, and thus the ratio R. The sample used consists of all CC candidates with an energy greater than 1 GeV found in about 40% of the films, namely 2584 events.

In what follows, we shall focus only on the main problems in each-method. More details can be obtained in reference [2]

III.- DETERMINATION OF R BASED ON INTERACTIONS ON FREE PROTONS.

In this method, R is calculated using the number N_f of interactions occuring on free protons and the total number N_t of all CC interactions in the same neutrino flux :

$$R = \frac{d_f}{d_n} \cdot \frac{Nt}{Nf} - \frac{d_p}{d_n} = 0.312 \frac{N_t}{N_f} - 1.264$$

where d_p , d_n and d_f are the proton, neutron and free proton densities in the liquid.

The number N_t is obtained from the number of CC-events observed in 40% of the photographs, using the measured neutrino flux.

The number N_f is obtained by a kinematical separation of events on free protons. These events can be classified in term of neutral particle multiplicity in the final state :

i) events with no neutral particle ; they must satisfy generally 3 kinematical constraints (3C) and sometimes 2 (2C) if the momentum of one particle is unknown.

REACTION	Number of constraints	Number of fitting events	Corrected events numbers
$\nu + p \rightarrow \mu^- + p + \pi^+$	3 2	259 98	353 ± 22
$\nu + p \rightarrow \mu^- + n + \pi^+ + \pi^+$	2	11	41 ± 13
$\nu + p \rightarrow \mu^- + p + \pi^+ + \pi^\circ$	2	32	130 ± 26
$\nu + p \rightarrow \mu^- + p + \pi^+ + \pi^+ + \pi^-$	3 2	13 8	21 ± 7
$\nu + p \rightarrow \mu^- + n + \pi^+ + \pi^+ + \pi^+ + \pi^-$	2	1	5 ± 5
$\nu + p \rightarrow \mu^- + p + \pi^+ + \pi^+ + \pi^- + \pi^\circ$	2	2	10 ± 8
$\nu + p \rightarrow \mu^-$ + multi-neutrals	-	-	39 ± 13
$\nu + p \rightarrow \mu^-$ + strange particles	-	-	18 ± 5

TABLE 2

Charged current interactions on free protons

ii) events with a neutron or a π° in the final state. $(31 \pm 4)\%$ [2] of the neutrons are observed by an interaction and $(30 \pm 2)\%$ [2] of the π° are detected by the conversion of the two decay gamma rays. These events must satisfy a 2C fit (the momentum of the neutron is unknown and the γ energy is considered as badly measured).

iii) multineutral channels are evaluated assuming the rate of "hydrogen events" in the sample of "hydrogen-like events" to be the same for these channels as for the preceeding ones ($30 \pm 5\%$).

Channels with more than 4 pions in the final state are negligible and the rate of events with strange particles is found to be $3 \pm 0.7\%$.

This kinematical analysis, corrected for nuclear events fitting the constraints, for the charged particle measurability and for π° or neutron detection efficiency yields to : $N_f = 627 \pm 41$ (see table 2).

Finally, we find :

$$R = 2.18 \pm 0.26$$

IV.- DETERMINATION OF R BASED ON THE OBSERVED CHARGE AND PROTON MULTIPLICITY DISTRIBUTION.

Since the sample used in this method consists mainly of neutrino interactions on bound nucleons, the total charge of the final state does not allow a direct separation of reactions on neutrons and protons. But, adding the information of the proton multiplicity, it is possible to account for nuclear effects.

Thus, for each event, we note the total visible charge (Q_V) and the number of proton(s) [1] in the final state (P_V).

---

(1) The problem of π^+/p ambiguity is detailed in ref [2] and is solved. In any case, it is not very important for determining the ratio R, the total charge being unaffected by this ambiguity.

P_V									
6							2	4	2
5						5	15	5	1
4					9	37	20	6	2
3				13	120	69	12	3	
2			11	310	168	26			
1		6	587	577	51	4			
0	2	42	321	149	1				
Q_V	-2	- 1	0	1	2	3	4	5	6

TABLE 3

The (Q_V , P_V) plot

Q_V = visible charge

P_V = number of visible protons.

In an ideal case (free nucleons) only the cells Q = 0,1 and P = 0,1 should be filled. The observed distorted distribution (see table 3) is due to nuclear reinteraction inside nucleus target (mainly carbon). Using in a highly constrained fit a small number of free parameters describing the nuclear effects, it is possible to determine the original numbers in the 4 cells Q = 0,1 , P = 0,1, and then the ratio R.

Observing table 3, it appears that a dominant effect seems to be transitions along the diagonal $M = Q_v - P_v$.

The only processes changing M are the following :

i) π^+ , π^- absorption

ii) π^+ , π^- , π° charge exchange

iii) production of additional π^+ or π^-.

The various probabilities for process i and ii are experimentally known [3] when a π interacts, and the third process is negligible (less than 1% of the total π production). Thus, we introduce the probability α_π for a π to reinteract inside the nucleus target as a free parameter in the fit. The fitted value is $\alpha_\pi = 0.36 \pm 0.06$.

The $\Delta M = 0$ processes (representing 83% of the events as it is shown by the fit) are explained with the following parameters :

i) the probability p for the reaction proton to remain undetected if its energy is too low (fitted value : p = 0.043 ± 0.011).

ii) the probabilities $p_0, \ldots, p_4$ for an event to exhibit 0,1,...,4 additional protons. The fitted values are observed to follow a Poisson law (mean value : 0.49 ± 0.02).

The 10C fit gives a good χ^2 probability of 57% and yields the following results :

$$R = \frac{\sigma(\nu + n \to \mu^- + \ldots)}{\sigma(\nu + p \to \mu^- + \ldots)} = 2.03 \pm 0.18$$

$$\rho_n = \frac{\sigma(\nu + n \to \mu^- + P + \ldots)}{\sigma(\nu + n \to \mu^- + \ldots)} = 0.70 \pm 0.02$$

$$\rho_P = \frac{\sigma(\nu + P \to \mu^- + P + \ldots)}{\sigma(\nu + P \to \mu^- + \ldots)} = 0.85 \pm 0.02$$

V.- CONCLUSION

The two determinations of R are in good agreement. The value $\rho_P = 0.89 \pm 0.03$ obtained by the first method is also in good agreement with the one of the second.

In the first method, the dominant error is due to the number of events on free protons. These events being a very small fraction of the sample used in the second method, we can combine the two results :

$$R = 2.08 \pm 0.15$$

This value agrees with the ANL result [1] but is in disagreement with the BNL one [1]

Due to the energy range of our neutrino spectrum (1 - 10 GeV) quasi elastic and one π channels represent about 50% of our statistics. Thus, we are not in the scaling region. Meanwhile, the prediction for R is [4] :

$$R = \frac{\int_0^1 x \left[u(x) + \frac{1}{3} \bar{d}(x) + \ldots \right] dx}{\int_0^1 x \left[d(x) + \frac{1}{3} \bar{u}(x) + \ldots \right] dx} = 1.3 - 2.4$$

This prediction is in good agreement with our low energy data.

Up to now, the value of R for neutral currents is not known and cannot be determined by kinematical constraints. The second method presented,

found to be in excellent agreement with the kinematical one for charged currents, can be, and will be,extended to the neutral current case.

REFERENCES.

1 - G. MYATT and D.H. PERKINS, Phys. Lett. 34B (1971) 542.
N. SAMIOS, in Proceedings of the 1975 International Symposium on Lepton and Photon Interactions at High Energies, Stanford (1975) p. 527.
S.J. BARISH et al., Phys. Lett. 66B (1977) 291.

2 - W. LERCHE et al., Measurement of the ratio of charged current neutrino cross-sections on neutrons and protons in the energy range 1 - 10 GeV. To be published in Nucl. Phys. B.

3 - E. FETT et al., Nucl. Instr. and Meth. 144 (1977) 109.

4 - G. ALTARELLI, N. CABIBBO, L. MAIANI and R. PETRONZIO, Nucl. Phys. B69 (1974) 531.
R. Mac ELHANEY and S.F. TUAN, Nucl. Phys. B72 (1974) 487.
V. BARGER and R.J.N. PHILIPPS, Nucl. Phys. B73 (1974) 269.

STUDY OF ν, $\bar{\nu}$ INTERACTIONS IN CERN BUBBLE CHAMBERS EXPERIMENTS AND ANALYSIS OF THE NUCLEON STRUCTURE FUNCTIONS

Aachen-Bonn-CERN-London-Oxford,Saclay Collaboration
(presented by B. TALLINI)
DPhPE, Centre d'Etudes Nucléaires de Saclay,
BP 2, 91190 Gif-sur-Yvette, France.

SUMMARY

Using the CERN bubble chamber data on ν, $\bar{\nu}$ interactions on nucleons in the energy range $2 < E_\nu < 200$ GeV, the structure functions F_2, $2xF_1$ and xF_3 are determined as a function of x and Q^2. The Callan-Gross ratio is measured to be $A = 2xF_1/F_2 = 0.89 \pm 0.12$ in the range $3 < Q^2 < 30$ GeV^2. The Gross-Llewellyn-Smith sumrule is tested : we measure $> 2.5 \pm 0.5$ valence quark per nucleon. Deviations from Bjorken scaling are observed in F_2 and xF_3 and their Nachtmann moments are quantitatively consistent with predictions of QCD. The value of the strong interaction parameter is $\Lambda = 0.74 \pm 0.05$ GeV. The moments of the gluon distribution indicate an x distribution of gluon comparable to that of the valence quarks.

RESUME

Les données des chambres à bulles du CERN sur les événements $\nu, \bar{\nu}$ -nucléons dans le domaine d'énergie $2 < E_\nu < 200$ GeV, ont permis de déterminer les fonctions de structures F_2, $2xF_1$ et xF_3 en fonction des variables x et Q^2. On a déterminé la relation de Callan-Gross : $A = 2xF_1/F_2 = 0.89 \pm 0.12$ dans l'intervalle $3 < Q^2 < 30$ GeV^2. La règle de somme de Gross-Llewellyn-Smith nous a permis de déterminer que le nombre de quarks de valence par nucléon est supérieur à 2.5 ± 0.5. On a observé des déviations du scaling à la Bjorken dans F_2 et xF_3 et les moments de Nachtmann de ces fonctions sont en accord quantitatif avec les prédictions de QCD. La valeur du paramètre Λ des interactions fortes est 0.74 ± 0.07 GeV. La distribution en x des gluons, déterminée à l'aide de ses moments, est comparable à celle des quarks de valence.

I - Introduction

In the following we present an analysis of the structure functions xF_1, F_2, xF_3, describing the charged current ν, $\bar{\nu}$ interactions on isoscalar targets, as a function of $x = Q^2/2ME_H$ and Q^2 in the widest possible range of Q^2 from 0.1 to 100 GeV^2, in order to study deviations from Bjorken scaling in ν, $\bar{\nu}$ interactions and compare them with both the results found in e, μ scattering and with QCD predictions. The list of the physicists who carried out this work is given in [1].

II - The Data

The data used are the published data from Gargamelle filled with Freon exposed to the CERN PS wide band beam [2,3] consisting of 3000 ν events and 2000 $\bar{\nu}$ events in the energy range $2 < E < 12$ GeV, together with the latest ν, $\bar{\nu}$ data from the CERN SPS narrow-band beam in BEBC filled with 74 % mole Ne-H_2 mixture. The BEBC data consists of 1160 ν events and 277 $\bar{\nu}$ events in the energy range $20 < E < 200$ GeV. Results on total cross sections from BEBC have been published in [4] where details concerning the narrow-band beam, BEBC itself and the EMI can be found. Here we summarize the points on experimental resolution, relevant for the present analysis. Both the angle and the momentum of the muons in the ν, $\bar{\nu}$ events are well measured in BEBC thanks to its magnetic field of 35 kGauss and space resolution $\varepsilon \simeq 200\ \mu$ in space ($\Delta\theta_\mu \sim 0.5$ mrad, $(\Delta p/p)_\mu \sim \pm 4$ % for $P_\mu = 100$ GeV/c). For μ's with short track lengths the additional information from the corresponding hit measured in the EMI was used to improve the $(\Delta p/p)_\mu$ with the lever-arm method. The result of this is a uniform $(\Delta p/p)_\mu$ throughout the fiducial volume.

Concerning the hadronic energy E_H, detailed study of the transverse momentum un-balance $P_T^\mu - P_T^H$ in the μ-ν plane in the ν, $\bar{\nu}$ events as well as the analysis of π^- interactions in Ne at 70 GeV taken in the same film and measured with the same criteria as ν, $\bar{\nu}$ events, resulted in an accurate determination of the energy resolution function and of the mean correction for energy loss :

$E_H^{CORRECTED} = E_H^{MEASURED} * f$ with $f = 1.20 \pm 0.04$ independent of the total hadron energy E_H and the same for ν and $\bar{\nu}$ events. These results, which were satisfactorily checked against the (known) beam energy values, were included in a Monte-Carlo program used to unfold the smearing effects due to measurement errors from the x, Q^2 distribu-

tions from which the structure functions are determined. These unsmearing factors are less than 10 % for $x < 0.6$ and at most 30 % for $x > 0.6$.

III - Evaluation of Structure Functions

Assuming charge-symmetry and taking $\theta_{CABIBBO} = 0$, the differential cross sections for inelastic reactions can be written as

$$\frac{d^2\sigma^{\nu,\bar{\nu}}}{dxdy} = \frac{G^2ME}{\pi}\left[(1-y-\frac{Mxy}{2E})F_2(x,Q^2)+\frac{y^2}{2}2xF_1(x,Q^2)\pm y(1-\frac{y}{2})xF_3(x,Q^2)\right] \quad (1)$$

with $x = Q^2/2ME_H$, $y = E_H/E$.

We assume for the time being the Callan-Gross relation $2xF_1 = F_2$[5] which, as shown below is compatible with our data. Using the known ν, $\bar{\nu}$ fluxes $\Phi(E)$, $\bar{\Phi}(E)$ one can integrate (1) over E and y (which in a given (x,Q^2) bin is function of E : $y \propto 1/E$) and we obtain for ν, $\bar{\nu}$ respectively

$$\begin{aligned} N_{obs} &= N_2(x,Q^2)\ F_2(x,Q^2) + N_3(x,Q^2)xF_3(x,Q^2) \\ \bar{N}_{obs} &= \bar{N}_2(x,Q^2)\ F_2(x,Q^2) - \bar{N}_3(x,Q^2)xF_3(x,Q^2) \end{aligned} \quad (2)$$

where N_{obs}, $\bar{N}_{obs}$ represent the number of ν, $\bar{\nu}$ events observed in a given bin of (x,Q^2), and N_2, N_3 are the flux integrals given by

$$\begin{aligned} N_2(x,Q^2) &= \iint \Phi(E)\ \frac{G^2ME}{\pi}\ (1-y-\frac{Mxy}{2E}+\frac{y^2}{2})\ dydE \\ N_3(x,Q^2) &= \iint \Phi(E)\ \frac{G^2ME}{\pi}\ y\ (1-\frac{y}{2})\ dydE \end{aligned} \quad (3)$$

and similarly for $\bar{\nu}$.

Solving equations (2) yields $F_2(x,Q^2)$ and $xF_3(x,Q^2)$ which are shown in Fig. 1 as a function of Q^2 in different intervals of x. We observe that :

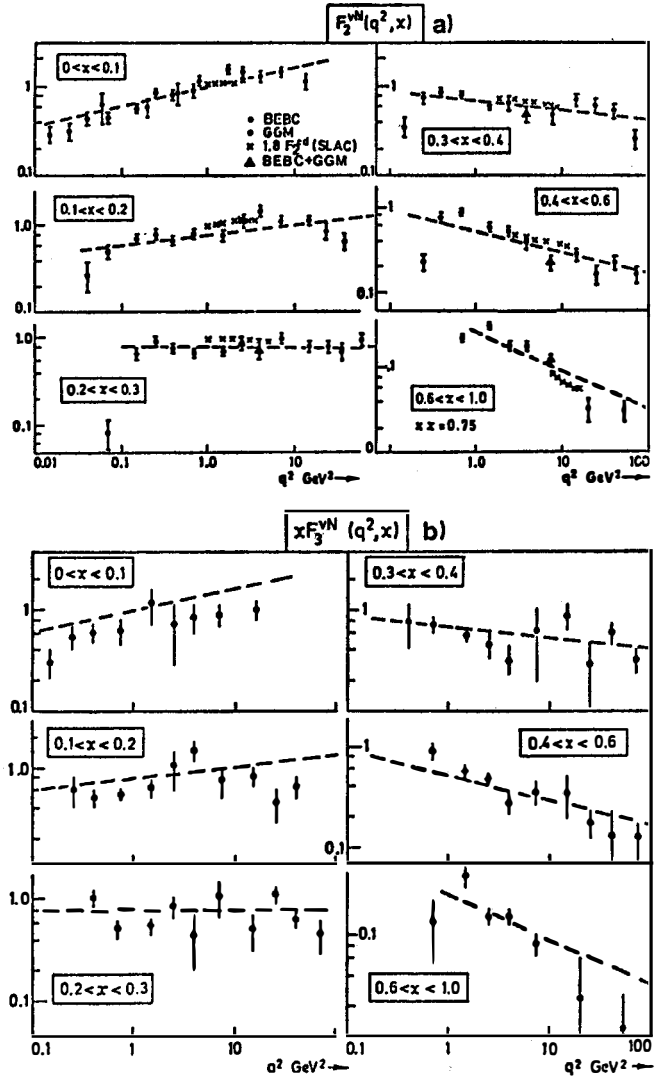

Figure 1

νN structure for various intervals of x plotted vs Q^2. a) $F_2^{\nu N}$; the dashed lines indicate the slopes of fits to $e^2$and μ data[6]. b) $F_3^{\nu N}$; the dashed lines are the same as in Fig. 1a.

a) wherever they overlap, the Gargamelle values of F_2 agree well (within 10 %) with the BEBC values; this represents a good test of the current-current interaction hypothesis implied in equ. (1) : for a given (x,Q^2) value, the F_2 function has a unique value independent of the incident ν energy which in the two experiments differ by a factor $\sim$ 30.

b) The BEBC data when compared to the lower Q^2 range covered by Gargamelle show a marked Q^2 dependence of F_2 which implies deviations from Bjorken scaling.

c) These deviations are similar to those found in e, μ scattering data also shown in Fig. 1 by the broken line from Ref.[6].

d) The values of $F_2^{ed}(x,Q^2)$ determined in e-deuterium scattering in Ref.[7], multiplied by the factor 9/5 predicted by the quark model, agrees satisfactorily well with $F_2^{\nu}(x,Q^2)$ in all intervals of x.

Fig. 1b presents $xF_3(x,Q^2)$ which shows the same general behaviour as $F_2(x,Q^2)$. The errors indicated, which are purely statistical, are larger for $xF_3(x,Q^2)$ since xF_3 is determined by the difference between ν and $\bar{\nu}$ data.

Finally Figs. 2a, 2b, 2c represent respectively the integrals $\int F_2 dx$, $\int xF_3 dx$ and their ratio $B = \int xF_3 dx \,/ \int F_2 dx$. We note that $\int F_2\, dx$ represents the fractional momentum of the quarks and anti-quarks whereas $\int xF_3\, dx$ represents that of the valence quarks; also the quantity $1 - \int F_2 dx$ represents the fraction of the nucleon momentum carried by the gluons. As expected in QCD we observe a gentle increase of $1 - \int F_2 dx$ and a decrease of B with increasing Q^2, which indicates that an increasing fraction of the momentum of the valence quarks is transferred to $Q\bar{Q}$ pairs and to gluons.

IV - Callan-Gross Relation

If one does not integrate equ. (1) over y it is possible to use the detailed shape of the y distributions

$\frac{1}{E}(\frac{d\sigma}{dy} + \frac{d\bar{\sigma}}{dy})$ in order to determine xF_1 and F_2 separately as a function of x and Q^2, in order to check the Callan-Gross relation. The result using all BEBC data is summarized in Fig. 3 and table I which give

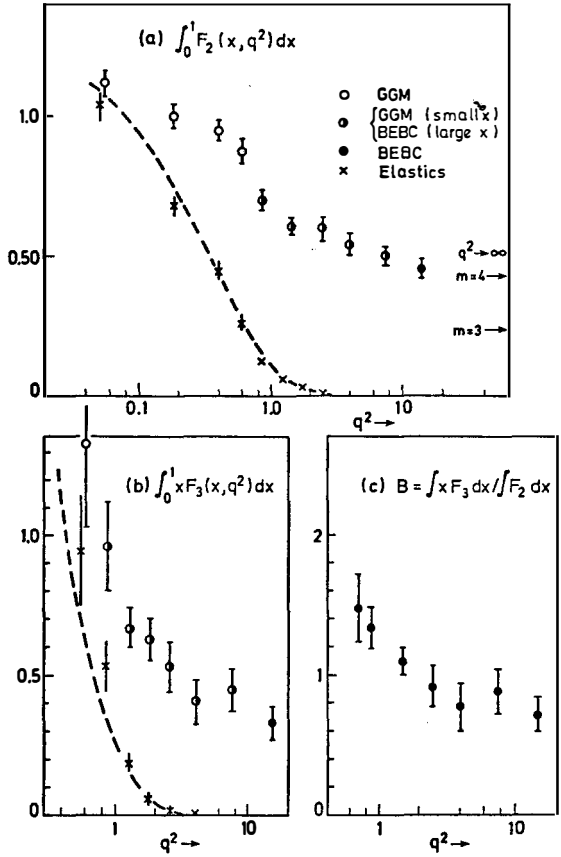

Figure 2

a) $\int F_2 dx$ vs Q^2; b) $\int xF_3 dx$ vs Q^2. The elastic events are shown separately. The dashed curves show the contribution expected from elastic events assuming dipole form factors.
c) $B = \int xF_3 dx \,/\, \int F_2 dx$ plotted versus Q^2.

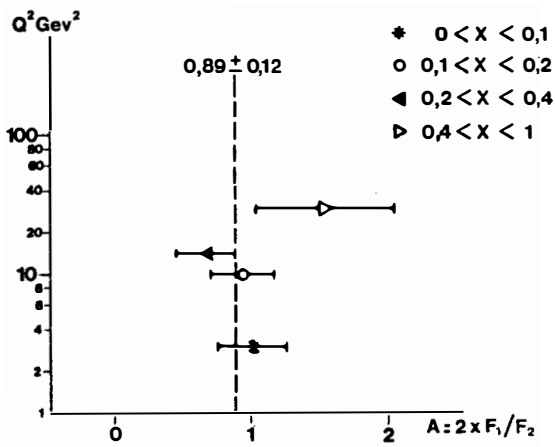

Figure 3

Callan-Gross ratio $A = 2xF_1/F_2$ plotted versus Q^2, for various intervals of x.

TABLE 1

Values of $A = 2xF_1/F_2$ from BEBC data

x	$Q^2(GeV^2)$	A
0 - 0.1	3	1.01 ± 0.25
0.1 - 0.2	10	0.93 ± 0.25
0.2 - 0.4	15	0.71 ± 0.19
0.4 - 1	30	1.53 ± 0.51
weighted average $\langle A \rangle = 0.89 \pm 0.12$		

TABLE II - GLS sumrule $\int_{x\,min}^{1} xF_3(x,Q^2)dx/x$ for different values of X_{min} as a function of Q^2

Q^2 (GeV^2)	$X_{min}= 0.02$	$X_{min}= 0.06$	$X_{min}= 0.10$
0.3 - 1	2.94 ± 0.56	2.33 ± 0.16	2.01 ± 0.15
1 - 3	2.79 ± 0.51	2.04 ± 0.33	1.38 ± 0.11
3 - 10	2.69 ± 0.41	1.96 ± 0.26	1.20 ± 0.21
10 - 40		1.39 ± 0.17	1.07 ± 0.11
40 - 100			0.94 ± 0.17

$A = 2xF_1/F_2$ for various values of x and Q^2. The weighted average is $A = 0.89 \pm 0.12$ and corresponds to a value of

$$R = \frac{\sigma_S}{\sigma_T} = \frac{1 + 4M^2x^2/Q^2 - A}{A} = 0.12 \begin{matrix} + 0.18 \\ - 0.14 \end{matrix}$$

V - Gross-Llewellyn-Smith Sumrule

From the values of xF_3 determined above one can determine $\int F_3 dx$ which is predicted by the G-L-S sumrule[8] :

$$\lim_{Q^2 \to \infty} \int_0^1 xF_3 \frac{dx}{x} = 3 \qquad (4)$$

and measures the number of quarks in the target. Table II summarizes the results of $\int_{x_{MIN}}^1 xF_3 \frac{dx}{x}$ for various values of x_{MIN}. As expected in QCD at fixed x_{MIN} the integral decreases with increasing Q^2 since the valence quarks slowly shrinks towards x = 0 and an increasingly large proportion of the integral is lost below x_{MIN}.

VI - Higher moments of F_2, xF_3

Fig. 4 shows the higher moments of F_2 and xF_3 with respect to the Bjorken x variable :

$$M_i(N,Q^2) = \int_0^1 x^{N-2} F_i(x,Q^2) dx$$

where $F_i = F_2$ or xF_3.

The strong Q^2 dependence of these moments for small Q^2 is mostly accounted for by the target nucleon mass correction terms as shown in Fig. 5 which represents the Nachtmann moments[9] with respect to the variable $\xi = \frac{2x}{(1 + \sqrt{1 + 4M^2x^2/Q^2})}$ (which tends to x for $Q^2 \to \infty$).

These latter moments have the form[10], for F_2 and xF_3 :

$$M_2(N,Q^2) = \int_0^1 \frac{\xi^{N+1}}{x^3} F_2(x,Q^2) \frac{(N^2+2N+3)+3(N+1)\sqrt{1+4M^2x^2/Q^2}+N(N+2)\frac{4M^2x^2}{Q^2}}{(N+2)(N+3)} dx$$

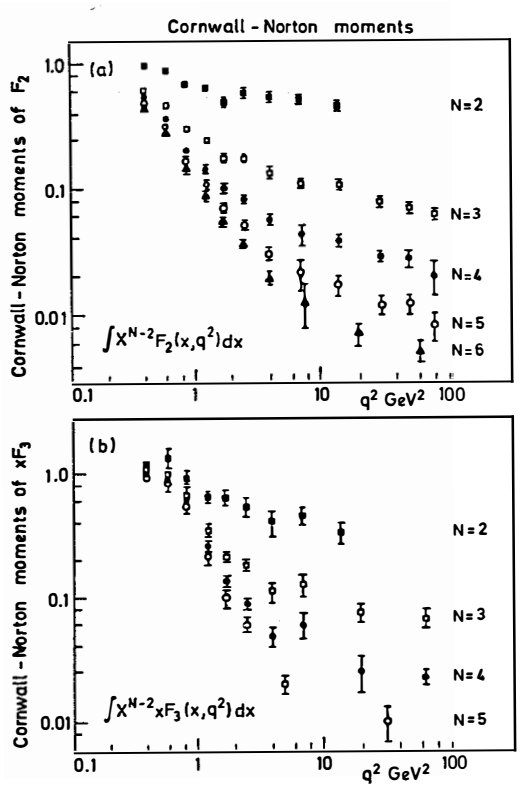

Figure 4

Structure function moments $\int X^{N-2} F_i(X,Q^2)dX$
a) for $F_i = F_2$
b) for $F_i = xF_3$.

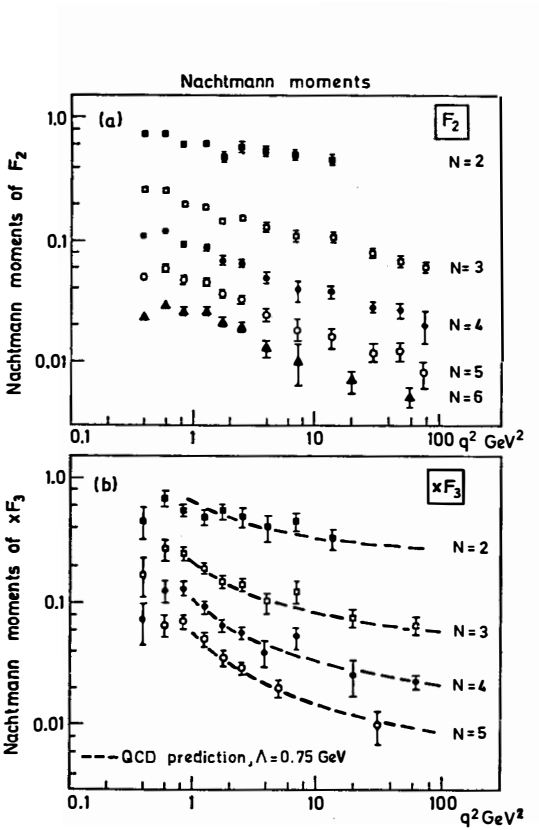

Figure 5

Nachtmann moments of a) F_2 and b) xF_3.

$$M_3(N,Q^2) = \int_0^1 \frac{\xi^{N+1}}{x^3} xF_3(x,Q^2) \frac{1+(N+1)\sqrt{1+4M^2x^2/Q^2}}{(N+2)} dx \qquad (5)$$

For N=2, moments are shown only up to $Q^2 \sim 20$ GeV^2 since for larger Q^2 the interval $x < 0.1$ is not accessible at our energies and thus F_2 and xF_3 are not determined. On the other hand for large $N > 7$ more than 50 % of the integral comes from $x > 0.6$ where smearing corrections are $\lesssim$ 30 %.

From a comparison of Figs. 4 and 5 we note that for $Q^2 > 2$ GeV^2 the two sets of moments are essentially the same and that for each N they slowly decrease as Q^2 increases. In what follows we will make a quantitative test of the Nachtmann moments determined in this experiment with the predictions of QCD.

VII - The moments of xF_3, tests of QCD and determination of Λ

In QCD the quark-gluon coupling constant is given by :

$$\frac{\alpha_S}{\pi} = \frac{12}{(33-2m)} \frac{1}{\ln(Q^2/\Lambda^2)} \qquad (6)$$

where Λ is an arbitrary parameter and m is the number of quark flavours. In what follows we have taken m=3 since c-quarks make only a small contribution to the cross sections in our energy range.

The moments of F_2 and xF_3 can be expressed as the sum of three terms[11], with arbitrary coefficients, each varying as a known power of α_S in the region $Q^2 \gg \Lambda^2$, where α_S is small. One term is non-singlet with respect to flavour (corresponding to the valence quarks) and two are singlets (for the gluon and sea quark contributions). Since xF_3 measures the valence quark distribution, only the non-singlet term contributes to its moments which have therefore the particularly simple form (valid for $Q^2 \gg \Lambda^2$) :

$$M_3(N,Q^2) = \frac{\text{constant}}{(\ln(Q^2/\Lambda^2)^{d_{NS}}} \qquad (7a)$$

$$\text{with } d_{NS} = \frac{4}{(33-2m)} \left[1 - \frac{2}{N(N+1)} + 4 \sum_2^N \frac{1}{j} \right] \qquad (7b)$$

Two specific predictions of equ. (7) can be tested experimentally :

- The different moments of xF_3 should follow a power law behaviour; this can be tested by showing that, independently of the parameter Λ, the ratios $\frac{M_3(N,Q^2)}{M_3(L,Q^2)^{P_{N,L}}}$ (where $P_{N,L} = \frac{d_{NS}(N)}{d_{NS}(L)}$) (7c) are independent of Q^2.

The result of this test for various values of N and L is presented in Fig. 6 where second order effects in α_s are indicated[12]; we see that, for $Q^2 > 1$ GeV^2, the appropriate ratios of different moments of xF_3 plotted vs. Q^2 are indeed constants within the statistical errors. Alternatively one can measure directly the $P_{N,L}$'s by plotting $\ln(M_3(N,Q^2))$ vs. $\ln(M_3(L,Q^2))$ as shown in Fig. 7; again we see that the points at different Q^2 lie on straight lines the slopes of which determine the $P_{N,L}$'s. In table III the $P_{N,L}$'s values thus determined are compared to those predicted from equ. (7) : in all cases the agreement with QCD is remarkably good.

- Equ.(7a) can be re-written as a linear relation

$$M_3(N,Q^2)^{-1/d_{NS}} = \ln Q^2 - \ln\Lambda^2 \qquad (8)$$

The data are presented in Fig. 8a for N=2 and N=4 and in Fig.8b for N=3 and N=5, and show that the linear relationship is satisfied in all cases. The value of the intercept with the $\ln Q^2$ axis gives Λ. Fitted values of Λ for various choices of m and N and for $Q^2 > 1$ GeV^2 and $Q^2 > 2$ GeV^2 are summarized in table IV where we also indicate the effect of possible systematic errors on the K/π ratio, and α_s^2 corrections. Our best estimate is $\Lambda = 0.74 \pm 0.05$ GeV.

VIII - The F_2 moments and study of the gluon distribution

Concerning F_2, the predictions of QCD are that all 3 terms mentioned above - two singlets and a non singlet - contribute to its Nachtmann moments[11]:

$$M_2(N,Q^2) = \frac{C_{NS}}{(\ln Q^2/\Lambda^2)^{d_{NS}}} + \frac{C_+}{(\ln Q^2/\Lambda^2)^{d_+}} + \frac{C_-}{(\ln Q^2/\Lambda^2)^{d_-}} \qquad (9)$$

If one neglects the contribution of the s and $\bar{s}$ quarks the 3 terms in (9) can be expressed in terms of the moments $Q(N)$, $\bar{Q}(N)$

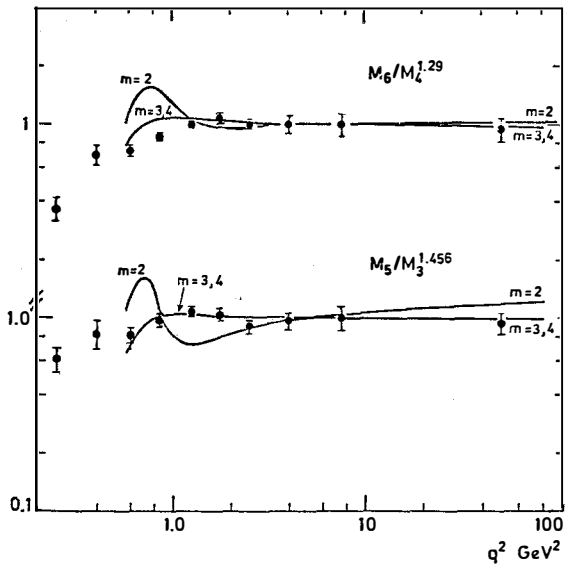

Figure 6

The N = 5 moment of xF_3 : (M_5) divided by the N = 3 moment : (M_3) to the power $p_{5,3} = 1.456$; and the N = 6 moment : (M_6) divided by the N = 4 moment : (M_4) to the power $p_{6,4} = 1.29$ as a function of Q^2. QCD predicts (equ.7) that these ratios should be constant, independent of Q^2. The lines indicate the effects of second order corrections in α_s^2 (Ref.12).

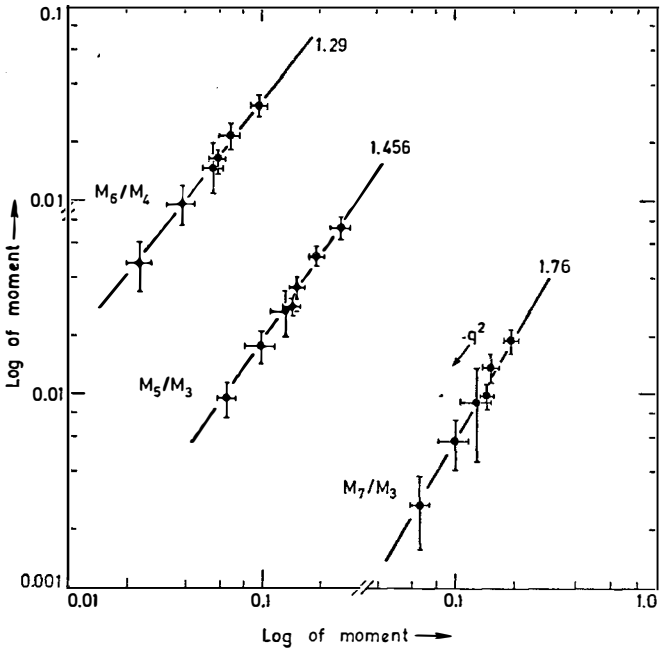

Figure 7

Test of the power-law behaviour of the Nachtmann moments of xF_3. Determination of the ratios $P_{N,L}$ (see equ.7) for various values of N and L. The values shown are those predicted by QCD.

TABLE III : xF_3 moment ratios ($Q^2 > 1$ GeV^2)

	observed slope	QCD prediction
d ln M(N=6)/ d ln M(N=4)	1.29 ± 0.06	1.290
d ln M(N=5)/ d ln M(N=3)	1.50 ± 0.18	1.456
d ln M(N=7)/ d ln m(N=3)	1.84 ± 0.20	1.760

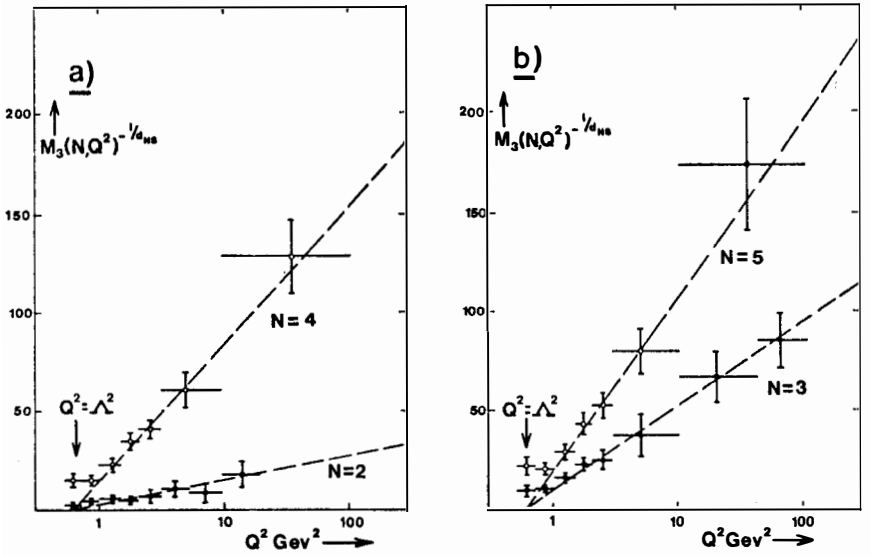

Figure 8

Nachtmann moments of xF_3. The reciprocal of the moments $M_3(N,Q^2)$ raised to the power $1/d_{NS}(N)$ plotted versus Q^2 (see equ.8).
a) even moments, N = 2 and N = 4; b) odd moments N = 3 and N = 5.
QCD predicts a linear relation with intercept $\ln\Lambda^2$ on the x axis.
The dashed lines represent the results of the fits for $Q^2 > 1$ GeV^2.

TABLE IV - Fitted values of Λ (in GeV) from the xF_3 Nachtmann moments (eqn.(8) in the text) for various values of N,m and with different cuts in Q^2.

Q^2 range	$Q^2 > 1$ GeV^2	$Q^2 > 2$ GeV^2
N = 3 , m = 3	0.70 ± 0.07	0.85 ± 0.18
$(K^{\pm}/\pi^{\pm})$ x 0.9	0.67 ± 0.07	
α_s^2 corrections	0.62 ± 0.07	0.82 ± 0.18
N = 5 m = 3	0.77 ± 0.07	0.70 ± 0.18
N = 7 m = 3	0.75 ± 0.07	0.95 ± 0.20

Table V : Gluon moment $G(N,Q_o^2)$ at $Q_o^2 = 5$ GeV^2 based on data with $Q^2 > 1$ GeV^2.

N	$G(N,Q_o^2)$	Q^2 range	Moment of xF_3
2	$+ 0.62 \pm 0.15$	1 - 20 GeV^2	0.45 ± 0.07
3	$+ 0.12 \pm 0.05$	1 - 100 "	0.12 ± 0.02
4	$+ 0.03 \pm 0.02$	1 - 100 "	0.045 ± 0.010
5	$+ 0.02 \pm 0.01$	1 - 100 "	0.027 ± 0.007

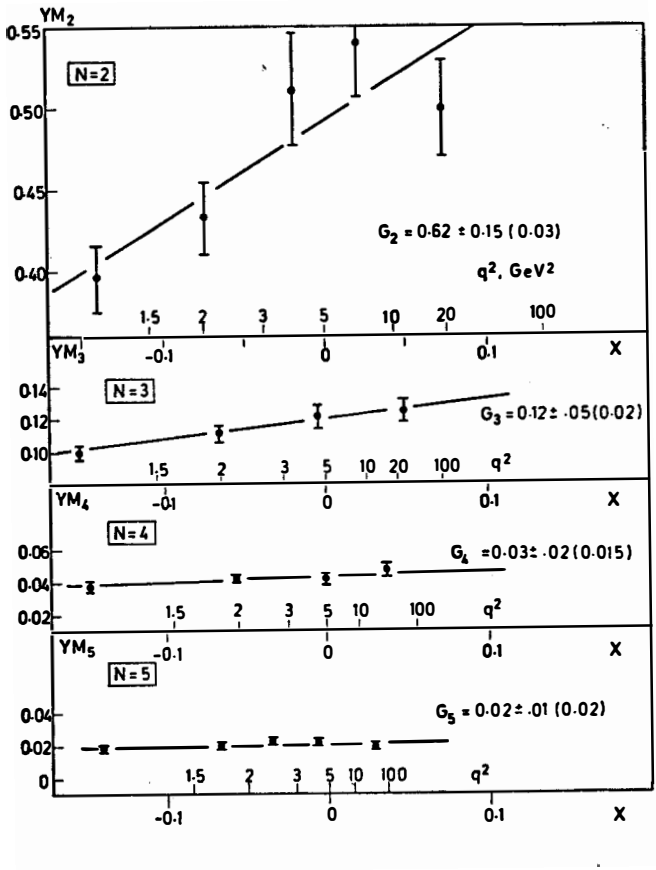

Figure 9

Determination of the gluon moments from the Nachtmann moments of F_2. Plot of $Y(Q^2).M_2(N,Q^2)$ against $X(Q^2)$. The data are evaluated at $Q_0^2 = 5$ GeV^2. The slopes of the distributions should be equal to the gluon moments $G(N,Q_0^2)$. The magnitudes of the N = 2,3,4 and 5 gluon moments are indicated in the figure and in table V. The errors indicated are statistical; those in brackets arise from the uncertainty (0.07 GeV) in the assumed value of Λ.

and G(N) of the quarks, antiquarks and gluons respectively at $Q^2=Q_o^2$:

$$\frac{C_{NS}}{(\ln Q_o^2/\Lambda^2)^{d_{NS}}} = \frac{1}{3}(Q+\bar{Q})$$

$$\frac{C_+}{(\ln Q_o^2/\Lambda^2)^{d_+}} = \frac{2}{3}\left[(1-A_N)(Q+\bar{Q}) + B_N G\right] \qquad (10)$$

$$\frac{C_-}{(\ln Q_o^2/\Lambda^2)^{d_-}} = \frac{2}{3}\left[A_N(Q+\bar{Q}) - B_N G\right]$$

where d_{NS} is given in (7b) above and d_+, d_-, A_N and B_N are parameters which depend only on N and m and are defined in the Appendix. It is convenient to recast equs. (9) and (10) in the linear form[13]

$$M_2(N,Q^2).Y = M_2(N,Q_o^2) + G(N,Q_o^2).X \qquad (11)$$

where X and Y are suitable functions of Q^2 and are also shown in the Appendix. Therefore, plotting $Y.M_2$ vs. X for a given N should give a straight line with slope given by the moment $G(N,Q_o^2)$ of the gluon distribution at Q_o^2. The results are shown in Fig. 9 and summarized in Table V where the values of the gluon moments are compared to those of the valence quarks. Thus we conclude that the gluons have approximately the same X distribution as that of the valence quarks.

Appendix

The anomalous dimensions appearing in Equs. (9) and (10) are given below, in the notation of Hincliffe and Llewellyn-Smith[11]:

$$d_{\pm} = \frac{1}{2}\left[d_{NS} + d_{GG} \pm \sqrt{(d_{NS}-d_{GG})^2 + 4d_{GQ}d_{QG}}\right]$$

$$d_{GG} = \frac{2m}{(33-2m)} + \frac{9}{(33-2m)}\left[\frac{1}{3} - \frac{4}{N(N-1)} - \frac{4}{(N+1)(N+2)} + 4\sum_{2}^{N}\frac{1}{j}\right]$$

$$d_{GQ} = \frac{-8(N^2+N+2)}{(33-2m)N(N^2-1)}$$

$$d_{QG} = \frac{-6m(N^2+N+2)}{(33-2m)N(N+1)(N+2)}$$

$$d_{NS} = \frac{4}{(33-2m)}\left[1 - \frac{2}{N(N+1)} + 4\sum_{2}^{N}\frac{1}{j}\right]$$

The quantities A_N and B_N are defined by

$$A_N = (d_+ - d_{NS})/(d_+ - d_-)$$

$$B_N = d_{QG}/(d_+ - d_-)$$

The quantities X and Y are defined by

$$X = \frac{2}{3} B_N(\chi^{d_+} - \chi^{d_-}).Y$$

$$\frac{1}{Y} = \frac{(2\chi^{d_+} + \chi^{d_{NS}})}{3} - \frac{2A_N}{3}(\chi^{d_+} - \chi^{d_-})$$

where $\chi = (\ln Q_o^2/\Lambda^2)/(\ln Q^2/\Lambda^2)$.

References

1) P.C. Bosetti, H. Deden, M. Deutschmann, P. Fritze, H. Grassler, F.J. Hasert, J. Morfin, H. Seyfert, R. Schulte and K. Schulte, III. Physikalisches Inst. der Techn. Hochschule, Aachen.

K. Bockmann, H. Emans, C. Geich-Gimbel, R. Hartmann, A. Keller, T.P. Kokott, E. Meincke, B. Nellen and R. Pech, Physikalisches Inst. der Universität Bonn, Bonn.

D.C. Cundy, J. Figiel, A. Grant, D. Haidt, P.O. Hulth, D.J. Kocher, D.R.O. Morrison, E. Pagiola, L. Pape, C.H. Peyrou, P. Porth, P. Schmid, W.G. Scott, H. Wachsmuth and K.L. Wernhard, CERN, Geneva.

S. Banerjee, K.W.J. Barnham, R. Beuselinck, I. Butterworth, E.F. Clayton, D.R. Miller and K.J. Powell, Imperial College of Science and Technology, London.

C.L. Davis, P. Grossmann, R. McGow, J.H. Mulvey, G. Myatt, D.H. Perkins, R. Pons, D. Radojicic, P. Renton, and B. Saitta, Department of Nuclear Physics, Oxford.

V. Baruzzi, M. Bloch, M. De Beer, W. Hart, Y. Sacquin, B.Tallini and D. Vignaud, DPhPE, Centre d'Etudes Nucléaires de Saclay.

2) T. Eichten et al, Phys. Letters 46B (1973) 281.
3) H. Deden et al, Nucl. Phys. B85 (1975) 269.
4) P. Bosetti et al, Phys. Letters 70B (1977) 273.
5) C.G. Callan and D.G. Gross, Phys. Letters 21 (1968) 211.
6) D.H. Perkins et al, Phys. Letters 67B (1977) 347.
7) E.M. Riordan et al, SLAC-PUB-1634 (1975).
8) D.J. Gross and C.H. Llewellyn-Smith, Nucl. Phys. B14 (1969) 337.
9) O. Nachtmann, Nucl. Phys. B63 (1973) 237; B78 (1974) 455.
10) B. Wandzura, Nucl. Phys. B122 (1977) 412.
11) I. Hincliffe and C.H. Llewellyn-Smith, Nucl. Phys. B128 (1977) 93.
12) I.G. Floratos et al, Nucl. Phys. B129 (1977) 66, A.J. Buras et al, Nucl. Phys. B131 (1977) 308.
13) P.C. Bosetti et al, the full lenght version of the present paper to be submitted shortly to Nucl. Phys. B.

QUARK FRAGMENTATION IN HIGH ENERGY NEUTRINO AND ANTINEUTRINO REACTIONS

Aachen-Bonn-CERN-London-Oxford-Saclay Collaboration
presented by Y. SACQUIN
DPhPE/SECB, Centre d'Etudes Nucléaires de Saclay,
BP 2, 91190 Gif-sur-Yvette, France.

SUMMARY

In a study of the hadronic system in $\nu(\bar{\nu})$ induced reactions in BEBC, the quark fragmentation functions are found to be essentially independent on Q^2, W, X for $Q^2 > 2$ GeV^2 and W > 4 GeV. A simple model by Feynman, Field and Fox gives an excellent description of all distributions, except for the correlation between transverse momentum and relative energy.

RESUME

Dans l'étude de la gerbe hadronique produite dans des interactions de neutrinos (d'antineutrinos) dans BEBC, les fonctions de fragmentation des quarks sont trouvées indépendantes de Q^2, W, X pour $Q^2 > 2$ GeV^2 et W > 4 GeV. Un modèle simple tel celui de Feynman, Field et Fox fournit une excellente description de toutes les distributions, à l'exception de la corrélation entre les impulsions transverses et l'énergie relative.

In this experiment performed at BEBC filled with heavy liquid[1], using the Narrow Band Neutrino Beam of the SPS (200 GeV transport momentum), we have looked for data at very high energy (E_ν > 100 GeV) on the hadronic system.

In the quark-parton model, hadron production by neutrinos is described by structure functions :

$$\frac{d^2\sigma}{dXdZ}(\nu N \rightarrow \mu h X) \propto G_{Nq}(X,Q^2)\, D^h_{q'}(Z) \qquad (1)$$

$$Z = \frac{P_h}{P_{q'}} \simeq \frac{E_h}{E_{had}} \qquad X = \frac{Q^2}{2M\nu}$$

where G gives the distribution of quarks q inside the nucleon and D is the fragmentation function of the quark q' to hadrons of type h.

We are interested here in the D function and due to the fact that in neutrino the flavour of the scattered quark is known, this function reveals itself most clearly.

We compare our results with one of the different models for the hadronic jet, the "standard jet model" by Feynman, Field and Fox[2]. This model is mainly a parametrization of electro- and neutrino-data at lower energies, and gives detailed predictions.

I - The quark fragmentation function

Following Feynman and Field we define the fragmentation function by

$$D^h_q = \frac{1}{N_E}\frac{dN}{dZ} \qquad (2)$$

with N_E : number of events

This function is a multiplicity. We first eliminate target fragments in the hadronic jet by a cut Z > 0.2. Then we define a kinematical region W > 4 GeV in order to eliminate the coherent quark scattering and Q^2 > 2 GeV^2 where the average multiplicity shows no variation. In this region the integrated function

$$\int_{0.2}^{1.0} D^h_{q'}(Z)\, dZ$$

shows no variation with the variable X (fig.1).

The quark fragmentation function $D^h_q(Z)$ for ν and $\bar{\nu}$ are given in fig.2 as a function of Z, with the prediction of Feynman and Field (dashed line) and points from ep [3] and e^+e^- [4] scattering. The agreement is excellent, indicating the universality of the D-function, for Z < 0.6. Above this value the comparison is meaningless due to the global correction applied on hadronic energy.

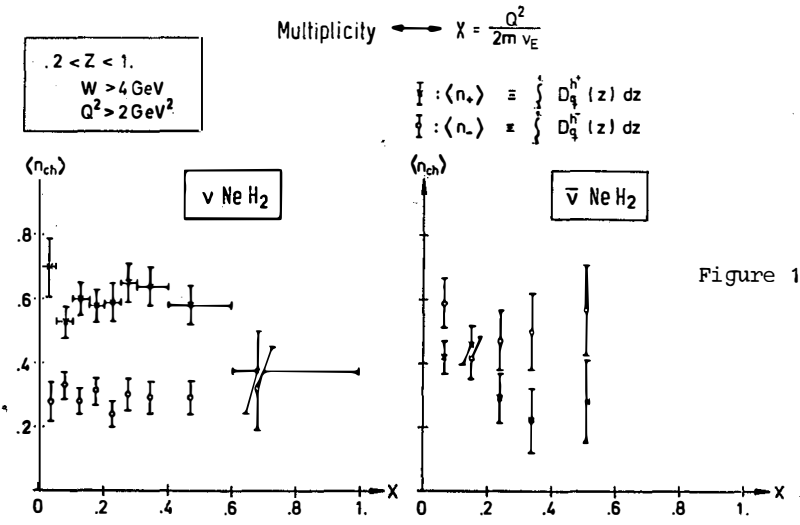

Figure 1

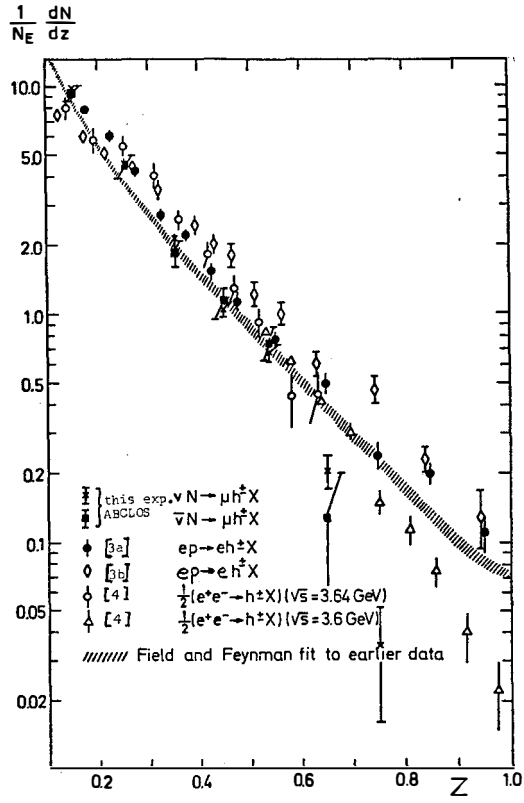

Figure 2

Looking in more details by separating positive and negative particle, we found a definite enhancement of positive over the negative in neutrino data, as predicted by the quark-parton model (fig.3a) and in antineutrino the effect is less conclusive, but consistent (fig.3b) with a slight enhancement of negative over positive particles.

Feynman and Field use also the function

$$\omega(Z) = \frac{D_u^{\pi^-}}{D_u^{\pi^+}} \tag{3}$$

As we are not able to separate charged pion and kaons, neither proton of high momentum (> 800 MeV), we note that isospin and charge symmetry imply

$$D_u^{\pi^+}(Z) = D_d^{\pi^-}(Z) \tag{4}$$

and, assuming a similar behaviour for kaons and pions, we approximate

$$\omega(Z) = \frac{D_u^{\pi^-}}{D_d^{\pi^-}} \simeq \frac{D_u^{h^-}}{D_d^{h^-}} \tag{5}$$

So we can compute this function undistorted by target fragments and obtain a good agreement with Feynman and Field at low Z (fig.4). The ratio ω' computed from neutrino data alone shows the effect of target fragments. A parametrisation by Sehgal[5] gives also a good agreement.

II - Comparison with a standard jet model

From definite assumptions on relative coupling strengths and relative amount of different produced mesons, Feynman and Field have predictions for the hadronic jet.

First we show the distribution in Z_R of the fastest and second fastest particles (fig.5). The variable $Z_R = \frac{E}{E_{had}^{charged}}$ is natural for this study and, as Feynman and Field refer to a 10 GeV fragmenting quark, we restrict our plot to the interval $5 < E_{had} < 40$ GeV. Without other cut, the agreement with the model is good, as well as the distribution of the sum of Z_R of the two fastest (fig.6).

Reflexions of the different flavours of the fragmenting quarks are studied in the Z_R distributions of the fastest positive and negative particle (fig.7). The leading charge effect is well pronounced and nicely reproduced by Feynman et al.

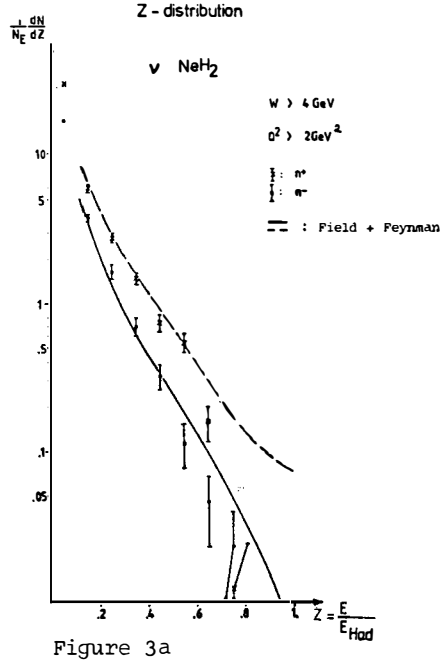

Figure 3a

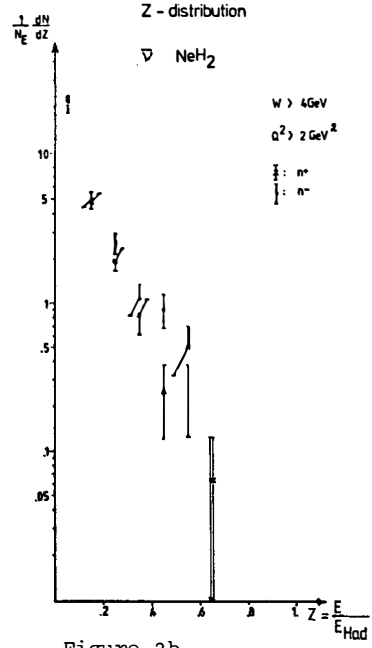

Figure 3b

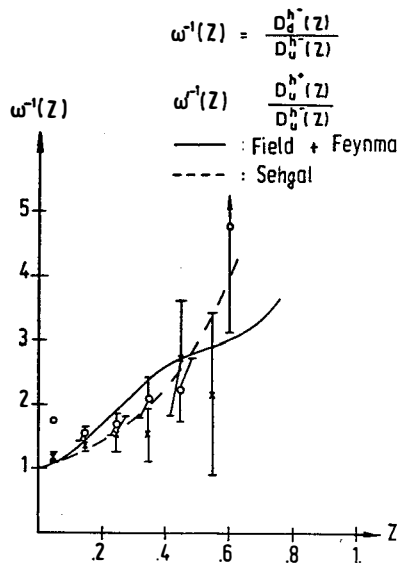

Figure 4

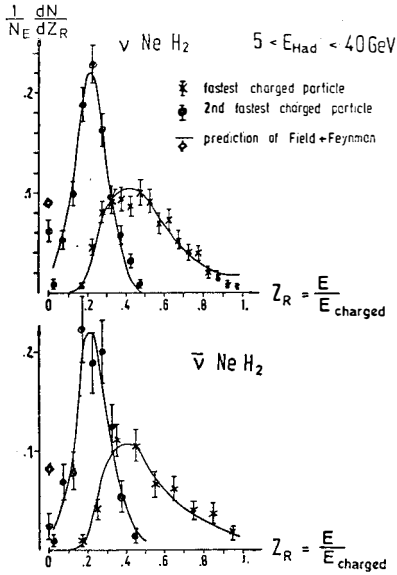

Figure 5

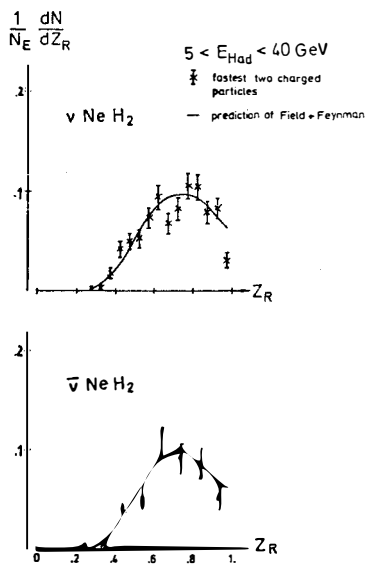

Figure 6

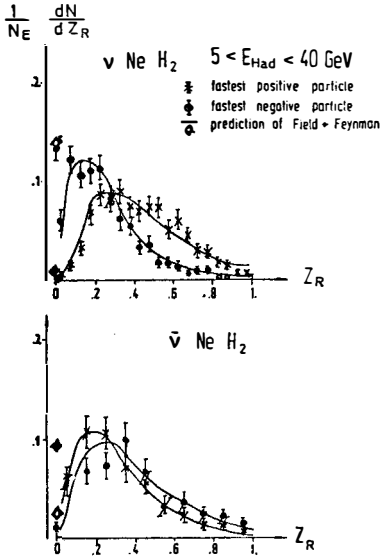

Figure 7

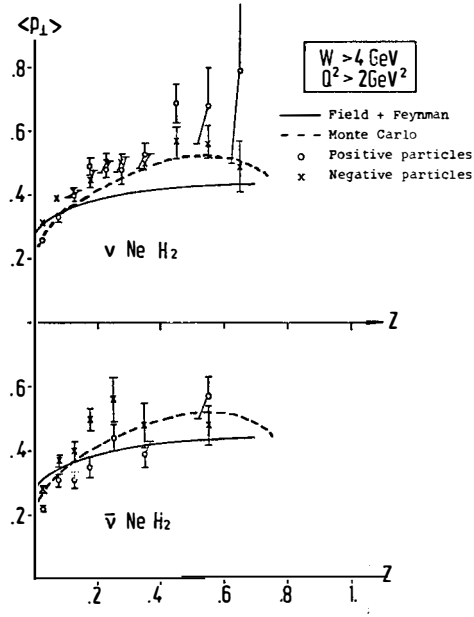

Figure 8

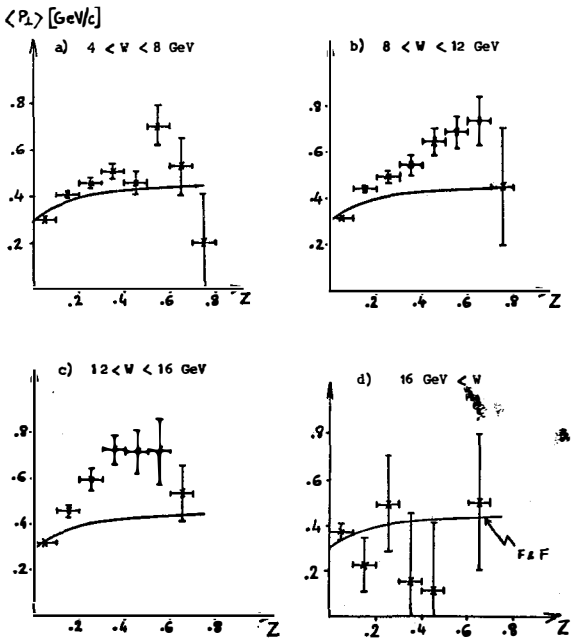

Figure 9

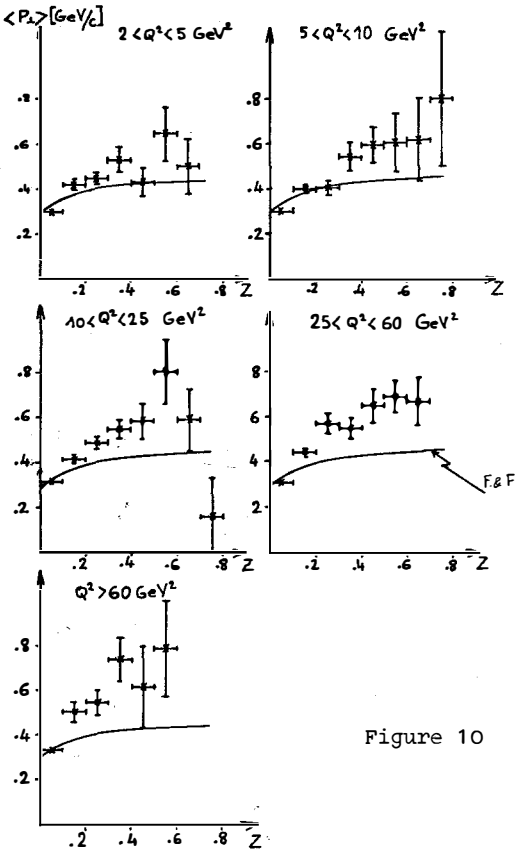

Figure 10

Table 1 gives the mean value of Z_R for the fastest tracks with the prediction of the model. In Table 2 we have the mean charge of the hadronic jet compared to the prediction. We see clearly an excess of positive charge for neutrino and anti-neutrinos data, probably caused by positive target fragments not yet removed by the cut $Z > 0.1$ made in Feynman model. Higher cut in Z or higher energy reduces this excess of positive charge and can be used for later comparison with the predictions corresponding to lower cut.

Table 1

Mean values of Z_R for hadrons fragmenting from u-, d-quarks
(Prediction of F.&F. for p_q = 10 GeV/c,
Experimental results for $5 < E_{had} < 40$ GeV)

	ν u-quark		$\bar{\nu}$ d-quark	
	F.&F.	exp.	F.&F.	exp.
fastest charged part.	0.54	0.53±0.01	0.53	0.53±0.02
2nd fastest charged	0.21	0.22±0.01	0.22	0.23±0.01
fastest two charged	0.75	0.74±0.01	0.75	0.75±0.01
fastest positive part.	0.45	0.47±0.01	0.31	0.33±0.02
2nd fastest positive	0.12	0.15±0.01	0.08	0.10±0.01
fastest two positive	0.57	0.62±0.01	0.39	0.42±0.02
fastest negative part.	0.27	0.22±0.01	0.41	0.39±0.02
2nd fastest negative	0.07	0.05±0.01	0.11	0.10±0.01
fastest two negative	0.34	0.27±0.01	0.52	0.49±0.02

Table 2

Mean charge of the hadronic jets in the fragmentation region
($Z \gtrsim 0.1$ except for last line).
The prediction of F.&F. is for p_q = 10 GeV/c.

	u	d	S
F.&F.	0.39	-0.22	-0.28
$5 < E_{had} < 40$ GeV	0.67±0.04	-0.07±0.08	
$40 < E_{had} < 100$ GeV	0.41±0.06		
$5 < E_{had} < 40$ GeV $Z \geq 0.15$	0.43±0.03	-0.15±0.07	

Finally we show a study of the Z distribution of the mean transverse momentum of the charged hadrons. Fig.8 shows a strong increase of $\langle p_T \rangle$ for $Z < 0.2$, whereas for $Z > 0.2$ the distributions flatten out. The plateau for the different charges agrees within the errors and reaches a mean transverse momentum of 600 MeV/c. The Feynman and Field description, based on limited transverse momentum ($\langle p_T \rangle = 323$ MeV/c) is consistent for the antineutrinos data but fails to describe the neutrino data. Averaged over Z, the mean value of p_T agrees with the model, but the explicit Z dependence clearly disagrees. We investigate this behaviour in slice of Q^2 and W for the combined positive and negative tracks and see that disagreement occurs for high Q^2 and W (figs. 9 and 10). This strong Q^2 and W dependence cannot be reproduced by Monte Carlo or explained by kinematical effects.

III - Conclusion

Our results show that the longitudinal dependence of the hadronic jet agrees with simple models using longitudinal phase space. The Feynman and Field parametrization of the quarks fragmentation is consistent with the data. We observe a rise of $\langle P_T \rangle$ with Q^2 which cannot be explained by kinematics or conventionnal quark fragmentation model.

References

1) B. Tallini, these Proceedings
and Bosetti et al., Phys. Letters 70B(1977)273. The list of people involved in this study is given in this reference.
2) R.D. Field and R.P. Feynman, Phys. Rev. D15(1977)2590,
R.D. Field and R.P. Feynman, report CALT-68-618(1977),
R.P. Feynman, Quark jets, Proc. of the VIII Intern. Symposium on Multiparticle Dynamics, Kaysersberg (1977) ,p.B-141,
R.P. Feynman, R.D. Field and G.C. Fox, Nucl. Phys. B128(1977)1.
3) a) I. Cohen et al., report DESY 77/71 (1977),
b) J.M. Scarr et al., report DESY 77/77 (1977).
4) R. Brandelik et al., report DESY 77/11 (1977).
5) L.M. Sehgal, Hadron production by leptons, Proc. of the 1977 Intern. Symposium on Lepton and Photon Interactions, Hamburg (1977), p.837.

MUON NEUTRINO - ELECTRON ELASTIC SCATTERING

G. Carnesecchi
EP Division, CERN, Geneva
WA14 Collaboration: Bari, CERN, Ecole Polytechnique, Milano, Orsay

Abstract: A search for the reaction $\nu_\mu + e^- \rightarrow \nu_\mu + e^-$ was performed in the bubble chamber Gargamelle, exposed to the wide-band neutrino beam of the CERN-SPS. Ten isolated e^- were found above 2 GeV energy with a background of 0.2 ± 0.2 events. Results on the cross-section are given in terms of vector and axial-vector coupling constants and a comparison is made with the standard SU(2) ⊗ U (1) model.

Résumé: La recherche de la réaction $\nu_\mu + e^- \rightarrow \nu_\mu + e^-$ a été effectuée dans la chambre à bulles Gargamelle exposée au faisceau neutrino à bande large du CERN-SPS. Dix e^- isolés ont été trouvés avec une énergie supérieure à 2 GeV et un bruit de fond de 0.2 ± 0.2 événements. Les résultats sur la section efficace sont donnés en fonction des constantes de couplage vecteur et vecteur-axial et une comparaison est faite avec le model standard SU(2) ⊗ U (1).

The purely leptonic reactions

$$\nu_\mu + e^- \rightarrow \nu_\mu + e^- \quad (1)$$

and

$$\bar{\nu}_\mu + e^- \rightarrow \bar{\nu}_\mu + e^- \quad (2)$$

are of great importance for the study of weak interaction processes induced by neutral currents since only the leptonic current is involved.

However, only limited results [1,2,3] have been obtained so far, due to the exceedingly low cross-section and to difficult background problems. Reaction (1) has been searched for in the heavy liquid bubble chamber Gargamelle exposed to the wide-band neutrino beam of the CERN-SPS which peaks at 25 GeV and extends up to 200 GeV (fig. 1). The chamber was filled with a mixture of propane (90.5% in moles) and Freon CF_3Br (9.5%), yielding a radiation length X_o = 61.5 cm. This value ensures an excellent efficiency for the signature of electrons, either by spiralization or by electromagnetic shower development, although large enough to allow a clear separation between γ-rays and electrons.

The experimental set-up was completed by two MWPC placed respectively upstream and downstream against the chamber body (fig. 2), for detecting particles entering or leaving the chamber and by two planes of MWPC interpersed with an iron shielding for the identification of muons above 2.5 GeV.

A sample of 128,000 pictures, taken during the end of 1977, was scanned for spiralizing tracks or electromagnetic showers, with no visible source in the chamber. The events were retained only if they occured in a fiducial volume of 5.09 m^3 inside a visible volume of 7.2 m^3 and if they satisfied the conditions E > 2 GeV and $\theta_{(beam-e)} < 3^o$. No good event is cut by the last condition which takes into account the kinematical constraint for reaction (1) $\theta^2_{(beam-e)} < \frac{2m_e}{E_e}$ and the angular resolution for electrons. The probability for an electron to be signed by electromagnetic processes is then > 98% at 90% CL. A sub-sample of 36% of the films was scanned twice giving a scanning efficiency of 85% per scan, within the cuts, or (90 ± 6)% on average in the total sample.

The events were classified as "isolated e^-" candidates if just a single track was at the interaction vertex. No bremsstrahlung e^+e^- pair above 30 MeV energy was allowed on the first 7 centimetres of the track and no e^+ above 2.5 MeV on the first centimetre of the track. Events which did not

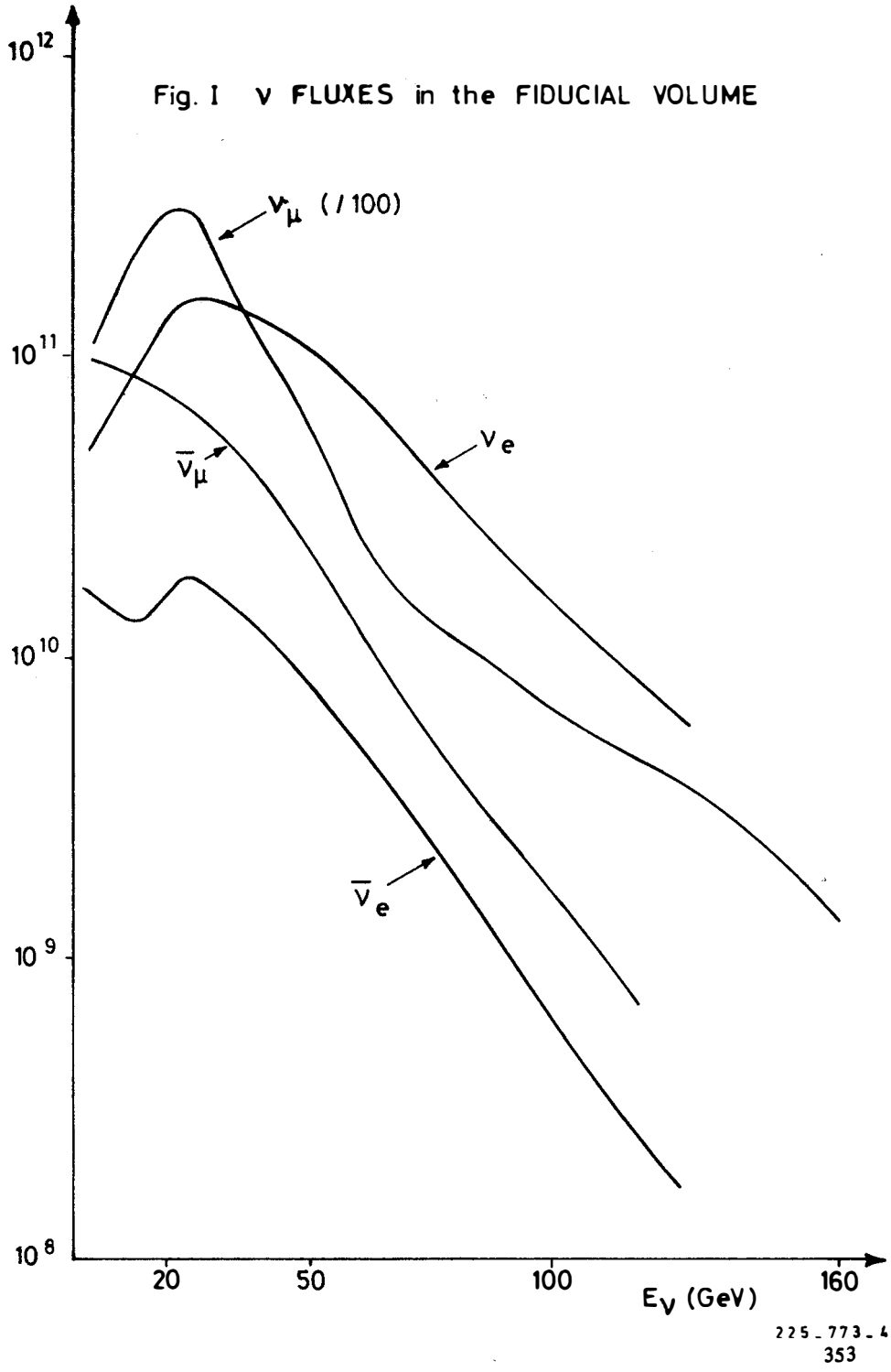
Fig. I ν FLUXES in the FIDUCIAL VOLUME
10^{12}
10^{11}
10^{10}
10^{9}
10^{8}
ν_μ (/100)
$\bar{\nu}_\mu$
ν_e
$\bar{\nu}_e$
20
50
100
160
E_ν (GeV)
225_773_4
353

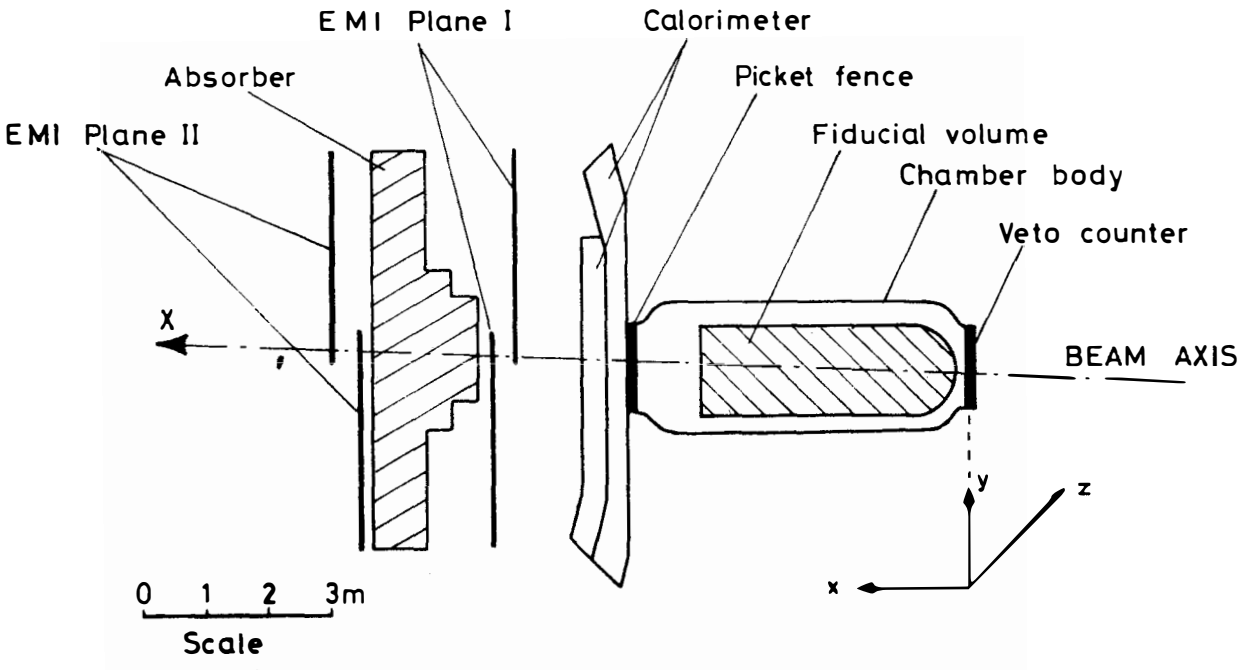

Fig. 2 Experimental set up

satisfy these two criteria were classified as "isolated γ-rays". The probability to misclassify as a γ-ray a genuíne electron by the selection criteria was estimated by a Monte-Carlo method and found to be equal to $(8 + 3.7 \text{ Log } E_e \text{ (GeV)})\%$.

Ten e^- and 13 γ-rays fulfilling these conditions were found (fig. 3).

The separation between events with 1 or 2 electrons at the vertex was checked by counting the bubble density near the vertex relatively to that of the electrons at minimum ionization in the same shower. A ratio between 0.8 and 1.2 was found for each of the 10 e^- candidates, while the same ratio was found to be greater than 1.5 for identified γ-rays. We can conclude that our 10 e^- candidates are true single electrons.

Three background processes could give rise to isolated single electrons:

i) high energy γ-rays, by asymmetric e^+e^- pair creation, Compton effect or annihilation of the e^+ close to the vertex of the e^+e^- created pair;

ii) isolated μ^-'s or π^-'s which by emission of δ-rays can develop an electromagnetic shower and simulate an electron;

iii) charged current interaction of ν_e (or $\bar{\nu}_e$) with nuclei in which hadrons escape detection.

The photon background was estimated experimentally using a sample of 183 e^+e^- pairs or $e^\pm$ in the 2 to 20 GeV energy range, associated with interactions of neutrinos in the chamber. Indeed, no signle e^- or e^+ was found is this sample, thus giving a limit on this background process of 1.2% at 90% CL, in excellent agreement with theoretical calculations. From the sample of isolated γ-rays, this background is thus found smaller than 0.13 events.

To estimate the background ii), it was checked that none of the 10 e^- candidates were associated with hits in the EMI. Since the EMI efficiency was already determined to be almost 100% for muons produced in the beam direction, it is concluded that the background from muons is negligible. All the negative leaving particles without any shower were found to hit the EMI, meaning that no leaving isolated π^-'s along the beam direction were observed. Since the probability for a π to give an electromagnetic shower was estimated to be $< 2\%$, also the background from π^- is negligible.

Fig. 3 ENERGY VERSUS ANGLE TO THE BEAM

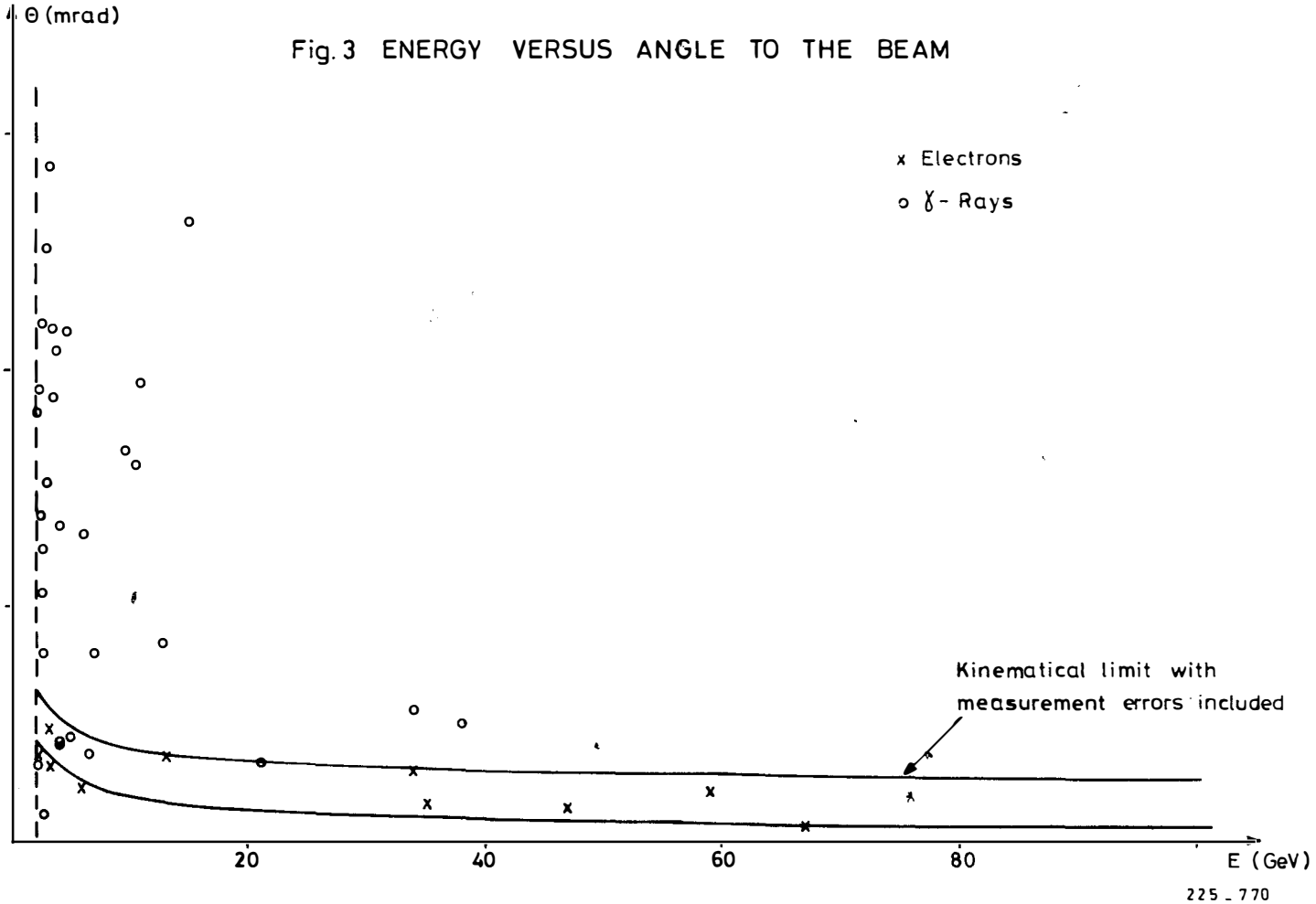

The charged current reaction $\nu_e + n \rightarrow e^- + p$ could fake a $\nu_\mu + e^- \rightarrow \nu_\mu + e^-$ reaction if no protons are seen. The probability that all protons escape detection has been computed from the similar reaction $\nu_\mu + n \rightarrow \mu^- + p$. The ratio

$$R_\mu = \frac{\mu^- \ (\theta_\mu < 3^o) + \text{unseen proton}}{\mu^- + p}$$

has been estimated in two ways. First, the q^2 distribution of $\mu^- p$ events was compared to the prediction of a Monte Carlo using $M_A^2 = 0.9$ GeV$^2/c^4$ for the axial mass M_A in the form factor and taking into account the nuclear re-interactions. From the loss of events at low q^2, attributed to event classified as isolated μ^-, we compute $R_\mu = (6 \pm 3)\%$. Secondly, R_μ was computed from the observed μ^- events. At energies above 11 GeV, some of the isolated μ^-'s are producted through the reaction $\nu_\mu + e^- \rightarrow \mu^- + \nu_e$. This contribution has been estimated 6 ± 3 events, using the theoretical cross-section, and it has been subtracted from the observed 15 μ^- events. We estimate with this method that $R_\mu = (5 \pm 3)\%$ in agreement with the previous determination. From the 3 $e^- p$ events observed in our films this background therefore amounts to 0.2 ± 0.2 events. Other background sources such as $n + e^- \rightarrow n + e^-$ have been found completely negligible.

Another source of isolated e^- is the reaction $\nu_e + e^- \rightarrow \nu_e + e^-$, which is allowed by charged and neutral current processes. Nevertheless, these events cannot be experimentally separated from the $\nu_\mu e^-$ events and furthermore the $\nu_e e$ contribution depends not only on the experimental cuts, but also on the vector and axial-vector constants which are related to those of $\nu_\mu e$ reactions. So it was chosen not to subtract a possible $\nu_e e$ contribution to our signal, but to compare the signal to the sum of predicted ν_μ and ν_e cross sections weighted by the corresponding fluxes.

To summarize, the signal of isolated e^- consists of 10 events; with a total background of 0.2 ± 0.2 events.

In order to obtain the cross-section, the neutrino flux has been computed by a Monte-Carlo method. The production spectra of the π and K parents of the ν's were taken from the thermodynamical model [4], taking also into account experimental points obtained by hadronic experiments at Fermilab [5].

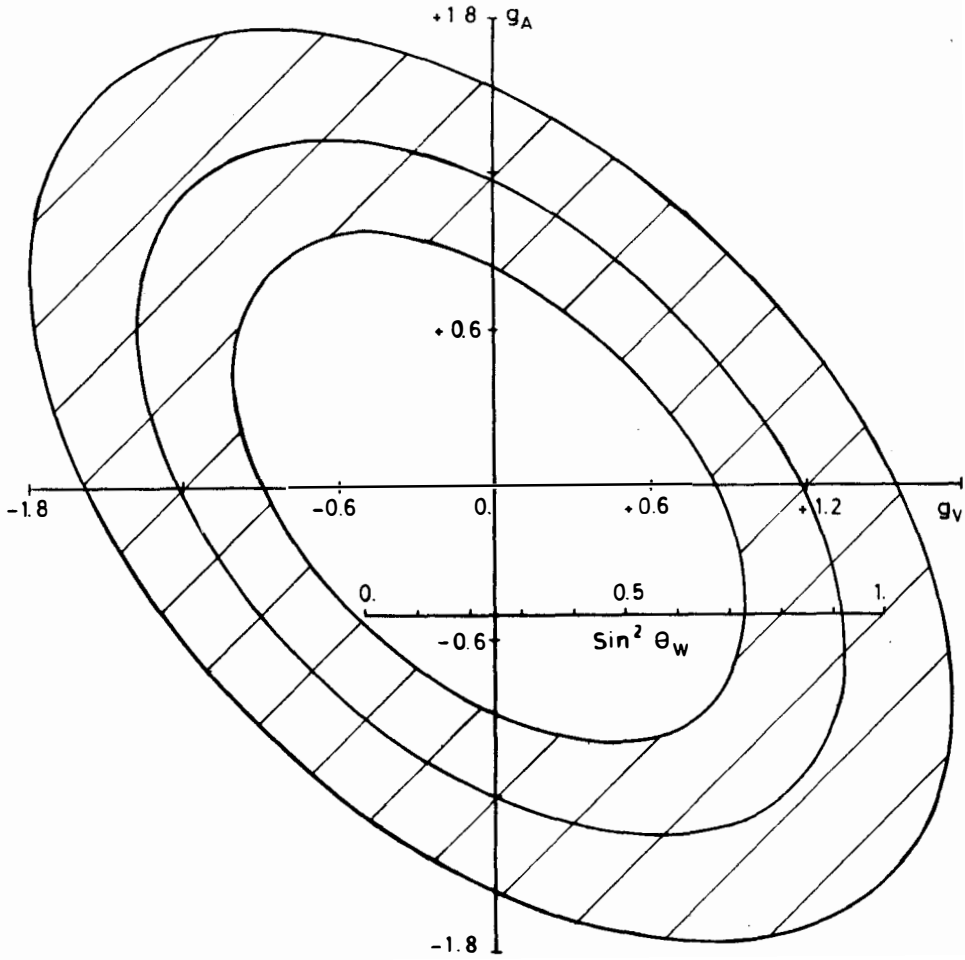

Fig.4 DOMAIN ALLOWED IN THE $g_V - g_A$ PLANE FROM THE REACTION $\nu_\mu + e^- \longrightarrow \nu_\mu + e^-$

225_775_4

From this flux, and using for the total cross-section the value

$$\sigma_{tot}\ (\nu_\mu + N \rightarrow \mu^- + x) = 0.7\ 10^{-38}\ E_\nu\ cm^2/nucleon$$

as measured in other high energy experiments [6]. The total number of expected inclusive charged current ν_μ events is 23 600 in the fiducial volume. This number was checked counting in a sample of pictures the number of interactions in the fiducial volume with a μ^- signed in the EMI. After normalization to the total number of pictures we find 24 500 ± 3 000 in excellent agreement with the previous estimate. The calculated flux is also in very good agreement with the observed μ^-p events. The error on the flux is estimated to be 10%. The calculated ν_e flux is about 2% of the ν_μ flux, confirmed by the observed rate of ν_e events.

Assuming that the weak current is made only of V and A terms, the cross-section is written as:

$$\frac{d\sigma}{dE_e} = \frac{G^2 m_e}{2\pi} \left\{ (g_V + g_A)^2 + (g_V - g_A)^2 \left(1 - \frac{E_e}{E_\nu}\right)^2 \right\}$$

where $g_{V,A}^{\nu_e} = 1 + g_{V,A}^{\nu_\mu}$, the constant 1 for the ν_e reaction being due to the charged current contribution. Thus, the number of expected events is

$$N\ (g_V,\ g_A)\ \alpha \iint_{Ee\ >\ 2} \left\{ \phi_{\nu_\mu}\ \frac{d\sigma^{\nu_\mu}}{dE_e} + \phi_{\nu_e}\ \frac{d\sigma^{\nu_e}}{dE_e} \right\} \beta(E_e)\ dE_e\ dE_\nu$$

where $\beta(E_e)$ is the electron detection function product of the different efficiencies defined above:

$$\beta(E_e) = 0.90\ (\text{scanning}) \times (0.92 - 0.037\ \text{Log}\ E_e)\ (\text{misclas}) \times 0.99\ (\text{ident.})$$

Fig. 4 shows the limits at 90% CL of the domain in the g_V, g_A plane allowed by the signal of 10 events, using the Poisson distribution.

Depending on the g_V/g_A ratio, the value of the slope

$$S = \frac{\sigma_{tot}\ (\nu_\mu + e^- \rightarrow \nu_\mu + e^-)}{E_\nu}$$

is always found in the range

$$(0.73\ ^{+0.33}_{-0.26})\ 10^{-41}\ cm^2/GeV \leq S \leq (0.82\ ^{+0.37}_{-0.28})\ 10^{-41}\ cm^2/GeV.$$

It must be remarked that the signal is higher than what was foreseen from the results on the same reaction at PS energies [2,3].

In the framework of the standard SU(2) ⊗ U (1) model, at 90% CL $\sin^2\theta_w$ is found to be greater than 0.74.

With the currently accepted value $\sin^2\theta_w \simeq 0.25$, 1.7 ± 0.2 events are expected whereas 10 are observed.

REFERENCES

1) J. Blietschau et al., Nuclear Physics B114 (1976) 189.

2) H. Faissner et al., to be published.

3) J. Blietschau et al., Phys. Lett. 73B (1978) 232.

4) H. Grote et al., Atlas of Particle Production Data, CERN 1970;
J. Ranft et al., CERN Lab II-RA/74-2 (1974).

5) W.F. Baker et al., Phys. Lett. 51B (1974) 303;
R. Stefansky, La Physique du Neutrino à Haute Energie, Paris (1975);
B. Aubert et al., Fermilab. Conference 1975/31-Exp (1975).

6) K. Schultze and F. Sciulli, Talks at the Symposium on Lepton and Photon Interactions, Hamburg (1977).

LEPTON AND CHARM PRODUCTION IN THE 15 FOOT FNAL BUBBLE CHAMBER

Report by R. B. Palmer
Brookhaven National Laboratory, Upton, NY, USA

A. M. Cnops, P. L. Connolly, S. A. Kahn, H. Kirk, M. J. Murtagh,
R. B. Palmer, N. P. Samios, M. Tanaka
Brookhaven National Laboratory, Upton, NY, USA

C. Baltay, D. Caroumbalis, H. French, M. Hibbs, R. Hilton,
M. Kalelkar, W. Orance, E. Schmidt
Columbia University, NY, USA

ABSTRACT

The report is on ν interactions in the FNAL 15 foot bubble chamber filled with heavy neon. Inclusive production of π^+, π^-, K^o and Λ^o is shown. Limits are given on the production and hadronic decay of Λ_c. The rate of D^o production and decay to $K^o\pi^+\pi^-$ is reported. Events containing a μ^- and e^+ are observed and interpreted as leptonic decay of charm. Events with single e^+ or e^- are reported and found to be consistent with $\bar{\nu}_e$ and ν_e interactions.

Le rapport traite des interactions ν dans la chambre a bulle FNAL de 15 pieds remplie de neon lourd. On y montre la production inclusive de π^+, π^-, K^o et de Λ^o. Des limites sont attribuées à la production et à la désintegration hadronique de Λ_c. Le taux de production de D^o et de desintegration en $K^o\pi^+\pi^-$ y est rapporté. On observe les évenements comportant un seul e^+ ou un e^- et on trouve qu'ils sont cohérents avec les interactions $\bar{\nu}_e$ et ν_e.

1. INTRODUCTION

The following report is on our experiment done at FNAL in the 15 foot bubble chamber filled with 64% (atomic) neon and 36% (atomic) hydrogen. The chamber was run in the FNAL two horn "wide band" neutrino beam whose energy distribution is shown in Figure 1. With this combination a charged current rate of about one event per two pictures was obtained, much higher than that obtainable with the quadruple triplet beam (again see Figure 1).

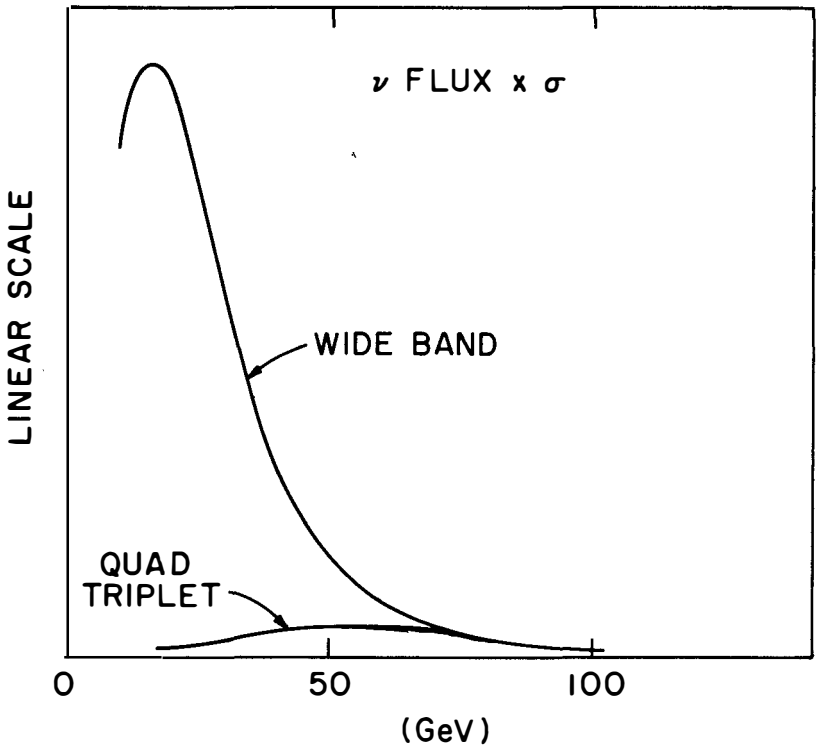

Figure 1. Energy distribution of flux times cross section, assuming cross section proportional to energy.

In addition, the use of neon provided good gamma and electron identification (the chamber is 3.6 meters diameter and the radiation length is 40 cm) and moderate hadron identification (the interaction length is 1.25 meter).

The following results were obtained from the analysis of 96,000 pictures containing 46,400 charged current events. All events containing a K^o, a Λ^o or an electron were measured (approximately 3,000 events). In addition a smaller sample of charged current events was measured without the above requirements. This report will cover data on inclusive production of π's, K's and Λ's and the search for hadronic decays of charmed particles. Events containing an e^+ or e^- will be analyzed in terms of contributions from charm decay, ν_e and $\bar{\nu}_e$ interactions and possible contributions from heavy leptons.

2. NON CHARMED HADRON PRODUCTION

For charged current events, Figure 2 shows the corrected $K^o + \bar{K}^o$ and $\Lambda + \Sigma^o$ production as a function of W_{vis} (the visible center of mass energy of all hadrons). The mean value of W_{vis} for this experiment was 3.3 GeV and the mean fractions of events with K^o's and Λ's/Σ's were 13.6 ± 1.5 and 5 ± .5%, respectively.

Figure 3, again for charged current events, shows the multiplicities of π^+, π^-, K^o and Λ/Σ^o as a function of Z, where Z is the corrected fraction of hadronic momentum carried by the particle in question. The correction is given by the formula:

$$Z = \frac{P_i}{E_{other} \times 1.4 + P_i} \quad . \qquad (1)$$

where P_i is the momentum of the particle in question and E_{other}, the total hadronic energy excluding P_i. This correction is not exact and will somewhat distort the resulting distributions shown in Figure 3. Nevertheless, one may note the general feature that as $Z \to 1$ the production of π^-, K^o's and Λ's are all similar and all a factor of about 10 below that for π^+'s. This may reflect the fact that the $\pi^+(u\bar{d})$ can be formed with one ocean quark, the other coming from the fast valence quark leaving the initial interaction ($\nu + d \to \mu^- + u$). For the π^-, K^o and Λ two quarks have to come from ocean in each case. It should be noted, however, that these characteristics may arise simply from mass and charge conservation considerations and do not of themselves prove anything about leaving quarks.

3. HADRONIC DECAYS OF CHARM

A search was made for hadronic decays of the D and Λ_c charmed hadrons.

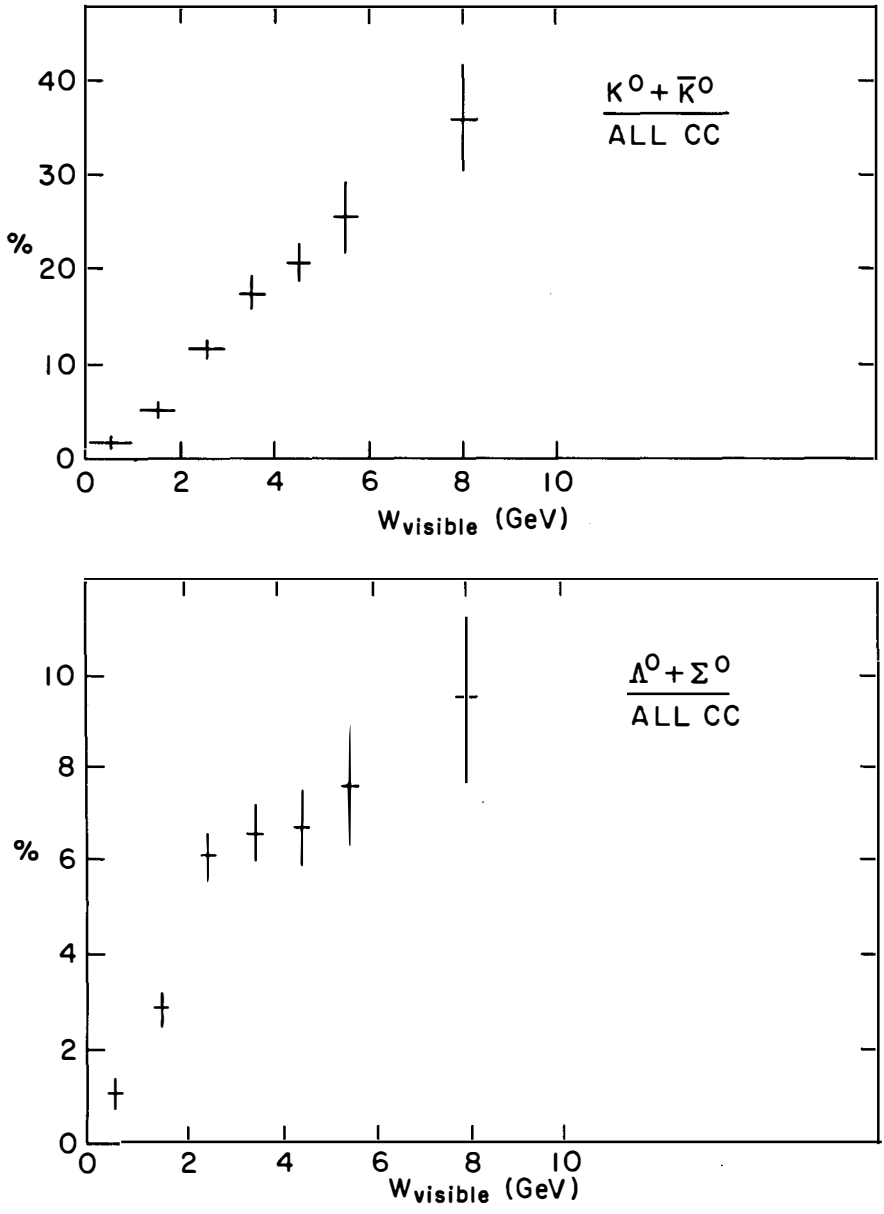

Figure 2. Multiplicities of strange particle production in charged current interactions versus the visible hadron energy for (a) K^0 and $\bar{K}^0$ and (b) Λ^0 and Σ^0.

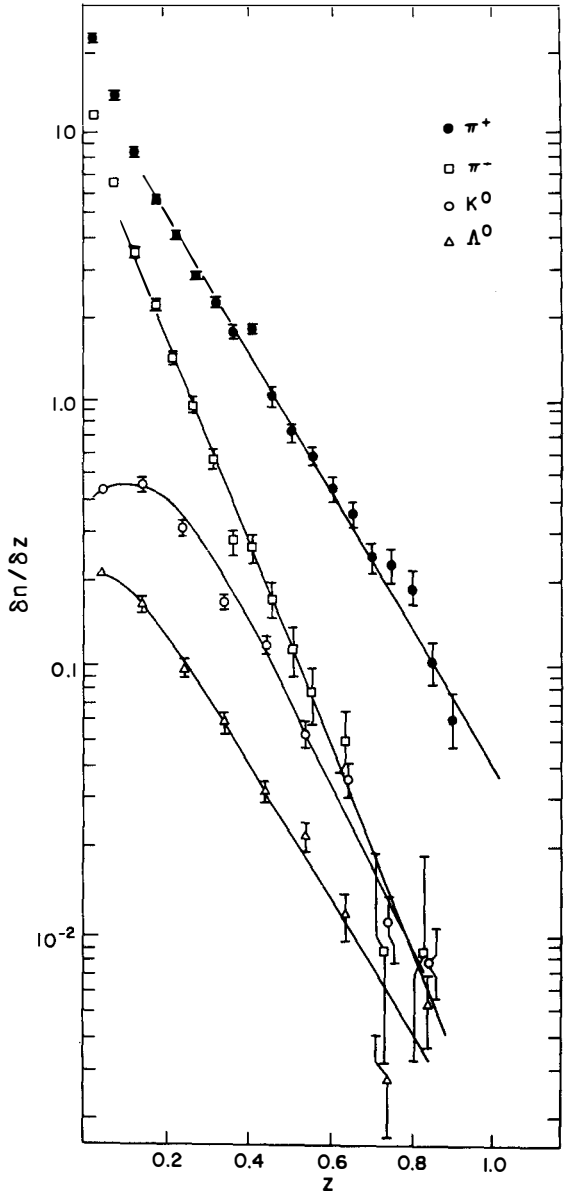

Figure 3. Multiplicities of particle production in charged current interactions versus Z the corrected fraction of the total hadron energy carried by the particle.

The modes studied were

$$\Lambda_c^+(2250) \rightarrow \Lambda\, \pi^+\pi^+\pi^- \qquad (2)$$

$$\Lambda_c^+ \rightarrow \Lambda\, \pi^+ \qquad (3)$$

$$D^+ \rightarrow K^o\pi^+ \qquad (4)$$

$$D^o \rightarrow K^o\pi^+\pi^- \qquad (5)$$

Plots of the observed effective mass distributions are shown in Figures 4 through 7. No signal is observed in reactions (2) and (4). A small signal is apparent in channel (3) but is not observed if a cut is made of helicity angle ($Cos\theta_H^* > -0.6$). This cut was chosen to remove the large background from events with a slow Λ and fast pion, and should have enhanced the signal to background ratio. The fact that this does not occur suggests that the observed enhancement is a fluctuation. From these results we obtain the following 90% confidence level limits for branching ratios times fraction of charged current production:

$$\Lambda_c \rightarrow \Lambda\, \pi^+\pi^+\pi^- \quad \leq .2\% \qquad (6)$$

$$\Lambda_c \rightarrow \Lambda\, \pi^+ \quad \leq .1\%$$

$$D^+ \rightarrow K^o\pi^+ \quad \leq .2\%$$

In reaction (5) $D^+ \rightarrow K^o\pi^+\pi^-$ (Figures 7a and 7b) a clear signal is observed at the expected mass value. A fit using a gaussian on a polynomial background gave a signal of 64 ± 15 events, a mass of 1850 ± 15 MeV. The width was 23 MeV which is consistent with our resolution. This signal corresponds to a branching ratio times fraction of charged current events of 0.7 ± .2%.

Comparing this with the limit on D^+ production and using the SLAC branching ratios of 4 ± 1.3% for $D^o \rightarrow K^o\pi^+\pi$ and 1.5 ± .6% for $K^o\pi^+$ we obtain the ratio

$$\frac{\sigma(D^+ \text{ production})}{\sigma(D^o \text{ production})} = .5 \pm .4 \leq .76 \text{ (90\% CL)} \qquad (7)$$

Using this sample of D^o's we have looked for evidence of D^*'s by plotting $D^o\pi^+$ and $D^o\pi^+\pi^-$ masses. No evidence of D^*'s were seen but an enhancement in the $D^o\pi^+\pi^-$ mass spectrum at 4.9 GeV is present (see Figure

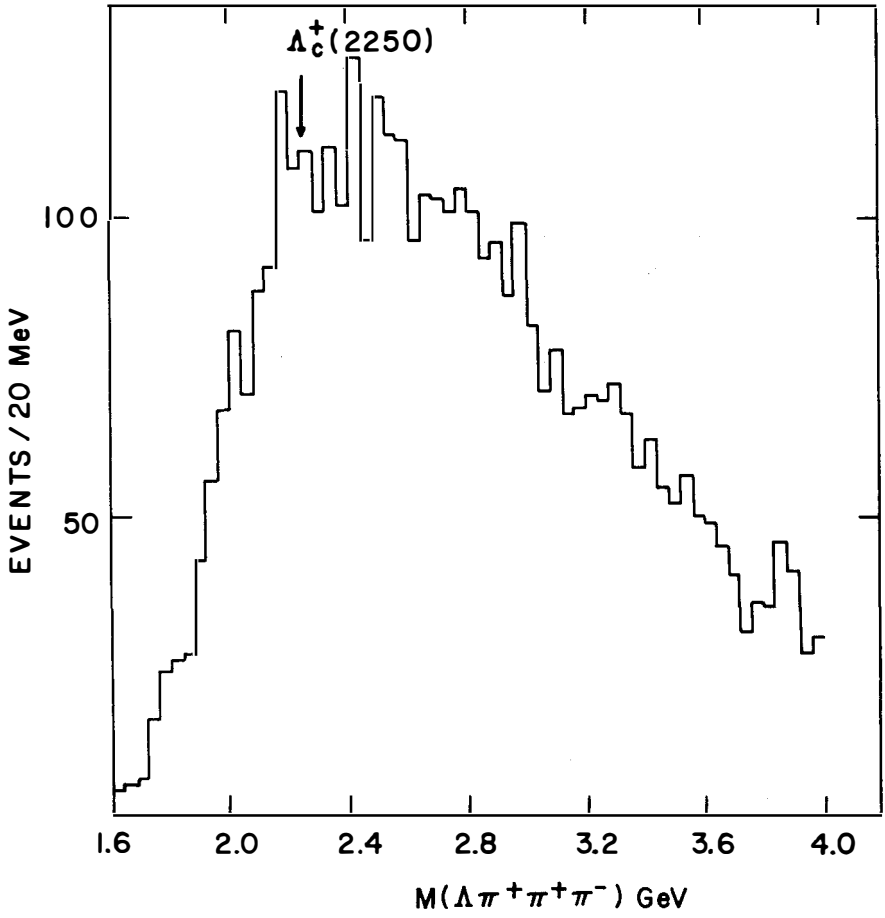

Figure 4. Effective mass distribution for $\Lambda\pi^+\pi^+\pi^-$ system.

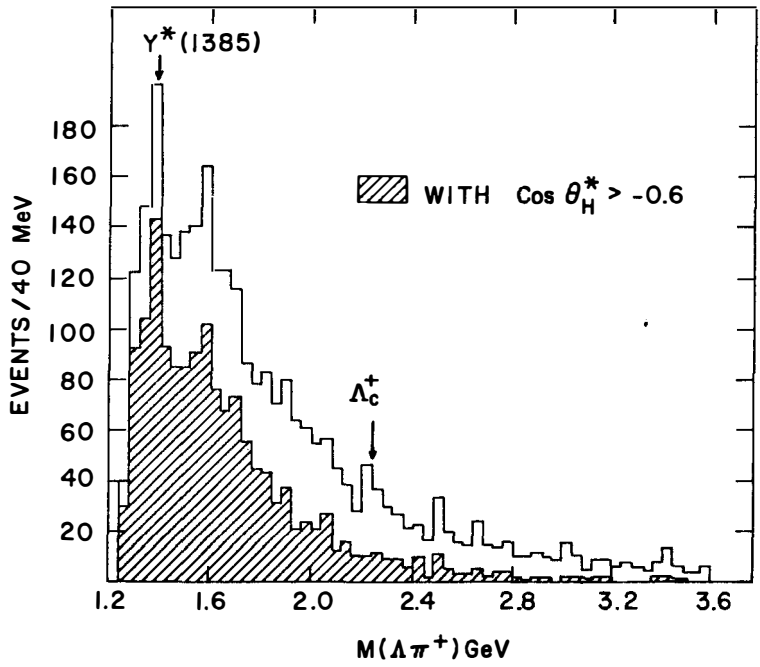

Figure 5. Effective mass distribution for $\Lambda\pi^+$ system. The shaded area indicates the distribution for events with $\cos\theta_H > -0.6$, where θ_H is the helicity angle of the Λ in the $\Lambda\pi$ system.

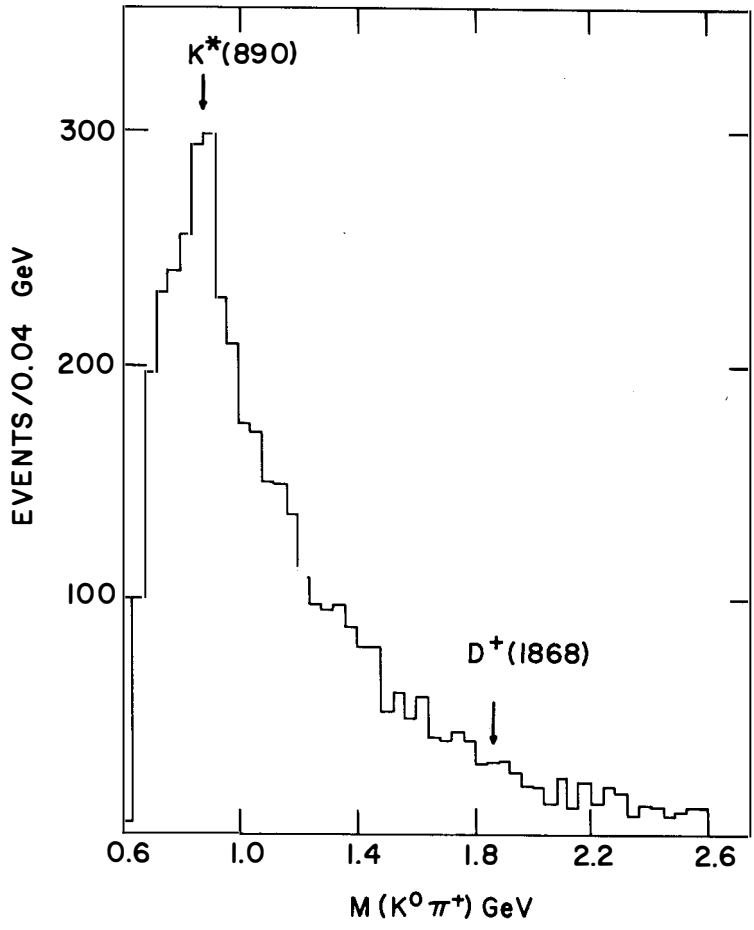

Figure 6. Effective mass distribution of $K^0\pi^+$ systems.

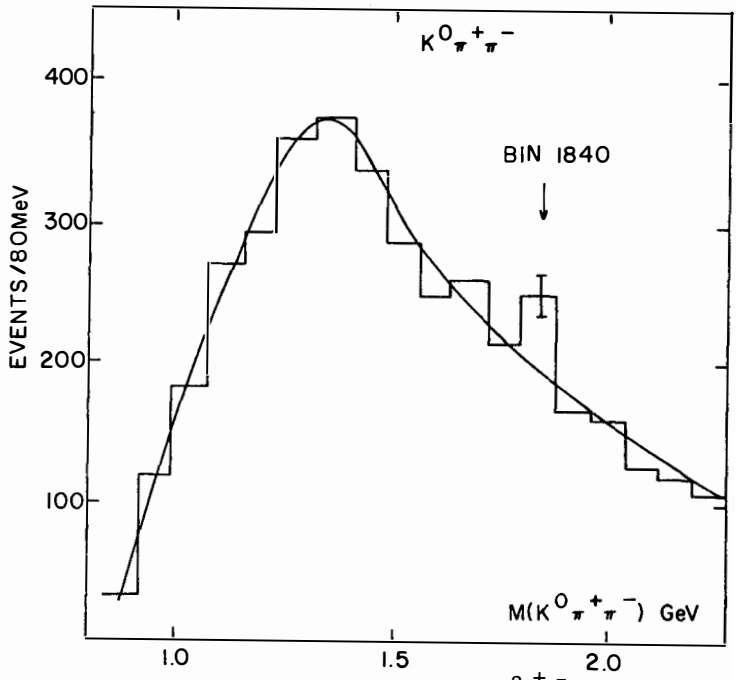

Figure 7a. Effective mass distribution of $K^0\pi^+\pi^-$ system plotted in 80 MeV bins.

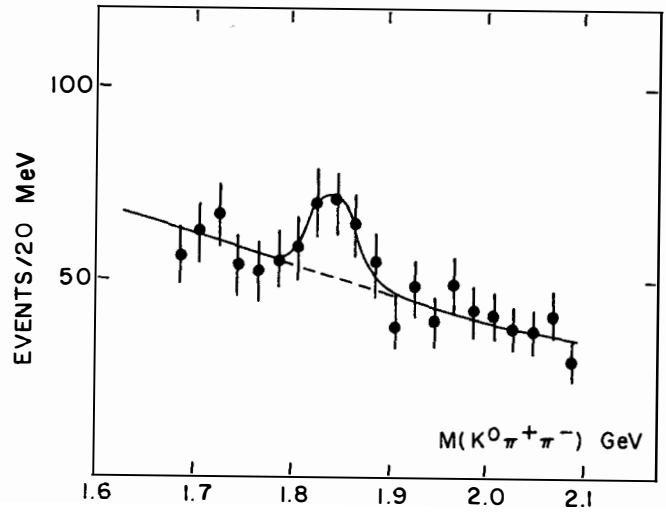

Figure 7b. Effective mass distribution of $K^0\pi^+\pi^-$ system plotted in 20 MeV bins. The polynomial plus gaussian fit is shown by the continuous line, the polynomial alone being indicated by the broken line.

8). This might be considered evidence for a meson containing a quark of the type present in the $\Upsilon(9.5)$. However, if the enhancement were of this origin then its branching ratio times fraction of charged current events is 2.5%. A branching ratio greater than 10% seems unlikely thus implying that the production of the state occurs in 25% of all charged current events: a very unlikely situation. We conclude that the effect is probably a statistical fluctuation.

4. LEPTONIC DECAY OF CHARM

Charm is expected to be produced only in charged current events and the $\Delta C = \Delta Q$ rule requires that with neutrinos only positive charm can be made and the leptonic decay will then give a positive lepton (e^+ or μ^+) and a neutrino. Thus production and leptonic decay of charm will appear as events with a μ^- and μ^+, or μ^- and e^+. The μ identification in the chamber is not sufficient to identify the former but the latter can be identified with high efficiency (85%) and low background ($\leq$ 14%). 164 events with μ^- and e^+ were found. When corrections are made for scanning efficiency and identification we obtain a ratio of $\mu^- e^+$ events to all charged current events of 0.5 ± .15%. The y ($\frac{\nu}{E_\nu}$) and x ($\frac{q^2}{2M\nu}$) distributions for these events are shown in Figures 9 and 10. The y distributions can be seen to be consistent with a normal V-A interaction and inconsistent with V + A. The x distribution may be compared with that expected (continuous line) for production from a valence quark:

$$\nu + d \rightarrow \mu^- + c \qquad (8)$$

The agreement is reasonable, but one does note a slight enhancement at low x which when fitted (broken line) indicates a 25 ± 25% contribution from the strange quarks in the sea reaction:

$$\nu\ s \rightarrow \mu^-\ c \qquad (9)$$

We now consider the strange particle content. 33 of the 164 events also contain a V^0 i.e. 20 ± 4%. This may be compared to the fraction of other charged current events with a V^0 which is 6%. The excess is explained if the events come from charm decay by the expected dominance of charm decay to strangeness. If reaction 8 dominates then the expected excess (after correction for decay modes, efficiencies, and assuming equal charged and neutral strange particles would to 15%. At higher energies reaction 9 should eventually become dominant, two strange particles would be made per event and the visible excess would be

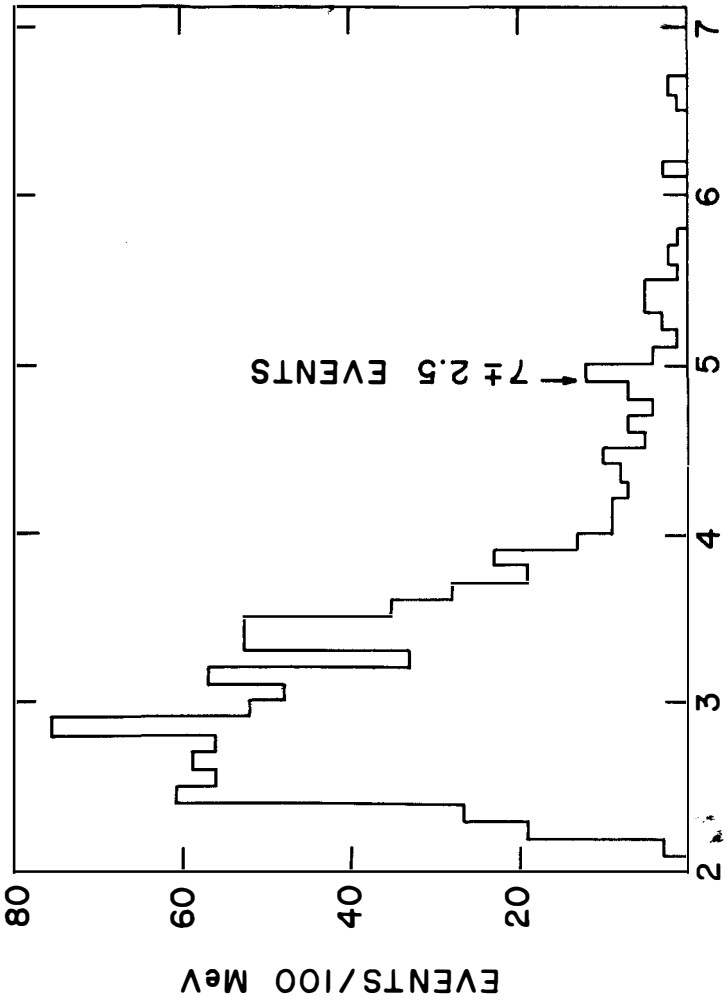

Figure 8. Effective mass distribution of the $D^{o}\pi^{+-}$ system.

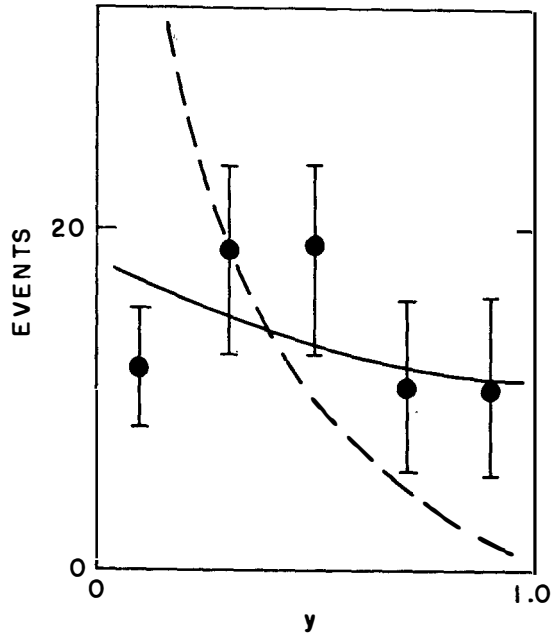

Figure 9. y distribution of events of the type ν_μ Ne → μ^- e^+ etc.

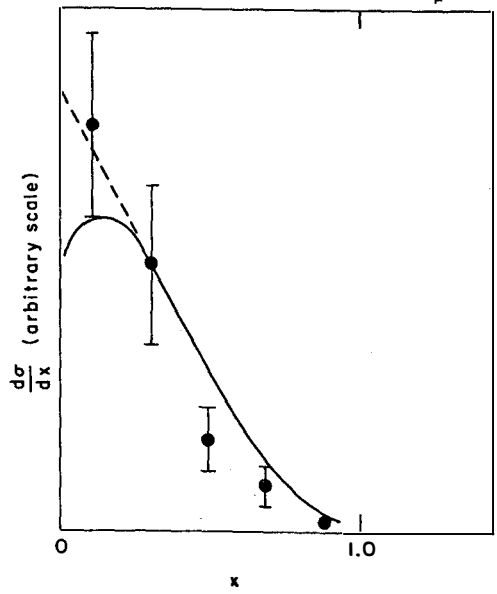

Figure 10. x distribution of events of the type ν_μ Ne → μ^- e^+ etc.

about 30%. In Figure 11 and Table I the fraction of V^o's observed by different experiments are plotted against an estimate of the mean neutrino energy in each case. The lowest dotted line indicates the expected contribution from associated strange particle production (unrelated to the charm); the second dotted line includes the contribution from reaction 1; and the dashed line is an arbitrary guess as to how the ratio might vary if production becomes dominated by reaction 2 above 60 GeV neutrino energy. This line is not the result of a calculation but shows that a higher ratio in the BEBC narrow band beam experiment (point 6) is consistent with what should be expected.

TABLE I

Fraction of V^o's Found in Dilepton Events from Different Experiments

#	Experiment	Beam	Average† E_ν	Total Dileptons	Total V^o's	Fraction* With V^o's
1	Gargamelle, Freon/propane	WB Ps	3	14 μ^-e^+	3	.21 ± .11
2	CERN BEBC, Heavy Neon	WB SPS	20	21 μ^-e^+	6	.29 ± .10
3	NAL 15', Light Neon	WB NAL	25	17 μ^-e^+	11	.65 ± .12
4	NAL 15', Heavy Neon (E 172)	WB NAL	25	6 μ^-e^+	1	.13 ± .12
5	NAL 15', Heavy Neon	QT NAL	40	9 $\mu^-\mu^+$	1	.11 ± .10
6	CERN BEBC, Heavy Neon	NB SPS	75	7 $\mu^-\mu^+$ 5 μ^-e^+	4 2	.5 ± .14
	THIS EXPERIMENT	WB NAL	25	164 μ^-e^+	33	.2 ± .03

Abbreviations: WB Wide band horn focus
QT Wide band quadruple triplet
NB Narrow band
NAL FNAL (Fermilab)

* Errors given are statistical only.

† These values are approximate only.

Of the 33 events with strange particles 23 ± 3 are K^o's and 10 ± 3 and Λ's or Σ^o's. The errors arise because of ambiguities. The expected numbers from associated production are 5 and 4, respectively from which we obtain a ratio of charm decay to K^o over that to Λ/Σ^o of 6 ± 4.7. The

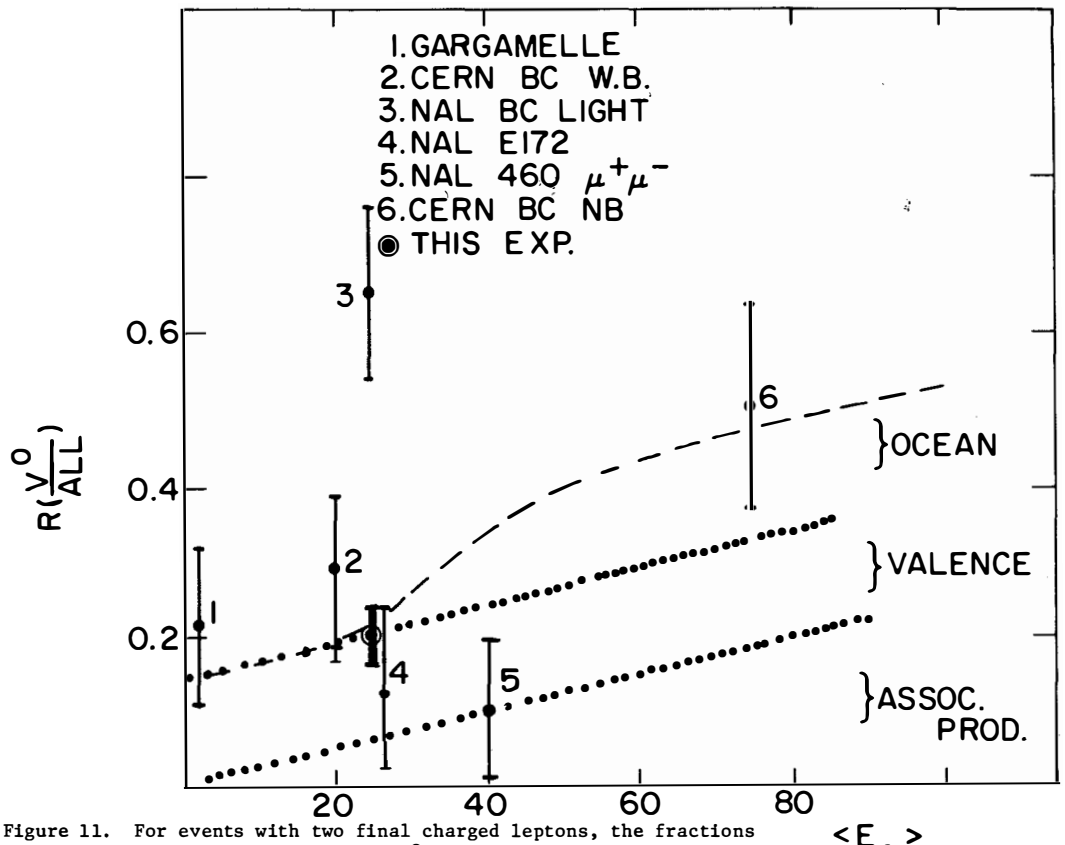

Figure 11. For events with two final charged leptons, the fractions (R) that have a visible V^o is plotted against the mean neutrino energies for seven experiments.

errors are large but suggest relatively small charmed baryon production relative to meson production, a result also suggested by the limits on hadronic decays (equations 6).

Assuming that the events with a K^o do come from D decay, we can plot the effective mass of the $K^o e^+$ system and compare the distribution with that expected for different decay modes. For this purpose only unambiguous K^o's are used (Figure 12b). If the decay were

$$D^+ \to e^+ \nu K^o \tag{10}$$

then the distribution should be as shown by the dashed line (the curve is 3 body phase space but calculations including guessed form factors give very similar curves). Alternatively if the decay were

$$D^+ \to e^+ \nu K^o \pi^o \tag{11}$$

or

$$D^o \to e^+ \nu K^o \pi^- \tag{12}$$

the distribution should be as given by the continuous line (four body phase space). The distribution strongly favors this latter hypothesis. One explanation would be that there are far more D^o's than D^+'s as suggested by the hadronic decays (equation 7). If this were the case then decay (12) is dominant and one should be able to find the π^- by requiring the $\pi^- K^o e^+$ mass to be less than the D mass. Of the 16 events with unambiguous K^o's, 12 have only one candidate π^- and 4 have two such candidates. The $\pi^- K^o$ mass for these events is plotted in Figure 12a. the distribution observed is consistent with the phase space curve indicated. There is little evidence for the $\pi^- K^o$'s being from the $K^*(890)$.

Finally we can compare the hadronic and leptonic decays branching ratios. We obtain

$$\frac{D^o \to K^o \pi^+ \pi^-}{D^o \to \nu e^+ \text{ etc}} \geq 1.4 \pm .7 \tag{13}$$

where the limit is reached when there is no D^+ production. The above limit may be compared with the SLAC observed ratio

$$\frac{D^o \to K^o \pi^+ \pi^- \ (4 \pm 1.3\%)}{D^{+/o} \to e\nu \ldots (7.2 \pm 2.8)} = 0.56 \pm 0.28 \tag{14}$$

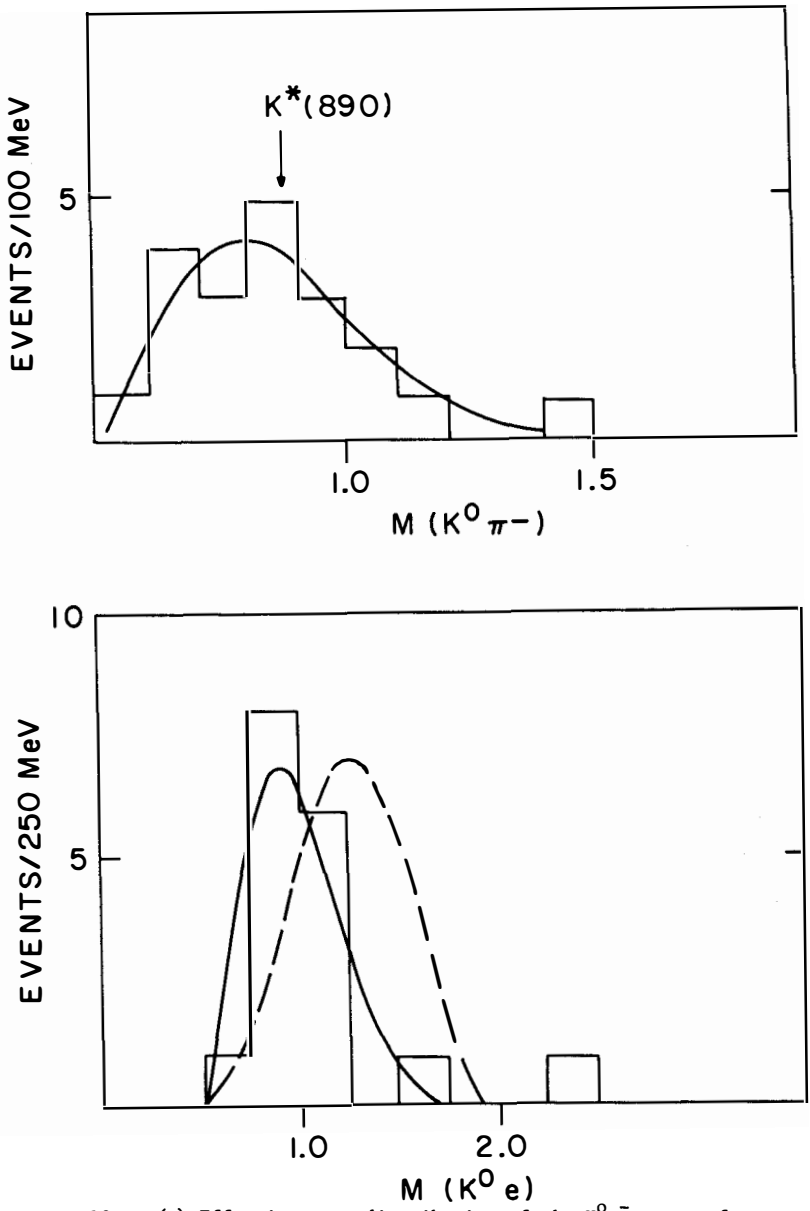

Figure 12. (a) Effective mass distribution of the $K^o\pi^-$ system for events of the type ν_μ Ne → μ^- e^+ $K^o\pi^-$ etc. for which the effective mass of e^+ $K^o\pi^-$ is less than 1.86 GeV. (b) Effective mass distribution of the K^oe^+ system for events of the type ν_μ Ne → μ^- e^+ K^o etc. Events with 2 V^o's or ambiguous Vo's have been removed.

The apparent discrepancy between equations (13) and (14) could be explained if the semileptonic decay rate of the D^o were much less than that for the D^+. One notes however that the errors are large.

5. ELECTRON NEUTRINO EVENTS

Events were selected with an e^+ or e^- but no μ^- candidate. 28 such events were seen with an e^+ and 187 with an e^-. Such events can come from $\bar{\nu}_e$ and ν_e respectively but could also come from the decay of heavy muon type leptons. In order to set a limit on this latter hypothesis the expected numbers of $\bar{\nu}_e$ and ν_e events were calculated and thus any excess calculated. We obtained:

$$\begin{aligned} \text{excess } e^- &= 187 \pm 14 \text{ (observed) } -215 \pm 60 \text{ (calculated) } = -28 \pm 60 \\ \text{excess } e^+ &= 28 \pm 6 \text{ (observed) } -23 \pm 8 \text{ (calculated) } = 5 \pm 10 \end{aligned} \tag{15}$$

Clearly there is no significant excess. An independent test as to whether these events are indeed due to ν_e and $\bar{\nu}_e$ is provided by the distributions of the events in y_{viz}, where $y_{viz} = (E_{viz} - E_e)/E_{viz}$. These distributions are given in Figures 13 and 14 where the continuous lines indicate the expectation for $\bar{\nu}_e$ and ν_e interactions and the broken lines indicate that expected if the e's were coming from the decay of a τ meson (eg., $\tau^- \to e^- \bar{\nu}_e \nu_\tau$), where the τ^- is assumed to have the same distribution as a μ^- in a normal charged current event. The events appear to be due to $\bar{\nu}_e$ and ν_e with no evidence of heavy leptons.

Quantitatively, these results give the following limits:

$$\frac{\text{No. of } e^\pm \text{ from heavy leptons}}{\text{all charged current events}} \begin{cases} \leq 3\ 10^{-3} \text{ for } e^- \\ \leq 1\ 10^{-3} \text{ for } e^+ \end{cases} \tag{16}$$

$$\text{Mass of heavy lepton } L^\pm \text{ (if } g_{L\nu_\mu} = g_{\mu\nu_\mu}) \begin{cases} \geq 7.5 \text{ GeV for } L^- \\ \geq 9 \text{ GeV for } L^+ \end{cases} \tag{17}$$

$$g_{\tau\nu_\mu}/g_{\mu\nu_\mu} \text{ (or } \tan^2\theta_M) \begin{cases} \leq .025 \text{ for } \tau^- \\ \leq .01 \text{ for } \tau^+ \end{cases} \tag{18}$$

The last result may be considered as a limit on a possible mixing angle θ_M between the ν_τ and ν_μ, in which case the limits apply to $\tan^2\theta_M$.

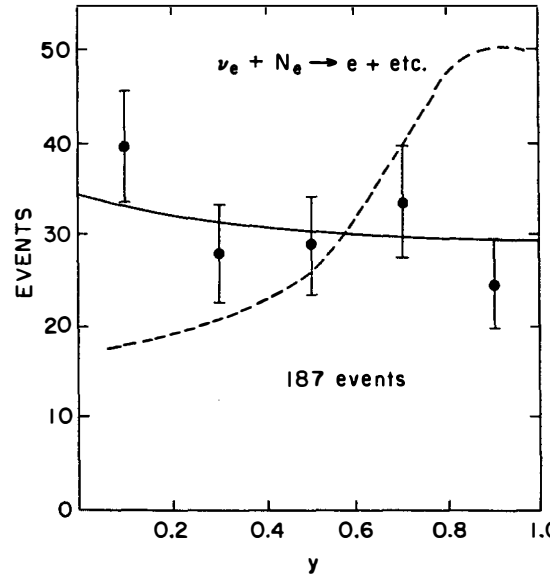

Figure 13. y distribution for events of the type ν_e Ne → e^- etc.

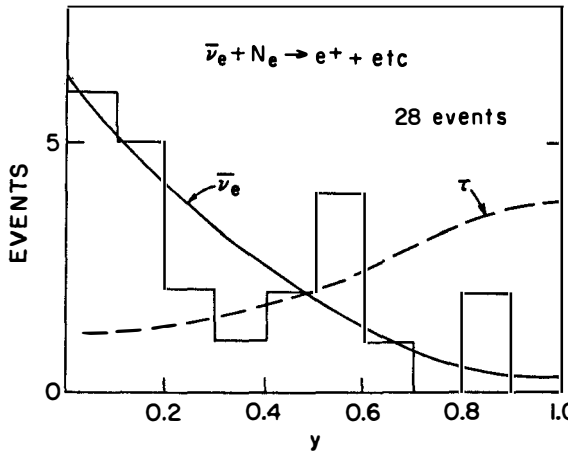

Figure 14. y distribution for events of the type $\bar{\nu}_e$ Ne → e^+ etc.

6. OTHER EXOTIC STATES

Finally we can report two non observations: We have seen no tri-lepton events of the type $\mu^- e^+ e^-$. From this we obtain:

$$\frac{\text{Rate } \nu_\mu \to \mu^- e^+ e^- \text{ etc.}}{\text{Total charged current rate}} \leq 10^{-4} \tag{19}$$

where $< E_\nu > \sim 20$ GeV and $M_{e^+e^-} \geq 500$ MeV. Such events would be made if there were neutral current charmed particle production. Thus we can obtain the limit:

$$\frac{\text{Neutral current charmed particle production}}{\text{Charged current charmed particle production}} \leq 2\% \tag{20}$$

The second non observation concerns long lived neutral particles of the type reported by the Serpukov bubble chamber group.[1] We have searched for neutral particles decaying in an e and μ with flight path greater than 5 mm. We have found no such event in 40,000 charged current events. Our scanning efficiency for such an event is greater than 50%.

This research was supported by the U.S. Department of Energy under Brookhaven National Laboratory Contract No. EY 76-C-02-0016.

REFERENCES

1. Physics Letters 70B, 269 (1977).

NEUTRINOS AND COSMOLOGY

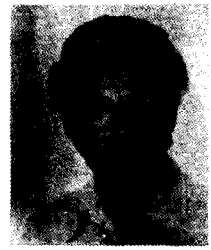

Gary Steigman
Astronomy Department, Yale University
New Haven, Connecticut 06520

ABSTRACT

In the early Universe weakly interacting particles were in thermodynamic equilibrium and neutrino-antineutrino pairs were copiously produced. These pairs subsequently annihilate in the course of the expansion but, some relic neutrinos survive to play a role in the evolution of the Universe. The confrontation of weak interaction theory and cosmology with astronomical data can lead to constraints of value to both disciplines.

The basic processes underlying the production and survival of relic neutrinos are outlined in this lecture; some specific cosmological consequences of such neutrinos are also discussed. It is shown that massive, stable neutrinos (neutral leptons) cannot have masses in the range 100 eV - 2 GeV. It is also shown, in some detail, how considerations of primordial nucleosynthesis and observations of the abundance of ^4He can constrain the number of neutrino flavors (including the e- and μ- neutrinos, $N_\nu \lesssim 7$).

INTRODUCTION

Recent developments in weak interaction physics have not escaped the attention of those whose research interests are in astrophysics and cosmology. To ignore these developments would be perilous since it is necessary to use as input in astrophysical calculations, the best available basic physics. The relation, however, between particle physics and astrophysics is not entirely unidirectional. Astrophysicists are not merely consumers of new developments in particle physics. There is, rather, a symbiotic relation in the sense that astronomical observations can provide a check on astrophysical predictions based, in part, on the latest innovations in particle physics. The distinction between particle physics and other branches of science is, to some extent artificial and, the Universe may, on occasion, provide an alternative to the accelerator as a laboratory in which to test new theories.

Neutrino astrophysics provides a specific example of the symbiotic relationship between particle physics and astrophysics. The role of neutrinos in cosmology has received much recent attention and is the subject to be reviewed in this lecture. Cosmological neutrinos have been dealt with in many recent papers[1)-12)]; here, the more limited goal is adopted of exposing and clarifying some of the details of this rapidly developing subject. Only a few specific results will be discussed; the interested reader is encouraged to consult the references for further details and references.

RELIC NEUTRINOS

If neutrinos play an important role in the physics of the early Universe then, the study of cosmology may provide information of value to the study of weak interaction physics. There is at present, however, no direct evidence for a universal background of primordial neutrinos. This is due, entirely, to the extraordinary difficulty associated with detecting neutrinos, especially low energy neutrinos. The neutrino counterparts to the relic photons of the well observed microwave background radiation, will elude detection in the forseeable future. Nevertheless, the glimpse of the early, hot, dense stages provided by the relic photons, strongly suggest that such neutrinos are present; if the right places are searched carefully enough, traces of their "footprints" may be found.

The bridge connecting particle physics and cosmology is provided by statistical mechanics. The crucial point is that, in thermodynamic equili-

brium, the physical state of a gas of elementary particles is described by macroscopic quantities (density, pressure, etc.) which are independent of the details of the specific interactions among those particles. As long as the interactions are capable of establishing and maintaining equilibrium, their detailed nature is irrelevant. This is a great simplification and it permits the analysis to be sufficiently general that the role of neutrinos in cosmology may be established with some confidence.

The approach, then, is to consider the early evolution of the Universe and to show that weakly interacting particles were once in thermodynamic equilibrium. Statistical mechanics provides us with the means of calculating the density of such particles during such equilibrium stages. The expansion of the Universe and the evolution of neutrino densities is followed until the weak interaction is too slow to maintain equilibrium; neutrino survival then depends on the competition between the expansion rate ($t^{-1} \approx$ the inverse of the age of the Universe) and the weak interaction rate ($\Lambda \approx n\sigma v$). The observable effects, the "footprints", depend on the abundance of surviving relic neutrinos (e.g.: on the ratio of relic neutrinos to relic photons).

EARLY EVOLUTION

A useful analog of the early expansion of the Universe is the free fall collapse of a homogeneous gas of noninteracting (except via gravity) particles. A gas in free fall with uniform density ρ at $t = 0$, will collapse to a singularity ($\rho \to \infty$) at $t = t(\rho)$ where $t(\rho) \sim \rho^{-1/2}$. Similarly, the age of the Universe (the time from the singularity) and the density are related by $\rho t^2 =$ constant. The basis of this simple result will now be reviewed in some detail.

On sufficiently large scales, the Universe is remarkably homogeneous and is expanding isotropically. These observational facts have led to the general adoption of the "Cosmological Principle": To a good approximation the Universe is and always was homogeneous and isotropic. It follows from the Cosmological Principle that the Universe is described by a unique metric, the Robertson-Walker metric (see, for example, the discussion in Weinberg[13]). Through the metric, the expansion of the Universe is described by one function of time, the scale factor a(t). The distance between particles (e.g.: atoms, galaxies, etc.) which are participating in the general expansion, changes in proportion to the scale factor (i.e.: $R(t) \sim a(t)$). The (observable) Hubble parameter is related to the (unobservable) scale factor through

$$H(t) = \frac{1}{a}\left(\frac{da}{dt}\right) . \qquad (1)$$

The present value of the Hubble parameter (often called the Hubble "constant") is uncertain. To reflect this uncertainty it is convenient to write: $H=100h_o$ ($kms^{-1}Mpc^{-1}$) with, $1/2 \lesssim h_o \lesssim 1$ (note that 1 Mpc $\gtrsim$ 3 x 10^{24}cm; it is conventional to indicate quantities measured at present by the subscript zero).

The Einstein equations (General Relativity) determine the time variation of the scale factor. Substituting the Robertson-Walker metric into the Einstein equations yields two differential equations which may be cast in the following suggestive forms

$$\frac{1}{2}\left(\frac{da}{dt}\right)^2 = \frac{GM}{a} + \text{constant}; \quad M = \frac{4\pi}{3} a^3\rho, \qquad (2)$$

$$d(\rho c^2 V) + pdV = 0 \quad ; \quad V \sim a^3. \qquad (3)$$

In terms of the Hubble parameter, (2) may be rewritten as

$$H^2 = \frac{8\pi}{3} G\rho + \frac{\text{constant}}{a^2} . \qquad (2')$$

From (2') it follows that there is a critical density $\rho_c = 3H^2(8\pi G)^{-1}$ such that for $\rho = \rho_c$, the constant term is zero; for $\rho \leq \rho_c$ the Universe will expand forever, for $\rho > \rho_c$ the expansion will ultimately cease to be followed by recollapse.

It is convenient to recast equation (3) as

$$d(\ln\rho) + 3\left(1 + \frac{p}{\rho c^2}\right) d(\ln a) = 0 \qquad (3')$$

Notice that there are three functions of time (a, ρ,p) and two equations; an equation of state $p = p(\rho)$ is needed to close the system. Two simple equations of state will suffice.

For a noninteracting gas of nonrelativistic particles

$$p = nkT \; ; \quad \rho = mn \qquad \frac{p}{\rho c^2} = \frac{kT}{mc^2} << 1. \qquad (4)$$

It follows from (3') and (4) that: $\rho_{NR} \sim a^{-3}$.

For a noninteracting gas of relativistic particles

$$p = \frac{1}{3}\rho c^2 \quad ; \qquad \rho \sim T^4. \qquad (5)$$

It follows from (3') and (5) that $\rho_R \sim a^{-4}$ and $T \sim a^{-1}$.

Returning to (2') and (3'), for early times and high densities

$$\rho^{1/2} \sim H = \frac{1}{a}\left(\frac{da}{dt}\right) \sim \frac{1}{\rho}\left(\frac{d\rho}{dt}\right). \tag{6}$$

As advertised then, in the early Universe $\rho t^2 =$ constant. Furthermore, although the Universe is a mixture of nonrelativistic particles (e.g.: nucleons, galaxies, etc.) and relativistic particles (e.g.: photons, neutrinos, etc.), the early Universe is "Radiation Dominated". Sufficiently early on ($a \to 0$), $\rho_{NR} \ll \rho_R$ (since $\rho_{NR} \sim a^{-3}$ and $\rho_R \sim a^{-4}$) so that $\rho \approx \rho_R$. Then, since $t \sim \rho^{-1/2}$ and $\rho \sim T^4$,

$$t(T) = \frac{A}{T^2} \quad ; \quad A \approx 1 \text{ sec MeV}^2. \tag{7}$$

Turning from the expansion rate to the weak interaction rate, consider as a prototype the following neutral-current weak interaction: $e^- + e^+ \rightleftarrows \nu + \bar{\nu}$. In the early Universe, for $kT \gtrsim m_e c^2$, $e^\pm$ pairs are copiously produced and are as common as photons[14]: $n_e \sim n_\gamma \sim T^3$. Neglecting any energy dependence in the cross section (the conclusions are strengthened if $\sigma \sim E^2 \sim T^2$), the reaction rate is

$$\Lambda = \Lambda(T) = n_e \sigma v \sim T^3. \tag{8}$$

Comparing the reaction rate with the expansion rate

$$\Lambda(T)t(T) \sim T^3 \cdot T^{-2} \sim T, \tag{9}$$

shows that, sufficiently early on ($t \to 0$, $T \to \infty$), the weak interaction is "fast" ($\Lambda t \to \infty$) and neutrinos will have been in equilibrium.

In equilibrium at temperature T, the number density and mass density of massive neutrinos are

$$n_\nu(T;m_\nu) = n_\nu(z_\nu) = g_\nu \left(\frac{1}{2\pi^2}\right)\left(\frac{kT}{\hbar c}\right)^3 \int_0^\infty \frac{x^2 dx}{\exp[(x^2+z_\nu^2)^{1/2}]+1}, \tag{10}$$

$$\rho_\nu(T;m_\nu) = \rho_\nu(z_\nu) = g_\nu \left(\frac{1}{2\pi^2}\right)\left(\frac{kT}{\hbar c}\right)^3 \int_0^\infty \frac{(x^2+z_\nu^2)^{1/2} x^2 dx}{\exp[(x^2+z_\nu^2)^{1/2}]+1}. \tag{11}$$

In the above, $z_\nu = m_\nu c^2/kT$ and g_ν is the statistical weight (one for each helicity state; e.g.: for ν_e and $\bar{\nu}_e$, $g_\nu = 2$). For photons (massless bosons with $g_\gamma = 2$), analogous expressions yield

$$n_\gamma = \frac{2\zeta(3)}{\pi^2}\left(\frac{kT}{\hbar c}\right)^3 \approx 20T^3(\text{cm}^{-3}); \quad \rho_\gamma \approx 2.7\left(\frac{kT}{c^2}\right)n_\gamma . \tag{12}$$

It is convenient to compare neutrinos to photons. For massless neutrinos and/or low mass neutrinos in the high temperature limit ($m_\nu c^2 << kT; z_\nu << 1$)

$$\frac{n_\nu}{n_\gamma} = \frac{3}{8} g_\nu \quad ; \quad \frac{\rho_\nu}{\rho_\gamma} = \frac{7}{16} g_\nu . \tag{13}$$

In equilibrium, then, "light" neutrinos are as important as photons ($n_\nu \approx n_\gamma$; $\rho_\nu \approx \rho_\gamma$).

For massive neutrinos in the low temperature limit ($kT << m_\nu c^2$; $z_\nu >> 1$)

$$\frac{n_\nu}{n_\gamma} \approx 0.26\, g_\nu z_\nu^{3/2} e^{-z_\nu} \quad ; \quad \frac{\rho_\nu}{\rho_\gamma} \approx 0.10\, g_\nu z_\nu^{5/2} e^{-z_\nu} . \tag{14}$$

"Heavy" neutrinos are always rare ($n_\nu << n_\gamma$; $\rho_\nu << \rho_\gamma$). In collisions when the average available energy is small compared to the rest mass, few pairs are produced.

The cosmological role played by neutrinos depends on the numbers surviving the early stages. Neutrino survival depends on the details of the departure from equilibrium. Though the basic physics is the same, there are quantitative as well as qualitative differences in the survival of "heavy" ($m_\nu c^2 \gtrsim 1$ MeV) and "light" ($m_\nu c^2 \lesssim 1$ MeV) neutrinos.

For $z_\nu \lesssim 1$, neutrinos are as abundant as photons and, in this case, the reaction rate and expansion rate become comparable for $kT \approx$ 1-10 MeV. The considerations here apply, then, to neutrinos with $m_\nu c^2 \lesssim$ 1MeV. For later times (kT < 1 MeV; t > 1 sec) the Universe expands too rapidly for the neutrinos to remain in equilibrium. Subsequently, then, the neutrinos are decoupled, they are neither created nor annihilated. If not for one complication, the "frozen-out" ratio of neutrinos to photons would be that given by equation (13). The reason that the present ratio of relic neutrinos to photons differs from (13) is that for $kT \lesssim 1/2$ MeV, electron-positron pairs annihilate and the associated energy is thermalized. In the process of thermalization, "extra" relic photons are created; the neutrinos, recall, have decoupled and cannot share this energy. By considering entropy conservation, the ratio of "new" to "old" photons may be found (see, for example, ref. 14).

$$n_\gamma(\text{now}) = (\tfrac{11}{4})\, n_\gamma(\text{then}). \tag{15}$$

Thus, the present ratio of light ($m_\nu c^2 \lesssim 1$ MeV) neutrinos to photons is

$$\left(\frac{n_\nu}{n_\gamma}\right)_{\text{now}} = \frac{3}{22} g_\nu . \tag{16}$$

If $T_0 \approx 2.7$ °K then, $n_\gamma \approx 400$ cm^{-3} and the present mass density in light neutrinos is

$$\rho_\nu(\text{now}) \approx 1 \times 10^{-31} g_\nu m_{ev} \ (\text{gcm}^{-3}). \tag{17}$$

In contrast, "heavy" neutrinos ($m_\nu c^2 \gtrsim 1$ MeV) are not very abundant (for $z_\nu \lesssim 1$) and, since their density is low, they decouple earlier at a higher "freeze-out" temperature which depends on the neutrino mass (and, on the strength of the weak interaction). For masses in the range of a few GeV, Lee and Weinberg[4] and Discus et al[5] find: $kT_f \approx m_\nu c^2/20$. The present ratio of heavy neutrinos (plus antineutrinos) to photons is found to be[4]

$$\left(\frac{n_\nu}{n_\gamma}\right)_{\text{now}} \approx 2 \times 10^{-7} m_{\text{GeV}}^{-3}. \tag{18}$$

The present mass density in heavy neutrinos is

$$\rho_\nu(\text{now}) \approx 8 \times 10^{-29} m_{\text{GeV}}^{-2} \ (\text{gcm}^{-3}) \tag{19}$$

Although rare compared to their light counterparts, heavy neutrinos may, nevertheless, dominate the present mass density.

LIMITS TO THE NEUTRINO MASS

The present total mass density may receive a significant contribution from massive relic photons. Limits, then, to the total density will constrain the mass of such neutrinos.[2),4),5)]

As a benchmark, consider the present critical density

$$\rho_{co} = \frac{3H_o^2}{8\pi G} \approx 2 \times 10^{-29} h_o^2 \ (\text{gcm}^{-3}) \tag{20}$$

The dimensionless density parameter $\Omega_o = \rho_o/\rho_{co}$ separates those models which expand forever ($\Omega_o \leq 1$) from those which will ultimately recollapse ($\Omega_o > 1$). To assess the importance of relic neutrinos, define $\Omega_\nu = \rho_\nu/\rho_{co}$. Then, for light neutrinos

$$g_\nu m_\nu \approx 200(\Omega_\nu h_o^2) \ ; \quad m_\nu c^2 \lesssim 1 \text{ MeV}. \tag{21}$$

In (21), m_ν is in eV and $g_\nu m_\nu$ is summed over all neutrino flavors. For heavy neutrinos

$$m_{\text{GeV}} \approx 2(\Omega_\nu h_o^2)^{-1/2} \ ; \quad m_\nu c^2 \gtrsim 1 \text{ MeV}. \tag{22}$$

Since $\Omega_\nu < \Omega_o$, upper limits to Ω_o provide constraints to Ω_ν and, through

equations (21) and (22), to m_ν. The absence of observable deceleration in the expansion of the Universe suggests that $\rho_o \lesssim 2 \times 10^{-29} gcm^{-3}$ ($\Omega_o h_o^2 \lesssim 1$). The neutrino mass is restricted thereby to

$$\begin{aligned} &\text{Light neutrinos:} && g_\nu m_\nu \lesssim 200 \text{ eV}, \\ &\text{Heavy neutrinos:} && m_\nu \gtrsim 2 \text{ GeV}. \end{aligned} \tag{23}$$

It has been assumed in this analysis that massive neutrinos are stable[4]. If, however, the neutrino decays in a time short compared to the present age of the Universe ($t_o \approx 1\text{-}2 \times 10^{10}$yr.), the restrictions on the neutrino mass are inapplicable.[5),7)] The cosmological consequences of unstable neutrinos have been studied by Dicus et al[5)] and by Gunn et al[7)] who relate the limiting masses to the assumed lifetime; the interested reader is encouraged to consult those references for specific results.

Neutrino degeneracy is another complication which has been swept under the rug in the foregoing analysis. The choice of a vanishing chemical potential in equation (10) guaranteed equal numbers of neutrinos and anti-neutrinos. It is not known, however, whether or not the Universe is symmetric between neutrinos and antineutrinos. In contrast, it is well known that the Universe is not baryon symmetric.[14)] Although, by analogy, neutrino asymmetry is not unreasonable, such an asymmetry would have associated with it an arbitrary free parameter for each neutrino flavor. For simplicity, the "standard" assumption is to choose zero for those parameters (equal numbers of neutrinos and antineutrinos); any other choice complicates the connection between particle physics and cosmology. If, however, there were a degenerate sea of relic, massive, stable neutrinos then, the limits to the mass would be even more restrictive than those given in (23).

A related question concerns the present momentum space distribution of the relic neutrinos; is it that of a degenerate Fermi gas? The answer is no for the following reason. The neutrino distribution in phase space was established early on when the neutrinos were hot; a Maxwellian distribution was set up. Afterwards, the neutrinos decouple and, as a collisionless gas, their distribution evolves remaining nondegenerate.

There is no observationally determined lower limit to the present mass density in neutrinos. Truly massless neutrinos play a negligible dynamical role at present ($\rho_\nu \approx \rho_\gamma \ll \rho_o$). For the nucleon contribution to the total density, it seems likely[15)] that: $\Omega_N h_o^2 \gtrsim 0.01$; $\rho_N \gtrsim 2 \times 10^{-31}$ gcm^{-3}. If neutrinos are to be dynamically important at present (there is no evidence which compells this assumption) then $\rho_\nu \gtrsim \rho_N$ which leads to the

restrictions

$$\begin{aligned} &\text{Light neutrinos:} \quad g_\nu m_\nu \gtrsim 10 \text{ eV} \\ &\text{Heavy neutrinos:} \quad m_\nu \lesssim 20 \text{ GeV}. \end{aligned} \tag{24}$$

To play a dynamically interesting role at present, massive, stable, relic neutrinos must have masses in either of the two narrow ranges: $10 \lesssim g_\nu m_\nu \lesssim 200$ eV, $2 \lesssim m_\nu \lesssim 20$ GeV.

PRIMORDIAL NUCLEOSYNTHESIS

During the early, radiation dominated epochs, light neutrinos contribute significantly to the total density ($\rho_\nu \gtrsim \rho_\gamma$). The quantitative effects of such neutrinos on the early evolution depend on the number of lepton flavors through the neutrino multiplicity g_ν (for 2-component neutrinos, $g_\nu = 2$ for each lepton flavor). The impact of these neutrinos is greatest on the abundances of the light nuclei produced in primordial nucleosynthesis 3),6),10)

To better appreciate the influence of "new" neutrinos, it will be of value to briefly review the basics of primordial nucleosynthesis in the "standard" model in which only e- and μ-neutrinos are considered ($g_\nu = 4$). For details, the reader is referred to the review article by Schramm and Wagoner[16].

Photons, electrons and neutrinos are in equilibrium ($T_\gamma = T_e = T_\nu$) for $kT \gtrsim 1$ MeV. The neutron-to-proton ratio is maintained at its equilibrium value

$$\frac{n}{p} = \exp\left(\frac{-\Delta Mc^2}{kT}\right) \tag{25}$$

by the reactions

$$p + e^- \rightleftarrows n + \nu_e, \quad p + \bar{\nu}_e \rightleftarrows n + e^+, \quad n \rightleftarrows p + e^- + \bar{\nu}_e. \tag{26}$$

For $kT \lesssim 1$ MeV, the reactions (26) can no longer maintain equilibrium and the neutron-to-proton ratio "freezes-out" at a value $n/p \approx 0.22$ corresponding to a neutron abundance by mass: $X_n = n(n + p)^{-1} \approx 0.18$.

All the while, neutrons and protons have been colliding and, occasionally, forming deuterons which are quickly photodissociated ($n + p \rightleftarrows D + \gamma$). The deuterium abundance is kept low for $kT \gtrsim 0.2$ MeV by the presence of large numbers of photons capable of destroying the deuteron. As a result, there is a bottleneck to the buildup of heavier nuclei. Only

Consider, now, the effect of "new" neutrinos (e.g.: the neutrino accompanying the τ-lepton; see Perl, this conference). The density differs from that in (28) due to the extra neutrinos.

$$\rho \to \rho' = \xi^2 \rho \; ; \quad \xi^2 = 1 + \frac{7}{72} \Delta g_\nu \; ; \quad g_\nu = 4 + \Delta g_\nu \; . \qquad (29)$$

The expansion rate changes in the sense that the age versus temperature relation is changed from t(T) to t'(T) where

$$\frac{t'(T)}{t(T)} = [\frac{\rho(t)}{\rho'(t)}]^{1/2} = \xi^{-1}. \qquad (30)$$

The speed-up in the expansion rate (t'(T) < t(T)) leads to an earlier freeze-out at a higher temperature ($T_f' > T_f$) and, therefore, to a larger neutron-to-proton ratio.[3),10)]

$$\frac{n}{p} \to \frac{n'}{p'} \gtrsim \exp\,[-\xi^{1/3}\,(\frac{\Delta Mc^2}{kT_f})] > \frac{n}{p} \; . \qquad (31)$$

A higher helium abundance results from enhanced neutron survival. The helium abundance by mass (Y) depends strongly on Δg_ν and weakly on the nucleon density ($\rho_N \gtrsim 2 \times 10^{-29}\ \Omega_N h_o^2\ \mathrm{gcm}^{-3}$). The detailed calculations of Yang et al[10)] may be fit by the relatively simple formula

$$Y = (0.276 + 0.005\Delta g_\nu) + (0.020 - 10^{-4}\ \Delta g_\nu)\ \log\ (\Omega_N h_o^2). \qquad (32)$$

For two component neutrinos, the number of neutrino flavors is: $N_\nu = g_\nu/2 = 2 + \Delta g_\nu/2$. In Table 1 (following Yang et al[10)]) the minimum abundance of primordial ^{4}He is presented for several values of $\Omega_N h_o^2$ and N_ν. The present cosmic abundance of helium is $Y \gtrsim 0.29$ but, there is strong evidence (reviewed by Yang et al[10)]) that the primordial abundance was $Y \lesssim 0.25$.

Several interesting conclusions may be drawn from the data in Table 1.

(i) If, indeed, $Y \lesssim 0.25$ then, the Universe is open and will expand forever ($\Omega_N h_o^2 \lesssim 0.1$; $\Omega_N \lesssim 0.4$). The e-, μ- and τ-leptons may be the only leptons ($N_\nu \lesssim 3$).

(ii) Even for the more conservative limit $Y \lesssim 0.29$, the number of lepton flavors is limited to $N_\nu \lesssim 7$ since $\Omega_N h_o^2 \gtrsim 10^{-2}$.

for kT $\lesssim$ 0.1 MeV will photodissociation become unimportant permitting an increase in the deuterium abundance. The formation of the other light nuclei can then proceed via reactions such as

$$p + n \rightarrow D + \gamma, \text{ ---}, \quad D + D \rightarrow {}^4He + \gamma, \text{ ---}. \tag{27}$$

The gap at mass-5 where there is no stable nucleus provides a bottleneck to the formation of heavier nuclei. As a result, virtually all the neutrons present at freeze-out are incorporated into ^{4}He nuclei. As the Universe expands and the temperature and density decrease, further nuclear reactions are rapidly suppressed by the low density and high coulomb barrier. The gap at mass-5 cannot be bridged and most of the action is over by t $\lesssim 10^3$ sec.

With the exception of ^{4}He, the abundances of the light nuclei are determined by the competition between the expansion rate ($\sim t^{-1}$) and the two-body reaction rates ($\sim n$). The abundances of nuclei such as D and ^{3}He, therefore, are very sensitive to the nucleon density at the time of nucleosynthesis. The higher the density the fewer D and ^{3}He survive and the more ^{4}He produced. In contrast, since virtually all neutrons available at freeze-out are incorporated into ^{4}He, the helium abundance is only weakly dependent on two-body reaction rates (and, hence, on the nucleon density) and is most strongly a function of the frozen-out neutron-to-proton ratio.

Observations, then, of the D-abundance constrain the nucleon density (since nucleons are conserved, the present nucleon density may be related to the nucleon density at the time of nucleosynthesis). In contrast, since the ^{4}He abundance is relatively independent of ρ_N, observations of ^{4}He can provide useful constraints on the physics of the early Universe. The point is that the ^{4}He abundance constrains the neutron abundance at freeze-out which, in turn, depends on the competition between the weak interaction reaction rates (known from beta decay; see equation (26)) and the expansion rate. During the radiation dominated era, the expansion rate depends on the number of different relativistic particles present (e.g.: the number of light neutrinos). The helium abundance, then, constrains the frozen-out neutron abundance which constrains the expansion rate which depends on the number of neutrino flavors.[3),10)]

With only e- and μ-neutrinos ($g_\nu = 4$), the total density at early times is

$$\rho = \rho_\gamma + \rho_e + \rho_{\nu e} + \rho_{\nu \mu} = 4.5\, \rho_\gamma. \tag{28}$$

Table 1: The minimum ^{4}He abundance as a function of the present nucleon density ($\rho_N = 2 \times 10^{-29}\ \Omega_N h_o^2$) and the number of neutrino flavors ($N_\nu \equiv 2 + \Delta g_\nu/2$).

$\log(\Omega_N h_o^2)$	Δg_ν	N_ν	Y_{MIN}
-2	0	2	0.24
	2	3	0.25
	4	4	0.26
	6	5	0.27
	8	6	0.28
	10	7	0.29
-1	0	2	0.26
	2	3	0.27
	4	4	0.28
	6	5	0.29
0	0	2	0.28
	2	3	0.29

FURTHER ASTROPHYSICAL CONSEQUENCES

It has not been the purpose of this lecture to present a complete survey of neutrino astrophysics. Two of the most important consequences of the symbiotic relationship between weak interaction physics and cosmology have been considered in some detail and limits were derived to the mass of stable neutrinos and to the number of neutrino flavors. In this concluding section, brief mention is made of some of the other interesting results which have emerged in this active field of research.

The dynamical consequences of a background of stable massive neutinos have been studied by Gunn et al[7] and by Steigman et al.[9] If heavy neutrinos dominate the universal mass density at present, they may contribute to the so-called "missing mass". Such neutrinos would participate in those stages of collapse of galaxies and clusters of galaxies which are dissipationless. Since, however, such neutrinos constitute a noninteracting (except for gravity) gas, they are left behind during any fragmentation and collapse involving dissipation (the neutrinos are unable to radiate away or transfer to other components their internal energy). This inflated gas of heavy neutrinos may, therefore, form halos around galaxies and may dominate the mass in clusters of galaxies. If our own Galaxy is surrounded by a halo of heavy $\nu\bar{\nu}$ pairs, occasional annihilation may produce

an observable flux of gamma rays.[7),8)]

It is fortunate that in the dissipative collapse of gas clouds to form stars, heavy neutrinos are left behind.[9)] The reason is that neutrinos could transport energy so efficiently that stellar structure and evolution would be altered by the presence of a neutrino component some ten orders of magnitude smaller than the nucleon component.[9)]

Finally, it is interesting to note the important work of Dicus et al[5)] on the consequences of unstable neutrinos (see, also, Gunn et al[7)]). If neutrino decay results in photons then the mass and lifetime are restricted to: $m_\nu \lesssim 10$ keV; $T_\nu \lesssim 1$ year. Weaker constraints apply if the heavy neutrino decay channels produce no photons.

REFERENCES

1) Zeldovich, Ya.B. (1970), Comm. Ap. & Sp. Phys. 2, 12.
2) Cowsik, R. and McClelland, J. (1972), Phys.Rev. Lett. 29, 669.
3) Steigman, G., Schramm, D.N., and Gunn, J.E. (1977), Phys.Lett. 66B,202.
4) Lee, B.W. and Weinberg, S. (1977), Phys.Rev. Lett. 39, 165.
5) Dicus, D.A., Kolb, E.N. and Teplitz, V.L. (1977), Phys.Rev. Lett. 39,168.
6) Hut, P. (1977), Phys. Lett. 69B, 85.
7) Gunn, J.E., Lee, B.W., Lerche, I., Schramm, D.N. and Steigman, G. (1978) Ap.J. (In Press).
8) Stecker, F.W. (1978), Ap.J. (In Press).
9) Steigman, G., Sarazin, C., Quintana, H. and Faulkner, J. (1978), AJ (submitted).
10) Yang, J., Schramm, D.N., Steigman, G. and Rood, R.T. (1978) In Preparation
11) Steigman, G. (1978), Proceedings of the Ben Lee Memorial Conference (D. Cline, ed.; In Press).
12) Steigman, G. (1979), Ann. Rev. Nucl. Sci. 29, In Preparation.
13) Weinberg, S. (1972), Gravitation and Cosmology (New York: Wiley Interscience).
14) Steigman, G. (1973), Cargese Lect. Phys. 6, 505.
15) Gott, J.R., Gunn, J.E., Schramm, D.N. and Tinsley, B.M. (1974) Ap.J. 194, 543.
16) Schramm, D.N. and Wagoner, R.V. (1977), Ann. Rev. Nucl. Sci. 27, 37(1977).

DEEP INELASTIC PROCESSES IN QUANTUM CHROMODYNAMICS

G. ALTARELLI
Istituto di Fisica - Università di Roma
Istituto Nazionale di Fisica Nucleare
Sezione di Roma.

Abstract :

An introduction is presented to the results of QCD concerning deep inelastic processes. We consider the predictions for the scaling violations, the longitudinal cross section and the transverse momentum of jets in leptoproduction. We also review the status of the Drell-Yan formula in QCD and the analysis of the transverse momentum distributions in lepton pair production from hadronic collisions.

1. INTRODUCTION

The quark parton model[1] provides us with a very useful and simple description of the physics of deep inelastic phenomena. On the other hand non abelian gauge theories are unique among renormalisable field theories to predict approximate Bjorken scaling. Thus the modern foundation for the parton model is the gauge theory of strong interactions based on the color degrees of freedom (Quantum Chromodynamics : QCD[2]). Indeed in QCD scaling is predicted to be broken by logarithms (a fact well consistent with present experiments), and these deviations from scaling are computable. The results can again be phrased in the parton language, by assigning a specified Q^2 dependence to the parton densities. Thus although the naive parton model, strictly speaking, fails in QCD, a suitably modified parton language remains the most effective and physically transparent way of phrasing the content of the theory.

The first part of the present lectures is devoted to a euristhic but quantitative derivation of the QCD predictions for scaling violations in leptoproduction in terms of parton concepts. For this part, I shall closely follow my lectures in the last of ref. 5 that the reader may find useful for further details and applications.

The standard approach to this problem[2] is somewhat more abstract and formal being founded on renormalization groups equations applied to the coefficient functions of the local operators which appear in the light cone expansion of the product of the two currents. Although less rigorous and general the method I shall follow here is more transparent and has the further advantage that it can provide useful insights to problems that cannot be solved by the operator method.

In the second part of these lectures I shall deal with some of the most recent developments in the direction of enlarging the set of predictions of QCD for deep inelastic processes. Precisely I shall consider the transverse momentum distributions of jets in leptoproduction, and the effect of gluon corrections to Drell-Yan processes.

2. BASIC VERTICES OF QCD

QCD[2] is a gauge theory, with gauge group SU(3) color (unbroken) of colored quarks and gluons. There are eight colored (spin one) gluons,

the gauge fields, one for each generator of SU(3) color (they transform as the regular representation $\underline{8}$). There are f flavors (p, n, λ, p'...) of quarks (the matter fields). For each flavor we have a triplet of colored quarks, belonging to a $\underline{3}$ of SU(3) color, and of course the antiquarks belong to $\overline{\underline{3}}$.

All vertices in the theory are specified in terms of a single coupling constant. The quark-gluon vertex is given by :

$$g\ \bar{q}_i \gamma^\mu \lambda^a\ q_i A^a_\mu \qquad (1)$$

where A^a_μ is the gluon field and sums over a and i are understood a = 1, ...,8 is the color index of gluons ; i = 1,...f is the flavor index for quarks , q is the quark field, λ^a are SU(3) color matrices with the normalization :

$$Tr(\lambda^a \lambda^b) = \frac{1}{2}\,\delta^{ab} \qquad (2)$$

They obey the commutation relations :

$$[\lambda^a, \lambda^b] = i\, f^{abc}\, \lambda c \qquad (3)$$

with f^{abc} the structure constants of SU(3) color.

In analogy with electrodynamics (QED) we define :

$$\alpha_s \equiv g^2/4\pi \qquad (4)$$

and the true expansion parameter of perturbation theory is α_s/π.

The quark gluon vertex, but for the λ matrices of color, is completely analogous to the QED vertex. However, in QCD we also have three gluon and four gluon vertices, typical of non abelian gauge theories. The difference is that in QED the photon is coupled to all charged particles while it does not carry charge. In QCD the gluons couple to all colored particles but they also carry color and therefore are self coupled. The three gluon vertex, of order g, is linear in the structure constants f^{abc}, which shows its relation to the commutator. On the other hand the four gluon vertex is of order g^2 and bilinear in the structure constants.

3. THE NAIVE PARTON MODEL AND QCD

In this section I shall review the physical content of the naive parton model and make clear why it fails in QCD and how it must be modified in this theory.

Consider the total cross section of a virtual photon of mass $-Q^2$ on a proton target. Since the virtual photon is spacelike we can choose a reference frame where its four momentum has the simple form :

$$q \equiv (0 ; -Q, \vec{0}) \tag{5}$$

The first entry is the energy, the second the z component of the three momentum, the third the bidimensional vector of transverse momentum. The proton four momentum can be parametrized as follows :

$$P \equiv (\frac{Q}{2X} ; \frac{Q}{2X} , \vec{0}) \tag{6}$$

where Q is assumed large enough that the proton mass M can be neglected. Note that :

$$(P.q) \equiv M\nu = \frac{Q^2}{2X} \tag{7}$$

Therefore X in eq. (6) is the familiar scaling variable :

$$X = \frac{Q^2}{2M\nu} \quad (0 \leqslant X \leqslant 1) \tag{8}$$

We now summarize the assumptions in the naive parton model. The naive parton model contains two crucial steps in its derivation that require for their validity a high degree of convergence in the underlying theory.

First the dominant contributions in the limit $Q^2 >> M^2$, X fixed, are identified with the class of diagrams in fig. 1. What is special about this class of diagrams is that no interaction takes place between the final parton k' and the lower blob. In the light cone language it corresponds to picking up the operators of minimum twist, i.e. those with most singular coefficients. In a sufficiently regular theory all other terms are suppressed by integral powers of m^2/Q^2, where m^2 is some typical mass.

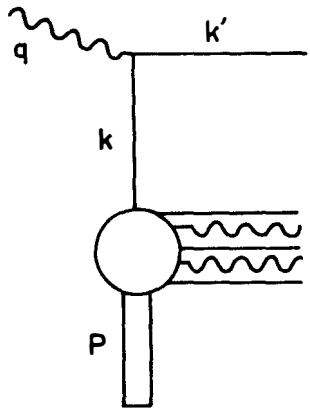

FIG.1

As a second step one focus on the intermediate virtual parton K. We assume the rest mass of K as negligible. Then its four momentum has the general form :

$$K = (E_K \; ; \; K_Z, \vec{P}_\perp) \; , \; E_K = \sqrt{K_Z^2 + P_\perp^2 + K^2} \qquad (9)$$

where K^2 is the virtual mass of the off-mass shell parton. K_Z is a given fraction y of the proton longitudinal momentum (see eq. (6)) :

$$K_Z = y \frac{Q}{2X} \qquad (10)$$

In the naive parton model one assumes the distributions of virtual masses and transverse moments for partons inside the proton to be enough damped that terms of order K^2/Q^2 and/or $p_\perp^2/Q^2$ can be safely neglected, i.e. they lead to corrections of order m^2/Q^2 after integration over the final state. When K^2 and $p_\perp^2$ can be neglected K acts as a real on mass shell quark and its momentum is proportional to the proton momentum :

$$K \simeq (\frac{y}{X}\frac{Q}{2} \; ; \; \frac{y}{X}\frac{Q}{2}, \vec{0}) \qquad (11)$$

Being K quasi real the diagram factorizes into two parts (before integrating over y). One factor is a function of y,q(y) which depends on

the lower blob in Fig. 1 and describes the probability of finding inside the proton that kind of parton with a fraction y of the proton momentum. The second factor is proportional to the point like total cross section for the scattering of the parton on the virtual photon and corresponds to the upper part of the diagram in Fig. 1. For the structure functions one thus obtains :

$$2\,F_1(X) \simeq F_2(X)/X \simeq \int \frac{dy}{y}\, q(y)\, \sigma_{point}\,(K+q) \qquad (12)$$

Moreover σ_{point} is proportional to a δ-function. This is because $(K+q)^2$ must be equal to the squared rest mass of the final parton. Taking this rest mass as negligible, we have :

$$(K+q)^2 = -Q^2\left(1-\frac{y}{X}\right) = 0 \qquad (13)$$

This means that only partons with a fraction X of momentum can interact with the photon in the reference frame of eq. (5). Taking all factors into account we get :

$$\sigma_{point}\,(K+q) = e^2\,\delta\left(\frac{y}{X}-1\right) \qquad (14)$$

where e is the parton charge (in units of the proton charge). We thus obtain from eq. (12) :

$$2\,F_1(X) \simeq F_2(X)/X = \int \frac{dy}{y}\, q(y)\, e^2\delta\left(\frac{y}{X}-1\right) = e^2\, q(X) \qquad (15)$$

which is the well-known result (we are dropping for simplicity the sum over all kinds of possible partons).

We now consider the parton model in the context of QCD.

About the dominance of diagrams in Fig. 1 in QCD one observation is crucial. The struck quark carries color and the same is true for the state emerging from the lower blob. But colored states are confined through a mechanism that we do not know precisely. Therefore some kind of final state interaction is indeed necessary to reshuffle the quantum numbers of the quark jet and of the proton fragmentation jet. Lacking a theory of confinement we must assume that this process of color neutralisation (presumably a long wavelenght phenomenon) does not alter the structure of singularities on the light cone.

The next question is whether QCD does indeed provide enough convergence in K^2 and $p_\perp^2$ to allow the neglect of terms of order $p_\perp^2/Q^2$ and K^2/Q^2. We cannot directly compute the $p_\perp$ distribution of quarks and gluons inside the proton because this task is beyond perturbation theory. But we can make a simple consistency check on the parton model assumptions. Consider the diagram in Fig. 2.

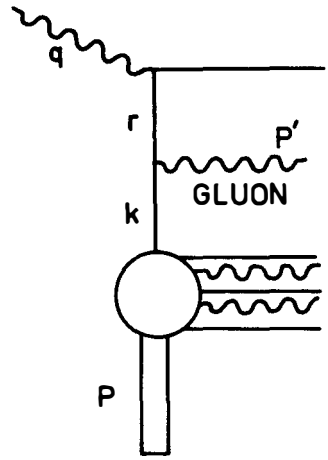

FIG. 2

This contribution is a particular case of Fig. 1 with a gluon being extracted from the blob and analyzed separately. We can compute this diagram assuming an initial parton k with negligible $p_\perp$ and check whether the parton r that interacts with the photon has a $p_\perp$ distribution sufficiently damped. More in general we can go back to eq. (12) and add to σ_{point}, which is of order zero in α_s, the next order contribution

$\sigma_{\text{order } \alpha_s}$ computed from all possible diagrams for γ + parton → all of which Fig. 2 is an example (we shall later list these diagrams). If the parton model works, these corrections should only add terms that are either non leading (i.e. of order m^2/Q^2) or that can be recast in the form of eq. (15). We therefore consider the modified equation :

$$2F_1 \simeq F_2/X \simeq \int \frac{dy}{y} q(y)\left[e^2\delta(\frac{y}{X} - 1) + \sigma_{\text{order } \alpha_s}(\frac{X}{y}, Q^2)\right] \quad (16)$$

As indicated $\sigma_{\text{order } \alpha_s}$ is a function of $\frac{X}{y}$ and in general of Q^2. In fact the total parton - γ cross section can only depend on the photon mass $-Q^2$ and the total center of mass energy squared $(k + q)^2 = -Q^2(1 - \frac{y}{X})$. We do not need at this stage the explicit form for $\sigma_{\text{order } \alpha_s}$. The essential point is that in QCD $\sigma_{\text{order } \alpha_s}$ has the following form.

$$\sigma_{\text{order } \alpha_s}(\frac{X}{y},Q^2) = \frac{\alpha_s}{2\pi} e^2 \left[t\, P(\frac{X}{y}) + f(\frac{X}{y}) + O(1/Q^2)\right] \quad (17)$$

with

$$t \equiv \ln Q^2/\mu^2 \quad (18)$$

where μ^2 is a convenient but arbitrary normalization mass.

The function P(X/y) is uniquely defined as the coefficient of $\ln Q^2$, while the definition of the scaling term f(X/y) depends on μ^2. Changing μ^2 into μ'^2 adds to f a term $\ln\mu'^2/\mu^2 P$. Note that terms of order $1/Q^2$ can be directly dropped, being of the same order as the already neglected non leading singularities on the light cone. Finally the factors of α_s and e^2 are obvious while $1/2\pi$ is inserted for convenience. Clearly the essential feature of eq. (17) for $\sigma_{\text{order } \alpha_s}$ is the presence of the factor of t. This term violates scaling and indicates the failure of the naive parton model in QCD. We can easily reconstruct its origin. It is the same as the term proportional to $\ln E/m_e$ in the total cross section for Compton scattering in QED, that one finds in books. For example consider the upper part of the diagram in Fig. 2. Let us parametrize the momenta of the initial quark and of the final gluon in the form (see eq. (11)) :

$$\begin{aligned} k &= (P\ ;\ P, \vec{0}) \quad (P = \frac{y}{X}\ \frac{Q}{2}) \\ p' &= (ZP + \frac{P_\perp^2}{2ZP}\ ;\ ZP\ ,\ -P_\perp) \end{aligned} \quad (19)$$

Note that by momentum conservation at the gluon vertex, $P_\perp$ is the transverse momentum of the virtual quark r. Also, the energy of p' has been expanded up to the first order term in $P_\perp^2/P^2$ which is sufficient for our discussion. We can compute the virtual square mass of the intermediate quark r :

$$r^2 \simeq (k - p')^2 = -2(Kp') = - P_\perp^2/Z \qquad (20)$$

The virtual mass and the $P_\perp^2$ distributions are thus related for the quark r. When the absolute value squared of the amplitude is taken, a factor $1/(r^2)^2$ arises from the propagator of the virtual quark (of negligible rest mass). By eq. (21) this is a factor of $1/(P_\perp^2)^2$. However this singularity in $P_\perp^2$ is partially removed in that the numerator vanishes as $P_\perp^2$. This is because helicity conservation at the lower vertex forbids the forward emission of the gluon. In fact the quark gluon vertex is of vector nature. It is a simple property of this coupling that a fast fermion conserves its helicity while emitting a gluon (or a photon) when terms of order m^2/P^2 are neglected. In the forward direction helicity and spin components in the Z direction coincide and the spin component (helicity) of the forward emitted gluon should be zero, which is impossible for a massless vector particle. Thus the total singularity in $P_\perp^2$ of the diagram is reduced to $1/P_\perp^2$. On the other hand the upper limit of the integration over $dP_\perp^2$ is of order Q^2, being Q^2 the order of the total energy squared in the center of mass. The effect of the upper limit is thus to induce a log. Q^2 dependence of the integral :

$$\sigma_{\text{order } \alpha_s} \sim \int^{\sim Q^2} \frac{dP_\perp^2}{P_\perp^2} = \ell n\, Q^2 + \ldots \qquad (21)$$

Note that the divergence at the lower limit of integration can be cured by restoring the physical mass for the quark, or by working with off mass shell quarks of zero rest mass (indeed the quark inside the nucleon is a virtual particle). All of these complicacies can be lumped inside f(X/y) by introducing the normalization mass μ^2 that appears in eq. (18). Thus while the function P(z) in eq. (18) is well defined even in the massless theory, the function f(z) depends on the regularisation of the infrared singularities of the massless theory. Since the precise regularization mechanism has to do with the nucleon wave function we shall always limit to properties of f(z) that are independent on that. For the moment we concentrate on the terms in log Q^2.

The moral of this discussion , which of course can be fully demonstrated by a totally explicit calculation, is that the $P_\perp^2$ distribution of the quark r is not sufficiently damped to suppress the effect of the upper limit of the $P_\perp^2$ integration which is of order Q^2. For the naive parton model to work a decrease in $P_\perp^2$ faster than $1/P_\perp^2$ is necessary and this is not the case in QCD.

How to cure this problem ? Let's start by trying to absorb the anomalous term into a modified parton density. We rewrite eq. (16) in more explicit form :

$$2\,F_1(X) \simeq \int_X^1 \frac{dy}{y}\left[e^2\,\delta\left(\frac{y}{X}-1\right) + \frac{\alpha_s}{2\pi}\,e^2.t.P\left(\frac{X}{y}\right) + \ldots\right] \qquad (22)$$

Note that the lower limit of integration is set equal to X. This is because in general $(k^+ + q)^2 \gtrsim 0$ (see eq. (13)). Precisely it is larger than zero when the final state is not simply a quark, but there is also a gluon.

We want to cast eq. (22) into the form

$$\begin{aligned} 2\,F_1(X) &\simeq \int_X^1 \frac{dy}{y} q(y)\,e^2\left[\delta\left(\frac{y}{X}-1\right) + \frac{\alpha_s}{2\pi}\,t\,P\left(\frac{X}{y}\right) + \ldots\right] \\ &= \int_X^1 \frac{dy}{y}\left[q(y) + \Delta q(y,t)\right] e^2\,\delta\left(\frac{y}{X}-1\right) \\ &= e^2\left[q(X) + \Delta q(X,t)\right] \end{aligned} \qquad (23)$$

This is certainly possible provided that :

$$\Delta q(X,t) = \frac{\alpha_s}{2\pi}\,t\int_X^1 \frac{dy}{y}\,q(y)\,P\left(\frac{X}{y}\right) + \ldots \qquad (24)$$

where the dots stand for the neglected terms with no factor of t in eq. (17). We see that lowest order perturbation theory suggests to replace the density of partons inside the proton by an effective density as seen by the photon which depends on t :

$$q(X) \longrightarrow q(X,t) \qquad (25)$$

We understand the t dependence as due to the fact that a photon with larger Q^2 explores a wider range of $P_\perp^2$ inside the proton. Furthermore the variation of q(X,t) for an increase dt, which is due to probing a new infinitesimal interval of $P_\perp^2$ is given by :

$$\frac{dq(X,t)}{dt} = \frac{\alpha_s}{2\pi} \int_X^1 \frac{dy}{y} q(y,t) P(\frac{X}{y}) \tag{26}$$

Note that this equation is insensitive to $f(\frac{X}{y})$ in eq. (17) and is exact up to terms of order α_s^2 . Eq. (26) with suitable generalizations will play a central role in what follows. An equation of this type for the densities is in fact the end result of the more conventional approach and was originally derived in ref. (3).

An important property of the integro-differential eq. (26) is that it implies a simple differential equation for the moments of the densities. Defining the moments as :

$$M_n(t) \equiv \int_0^1 dX\, X^{n-1} q(X,t) \tag{27}$$

We can multiply both sides of eq. (26) by x^{n-1} and integrate from zero to one :

$$\frac{d}{dt} M_n(t) = \frac{\alpha_s}{2\pi} \int_0^1 dX\, X^{n-1} \int_X^1 \frac{dy}{y} q(y,t) P(\frac{X}{y})$$

By inverting the order of integration on the right hand side, we obtain :

$$\frac{dM_n(t)}{dt} = \frac{\alpha_s}{2\pi} \int_0^1 \frac{dy}{y} q(y,t) \int_0^y dX\, X^{n-1} P(\frac{X}{y})$$

By the change of the variable Z = X/y in the second integral we get :

$$\frac{dM_n(t)}{dt} = \frac{\alpha_s}{2\pi} \int_0^1 dy\, y^{n-1} q(y,t) \int_0^1 dZ\, Z^{n-1} P(Z)$$

Recalling the definition of moments in eq. (27) we finally obtain

$$\frac{dM_n(t)}{dt} = \frac{\alpha_s}{2\pi} A_n M_n(t) \tag{28}$$

where

$$A_n \equiv \int_0^1 dZ\, Z^{n-1} P(Z) \tag{29}$$

We thus see that the moments satisfy a simpler differential equation. For each n a constant A_n appears and the function P(Z) is the generating function for the entire set of A_n. As we shall see this is the origin of the known result that the predictions of QCD on scaling violations are much simpler for moments.

4. IMPROVING PERTURBATION THEORY

The reader may wonder at this stage why I am so much interested in results, like eqs. (26, 28) which are only true in first order perturbation theory. Even for α_s small, terms of order $\alpha_s^2 t$ for large enough t become eventually larger than terms of order α_s. Thus lowest order perturbation theory cannot be directly relevant. The reason is that eqs. (26,28, 29) become exact asymptotic results by the simple replacement of α_s with $\alpha_s(t)$, i.e. the running coupling constant of QCD. $\alpha_s(t)$ is the effective coupling constant for any quantity that obeys the renormalization group equations for the massless theory. In turn the massless theory is the relevant asymptotic limit of the actual theory in the deep Euclidean region[4].

The precise definition of $\alpha_s(t)$ is given by :

$$t = \int_{\alpha_s}^{\alpha_s(t)} \frac{d\alpha'}{\beta(\alpha')} \qquad (t = \ln Q^2/\mu^2) \tag{30}$$

where the function $\beta(\alpha)$ is computable in perturbation theory :

$$\beta(\alpha) \simeq - b\alpha^2 \left(1 + O\left(\frac{\alpha}{\pi}\right)\right) \tag{31}$$

and

$$b = \frac{33 - 2f}{12\pi} \tag{32}$$

The negative sign in front of b is crucial and implies that the theory is asymptotically free. In fact from eq. (30) it follows that :

$$\frac{d\alpha_s(t)}{dt} = \beta\left[\alpha_s(t)\right]$$

For $\alpha_s(t)$ small enough β is negative by eq. (31) and so is the derivative. Then increasing t makes $\alpha_s(t)$ still smaller. Note that the lower limit α_s in the integral eq.(30) is the value of $\alpha_s(t)$ for $t = 0$ i.e. at $Q^2 = \mu^2$. By choosing μ^2 large enough so that α_s/π is small, we can explicitly perform the integration in eq. (30) and obtain :

$$t \simeq \int_{\alpha_s}^{\alpha_s(t)} \frac{d\alpha}{-b\alpha^2} = \frac{1}{b} \left(\frac{1}{\alpha_s(t)} - \frac{1}{\alpha_s} \right)$$

and therefore

$$\alpha_s(t) \simeq \frac{\alpha_s}{1 + b\alpha_s t} \tag{32}$$

We thus see that $\alpha_s(t)$ decreases asymptotically as $1/t$.

An alternative form for $\alpha_s(t)$ which is much used in the literature is the following :

$$\alpha_s(t) = \frac{1}{b \ln Q^2/\Lambda^2} \tag{33}$$

By comparison with eq. (32) we see that Λ^2 is in fact independent of Q^2 :

$$\Lambda^2 = \mu^2 \exp - 1/b\alpha_s \tag{34}$$

We anticipate that the observed pattern of scaling violations implies for Λ the range of values :

$$\Lambda \simeq (0.2 \div 0.6) \text{ GeV} \tag{35}$$

or equivalently

$$\alpha_s(1 \text{ GeV})^2 \simeq 0.5 \div 1.5 \tag{36}$$

Note that α_s/π is already small in the few GeV range (precocious scaling).

By replacing α_s with $\alpha_s(t)$ the basic equations for the densities and their moments become :

$$\frac{dq(X,t)}{dt} = \frac{\alpha_s(t)}{2\pi} \int_0^1 \frac{dy}{y}\, q(y,t)\, P\left(\frac{X}{y}\right) \tag{37}$$

$$\frac{dM_n(t)}{dt} = \frac{\alpha_s(t)}{2\pi}\, An\, Mn(t) \tag{38}$$

with Mn(t) defined in eq. (27) and An determined from the function P(Z) by eq. (29).

By taking $\alpha_s(t)$ from eq. (32) we can easily solve eqs. (38) for the moments. The solution is :

$$Mn(t) = M_n(0) \left[\frac{\alpha_s}{\alpha_s(t)}\right]^{\frac{A_n}{2\pi b}} \tag{39}$$

Note that by eq. (33) the ratio $\frac{\alpha_s}{\alpha_s(t)}$ can be written as :

$$\frac{\alpha_s}{\alpha_s(t)} = \frac{\ln Q^2/\mu^2}{\ln \mu^2/\Lambda^2} \tag{40}$$

The moments behave as powers of logarithms of Q^2 and the exponents are generated by P(Z) which is determined by lowest order perturbation theory. The initial value $M_n(0)$ must however be fixed empirically. It corresponds to our ignorance of the matrix elements between protons of the local operators in the light cone expansion.

5. PHYSICAL INTERPRETATION OF P(Z)

Going back to the integro differential equation for the densities eq. (37) we point out an illuminating physical interpretation of the functions P(Z)[5]. This intuitive picture will be very useful in the following and in particular can serve as a basis for a very direct calculation of the P function and of other similar quantities that will be introduced shortly.

The results of first order perturbation theory in eq. (24) can be cast in a slightly different form as follows :

$$q(X,t) + \Delta q(X,t) = \int_0^1 dy \int_0^1 dZ\, \delta(Zy - X)\, q(y,t) \left[\delta(Z-1) + \frac{\alpha_s}{2\pi} t\, P(Z)\right] \tag{41}$$

The quantity

$$P(Z,t) = \delta(Z - 1) + \frac{\alpha_s}{2\pi}\, t\, P(Z) + \ldots \tag{42}$$

can be interpreted as an expansion of the probability density of finding a quark inside a quark with fraction Z of the parent quark momentum. Consequently $\frac{\alpha s}{2\pi} P(Z)$ appears as the lowest order variation of the probability density for unit t. The variation of q(X,t) is given by the number of quarks of momentum y larger than X times the variation of the probability of finding a quark inside a quark with momentum lower by a fraction X/y.

We point out that with our definition of P(Z), it also contains terms proportional to $\delta(Z - 1)$. The coefficient of $\delta(Z - 1)$ in eq. (42) is in fact modified by terms of order α_s because the probability for a quark to remain a quark with the same energy is lowered by the interaction. These terms are included in P(Z). In our gedanken derivation of P(Z) from $\sigma_{\text{order } \alpha_s}$, the $\delta(Z - 1)$ contributions arise from the interference of the point like diagram with the radiatively corrected (to order α_s) amplitude for a final state with a single quark and no gluons (see fig. 3a where gluons are marked by a G). If therefore follows that P(Z) is directly proportional to a probability (in particular is positive definite) only at $Z < 1$; while at $Z = 1$, $\delta(Z - 1)$ contributions are present which spoil the positive definiteness. At all Z the real probability density is P(Z,t) and not P(Z).

6. THE GENERAL MASTER EQUATIONS

In this section we start from our prototype eq. (37) for the densities and generalize it to the actual level of complication of QCD by taking into account the effects of the gluons and of the presence of several flavors.

First of all it is immediate to realize that there must also be a gluon term in dq/dt. The effective number of quarks inside the proton as seen by the photon may take a contribution from a gluon in the proton that makes a quark-antiquark pair and one of them interacts with the photon. This is seen by observing that both the diagrams in fig. 3b and 3c are contributions of the same order to $\sigma_{\text{order } \alpha_s}$. Correspondingly in dq/dt we shall find two terms. One is proportional to the number of quarks times the probability for finding a quark in a quark. The second is proportional to the number of gluons in the proton times the probability of finding a quark in a gluon :

$$\frac{dq(X,t)}{dt} = \frac{\alpha_s(t)}{2\pi} \int_X^1 \frac{dy}{y} \left[q(y,t)\, P_{qq}\left(\frac{X}{y}\right) + G(y,t)\, P_{qG}\left(\frac{X}{y}\right) \right] \qquad (43)$$

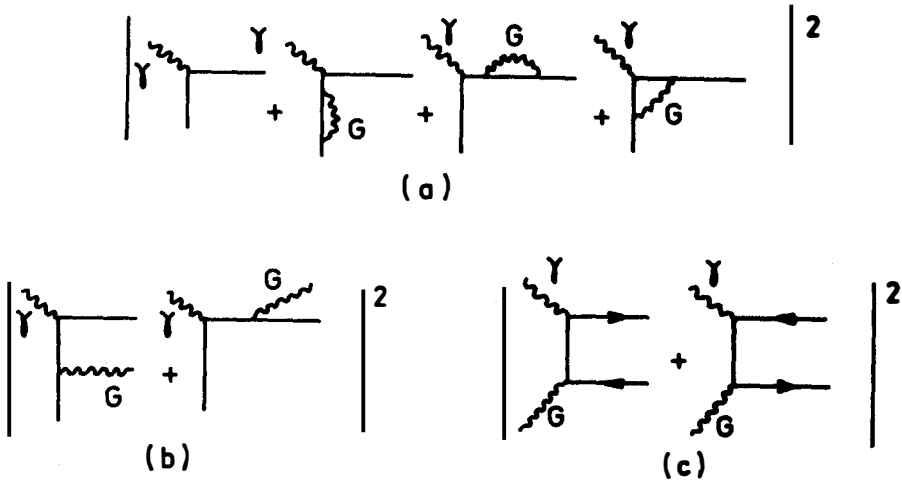

FIG. 3

We have thus introduced a new P function, which is non diagonal. With no interaction there would be no chance of finding a quark in a gluon. Therefore the corresponding probability density $P_{qG}(Z,t)$ starts with $P_{qG}(Z)$ (with no $\delta(Z-1)$ term) :

$$P_{qG}(Z,t) = \frac{\alpha_s}{2\pi}\, t\, P_{qG}(Z) + \ldots \qquad (44)$$

We observe that eq. (43) by itself cannot be solved because the variation of the quark density also involves the gluon density. An equation for the variation of the latter is also needed in order for the system to be closed. An equation for the gluon density is readily obtained by following the same logic as above. Only we must imagine a different probe because the photon is not coupled to color. But we can imagine a virtual spacelike gluon of mass $-Q^2$ probing the proton structure. It is than straight forward to write down the master equation for the variation of the effective gluon density :

$$\frac{dG(X,t)}{dt} = \frac{\alpha_s(t)}{2\pi} \int_X^1 \frac{dy}{y} \left[(\bar{q}(y,t) + q(y,t))\, P_{Gq}\left(\frac{X}{y}\right) + G(y,t)\, P_{GG}\left(\frac{X}{y}\right) \right] \qquad (45)$$

The first term is proportional to the total number of quarks and antiquarks times the probability of finding a gluon in a quark or in an antiquark.

The two probabilities are the same by charge conjugation :

$$P_{Gq}(Z) = P_{G\bar{q}}(Z) \tag{46}$$

The second term is proportional to the number of gluons times the probability of finding a gluon inside a gluon.

Up to now we made no reference to the variety of flavors that exists. There is no difficulty in taking it into account. Let us label by q_i (i = 1, ..., 2f) any quark or antiquark of all flavors. In full generality we should write :

$$\frac{dq_i(X,t)}{dt} = \frac{\alpha_s}{2\pi} \int_X^1 \frac{dy}{y} \left[\sum_j^{2f} qj\, P_{qjqi} + GP_{qiG} \right] \tag{47}$$

$$\frac{dG(X,t)}{dt} = \frac{\alpha_s}{2\pi} \int_X^1 \frac{dy}{y} \left[\sum_j^{2f} qj\, PG_{qi} + GP_{GG} \right] \tag{48}$$

However a great simplification is introduced by the facts that color and flavor commute and that a sufficiently large Q^2, masses can be neglected. Thus P_{qjqi} is really diagonal because the emission of gluons can neither change the flavor of the quark, nor transform a quark into an antiquark. Furthermore in presence of no mass effects the diagonal terms are independent of i :

$$P_{qiqj}(Z) = \delta_{qiqj}\, P_{qq}(Z) \tag{49}$$

Similarly the probability of finding a quark in a gluon is independent of the flavor of the quark (or antiquark) :

$$P_{qiG}(Z) = P_{qG} \qquad \text{independent of i} \tag{50}$$

The same applies to the probability of finding a gluon in a quark :

$$P_{Gq_i}(Z) = P_{Gq} \qquad \text{independent of i} \tag{51}$$

When eqs. (49,50,51) are taken into account the master equations eqs. (47) and (48) take the simpler form :

$$\frac{dq_i(X,t)}{dt} = \frac{\alpha_s(t)}{2\pi} \int_X^1 \frac{dy}{y} \left[qi(y,t)\ P_{qq}\left(\frac{X}{y}\right) + G(y,t)\ P_{qG}\left(\frac{X}{y}\right) \right] \qquad (52)$$

$$\frac{dG(X,t)}{dt} = \frac{\alpha_s(t)}{2\pi} \int_X^1 \frac{dy}{y} \left[\left(\sum_j^{2f} qj \right) P_{Gq}\left(\frac{X}{y}\right) + G(y,t)\ P_{qG}\left(\frac{X}{y}\right) \right] \qquad (53)$$

All the information on scaling violations in QCD is contained in the above equations, when the functions P(Z) are explicitly evaluated (from first order perturbation theory).

It is convenient to write down separate equations for singlet and non singlet quark components. A non singlet component (under the flavor group) is any difference $q_i - q_j$ for whatever i and j (i,j = 1, ..., 2f) or any linear combination of differences.

Denoting by p, n, λ, p' the densities of up, down, strange and charmed quarks in the proton (sumed over colors), examples of non singlet components are the "valence" quark densities :

$$p_V(X,t) \equiv p(X,t) - \bar{p}(X,t) \qquad (54)$$

$$n_V(X,t) \equiv n(X,t) - \bar{n}(X,t) \qquad (55)$$

Let $q_{ij} = q_i - q_j$. By substracting the equation (52) for q_j from the equation for q_i we remark the cancellation of the gluon contribution and obtain the diagonal equation :

$$\frac{dq_{ij}(X,t)}{dt} = \frac{\alpha_s(t)}{2\pi} \int_X^1 \frac{dy}{y}\ q_{ij}(y,t)\ P_{qq}\left(\frac{X}{y}\right) \qquad (56)$$

The simplest equation discussed in the previous sections is thus obtained as appropriate for all non singlet densities. Note that $P_{qq}(Z)$ is a single function that determines the same scaling violations for all non singlet densities. In particular all moments of any non singlet density are of the form in eq. (39) with exponents An determined by $P_{qq}(Z)$, through eq. (29).

To extract the remaining content of eqs. (52,53), it is sufficient to sum the equations for dq_i/dt over all i. Denoting the sum of all quarks and antiquarks by Σ :

$$\Sigma(X,t) = \sum_{i}^{2f} q_i(X,t) \tag{57}$$

We obtain a closed system of two equations :

$$\frac{d\Sigma(X,t)}{dt} = \frac{\alpha_s(t)}{2\pi} \int_X^1 \frac{dy}{y} \left[\Sigma(y,t)\, P_{qq}(\frac{X}{y}) + 2f\, G(y,t)\, P_{qG}(\frac{X}{y})\right] \tag{58}$$

$$\frac{dG(X,t)}{dt} = \frac{\alpha_s(t)}{2\pi} \int_X^1 \frac{dy}{y} \left[\Sigma(y,t)\, P_{Gq}(\frac{X}{y}) + G(y,t)\, P_{GG}(\frac{X}{y})\right] \tag{59}$$

Correspondingly for the moments of $\Sigma(X,t)$ and $G(X,t)$ one obtains a system of two linear differential equations :

$$<\Sigma(t)>_n \equiv \int_0^1 dX\, X^{n-1}\, \Sigma(X,t) \tag{60}$$

$$<G(t)>_n \equiv \int_0^1 dX\, X^{n-1}\, G(X,t) \tag{61}$$

$$\frac{d}{dt}\begin{pmatrix} <\Sigma(t)>_n \\ <G(t)>_n \end{pmatrix} = \frac{\alpha_s(t)}{2\pi} \begin{pmatrix} A^n_{qq} & 2f\, A^n_{qG} \\ A^n_{Gq} & A^n_{GG} \end{pmatrix} \begin{pmatrix} <\Sigma(t)>_n \\ <G(t)>_n \end{pmatrix} \tag{62}$$

with :

$$A^n = \int_0^1 dZ\, Z^{n-1}\, P(Z) \tag{63}$$

as in eq. (29).

It is straight forward to derive the expressions of a given parton density in terms of singlet and non singlet components. Assume for example SU(3) symmetry for the sea and define :

$$
\begin{aligned}
p_V(X,t) &\equiv p(X,t) - \bar{p}(X,t) \\
n_V(X,t) &\equiv n(X,t) - \bar{n}(X,t) \\
S(X,t) &\equiv \bar{p}(X,t) \simeq \bar{n}(X,t) \simeq \lambda(X,t) \simeq \bar{\lambda}(X,t) \\
C(X,t) &\equiv p'(X,t) \simeq \bar{p}'(X,t)
\end{aligned} \tag{64}
$$

The evolution of the sea and charm densities is easily obtained in terms of that of Σ and of non singlet components. Defining :

$$
V(X,t) = p_V(X,t) + n_V(X,t) \tag{65}
$$

$$
\Delta(X,t) = S(X,t) - C(X,t) \tag{66}
$$

We immediately have :

$$
\Sigma(X,t) = V(X,t) + 6S(X,t) + 2C(X,t) \tag{67}
$$

and

$$
S(X,t) = \frac{1}{8}\left[\Sigma(X,t) - V(X,t) + 2\Delta(X,t)\right] \tag{68}
$$

$$
C(X,t) = \frac{1}{8}\left[\Sigma(X,t) - V(X,t) - 6\Delta(X,t)\right] \tag{69}
$$

The t behavior of p_V, n_V, V and Δ is obtained by the diagonal equations (56) while for Σ the system eqs. (58,59) has to be solved. Finally from the evolution of the parton densities the t behavior of structure functions is obtained by the familiar parton expressions for them.

7. CONSTRAINTS ON THE P FUNCTIONS

In this section we shall introduce a number of simple constraints[5] on the P functions which are important in themselves and can be used to simplify their computation.

The parton densities are positive definite functions of X for all t

that are only bound a priori to satisfy the sum rules of conservation for the proton quantum numbers and of momentum. These sum rules read (see eqs. (54) (55))

$$\int_0^1 dX\ p_V(X,t) = 2\ ;\ \int_0^1 dX\ n_V(X,t) = 1 \tag{70}$$

$$\int_0^1 dX(\lambda(X,t) - \overline{\lambda}(X,t)) = 0\ ;\ \int_0^1 dX(p'(X,t) - \overline{p}'(X,t)) = 0 \tag{71}$$

and

$$\int_0^1 dX.X\ (\Sigma(X,t) + G(X,t)) = 1 \tag{72}$$

where Σ is defined in eq. (57). Conservation of charges and of momentum at the basic vertices of QCD preserves these sum rules from being spoilt by changes of Q^2 so that they provide constraints on the P functions that determine the Q^2 dependence of the densities and their moments. The sum rules for the conservation of charges involve the moments with n = 1 of non singlet densities. The exponent A_{qq}^n with n = 1 given by eq. (63) in terms of $P_{qq}(Z)$ must vanish in order for the charges to be Q^2 independent. We thus derive the result :

$$\int_0^1 dZ\ P_{qq}(Z) = 0 \tag{73}$$

Recalling that for a diagonal P function the relation with a probability density involves a $\delta(Z-1)$ term (see eq. (42)) :

$$P_{AB}(Z,t) = \delta_{AB}\,\delta(Z-1) + \frac{\alpha_s}{2}\,t\,P_{AB}(Z) + \ldots \tag{74}$$

We explicitly see from eq. (73) that the terms proportional to $\delta(Z-1)$ of order α_s in $P_{qq}(Z)$ make this function not definite positive. $P_{qq}(Z)$ is made up of a regular definite positive term and a δ function at $Z = 1$ with negative coefficient. Eq. (73) can be used to fix this coefficient with no need of diagrammatic calculations, which however can well be done as a useful exercise.

From the above discussion we also obtain the following set of inequalities for $n > 1$:

$$0 > \int_0^1 dZ\, Z^{n-1}\, P_{qq}(Z) > \int_0^1 dZ\, Z^n\, P_{qq}(Z) \qquad (75)$$

In fact the regular term at $Z < 1$ gives a positive contribution to the integral which is smaller when n is larger, while the negative term from the $\delta(Z - 1)$ contribution is independent of n. Therefore from the vanishing of the $n = 1$ moment of $P_{qq}(Z)$ the whole set of eqs. (75) is obtained. This fact implies through eqs. (32) (39) and (63) that all non singlet moments with $n > 1$ go to zero at $t \to \infty$ (faster for larger n).

We now consider the momentum conservation sum rule in eq. (72). The corresponding contraint is obtained by going to eqs. (62). Taking the $n = 2$ moment, summing the equations for $\frac{d <\Sigma(t)>_2}{dt}$ and $\frac{d <G(t)>_2}{dt}$ and imposing the separate vanishing of the coefficients of $<\Sigma(t)>_2$ and $<G(t)>_2$ on the right hand side leads to :

$$\int_0^1 dZ.Z \left(P_{qq}(Z) + P_{Gq}(Z)\right) = 0 \qquad (76)$$

$$\int_0^1 dZ.Z \left(2f\, P_{Gq}(Z) + P_{GG}(Z)\right) = 0 \qquad (77)$$

Eq. (77) can be used to fix the coefficient of the $\delta(Z - 1)$ term in $P_{GG}(Z)$.

8. AN ALTERNATIVE CALCULATION OF THE P FUNCTIONS

We have seen in the previous sections that as a matter of principle the functions P_{qq} and P_{qG} can be obtained from a calculation of the diagrams in Fig. 3a, b, c that contribute to $\sigma_{\text{order } \alpha_s}$. This method can also be extended to the calculation of P_{Gq} and P_{GG}. On the other hand we have given a physical interpretation of $\frac{\alpha s}{2\pi} t$. $P_{BA}(Z)$ in terms of probabilities of finding the parton B in the parton A with a fraction Z of the A momentum. This interpretation suggests that it should be possible to extract $\frac{\alpha s}{2\pi} t\, P_{BA}(Z)$ directly from the lowest order basic vertex of QCD involving the fields A and B. This is in fact necessary for the consistency of this interpretation which asserts the independence of P_{BA} from the probe that interacts with the

with the given parton B, which only determines the value of t. In other words we stated that the effect of the P terms can be taken into account by a redefinition of parton densities that thus acquire a Q^2 dependence. But parton densities are useful if we can relate different structure functions for the same process or the same structure functions for different processes, say electroproduction and ν or $\bar{\nu}$ scattering. It is thus important to show that the P functions and consequently the effective Q^2 dependent parton densities, only depend on the target and for each fixed Q^2 are insensitive to whether the probe is a photon with one or another polarization, or a weak current with any mixture of vector and axial vector couplings. This fact was explicitely demonstrated in the second article of ref. (5) where the whole set of P functions was derived from the basic vertices of QCD and the constraints introduced in Sect. 7. The method is a generalization in QCD of the well-known Weizsacker-Williams calculation of the equivalent number of photons in an electron in QED.

The strategy is to compute the regular part of $P_{BA}(Z)$ at $Z < 1$. The $\delta(Z - 1)$ singularities that are present for the diagonal cases ($A = B$) can then be fixed by the constraints derived in the previous section. The diagrams in Fig. 3a and b contribute to $P_{qq}(Z)$. Those in Fig. 3a can only contribute $\delta(Z - 1)$ terms and we can avoid to compute them. As for the diagrams in Fig. 3b, the one with the gluon emitted by the final quark (after interaction with the photon), seems superficially to contradict our philosophy for the P functions, while the other one is directly of parton type in that the emitted gluon could be considered as part of the proton blob. Actually both diagrams are necessary in a general gauge to ensure gauge invariance of the amplitude. But looking more closely one discovers that the second diagram is only necessary to cancel the contribution of the unphysical longitudinal and scalar gluons in the parton like diagram which are present in a general gauge. In other words if we only sum over transverse gluons the contribution of the parton diagram is the only relevant one for the terms which contain t i.e. are logarithmically dominant. Moreover the parton diagram factorizes into a contribution from the current vertex and one from the gluon vertex and the latter is the one relevant for $P_{qq}(Z)$. A similar discussion applies for all $P_{BA}(Z)$.

More recently the universality of the P functions and the possibility of factorizing their effect by a redefinition of parton densities has been further elucidated in refs. 6 and 7.

9. TRANSVERSE AND LONGITUDINAL STRUCTURE FUNCTIONS

We now pause for a moment in order to summarize the main points in the long argument in the previous sections.

We started from the lowest order result (naive parton model) :

$$2\,F_1(X) = e^2 q(X) = \int \frac{dy}{y}\, q(y)\, e^2\, \delta(\frac{X}{y} - 1) \tag{78}$$

(the non singlet structure function is considered for simplicity). We then added the correction of order α_s to the point like cross section :

$$2\,F_1(X,t) = \int_X^1 \frac{dy}{y}\, q(y)\, e^2 \left[\delta(\frac{X}{y} - 1) + \frac{\alpha_s}{2\pi}\, t\, P(\frac{X}{y}) + \frac{\alpha_s}{2\pi}\, f\, (\frac{X}{y})\right] \tag{79}$$

The necessity of including the t dependent term in q(y,t) arises because $\alpha_s t$ cannot be considered as a small parameter (even if we could replace α_s with $\alpha_s(t)$). On the other hand, the independence of the P functions from the detailed structure of the probe leads to effective parton densities that only depend on t and on the target. In turn the t derivatives of the effective parton densities start with α_s and are small when α_s is replaced by $\alpha_s(t)$. By replacing q(y) by q(y,t), one obtains from eq. (79)

$$2\,F_1(X,t) = \int_X^1 \frac{dy}{y}\, q(y,t)\, e^2 \left[\delta(\frac{X}{y} - 1) + \frac{\alpha_s(t)}{2\pi}\, f\, (\frac{X}{y})\right] \tag{80}$$

The possibility of implementing the above factorization to all orders is the key result of the renormalization group approach.

In most cases, for Q^2 large, we can neglect the f term and the naive parton model form of the structure function is restored in terms of t dependent effective parton densities satisfying the integro-differential equations (52,53). However, in some cases the f terms are important and we shall now discuss this matter.

First one may ask why we do not absorb the f terms in the definition of q(X,t) as well. The answer is that the f functions contrary to the P functions are not independent on the detailed properties of the current. Thus if we were to compute F_2/X instead of $2F_1$ we would have found the same P functions but a different f term. In fact the complete result for the two structure functions would be (we restored the non singlet components as well) :

(81)

$$\frac{F_2(X,t)}{X} = \int_X^1 \frac{dy}{y} \left\{ \sum_i e_i^2 \, q_i(y,t) \left[\delta\left(\frac{X}{y} - 1\right) + \frac{\alpha_s(t)}{2\pi} f_2^q\left(\frac{X}{y}\right) \right] + \sum_i e_i^2 \, G(y,t) \, \frac{\alpha_s(t)}{2\pi} f_2^G\left(\frac{X}{y}\right) \right\}$$

$$2F_1(X,t) = \int_X^1 \frac{dy}{y} \left\{ \sum_i e_i^2 \, q_i(y,t) \left[\delta\left(\frac{X}{y} - 1\right) + \frac{\alpha_s(t)}{2\pi} f_1^q\left(\frac{X}{y}\right) \right] + \sum_i e_i^2 \, G(y,t) \, \frac{\alpha_s(t)}{2\pi} f_1^G\left(\frac{X}{y}\right) \right\}$$

(82)

where the index i runs over both quarks and antiquarks of all flavors. The importance of the f terms becomes manifest if we are interested in the longitudinal structure function :

$$F_L(X,t) = \left[F_2(X,t) - 2 \, X \, F_1(X,t) \right] \tag{83}$$

In fact F_L is zero to lowest order, while to order $\alpha_s(t)$, by subtracting eqs (81, 82), we find :

$$\frac{F_L(X,t)}{X} = \frac{\alpha_s(t)}{2\pi} \int_X^1 \frac{dy}{y} \left\{ \sum_i e_i^2 \, q_i(y,t) \, f_L^q\left(\frac{X}{y}\right) + \left(\sum_i e_i^2 \right) G(y,t) \, f_L^G\left(\frac{X}{y}\right) \right\} \tag{84}$$

where

$$f_L^{q,G} = f_2^{q,G} - f_1^{q,G} \tag{85}$$

This is a very important result that shows that the longitudinal structure function in QCD is only expected to vanish logarithmically at $Q^2 \to \infty$. This is to be confronted with the prediction of the naive parton model of a power behavior at large Q^2 : $F_L \sim m^2/Q^2$.

We alreday mentioned in Sect. 3 that the f functions are not well defined in that they depend on the regulator mass that makes the integral over $P_\perp^2$ in eq. (21) finite near $P_\perp^2 \simeq 0$. But this dependence on the regulator mass cancels in the differences in eq. (85). In fact f_L^q and f_L^G can be directly related to the longitudinal structure functions for parton-virtual photon scattering and computed from the diagrams in Fig. (3) (referred to a longitudinal photon). The independence on the infrared cut off manifests itself in that the parton longitudinal structure functions are well defined even in the massless theory and one finds[8] :

$$f_L^q(Z) = \frac{8}{3} Z$$
$$f_L^G(Z) = 2Z(1 - Z) \tag{86}$$

For an arbitrary process (e-P or ν, $\bar{\nu}$ scattering) we then obtain the results[9] (a part from terms of higher order in $\alpha_s(t)$) :

$$F_L(X,t) = \frac{\alpha_s(t)}{2\pi} X^2 \int_X^1 \frac{dy}{y^3} \left\{ \frac{8}{3} F_2(X,t) + 2A \left(1 - \frac{X}{y}\right) y\, G(y,t) \right\} \quad (87)$$

$$\sigma_L(t) \equiv \int_0^1 dZ\, F_L(Z,t) = \frac{\alpha_s(t)}{2\pi} \left\{ \frac{8}{9} \int_0^1 dX\, F_2(X,t) + \frac{A}{6} \int_0^1 dX\, G(X,t) \right\} \quad (88)$$

where A is the sum of all coefficients of quarks and antiquarks in the naive parton model expression for F2/X. For example, with four flavors beyond charm threshold, A = 20/9 in electroproduction, and A = 8 for ν or $\bar{\nu}$ scattering on matter.

We can easily understand why QCD leads to $\sigma_L \sim \alpha_s(t)$ and why the infrared singularities cancel in this case. In the naive parton model, (i.e. for α_s set to zero), the point like longitudinal cross-section is zero in the limit of zero $P_\perp$ for the quark in the nucleon. In fact in the frame where the spacelike current carries no energy (see eq. (5)), the hit parton reverses its momentum and since the helicity is conserved (vector and axial vector interactions for mass less fermions) the spin is also reversed. Thus, being the process collinear the current must carry a unit of spin component in order to conserve angular momentum and the longitudinal cross section is zero. If $P_\perp^2$ (or m^2) is not exactly zero, but the $P_\perp^2$ distribution is sufficiently damped, as one assumes in the naive parton model, then one obtains by a precise calculation :

$$\frac{\sigma_L}{\sigma_T} \simeq 4 \frac{\langle P_\perp^2 \rangle + m^2}{Q^2} \qquad \text{(Naive parton model)} \quad (89)$$

If we now allow for correction of order α_s as in the diagrams of Figs. 3, then the intermediate quark that actually interacts with the current has a $P_\perp^2$ distribution that only drops as $P_\perp^{-2}$ (recall the discussion in Sect. 3 and especially eq. (21)). We then have schematically in QCD

$$\sigma_T \sim 1 + \alpha_s \int^{Q^2} \frac{dp_\perp^2}{p_\perp^2} \sim 1 + \alpha_s \ell_n Q^2 \quad (90)$$

$$\langle p_\perp^2 \rangle \sim \alpha_s \int^{Q^2} p_\perp^2 \frac{dp_\perp^2}{p_\perp^2} \sim \alpha_s Q^2 + \text{constant} \quad (91)$$

$$\frac{\sigma_L}{\sigma_T} \sim \alpha_s \int^{Q^2} \frac{p_\perp^2}{Q^2} \frac{dp_\perp^2}{p_\perp^2} \sim \alpha_s + 0\,(1/Q^2) \qquad (92)$$

We thus expect in QCD $\sigma_L/\sigma_T \sim < p_\perp^2 > /Q^2 \sim \alpha_s(t)$. We also understand why σ_L is regular in the massless theory for partons : the singularity at $P_\perp = 0$ is cancelled by the vanishing of the numerator for a collinear process.

We stress that the verification of this QCD prediction is of the utmost importance. Unfortunately, the present experimental situation on F_L and σ_L is confuse. A precise experimental determination of these quantities is also a most direct way of measuring the gluon content of the nucleon.

10. JETS IN LEPTOPRODUCTION AND THEIR $P_\perp$ DISTRIBUTIONS

A strictly related set of consequences following from the above discussion is about the $P_\perp$ distribution of jets in electroproduction. Here we deal with the first example of more recent problems attacked in QCD, which were not solved by the renormalization group method. As we shall see the relevant QCD predictions are quite naturally derived by the present approach.

In the naive parton model, neglecting the $P_\perp$ spread of quarks in the nucleon, which is damped by the wave function and does not increase with Q^2, we expect two hadronic jets opposite in rapidity, arising from the fragmentation of the quark parton on one side (current region) and from the debris of the nucleon on the other side (target fragmentation). This is a two jet process with small $P_\perp$. The $P_\perp$ of hadrons in the jets arises from two effects : the $P_\perp$ of the quark parton and the $P_\perp$ with respect to the parton axis from the fragmentation of the quark into hadrons.

But we have seen that in QCD the possibility of gluon interactions provides the intermediate quark (and therefore the final quark because the current carries no $P_\perp$) with a hard tail in its $P_\perp$ distribution. This tail is small (because it arises from a fraction of events of order $\alpha_s(t)$) but extends up to $P_\perp^2 \sim Q^2$. The leading term of $< P_\perp^2 >$ in eq. (91) is due to this effect and can be predicted perturbatively, while the constant term depends on the wave function effects and cannot be evaluated. One thus expects a

fraction of events of order $\alpha_s(t)$ with the topology of three jet events : the target fragmentation jet with small $P_\perp$ and two jets with large and almost opposite $P_\perp$ from the quark and gluon fragments or from quark and antiquark fragments for parton processes started by a gluon in the nucleon).

For a quantitative discussion[9,10], suppose we want to compute a moment of the $P_\perp$ distribution for the parton jets for three jet events in electroproduction, for example $\langle P_\perp^2 \rangle$ as a function of Q^2, X and y. y is defined by :

$$y = \nu/E_\ell \tag{93}$$

where E_ℓ is the laboratory energy for the incoming electron. As well-known y enters because it rules the proportion of longitudinal and transverse photons according to :

$$\frac{d\sigma}{dX\,dy} \equiv \left[1 - y + y^2/2\right] (2X\,F_1) + (1 - y)\,F_L \tag{94}$$

with F_L defined in eq. (83). From the previous discussion, it follows that we can compute the leading term at large Q^2 of $\langle P_\perp^2 \rangle$ (i.e. the one proportional to Q^2). We saw that the physical origin of σ_L and of $\langle P_\perp^2 \rangle$ are related. Their computation is also very similar. Just as σ_L is obtained by computing σ_L for partons in lowest non vanishing order, i.e. order α_s, then convoluting the result with t dependent parton densities and finally replacing α_s with $\alpha_s(t)$, the same strategy is followed in evaluating $\langle P_\perp^2 \rangle / Q^2$. We evaluate the angular distributions $\frac{d\sigma}{dp_\perp^2}$ off transverse and longitudinal photons for both an initial quark (antiquark) or a gluon. We then obtain the relevant moment. In particular for $\langle P_\perp^2 \rangle$ we define :

$$\frac{\alpha_s}{2\pi}\; {}^{L,T}_{q,G}T\,(Z) = \int \frac{P_\perp^2}{Q^2}\,\frac{d\sigma}{dp_\perp^2}\,dp_\perp^2 \tag{95}$$

with the integration from zero to the maximum allowed $P_\perp^2$ of order Q^2. We finally convolute with t dependent effective parton densities and replace α_s with $\alpha_s(t)$. The final result has the form :

$$\frac{\langle p_\perp^2 \rangle}{Q^2} \equiv \alpha_s(t)\; g(X,y,t) = \frac{\alpha_s(t)}{2\pi}\,\frac{X}{F_2(X,t)} \left\{ \int_X^1 \frac{du}{u^2} \left[F_2(u,t)\; T_q^T\left(\frac{X}{u}\right) + \right.\right.$$

$$\left. + \left(\sum_i e_i^2\right)\left(u\,G(u,t)\right)\; T_G^T\left(\frac{X}{u}\right)\right] + \frac{1-y}{1-y+y^2/2} \int_X^1 \frac{du}{u^2} \left[F_2(u,t)\; T_q^L\left(\frac{X}{u}\right) + \left(\sum_i e_i^2\right)\left(uG(u,t)\right) T_G^L\left(\frac{X}{u}\right)\right] \Bigg\} \tag{96}$$

The T functions are explicitely evaluated in ref. (9). As is clear from eqs. (21, 95), they are well defined even in the massless theory and consequently no infrared cut off dependence affects them. Note that the t dependence of the function g in the previous equation only arises from the effective parton densities. The main results of the detailed computation can be read from Fig. (4,5). There we neglected the t dependence of parton densities and inserted standard parton fits in the present range of Q^2. One finds that the result is fortunately not very sensitive to the badly known gluon density in the nucleon (this is not the case for σ_L/σ_T). The naive parton model prediction in eq. (89) (with m = 0) is found not to be true quantitatively, but only as an order of magnitude relation. As for the properties of g(X,Y) in eq. (96) the y dependence is generally negligible, while the X dependence is very important but can almost completely be taken into account by saying that $< P_\perp^2 >$ is not proportional to Q^2 but rather to W^2, the total hadronic invariant mass squared :

$$W^2 = (P + q)^2 \tag{97}$$

with P the nucleon momentum. For almost all X, we roughly obtain :

$$< p_\perp^2 > \sim \alpha_s(t)\, W^2/32 \tag{98}$$

Recall that to this linearly rising (in W^2) component, one should add a constant contribution (a part from logs) originating from the intrinsic $P_\perp$ of partons in the nucleon. At small W^2 the constant component is expected to be dominant while at sufficiently large W^2 the first term takes over. Note however that the slope in W^2 of the linearly rising term is small, as apparent from eq. (98). Thus it is not a surprise that at present energies ($W^2 \lesssim 200\ GeV^2$) the presence of the hard component is still not visible.

Note also that the available data[11] refer to $< P_\perp^2 >$ of one given hadron in the jet, while the QCD result in eqs. (96,98) concerns the $< P_\perp^2 >$ of the parton that produces the jet. The $P_\perp$ distribution of the hadrons in the jet is also dependent on the fragmentation properties of the parton into hadrons which cannot be calculated in perturbation theory. By summing the $\vec{P}_\perp$ of the hadrons in the jet, one can in principle reconstruct the $\vec{P}_\perp$ of the parton and be freed from the dependence on the fragmentation functions[12].

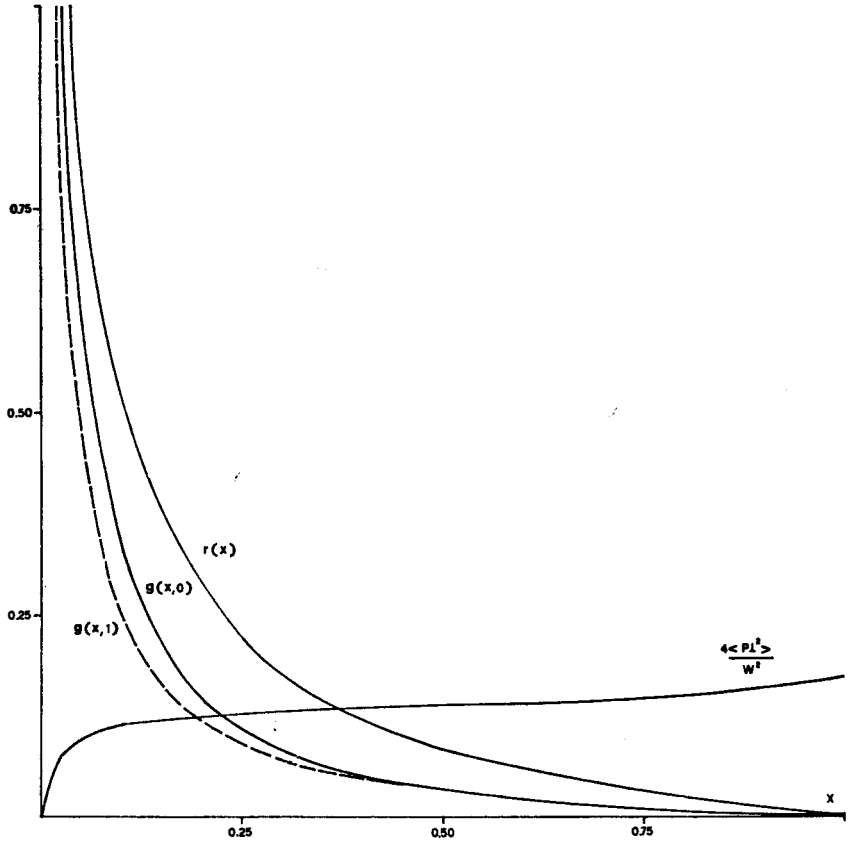

Fig. 4 : Plots of $(p_\perp^2>/Q^2 \propto \alpha_s(Q^2)g(x,y)$ for y = 0 (——), y = 1 (---), of $F_L(x,Q^2)/F^2(x,Q^2) \sim \alpha_s(Q^2)r(x)$ and of $4(p_\perp^2)/W^2$ for y = 1 (and with $\alpha_s(Q^2) = 1$).

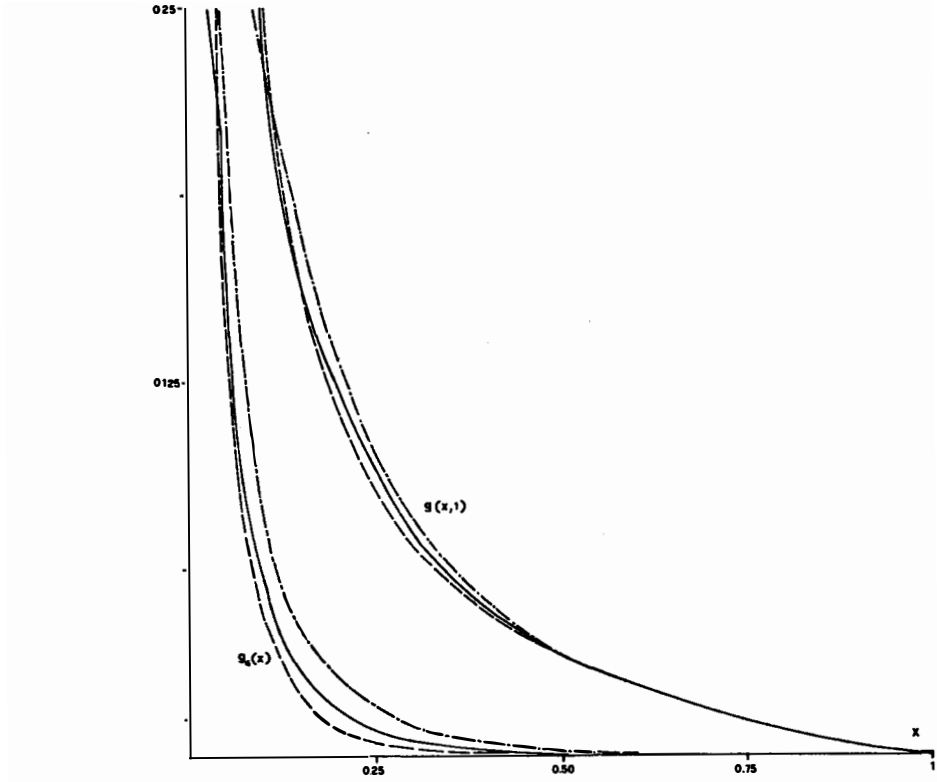

Fig. 5 : With $(p_\perp^2>/Q^2 \approx \alpha_s(Q^2)g(x,y)$ we separate at y = 1 the contributions of quarks and gluons, $g_G(x)$, in the nucleon.

11. DRELL-YAN PROCESSES

In this section we consider lepton pair production in hadron-hadron collisions. The usefulness of the QCD improved parton language is best seen in this case which is outside the range of application of renormalization group methods.

In the naive parton model lepton pair production in hadron-hadron collisions is described by the famous Drell-Yan formula[13]. A quark in one hadron annihilates with an antiquark in the other hadron and produces a lepton pair with point like cross-section :

$$\frac{Q^2 \, d\sigma^{DY}}{dQ^2} = \frac{4\pi\alpha^2}{9S} \int \frac{dX_1 \, dX_2}{X_1 \, X_2} \left[\sum_{j=1}^{f} e_j^2 \, q_j^1(X_1) \, \bar{q}_j^2(X_2) + 1 \leftrightarrow 2 \right] \delta(1 - \frac{\tau}{X_1 X_2}) \tag{99}$$

where $Q^2 > 0$ is the invariant mass squared of the lepton pair, S the invariant mass squared of the incoming hadrons, $\tau = Q^2/S$, $X_{1,2}$ are the fractions of longitudinal momentum carried by the parton quark or antiquark in hadron 1 or 2, the labels 1 and 2 on the parton symbols refer to the hadron they belong and the sum over j runs on quark flavors (i.e. $j = 1, \ldots 4$). Starting from the Drell-Yan formula, we can compute the effects induced by gluon corrections in QCD, just as we did in leptoproduction where we also started from the naive parton model approximation. In particular, two problems can be considered. The first deals with the relation of the parton densities that appear in the Drell-Yan formula with those measured in leptoproduction. The result[14] is that in the Drell-Yan case also t dependent effective parton densities are induced by gluon corrections which turn out to be the same, in the leading logarithmic approximation, as in leptoproduction at the same $|q^2|$ (i.e. there is no influence of the current being spacelike in one case and timelike in the other). The second problem is the study of the $P_\perp$ distribution of the produced lepton pair. In this case the $P_\perp$ of the pair is directly related to the transverse momentum of the incoming partons with no hadronic fragmentation function obscuring the result. The problem is solved by computing the angular distributions for the parton processes and then convoluting with the effective parton densities and replacing α_s with $\alpha_s(t)$[10,15,16].

Gluon corrections are evaluated from the basic processes :

$$\begin{aligned} q + \bar{q} &\longrightarrow G + \gamma^* \\ q(\bar{q}) + G &\longrightarrow q(\bar{q}) + \gamma^* \end{aligned} \tag{100}$$

where γ^* is the virtual photon of mass $\sqrt{Q^2}$. One must also take into account virtual corrections of order α_s to the lowest order process $q + \bar{q} \to \gamma^*$. As we did for electroproduction we add to the point like cross-section appearing in the Drell-Yan formula the result for $\sigma_{\text{order } \alpha_s}$. Ignoring povers of m^2/Q^2, $\sigma_{\text{order } \alpha_s}$ for both processes in eqs. (100) has a term that increases logarithmically with Q^2 and a finite term. By omitting all obvious factors and sums the result for the corrected Drell-Yan formula is of the form

$$Q^2 \frac{d\sigma^{DY}}{dQ^2} \sim \int_\tau^1 \frac{dX_1}{X_1} \int_{\frac{\tau}{X_1}}^1 \frac{dX_2}{X_2} \left\{ \left[q^1(X_1)\, \bar{q}^2(X_2) + 1 \leftrightarrow 2 \right] \left| \delta(1 - Z_{12}) \right. \right.$$

$$\left. + \frac{\alpha_s}{2\pi} t\, 2\, P_{qq}^{DY}(Z_{12}) + \frac{\alpha_s}{2\pi} f_q^{DY}(Z_{12}) \right] + \left[(q^1(X_1) + \bar{q}^1(X_1)) G^2(X_2) + 1 \leftrightarrow 2 \right] \frac{\alpha_s}{2\pi}$$

$$\left. \left[P_{qG}^{DY}(Z_{12})\, t + f_G^{DY}(Z_{12}) \right] \right\} \tag{101}$$

where

$$Z_{12} = \frac{\tau}{X_1 X_2} = \frac{Q^2}{s} \leq 1 \tag{102}$$

with $s = X_1 X_2 S$ the invariant mass squared of the incoming partons. It is clear that the total cross sections for the parton processes in eqs. (100) can only depend on Q^2 and s, and thus when an appropriate dimensional factor is extracted they are just functions of Z_{12}.

An explicit calculation[14] shows the identities

$$\begin{aligned} P_{qq}^{DY}(Z) &= P_{qq}(Z) \\ P_{qG}^{DY}(Z) &= P_{qG}(Z) \end{aligned} \tag{103}$$

where on the right hand side we have the familiar functions introduced for leptoproduction. If we neglect for a moment $f_{q,G}^{DY}$ in eq. (101) it is a simple matter to show that we can reabsorb the terms in $\alpha_s t$ into effective parton densities, as we did for leptoproduction ;

$$Q^2 \frac{d\sigma^{DY}}{dQ^2} \sim \int_\tau^1 \frac{dX_1}{X_1} \int_{\frac{\tau}{X_1}}^1 \frac{dX_2}{X_2} \left\{ (q^1(X_1) + \Delta q^1(X_1,t))(\bar{q}^2(X_2) + \Delta \bar{q}^2(X_2,t)) \delta(1-Z_{12}) \right\} \tag{104}$$

with

$$\Delta q(X,t) = \frac{\alpha_s}{2\pi} \; t \int_X^1 \frac{dy}{y} \left[q(y) \; P_{qq}\left(\frac{X}{y}\right) + G(y) \; P_{qG}\left(\frac{X}{y}\right) \right] \qquad (105)$$

We thus obtained the quoted result that the same effective parton densities describe both leptoproduction and Drell-Yan processes when the same $Q^2 = |q^2|$ is considered. By taking the $f^{DY}_{q,G}$ terms also into account and replacing α_s with $\alpha_s(t)$ we then end up with the modified Drell-Yan formula :

$$Q^2 \frac{d\sigma^{DY}}{dQ^2} = \frac{4\pi\alpha^2}{9S} \int_\tau^1 \frac{dX_1}{X_1} \int_{\frac{\tau}{X_1}}^1 \frac{dX_2}{X_2} \left\{ \left[\sum_{j=1}^{f} e_j^2 \; q_j^1(X_1,t) \; \bar{q}_j^2(X_2,t) + 1 \leftrightarrow 2 \right] \left[\delta(1-Z_{12}) + \frac{\alpha_s(t)}{2\pi} \; f_q^{DY}(Z_{12}) \right] + \left[2F_1^1(X_1,t) \; G^2(X_2,t) + 1 \leftrightarrow 2 \right] \frac{\alpha_s(t)}{2\pi} \; f_G^{DY}(Z_{12}) \right\} \qquad (106)$$

where F_1^1 is the electroproduction structure function, F_1 for hadron 1 (that originates from $\sum_j e_j^2(q_j + \bar{q}_j)$ in eq. (10)).

While the f corrective terms proportional to $\alpha_s(t)$ are certainly negligible for $\bar{P}$-Nucleus collisions they may be important[17] for P-Nucleus collisions, where the leading term is small being proportional to the sea densities. The precise determination of these corrections depends somewhat on the definition of parton densities beyond the leading order, as a consequence of the infrared subtelies connected with the f terms. After this meeting this matter has been discussed in Ref. (18).

We finally consider the problem of the $P_\perp$ distributions of muon pairs. As for the $P_\perp$ of jets in leptoproduction, one obtains from QCD a detailed prediction for the hard component of the $P_\perp$ spectrum. That is to say that for example we can predict the coefficient of S in the expression of $< P_\perp^2 >$. This is of order $\alpha_s(t)$ and is a function of τ :

$$< P_\perp^2 > = \alpha_s(t) \; S \; G(\tau, \alpha_s(t)) + \ldots \qquad (107)$$

A part for terms of order α_s^2 (t), the dots stand for terms with no factor of S, which cannot be predicted because they contain the information about the intrinsic component of $P_\perp$ from the nucleon wave function. At sufficiently large S the first term dominates, but the

magnitude of the terms in the dots at present energies is still non negligible, because the linearly rising term has a small derivative of order $\alpha_s(t)$.

One starts by computing[15] the angular distributions for the parton processes in eqs. (100). From these one obtains the moments of the $P_\perp$ distribution :

$$\int \left(\frac{P_\perp}{S}\right)^n \frac{d\sigma^{DY}}{dQ^2 dp_\perp^2}\, dp_\perp^2$$

that are well defined and convergent even in the massless theory (for $n > 1$). Convoluting with the effective parton densities and replacing α_s with $\alpha_s(t)$, one ends up with the result (for $P_\perp^2$ for example)[15] :

$$< p_\perp^2 > Q^2 \frac{d\sigma^{DY}}{dQ^2} = \frac{\alpha^2\, \alpha_s(t)}{27} \int_\tau^1 \frac{dX_1}{X_1} \int_{\frac{\tau}{X_1}}^1 \frac{dX_2}{X_2} (1 - Z_{12})^3 \left\{ \left[\sum_{j=1}^{f} e_j^2\, q_j^1(X_1,t)\, \bar{q}_j^2(X_2,t) + 1 \leftrightarrow 2 \right] \right.$$

$$\left. .16 \left(\frac{1}{3} + \frac{Z_{12}}{(1-Z_{12})^2}\right) + \left[2F_1^1(X_1,t)\, G^2(X_2,t) + 1 \leftrightarrow 2 \right] \left[\frac{3}{2} \frac{1}{1-Z_{12}} + \frac{1}{4}(1-Z_{12}) - 2Z_{12} \right] \right\}$$

(108)

I shall not go here in the details of a comparison of the above formula with the data because this subject is discussed in full in the lecture by PETRONZIO at this Meeting that can be found in the companion volume of the Proceedings. The conclusion is that the component due to the intrinsic $P_\perp$ of partons in the nucleon is still substantial at present energies, but evidence already exists for an hard component that increases with S at fixed τ.

REFERENCES

(1) See for example :
R.P. FEYNMAN : "Photon Hadron Interactions"
W.A. BENJAMIN, New York (1972)
J. KOGUT, L. SUSSKIND : Physics Reports C8 (1973) 76
G. ALTARELLI - Rivista Nuovo Cimento 4 (1974) 335
G. ALTARELLI : "Deep Inelastic Processes and the Parton Model",
Ecole d'Eté de Physique des Particules, Gif-sur-Yvette, 1974, II.

(2) See for example : H.D. POLITZER, Physics Reports 14C (1974) 129
and references therein.

(3) G. PARISI, Physics Letters 43 B (1973) 207 and 50 B (1974) 367.
See also J. KOGUT, L. SUSSKIND; Physics Rev. D9 (1974) 697 and
D9 (1974) 3391.

(4) For a review on the Renormalisation Group Equations and their
Application to Deep Inelastic Scattering, See for example :
W. MARCIANO, H. PAGELS "Quantum Chromodynamics", Rockefeller
University, Preprint (1977), and Ref. (2).

(5) G. PARISI, Proc. 11th Rencontre de Moriond on Weak Interactions
and Neutrino Physics (1976), Ed. by J. TRAN THANH VAN.
G. ALTARELLI, G. PARISI, Nuclear Physics, B 126 (1977) 298.
G. ALTARELLI "Partons in Quantum Chromodynamics", Ecole d'Eté
de Physique des Particules", Gif-sur-Yvette (1977).

(6) D. AMATI, R. PETRONZIO, G. VENEZIANO, CERN Preprint TH-2470 (1978).

(7) L. BAULIEU, C. KOUNNAS, Ecole Normale Supérieure, Preprint,
Paris (1978).

(8) A. ZEE, F. WILCZEK, S.B. TREIMAN, Physical Rev. D10 (1974) 2881.
D.V. NANOPOULOS, G.G. ROOS, Phys. Letters 58B (1975) 105
See also E. WITTEN, Nucl. Phys. B 120 (1977) 189, eqs.(11) and (13).

(9) G. ALTARELLI, G. MARTINELLI, Phys. Letters 76B (1978) 89

(10) K.H. CRAIG, C.H. LLEWELLYN SMITH, Oxford University Preprint (1977).

(11) See for example, L. HAND, in Proceedings of the Hambourg Conference (1977).

(12) Other tests of QCD in μP Scattering, can be found in H. GEORGI, H.D. POLITZER, Harvard University, Preprint (1977).

(13) S.D. DRELL, T.M. YAN, Phys. Rev. Letters 25 (1970) 316.

(14) H.D. POLITZER, Nuclear Physics B 129 (1977) 301 ; see also C.T. SACHRAJDA, CERN Preprint TH 2416 (1977).

(15) G. ALTARELLI, G. PARISI, G. PETRONZIO, CERN Preprint TH 2413 (1977) and TH 2450 (1978).

(16) A.V. RADYUSHKIN, Phys. Letters 69B (1977) 245.
H. FRITZSCH, P. MINKOWSKI, Physics Letters 73B (1978) 80.
K. KAJANTIE, R. RAITIO, Helsinki Preprint (1977).

(17) H. GEORGI, Harvard University Preprint (1978).

(18) G. ALTARELLI, R.K. ELLIS, G. MARTINELLI, MIT Preprint (1978).

QUARK JETS

U.P. Sukhatme

Laboratoire de Physique Théorique et Particules Elémentaires
Université de Paris - Sud, Orsay, France

Abstract : We discuss various aspects of jets resulting from quark fragmentation in the framework of the cascade model, in which the jet is formed by a succession of breakups (quark → meson+quark). Among the topics discussed are jet multiplicities, inclusive momentum distributions, the leading particle effect in jets, the behavior of fragmentation functions as $x \to 1$, a comparison of various methods for finding the jet axis, and how the jet angular distribution in e^+e^- collisions can be used to discover new quark or lepton thresholds.

Résumé : Nous discutons les divers aspects des jets produits par la fragmentation des quarks. Dans le cadre du modèle de cascade, le jet est formé par des "breakups" (quark → meson + quark) successifs. Les sujets traités sont les suivants : les multiplicités des jets, les distributions inclusives, la présence d'une particule dominante, le comportement des fonctions de fragmentation quand $x \to 1$, la comparaison de diverses méthodes pour trouver l'axe d'un jet, et comment peut-on découvrir des nouveaux seuils de quarks ou de leptons en observant la distribution angulaire des jets dans les collisions e^+e^-.

I - INTRODUCTION.

This article deals with several aspects concerning jets of particles arising from quark fragmentation. First, we provide a theoretical framework for the discussion by briefly describing the popular cascade model for jets (Sec.II), and formulating it in terms of integral equations.[1-4] This enables the calculation of all quantities of physical interest. In particular, one obtains logarithmic multiplicities with a universal slope and the inclusive momentum distribution for mesons (Sec. III). From this, it is easy to compute how often the leading particle in a jet contains the jet-initiating quark (Sec. IV).[2] This question is of experimental importance, since one would like to be able to identify the flavor of the quark which produced the jet. Sec. V contains a derivation of "power counting rules" which give the behavior of various quark fragmentation functions as $x \to 1$.[4] These rules are different from "dimensional counting",[5] and are in good agreement with available experiments. In Sec. VI, we discuss various possible methods for finding the jet axis in a given jet-like event.[6,7] The inherent uncertainty in such determinations is estimated. Finally, in Sec. VII, we show that the observation of structure in the eccentricity of jet angular distributions is probably the quickest way of establishing the existence and position of new physics at PETRA and PEP.[8]

II - CASCADE MODEL FOR JETS.

Let us first give a qualitative description of jet formation. Quarks and antiquarks in a hadron can be regarded as relatively free to move around in a region whose spatial extent is the hadronic size. Suppose that for some reason (typically a high energy collision) a quark acquires a large momentum and tries to escape from the system. A complete escape would result in the observation of fractional quark-like quantum numbers. Since they are not seen, it follows that the confinement forces must be responsible for sorting out quantum numbers - the final result being the transformation (or fragmentation) of the escaping quark into a jet of particles. Thus, jets are a consequence of confinement.

More specifically, jet formation is assumed to proceed via a succession of fundamental "breakups" of the form quark → "meson" + quark. For example, the first breakup is

$$q_i(P) \rightarrow M_1(xP) + q_{i'}(P - xP) \qquad (1)$$

Here, the initial quark q_i with flavor i and momentum P undergoes a breakup into a "meson" $M_1 \equiv q_i\bar{q}_{i'}$ with momentum xP and a left-over quark $q_{i'}$ with flavor i' and momentum (1 - x)P (see Fig. 1). At each breakup, the quark momentum decreases. When it falls below a critical value μ[presumably of $O(m_\pi)$], the quark remains comfortably in a hadronic system, without any tendency to escape. At this stage, jet formation is complete.

It is important to note that in principle, all properties of a jet should be derivable, if one knows the fundamental breakup process. We now demonstrate how this is done quantitatively.

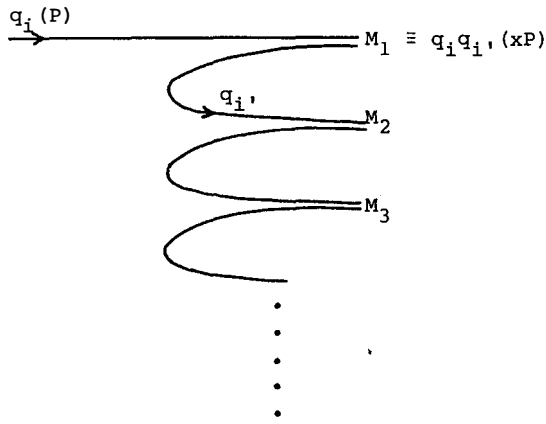

Figure 1 : The fragmentation of a quark $q_i(P)$ into a jet of mesons $M_1, M_2, M_3, \ldots$ in a standard cascade model. The mesons are formed in successive breakups of the form quark → "meson" + leftover quark.

For simplicity, let us first consider the case of one quark flavor only. Furthermore, for now, we ignore the complications due to quark masses and spins, the production of resonances and baryons, and the transverse momenta of particles in the jet. These complications can all be satisfactorily handled.[3,4] For our simplified, one-dimensional jet, the breakup process is fully described by a single function f(x), for which we have assumed scaling. Note that f(x)dx is the probability that a breakup yields a "meson" M with momentum fraction in the interval (x,x + dx). Since f(x) describes how the incident quark momentum is shared between the meson and leftover quark, we shall henceforth call it the "momentum sharing function". Clearly

$$\int_0^1 f(x)\,dx = 1 \ , \tag{2}$$

since each breakup gives one meson.

III - JET MULTIPLICITY, MOMENTUM DISTRIBUTIONS.

Since the cascade model is a recursive process, it is reasonable to expect that all quantities of physical interest satisfy appropriate integral equations. This is in fact the case. The meson multiplicity n(P) in a jet initiated by a quark with momentum $P \geq \mu$ satisfies the integral equation

$$n(P) = 1 + \int_{\mu/P}^1 dx' f(1-x') n(x'P) . \tag{3}$$

The term unity on the right hand side corresponds to the meson produced in the first breakup, and the integral corresponds to the multiplicity coming from the leftover quark, which has momentum x'P.

Similarly, if we denote the inclusive single-meson momentum distribution dn/dx by F(x), then for $P \geq \mu$, we have

$$F(x) = f(x) + \int_x^1 \frac{dx'}{x'} f(1-x') F(x/x') . \tag{4}$$

Again, the two terms in eq.(4) have a simple physical interpretation. The term f(x) corresponds to the possibility that a meson with momentum fraction x is formed in the first breakup. The integral corresponds to the possibility that the first breakup produces a

quark with momentum fraction $x' \geq x$, and this quark yields a meson at x in a subsequent breakup. Note that integrating eq. (4) over x yields the multiplicity integral eq. (3).

Similarly, the two-meson inclusive momentum distribution $dn/dx_1dx_2 \equiv G(x_1,x_2)$ satisfies the integral equation

$$G(x_1,x_2) = \frac{f(x_1)}{1-x_1} F\left[\frac{x_2}{1-x_1}\right] + \frac{f(x_2)}{1-x_2} F\left[\frac{x_1}{1-x_2}\right]$$

$$+ \int_{x_1+x_2}^{1} \frac{dx'}{x'^2} f(1-x') G\left[\frac{x_1}{x'}, \frac{x_2}{x'}\right] \qquad (5)$$

We now present the salient features of the solutions to integral eqs. (3) - (5). The general solution to the multiplicity integral equation (3) is

$$n(P) = \alpha \ell n\left(\frac{P}{\mu}\right) + 0\left(\frac{\mu^2}{P^2}\right) \; ; \quad \alpha = \frac{-1}{\int_0^1 dx' \, f(1-x') \ell n x'} \qquad (6)$$

Note the very general result that one always obtains logarithmic multiplicities at large energies for any choice of the momentum sharing function f(x). The slope α depends on f(x), and one can see that if f(x) is such that the meson tends to take a larger share of momentum in a breakup, then a smaller slope α results. Since $\ell n x'$ is large near $x' = 0$, the slope α is sensitive to the behavior of f(x) near $x = 1$.

Next, we solve integral eq.(4) for the meson distribution F(x). It is a linear Volterra equation of the second kind and a convergent solution is obtained by successive iteration.

$$F(x) = \sum_{j=1}^{\infty} F^{(j)}(x) \qquad (7)$$

where,

$$F^{(1)}(x) = f(x),$$

$$F^{(j+)}(x) = \int_x^1 \frac{dy}{y} f(1- x/y) F^{(j)}(y); (j=1,2,\ldots) \; . \qquad (8)$$

The index j in eq. (7) labels the breakup, in the sense that $F^{(j)}(x)$ is the contribution of the j^{th} breakup. Similarly, eq.(5) can also be solved iteratively to give $G(x_1,x_2)$.

The jet-initiating quark is of course a part of the "meson" M_1 produced in the first breakup. Let us note that if the contribution of the first breakup $F^{(1)}(x)$ behaves like $(1-x)^{\beta}$ as $x \to 1$, then it is easy to see that the contribution of the second breakup $F^{(2)}(x) \xrightarrow{x\to 1} (1-x)^{\beta+1}$, and in general $F^{(j+1)}(x) \xrightarrow{x\to 1} (1-x)^{\beta+j}$. Thus, one gets an extra factor of (1-x) at each breakup. We will make use of this simple rule later [in Sec. V] , when we examine the behavior of fragmentation functions as $x \to 1$.

In order to get a feel for the behavior of the inclusive distribution, let us consider the following simple but realistic choice for the momentum sharing function :

$$f(x) = (1+\beta)(1-x)^{\beta} \qquad (\beta \geq 0). \tag{9}$$

For this example, the multiplicity and momentum distributions are :

$$n(P) = (1+\beta)\ell nP + \text{constant} \tag{10}$$

$$dn/dx \equiv F(x) = (1+\beta)(1-x)^{\beta}/x \tag{11}$$

$$dn/dx_1dx_2 \equiv G(x_1,x_2) = (1+\beta)^2(1-x_1-x_2)^{\beta}/x_1x_2 \tag{12}$$

For concreteness, take the case $\beta = 1$ [which is roughly in agreement with e^+e^- inclusive meson distributions]. Fig. 2 shows how the full meson distribution $F(x) = 2(1-x)/x$ is built up from the contributions of successive breakups : $F^{(1)}(x) = f(x) = 2(1-x)$, $F^{(2)}(x) = 4(1-x+ x\ell nx)$, etc. Note that for $x \gtrsim .5$, truncation of the series solution [eq.(8)] after 2 breakups is adequate.

In the discussion above, we have solved integral eq.(4) by successive iteration, since each iteration corresponded physically to an additional breakup. An alternative mathematical procedure is to take Mellin transforms and treat the resulting algebraic equations.[1] This procedure can be profitably used in obtaining eqs. (10)-(12).

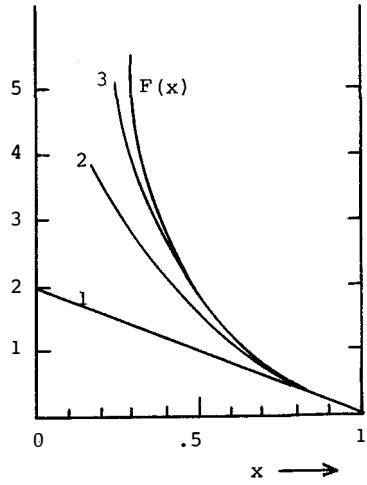

Figure 2 : A plot of the meson distribution for the momentum sharing function $f(x) = 2(1-x)$. The graph illustrates how successive breakups build up the full distribution $F(x) = 2(1-x)/x$. The first breakup gives curve 1, the first two breakups give curve 2, etc.

IV - LEADING PARTICLE EFFECT.

For this article, a leading particle is defined to be that having $x \geqslant \frac{1}{2}$. Consider those jets which contain a leading particle, and let us ask for the probability that the leading particle came from the first breakup and hence contains the jet-initiating quark. This probability r is given by[2]

$$r = \int_{1/2}^{1} f(x)dx \Big/ \int_{1/2}^{1} F(x)dx. \qquad (13)$$

For the realistic choice $f(x) = 2(1-x)$ of the previous section, $r = \cdot 6$. Therefore, in 4 events out of 10, the $x \geqslant \frac{1}{2}$ particle came from the second or subsequent breakup, and does not contain the quark which initiated the jet. By a similar calculation, it is easy to check that there is a high probability ($\simeq$ 85 %) that the

jet-initiating quark is contained in the fastest particle only if it has $x \gtrsim .75$. This is a useful, practical criterion which experimentalists can use for identifying the quark origin of a jet by looking at the fastest meson.

V - QUARK FRAGMENTATION FUNCTIONS AS $x \to 1$.

We now make the cascade model more realistic by allowing the quarks to have several possible flavors. [The treatment given below is for an arbitrary number N of quark flavors]. The momentum sharing function $f_{ii'}(x)$ acquires flavor indices [see eq.(1)], and this leads to matrix integral equations for quantities of physical interest. A detailed discussion can be found in Ref. (4).

It can be shown that the multiplicity of "mesons" $q_j\bar{q}_k$ produced from an initial quark q_i with momentum P is

$$n_{jk;i}(P) \sim (\alpha \, \mathbb{P}_{jk}/N) \ell n(P/\mu) \tag{14}$$

where,

$$\alpha = -N\Big[\sum_{i,i'=1}^{N} \int_0^1 dx \, f_{ii'}(x) \ell n(1-x)\Big]^{-1} \tag{15}$$

$$\mathbb{P}_{jk} \equiv \int_0^1 f_{jk}(x)dx. \tag{16}$$

The quantity $\mathbb{P}_{jk}$ is the probability of having a $(q_j \to q_k + "q_j\bar{q}_k")$ breakup, which corresponds to a connection between flavors j and k. Eq.(14) for the multiplicity is a generalization of eq.(6) to an arbitrary number of flavors. Note that the multiplicity is logarithmic and has a universal slope independent of the initial quark flavor i. This is a reasonable result when the multiplicity is large, since information about the initial flavor i gets diluted with each successive[9] breakup.

The momentum distributions (fragmentation functions) $F_{j\bar{k};i}(x)$ for various "mesons" $q_j\bar{q}_k$ can be found[4] by successive iteration. This gives a generalization of eqs. (7) and (8). Here, we wish to point out a simple general result as $x \to 1$. The point is more clearly made with an example. Consider the fragmentation functions of a d quark into π^+ and π^-. A $\pi^- = (\bar{u}d)$ can be produced in the first breakup, but in order to form a $\pi^+ = (u\bar{d})$, at least two

breakups are necessary. As we have seen in Sec. III, one gets an extra factor of (1-x) with each breakup. Therefore, as $x \to 1$, we have the simple rule

$$\frac{F_{\pi^+;d}}{F_{\pi^-;d}} \to p_{ud}(1-x) \qquad (17)$$

More generally, one can say that "unfavored" mesons have one power of (1-x) more than "favored" mesons - where "unfavored" refers to a meson which cannot be produced in the first breakup. This result is not affected by the presence of resonances in the jet[4]. Eq. (17) is very different from dimensional power counting,[5] where a ratio $(1-x)^4$ would be expected in the absence of resonances. However, phenomenological determinations of fragmentation functions[10] are consistent with the power of unity in eq.(17).

VI - FINDING THE JET AXIS.

Given a multiparticle event (for concreteness, we consider an e^+e^- collision), one would like to find the jet axis. The customary procedure[6,11] has been to compute the sphericity = $3 \Sigma_i p_{\perp i}^2 / 2 \Sigma_i p_i^2$ and define the jet axis to be that which minimizes the sphericity. Another recent proposal[7] has been to find the jet axis by minimizing the spherocity = $[4 \Sigma_i | p_{\perp i} | / \pi \Sigma_i p_i]^2$. So, it is very relevant to ask whether both methods give the same results, and to re-examine the criteria for finding the jet axis.

The sphericity method minimizes a quadratic expression $\Sigma_i p_{\perp i}^2$, whereas the spherocity method minimizes a linear combination $\Sigma_i | p_{\perp i} |$. In principle, an expression of any power $\Sigma_i p_{\perp i}^n$ can be minimized. However, note that if a particle with momentum $\vec{P}$ fragments into a jet, conservation of momentum implies that the particles in the jet have no net transverse momentum. In other words, the physics criterion for determining the jet axis is to require conservation of transverse momentum - the jet axis being the one such that $\Sigma_i p_{\perp i} = 0$. This is the correct procedure if one knows all the particles in a jet.

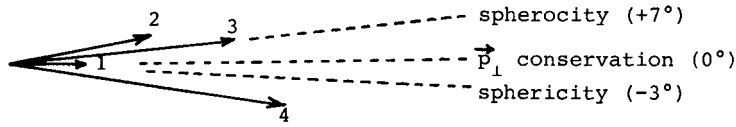

Figure 3 : A two-dimensional, four-particle jet with total momentum P = 10 GeV/c at 0°, and $< p_\perp >$ = .5 GeV/c. The components of momentum parallel and perpendicular to the 0° line are (1,0), (2,.5), (3,.5) and (4,-1). The axes obtained by minimizing sphericity and spherocity are marked.

As an illustrative example, consider the four-particle jet shown in Fig. 3. It has a total momentum P = 10 GeV/c and $<p_\perp>$ = .5GeV/c. Note the discrepancy between the true jet axis (0°) and the axes determined by minimizing sphericity (-3°) and spherocity (+7°). Although we have not made a detailed study of jets generated via Monte Carlo methods, it seems from numerous simple examples of jets with P = 10 GeV/c that the axis from minimizing sphericity is usually not too far from the true axis ($\Delta\theta \simeq 3°$), whereas spherocity minimization gives poor results ($\Delta\theta \simeq 8°$). This is presumably related to the fact that spherocity is not an analytic function of $p_{\perp i}$.

In principle, requiring $\sum_i p_{\perp i} = 0$ is the proper way of finding the jet axis if all the particles in a jet are known. In practice, in an e^+e^- event, one would need to cut each event into two hemispheres by a plane perpendicular to a trial jet axis, and take all particles in the hemisphere on the side of the axis as belonging to the jet. The true axis would be that trial axis which has $\sum_i p_{\perp i} = 0$. In such a procedure, there will often be an ambiguity about whether a particle in the middle (near the flat boundary between the two hemispheres) belongs to the jet

or not. This will always be the case in an e^+e^- collision, since a quark (or antiquark) jet must have a connection with the other hemisphere in order to conserve quantum numbers. This intrinsic uncertainty will give rise to a typical angular error given by

$$\Delta\theta \simeq \frac{\langle p_\perp \rangle}{|\vec{P}|} \tag{18}$$

and this could be present in most events. For $\langle p_\perp \rangle = .3\text{GeV/c}$ and a SPEAR energy $\sqrt{s} = 7.6$ GeV, $\Delta\theta_{SPEAR} \simeq 4.5^\circ$ whereas at a PETRA energy $\sqrt{s} = 20$ GeV, $\Delta\theta_{PETRA} \simeq 2^\circ$. This estimate indicates that, in practice, transverse momentum conservation and sphericity give reasonable determinations of the jet axis, but spherocity is not good. One must also keep in mind, that event by event there is an uncertainty in the jet axis given by eq.(18).

VII - FINDING NEW THRESHOLDS.

In this section, we discuss how the angular distribution of jets in e^+e^- collisions can be used to locate new thresholds at PETRA and PEP.[8] Assuming one photon exchange, the angular distribution of jets is given by[12]

$$\left.\frac{d\sigma}{d\Omega}\right|_{JETS} = \sum_i \left[A_i(s) + \cos^2\theta_J B_i(s)\right] \tag{19}$$

where, for spin $\frac{1}{2}$ quarks,

$$\begin{matrix} A_i(s) \\ B_i(s) \end{matrix} = \frac{q_i^2}{4s}\left[1 \pm \frac{4m_i^2}{s}\right]\left[1 - \frac{4m_i^2}{s}\right]^{\frac{1}{2}} \tag{20}$$

θ_J is the angle between the jet (i.e. quark) direction and the e^+e^- beams. The index i runs over all active flavors at energy $\sqrt{s}$. Note that when the energy is just above a new threshold at $s = 4m^2$, the contribution of the new quarks is spherically symmetric, whereas when $s >> 4m^2$, the contribution is $1 + \cos^2\theta_J$. In general,

$$\left.\frac{d\sigma}{d\Omega}\right|_{JETS} \sim \left[1 + \alpha_J(s)\cos^2\theta_J\right] \; ; \; \alpha_J(s) \equiv \sum_i B_i(s) / \sum_i A_i(s), \tag{21}$$

where $\alpha_J(s)$ is the eccentricity of the jet angular distribution.

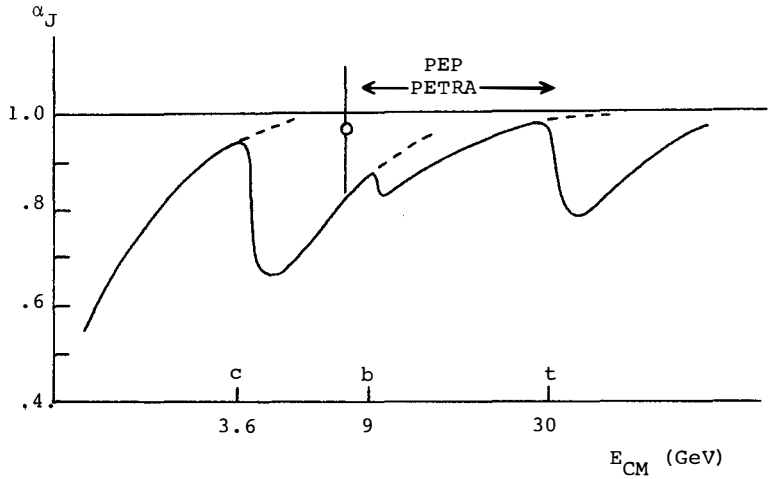

Figure 4 : A plot of the eccentricity α_J of the jet angular distribution (from quarks only) as a function of CM energy (on a logarithmic scale). Note that α_J takes a downward jump whenever a new threshold is crossed.

A reasonable choice for the masses of the strange, charm, and bottom quarks is m_s = .5GeV, m_c = 1.9 GeV, m_b = 4.5 GeV. This gives an eccentricity $\alpha_J(s)$ as shown in Fig. 4. The figure also shows the expected behavior of $\alpha_J(s)$ assuming the existence of a "top" quark of mass m_t = 15 GeV and charge + $\frac{2}{3}$. Note that whenever a new flavor threshold is passed, the angular distribution becomes more spherically symmetric and α_J takes a noticeable downward jump $\Delta\alpha_J$. This jump is not a local effect - the dashed lines in Fig. 4 show how α_J would have behaved if a new threshold had not appeared. The effect of a decrease in α_J due to a new threshold persists over a large energy range [the scale is set by $4m_i^2$ - see eq. (20)].

The sawteeth in $\alpha_J(s)$ correspond to the steps seen in the more conventional quantity $R \equiv \sigma(e^+e^- \rightarrow \text{hadrons})/\sigma(e^+e^- \rightarrow \mu^+\mu^-)$.

From eqs. (19) to (21), it follows that

$$\frac{\Delta\alpha_J}{\alpha_J} \simeq -\frac{\Delta R}{R} \tag{22}$$

Thus, detecting $\Delta\alpha_J$ is not a more sensitive method of finding new flavors than R, but as we shall see, it is an alternative method with numerous advantages.

How can α_J be determined from e^+e^- data ? The procedure used at SPEAR consists of an event-by-event sphericity analysis to find the jet axis.[6] This is tedious and not very accurate, but the value $\alpha_J = 0.97 \pm 0.14$ at $\sqrt{s} = 7.4$ GeV is consistent with Fig. 4. At higher energies, one expects jet structure to become more obvious and it should be possible to have a precise determination of α_J. However, we will now show that a considerably simpler method of finding α_J can also be used at high energies.

Consider the eccentricity α_M of the meson angular distribution $1 + \alpha_M(s)\cos^2\theta$ in e^+e^- collisions, and let us study how it is related to $\alpha_J(s)$. To do this, we take a simple factorized model for quark fragmentation into a meson jet.

$$D^{q\to M}(x, \mathbf{p}_\perp) = F(x) \exp\left[\frac{-\pi \mathbf{p}_\perp^2}{4\langle \mathbf{p}_\perp\rangle^2}\right] \tag{23}$$

For the one-dimensional case, $\langle \mathbf{p}_\perp\rangle = 0$, the mesons are aligned along the jet axis, and α_M equals α_J. This simple result is slightly altered in the realistic situation where $\langle \mathbf{p}_\perp\rangle$ is finite. One finds that the eccentricity of mesons with momentum $\mathbf{p} >> \langle \mathbf{p}_\perp\rangle$ is essentially equal to α_J. Physically, this result is qualitatively evident, and corresponds to saying that the fast particles in a jet are approximately on the jet axis. More quantitatively, if $\langle \mathbf{p}_\perp\rangle = .3$GeV/c, then $\alpha_M(\mathbf{p}) > .98\ \alpha_J$ for mesons with momenta $\mathbf{p} \gtrsim 3$ GeV/c. This provides an easy method of determining α_J.

If two identical hadronic detectors are placed at angles $\theta = \pi/2$ and θ, and mesons with $p \gtrsim 3$ GeV/c are counted, then the meson eccentricity is determined

$$\alpha_M(\mathbf{p} \gtrsim 3) = \frac{N(\theta) - N(\pi/2)}{N(\pi/2)\cos^2\theta} \tag{24}$$

It will show a drop in value with the appearance of each new threshold. Qualitatively, this remark is independent of all detailed assumptions going into our analysis. It simply says that the contribution of a specific particle-antiparticle pair just above its threshold is isotropic, but at higher energies becomes $(1 + \cos^2\theta)$. Quantitatively, the magnitude of the drop in $\alpha_M(p \gtrsim 3)$ is essentially given by eq. (22), but it also depends to some extent on our assumptions about quark fragmentation and jet multiplicities. This is, of course, a disadvantage compared to the traditional quantity R. However, there are numerous advantages too. In particular (i) one does not need 4π detection and no extrapolation into the blind regions of the detector (as is required for R). The angle θ can be chosen slightly away from the forward direction so as to avoid troublesome background problems, which are a major source of error in R ; (ii) one does not need to detect all the produced hadrons, and in fact the type of trigger mesons can be chosen at the experimenter's convenience (it is probably most easy to detect either all charged hadrons or only π°'s); (iii) since one only takes the ratio of hadronic quantities in eq.(24) to obtain $\alpha_M(p \gtrsim 3)$, normalization errors will be small. In particular, we will not have energy-dependent systematic effects (which cause considerable uncertainty in the determination of R).

The observation of structure in $\alpha_M(p \gtrsim 3)$ will correctly indicate the location in energy where interesting new physics lies. However, the interpretation of this structure (in terms of new quark flavors, new heavy leptons, resonances, etc.) will need further work.[8] Since α_M measurements have less energy-dependent systematic errors than R and can be carried out with available detection equipment, they are sepecially suitable for an initial energy scan at a new accelerator like PETRA or PEP in order to establish the existence of new physical effects.

I have profited from numerous discussions with my colleagues at Cambridge University and at Orsay. In particular, it is a pleasure to thank Prof. P.V. Landshoff, Prof. J.C. Polkinghorne and Prof. J. Tran Thanh Van for collaboration and helpful discussions on several topics treated in this article.

REFERENCES AND FOOTNOTES

1. A. Krzywicki and B. Petersson, Phys. Rev. D6, 924 (1972) ; J. Finkelstein and R. Peccei, Phys. Rev. D6, 2606 (1972) ; R. Jengo, A. Krzywicki and B. Petersson, Nucl. Phys. B65, 319 (1973) ; F. Niedermayer, Nucl. Phys. B79, 355 (1974) ; S. Matsuda, Phys. Rev. D12, 1940 (1975) ; H. Fukuda and C. Iso, Prog. Theo. Phys. 57, 483 (1977) ; O. Sawada and G. Takeda, Tohoku Univ. Preprint TU/77/166 (1977) ; A. Seiden, Phys. Lett. 68B, 157 (1977).

2. ". Sukhatme, Cambridge Univ. report DAMTP 77/25 (1977).

3. R. Feynman, Proc. VIII Int. Symposium on Multiparticle Dynamics, Kaysersberg (1977) ; R. Field and R. Feynman, Caltech preprint (1977).

4. U. Sukhatme, Phys. Lett. 73B, 478 (1978).

5. See, for example, S.J. Brodsky and J.F. Gunion, Phys. Rev. D17, 848 (1978).

6. G. Hanson, Proc. VII Int. Colloquium on Multiparticle Reactions, Tutzing (1976).

7. H. Georgi and M. Machacek, Phys. Rev. Lett. 39, 1237 (1977).

8. U. Sukhatme and J. Tran Thanh Van, Orsay preprint LPTPE 78/4 (1978) ; to be published in Phys. Lett.B.

9. The word "successive" refers to the ordering of breakups starting from the initial quark ; it is not meant to imply anything about the time development of a jet.

10. R. Field and R. Feynman, Phys. Rev. D15, 2590 (1977) ; L. M. Sehgal, Proc. Int. Symposium on Lepton and Photon Interactions, Hamburg (1977).

11. J.D. Bjorken and S. Brodsky, Phys. Rev. D1, 1416 (1970).

12. See, for example, J. Perez-Y-Jorba and F. Renard, Phys. Rep. 31C, 1(1977).

RL-78-030

T.216

MECHANISMS FOR TETRALEPTON PRODUCTION

R. J. N. Phillips

Rutherford Laboratory, Chilton, Didcot, Oxon, England.

Abstract: Mechanisms that might explain the reported tetralepton events in neutrino scattering are evaluated and compared. The CDHS $\nu N \to \mu^-\mu^-\mu^+\mu^+X$ event looks like normal charm production plus an electromagnetic $\mu^+\mu^-$ pair. The BHFSW $\bar{\nu}N \to \mu^+e^+e^-e^-X$ event may also be charm production plus vector meson decay to e^+e^-.

Résumé: Quelques mécanismes qui pourraient expliquer les événements tetraleptoniques sont évalués et confrontés aux résultats expérimentaux. L'événement $\nu N \to \mu^-\mu^-\mu^+\mu^+X$ du groupe CDHS, ainsi que l'événement $\bar{\nu}N \to \mu^+e^+e^-e^-X$ du groupe BHFSW, peut être interpreté comme production du charme plus une paire $\ell^+\ell^-$ d'origine électromagnétique ou hadronique.

Several tetralepton events have been reported; two $\nu N \to \mu^-\mu^-\mu^+\mu^+X$ from the CDHS and FHPRW groups and one $\bar{\nu}N \to \mu^+e^+e^-e^-X$ from the BHFSW group.[1)-3)] All so far have lepton charge signature --++. The rate is

$$\sigma(\nu \to 4\mu)/\sigma(\nu \to \mu) \sim 10^{-6} \tag{1}$$

within a factor 10 anyway, since CDHS see one 4μ to seventy 3μ events [4)] and quote a rate $\sim 5 \times 10^{-5}$ for the latter, for E > 30. Let us look at mechanisms that could give this signature and rate, concentrating mostly on the $\nu \to 4\mu$ case. (The results presented come from a collaboration with Vernon Barger and Tom Gottschalk at UW Madison.[5)])

Note that the 4μ mechanism does not have to explain the 3μ events too (the latter are pretty well understood already [4)]) but it must not predict 3μ too copiously or with wrong properties.

Quark Cascade (QC)

Suppose we have a third quark doublet

$$\begin{pmatrix} u \\ d \end{pmatrix}_L \quad \begin{pmatrix} c \\ s \end{pmatrix}_L \quad \begin{pmatrix} t \\ b \end{pmatrix}_L \tag{2}$$

where $m_b \sim 4.8$ GeV (so that T-resonances are $b\bar{b}$ composites) and $m_t \sim 8$ GeV say. Mixing of d,s,b is understood. Then neutrino production of t followed by cascade decay $t \to b \to c \to s$ can give 4-lepton events as shown in Fig. 1; there is a similar story for antineutrino production of $\bar{t}$. Other quark cascade possibilities exist [6)] but seem much less promising.

Some remarks.

i) Cascade decay is not inevitable; there are short-cuts like $t \to s$ or $t \to d$ (the couplings that manufactured t in the first place). Model-builders must take care with mixing angles and masses, to keep the cascade competitive.

ii) Tetralepton production is suppressed at low E by many things: by threshold kinematics (t is massive), by the slow-rescaling variable [7)] $x' = x + m_t^2/(2ME_\nu)$ that puts small-x' regions out of reach, and by lepton acceptance cuts $E_\ell > E_{min}$. Averaging over the CDHS or FHPRW spectra with E > 100 GeV, the QC mechanism can give a $\nu \to 4\mu$ rate of order 10^{-6} (the

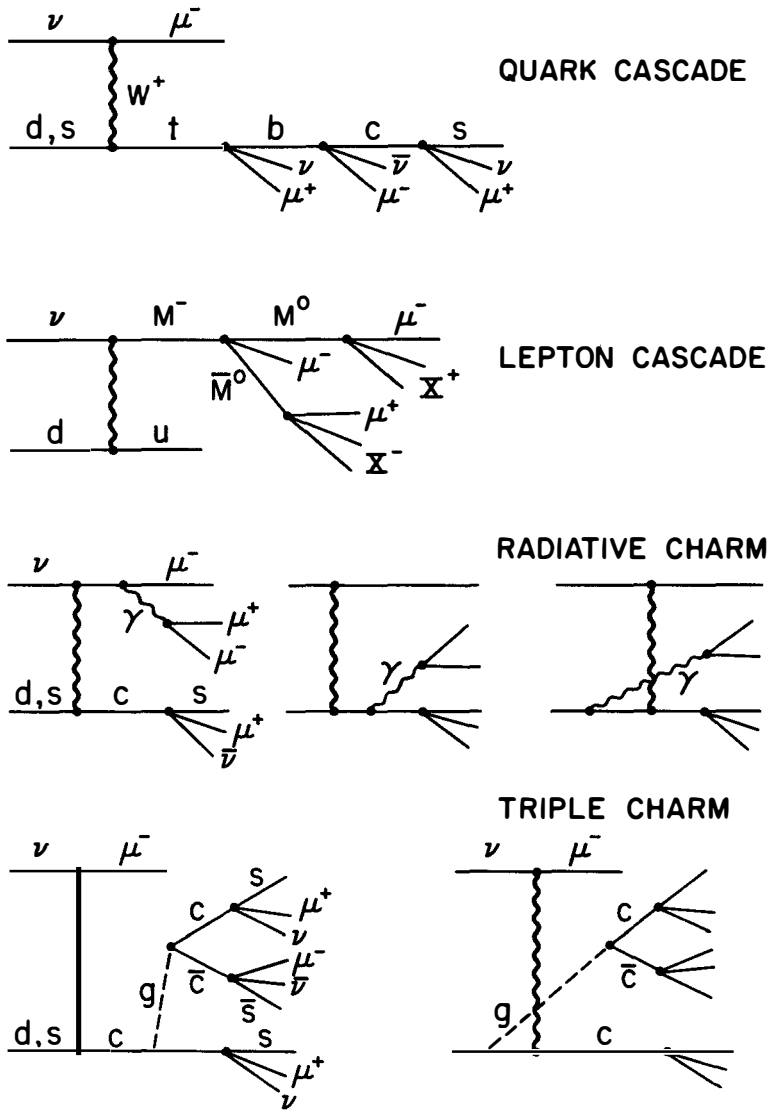

Figure 1: Mechanisms for $\nu \rightarrow 4\mu$ production.

asymptotic rate would be much more, the $\bar{\nu} \to 4\mu$ rate would be less).

iii) Wrong-sign trimuons. Because one of the decay steps could be hadronic instead of semileptonic, QC predicts

$$\sigma(\nu \to \mu^-\mu^+\mu^+)/\sigma(\nu \to 4\mu) \simeq 5 - 10 . \qquad (3)$$

CDHS sees essentially no wrong-sign trimuons (4 events with an expected contribution of 5 from dimuons plus π, K decays) compared to one tetramuon, which is bad news for QC.

iv) QC has a high threshold. For $m_t = 8$ it requires $E > 40$, $W > 8$ and cannot easily accommodate the BHFSW event [3] with $E_{vis} = 32$, $W_{vis} = 4$. (If $m_t < 8$ Lederman should have found toponium; if $m_t \approx m_b$ the cascade would not go.)

v) Calculated invariant mass distributions are shown in Fig. 2. The arrows correspond to the CDHS 4μ event : QC has difficulty explaining the lower of the $m(\mu^-\mu^-\mu^+)$ values.

In short QC is not very happy, either with wrong-sign trimuons or with the two tetralepton events for which we have numbers.

Lepton Cascade (LC)

Given two new heavy leptons M^-, M^o in the muon sector, we can get 4ℓ and 5ℓ events from $\nu N \to M^- X$ followed by $M^- \to M^o\mu^-\bar{\nu}^o$, $M^o \to \mu^- X^+$, $\bar{M}^o \to \mu^+ X^-$ (where $X^\pm$ can be $\mu^\pm\nu$, $e^\pm\nu$, or hadronic) as in Fig. 1.

Some remarks.

i) This can give a substantial $\nu \to 4\mu$ rate, as high as 10^{-5}, but only in a fancy scheme [8] with an extra lepton and right-handed couplings

$$\begin{pmatrix}\nu\\ \mu^-\end{pmatrix}_L \quad \begin{pmatrix}\mu^o\\ M^-\end{pmatrix}_L \quad \begin{pmatrix}M^o\\ \mu^-\end{pmatrix}_R \quad \begin{pmatrix}\mu^o\\ M^-\end{pmatrix}_R \qquad (4)$$

with mixing of the two L and two R doublets understood.

ii) Pentamuons: LC predicts

$$\sigma(\nu \to 5\mu)/\sigma(\nu \to 4\mu) \sim 0.1 - 0.2 . \qquad (5)$$

iii) "Wrong-sign" tetramuons: none have been reported but the statistics are small! LC predicts

$$\sigma(\nu \to \mu^-\mu^-\mu^-\mu^+) = \sigma(\nu \to \mu^-\mu^-\mu^+\mu^+) \qquad (6)$$

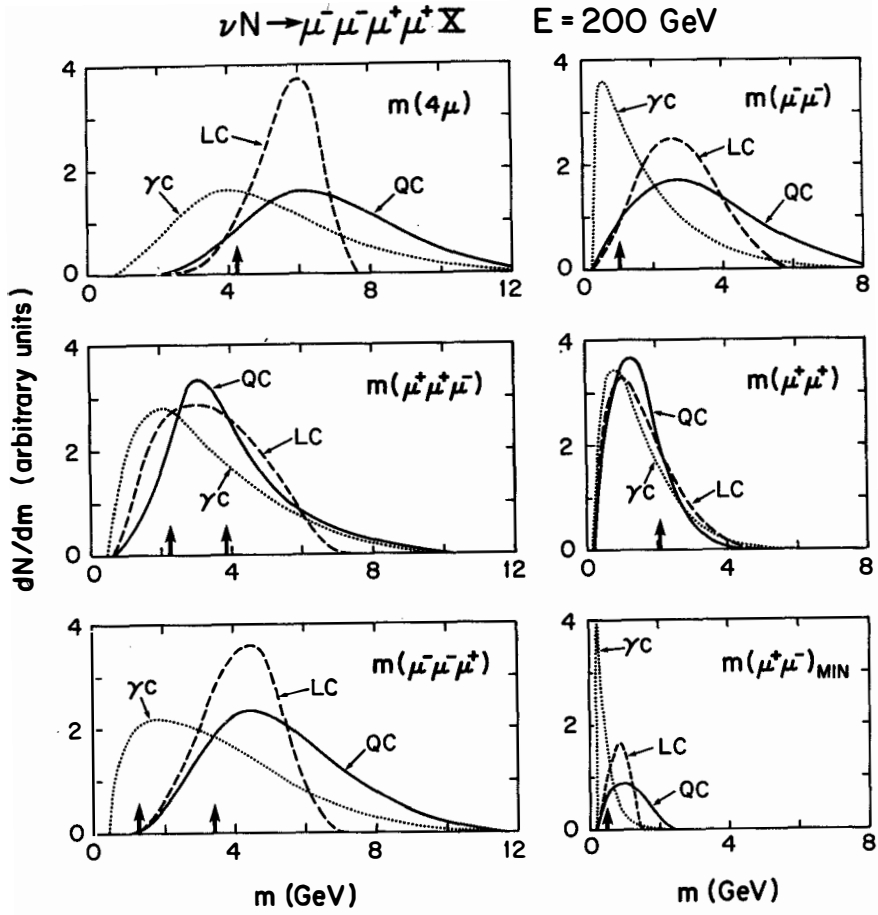

Figure 2: Invariant mass distributions in 4μ events for the QC, LC and γc mechanisms at E = 200 GeV (the E-dependence is not very strong for QC and γc, zero for LC). The arrows denote the corresponding values for the CDHS event with E_{vis} = 91 GeV.

iv) Since the scheme above does not allow $\bar{M}^o \to e^+X^-$ it does not give $\nu \to \mu^-e^-e^+e^+$ nor $\bar{\nu} \to \mu^+e^+e^-e^-$ like the BHFSW event. (We should have to introduce an extra E^o with $M^- \to M^oe^-\bar{E}^o$ and $\bar{E}^o \to e^+X^-$).

v) High threshold: with $m(M^-) > 5$ GeV as suggested by the CDHS event (where $m(4\mu) = 4.1$ GeV), the BHFSW event cannot be far above threshold with $E_{vis} = 32$.

vi) Invariant mass distributions are shown in Fig. 2, for $m(M^-) = 8$, $m(M^o) = 1.5$. The lower $m(\mu^-\mu^-\mu^+)$ value of the CDHS event looks incompatible with LC, but would look better with a lighter M^-.

Thus LC has theoretical and experimental drawbacks; it needs a lot of new leptons plus unfashionable right-handed couplings, and has threshold problems with the BHFSW event. The predicted 5μ and wrong-sign 4μ events are unique and characteristic, but remain to be seen.

Radiative Charm (γc)

Normal charm dimuon production $\nu d(s) \to \mu^- c$, $c \to d(s)\mu^+\nu$ becomes 4μ production when accompanied by a radiative $\mu^+\mu^-$ pair.

i) For gauge invariance, the calculation must include radiation from the initial and final interacting quarks as well as the direct μ^-, as shown in Fig. 1: these are the results reported here. This calculation [5] gives a rate

$$\sigma(\nu \to 4\mu)/\sigma(\nu \to \mu^-) \simeq 10^{-7} \qquad (7)$$

averaged over the CDHS or FHPRW spectrum with $E > 100$ GeV.

ii) In azimuthal correlations with the fast μ^-, which is usually the direct μ^-, γc gives a peak near $\Delta\phi = 0$ unlike QC or LC: see Fig. 3. This peak can be thought of loosely as coming from radiation off the direct μ^- (though in fact all three diagrams and their interference crossterms contribute nontrivially to produce the effect).

iii) Another γc characteristic is a narrow low-mass peak in the lowest of the four $\mu^+\mu^-$ invariant mass combinations, labelled $m(\mu^+\mu^-)_{MIN}$ in Fig. 2, due to the photon propagator that holds down the electromagnetic pair mass.

iv) The CDHS event accords quite well with this γc calculation; see especially the invariant masses in Fig. 2.

v) In addition to the above calculation, we expect further electromagnetic

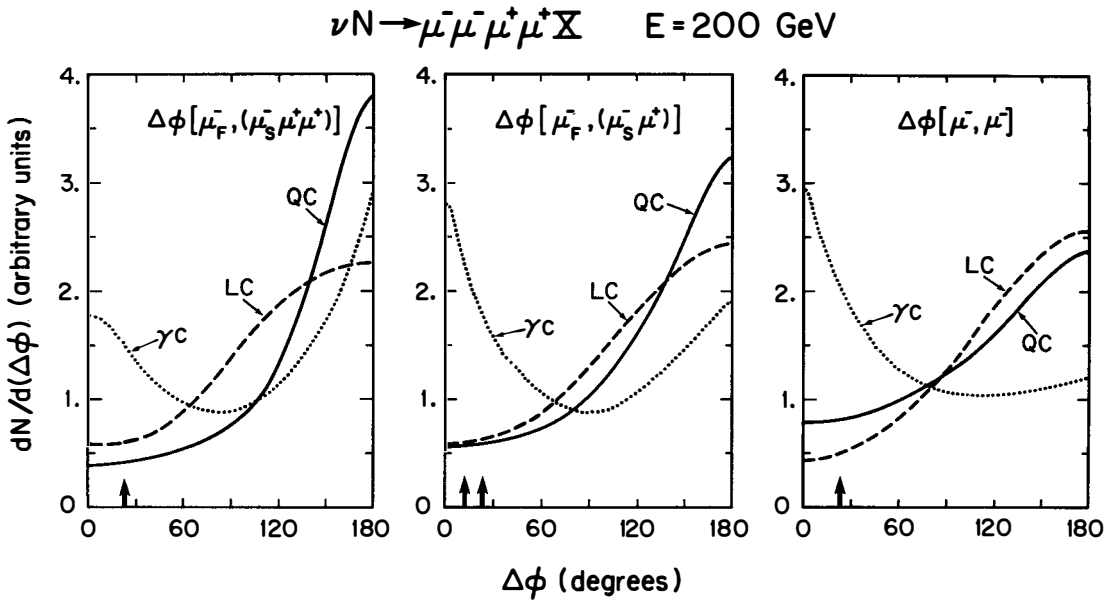

Figure 3: Azimuthal correlations about the beam axis in 4μ events, between the fast μ^- and the vector sum of other muon combinations, calculated at E = 200 GeV (the E-dependence is weak). The arrows denote values for the CDHS event.

pair contributions from the hadron vertex - from spectator quarks, from final-state enhancements, from vector meson production and decay $V^o \to \mu^+\mu^-$. These have not yet been calculated. In azimuthal correlations with the direct μ^- (Fig. 3), the additional contributions should appear near $\Delta\phi = 180^o$.

vi) γc has a low threshold, with or without hadron enhancement.

vii) The BHFSW event does not match the minimal γc calculation in (i) above, since the two possible e^+e^- pairings each have invariant mass of order 0.8 - 1.0 GeV. However it might be explained by charm plus hadronic pair enhancement as described in (v) with ρ, ω or $\phi \to e^+e^-$.

viii) Interpretation of the BHFSW event as charm plus $V \to e^+e^-$ is supported by some happy coincidences among the visible particles $\mu^+e^+e^-e^-K_s + 6\gamma$:

The six gammas reconstruct $3\pi^o$

One π^o with K_s reconstructs K^*

(Now add e^- and missing $\bar{\nu}$ to make $D \to K^*e\bar{\nu}$)

One π^o with D reconstructs D^*

A possible interpretation is then

$\bar{\nu}\bar{s} \to \mu^+\bar{c}$

$\quad \hookrightarrow$ fragments to $D^{*-} \to D^-\pi^o$

$\qquad\qquad \hookrightarrow K^{*o}e^-\bar{\nu}$

$\qquad\qquad\qquad \hookrightarrow K_s\pi^o$

additional fragment $V^o \to e^+e^-$

spectator sea quark $s \to$ fragments to $\Lambda \to n\pi^o$

[This was worked out during the Meeting, with Henry Lubatti and Toby Burnett.]

xi) Adding in the missing $\bar{\nu}$ energy above, the BHFSW event can have E = 40, x = 0.14 which look healthier for charm production from the sea than the raw $E_{vis} = 32$, $x_{vis} = 0.21$.

In short, charm production plus an electromagnetic pair (either from internal bremsstrahlung as in Fig. 1 or from a hadronic enhancement) seems the most promising explanation so far.

Triple-Charm

Normal charm production, accompanied by associated charm pair production via a gluon, can lead to 4-lepton events as in Fig. 1. However, calculation [5)]

in lowest-order QCD gives a very small rate

$$\sigma(\nu \to 4\mu)/\sigma(\nu \to \mu) \simeq 10^{-9} \qquad (8)$$

averaging over the CDHS or FHPRW spectrum with E → 100 GeV. We can ignore this mechanism.

Summary

i) Charm production plus a lepton pair (with or without hadronic enhancement) seems the most promising explanation.

ii) Both the 4-lepton events for which we have details seem compatible with the above interpretation, whereas they pose problems for QC and LC.

iii) Absence of wrong-sign trimuons is another bad sign for QC.

iv) Absence of wrong-sign tetramuons and pentamuons (not yet established) would be further bad signs for LC.

v) LC needs numerous new leptons and V + A currents - an aesthetic bad sign?

vi) Triple-charm gives a negligible 4-lepton rate, at least with present methods of calculation.

References

1) CERN-Dortmund-Heidelberg-Saclay group: Phys. Letters 73B, 105 (1978).
2) FNAL-Harvard-Pennsylvania-Rutgers-Wisconsin group: private communications from D. Cline and T. Y. Ling. There are said to be further 4μ candidates too.
3) Berkeley-Hawaii-FNAL-Seattle-Wisconsin collaboration: see report to this meeting by H. Lubatti.
4) See report to this meeting by K. Kleinknecht.
5) V. Barger, T. Gottschalk and R. Phillips, "Sources of tetramuon production by neutrinos", to be published in Phys. Letters B.
6) J. Ellis et al., Nucl. Phys. B131, 285 (1977).
7) R. Barnett, Phys. Rev. Letters 36, 1163 (1976); H. Georgi and H. D. Politzer, Phys. Rev. Letters 36, 1281 (1976).
8) A. De Rujula et al., Phys. Rev. D17, 151 (1978).

THEORETICAL MODELS FOR MULTIMUON EVENTS

J. Smith
Institute for Theoretical Physics
State University of New York at
Stony Brook, N.Y. 11794

ABSTRACT: We discuss the consistency between the trimuon event rates reported by the CDHS and FHPRW groups. Then we make some comments on models for the electromagnetic and hadronic production of trimuons.

RESUME: Nous presentons une comparaison entre les resultats des groupes CDHS et FHPRW sur les mesures de la fraction $\sigma(3\mu)/\sigma(\mu)$. Ensuite nous ferons quelques remarques sur les models théorique pour la production des événements avec trois μ par les mechanismes électromagnetiques et hadroniques.

1. INTRODUCTION

Multimuon events have been reported by several experimental groups, using both narrow- and wide-band neutrino and antineutrino beams. The first trimuon events were found in 1976 by the Caltech-Fermilab (CF) group.[1] Then thirteen events were recorded by the Fermilab-Harvard-Pennsylvania-Rutgers-Wisconsin (FHPRW) collaboration[2] and three were detected by the CERN-Dortmund-Heidelberg-Saclay (CDHS) group.[3] This morning we heard a report from the CDHS group[4] on the analysis of the 76 events recorded using wide-band neutrino beams. Both the CF and FHPRW groups have substantially enlarged their original detectors and are purported to have considerably increased their trimuon event samples. However, no results on rates or distributions are available yet.

Opposite sign dimuon events have been detected in considerable numbers. The origin of these events is now well understood to be due to the production and subsequent decay of charmed particles[5] so we will not discuss them further. The existence of a mechanism responsible for the production of like-sign dimuon events ($\mu^-\mu^-$ in a ν beam and $\mu^+\mu^+$ in a $\bar{\nu}$ beam) is not yet firmly established. Ling[7] has presented evidence for a $\mu^-\mu^-$ signal in the FHPRW experiment yielding $\sigma(\mu^-\mu^-)/\sigma(\mu^-) = (6\pm4) \times 10^{-4}$. More statistics are necessary to clarify the situation. This is an important question which, as we will see later, has direct bearing on the source of the trimuon events.

Tetramuon events[8] have also been seen. The rate for these events is very low and there are many possible production mechanisms. Further progress in understanding these events must await much higher statistics. Therefore in this talk I will discuss questions which are related primarily to the production of trimuon events. I will begin by discussing the compatibility between the experimental rates from the CDHS and FHPRW groups, then make some comments on the interpretation of the CDHS trimuon events presented this morning and finish by discussing the FHPRW super events.

2. EXPERIMENTAL RATES FOR $\mu^-\mu^-\mu^+$ EVENTS.

This morning both Ling and Kleinknecht gave sufficient information to allow us to make a careful comparison between the rates for trimuon production at Fermilab and at CERN. I remind you that the original uncorrected rate from the FHPRW group was $\sigma(3\mu)/\sigma(\mu) = 5 \times 10^{-4}$ for $E > 100$ GeV, with cuts of 4 GeV on each muon energy while the CDHS result was much smaller ($\sim 1 \times 10^{-4}$ based

on 3 events). The calculated single muon event rates (spectra multiplied by E) are shown in Fig. 1 for the FNAL quadrupole-triplet (QT) beam with 400 GeV protons and for the CERN wide-band beam (WBB) with 350 GeV protons, assuming 10^{13} protons on target. To normalize we scale the QT rate

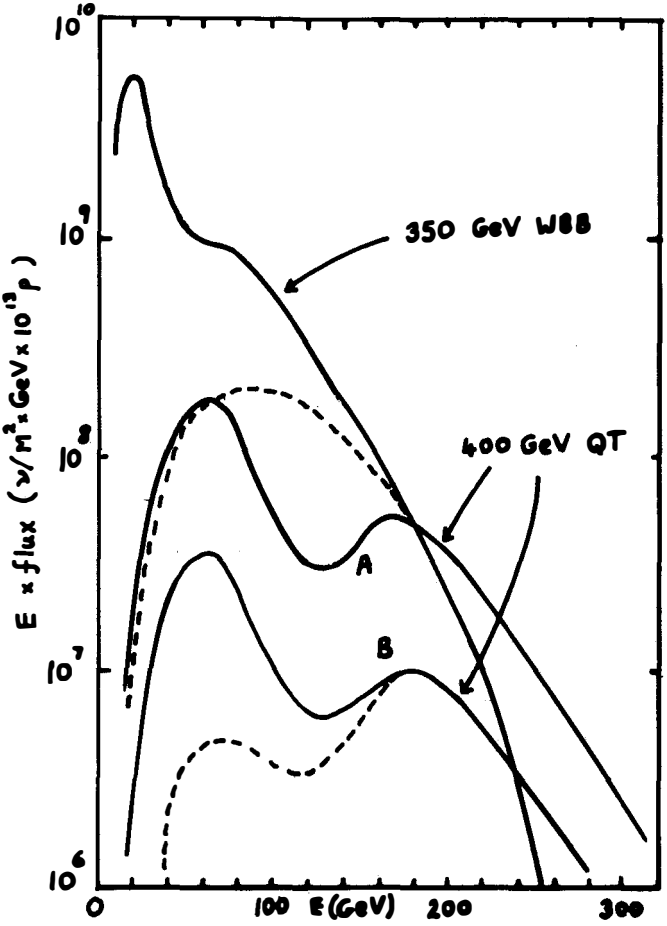

Fig.1 Single muon event rate for the CERN WBB (350 GeV protons) and the Fermilab QT beam (400 GeV protons). Curve A is normalized per 10^{13} incident protons for the same target mass. Curve B includes the ratio of fiducial volumes and the ratio of numbers of incident protons (see text). The dashed curves include trimuon acceptance factors and give the relative numbers of trimuon events.

down by a factor of 5.3 to take into account the relative differences in fiducial volume (660 tons for CDHS versus 300 tons for FHPRW) and protons on target (1.7×10^{18} for CDHS in the 350 GeV WBB run versus 0.7×10^{18} for FHPRW in the 400 GeV QT run.) Now to compare trimuon event rates, we still have to correct for the detection efficiency. This morning Kleinknecht showed the ratio of the trimuon acceptance as compared with the single muon acceptance for the CDHS experiment. The acceptance is essentially 100% at E =180 GeV and falls to 10% at E = 50 GeV. If we assume the same acceptance correction for the FHPRW experiment, which is a reasonable assumption because the energy cuts on the muons are similar, then the relative trimuon event rates can be plotted in Fig. 1 as a function of the neutrino energy. These are shown by the dashed lines up to E = 180 GeV and the solid lines above that energy. The two curves intersect at E = 240 GeV. Above this energy the FHPRW experiment can still see trimuon events in a small window out to E = 280 GeV.

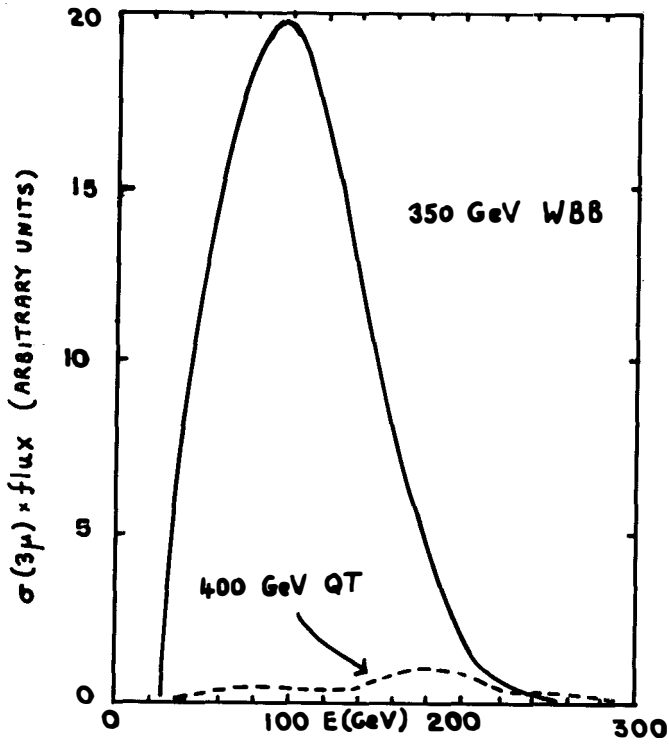

Fig. 2. Trimuon event rates for the CERN WBB (350 GeV protons) and the Fermilab QT beam (400 GeV protons).

To compare the rates we convert the semilogarithmic scale to a linear scale and replot the final curves in Fig. 2. Using the result that the CDHS group found 63 events in their 350 GeV WBB run and scaling by the relative area under the curves (factor of 17) we find that the FHPRW group should have seen 4 events in their 400 GeV QT run. They actually found 6 events which is consistent considering the small number of events expected. The rates reported in the previous talks are $\sigma(3\mu)/\sigma(\mu) = (26 \pm 15)\times 10^{-5}$ for FHPRW with $E > 100$ GeV which compares favorably with $\sigma(3\mu)/\sigma(\mu) = (9 \pm 2) \times 10^{-5}$ for CDHS with the same energy cut. These ratios decrease when we lower the neutrino energy cut due to the denominator becoming larger. The FHPRW group reported that $\sigma(3\mu)/\sigma(\mu) = (9 \pm 5) \times 10^{-5}$ for all E while CDHS reported $\sigma(3\mu)/\sigma(\mu) = 3.0 \times 10^{-5}$ for $E > 30$ GeV. We therefore conclude that the initial difference between the uncorrected FHPRW trimuon event rate and the CDHS trimuon event rate has essentially disappeared.

3. THEORETICAL MODELS FOR THE TRIMUON EVENTS

Many models have been proposed to explain the trimuon events and one can divide them into two broad classifications: namely, those that invoke new particles, leptons[9] or quarks[10] or both[11], and those that invoke more conventional production mechanisms.[12,13,14] The associated production of pairs

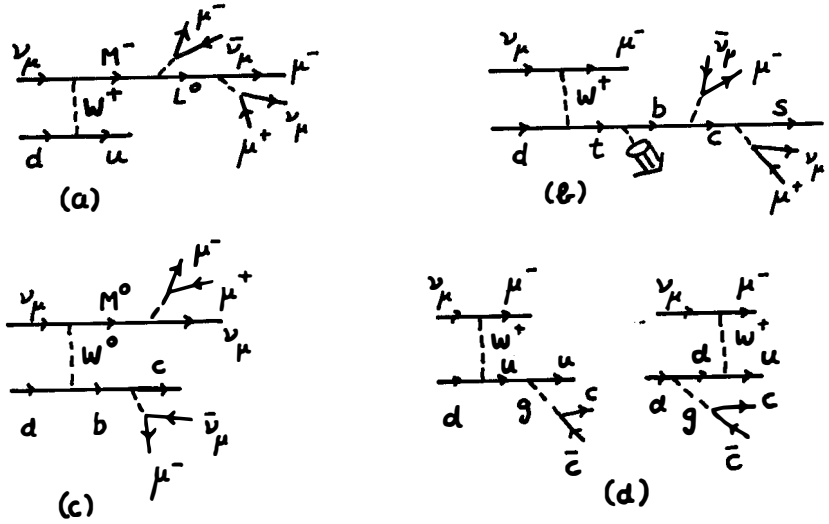

Fig. 3. Feynman diagrams for (a) heavy lepton production, (b) heavy quark production, (c) flavor changing M^0 and b production, and (d) associated production of pairs of charmed particles.

of charmed particles[13,14] will be included in the latter category because charm is by now reasonably well understood and is really part of old physics rather than new physics. Fig. 3 shows some of the mechanisms proposed.

The distributions presented by the CDHS group seem to rule out the necessity of invoking exotic explanations for the bulk of their events. We have seen that the transverse momenta of the muons with respect to the hadron shower direction are much smaller than one would expect from the decay of a heavy object (either lepton or quark). Also, the azimuthal correlation in $\phi = \phi_{1,(2+3)}$ between the leading μ^- and the vector sum of the other muon momenta, presented in Fig. 4, shows distinct forward and backward peaks (with respect to a z-axis along the direction of the neutrino). The backward peak agrees with the expectations from a hadronic source for the trimuon events because the slow dimuon pair would tend to follow the hadron

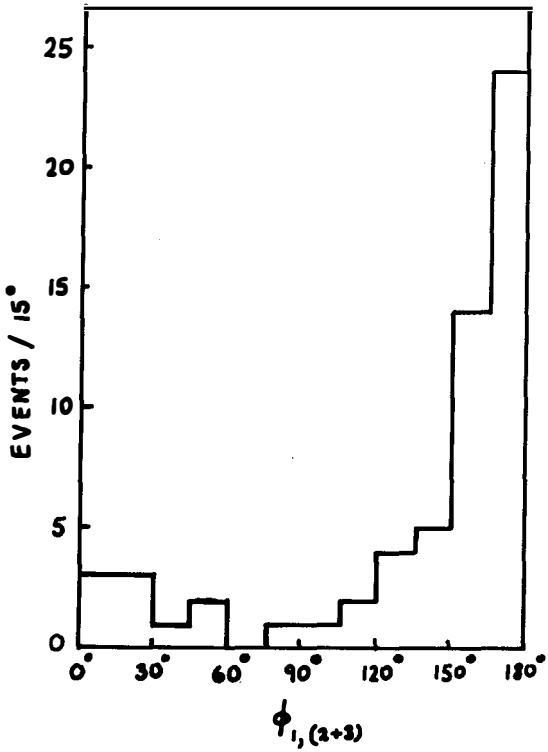

Fig. 4. Plot of the $\phi = \phi_{1,(2+3)}$ distributionfor the CDHS events.

shower (W-boson) direction which is oppositely correlated to the fast μ^- direction. Such a mechanism is depicted in Fig. 5. The forward peak is consistent with that expected from the electromagnetic radiation of a muon pair from the fast μ^-. However, in order to make the latter process satisfy the stringent requirement of electromagnetic gauge invariance one must calculate it[12] from the graphs shown in Fig. 6. Some radiation must be emitted by the accelerated hadrons (or quarks) so that there is a possibility of overcounting if one simply adds the cross sections calculated from the processes depicted in Figs. 5 and 6. The theoretical models all assume a

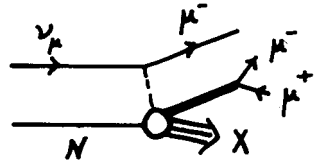

Fig. 5. Hadronic production of muon pairs in neutrino collisions.

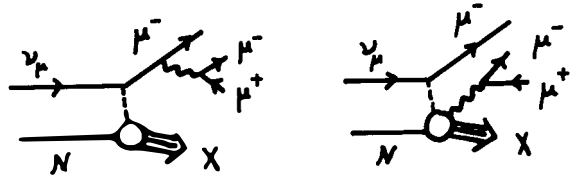

Fig. 6. Electromagnetic production of muon pairs in neutrino collisions.

bremsstrahlung type radiation from the up and down quarks and work in the quark parton model framework.

The CDHS group claim that the trimuon rates and distributions are consistent with the sum of the two processes given above. In particular they use a theoretical calculation for the electromagnetic reaction to fit their events at low ϕ and take over experimental data from hadronic dimuon production (reference 15) to fit their events at large ϕ. One needs an approximate event rate $\sigma(3\mu)/\sigma(\mu) \simeq 0.5 \times 10^{-5}$ to fit the low ϕ events (this checks with the fraction of the total electromagnetic trimuon production rate as calculated from Fig. 6) and $\sigma(3\mu)/\sigma(\mu) \simeq 2.5 \times 10^{-5}$ to fit the large ϕ events (i.e., the hadronic contribution.)

Regarding the electromagnetic rate for Dalitz pairs, there is little one can say. The calculations include the emission of soft photons, because all

the authors have taken a bremsstrahlung type approximation, in which only radiation from external charged particles (muons or quarks) is included, giving rise to a typical "soft photon" peak in the mass of the slow $\mu^+\mu^-$ pair. The precise nature of the hard photon coupling to the quarks in the parton model (or to the physical hadrons) is left unanswered because these are contributions to the large ϕ region where the hadronic rate is probably much larger. Here there are some unanswered questions. Both the vector and axial vector couplings of the W-boson presumably contribute to the trimuon production rate as calculated from Fig. 5, so, via vector dominance, one needs information on the production of $\mu^+\mu^-$ pairs by ρ, A_1 and π mesons. Although the CDHS group has used data from $\pi + p \to \mu^- + \mu^+ + X$ to fit their distributions, it would be more satisfactory to construct a model which fits the pion production of low mass muon pairs and then use this model in the neutrino channel. If the trimuon rate can be fitted in such a model then we can rule out the need for other contributions such as the associated production of charmed mesons.

Let us examine the recent data on the production of low mass muon pairs in πp collisions by Bunnell et al.[16] shown in Fig.7, (higher energy data are also available from Anderson, et al.[15], and have the same general features.)

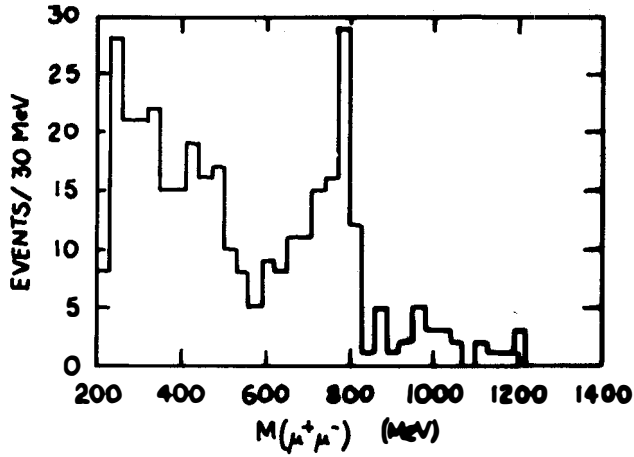

Fig.7. The $\mu^+\mu^-$ invariant mass distribution in $\pi p \to \mu^+\mu^- X$.

It is clear that the region in dimuon mass above 0.6 GeV is dominated by the production and decay of ρ mesons, while there is another large enhancement at very low masses. The physics in the latter region is presumably rather

complicated and must include contributions from the decays of ω- and η-mesons as well as direct photons. The dimuon invariant mass spectrum in pp collisions is very similar to that in πp collisions, as is presumably the case in ρp collisions. If we now assume that the vector and axial vector currents are dominated by almost on-shell ρ , A_1 and π mesons then the dimuon invariant mass spectrum in the trimuon events should possess similar features. This distribution is given in Fig. 8 for the CDHS events. Although there is evidence for an enhancement around the ρ mass, the resolution is not good enough to make any conclusive statement. However, a check on ρ-meson production will clearly be available soon from bubble chamber experiments. For instance, suppose that $\sigma(\nu N \to \mu^- \rho X)/\sigma(\nu N \to \mu^- X) = 15\%$ then using $\Gamma(\rho \to \mu^+\mu^-)/\Gamma(\rho \to \text{all}) = 7 \times 10^{-5}$, we would expect a trimuon event rate of $\sigma(3\mu)/\sigma(\mu) \sim 1 \times 10^{-5}$.

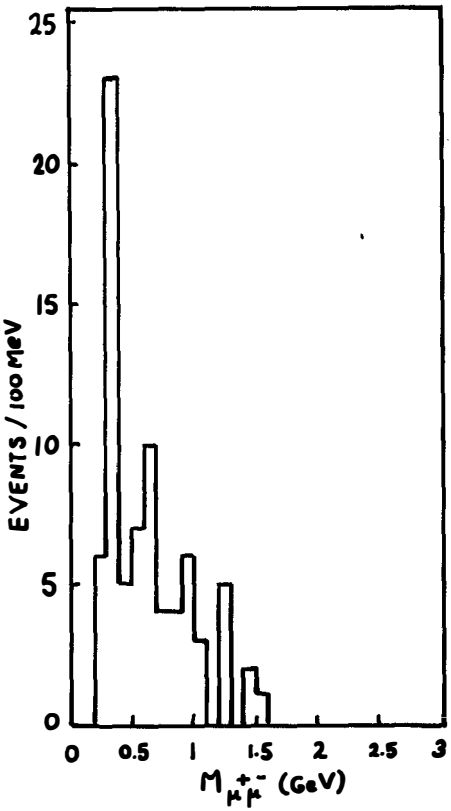

Fig. 8. The invariant mass of the nonleading μ^- and μ^+ in the CDHS experiment.

Unfortunately the only data on ρ mesons reported so far is on the diffractive production of ρ^+ mesons at Fermilab[17], whereas we need the cross section for the non-diffractive inclusive production of ρ^0-mesons.

Nevertheless, theoretical attempts should be made to calculate the excitation of dimuon pairs by the off-shell components of the vector and axial currents. The data can then be used to place restrictions on models and perhaps help us to check, via CVC, the amount of hadronic $\mu^+\mu^-$ production cross section expected in trimuon production by high energy muon and electron beams. The results for antineutrino production of $\mu^+\mu^+\mu^-$ events will also yield a check on the presence or absence of exotic mechanisms such as heavy quark or heavy lepton production. The hadronic plus electromagnetic explanation of these events will lead to $\sigma(\mu^+\mu^+\mu^-)/\sigma(\mu^+) \simeq \sigma(\mu^-\mu^-\mu^+)/\sigma(\mu^-)$.

Now we turn to a discussion of whether there is any evidence for the associated production of charm in the trimuon events. This question has not been addressed by the CDHS group because QCD calculations by both Goldberg and by Young, et al.,[14] reported rather low rates which, if taken at full value, are too small to explain the signal. However, it could be that associated production of charmed particles is larger than this QCD estimate. Remember that the associated production of pairs of strange particles has a relatively large rate in neutrino interactions. Nieh[13], in particular, has advocated that the diffractive production of pairs of charmed particles may account for the trimuon events. Now that there is a substantial number of events available, it is possible to compare results from Monte Carlo calculations of associated charm production and decay to see if the models can be excluded. Such a comparison has not yet been made.

Experimental results on the $\mu^-\mu^-$ event rate will be decisive in answering this remaining question. If all the trimuon event rate were due to $c\bar{c}$ production then we expect $\sigma(\mu^-\mu^-)/\sigma(\mu^-\mu^-\mu^+) \simeq 10$ because the branching ratio for a charmed meson to decay leptonically is approxiamtely 10%. This number is consistent with Ling's result that $\sigma(\mu^-\mu^-\mu^+)/\sigma(\mu^-) = (9\pm5) \times 10^{-5}$ and $\sigma(\mu^-\mu^-)/\sigma(\mu^-) = (6\pm4) \times 10^{-4}$. Further work is needed to either verify the latter number or reduce the limit on $\mu^-\mu^-$ production. If all the trimuon events are explained by either electromagnetic or hadronic production processes then $\sigma(\mu^-\mu^-)/\sigma(\mu^-\mu^-\mu^+)$ must be much lower than unity.

Before finishing this talk I would like to comment on the possibility that there is another source for some trimuon events which have been labelled "super-events" in the literature. Two events were found by the FHPRW group where the observed muon energies are large (157, 32 and 47 GeV) and (96, 73 and 83 GeV) respectively, while the observed hadron energies are small

(E_{had} = 13 GeV) and (E_{had} < 30 GeV), respectively. The first event, namely event 119, has a total visible energy of 249 GeV and the second event, let us call it 281, has $E_{vis} \simeq$ 260 GeV. From Fig. 1 we see that the QT neutrino flux is larger than the CERN WBB flux in this energy range. Is there possibly a new threshold at very large E so that events 119 and 281 signify the onset of some new physics?

Unfortunately the CDHS 400 GeV WBB run was so limited in terms of the number of protons on target that it did not settle the issue. When the larger sample of FHPRW trimuons are analyzed we will see if there is evidence for more events of this type. At present one can only examine the other more conventional physics processes to see the probability with which they can explain these events. Neither the electromagnetic nor the hadronic

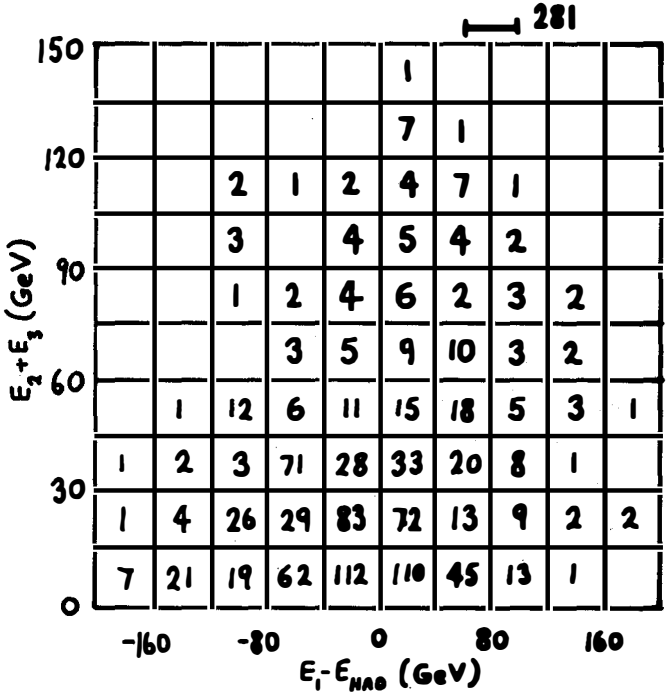

Fig. 9. Scatter plot of E_1-E_{had} versus $E_2 + E_3$ (the slow muon pair) for the electromagnetic production of muon pairs. We have folded the cross section with the QT spectrum but have not imposed any cuts on the muon energies or angles.

explanations are very successful. Regarding event 119, it is remarkable that the slow dimuon invariant mass is ≃ 3.1 GeV, so it cannot be of electromagnetic origin, but it could be the hadronic production of the J/ψ followed by its decay in a dimuon pair. In the data of Anderson et al.[15] the J/ψ peak in $M_{\mu^+\mu^-}$ is approximately two orders of magnitude below the ρ peak. If this explanation is correct, then we expect a rate of roughly one trimuon event in one thousand. The event 281 has a dimuon mass of ≃ 1.2 GeV so it could be of either electromagnetic or hadronic origin. If we examine our Monte Carlo results to find the probability that event 281 is of electromagnetic origin, then again we find probabilities of around one in one thousand. To demonstrate this probability we show in Fig. 9 a scatter plot of $E_1 - E_{had}$ versus $E_2 + E_3$, where E_1 equals the energy of the leading μ^-, to demonstrate that event 281 is on the edge of the allowed kinematic region for producing trimuon events.

We conclude by summarizing the main points of this talk.

1. The trimuon event rates reported by the FHPRW and CDHS experiments are now consistent.

2. The bulk of the events can be explained by electromagnetic and hadronic production mechanisms. More theoretical work is needed on hadronic models.

3. The associated production of charm is not necessary to explain the trimuon events but it could also be present. More experimental work is needed on the $\mu^-\mu^-$ event rate.

4. Super events occur with a very low probability. If more are found then probably some new process is responsible for them.

REFERENCES:

1. B. C. Barish, *et al.*, Phys. Rev. Letters 38, 577 (1977).
2. A. Benvenuti, *et al.*, Phys. Rev. Letters 38, 1110 (1977), 40, 432, 488 (1978).
3. M. Holder, *et al.*, Phys. Lett. 70 B, 393 (1977).
4. See contribution by K. Kleinknecht.
5. M. Holder, *et al.*, Phys. Lett. 69 B, 377 (1977).
6. M. Holder, *et al.*, Phys. Lett. 70 B, 396 (1977).
7. See contribution by T. Y. Ling.
8. M. Holder, *et al.*, Phys. Lett. 73B, 105 (1978).

9. C. H. Albright, J. Smith and J. A. M. Vermaseren, Phys. Rev. Letts. 38 1187 (1977); Phys. Rev. D16, 3182, 3204 (1977); Phys. Rev. (to be published); V. Barger, T. Gottschalk, D. V. Nanopoulos, J. Abad and R. J. N. Phillips, Phys. Rev. Letts. 38, 1190 (1977), Phys. Rev. D16, 2141 (1977).

10. A. Soni, Phys. Lett. 71B, 435 (1977).

11. R. M. Barnett and L. N. Chang, Phys. Lett. 72B, 233 (1977). V. Barger, T. Gottschalk, and R. J. N. Phillips, Phys. Lett. 70B, 243 (1977).

12. J. Smith and J. A. M. Vermaseren, Phys. Rev. D (to be published). V. Barger, T. Gottschalk and R. J. N. Phillips, Phys. Rev. D (to be published).

R. M. Barnett, L. N. Chang and N. Weiss, Phys. Rev. D. (to be published).

13. F. Bletzacker, H. T. Nieh and A. Soni, Phys. Rev. Letts. 38, 1241 (1977); F. Bletzacker and H. T. Nieh, Phys. Rev. D (to be published).

14. H. Goldberg, Phys. Rev. Lett. 39, 1598 (1977).

15. K. J. Anderson, *et al.*, Phys. Rev. Letts. 37, 799 (1976).

16. K. Bunnell, *et al.*, Phys. Rev. Letts. 40, 136 (1978).

17. J. Bell, *et al.*, Fermilab report, FERMILAB-pub-78/24.

TWO BODY DECAYS OF CHARMED PARTICLES

L. MAIANI +

Laboratoire de Physique Théorique de l'Ecole Normale Supérieure, PARIS, France

and

Istituto Nazionale di Fisica Nucleare, ROMA, Italia

Abstract :

Exclusive weak decays of charmed mesons and baryons into simple two body channels are discussed within the framework of the parton model.

On discute les désintégrations faibles des mésons et des baryons charmés en états finals simples à deux particules dans le cadre du modèle des partons.

+ On leave of absence from : Istituto di Fisica G. Marconi,
Universita di Roma, Roma, Italia

INTRODUCTION :

A theory of weak non leptonic decays must necessarily overcome three different problems :

i) the determination of the weak currents which take part in the transition ;

ii) the construction of the effective Hamiltonian H_{eff} ;

iii) the computation of the matrix elements of H_{eff}, in the presence of strong interactions.

In a gauge theory of weak interactions, the weak currents are fixed by the choice of the gauge group and by the assignment of the different quark fields to group multiplets. The structure of the weak currents thus obtained can be subjected to independent tests in semileptonic processes, and it can thus be regarded as an independent input.

Furthermore, the effective Hamiltonian H_{eff} is also given in terms of intermediate boson exchange [1]:

$$H_{eff} = g_W^2 \int d^4x \; T(J_\mu(x) \; J^+_\nu(o)) \; \Delta(x^2, M_W^2) \, g^{\mu\nu} \qquad (1)$$

g_W is the weak gauge coupling constant, $g^{\mu\nu}\Delta(x^2, M_W^2)$ the relevant W propagation function (eq. (1) applies to flavour changing processes in the standard $SU(2) \otimes U(1)$ model, [2] where only the charged W contributes ; in more complicated cases, one might have to add further terms corresponding to the exchange of additional W 's and possibly of Higgs mesons).

The non local Hamiltonian eq. (1) reduces to a local one if we are interested (as we are) only in the leading terms, in the limit $M_W \to \infty$ It was pointed out long ago by K. Wilson [3] that the resulting H_{eff} is determined by the short-distance behaviour of the strong interactions. This is so because the propagation function $\Delta(x^2, M_W^2)$ cuts off all contributions coming from distances $x^2 > M_W^{-2}$. In an asymptotically free theory of the strong interactions, such as QCD, the short-distance renormalization effects can in turn be controlled [4] and therefore, one can complete step ii) arriving at a well defined, local, effective Hamiltonian.

Step iii) is at present the most difficult to accomplish. For the decays of the particles associated with a heavy flavour (such as charmed particles), one can resort to the parton model. The parton picture has indeed been applied to predict the inclusive non leptonic and semileptonic rates [5-9].

In this lecture, I will discuss the predictions one can obtain for the decay amplitudes of a charmed particle into some exclusive channels. The

channels considered are those which can be formed by a simple rearrangement into uncoloured hadrons of the quarks and antiquarks present after the point-like interaction induced by H_{eff} has taken place (to a good approximation, the interaction will be just the point-like decay of the heavy quark).

The decays that can be treated in this way include :
i) the decay of a charmed pseudoscalar (D,F) into two pseudoscalar mesons (PP), into one pseudoscalar and one vector meson (PV) and into two vector mesons (VV) ;
ii) the decay of a charmed baryon into one stable baryon and one pseudoscalar meson (BP).

It turns out that, within the quark rearrangement model [10,11,12] the ratios of the amplitudes in a channel of a given type are determined in terms of the structure of H_{eff} and of a few phenomenological parameters. In particular, no new parameter is needed for the PP channels which thus offer the cleanest test of the model. Many predictions result, which, hopefully will be tested in the near future. At the moment, the only test of the model is given by the ratio of $B(D^+ \to \bar{K}^0 \pi^+)$ versus $B(D^0 \to K^- \pi^+)$. The experimental ratio agrees, within errors, with what is predicted.

If one is willing to introduce further more questionable assumptions, the relative normalization of (PV) and (VV) with respect to (PP) amplitudes can be estimated. Eventually, one might be able to obtain an absolute determination of the (PP) amplitudes, such as that given in ref. 10 , although at present this is on a much less secure ground than the predictions of relative ratios within channels of a given type.

In accomplishing both steps ii) and iii), a crucial role is played by the energy scale at which the process takes place (i.e. the mass m of the decaying quark). The larger m is, and provided $m \ll M_W$, all the approximations we shall make are better satisfied . At the charm mass, one should already be safe, and this is why a simple picture of $\Delta C \neq 0$ non leptonic decays can be achieved. Of course, the same picture should work even better for the heavier flavour which is to be associated with the Y resonance. On the other side of the energy scale, there are strange particle decays for which all the approximations become dubious. The situation is still somewhat controversial and it would not be appropriate to discuss it here (see nonetheless ref. 13 for recent remarkable progress).

1. The weak current :

Without discussion, I will accept the standard $SU(2) \otimes U(1)$ model Neglecting any mixing of the charmed quark with further heavier flavours (t, t' etc), and setting to zero the Cabibbo angle, the relevant charged

current is :

$$J_\mu(x) = \sum_i \left[\bar{u}^i(x)\,\gamma_\mu\,(1-\gamma_5)\,d_i(x) + \bar{c}(x)^i\,\gamma_\mu\,(1-\gamma_5)\,s_i(x)\right] \equiv$$

$$\equiv \bar{u}_L\gamma_\mu d_L + \bar{c}_L\gamma_\mu s_L \qquad (2)$$

where i = 1,2,3 is the colour index.

2. The effective Hamiltonian :

Inserting eq. (2) into eq. (1), one obtains :

$$H_{eff} = g^2_W \int d^4x\; T\left[(\bar{c}_L\gamma_\mu s_L)(x)\,(\bar{d}_L\gamma_\mu u_L)(o)\right]\;\Delta(x^2, M^2_W) \qquad (3)$$

The derivation of the $M_W \to \infty$ behaviour of eq.(3) is by now well known [4] I shall give directly the final result for two cases.

a) No strong interactions : Eq. (3) yields the naive current-current interaction

$$H^{(o)}_{eff} = \frac{G}{\sqrt{2}}\,(\bar{c}_L\gamma_\mu s_L)\,(\bar{d}_L\gamma_\mu u_L)$$

$$\frac{G}{\sqrt{2}} = \frac{g^2_W}{M^2_W} \qquad (4)$$

Eq. (4) can be also rewritten as (we drop from now on the γ_μ 's and the subscript L) :

$$H^{(o)}_{eff} = \frac{G}{\sqrt{2}}\,(H_+ + H_-)$$

$$H_\pm = \frac{1}{2}\left[(\bar{c}\,s)\,(\bar{d}\,u) \pm (\bar{c}\,u)\,(\bar{d}\,s)\right] \qquad (5)$$

b) Quantum chromodynamics : The resulting H_{eff} is again a superposition of $H_\pm$

$$H_{eff} = \frac{G}{\sqrt{2}}\,(f_+ H_+ + f_- H_-) \qquad (6)$$

with $f_+ < 1 < f_-$, as a result of strong interaction renormalization. The coefficients $f_\pm$ are given explicitly by the expressions :

$$f_{\pm} = \left[\frac{\alpha_S (m^2)}{\alpha_S (M^2_W)} \right]^{\gamma_{\pm}} \left[1 + 0 (\alpha_S(m^2)) \right]$$

$$\gamma_- = -2\gamma_+ = \frac{12}{33 - 2F} \qquad (7)$$

$\alpha_S(m^2)$ is the strong quark-gluon fine structure constant evaluated at the mass of the charmed quark ; F is the number of quark flavours with masses far below M_W. Furthermore :

$$\frac{\alpha_S (m^2)}{\alpha_S (M^2_W)} = 1 + \frac{33 - 2F}{12\pi} \alpha_S (m^2) \ln \frac{M^2_W}{m^2} \qquad (8)$$

We shall use $m \sim 1.5$ GeV, $\alpha_S(m) \sim 0.7$ (as taken form the scaling departures in deep inelastic scattering [14] and F = 6. From eqs.(7) and (8), and neglecting $O(\alpha_S(m^2))$ corrections, we obtain :

$$f_+ \simeq 0.68 \qquad f_- \simeq 2.15 \qquad (9)$$

It is necessary to stress that the above results are reliable provided :

i) $\ln \frac{M^2_W}{m^2} >> 1$

ii) $\frac{\alpha_S (m^2)}{\pi} << 1$

while condition i) is obeyed for all known flavours, condition ii) starts being reasonably satisfied at about the charm mass.

The two components of H_{eff}, namely $H_{\pm}$, behave differently under flavour SU(4) transformations [15]. H_- belongs to a 20-dimensional SU(4) representation, while H_+ belongs to a 84-dimensional one. At an earlier stage of the theory, a strong "20" dominance was assumed [5,6,7,16], in analogy with octet dominance for $\Delta S = 1$ decays. This would correspond to $f_- >> f_+$ and it is not considered any more as a valid approximation both theoretically (eq. (9) gives only a mild 20 dominance) and experimentally (see section 4).

3. Parton model description of inclusive rates :

The decay of a hadron containing a c-quark is described in the parton model as a two step process :

i) a hard interaction, induced by H_{eff} whereby the c-quark either decays into a $s\,u\,\bar{d}$ state or interacts with another quark (antiquark) in the initial hadron, to produce an uncharmed qq ($q\bar{q}$) pair.

ii) a soft, dressing process, where the parton final state evolves into normal hadrons.

Inclusive rates equal the total rate of step i). This picture should become increasingly more accurate, the larger the heavy quark mass.

Actually, as m becomes large, one gets a further simplification in that the quark-decay mechanism becomes increasingly more important than the quark interaction. This can be seen as follows. The rate for the quark-decay mechanism, computed form eq. (6) is :

$$\Gamma_{q\text{-decay}} \equiv \Gamma_{NL} = \Gamma(\mu \to e\,\nu\bar{\nu}) \left(\frac{m_c}{m_\mu}\right)^5 (2f_+^2 + f_-^2) \tag{10}$$

On the other hand, the rate for the quark-interaction mechanism must be proportional to $|\psi(o)|^2$, $\psi(o)$ being the wave function of the light quark (antiquark) at the origin, where the c-quark is. By dimensional arguments we see therefore that :

$$\Gamma_{q\text{-int}} \sim \frac{|\psi(o)|^2}{m_c^3}\ \Gamma_{q\text{-decay}} \tag{11}$$

We do not expect charmed hadrons to have a much smaller radius than uncharmed hadrons, so that

$$|\psi(o)|^2 \sim 1/R^3_{Nucleon} \sim m_\pi^3 \text{ (or perhaps } m_\rho^3 \text{)}$$

and therefore $\Gamma_{q\text{-int}} \ll \Gamma_{q\text{-decay}}$

The consequences of quark decay dominance are :

i) equal lifetimes of all weakly decaying particles : one finds[17]

$$\tau_c = \tau(\mu \to e\,\nu\bar{\nu}) \left(\frac{m_\mu}{m_c}\right)^5 \frac{1}{2 + 2f_+^2 + f_-^2} \sim 5.10^{-13}\text{sec} \left(\frac{1.5\ \text{GeV}}{m_c}\right)^5 \tag{12}$$

ii) the semileptonic inclusive branching ratio can be computed to be :

$$B_{SL} = \frac{\Gamma(c \to e + \ldots)}{\Gamma_{tot}} = \frac{1}{2 + 2f_+^2 + f_-^2} \sim 13\ \% \tag{13}$$

The numerical values have been obtained by using eq. (9). While eq. (12) is as yet untested, the measured value of B_{SL} ranges at present [18] from 9% to 12%.

I shall assume in what follow that i) is satisfied. As a practical consequence, ratios of branching ratios are equal to ratios of absolute rates, even for different decaying particles.

4. Two body decays of charmed mesons :

We proceed now to study the decay of charmed particles into those exclusive final states which have a "nominal" quark and antiquark composition [19] equal to that of the parton quark state which results after the charmed quark disintegration. The simplest cases are those where a charmed meson decays into a pair of uncharmed pseudoscalar (P) or vector (V) mesons.

A computation of the absolute decay amplitudes would require a knowledge of the recombination amplitude of $q\bar{q}$ pair into a given meson, in the presence of strong interactions both between the members of the $q\bar{q}$ pair and with the other quarks. This is beyond present capabilities. We obviously must find some further simplification.

Let us preliminary rewrite eq. (6) as :

$$H_{eff} = \frac{G}{2\sqrt{2}} \left[(f_+ + f_-) \ (\bar{c}\, s) \ (\bar{d}\, u) \ + \right.$$

$$\left. (f_+ - f_-) \ (\bar{c}\, u) \ (\bar{d}\, s) \right] \equiv$$

$$\equiv \frac{G}{2\sqrt{2}} \left[(f_+ + f_-) \ H_1 \ + \ (f_+ - f_-) \ H_2 \right] \qquad (14)$$

and consider the contribution of H_1 to a given decay, say $D^0 \to \pi^+ K^-$. The parton process is given in Fig.1(a).

To form a π^+, the u and $\bar{d}$ quarks, which are in a colour singlet state, must be emitted together, with a small relative momentum, while the s quark picks up the spectator $\bar{u}$. The relative momentum between the two pairs is large (of order m_c). It may be reasonable, therefore, to neglect final state interactions (i.e. gluon exchange) between the $(u\bar{d})$ and the $(\bar{u}s)$ pairs. We are actually neglecting soft gluon exchange only. Hard gluons (energy $\gtrsim m_c$) have been taken into account in H_{eff}. This approximation does not give yet a means to compute the absolute amplitude, but, as we shall see in a moment, it allows us to compute the ratios of different amplitudes (neglecting flavour SU(3) breaking).

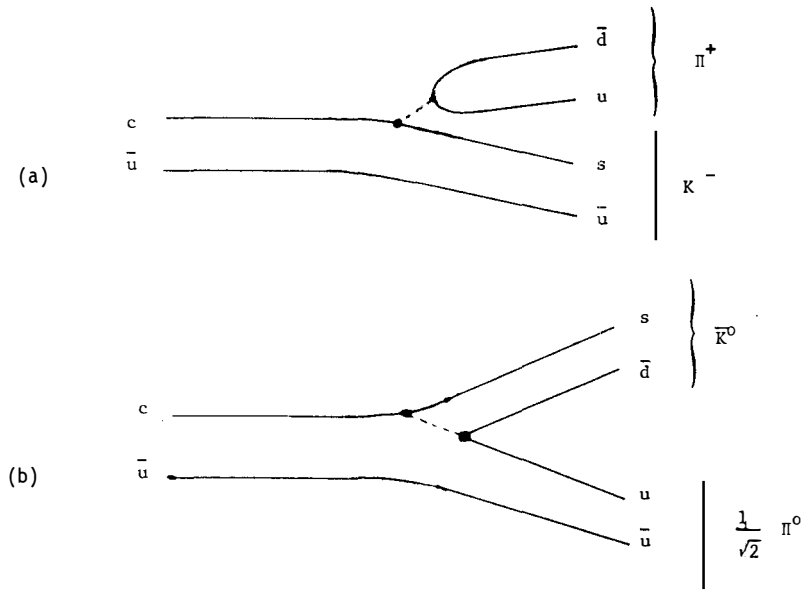

Fig. 1

Diagrams representing the contribution of H_1. Eq. (14) to $D^0 \to \pi^+ K^-$ (a) and to $D^0 \to \bar{K}^0 \pi^0$ (b). The quark pair originating from the dotted line is in a colour singlet state.

Let us denote by :

$$(f_+ + f_-)\ A \tag{15}$$

the contribution of $(f_+ + f_-)H_1$ to the amplitude for $D^0 \to \pi^+ K^-$, and consider $D^0 \to \pi^0 \bar{K}^0$ (Fig. 1(b)). The pairs with large relative momentum are now $(s\bar{d})$ and $(u\bar{u}) \equiv \frac{1}{\sqrt{2}} \pi^0$. To find the amplitude for this, we Fierz rearrange H_1, according to :

$$H_1 = (\bar{c}\ s)\ (\bar{d}\ u) = \frac{1}{3}\ (\bar{c}\ u)\ (\bar{d}\ s) + \frac{1}{2} \sum_{a=1}^{8} (\bar{c}\ \lambda^a\ u)\ (\bar{d}\ \lambda^a\ s)$$

The second term in the r.h.s. creates a $(\bar{d}s)$- pair in a colour octet, and this cannot be changed by final state interactions between $\bar{d}$ and s only. This term is therefore ineffective. The first one on the other hand contributes (apart from the colour factor 1/3) precisely in the same way as the full H_1

to $D^0 \to \pi^+ K^-$. We conclude that the contribution of $(f_+ + f_-)H_1$ to $D^0 \to \pi^0 \bar{K}^0$ is :

$$\frac{1}{3\sqrt{2}} (f_+ + f_-) \quad A \tag{16}$$

A being the same as in eq. (15) (in the limit of exact flavour SU(3) where we may neglect the difference between u and s quarks).

Along the same line, one can include the contribution of H_2 (see ref. 11 for more details) with the final result that all PP amplitudes of D^+, D^0 and F^+ can be given in terms of the single unknown amplitude A, the ratios depending only on the coefficients f_+ and f_-. The complete results are given in Table 1 where we also have reported the predicted branching ratios using $B(D^0 \to K^- \pi^+)$ as input, and allowing for a SU(3) breaking phase space factor proportional to the decay momentum. For convenience, we have used in Table 1 the combinations

$$X_+ = \frac{2}{3} f_+ + \frac{1}{3} f_- \quad \sim \quad 1.2$$

$$X_- = \frac{2}{3} f_+ - \frac{1}{3} f_- \quad \sim \quad -0.26 \tag{17}$$

TABLE 1 :

Amplitudes and branching ratios for PP decay modes. The amplitudes are given in units of A, eq. (15). Branching ratios are computed form the values of $X_\pm$ given in eq. (17) and using as an input the experimental value [22]
$B(D^0 \to K^- \pi^+) = (2.2 \pm 0.6)\%$. A phase space correction proportional to $|\vec{P}_{Decay}|$ has been included. The η meson has been taken to be a pure octet.

Decay mode	Amplitude	Branching ratio (%)
$D^+ \to \bar{K}^0 \pi^+$	$2(X_+ + X_-)$	1.3
$D^0 \to K^- \pi^+$	$2X_+$	2.2 (input)
$D^0 \to \bar{K}^0 \pi^0$	$\sqrt{2}X_-$	0.054
$D^0 \to \bar{K}^0 \eta$	$\sqrt{2/3}X_-$	0.016
$F^+ \to \eta \pi^+$	$-2\sqrt{2/3}X_+$	1.6
$F^+ \to K^+ \bar{K}^0$	$2X_-$	0.11

Concerning the results of Table 1, one may make the following observations :

i) the ratio of $D^0 \to K^- \pi^+$ to $D^+ \to \bar{K}^0 \pi^+$ is uniquely predicted [10,11] to be :

$$\frac{B(D^0 \to K^- \pi^+)}{B(D^+ \to \bar{K}^0 \pi^+)} = \frac{1}{4}\left(1 + \frac{f_-}{2 f_+}\right)^2 \sim 1.6 \qquad (18)$$

to be compared with the experimental value [22]: 1.5 ± 0.6.

The free Hamiltonian, eq. (4), would lead to a value of about 0.6, which seems excluded. Pure "20" dominance would predict $B(D^+ \to \bar{K}^0 \pi^+) \sim 0$ which is also excluded. Eq. (18) lends further support to the picture embodied in eqs. (6) and (9).

ii) given that $X_- << X_+$, one predicts a very peculiar pattern of suppressed transitions (the pattern would be similar in the free case, eq. (4)). In particular, $B(D^0 \to \bar{K}^0 \pi^0)$ should be very small [20], at variance with what is expected in the scheme of ref. (21). The observed decay $F^+ \to \eta \pi^+$ is not suppressed. We turn now to PV decays. If one repeats the previous arguments, one discovers that two amplitudes are needed. To see this consider again Fig. 1(a) and (b), as representing the contributions of $(f_+ + f_-)H_1$ to the decays $D^0 \to K^- \rho^+$ and $D^0 \to \bar{K}^0 \rho^0$, respectively. Call $(f_+ + f_-)B$ the amplitude from Fig. 1(a). Going again through the previous analysis, one sees that the contribution of Fig. 1(b) is

$$\frac{1}{3\sqrt{2}}(f_+ + f_-)B'$$

where B' differs from B in only one respect : in B, the spectator $\bar{u}$ goes into the P-meson, while in B' it goes into the V-meson. Setting $B' = Z\,B$, all ratios of PV amplitudes are given in terms of $f_\pm$ and Z (Table 2). No PV decay has been clearly seen yet. We postpone a further discussion of PV modes to the next section.

TABLE 2 :

Amplitudes and branching ratios for PV decay modes. The amplitudes are in units of B as defined in the text. Branching ratios are computed from $B(D^0 \to K^- \pi^+)$ according to the normalization factor, eq. (21) and with Z = 1. A phase space correction proportional to $|\vec{P}_{Decay}|^3$ has been included.

Decay mode	Amplitude	Branching ratio (%)
$D^+ \to \rho^+ \bar{K}^0$	$2(X_+ + ZX_-)$	1.4
$D^+ \to \bar{K}^{*0} \pi^+$	$2(ZX_+ + X_-)$	1.7
$D^0 \to K^{*-} \pi^+$	$2ZX_+$	2.7
$D^0 \to \rho^+ K^-$	$2X_+$	2.3
$D^0 \to \bar{K}^{*0} \pi^0$	$\sqrt{2}X_-$	0.067
$D^0 \to \bar{K}^{*0} \eta$	$\sqrt{2/3}X_-$	0.012
$D^0 \to \rho^0 \bar{K}^0$	$\sqrt{2}ZX_-$	0.058
$D^0 \to \omega \bar{K}^0$	$\sqrt{2}ZX_-$	0.056
$F^+ \to \varphi \pi^+$	$2ZX_+$	3.2
$F^+ \to \rho^+ \eta$	$-2\sqrt{2/3}X_+$	2.3
$F^+ \to K^{*+} \bar{K}^0$	$2ZX_-$	0.14
$F^+ \to \bar{K}^{*0} K^+$	$2X_-$	0.14

Finally, we consider VV decays. For each decay we have three helicity amplitudes corresponding to the two V mesons emitted both with helicity +1 or -1 or 0. Up to a common factor (A_+ , A_- , A_0) the decay amplitudes for a given helicity are given in terms of $f_\pm$ only, similarly to the PP case (see Table 3).

TABLE 3 :

VV decays of D and F. The first column gives the relative amplitudes for each halicity state. Branching ratios, second column, are computed as illustrated in the text. The last column gives the predicted values for the ratio R, defined in eq. (26).

Decay mode	Amplitude	Branching ratio (%)	R
$D^+ \to \rho^+ \bar{K}^{*0}$	$2(X_+ + X_-)$	2.1	2.3.
$D^0 \to \rho^+ K^{*-}$	$2X_+$	3.3	2.3
$D^0 \to \rho^0 \bar{K}^{*0}$	$\sqrt{2}X_-$	0.083	2.3
$D^0 \to \omega \bar{K}^{*0}$	$\sqrt{2}X_-$	0.078	2.2
$F^+ \to \rho^+ \varphi$	$2X_+$	4.1	2.6
$F^+ \to K^{*+} \bar{K}^{*0}$	$2X_-$	0.21	2.6

5. Relative normalizations :

By making further dynamical assumptions, one may obtain an estimate of the relative magnitudes of PV and VV with respect to PP amplitudes. The assumptions I will make [11] cannot be easily controlled, and the consequences we shall derive have to be taken with caution.

Consider the case of the D^0 meson. It is an S-wave bound state, so that, in some approximate sense, we may consider the spectator $\bar{u}$ quark to be localized at the position of the c-quark. If this makes sense, then the four final partons (after c-decay) can be considered to be emitted from the same space-time point, as if they were created by some local 4-fermion operator (a Lorentz scalar, since the initial state has zero spin). Given the chiral structure of the fields involved, there is only one possible operator, namely :

$$(f_+ + f_-)\ [\bar{u}\gamma_\mu(1-\gamma_5)s][\bar{d}\gamma^\mu(1-\gamma_5)u] \quad + \quad (f_+ - f_-)\ [\bar{u}\gamma_\mu(1-\gamma_5)u][\bar{d}\gamma^\mu(1-\gamma_5)s] \tag{19}$$

Our approximation consists in replacing (up to a normalization factor) the matrix elements of H_{eff} between a D^+ and PP, PV or VV state, by the matrix elements of the operator eq. (19) between the vacuum and the corresponding PP or PV or VV state. If we compute the latter matrix elements under the same approximation as in the previous section, we find e.g.

$$m(D^0 \to K^- \pi^+) = C(2X_+)\frac{M_D^2}{2} f_\pi f_K \tag{20}$$

$$m(D^0 \to K^- \rho^+) = C(2X_+)\frac{M_D^2}{2} \frac{\sqrt{2}\, m_\rho}{f_\rho} f_K \left[\frac{2|\vec{P}_\rho|}{M_D}\right] \tag{21}$$

$$m(D^0 \to K^{*-} \pi^+) = C(2X_+)\frac{M_D^2}{2} \frac{\sqrt{2}\, m_{K^*}}{f_{K^*}} f_\pi \left[\frac{2|\vec{P}_{K^*}|}{M_D}\right] \tag{22}$$

$$m(D^0 \to K^{*-} \rho^+) = C(2X_+)\frac{M_D^2}{2} \frac{2m_\rho\, m_{K^*}}{f_\rho\, f_{K^*}} \frac{2m_\rho\, m_{K^*}(\varepsilon_\rho \cdot \varepsilon_{K^*})}{M_D^2} \tag{23}$$

In the previous equations, we have used the definitions :

$$\langle \pi^+ | (\bar{u}\gamma_\mu\gamma_5 d) | 0 \rangle = f_\pi (P^\pi)_\mu$$

$$\langle \rho^+ | (\bar{u}\gamma_\mu d) | 0 \rangle = \sqrt{2}\langle \rho^0 | J_\mu^{e.m} | 0 \rangle = \frac{\sqrt{2}\, m_\rho^2}{f_\rho} \varepsilon_\mu$$

etc.

$\vec{P}_\rho$ ($\vec{P}_{K^*}$) is the appropriate rest-frame decay momentum, and C is an unknown normalization factor. The factors in square brackets, in eqs. (21) to (23), would be equal to one, in the limit $M_D \to \infty$, and give the dependence of the matrix element upon $\vec{P}_{Decay}$. The remaining factors, in the exact SU(3) limit, are to be identified with the amplitudes A, B, ZB, and A_+, A_-, A_0 previously introduced.

Comparing eqs. (21) and (22), in the SU(3) limit to the amplitudes of Table 2, we see that Z = 1 and that, furthermore :

$$\frac{B}{A} = \frac{\sqrt{2}\, m_\rho}{f_\rho\, f_\pi} \approx 1.6 \qquad (24)$$

The last column of Table 2 gives the predicted branching ratios for PV channels, computed from $B(D^0 \to K^- \pi^+)$ using both Z = 1 and the normalization factor, eq. (24) and allowing a phase space correction proportional to $|\vec{P}|^3$.

The contribution of PV channels to three-body D-decays (e.g. $D^+ \to K^- \pi^+ \pi^+$) can be easily computed from the tables [11]. The predictions thus obtained are compatible with the present lack of experimental evidence [23,24] for a PV signal in $D \to K \pi \pi$.

To compute the branching ratios for VV channels, we need f_{K^*}. One possibility is to assume :

$$\frac{m_{K^*}}{(f_{K^*})^2} = \frac{m_\rho}{(f_\rho)^2}$$

as suggested by the fact that the leptonic widths of ρ, ω, φ (and ψ) are in the SU(3) (SU(4)) ratios. Taking $f_K \sim 1.28\, f_\pi$ from experiment, one can use eq. (23) to compute the branching ratio for $D^0 \to \rho^+ K^{*-}$. The result is given in Table 3. For the branching ratios of the other channels, we have allowed for a phase space correction proportional to :

$$|\vec{P}_{Decay}| \cdot \Sigma\, (\varepsilon_1 \varepsilon_2)^2$$

From Tables 1 to 3, we see that comparable branching ratios are expected for similar PP, PV and VV channels (e.g. $F \to \varphi \pi$ and $F \to \varphi \rho$)

VV decays contribute to D and F decays into four pseudoscalar mesons. The only case where there is some experimental information is $D^0 \to K^- \pi^+ \pi^+ \pi^-$ where, essentially, no VV signal has been seen [23]. However, the only channel relevant here is $\bar{K}^{*0} \rho^0$, which is suppressed. The prediction is therefore not inconsistent with the observed null result.

Finally, eq. (23) can be used to estimate the ratio of the different helicity amplitudes in VV decay. Indeed, eq. (23) implies that :

$$|A_+|^2 : |A_-|^2 : |A_0|^2 = 1 : 1 : \frac{(M^2 - m_1^2 - m_2^2)^2}{4m_1^2 m_2^2} \qquad (25)$$

Therefore, we expect no parity violation (the probability for the two-V meson to be emitted both with helicity +1 equals that for helicity -1) and a dominance of the zero helicity amplitude. The latter feature could be tested by studying the angular distribution of the V-meson decay products where the quantity :

$$R = \frac{2|A_0|^2}{|A_+|^2 + |A_-|^2} \qquad (26)$$

can be determined. The values of R expected from eq. (25) are also given in Table 3. It is amusing that a predominance of the zero helicity amplitude results also from a different argument, based more directly on the quark parton picture. Consider $F \to \varphi \rho$. If we ignore the spectator $\bar{s}$ the helicity distribution of the $u\bar{d}$ pair which recoils against the s-quark in the point-like c-decay can be computed as a function of its invariant mass (μ). One finds:

$$|A_-|^2 = 0 \quad ; \quad |A_+|^2 = \frac{2\mu^2}{m_c^2} |A_0|^2$$

Setting $\mu = m_\rho$ and $m_c \sim 1.5$ GeV, one obtains a larger but similar value of $R (R \sim 3.8)$.

6. Charmed baryon two body decays :

Charmed baryon weak decays into a stable baryon and a pseudoscalar meson can also be analyzed within the quark rearrangement scheme sketched in section 4. I will just present the results [11].

Stable charmed baryons are expected to form an SU(3) antitriplet :

Λ_c^+ (c u d) ; N_c^+ (c u s) ; N_c^o (c d s)

For each decay channel, there are, as usual, two partial waves (S and P waves) and for each partial wave, two independent recombination amplitudes. Indeed the $\bar{d}$ emitted in c-decay must go into the meson, either with one of the quarks emitted in c-decay, or with one of the two spectator quarks. In the exact SU(3) limit, each partial wave amplitude is thus a combination of two unknown quantities, with coefficients given in Table 4.

TABLE 4

Coefficients of the amplitudes for charmed baryon BP decays. The S and P wave amplitudes of each mode are given by the combination

$$C_1 A_1^{S,P} + C_2 A_2^{S,P}$$

Decay mode	C_1	C_2
$\Lambda_c^+ \to \Lambda \pi^+$	$-2/\sqrt{6} X_+$	$f_- /\sqrt{6}$
$\Lambda_c^+ \to \Sigma^0 \pi^+$	0	$-f_- /\sqrt{2}$
$\Lambda_c^+ \to p \bar{K}^0$	X_-	0
$\Lambda_c^+ \to \Sigma^+ \eta$	0	$f_- \sqrt{6}$
$N_c^+ \to \Sigma^+ \bar{K}^0$	X_+	$-f_-$
$N_c^+ \to \Xi^0 \pi^+$	X_-	f_-
$N_c^0 \to \Lambda \bar{K}^0$	$X_- /\sqrt{6}$	$-f_- /\sqrt{6}$
$N_c^0 \to \Sigma^0 \bar{K}^0$	$X_- /\sqrt{2}$	$f_- /\sqrt{2}$
$N_c^0 \to \Xi^- \pi^+$	X_+	0
$N_c^0 \to \Xi^0 \pi^0$	0	$-f_- /\sqrt{2}$
$N_c^0 \to \Xi^0 \eta$	0	$f_- /\sqrt{6}$

Table 4 must be completed by the relations :

$$A(\Lambda_c^+ \to \Sigma^+ \pi^0) = A(\Lambda_c^+ \to \Sigma^0 \pi^+) \quad (\Delta I = 1 \text{ rule}) \tag{27}$$

$$A(\Lambda_c^+ \to \Xi^0 K^+) = 0 \quad (\text{Zweig rule}) \tag{28}$$

Many triangular relations can be obtained from Table 4. One such relation is interesting, namely :

$$A(\Lambda_C \to P\bar{K}_o) + \left(\frac{X_-}{\sqrt{2}\, X_+}\right)\left[\sqrt{3}\, A(\Lambda_C \to \Lambda\pi^+) + A(\Lambda_C \to \Sigma^o\pi^+)\right] = 0 \qquad (29)$$

(valid for both S and P waves). Since $X_- << X_+$, eq. (29) implies that the $P\bar{K}^o$ mode of the Λ_C^+ (which is expected to be the lightest charmed baryon) cannot dominate over the two-body decays involving a strange (Λ or Σ) baryon). This is the opposite of what has been seen in inclusive decays [24] where the Λ or Σ signals are much smaller than the P signal. Our model insists that, in spite of this, narrow two-body peaks should be more easily found in $\Lambda\pi$ or $\Sigma\pi$ states, rather than in $P\bar{K}$ states.

REFERENCES AND FOOTNOTES :

1 S. Weinberg, Phys. Rev. D8 (1973) 605 ; ibidem D8 (1973) 4482
D.V. Nanopoulos, Nuovo Cimento Lett. 8 (1973) 873
2 S. Weinberg, Phys. Rev. Letters 19 (1967) 1264
A. Salam, Proc. of the 8th Nobel Symposium, Stockholm 1968 (Amqvist and Wiksell, Stockholm 1968)
S.L. Glashow, J. Iliopoulos, L. Maiani, Phys. Rev. D2 (1970) 1285
3 K. Wilson, Phys. Rev. 179 (1969) 1499
4 M.K. Gaillard, B.W. Lee, Phys. Rev. Letters 33 (1974) 108
G. Altarelli, L. Maiani, Phys. Letters 52B, (1974) 351
5 M.K. Gaillard, B.W. Lee, J. Rosner, Rev. Mod. Phys. 47 (1975) 277
6 G. Altarelli, N. Cabibbo, L. Maiani, Nucl. Phys. B88 (1975) 285
7 S.R. Kingsley, S. Treiman, F. Wilczeck, A. Zee, Phys. Rev. D11 (1975) 1919
8 J. Ellis, M.K. Gaillard, D. Nanopoulos, Nucl. Phys. B100 (1975) 313
9 G. Altarelli, N. Cabibbo, L. Maiani, Phys. Rev. Letters 35 (1975) 635
10 D. Fakirov, B. Stech, Nucl. Nucl. Phys. B133 (1978) 315
11 N. Cabibbo, L. Maiani, Phys. Letters, 73B (1978) 418 ; the analysis given here of VV decays of D and F, and of BP decays of charmed baryons has been done in collaboration with N. Cabibbo and has also been reported by him at the SIN Spring School, Zuoz (Switzerland) March 1978.
12 T. Walsh, Proc. of the 1977 Int. Symp. on Lepton and Photon Int. at High Energy, Hamburg, 1977
13 M.A. Shifman, A.I. Vainshtein, V.I. Zakharov, Nucl. Phys. B120 (1977) 316 and ITEP preprints n. 63, 64 (JETP in press)
14 See e.g. G. Altarelli lectures, Proceedings of this meeting
15 This is why they can be differently affected by strong interactions even though at short distances QCD is SU(4) symmetric.
16 Predictions for the exclusive decays of charmed particles under the "20" dominance hypothesis have been reviewed by G. Altarelli, Xth Rencontre de Moriond 1975, vol. II.
17 In presence of a mixing of the charmed quark with heavier flavours τ_c should be multiplied by $(\cos\gamma)^{-2}$ γ being the mixing angle. See e.g. L. Maiani, Proc. of the 1977 Int. Symp. on Lepton and Photon Int. at High Energy, Hamburg 1977 and references therein
18 B_{SL} has been measured in various experiments performed at DORIS and SPEAR as discussed in the Proceedings of this meeting.
19 Counting, e.g. a $q\bar{q}$ pair for each meson etc.

20 The weak Hamiltonian eq. (6) (or eq. (4)) has pure $\Delta I = 1$, so that the amplitudes for $D^+ \to \bar{K}^0\pi^+$, and $D^0 \to K^-\pi^+$ or $\bar{K}^0\pi^0$ satisfy the triangular relation $\sqrt{2}\, A(D^0 \to \bar{K}^0\pi^0) = A(D^+ \to \bar{K}^0\pi^+) - A(0^0 \to K^-\pi^+)$. For $\Gamma(D^+ \to \bar{K}^0\pi^+)$ and $\Gamma(D^0 \to K^-\pi^+)$ nearly equal we have two solutions for $\Gamma(D^0 \to \bar{K}^0\pi^0)$: a large one which is the one selected in ref. (21) and a small one which is selected here.

21 H.R. Rubinstein, L. Stodolsky, F. Wagner, U. Wolff, Phys. Letters 73B (1978) 433
22 J.E. Wiss et al., Phys. Rev. Letters 37 (1976) 1531
23 M. Piccolo et al. Phys. Letters 70B (1977) 260
24 M. Piccolo et al. Phys. Rev. Letters 39 (1977) 1503

WEAK INTERACTIONS

J. D. Bjorken

Stanford Linear Accelerator Center
Stanford University, Stanford, California 94305, U.S.A.

In this talk we shall look at weak interactions from a phenomenological point of view.[1] Our aim is to describe the present situation concisely, using a minimal number of theoretical hypotheses. We first discuss charged-current phenomenology, and then neutral-current phenomenology. This all can be described in terms of a global SU(2) symmetry plus an electromagnetic correction. We then introduce the intermediate-boson hypothesis and infer lower bounds on the range of the weak force. (This inference turns out to be more general than the intermediate-boson hypothesis, but that is not discussed here in detail.)

It happens that this phenomenology does not yet reconstruct all the predictions of the conventional SU(2)×U(1) gauge theory. To do that requires an additional assumption of restoration of SU(2) symmetry at asymptotic energies. Finally we comment on the connection of this work to the usual point of view.

I. Charged Currents

All data on charged-current weak processes can be summarized in terms of an effective Lagrangian

$$\mathscr{L}_{\text{eff}} = \frac{G}{\sqrt{2}} J_\mu^+ J^{\mu-} \tag{1.1}$$

where the charged current $J_\mu^\pm$ is given by

$$J_\mu^\pm = \sum_F \bar{\psi}_F \gamma_\mu (1-\gamma_5) \tau^\pm \psi_F \tag{1.2}$$

and the fermion doublets ψ_F include

$$\psi_F = \begin{pmatrix} \nu_e \\ e^- \end{pmatrix}, \begin{pmatrix} \nu_\mu \\ \mu^- \end{pmatrix}, \begin{pmatrix} \nu_\tau \\ \tau^- \end{pmatrix}, \left(d\cos\theta_c^{\,u} + s\sin\theta_c \right), \left(s\cos\theta_c^{\,c} - d\cos\theta_c \right) \tag{1.3}$$

Not all of these terms are fully established, although there is good evidence in τ-decay, as presented at this meeting, for the left-handed V minus A assignment. Likewise the existence of the $\begin{pmatrix} c \\ s \end{pmatrix}$ left-handed current, of approximately universal strength, follows from the combined evidence from e^+e^- annihilation into $D\bar{D}$, followed by the semileptonic decay of the D, and from ν and $\bar{\nu}$ production of opposite-sign dileptons, with accompanying K-mesons. We do not know the precise normalization of the $\begin{pmatrix} \nu_\tau \\ \tau^- \end{pmatrix}$ and $\begin{pmatrix} c \\ s \end{pmatrix}$ contributions, nor do we yet know whether the s and d have the proper Cabibbo mixture in the charm-changing charged current. Nevertheless it is reasonable to assume these currents are also of universal strength, and that the degree of freedom s′ coupled to c is orthogonal to the degree of freedom d′ coupled to u. We do make these assumptions here.

II Neutral Currents

Given the above phenomenology for charged currents, two options for neutral current processes naturally present themselves. The first ("YES") option "completes" the current-current structure exhibited in Eq. (1.1) by supposing a global SU(2) symmetry controls the form of the total effective Lagrangian.[2]

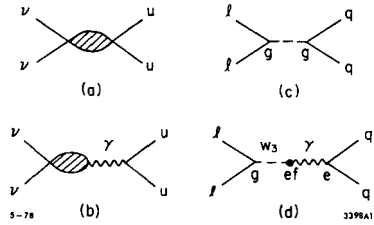

Fig. 1. Contributions to the weak interactions:
(a) "YES": intrinsic SU(2) invariant weak amplitude
(b) "NO": electromagnetic contribution
(c) "YES": intermediate boson hypothesis (pole dominance)
(d) "NO": intermediate boson hypothesis (pole dominance).

That is,

$$\mathscr{L}^{\text{"YES"}} = \frac{G}{4\sqrt{2}} \vec{J}_\mu \cdot \vec{J}^\mu \tag{2.1}$$

with

$$\vec{J}_\mu = \sum_F \bar{\psi}_F \gamma_\mu (1-\gamma_5) \vec{\tau} \psi_F \tag{2.2}$$

There appear no $\Delta S = 1$ neutral currents, because the GIM mechanism[3] applies: only the combination $\bar{s}\Gamma_\mu s + \bar{d}\Gamma_\mu d$ occurs in the neutral current, and this is invariant with respect to s-d mixing.

The second ("NO") option presumes no such intrinsic neutral current exists. In earlier times this option was prevalent because of the empirical absence of $\Delta S = 1$ neutral currents as well as the absence (in those times) of the GIM cancellation mechanism. However, even in this "NO" option, neutral currents will exist if only because of photon exchange.[4] The neutrino should possess a charge radius, i.e. its electromagnetic vertex function should not be identically zero:

$$e\Gamma_\lambda^{em}(q) \tilde{=} \bar{\nu}\gamma_\lambda \left(\frac{1-\gamma_5}{2}\right)\nu \cdot \frac{eq^2}{\Lambda^2} \tag{2.3}$$

This leads to a contact interaction between neutrino and charged matter quite analogous to the low-energy neutron-electron interaction. We easily obtain

$$\mathscr{L}_{NC}^{\text{"NO"}} = \frac{e^2}{2\Lambda^2} \bar{\nu} \gamma_\lambda (1-\gamma_5) \nu \, J_{em}^\lambda + \ldots \tag{2.4}$$

with J_λ^{em} the electromagnetic current-operator (at small momentum-transfer) for all charged matter, and the remaining terms (+...) describing similar contributions not involving neutrinos.

What is the right answer? Neither the "YES" answer (pure left-handed quark couplings) nor the "NO" answer (pure vector quark couplings) agrees with deep-inelastic neutrino-induced neutral-current data. Probably the right answer is the phenomenologically successful Weinberg-Salam effective Lagrangian.[5] For neutrino-induced neutral current processes it is given by

$$\mathscr{L}_{NC}^{W-S} = \frac{G}{2\sqrt{2}} \bar{\nu}_\mu \gamma_\lambda (1-\gamma_5) \nu_\mu \left\{ J_3^\lambda - 4 \sin^2\theta_W J_{em}^\lambda \right\} \tag{2.5}$$

However, inspection of Eqs. (2.1) and (2.4) shows that this is simply the sum of the "YES" and "NO" Lagrangians

$$\mathscr{L}_{NC}^{W-S} = \mathscr{L}^{"YES"} + \mathscr{L}^{"NO"} \tag{2.6}$$

provided one identifies the neutrino charge radius Λ^{-1} with the Weinberg-angle θ_W as follows

$$\left|\frac{1}{\Lambda}\right| = \left(\frac{G}{\pi\alpha\sqrt{2}}\right)^{1/2} \sin\theta_W \cong \frac{\sin\theta_W}{53\text{GeV}} \approx 10^{-2}\ \text{GeV}^{-1} \tag{2.7}$$

This is a rather large electromagnetic radius; from this point of view one might have a priori expected[6] $\sin^2\theta_W \sim O(\alpha) \sim$ a few %, not the observed 20-25%.

III. Intermediate-boson Hypothesis

Let us assume the intrinsic SU(2)-invariant weak interaction "YES" described by Eq. (2.1) is mediated by a triplet of intermediate bosons $W^\pm$, W_3, necessarily degenerate in mass. We define the (universal) Yukawa coupling constant g for the W such that

$$\frac{G}{\sqrt{2}} = \frac{2g^2}{m_W^2} \tag{3.1}$$

Then, just as we might imagine the neutron charge-radius to be dominated (in the dispersion-relation sense) by ρ^o and ω^o exchange, we may suppose the neutrino charge-radius to be dominated by exchange of the intermediate W_3 boson. Defining ef to be the direct coupling of W_3 to photon, the neutrino charge radius is then given by (c.f. Fig. 1d)

$$g \cdot \frac{1}{m_W^2} \cdot \frac{q^2}{m_W^2} \cdot f \cdot \frac{e^2}{q^2} = \frac{ge^2f}{m_W^4} = G\sqrt{2} \sin^2\theta_W \tag{3.2}$$

There is one additional effect of importance. The mixing of W_3 and photon produces a charge-renormalization and also splits the mass of the neutral boson from the $W^\pm$. The photon propagator $D(q^2) \sim e^2/q^2$ becomes, after including all proper W_3-insertions (c.f. Fig. 2).

$$D(q^2) = \frac{e_o^2}{q^2\left[1 - \frac{e_o^2 f^2}{m_W^2(q^2-m_W^2)}\right]} \tag{3.3}$$

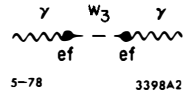

Fig. 2. Electromagnetic mixing of W_3 with photon.

This allows us to express the charge-renormalization as

$$\frac{1}{e_o^2} \equiv \frac{Z_3}{e^2} = \frac{1}{e^2} - \frac{f^2}{m_W^4} \tag{3.4}$$

Likewise, the nontrivial pole in $D(q^2)$ at $q^2 = m_Z^2$ gives the mass m_Z of the physical Z-boson

$$m_Z^2 = m_W^2 + \frac{e_o^2 f^2}{m_W^2} \tag{3.5}$$

Elimination of the coupling constants e_0, g, and f from Eqs. (3.1), (3.2), (3.4) and (3.5) leads to the results

$$m_W = \frac{37 \text{ GeV}}{\sin^2\theta_W} \sqrt{1-Z_3} \tag{3.6}$$

$$\frac{m_W^2}{m_Z^2} = Z_3 \tag{3.7}$$

However, Z_3 is not yet determined.

IV. Range of the Weak Force

Equation (3.6) shows that

$$m_W \leq \frac{37 \text{ GeV}}{\sin^2\theta_W} \lesssim 150 \text{ GeV} \tag{4.1}$$

Thus the range of the weak force must be large compared to the unitarity cutoff[7] $G_F^{-1/2}$. The bound is in fact comparable to that expected for the unified gauge theories. This result is much more general[8] than derived in Section III. Even if the single W-exchange is replaced by exchange of a general continuum (which need not even contain discrete quanta), the same result, Eq. (4.1), can be still obtained. One writes dispersion relations for the intrinsic weak amplitude, for the neutrino charge form-factor, and for the contribution of weak quanta to vacuum polarization. The result (Eqns. (3.6) and (4.1)) then follows from application of the Schwartz-inequality to the absorptive parts of the dispersion integrals. The parameter m_W is now a general measure of the range of the weak force, and controls the dependence of G_F on momentum transfer according to the definition

$$G_F(q^2) = G_F\left(1 + \frac{q^2}{m_W^2} + \ldots\right) \tag{4.2}$$

We also see from Eq. (3.6) that as m_W increases, Z_3 decreases. The quantity Z_3^{-1} measures the yield of weak quanta produced in e^+e^- annihilation. This implies a connection, again obtained via dispersion-relations and Schwartz inequalities, between the colliding-beam R_{weak}

$$R_{weak} = \frac{\sigma(e^+e^- \to \text{weak quanta})}{\frac{4}{3}\pi\alpha^2 s^{-1}} \tag{4.3}$$

and the parameters m_W^2, $\sin^2\theta_W$, G_F, etc. The resulting inequality is plotted in Fig. 3 and shows that the yield of weak quanta in e^+e^- annihilation is very large. Of course, given the intermediate boson hypothesis, this yield is dominated[9] by the resonant production of Z^0.

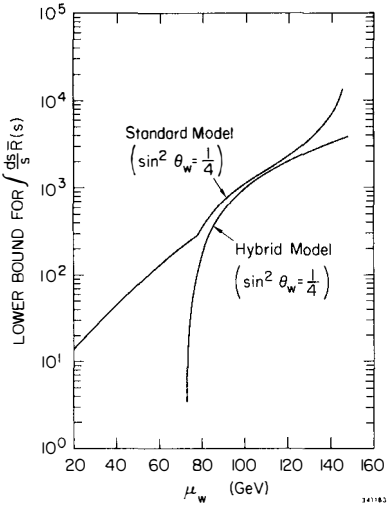

Figure 3: Lower bound for $\bar{R} = \int \frac{ds}{s} R(s)$, which measures the production of weak quanta by colliding e^+e^- beams. [Note: a similar plot given in Reference 1 is incorrect.]

We must caution the reader that although m_W is bounded above, implying that the threshold for the process $e^+\nu_e \to$ weak quanta lies no higher than $m_W \lesssim 150$ GeV, we have not succeeded in making such a statement for the threshold in e^+e^- annihilation. Indeed, as Eq. (3.7) shows, we do not have a bound on m_Z, even given the intermediate-boson hypothesis.

V. Asymptotic SU(2) Symmetry

Despite the use of the intermediate-boson hypothesis, not all of the predictions of the gauge theories, in particular those for m_W and m_Z, have been recovered. What is missing is the statement of symmetry at short distances, basic to gauge theories. We may, in the phenomenological language, express this as requirements that the single-intermediate-boson-exchange dominate the weak

amplitude at all energies, and that as $q^2 \to \infty$, the SU(2) symmetry of the intrinsic weak force (broken in general by the electromagnetic contribution) is restored.

For any charged elementary fermion of weak-isospin 1/2, the electromagnetic vertex function analogous to Eq. (2.3) is written

$$e\Gamma_\lambda(q) = \bar{u}\gamma_\lambda \left[\left(\frac{1-\gamma_5}{2} \right) \left\{ eQ + \frac{4T_{3L}gef}{(m_W^2 - q^2)} \cdot \frac{q^2}{m_W^2} \right\} + \left(\frac{1+\gamma_5}{2} \right) \left\{ eQ + \frac{4T_{3R}gef}{(m_W^2 - q^2)} \cdot \frac{q^2}{m_W^2} \right\} \right] u \quad (5.1)$$

Writing $Q = T_{3L} + Y_L = T_{3R} + Y_R$, the condition of asymptotic symmetry is that the coefficients of T_{3L} and T_{3R} in the electromagnetic vertex operator vanish as $q^2 \to \infty$:

$$1 = \frac{4gf}{m_W^2} \quad (5.2)$$

When this condition is combined with those already obtained, one finds

$$Z_3 = \cos^2\theta_W \quad (5.3)$$

and consequently

$$m_W = \frac{37 \text{ GeV}}{\sin\theta_W} \qquad \frac{m_W}{m_Z} = \cos\theta_W \quad (5.4)$$

The simple gauge-theory results are reconstructed. Assumption of pole-dominance of these weak amplitudes at all energies may be tantamount to assuming the gauge theories *in toto*,[10] although this point is not completely clear to me.

VI. Comments and Conclusions

1. The phenomenological picture of the weak effective Lagrangian as sum of an intrinsic SU(2)-invariant interaction plus electromagnetic correction is compatible with the conventional description using the gauge theories. This is seen especially clearly in a generalization of the standard model to $SU(2) \times U(1) \times G$ as constructed by Georgi and Weinberg.[11] They show that if the spontaneous symmetry breakdown is produced by Higgs bosons which transform as $(2,1) + (1,X)$ and if the neutrino is a singlet under G, the effective Lagrangian for neutrino-induced neutral currents is the same as in the standard model. In fact it can be shown[8] that the structure of this model is the same as the phenomenological picture: the weak amplitude decomposes into the two pieces, "intrinsic" and "electromagnetic", just in the way we have discussed.

2. If there does exist an alternative to the gauge theories, what might it mean? Such a question can be rephrased in terms of the analytic properties of the intrinsic weak interaction as function of squared momentum transfer q^2. In gauge theories this amplitude is dominated by poles. Pole-dominance may in fact imply the gauge theories. Alternatives (which most likely are nonrenormalizable) probably contain strong cuts as well as poles. Such a possibility could correspond to composite degrees of freedom,[12] either for intermediate bosons or for fermions, or both. But we have little of a concrete nature to offer here.

3. The general neutral-current coupling for charged as well as neutral fermions is not quite the same as for the standard model. In momentum-space the generalized effective Lagrangian for neutral-currents is, at low energies:

$$\mathscr{L}_{\text{eff}}^{\text{NC}} = \frac{G}{4\sqrt{2}}\left[J_3^\lambda - 4\sin^2\theta_W J_{\text{em}}^\lambda\right]\left[J_\lambda^3 - 4\sin^2\theta_W J_\lambda^{\text{em}}\right] + \frac{1}{2}J_\lambda^{\text{em}} J_{\text{em}}^\lambda\left\{-\frac{e^2}{q^2} + 4\lambda G\sqrt{2}\sin^4\theta_W\right\} \quad (6.1)$$

The first term is the result for the standard model. Only the last term proportional to λ differs: it is parity-conserving and vanishes, given the (single) intermediate-boson hypothesis. Under general circumstances λ is nonvanishing owing to an unknown contribution from vacuum-polarization via weak quanta. However, from Schwartz inequalities it is possible to show that $\lambda \geq 0$.

4. We have not written the most general SU(2)-invariant effective Lagrangian for the intrinsic weak force. There might also be contributions from $I_W = 0$ exchange as well as from $I_W = 1$, especially were the W to be a composite of $I_W = 1/2$ constituents. At present, probably the best test for such a component comes from the deep inelastic neutral-current data. If we write for this case

$$\begin{aligned}\mathscr{L}_{\text{NC}} = \frac{G}{2\sqrt{2}}\bar{\nu}_\mu\gamma_\lambda(1-\gamma_5)\nu_\mu\Big\{&\left[\bar{u}\gamma^\lambda(1-\gamma_5)u - \bar{d}\gamma^\lambda(1-\gamma_5)d\right] \\ &-4\sin^2\theta_W\left[\tfrac{2}{3}\bar{u}\gamma^\lambda u - \tfrac{1}{3}\bar{d}\gamma^\lambda d\right] \\ &+\xi\left[\bar{u}\gamma^\lambda(1-\gamma_5)u + \bar{d}\gamma^\lambda(1-\gamma_5)d\right]\Big\} \end{aligned} \quad (6.2)$$

then a crude estimate indicates that $|\xi| \leq 0.2$ is probably still allowed from experiment. It is of interest to test in general for such weak-isoscalar terms.

5. At present, the situation with regard to the atomic parity-violation experiments in Bi is unclear.[14] But even were there to be a vanishing effect, this would not affect the considerations here in a very basic way. For example, reassignment of right-handed e^- from singlet to an SU(2) doublet is sufficient to remove the problem.[15]

6. Central to the phenomenological approach presented here is the global SU(2) symmetry of the intrinsic weak interaction at low energies. From the conventional gauge-theory point of view, this symmetry occurs as a consequence of the assumption of only Higgs-doublets contributing to the intermediate-boson mass, an assumption of not an especially basic character. Perhaps the global SU(2) symmetry at low energies is a property of more fundamental origin. In any event, it would appear that there still is considerable room for alternatives to the renormalizable gauge theories of weak and electromagnetic interactions.

REFERENCES

1. An earlier version of these ideas was presented at the Ben Lee Memorial International Conference, Fermilab, Oct. 20-22, 1977. See also Ref. 8.
2. S. Bludman, Nuovo Cimento 9, 433 (1958).
3. S. Glashow, J. Iliopoulos, and L. Maiani, Phys. Rev. D2, 1285 (1970).
4. J. Bernstein and T.D. Lee, Phys. Rev. Letters 11, 512 (1963).
5. S. Weinberg, Phys. Rev. Letters 19, 1264 (1967). A. Salam, "Elementary Particle Physics" (Nobel Symposium No. 8, ed. N. Svartholm, Almquist and Wiksell (Stockholm), 1968.
6. Bernstein and Lee (Ref. 4) estimated $\sin^2\theta_w \sim \alpha \log \alpha$ in a nonrenormalizable charged intermediate-boson theory, given a vanishing anomalous magnetic moment κ of the $W^{\pm}$. However, for $\kappa \neq 0$, they estimated $\sin^2\theta_w \sim Q(\sqrt{-\alpha})$ and commented that this "seems to lead to a physically unacceptable result for the charge radius of the neutrino."
7. T. D. Lee and C. N. Yang, Phys. Rev. Letters 4, 307 (1960).
8. J. D. Bjorken, in preparation. See also Ref. 1.
9. In that case, the Schwartz inequality becomes an equality, and the yield shown in Fig. 2 agrees with the known results; c.f. e.g. B. Ioffe and V. Khoze, Leningrad preprint 76-274 (1976).
10. See J. Cornwall, D. Levin, and G. Tiktopoulos, Phys. Rev. D10, 1145 (1974), and references cited therein.
11. H. Georgi and S. Weinberg, Phys. Rev. D17, 275 (1978), HUTP 77/A052.
12. For example, see H. Terazawa, Phys. Rev. D7, 3663 (1973), D16, 2373 (1977).
13. P. Hung and J. Sakurai, Phys. Letters 72B, 208 (1977). L. Abbott and M. Barnett, SLAC-PUB-2097.
14. L. Lewis, J. Hollister, D. Soreide, E. Lindahl, and E. Fortson, Phys. Rev. Letters 39, 795 (1977). P. Baird, M. Brimicombe, R. Hunt, G. Roberts, P. Sanders, and D. Stacey, Phys. Rev. Letters 39, 798 (1977). L. Barkov and M. Zolotorev, JETP 26, 379 (1978).
15. S. Glashow has presented a nice review of the options, Proceedings of the Ben Lee Memorial International Conference, Fermilab, Batavia, Ill., 1978 (to be published).

COMMENTS ON THE OBSERVABILITY OF LARGE WEAK INTERACTIONS AT VERY HIGH ENERGIES*

G.L. Kane**
Physics Department, University of Michigan
Ann Arbor, MI 48109

ABSTRACT

We consider which weak interaction effects might be experimentally observable at very high energies in pp or $p\bar{p}$ colliding beams, and whether any weak cross sections get large at high energies. Apart from direct production of W's and Z's, the possibility of observable weak effects depends on the properties of the Higgs bosons. Weak cross sections could get large at high energies only if the Higgs mass is much larger than the mass of the vector bosons. However, for feasible experiments, such effects are suppressed in conventional gauge theories. Thus, we expect that observable weak cross sections will not get large at high energies. We also discuss a way to look for weak effects which has not been studied much: parity violation effects in the production of hadron resonances. Numerical results indicate that such effects due to the production of W's and Z's should be observable at Isabelle energies. We also consider the possibility of observing unconventional kinds of weak effects experimentally, and their implications for the gauge theories.

At low energies, weak interaction total cross sections rise linearly with lab energy; it is commonly stated that weak cross sections will get large at very high energies. In the context of gauge theories the situation becomes more precise. It has been discussed most thoroughly by Veltman[1] in terms of two thresholds. In any case one expects massive gauge vector bosons, charged $W^{\pm}$'s and neutral Z°'s. These will be produced directly, giving large cross sections in e^+e^- collisions at the Z° mass, and enhancements in $\nu p \to Z° + \ldots$, $pp \to Z° + \ldots$, etc. Their mass range constitutes the first threshold.

But the theory is not renormalizable with only the massive vector bosons, and additional physics must enter.[1] In the conventional versions this occurs through the Higgs bosons. To observe experimentally the differences between the basic theory with vector bosons and the renormalizable gauge theories, and to test the gauge theories, one must observe effects due to the additional physics. If the Higgs boson mass is large compared to m_W it gives the second threshold.

Veltman[1,2] has studied the possibility of testing the gauge theories at low energies, and found that is is not easy. In the present paper we discuss whether some observable effects might be expected at high energies. Unfortunately, the answer is probably negative.

We can understand this as follows. In the conventional gauge theories the new physics enters at high energies essentially by replacing a factor of s, which would lead to a large amplitude, by m_H^2 (m_H is the Higgs boson mass). Veltman,[1] and Lee, Quigg, and Thacker,[3] have observed that there are two situations. If m_H is less than or comparable to m_W, m_Z, then all weak amplitudes stay rather small in all circumstances and higher order effects which will test the structure of the theory are essentially undetectable. However, if m_H is large, so that some weak amplitudes are large, then higher order effects are large and perhaps some are observable.

Both from the requirements that radiative corrections were of order unity,[1] and from the unitarity limit[3,4], it was argued that perturbative arguments would break down and weak amplitudes would behave strongly for $m_H \sim 10^3$ GeV. Unfortunately, when one wishes to observe such effects experimentally at high energies one must begin with fermion states, e.g. in e^+e^- collisions or in $q\bar{q}$ collisions (where the quarks are in p or $\bar{p}$ beams). To get Higgs contributions one can see that in general the Higgs particles will couple to fermions. Since Higgs particles with non-zero vacuum expectation values will contribute to the fermion mass, their coupling strength is proportional to the fermion mass, m_f. In fact, the corrections due to higher order effects in observable processes turn out to be at most of order $g^4(m_f/m_W)^2 \ln m_H^2$. This is numerically negligible since $m_f/m_W \leq 10^{-3}$. We conclude that within the framework of conventional gauge theories with scalar Higgs mesons and fermion masses determined in part by coupling to the Higgs particles, no large weak interaction amplitudes will be ovserved, apart from those directly due to production of W's and Z's.

Producing two intermediate vector bosons from an $f\bar{f}$ pair is easily done kinematically with expected $\bar{p}p$ or pp colliding beams, and gives a cross section that grows with energy in a nonrenormalizable theory.[5,6] Might we expect a large rate experimentally? Again, unfortunately, the fermion mass factor enters and makes the rate negligible. This comes about as follows. At the tree level the diagrams of figure 1 contribute. As is well known, the Z^0 and photon contributions, (b), provide a cancellation of the term growing like s in (a). But (a)+(b) still leave a piece of order $\sqrt{s}$, which is cancelled by the Higgs boson contribution, (c). A factor of m_f comes from the Higgs

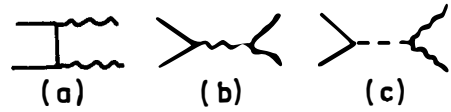

FIGURE 1: $f\bar{f} \to W^+W^-$
(a) fermion exchange
(b) Z^0, γ exchanges
(c) Higgs exchange

coupling in (c) and from the propagator or use of the Dirac equation on the spinors in (a) and (b). Thus the cross section for $f\bar{f} \to W^+W^-$ is proportional to $(m_f/m_W)^2$ (as compared to single W production) and is negligible.

Next we discuss in general how weak interactions can be studied at high energies. The usual methods involve the production of W's and Z's and their decays into leptons or hadron jets. These may well be the best methods, particularly to detect a Z^0 by its $\mu^+\mu^-$ decay, and they have been studied in some detail.[7,8] The method we want to emphasize here is the detection of weak effects via the parity-violating production of hadron resonances.

One can see very simply that such effects should occur. For example, a W decay into $q\bar{q}$ will give a left handed q in a V-A theory. When making a meson resonance by picking up a $\bar{q}$ from the vacuum it will form (say) ρ's only of helicity 0 and -1, while the strong interactions give equal amounts of helicity 1 and -1. Thus comparison of the amounts of helicity 1 and -1 ρ's can signal a weak effect.

To see what to expect we use a model[9,10] as shown in Figure 2, with the basic scattering a weak one, dominated by direct production of a W. To estimate the relative production of various resonances, we note some current opinions. The W^+ should decay equally into $u\bar{d}$ and $c\bar{s}$. When a quark fragments into a hadron, the probability of getting an $s\bar{s}$ pair from the vacuum is thought to be 1/2 the probability of getting $u\bar{u}$ or $d\bar{d}$.[11] An SU(6) argument suggests there will be three ρ's for each directly produced π, from equal population of helicity states. Thus, there should be (approximately) equal production of ρ's and K*'s of each helicity and of π's.[12] Perhaps, most important, φ's are expected with only a reduction of about 50% relative to K*'s. Since the φ background is quite small, they may give a large signal-to-noise ratio.

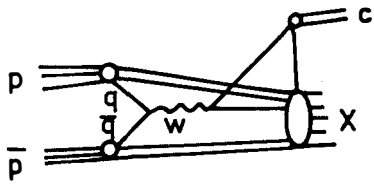

FIGURE 2: Inclusive production of resonance c by direct production of a W.

In addition, with a small Q value in the decay, they may be easy to detect (assuming $K^{\pm}$ identification).

Some of the results are shown in Figure 3. Thus, if appropriate cuts are made on the data to reduce the strong interaction background (say, by looking at $p_T \geq 10$ GeV and $\theta_{cm} \approx 90°$), a rise in the φ/π ratio, for example, would signal something new. To prove the signal is a weak interaction effect, one needs to detect a parity violation. In the case of φ decay, one needs to see a term[14] $\mathrm{Im}(\rho_{10}+\rho_{-10})$ which is present if there is a non-zero angular correlation for $\langle \sin^2\theta \sin\varphi \rangle$.

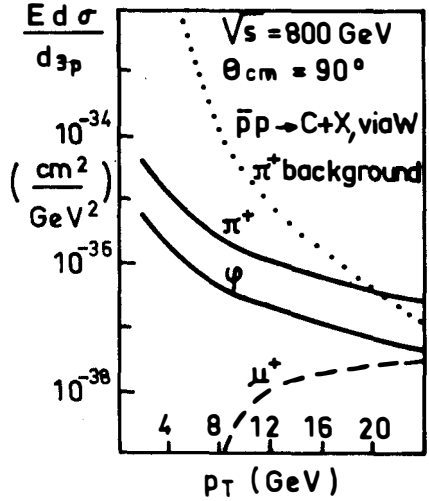

FIGURE 3: Inclusive production of π^+(———) $\varphi°$(—·—·) and μ+(----) in pp collisions due to direct production of W. The strong interaction background expected for π+(....) is estimated from Reference 13.

Parity violation can be identified in a similar manner by studying inclusive production of ρ, ω, and K*. Perhaps even more fruitful is to study inclusive Λ production[15] where parity violation in its production is signaled by either a $\langle \cos\theta \rangle$ or a $\langle \sin\theta \cos\varphi \rangle$ term in its decay. Our numerical results are encouraging[16], and one can find situations where background effects and experimental considerations appear to favor hadron resonance detection over other methods. Further, the method does seem to have one unique and eventually potentialy powerful advantage: by detecting resonances with different charge, strangeness, etc. one can study the flavor dependence of the W and Z spectrum, and of high energy weak effects in general.

Finally, we consider the implications of finding or not finding high energy weak effects not attributable to W's or Z's. For example, suppose bound states of Higgs, W's and Z's exist and lie on Regge trajectories.[17] The exchange of such

objects could lead to unconventional weak interaction effects at high energy. If such effects are observable, one will have evidence that m_H is large[1,3] and that a Higgs-fermion coupling exists which is not proportional to m_f/m_W.

REFERENCES AND FOOTNOTES

*Research supported in part by Department of Energy
** This paper was done in collaboration with H. Haber.

1. M. Veltman, Acta Phys. Polon. B8, 475 (1977).
2. M. Veltman, Phys. Lett. 70B, 253 (1977).
3. B.W. Lee, C. Quigg, and H.B. Thacker, Phys. Rev. D16, 1519 (1977); Phys. Rev. Lett. 38, 883 (1977).
4. D.A. Dicus and V.S. Mathur, Phys. Rev. D7, 3111 (1973).
5. S. Weinberg, Phys. Rev. Lett. 27, 1688 (1971).
6. C.H. Llewellyn-Smith, Phys. Lett. 46B, 233 (1973).
7. C. Quigg, Rev. Mod. Phys. 49, 297 (1977).
8. R.F. Peierls, T.L. Trueman, and L.-L. Wang, Phys. Rev. D16, 1397 (1977).
9. S.M. Berman, J.D. Bjorken, and J.B. Kogut, Phys. Rev. D4, 3388 (1971).
10. S.D. Ellis and M.B. Kislinger, Phys. Rev. D9, 2027 (1974).
11. R.D. Field and R.P. Feynman, Phys. Rev. D15, 2590 (1977).
12. However, the number of π's seen by an experiment is obtained by adding these directly produced π's and the π's which are decay products of resonances.
13. R.D. Field, CALT-68-633, (1977).
14. J.D. Jackson, lectures given at Les Houches 1965, edited by C. DeWitt and M. Jacob (Gordon and Breach, New York, 1965).
15. G.W. Look and E. Fischbach, Phys. Rev. D16, 1369 (1977).
16. Details are given in a longer paper: H.E. Haber and G.L. Kane UM HE 78-11, (1978).
17. T. Appelquist and J.D. Bjorken, Phys. Rev. D4, 3726 (1971).

THE IMPACT OF GAUGE THEORY

ON ELEMENTARY PARTICLE PHYSICS

N. CABIBBO
Laboratoire de Physique Théorique et Hautes Energies*
4, place Jussieu - Tour 16 - 1er étage
75230 PARIS cedex 05 - FRANCE

On leave of absence from : Istituto di Fisica G. Marconi
Universita di Roma. Roma. ITALY.

* Laboratoire Associé au CNRS

ABSTRACT :

Gauge theory has acquired a central role in our understanding of elementary particles. We give an assessment of the achievements and prospects for future development.

La théorie de jauge a acquis un rôle central dans notre compréhension des particules élémentaires. Nous donnons un état des réalisations et des perspectives de développement futur.

Recent developments, both experimental and theoretical, add new arguments for singling out gauge theories in the unique tool for understanding the interactions of elementary particles. From a philosophical point of view, the overwhelming merit of gauge theories is that they lead to unique interaction schemes, approaching the ideal of a theory with a minimum of arbitrary (i.e. experimentally determined) parameters. The essential element for the wide acceptance of non-abelian gauge theories was given by the relatively recent proof of their renormalizability, which opened the possibility that they can give models of elementary particle interactions which are not only aesthetically satisfactory, but also mathematically meaningful. Renormalization theory remains in fact the main tool for giving mathematical sense to realistic (i.e. four dimensional) models.

An exciting consequence of the advent of gauge theories is the unification of interactions which were previously considered as independent. We have already a unification of weak and e.m. interactions, and the process can continue. At each new level of unification we reduce the number of independent couplings, and we approach the ideal goal of a theory with no arbitrary parameters. At present, we think in terms of three types of interactions, each associated with a gauge group : i) Strong interaction, arising from the colour gauge symmetry $SU(3)_c$.

ii) Weak and electromagnetic interactions, arising from a gauge group, G, which contains at least $SU(2) \otimes U(1)$.

iii) Gravitational interactions (which I will not discuss here).

According to the more widely accepted scheme, strong interactions and weak-electromagnetic ones are independent of each other, i.e. they arise from "gauging" two symmetry groups, $SU(3)_c$ and G, which commute among themselves. In simple terms, gluon carries neither electric charge nor weak isospin. The opposite view, which can accomodate integrally charged quarks, is also being actively explored.

The unification of i) and ii) in a single gauge group is an attractive possibility, and a few interesting schemes have been proposed. Gauge theories lead to an interpretation of bosonic dynamical variables as variables which are related to local symmetry properties. Fermion fields are added on, much in the same way as "matter fields" are added in Einstein's theory of gravitation. This situation could be drastically changed by the emergence of supersymmetries, which involve transformations of boson into fermions and viceversa. Supersymmetry has not yet had an impact on our understanding of experimental data, but specta-

cular developments are well possible in the near future.

For weak interactions the advent of gauge theories has meant the passage from a phenomenological model - useful only at lowest order in the Fermi coupling constant - to a theory where any process can be computed to any desirable order. The list of physical effects which can now be computed in finite terms contains three main headings :

i) Second order weak processes, such as $K^\circ \to \mu^+ \mu^-$, and the $K_L - K_S$ mass difference.

ii) Weak corrections to e.m. effects, such as the (g - 2) of the muon.

iii) E.m. (radiative) corrections to weak processes.

We need not emphasize the importance of these achievements : as an example, radiative corrections to beta decay play an essential role in the verification of the relation between the muon coupling constant, G and the beta decay vector coupling constant, G_V :

$$\frac{G - G_V}{G} = 1 - \cos\theta \approx 2.5\ \%$$

A second feature of gauge theories is asymptotic freedom. This has proved essential for the success of QCD. Renormalizability in fact guarantees the existence of a perturbative series, with finite coefficients, for any physical quantity, A :

$$A = \sum a_n \alpha^n$$

on the contrary, renormalizability does not guarantee that the above series can be the basis of an effective approximation scheme, one where a specified accuracy can be reached with a computation of manageable proportions. This was a serious problem with the old theories of strong interactions, such as that based on the π- N Yukawa coupling.

The asymptotic freedom of QCD means that effective perturbative calculations can now be carried on for physical processes involving short distance, or high q^2, interactions. This possibility has an important fallout for weak and electromagnetic interactions of hadrons. Deep inelastic processes give an important example which has been extensively discussed during the meeting. Another important instance of this new possibility is given by explicit calculations of non leptonic weak processes, especially those involving the decay of charmed particles, and particles containing new types of heavy quarks (see Maiani's talk).

QCD - a unique theory of hadrons

Quantum chromodynamics has emerged as the unique theory of hadrons.

This unicity follows from the requirement of saturation of quark-quark forces in the singlet $q\bar{q}$ and qqq states, as well as from the requirement of approximate scaling in deep inelastic phenomena.

QCD is an asymptotically free theory : the effective fine structure constant α_s decreases at short distances, (i.e. at large Q^2), according to

$$\alpha_s(Q^2) = \left(\frac{33 - 2F}{12\pi}\right)^{-1} \left(\ln \frac{Q^2}{\Lambda^2}\right)^{-1} \qquad \text{for } Q^2 >> \Lambda^2$$

where F is the number of quark flavours.

This expression is valid for large Q^2 , i.e. $Q^2 >> \Lambda^2$, i.e. for values of Q^2 where α_s is small. Λ^2 gives the mass scale in which α_s becomes very large, i.e. the scale where quark interactions become strong. We note that Λ is the only parameter in this expression. Since Λ has the dimension of mass, we can always eliminate it by choosing Λ as the unit of mass, i.e. by choosing units in which $\Lambda = 1$. In such units QCD becomes a theory without arbitrary parameters !

The value of Λ can be determined by studying the violation to Bjorken scaling in deep inelastic scattering. The preferred value is now $\Lambda \approx 0.5$ GeV. This means that for Q = 3 GeV we have $\alpha_s \approx 0.4$, a smallish value which allows meaningful perturbative calculations. The situation is even better since first order corrections are typically proportional to α_s/π, rather than to α_s itself. The operational definition of a Q^2 dependent coupling constant, as well as the technology necessary for doing computations is a rather technical subject, as it involves the theory of renormalization and an extensive use of the renormalization group, and I will not discuss it here. Actual computations are not very different from similar computations in QED, and in many instances one finds that it is possible to adapt with little extra work results obtained a few decades ago.

The above expression of α_s is strictly valid only if quarks are massless. One can take roughly into account the effect of the quark masses by taking for F the number of quark flavours with mass less than Q^2. We would then put F = 4 in the range $2 < Q^2 < 25$ GeV^2, which is relevant for most of the present work.

Asymptotic freedom implies that there is a large body of physical phenomena which can be computed, essentially by perturbative methods, with a controllable accuracy. These phenomena yield meaningful tests of the theory. To list a few :

1) Predictions for the total hadronic cross sections in e^+e^-.

2) Predictions on the scaling violation in deep inelastic

phenomena.

3) Spectroscopy of bound states of heavy quarks.

4) Weak decays of particles including heavy quarks.

Inroads are being made into different ways of testing QCD, through the study of elementary gluon processes, the counterpart of QED processes such as e^+e^- scattering, $e^+e^- \to \gamma\gamma$, $e^+e^- \to e^+e^-\gamma$, etc. The doctrine behind these tests is that whenever an elementary process, such as

$$q + q \to q + q + \text{gluon}$$

takes place at high energy and large momentum transfer, each of the emitted quarks and gluons gives rise to a jet of hadrons carrying the energy and momentum of the originating quark or gluon. One can thus measure the cross section for an elementary process by measuring the cross section of the corresponding multijet event.

This area of physics is now at the beginning, but promises to become one of the active areas of research in machines such as PETRA, PEP, or the $\bar{P}P$ collider at CERN.

We thus have, in the upper reaches of the Q^2 spectrum, a rich area of collaboration of theory and experiment for the testing of QCD. The great challenge for theoreticians lies now at the other end of the spectrum : understanding quark confinement, and, more in general, developping the calculational techniques needed to apply QCD to low and intermediate energy phenomena, i.e. to the main body of classical hadron physics.

In this field we are far from a satisfactory situation and there are no results that would be presented in a meeting devoted to new experimental results and to the interaction of theory and experiment. The progress is nevertheless quite impressive. We have learned many unsuspected facts on the behaviour of classical gauge theory, in particular on the existence of exact localized solutions of the classical equations of motion, called the instantons. The existence of these solutions is now revolutionizing our views on the nature of quantized gauge theories at large distances, and these developments might lead to a convincing demonstration that QCD leads to colour confinement.

A consequence of the existence of instantons which is highly relevant to the comparison of theory and experiment is the solution of the η puzzle. It was thought that QCD led to the prediction of the existence of four very light pseudoscalars. Three of them were identified with the pion. The fourth had the quantum numbers of the η , which is however not light at all. It has been recently shown by 'T Hooft that the puzzle is not there : a subtle consequence of the existence of instantons is that QCD predicts the existence of only three, not four, light pseudoscalars. In conclusion QCD already offers specific predictions in a large area of high energy physics, and we hope that continued

effort will enlarge this area ; we have good hopes to achieve a number of important qualitative results, such as the proof of colour confinement.

Weak and electromagnetic interactions

In this field theoretical physics has scored two undeniable successes : the prediction of charm, the prediction of neutral currents.

Where we proceed from the present SU(2) ⊗ U(1) model ? We have no overwhelming indications on how to develop the model, and wether we should. The problem we are facing has been clearly stated by Bjorken : gauge theories of weak interactions are flexible while QCD is essentially unique. A possible way of reducing this flexibility comes from the idea of a super unification which derives weak, e.m. and strong interactions from the gauging of a single group. The requirement of unification does not lead to a unique solution, and different weak-electromagnetic theories could be unified with QCD. The present SU(2) x U(1) model is compatible with unification without further extensions, for instance in an overall SU(5) symmetry (Georgi and Glashow).

In this situation the strongest incitements to modify the present model come from new experimental results, often from rumours. Many new models are born of experimental rumours, and often die with them. There have been two new developments which suggest an enlargement of the standard four quarks-four lepton scheme, one very firm, consisting in the discovery of τ and of the γ resonance, the other being the persistent, although still not conclusive, lack of parity violation in atomic physics.

Recent results, presented here, indicate that τ decays into its own light neutrino, ν_τ , to which it couples in a V - A way with essentially full strength.

The very useful limit on the τ lifetime given by Pluto is very close to excluding the possibility that τ decays through ν_e , ν_u mixing. It seems that we have found the third replica of the e - νe doublet, and that we should abandon theoretical ideas of using τ in more exotic structures. The discovery of new quark doublet was then not only expected, but required in the SU(2) ⊗ U(1) scheme : the γ resonance was quickly accepted as the first manifestation of the new quark doublet and tentatively classified as a $b\bar{b}$ state.

The third lepton and quark doublets, however, are not mere replicas, in that they open new possibilities, namely that of giving a natural explanation of superweak CP violating forces which can now be explained through complex mixing between d, s, and b quarks. If neutrinos are not exactly massless a similar mixing would lead to CP violating neutrino oscillations - an exotic possibility, but worth looking into.

In conclusion, we have excellent results, but we still lack a

theory of weak interactions which forces itself on us because of its unique elegance and adherence to experimental facts. In this condition theoreticians will be largely led by the new experimental developments. And these are sure to come since the instrumental premises are there, both with machines now operating or being built, like PETRA and PEP, and with projects such as the $p\bar{p}$ colliders, and ISABELLE, and the future projects on large e^+e^- machines which are now taking shape.

An Experimental Summary of the XIII Rencontre de Moriond*

Martin L. Perl
Stanford Linear Accelerator Center
Stanford, California 94301

Abstract

This is the written version of a summary talk on some of the experimental results presented at the XIII Rencontre de Moriond. Results are reviewed in the following areas: (a) studies of the quark-parton model, Bjorken scaling, and quark fragmentation using virtual photons, neutrinos, and e^+-e^- annihilation; (b) properties of the τ lepton, D charmed meson, and F charmed meson as measured in e^+-e^- annihilation; (c) production of charmed particles by photons, neutrinos, and hadrons, including the CERN beam dump experiments; and (d) ongoing searches for new particles.

* Work supported by the Department of Energy.

TABLE OF CONTENTS

1. INTRODUCTION

At this XIIIth Rencontre de Moriond a tremendous amount of experimental and theoretical information had been presented — some new and some in the form of review. It is not possible in a summary talk to cover all this material or to do justice to the many fine presentations. Therefore, I have adopted two limits on the material I will discuss. First, I will not review any theory; a general theoretical talk has been presented by Cabibbo[1], and, in any case, I am not competent to report on much of the theoretical work presented here. Second, I have limited this talk to those experimental topics which seemed most in need of review either because a large amount of new material was presented; or because it seemed worthwhile to compare results from different areas such as neutrino physics and virtual photon physics; or because the topic still seemed to have a large amount of experimental uncertainty and incoherence. I hope that my use of this last criterion has not introduced too much incoherence into this talk.

2. VIRTUAL PHOTONS, NEUTRINOS, AND THE QUARK-PARTON MODEL

2A. The Interaction of Spacelike Virtual Photons with Quarks

As we all know, deep inelastic electroproduction or muoproduction occurs in the quark-parton model, Fig. 1a, through the fundamental reaction[2),3)]

$$\gamma_{\text{virtual, spacelike}} + \text{quark} \rightarrow \text{quark} \tag{1}$$

We also know that this reaction is described by three structure functions

$$F_1^{em}(\nu,q^2),\ F_2^{em}(\nu,q^2),\ F_3^{em}(\nu,q^2) \tag{2}$$

where ν is the energy of the virtual photon in the laboratory system and q^2 is the square of its four-momentum. Bjorken scaling says that these F's for sufficiently large ν and $|q^2|$ should only be a function of a single variable called x or ω where

$$x = \frac{1}{\omega} = \frac{Q^2}{2M\nu} \tag{3}$$

with $Q^2 = |q^2|$ and M the proton mass. Electroproduction experiments at SLAC by SLAC and MIT groups first established the validity of Bjorken scaling for F_1^{em} and F_2^{em} when $Q^2 \gtrsim 1(\text{GeV/c})^2$. ($F_3^{em}$ can only be determined through the inelastic scattering of polarized leptons on polarized nucleons; and this has only been accomplished recently.[4)]) The acceptance of the validity of

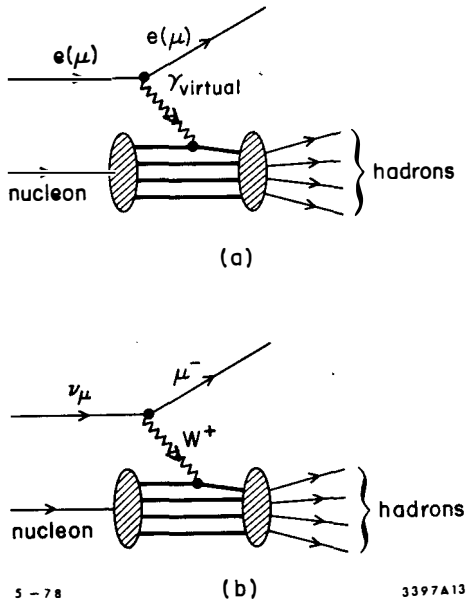

Fig. 1. The quark-parton model for (a) deep inelastic electroproduction or muoproduction; and (b) deep inelastic neutrinoproduction.

Bjorken scaling for Reaction 1 has meant that we could simply regard Reaction 1 as the absorption of a virtual photon by a free quark — the quark being simply a charged point particle.

While this picture has proved to be very useful, we must now accept the fact that violations of Bjorken scaling have been found experimentally using electrons at SLAC[5] and muons at Fermilab.[6),7] The explanation for these violations is simply that the quark is not free; rather the quark interacts with other quarks and with gluons in the nucleon. We should not be surprised at this; indeed, we should be more surprised the Bjorken scaling and the free quark concept work as well as they do. The concept of asymptotic freedom and the theory of quantum chromodynamics provide a framework for understanding why Bjorken scaling works and for studying the violations of Bjorken scaling. These ideas have been reviewed by G. Alterelli[8] at this conference; and, as I stated in the Introduction, I will not discuss these theoretical ideas again here. However, at the end of the next section I will use a bit of parameterization from quantum chromodynamics, the Λ parameter, to compare neutrino data with muoproduction data.

The most recent measurements of Bjorken scaling violations in muoproduction, TABLE I, were presented by T. Quirk[9] and W. Chen[10]. Figure 2 shows $F_2^{em}(x)$ for the 147 GeV μ-p data[9] compared to a fit to the lower energy electron data. We note that over this ν range it is a useful approximation to think of $F_2(x)$ at fixed Q^2 as independent of ν. The curves from Fig. 2 are superimposed in Fig. 3. We see that for

$$x \lesssim 0.25 \quad F_2(x) \text{ increases as } Q^2 \text{ increases} \tag{4a}$$

$$x \gtrsim 0.25 \quad F_2(x) \text{ decreases as } Q^2 \text{ increases} \tag{4b}$$

This observation has been made quantitative by Perkins et al[11] who used the scaling violation parameterization

$$F_2(x,Q^2) = F_2(x,Q_o^2) \left(\frac{Q^2}{Q_o^2}\right)^b \tag{5}$$

Fig. 4 prepared by T. Quirk[9] shows that the simple rule[11]

$$b = 0.25 - x \tag{6}$$

is a useful approximation. There are no corresponding measurements on $F_1(x)$ violations of scaling because $F_1(x)$ is multiplied by $\sin^2 \theta/2$ (θ is the electron scattering angle in the laboratory) and is therefore very difficult to measure.

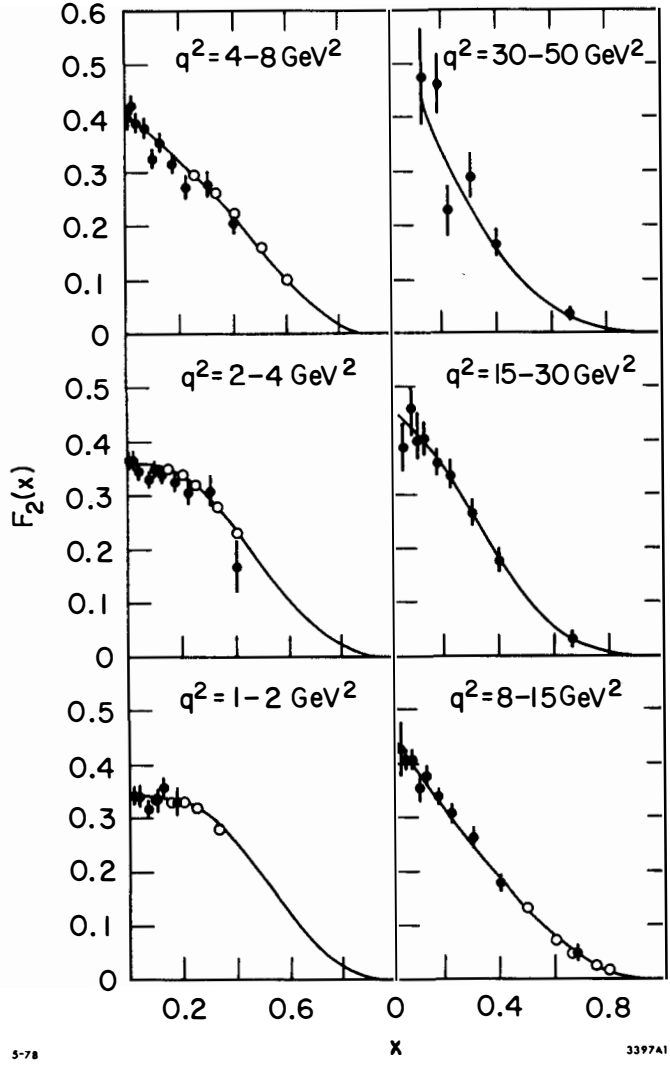

Fig. 2. F_2^{em} versus x. The solid circles are from μ-p deep inelastic scattering at 147 GeV (Ref. 9). The curves are fits (Ref. 9) to the lower energy electron data shown by the open circles (Ref.5).

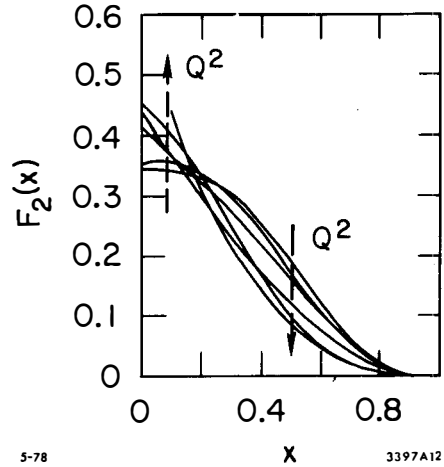

Fig. 3. A superposition of the curves from Fig. 2.

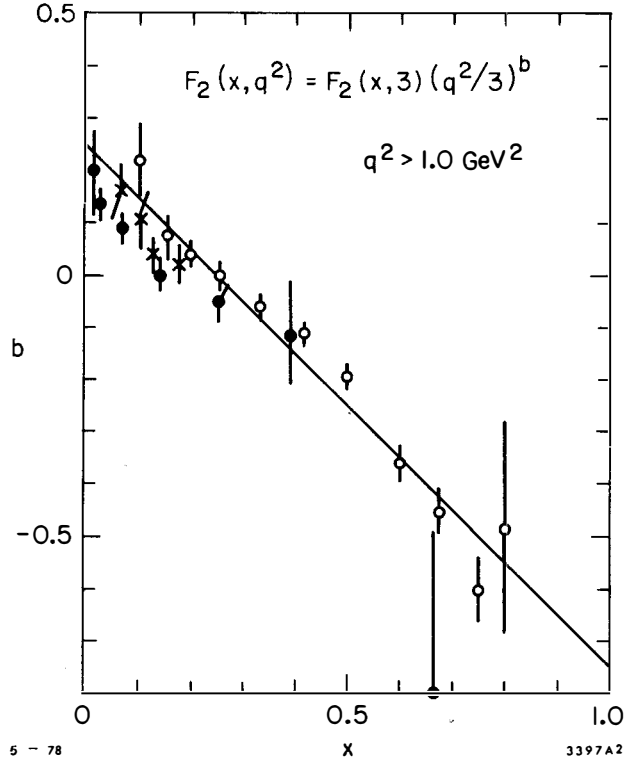

Fig. 4. Comparison of Eq. 6 using q_0^2=3 and b=0.25-x for: lower energy e-p data (open circles, Ref. 5); 147 GeV μ-p data (solid circles, Ref.9); 147 GeV μ-Fe data (x's, Ref. 6). Prepared by T. Quirk.

TABLE I

Muoproduction Experiments

Speaker	T. Quirk	W. Chen	W. Chen
Experimental parameters	μ-p, μ-D E_μ = 96,147 GeV $0.3 \lesssim Q^2 \lesssim 50.$ $(GeV/c)^2$	μ-Fe E_μ = 56,150 GeV $1 \lesssim Q^2 \lesssim 40$ $(GeV/c)^2$	μ-Fe E_μ = 270 GeV $5 \lesssim Q^2 \lesssim 150$ $(GeV/c)^2$
Reference	6, 9	7	10
Groups	Chicago, Harvard, Illinois, Oxford	Cornell, LBL, Mich. State, UCSD	Mich. State, Fermilab
Laboratory	Fermilab	Fermilab	Fermilab

Chen[10] presented very large Q^2 muoproduction data, Fig. 5, using an iron target. The curves are Chen's fits[10] to the SLAC-MIT data[5] at lower ν and Q^2 extrapolated to higher Q^2. The $5 < Q^2 < 15$ $(GeV/c)^2$ data is in fairly good agreement with the corresponding μ-p data, Fig. 2. And, as Q^2 increases, F_2 also appears to continue to increase for $x \lesssim .2$. This is a further illustration of Eq. 4a. Chen[10] also presented his data for fixed intervals in ω, Fig. 6. When $\omega > 5$ (that is $x < .2$) the increase of F_2 with Q^2 is clear. The $3 < \omega < 5$ plots show a non-monatonic behavior that can be interpreted, as pointed out by Chen, as an indication of a threshold for some new particle production at a total hadronic energy of about 10 GeV. However, this phenomenon and its threshold interpretation are probably best regarded as a stimulus for further measurements of F_2 in this high Q^2 range.

Incidently, a comprehensive review of electroproduction and muoproduction has been given recently by Hand.[3]

2B. The Interaction of Neutrinos with Quarks

Figure 1b reminds us that the fundamental reaction

$$W + \text{quark} \rightarrow \text{quark} \qquad (7)$$

where W is the intermediate boson which carries the weak interactions, is analogous to Reaction 1. If we accept the unification of weak interactions and electromagnetic interactions, then Reaction 7 should also show (a) approximate Bjorken scaling, and (b) violations of that scaling analogous to those

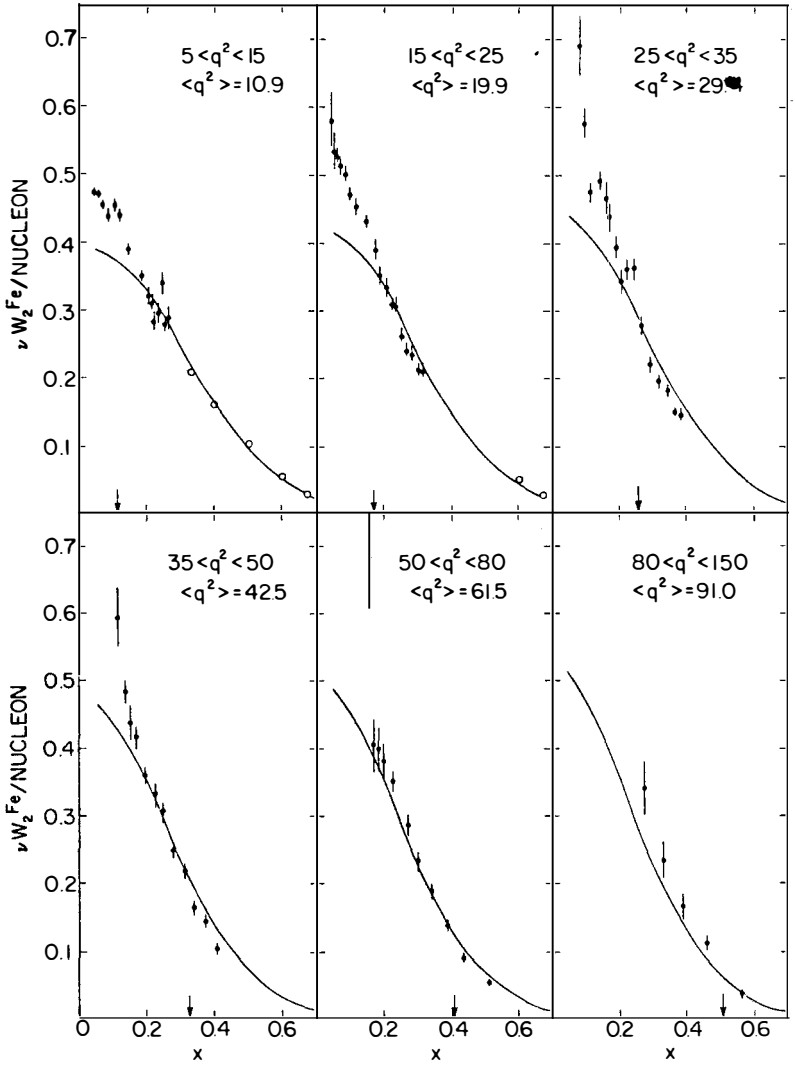

Fig. 5. $\nu W_2 = F_2^{em}$ versus x from μ-Fe data at 270 GeV. νW_2 is given per nucleon. The μ-Fe data and the curves which fit lower energy e-p data are from W. Chen, Ref. 10.

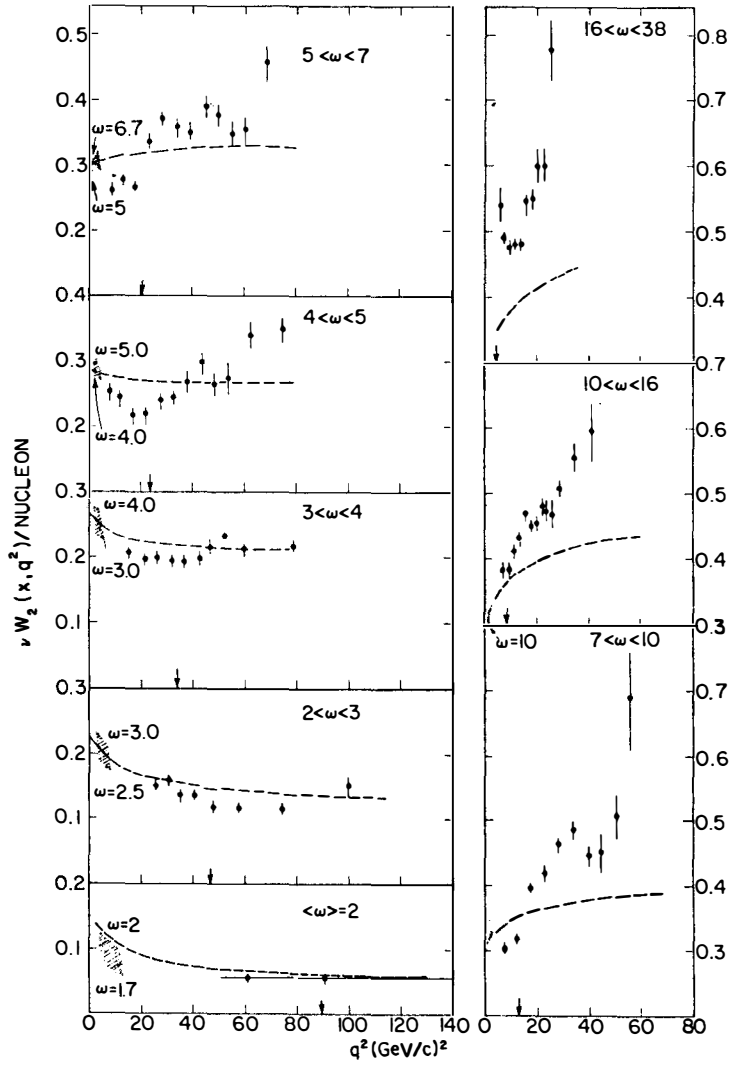

Fig. 6. $\nu W_2 = F_2^{em}$ versus q^2 for μ-Fe data at 270 GeV, from W. Chen, Ref. 10.

exhibited by Reaction 1. Point (a) is now well extablished[12),13),14)] for both neutrinos and anti-neutrinos, and so we can immediately turn to point (b) — the violations of Bjorken scaling.

B. Tallini[14)] presented measurements, Fig. 7, of the scaling violation of F_2^{ν} from BEBC and Gargamelle data (TABLE II). The dashed lines are fits to lower energy

TABLE II

Neutrino experiments on Bjorken scaling violations

Speaker	B. Tallini	A. Savoy-Navarro
Experimental parameters	ν and $\bar{\nu}$ in Gargamelle with $2 < E_\nu < 12$ GeV ν and $\bar{\nu}$ in BEBC with $20 < E_\nu < 200$ GeV	ν and $\bar{\nu}$ in CDHS counter, drift chamber experiment with $30 < E_\nu < 200$ GeV
Reference	14	13
Laboratory	CERN	CERN

electroproduction data; they show that very similar scaling violations are observed in F_2^{ν} and F_2^{em}. The difference between ν and $\bar{\nu}$ deep inelastic scattering yields directly F_3^{ν}; and, as shown in Fig. 8, xF_3^{ν} shows violations similar to F_2^{ν}. (We use xF_3^{ν} because in the simple quark-parton model $|xF_3^{\nu}| = F_2^{\nu}$.)

The CDHS data as presented by A. Savoy-Navarro[13)] is not yet in a form for direct comparisons with Fig. 7. However, Fig. 9 shows that there are scaling violations in $F_2(x)$ in quantitative agreement with Fig. 7 and Eq. 4. This follows from Fig. 10 which shows that in the CDHS data $\langle Q^2/E_{\nu,\bar{\nu}}\rangle$ is constant. Hence in Fig. 9 the larger E_ν curve is on the average a larger Q^2 curve. Incidently, Fig. 10 shows that the change in $\langle Q^2/E_{\nu,\bar{\nu}}\rangle$ which is apparent in the combined GGM-BEBC data (and which is also an indication[12)] of a scaling violation) is not seen in the exclusively high energy CDHS data. A similar remark applies to Fig. 11.

It has become conventional[15)] to describe scaling violations in quantum chromodynamics through a scale parameter Λ (GeV/c) which enters the theory through the function $\ln(Q^2/\Lambda^2)$. For example: Buras and Gaemers[15)] replace the usual expressions

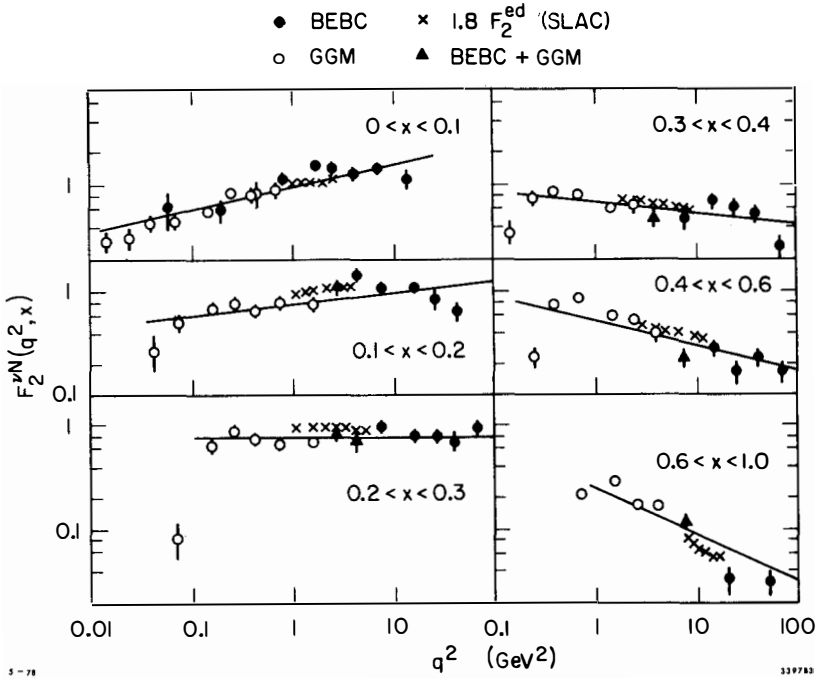

Fig. 7. Comparison of F_2 for neutrinoproduction and electroproduction versus q^2 presented by B. Tallini, Ref. 14. F_2^{em} is multiplied by 1.8 in accordance with the quark model.

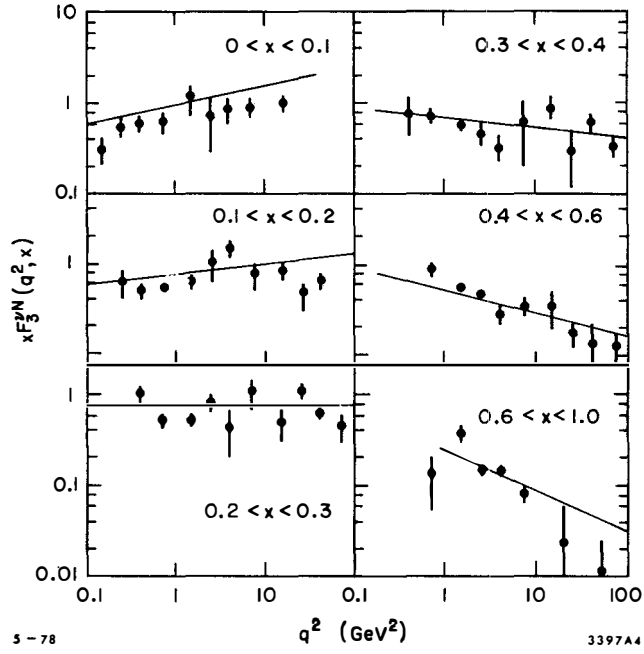

Fig. 8. $xF_3^{\nu N}$ versus q^2 from Ref. 14.

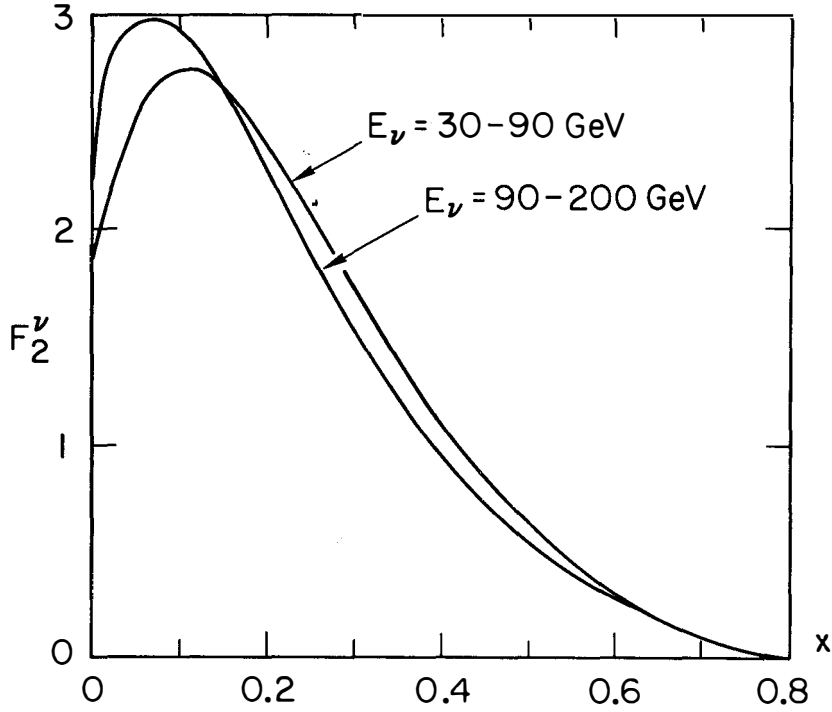

Fig. 9. F_2^ν versus x for two different E_ν regions from Ref. 13.

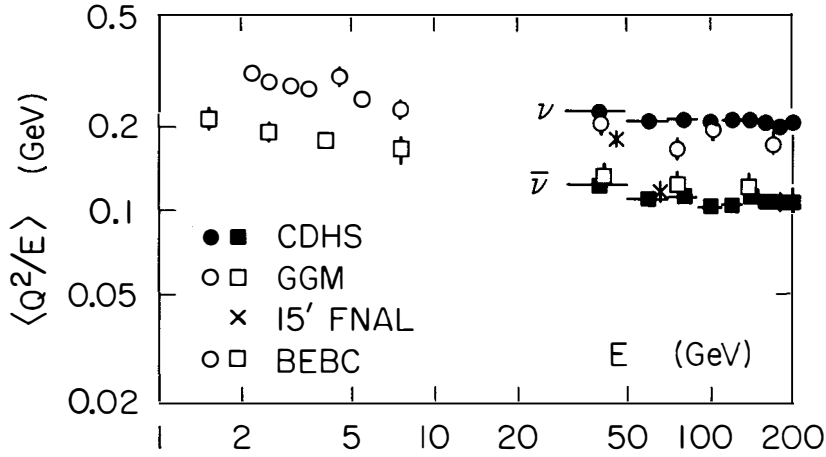

Fig. 10. $\langle Q^2/E_{\nu,\bar{\nu}} \rangle$ versus the neutrino energy E presented by A. Savoy-Navarro, Ref. 13.

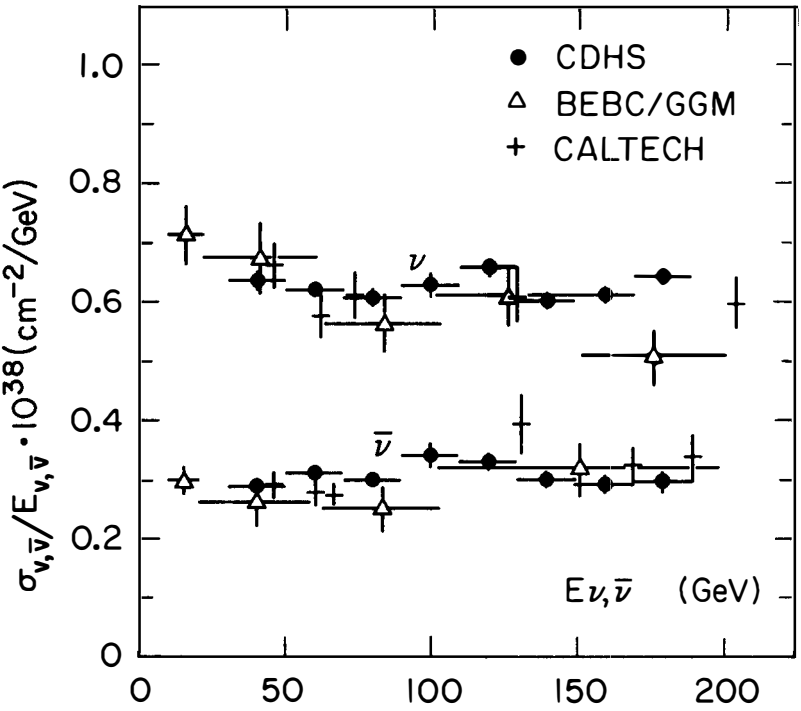

Fig. 11. $\sigma_{\nu,\bar{\nu}}/E_{\nu,\bar{\nu}}$ versus the neutrino energy E from Ref. 13.

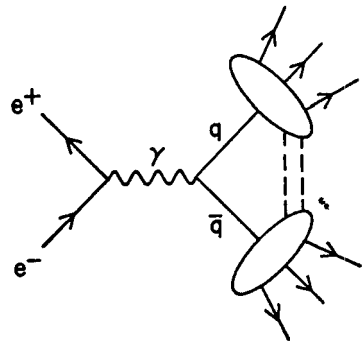

Fig. 12. Timelike virtual photon production of hadrons.

$$F_2(x) = \sum_i x^{a_i} (1 - x)^{b_i}; \; a_i, \; b_i \text{ constants,} \tag{8a}$$

which obey Bjorken scaling, by

$$F_2(x, Q^2) = \sum_i x^{a_i(\bar{s})} (1-x)^{b_i(\bar{s})} \tag{8b}$$

In this latter expression

$$\bar{s} = \ln \left| \frac{\ln \frac{Q^2}{\Lambda^2}}{\ln \frac{Q_o^2}{\Lambda^2}} \right| \tag{8c}$$

Electroproduction and muoproduction data gives values of Λ in the range of 0.3 to 0.66 GeV/c depending on the fitting method[15]. Tallini[14] gives $\Lambda = 0.75 \pm 0.1$ GeV/c for the neutrino data. It is too soon to say whether this difference has any significance because: (a) different ranges of ν and Q^2 occur in the different experiment, (b) the various experiments may have different systematic errors, and (c) different fitting methods have been used. However, as virtual photon and neutrino experiments improve in statistics, it will be interesting to test just how precisely the scaling violations agree.

2C. The Interaction of Timelike Virtual Photons with Quarks

The fundamental reaction, Fig. 12, is

$$\gamma_{\text{virtual, timelike}} \rightarrow \text{quark + anti-quark} \tag{9}$$

and this reaction is most easily studied through electron-positron annihilation,

$$e^+ + e^- \rightarrow \text{hadrons} \tag{10}$$

The analogy to Bjorken scaling in Reaction 9 is the statement[16] that

$$R = \sigma_{e^+e^- \rightarrow \text{hadrons}} \; / \; \sigma_{e^+e^- \rightarrow \mu^+\mu^-} = \text{constant} \tag{11}$$

Of course this can only be tested in an energy region where there are no thresholds for new particle production. Such a region appears to be $5 \lesssim E_{cm} \lesssim 9$ GeV; just below 5 GeV there are presumably charmed baryon thresholds, and above 9 GeV thresholds associated with the upsilon will occur. G. Wolf[17] presented new measurements of $\sigma_{e^+e^- \rightarrow \text{hadrons}}$ from the DASP collaboration Fig. 13; and Fig. 14 is a recent SLAC-LBL compilation[18] of $\sigma_{e^+e^- \rightarrow \text{hadrons}}$. Above 5 GeV $R_{exp} = 5.3$ to 5.5 and in the SLAC-LBL data is a constant. Thus we do see Bjorken scaling. However, the magnitude of R_{exp}

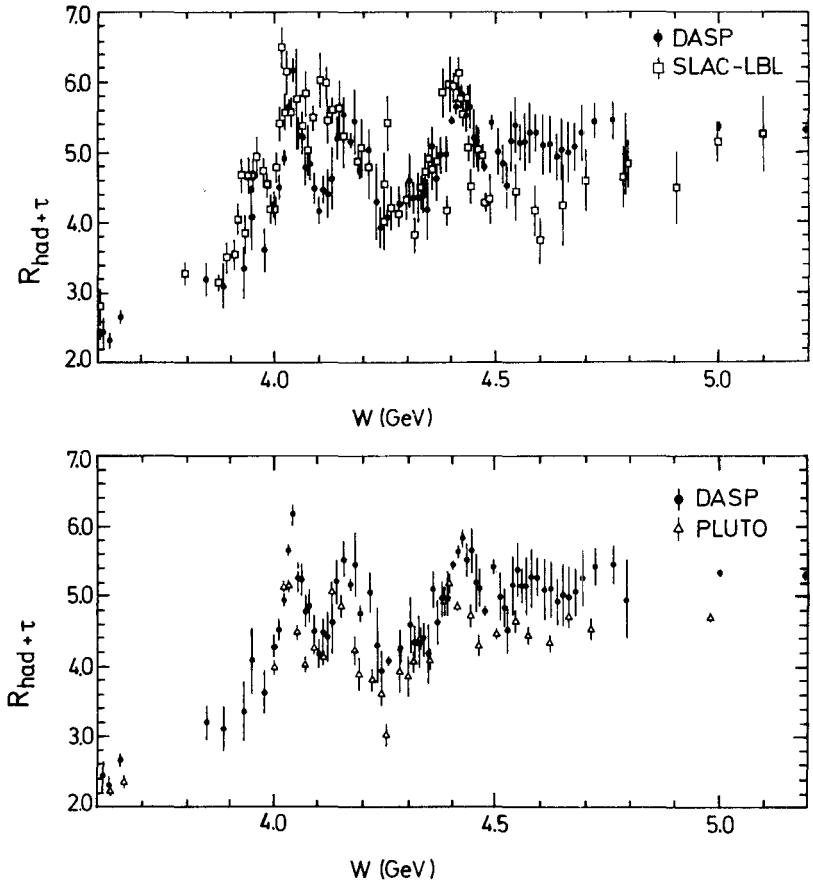

Fig. 13. The total $R=R_{had} + R_{\tau}$ versus the total center-of-mass energy W from DASP; presented by G. Wolf (Ref. 17).

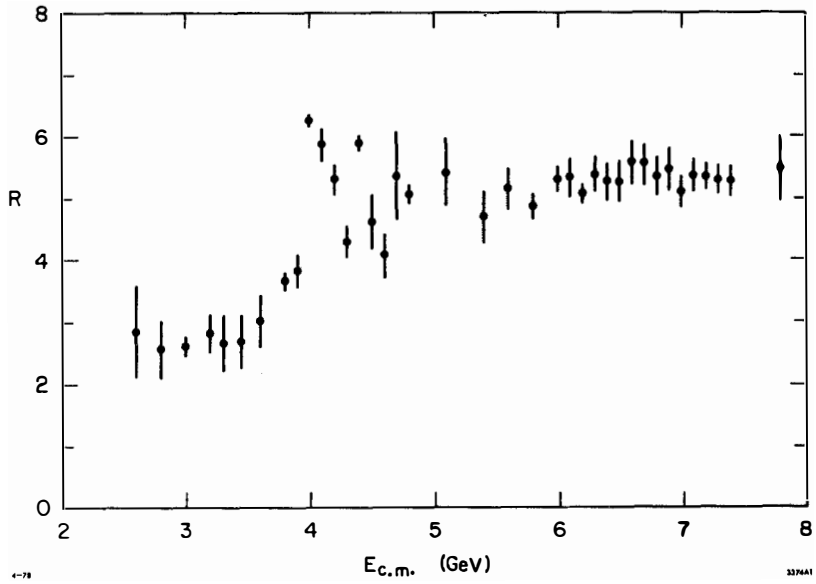

Fig. 14. The total R versus the total center-of-mass energy $E_{c.m.}$ from the SLAC-LBL Collaboration; presented by G. Hanson (Ref. 18).

is higher than the simple quark model prediction[19] of R = 4.33, which includes the u, d, s, and c quarks, and the τ lepton. Thus

$$R_{exp} - R_{theor} \sim 1 \text{ for } E_{cm} > 5 \text{ GeV} \tag{12}$$

We do not know the reason for this discrepancy.

2D. Quark Fragmentation

Here we are concerned with comparing how

$$\text{quark} \rightarrow \text{hadrons} \tag{13}$$

after the quark is excited or created in Reactions 1, 7, or 9. I shall limit my discussion here to the single hadron inclusive distribution, Eq. 14, and I shall neglect the mass

$$\text{quark} \rightarrow h + \text{other hadrons} \tag{14}$$

of the produced hadron (h). Then in all three of the reactions there is a maximum momentum p_{max} which can be given to h; and we define the longitudinal variable

$$z = p_{longitudinal}/p_{max} \tag{15}$$

and the transverse momentum p_T; relative to the direction of motion of the fragmenting quark.

As has been demonstrated beautifully by G. Hanson[18], the proper determination of z in e^+e^- annihilation (Eq. 9) requires the finding of a jet axis; and then the calculation of z and p_T relative to that axis. These variables are used in Fig. 15, prepared by T. Quirk[9], in which e^+e^- annihilation is compared with μ-p deep inelastic scattering (TABLE I). This is an absolute comparison. We see the pleasing result that the distribution functions $(z/\pi\sigma)(d\sigma/dz)$ are the same except in the lowest z bin.

Y. Sacquin[20] used ν and $\bar{\nu}$ data with $E_\nu > 100$ GeV from BEBC to show, Fig. 16, that the z distributions for ν and $\bar{\nu}$ reactions are quite similar[22] to those for electroproduction[21] and e^+e^- annihilation.[23] (The e^+e^- data here is not relative to the jet axis.)

Turning to the p_T distributions we first look at some interesting new results in the ν and $\bar{\nu}$ data presented by Y. Sacquin[20], Fig. 17. Here as Q^2 increases, $\langle p_T \rangle$ at fixed z increases. This is the first demonstration, to my knowledge[24], of an effect of Q^2 on $\langle p_T \rangle$ in inclusive hadron production properties in deep inelastic lepton scattering.

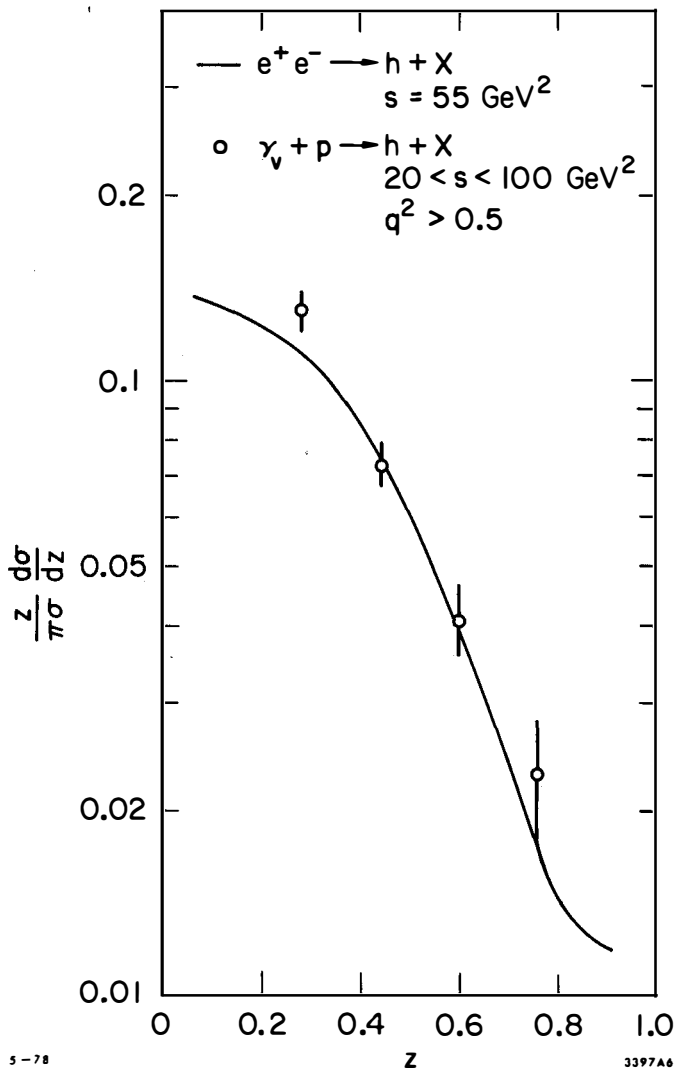

Fig. 15. Comparison of $(z/\pi\sigma)(d\sigma/dZ)$ versus z for the single hadron inclusive distributions from e^+e^- annihilation and muoproduction. Prepared by T. Quirk, Ref. 9.

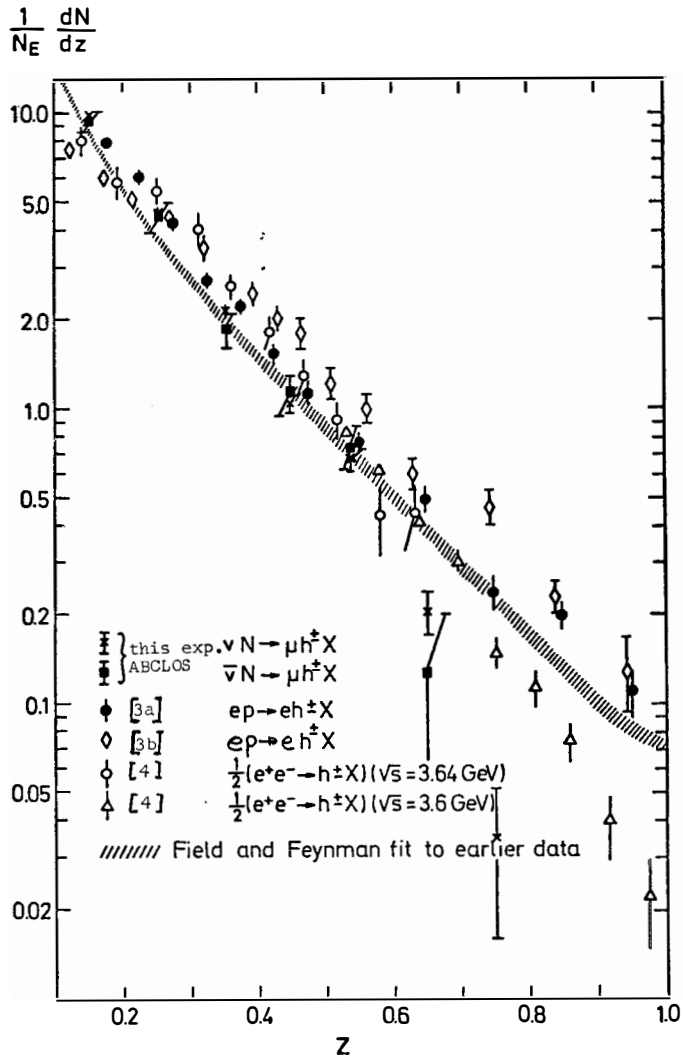

Fig. 16. Comparison of (1/N)(dN/d) versus z for neutrinoproduction, electroproduction, and e^+e^- annihilation from Y. Sacquin, Ref. 20.

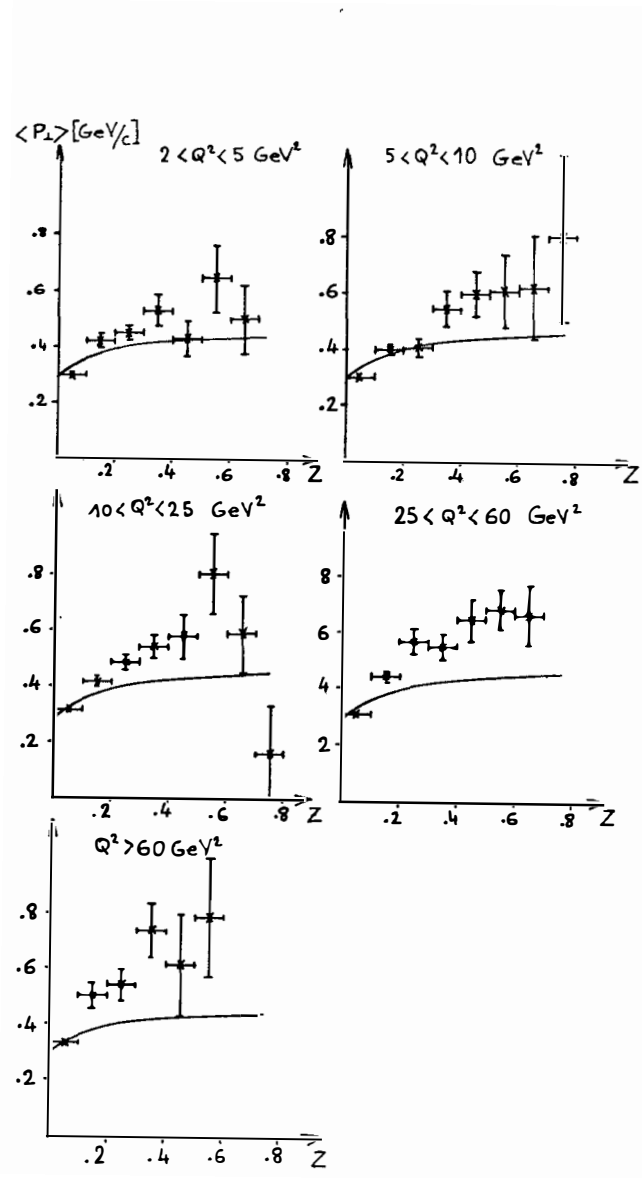

Fig. 17. $\langle P_\perp \rangle$ versus z for neutrinoproduction in various Q^2 ranges, Ref. 20.

Finally, in Fig. 18 we compare $\langle p_T \rangle$ for e^+e^- annihilation[18], muoproduction[9], and ν deep inelastic scattering. For the latter we use the $5 < Q^2 < 10$ $(GeV/c)^2$ data of Sacquin[20]. We see quite similar $\langle p_T \rangle$ values.

2E. Conclusions for Section 2

(a) Deep inelastic electron, muon and neutrino scattering all show similar violations of Bjorken scaling which qualitatively follow Eq. 4. For $Q^2 > 20$ $(GeV/c)^2$ and $\omega \sim 4$ there may be more complicated behavior versus Q^2.

(b) In e^+e^- annihilation above $E_{cm} = 5$ GeV, R shows Bjorken scaling but simple theory does not explain the high value of R.

(c) Quarks change into hadrons in the same way whether produced by deep inelastic lepton scattering or in e^+e^- annihilation; as we expect from the quark model. An interesting effect of Q^2 on $\langle p_T \rangle$ has been seen in ν experiments.

3. PROPERTIES OF NEW PARTICLES FROM e^+e^- ANNIHILATION

This discussion of the τ lepton, D charmed meson, F charmed meson, and charmed baryons is based on the electron-positron annihilation experiments listed in TABLE III.

TABLE III

e^+e^- Experiments Presented at this Conference

Speaker	Apparatus or Group Name	Storage Ring
J. Bürger	PLUTO	DORIS
G. Grindhammer	DASP	DORIS
G. Wolf	DASP	DORIS
G. Hanson	SLAC-LBL Mark I	SPEAR
M. Perl	SLAC-LBL Mark I	SPEAR
	LBL-SLAC Lead Glass Wall Detector	
A. Diament-Berger	DELCO	SPEAR

3A. Properties of the τ Lepton

All the known properties of the τ, (TABLE IV) are consistent with it being a lepton.

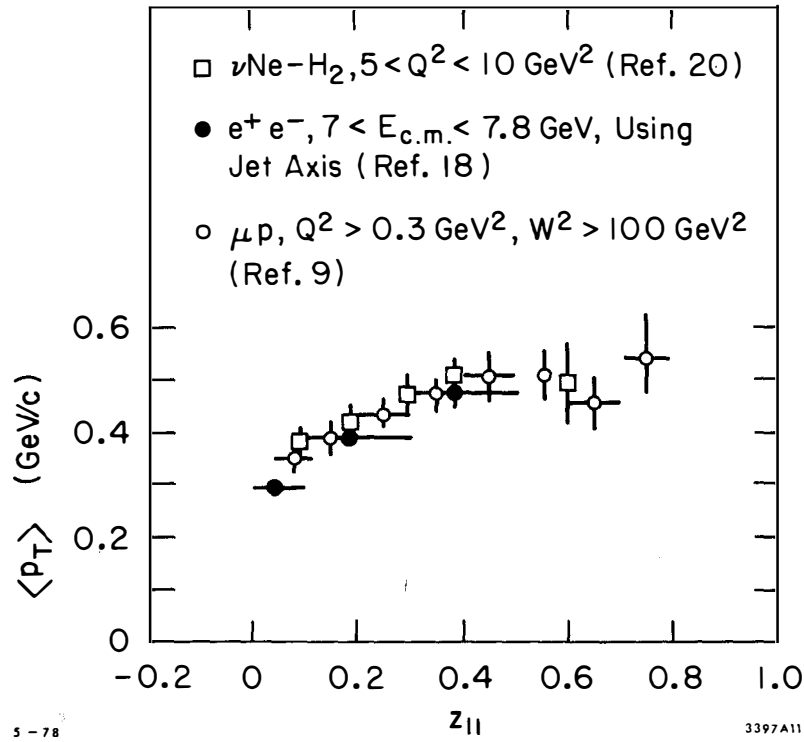

Fig. 18. Comparison of $\langle P_T \rangle$ versus z for neutrinoproduction, muoproduction and e^+e^- annihilation.[7]

TABLE IV

Properties of the τ lepton. Some of these properties were presented or published after this conference. Decay modes are always written for the τ^- to simplify the notation.

General Property	Value or Specific Property or Comment	Reference
τ Mass (GeV/c^2)	1807 ± 20 $1782 \begin{smallmatrix}+2\\-7\end{smallmatrix}$	(DASP) 17, 28 (DELCO), 27, 29
ν_τ Mass	<250 MeV/c^2 with 90% confidence	(DELCO) 27
τ-ν_τ Coupling	V+A excluded V+A excluded, Michel parameter $\rho = 0.73 \pm 0.15$	(SLAC-LBL) 30 (DELCO) 27
Lepton Type	Sequential or τ^- has lepton number of e^-	30, 31, 32, 33, 34, 35
Lifetime	$<10^{-11}$ sec. with 95% confidence $<4 \times 10^{-12}$ sec. with 95% confidence	(SLAC-LBL) 30 (PLUTO) 36
Leptonic Branching Ratio	$B(\tau^- \to \nu_\tau e^- \bar{\nu}_e) = B(\tau^- \to \nu_\tau \mu^- \bar{\nu}_\mu)$ to within 10 or 20% $B(\tau^- \to \nu_\tau e^- \bar{\nu}_e) = 18.2 \pm 2.8 \pm 1.4\%$ $B(\tau^- \to \nu_\tau e^- \bar{\nu}_e)\ 1 = 18.6 \pm 1.0 \pm 2.8\%$ $B(\tau^- \to \nu_\tau e^- \bar{\nu}_e) = 16.3 \pm 1.0\%$	 (DASP) 17, 28 (SLAC-LBL) 30,37 (DELCO) 27, 29
$\tau^- \to \nu_\tau + \pi^-$	$B(\tau^- \to \nu_\tau \pi^-) = 8.3 \pm 3\%$ General evidence for this decay mode has been found by G. Hanson. This mode has not been seen by a small statistics DASP search	(DELCO) 29 (SLAC-LBL) 38 (DASP) 17
Other Hadronic Decay Modes	$B(\tau^- \to \nu_\tau \rho^-) = 24 \pm 9\%$ $B(\tau^- \to \nu_\tau \pi^- \pi^+ \pi^-) = 5 \pm 1.5\%$ with evidence for A_1 $B(\tau^- \to \nu_\tau \pi^- \pi^+ \pi^-) = 6 \pm 4.5\%$; this data is consistent with A_1 but does not require it. $B(\tau^- \to \nu_\tau \pi^- \pi^+ \pi^- \pi^0) = 10 \pm 7\%$	(DASP) 17, 28 (PLUTO) 25, 39 (SLAC-LBL) 40 (SLAC-LBL) 40
Other Decay Modes	No other decay modes such as $\tau^- \to e^- \gamma, \tau^- \to \mu^- \gamma$ $\tau^- \to \nu_\tau e^- e^+ e^-$ have been seen	For a summary see Ref. 30
Spin	The energy dependence of the production cross section is consistent with spin = ½ and appears to be inconsistent with other spins; although more quantitative work needs to be done here	41

3B. D Charmed Mesons

The hadronic decay modes

$$D^o \to K^-\pi^+, \bar{K}^o\pi^+\pi^-, K^-\pi^+\pi^o, K^-\pi^+\pi^-\pi^+$$
$$D^+ \to \bar{K}^o\pi^+, K^-\pi^+\pi^+ \qquad (16)$$

have been seen. A thorough review has been given by Feldman[42] and we only note here that all the properties of these hadronic decays are consistent with the conventional theory of weak interactions and charmed quarks[19].

The semi-leptonic decay modes, Eq. 17, branching ratios

$$D^o \to e^+ + \nu_e + (\text{hadrons})^-$$
$$D^+ \to e^+ + \nu_e + (\text{hadrons})^o \; ; \qquad (17)$$

and more general

$$\text{charm particle} \to e + \nu_e + \text{hadron} \qquad (18)$$

branching ratios are given in TABLE V.

TABLE V

Energy Range	Branching Ratio	Reference
At $\psi(3772)$	$B(D \to e + X) = 7.2 \pm 2.8\%$ averaged over D^o and $D^\pm$	(LBL-SLAC)43
$3.9 \leq E_{cm} \leq 7.8$ GeV	$B(\text{charm} \to e + X) = 8.2 \pm 1.9\%$	(LBL-SLAC)43
$4 \leq E_{cm} \leq 5.2$ GeV	$B(\text{charm} \to e + X) = 7.2 \pm 2.0\%$	(DASP)17
At $\psi(3772)$	$B(D \to e + X) = 11 \pm 2\%$ averaged over D^o and $D^\pm$	(DELCO)27, 44

The $e^\pm$ momentum spectrum for Eq. 17 is given in Fig. 19. This is DELCO data[27] obtained at the $\psi(3772)$ and averaged over D^o and $D^\pm$ decays. The spectrum is consistent with a mixture of $D \to e\nu K$ and $D \to e\nu K^*(890)$ decay modes with V-A coupling.

3C. F Charmed Mesons

Information on the F meson is still scanty. DASP[17), 45] has previously reported seeing the

$$F^\pm \to \eta + \pi^\pm \qquad (19)$$

decay mode at $E_{cm} = 4.4$ GeV. This data yields masses of

$$M_F = 2030 \pm 60 \text{ MeV/c}^2, \; M_{F^*} = 2140 \pm 60 \text{ MeV/c}^2 \; ; \qquad (20)$$

and at this conference G. Wolf[17] reported an inclusive η peak at E_{cm} = 4.16 GeV, Fig. 20. This appears to be evidence for

$$e^+ + e^- \rightarrow F + \bar{F} \tag{21}$$

at 4.16 GeV since the η peak is not seen at 4.03 GeV, Fig. 21.

D. Lüke[46] has discussed searches for the F using all charged particle decay modes such as

$$F^{\pm} \rightarrow K^+ + K^- + \pi^{\pm} \tag{22}$$

3D. Charmed Baryons

No direct evidence for the production of charmed baryons in e^+e^- annihilation has been found. Figure 22 from the SLAC-LBL collaboration[47] presents indirect evidence for a threshold for charmed baryon production at an E_{cm} of roughly 4.5 GeV.

3E. Conclusions for Section 3

(a) All measured properties of the τ are consistent with it being a lepton and no other hypothesis as to the nature of the τ fits the data.

(b) The known decay modes of the D meson are consistent with conventional theory.

(c) The branching ratio for charmed particle $\rightarrow$ e + X is in the 7 to 11% range, averaged over the production cross section for charmed particles in e^+e^- annihilation.

(d) Much more work remains to be done on F production in e^+e^- annihilation; and charmed baryons have not yet been found directly in e^+e^- annihilation.

4. PRODUCTION OF CHARMED PARTICLES BY PHOTONS, HADRONS, AND NEUTRINOS

4A. Photoproduction of Charmed Particles

F. Richard[48] reported that 8 events of the form

$$\gamma + p \rightarrow D + X \qquad (D \rightarrow K^-\pi^+) \tag{23}$$

have been found using the Omega Facility at CERN with $25 < E_\gamma < 72$ GeV. This corresponds to a production cross section for the D in the range of one to

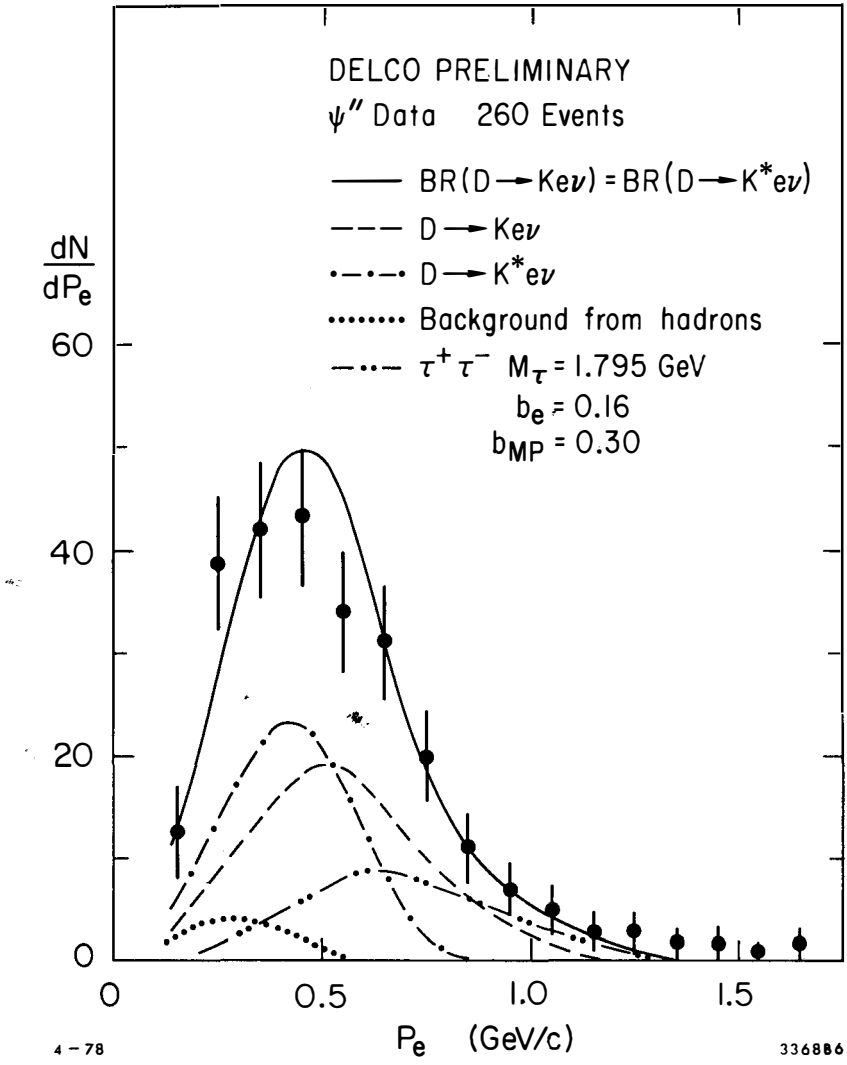

Fig. 19. The $e^{\pm}$ momentum spectrum for D decay from DELCO, Ref. 27.

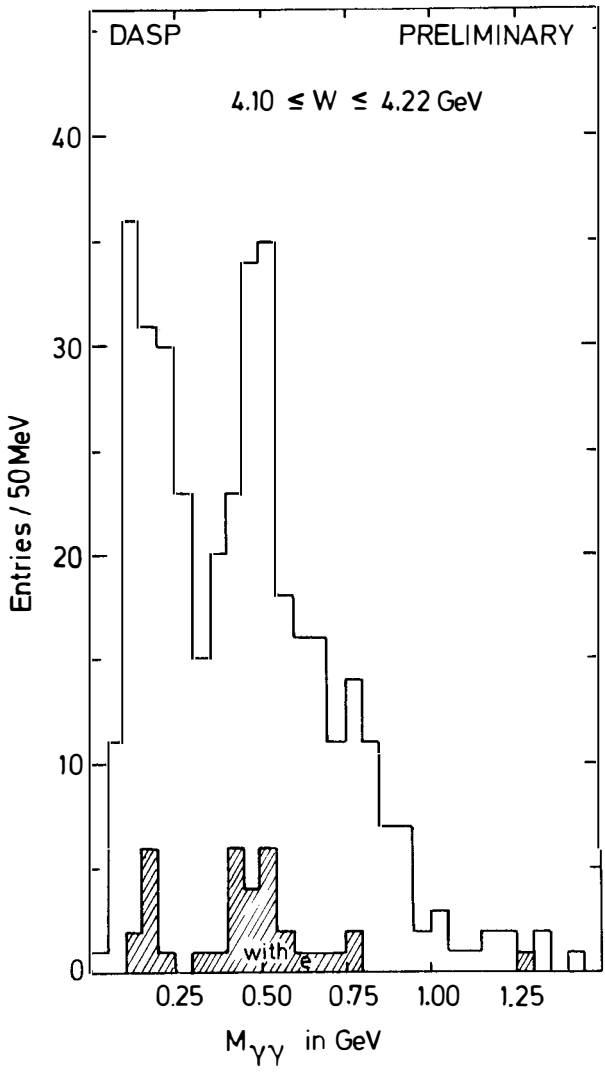

Fig. 20. The 2γ invariant mass spectrum in the energy range of 4.10 to 4.22 GeV showing a π^0 and an η peak; from DASP, Ref. 17.

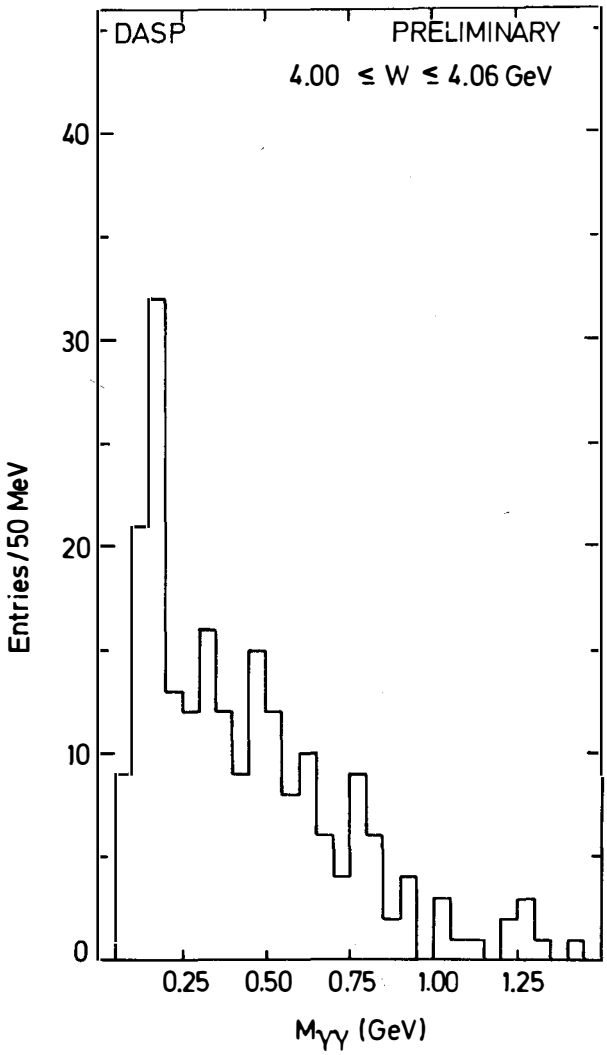

Fig. 21. The 2γ invariant mass spectrum in the energy range of 4.00 to 4.06 GeV showing only a π^0 peak; from DASP, Ref. 17.

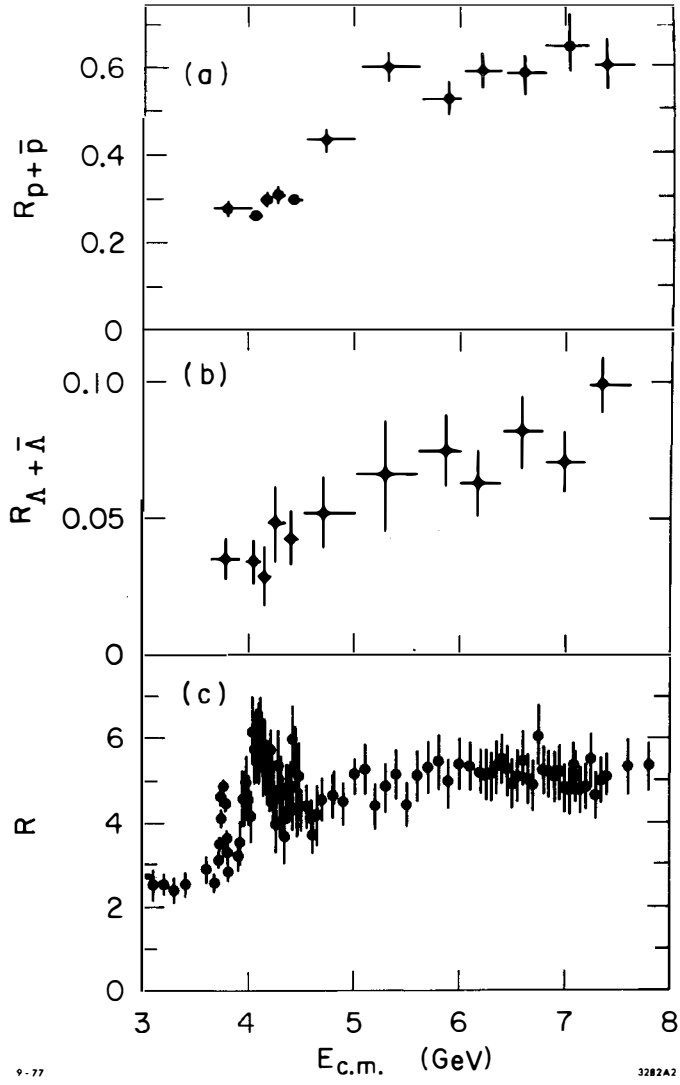

Fig. 22. R for (a) inclusive p + $\bar{p}$ production, (b) inclusive $\Lambda+\bar{\Lambda}$ production, and (c) total particle production versus $E_{c.m.}$ (Ref. 47).

several microbarns. This is a reasonable value because the total hadronic cross section is about 100 microbarns. This is the first report of photoproduction of charmed mesons.

4B. Direct Experiments on Hadroproduction of Charmed Particles

In this section we review experiments which have looked for hadronic production of charm by searching for

$$D \to K^{\pm} + \pi \tag{24}$$

$$\text{charm particle pair} \to e^{\pm} + \mu^{\mp} + X \tag{25}$$

$$\text{charm particle pair} \to \mu^{\pm} + \mu^{\mp} + X \tag{26}$$

$$\text{charm particle} \to \mu^{\pm} + X \tag{27}$$

TABLE VI gives published results on some experiments which have not found a charmed particle signal and so can only give upper limits. These upper bounds depend upon combining the acceptance of experiment with a model for the x and p_T distributions of charmed particles produced in hadronic interactions. This of course leads to an uncertainty in how to interpret these upper limits. I have not made a study of this problem; and so looking at TABLE VI I simply estimate that the cross section for the hadronic production of D^o mesons is less than several tens of μb in the energy range of the table. The cross sections for $D^o + D^{\pm}$ production could be twice as large; and the limit on the hadronic production of all types of charmed particles seems to be of the order of magnitude of 100 μb. The reader should make his or her own estimates.

This is now one experiment[49] which has finally detected charmed particle production by hadrons. This experiment carried out at Fermilab by a CIT-Stanford collaboration[49], used the apparatus in Fig. 23 with a 400 GeV proton beam. One part of the data collection consists of looking for events with a prompt, single muon. This data was corrected for feed-down from dimuon events and for contamination by muons from the decay of conventional particles-pions and kaons. The latter correction was made by varying the density of the target. The experimenters find a non-zero, prompt, single muon signal. If they assume the single muons come from the decay of a D meson produced with the distribution $dN/dx_F dp_T^2 = e^{-2.04 p_T (1-|x_F|)^{4.67}}$ and that the nuclear production cross sections is proportional to A then their preliminary result is

$$\sigma(\text{charm}) \sim 40\ \mu b \quad . \tag{28}$$

TABLE VI

Published limits in μb/nucleon for some searches for hadronic production of charmed particles. All limits assume that the nuclear production cross section is proportional to A

Experiment	Method	Limit and Comments	Reference
M.A. Abolins et al.	$n + Be \rightarrow D^o + X$ $D^o \rightarrow K^\pm + \pi^\mp$ $<E_n>$=250 GeV	No signal found. A 4 s.d. effect would require $\sigma_{D^o}(x>0)$=14 μb/nucleon	Phys.Lett. 73B, 355 (1978)
W.R. Ditzler	$p + Be, CH_2, Pb \rightarrow$ $D^o + X$ $D^o \rightarrow K^\pm + \pi^\mp$ E_p= 400 GeV	No signal found. $d\sigma_{D^o}/dy(y_{cm}=-0.4)$ <23 μb/nucleons with 95% confidence.	Phys.Lett. 71B, 451 (1978)
J.C. Alder et al.	$p + p \rightarrow D^o + X$ $D^o \rightarrow K^\pm + \pi^\mp$ E_{cm} = 53 GeV	No signal found. σ_{D^o}<770 μb/nucleon with 95% confidence. σ was measured for .9<y<1.2 and a model used to obtain the total σ.	Phys.Lett. 66B, 401 (1977)
A.M. Johckheere et al.	$\pi^- + C,H_2 \rightarrow$ $\mu^+ + \mu^- + X$	No signal found. $\sigma_{D\bar{D}}$ < 10.4 μb/nucleon with 90% confidence. $D\bar{D}$ production assumed similar to ψ production to calculate acceptance.	Phys.Rev. D16, 2073 (1977)
D. Spelbring et al.	$n + Be \rightarrow \mu + D^o + X$ $D^o \rightarrow K^\pm + \pi^\mp$ $<E_n>$=300 GeV	σ_{DC} < 64 μb/nucleon with 95% confidence. Used e^{-5x} and $\exp(-1.5\ p_T^2)$ to calculate acceptance.	Phys.Rev. Lett. 40, 607 (1978)
R. Lipton et al.	$n + Be \rightarrow \mu^\pm + e^\mp + X$ $<E_n>$ = 300 GeV	$\sigma_{c\bar{c}}$ <34 μb/nucleon with 95% confidence.	Phys.Rev.Lett. 40, 60B (1978)
G. Coremans-Bertrand et al.	p + emulsion → two particles with visible decays. E_p=300 GeV	σ <1.5 μb/nucleon with 90% confidence. However if a D lifetime of 3×10^{-13} sec and $<E_p>$=20 GeV is assumed, the limit becomes 10 μb/nucleon. This assumes 100% scanning efficiency.	Phys.Lett. 65B, 480 (1976).

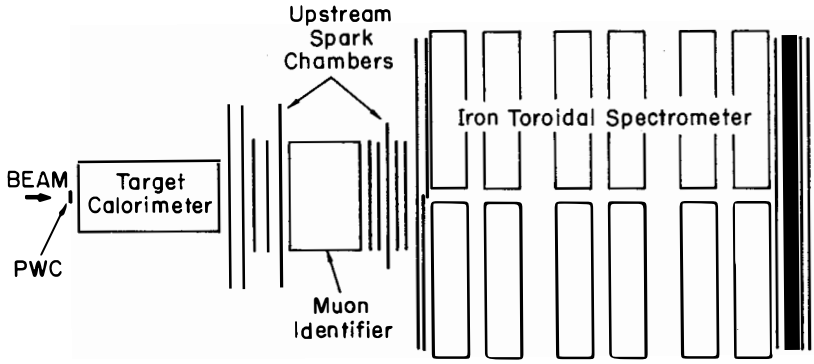

Fig. 23. The apparatus (not to scale) used for the CIT-Stanford measurement of charmed particle production by observation of a single prompt muon (Ref. 49).

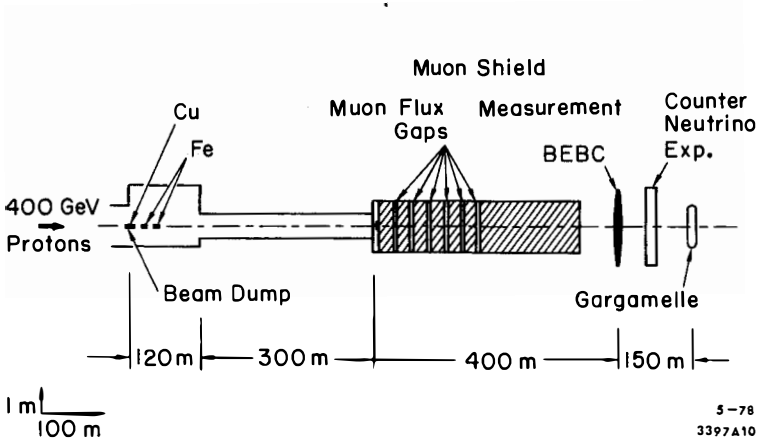

Fig. 24. The layout of the CERN beam dump experiments.

If other D production models are used or if an $A^{2/3}$ nucleon production cross section is used, then σ(charm) can be in the range of 20 to 80 μb. In comparing Eq. 28 with TABLE VI the reader should remember that Eq. 28 includes $D^{o}\bar{D}^{o}$ pairs, $D^{\pm}D$ pairs, $F^{+}F^{-}$ pairs, charm baryon pairs, and associated charm production.

4C. The CERN Beam Dump Experiments

The beam dump experiments recently carried out at CERN are closely connected with the hadronic production of charmed particles because part or all of the observed signal can come from the neutrinos produced in charmed particle semi-leptonic decays. In these experiments, Fig. 24, a 400 GeV proton beam was dumped at zero degrees into a very thick target of copper followed by an iron absorber. About 400 m downstream there was the usual 400 m long muon shield used for the neutrino experiments. And further downstream was the three neutrino dectors (TABLE VII) BEBC, CDHS, and Gargamelle. The copper and iron dump suppresses the usual neutrino beam flux by a factor of 3000. Hence the three detectors are sensitive to these neutrinos (usually called prompt neutrinos) or other weakly interacting neutral particles which can be produced within an hadronic absoprtion length in the dump. The only presently known and sufficiently copious production mechanism is the creation and decay of charmed particles.

All three experiments observed events which had the characteristics of events produced in normal neutrino experiments. Hence the observed events are labeled ν_{μ}, ν_{e}, neutral current, and so forth. Most of the thinking about these events has indeed assumed that they are produced by ordinary neutrino; however we should keep in the back of our minds the thought that there is no direct proof that these are ordinary neutrinos or that they are neutrinos at all. The last line of TABLE VII gives the

$$p + \text{nucleon} \rightarrow D+\bar{D}+X \qquad (29)$$

production cross sections required to yield the anomalous portion of the observed events: the so-called prompt neutrino events. These calculations are model dependent and the individual references[50-55] must be consulted for the details.

The correctness of the hypothesis that the prompt neutrinos come from $D\bar{D}$ production can be examined by comparing the last line of TABLE VII with TABLE VI and with Eq. 28. I will make a few comments, but readers should make their own comparisons.

TABLE VII

CERN beam dump experiments. $\sigma_{D\bar{D}}$ which include $D^0\bar{D}$ and D^+D^- is calculated assuming that the nuclear $D\bar{D}$ production cross section is proportional to A. Note that some of the observed events are from conventional sources such as π's and K's which decay before interacting in the dump. The reference must be consulted to learn what fraction of the events are attributed to prompt neutrinos.

Detector		Gargamelle	BEBC	CDHS
Speaker at this conference.		F. Jacquet[50]	K. L. Wernhard[52]	P. Bloch[54]
Reference		51	53	55
Acceptance (10^{-6} sr		1.71	11.2	10.2
Mass of detector (metric tons)		10.5	13	450
Observed Events	ν_μ	12	29	727
	$\bar{\nu}_\mu$	2	5	160
	ν_μ or $\bar{\nu}_\mu$	2		
	ν_e		11	
	$\bar{\nu}_e$		4	
	ν_e or $\bar{\nu}_e$	9		
	Neutral current	7	21	
	Neutral current or ν_e or $\bar{\nu}_e$			261
$\sigma_{D\bar{D}}$ (μb/nucleon)		$80\ ^{+40}_{-25}$ (Ref.50)	120 ± 54 (Ref.56)	∿ 30 (Ref.55) 40 ± 8 (Ref. 56)

(a) The $\sigma_{D\bar{D}}$'s required to explain the beam dump experiments prompt neutrino events, TABLE VII, are compatible with TABLE VI and Eq. 28 given the difficulties of the experiment and the uncertainties of the model used to calculate the cross sections. Furthermore the $\sigma_{D\bar{D}}$ in TABLE VII are overestimates because there will be some contributions to prompt neutrino events from F meson and charm baryon production.

(b) On the other hand, one should not get too comfortable with the comparison because the 95% confidence and 4 standard deviation upper limits in TABLE VI are the same size as the required cross

sections in TABLE VII. Clearly anomalous sources beyond charmed particle production are not excluded.

(c) There is a possible discrepancy between the bubble chamber measurements, BEBC and Gargamelle, and the CDHS measurement. This is most clearly seen in TABLE VIII taken from Jacquet's paper[50]. He defines

N_e = number of ν_e and $\bar{\nu}_e$ type events found.

$n_{e,prod}$ = number of ν_e and $\bar{\nu}_e$ neutrinos which had to be produced per proton in the beam dump to yield N_e

N_p = total number of protons

Ω = angular acceptance of detector with reference to beam dump (given in TABLE VII)

Since the ν_e and $\bar{\nu}_e$ total cross sections are proportional to E_ν, the neutrino energy, we can write

$$N_e = K \langle E_\nu \rangle n_{e,prod} N_p \quad , \tag{30}$$

where K is a constant for each detector. Then

$$\frac{n_{e,prod}}{\Omega} = \frac{N_e}{K\langle E_\nu \rangle N_p \Omega} \tag{31}$$

should be the same for all experiments.

TABLE VIII

Comparison of $n_{e,prod}/\Omega$. The errors are statistical and based only on N_e.

Detector	Gargamelle	BEBC	FHPRW
$K(GeV^{-1})$	2.45×10^{-12}	0.62×10^{-12}	20.1×10^{-12}
N_p	3.5×10^{17}	3.5×10^{17}	4.3×10^{17}
N_e	7.3	12	112*
$n_{e,prod}/\Omega$	$(4.6 \pm 1.7) \times 10^{-12}$	$(4.6 \pm 1.3) \times 10^{-2}$	$(1.2 \pm .11) \times 10^{-2}$

*Calculated from muonless events in Ref. 55

The combined results of the two bubble chambers differ from the CDHS result by 3 standard deviations.

4D. Neutrino Production of Charmed Particles

It is now well established[31),57)] that unlike sign dileptons events of the form

$$\nu_\mu + N \rightarrow \mu^- + \mu^+ + X \tag{32a}$$

$$\nu_\mu + N \rightarrow \mu^- + e^+ + X \tag{32b}$$

$$\nu_\mu + N \rightarrow \mu^- + \mu^+ + V^o + X \tag{32c}$$

$$\nu_\mu + N \rightarrow \mu^- + e^+ + V^o + X \tag{32d}$$

demonstrate the production of charmed particles in neutrino-hadron interactions. I shall not review this subject except to reproduce the nice compilation of Palmer[31)], Fig. 25, on the ratios

$$\frac{\text{Number } (\mu^- e^+ V^o)}{\text{Number } (\mu^- e^+)} \quad , \quad \frac{\text{Number } (\mu^- \mu^+ V^o)}{\text{Number } (\mu^- \mu^+)} \tag{33}$$

There has been some discussion[57)] as to whether the various measurements are consistent. Figure 25 makes two points.

(a) Given the large errors the various results are compatible.

(b) These ratios should increase as E_ν increases due to increased contributions from associated production of charmed particles and production of single charmed particles on quarks in the ocean.

Although events of the form of Eq. 32 are indirect evidence for charmed particle production; there is still a need for direct evidence based on reconstructing charmed particle invariant masses. Palmer[37)] reported that the decay mode $D^o \rightarrow K^o \pi^+\pi^-$ has been seen, Fig. 26, in the Columbus-BNL experiment using the 15 ft Fermilab bubble chamber in the wide band ν_μ beam. Their measured mass of $M_{Do} = 1850 \pm 15$ MeV/c^2 agrees with the SLAC-LBL measurement[42)] of $M_{Do} = 1863.3 \pm 0.9$ MeV/c^2.

4E. Conclusions for Section 4

The conclusions are obvious:

(a) A great deal more work must be done so that we have definitive measurements of the cross sections for the photoproduction, hadroproduction and neutrinoproduction of charmed particles.

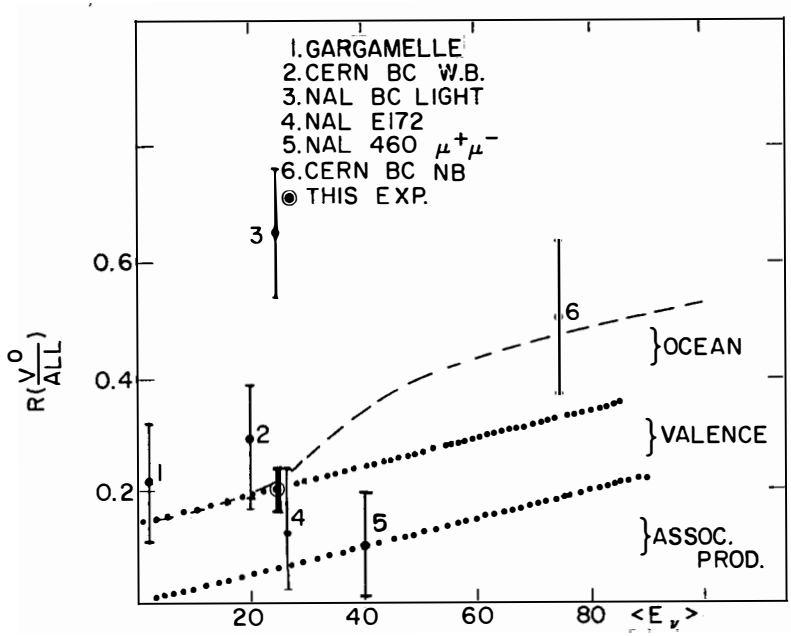

Fig. 25. Comparison of the number of unlike-sign dilepton neutrino events with and without V0's versus the neutrino energy for various experiments. Compiled by R. Palmer, Ref. 31.

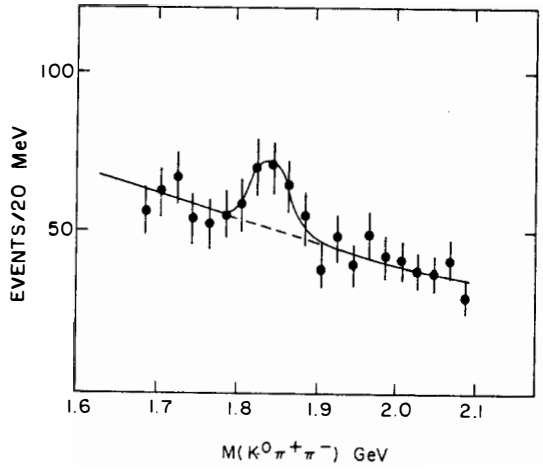

Fig. 26. Evidence for neutrino production of a D^0 which decays into the $K^0\pi^+\pi^-$ state (Ref. 31).

(b) On the basis of the scanty existing measurements there is nothing obviously in conflict with our expectations as to the size or behavior of these cross sections.

(c) The events found in the CERN beam dump experiments may be completely explainable as due to prompt neutrinos from the decay of charmed particles, but that hypothesis is not yet proven.

5. SEARCHES FOR NEW PARTICLES

5A. Multilepton Events Produced by Neutrinos

In the past few years there has been a great deal of interest as to whether particles other than ordinary or charmed mesons are responsible for events of the form:

$$\nu_\mu + \text{Nucleon} \rightarrow \mu^- + \mu^+ + X, \text{ (unlike-sign dimuons);} \tag{34a}$$

$$\nu_\mu + \text{Nucleon} \rightarrow \mu^- + \mu^- + X, \text{ (like-sign dimuons);} \tag{34b}$$

$$\nu_\mu + \text{Nucleon} \rightarrow \mu^- + e^+ + X, \ (\bar{\mu}e^+ \text{ events}); \tag{34c}$$

$$\nu_\mu + \text{Nucleon} \rightarrow \mu^- + \mu^+ + \mu^- + X, \text{ (trimuons);} \tag{34d}$$

and similar ν_μ induced events with more or other combinations of muons and electrons. By the time of this conference it had been generally agreed that the unlike sign dimuons and the μ^-e^+ events could be completely explained by the production and decay of a charmed particle. This left the like-sign dimuons, Eq. 34b; the trimuons, Eq. 34d and events of the form

$$\nu_\mu + \text{Nucleon} \rightarrow \ell_1 + \ell_2 + \ell_3 + \ell_4 + X \tag{(34e)}$$

(where ℓ_1, ℓ_2, ℓ_3, and ℓ_4 are muons or electrons) as the most intriguing places to search for new particles.

(a) Trimuon Events: These events were first reported in 1977 by Barish et al.,[58] and an important sample of 13 events has been described by the Fermilab-Harvard-Pennsylvania-Rutgers-Wisconsin (FHPRW) collaboration[59]. At this conference, K. Kleinknecht from the CERN-Dortmund-Heidelberg-Saclay (CDHS) collaboration reported[60] on 76 events. J. Smith[61] has presented a very thorough analysis of the trimuon events and my brief discussion here relies on his work.

Figure 27, the CDHS data[60], gives a beautiful overall picture of the relative rates of trimuon to single muon production. The rate $R(3\mu/1\mu)$ is given as a function on energy for their data in Fig. 28. Note that when corrected for the relative efficiency $R(3\mu/1\mu) \sim 10^{-4}$ for all E_{vis}. The

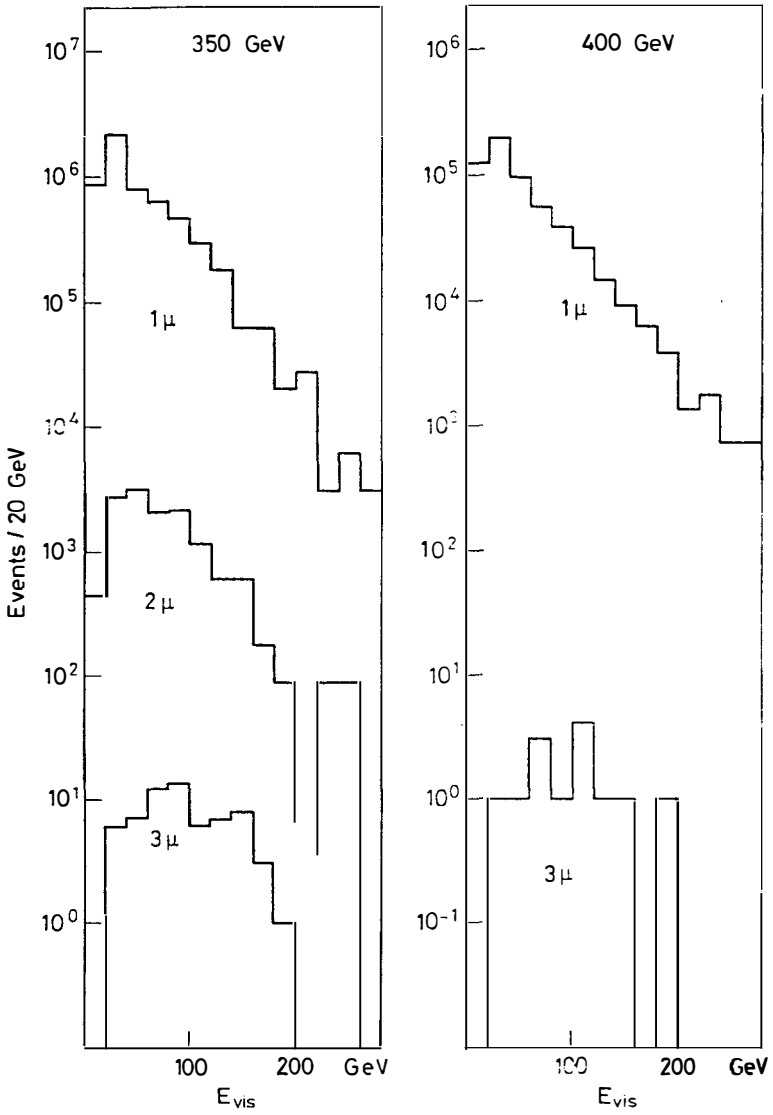

Fig. 27. Relative production of 1μ, 2μ, and 3μ events versus E_{vis} from the CDHS experiment (Ref. 60). These production rates are not corrected for detection efficiency.

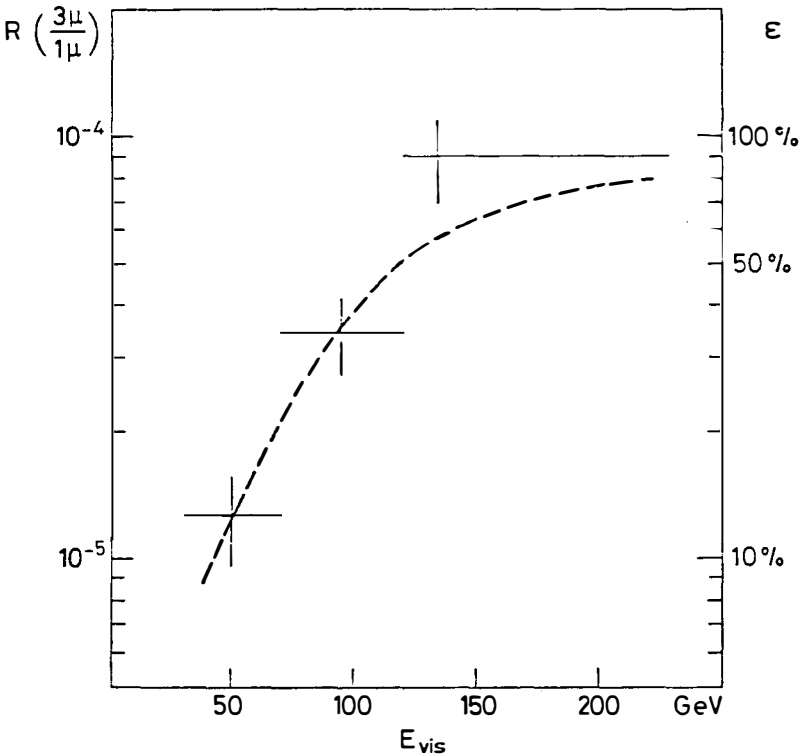

Fig. 28. Comparison of the ratio of 3μ to 1μ event production with the 3μ detection efficiency for the CDHS experiment (Ref. 60).

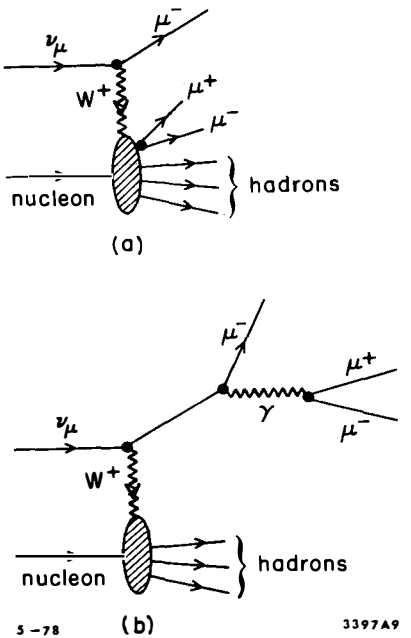

Fig. 29. Diagrams for production of trimuon events by (a) $\mu^+\mu^-$ pair production at the hadron vertex; and by (b) $\mu^+\mu^-$ pair production thru bremsstrahlung of the primary μ^-.

question is then whether this rate of trimuon events and their various kinematic distributions can be explained by conventional processes.

Two conventional processes are diagrammed in Fig. 29. In Fig. 29a a $\mu^+\mu^-$ pair is produced at the hadron vertex; the size and behavior of the pair production cross section being taken from experimental data on

$$\text{hadron} + N \rightarrow \mu^+ + \mu^- + X \tag{35}$$

These μ pairs tend to move in the direction of the produced hadrons; therefore in the transverse momentum plane they tend to move opposite in direction to the fast μ^-. The other conventional process, Fig. 29b is primarily μ pair production by internal bremsstrahlung from the first μ^-; hence these pairs move in the direction of the first μ^-. Smith[61] and Barger et al.[62] have discussed these diagrams in more detail.

Kleinknecht[60] and Smith[61] say that the number of trimuon events in the CDHS data can be explained by the processes in Fig. 29, and that these processes also explain the kinematic distributions of these events. For example: Fig. 30 shows that the very large 180° peak and smaller 0° peak in $\Delta\phi_{1,23}$ can be explained as the sum of these two processes. There is no need in the CDHS trimuon data to involve any new particles or unconventional processes.

Most of the published FHPRW trimuon events can be explained[62] by the two conventional processes in Fig. 29. However there are two so-called "super-events" with very large total muon energies and small total hadron energies in the FHPRW sample;[57),63] and these cannot be explained in this way. These events will remain a mystery unless more can be found.

(b) Like-sign Dilepton Events: T. Y. Ling[64] presented an extensive discussion of

$$\nu_\mu + N \rightarrow \mu^- + \mu^- + X \tag{36a}$$

events in the FHPRW data. The problem with these events is to show that they are not from

$$\nu_\mu + N \rightarrow \mu^- + \underbrace{\pi^- \text{ or } K^-}_{\hookrightarrow \mu^- + \bar{\nu}_\mu} + X \tag{36b}$$

FHPRW[64] finds that after correction of the background of Eq. 37

$$\frac{\text{Number}(\mu^-\mu^-)}{\text{Number}(\mu^-\mu^+)} = .10 \pm .07 \tag{37}$$

The simplest conventional explanation for $\mu^-\mu^-$ events is that they result from associated production of charmed particles (c and $\bar{c}$):

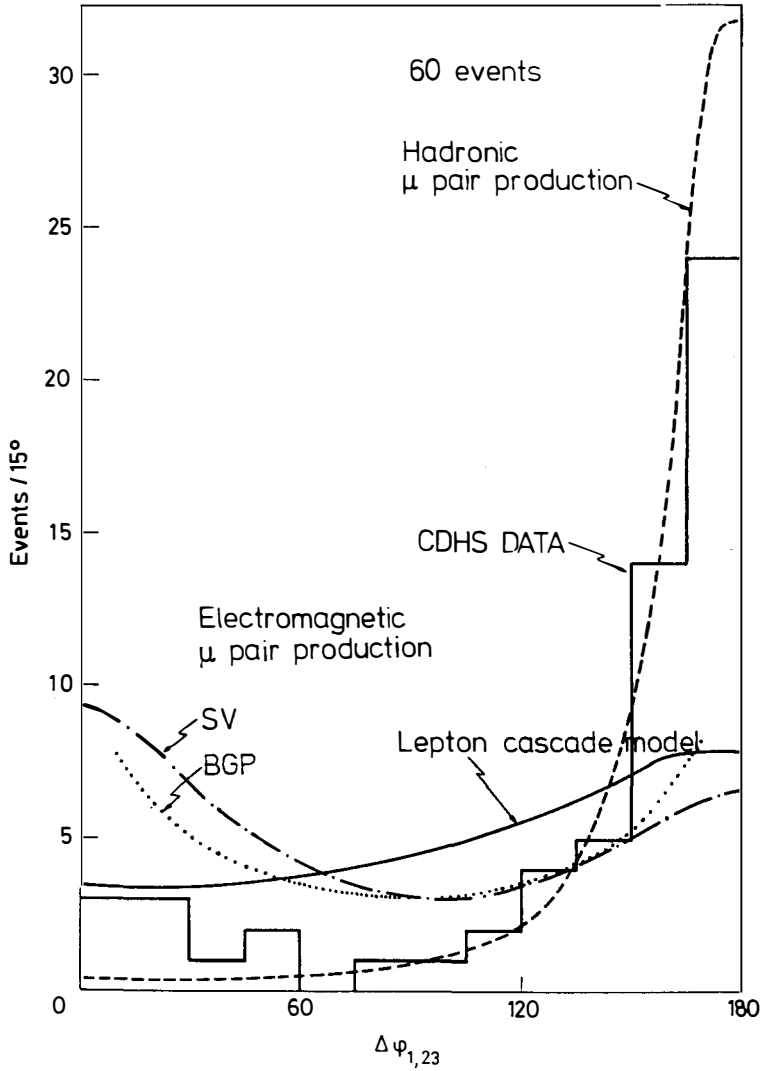

Fig. 30. The trimuon event distribution in $\Delta\phi 1,23$; the angle between the transverse momentum vector of the primary μ^- and the total transverse momentum vector of the $\mu^+\mu^-$ pair. The 0^o peak is ascribed primarily to electromagnetic μ pair production (the process in Fig. 29b), and the 180^o peak is ascribed primarily to hadronic μ pair production (the process in Fig. 29a).

$$\nu_\mu + N \rightarrow \mu^- + \bar{c} + c + X \qquad (38)$$
$$\downarrow$$
$$\mu^-$$

where the c does not go to a detectable μ^+. CDHS has not yet published their data on $\mu^-\mu^-$ events and there is not yet enough other data on $\mu^-\mu^-$ events to decisively test this explanation[65].

(c) Four-lepton Events: Only a few four-lepton events are known. M. Holder et al.[66] have described a four-muon event; and H. J. Lubatti[67),68] at this conference described an event of the form

$$\bar{\nu}_\mu + N \rightarrow \mu^+ + e^- + e^+ + e^- + X \qquad (39)$$

The authors report[68] that they have no plausible interpretation of this event.

5B. New Vector Mesons

I have devoted this summary talk to relatively high energy phenomena and high mass particles. However in concluding this talk I want to emphasize that there are still new particles to be found in the lower mass range. In particular there is much work to be done in elucidating the number and properties of vector mesons in the 1 to 3 GeV/c^2 mass range. F. Laplanche[69] reviewed the research at the D.C.I. e^+e^- colliding beams facility; and M. Spinetti[70] described the work at ADONE. This area was recently reviewed at the Hamburg Conference[71] and therefore I will not review it here. However as an example of the kind of intricate structure that can exist I have reproduced (Fig. 31) preliminary results from the "$\gamma\gamma$" group[70] emphasizing the various structures near 1500 MeV. It was exciting to learn of the plans at Frascati to build a new high luminosity e^+e^- colliding beam facility ALA with a peak luminosity of 10^{31} cm^{-2}sec^{-1}, and capable of operating down to 1 GeV total energy.

5C. Conclusions for Section 5.

(a) Almost all trimuon events can be explained by conventional processes

(b) There may be a net $\mu^-\mu^-$ signal above background; however its size and properties require study and verification.

(c) We do not know if the trimuon "super-events" and the four-lepton events will lead us into the discovery of new particles.

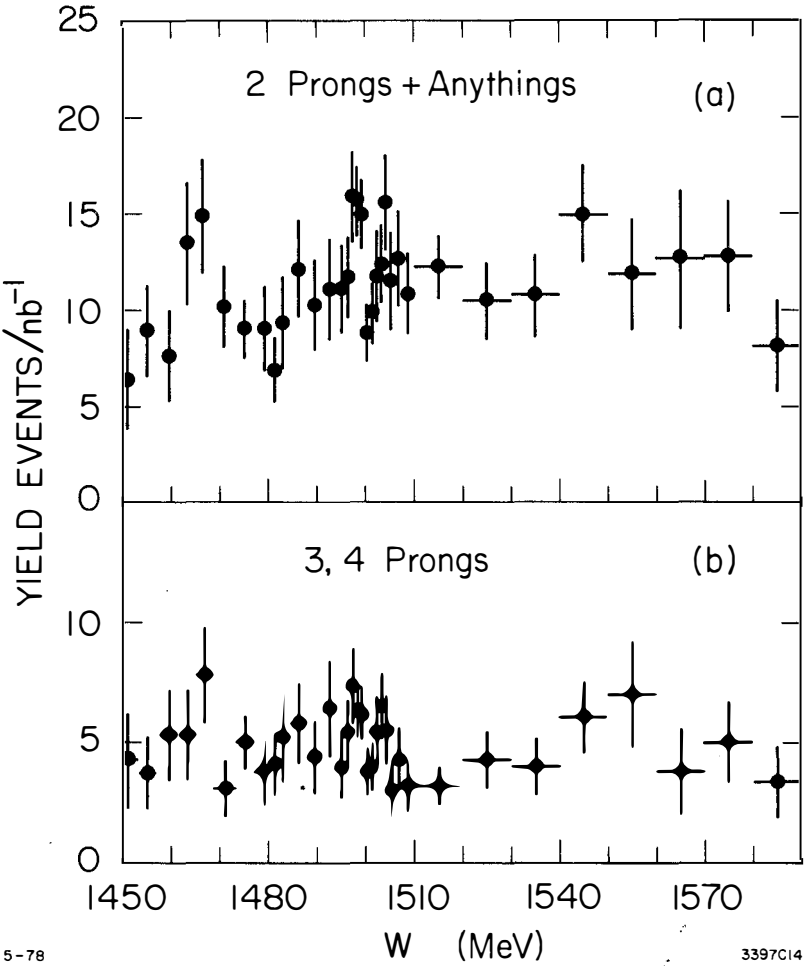

Fig. 31. Structure in various topological cross sections in hadrons produced in e^+e^- annihilation near 1500 MeV. From the $\gamma\gamma$ Group at Frascatti and presented by M. Spinetti, Ref. 70.

6. ACKNOWLEDGEMENTS

I am very grateful to the many speakers at the conference who sent me advanced copies of their papers and figures so that I could write this talk.

7. REFERENCES

1. N. Cabibbo, these proceedings.
2. M. L. Perl, High Energy Hadron Physics (Wiley, New York, 1974), Chapter 20.
3. L. Hand in Proc. of 1977 Int. Symp. on Lepton and Photon Interactions at High Energy (DESY, Hamburg, 1977).
4. M. J. Alguard et. al., Phys. Rev. Lett. 37, 1261 (1976).
5. E. M. Riordan et al., SLAC-PUB 1634 (1975), W. E. Atwood, SLAC-185 (1975).
6. H. L. Anderson et al., Phys. Rev. Lett. 38, 1450 (1977).
7. C. Chang et al., Phys. Rev. Lett. 35, 901 (1975).
8. G. Alterelli, these proceedings.
9. T. Quirk, these proceedings.
10. W. Chen, these proceedings.
11. D. H. Perkins et al., Phys. Lett. 67B, 347 (1977).
12. For recent reviews see the papers by B. Barish and by P. Musset in Proc. of 1977 Int. Symp. on Lepton and Photon Interactions at High Energy (DESY, Hamburg, 1977).
13. A. Savoy-Navarro, these proceedings.
14. B. Tallini, these proceedings.
15. H. L. Anderson, H. S. Matis, and L. C. Myrianthopoulos, submitted to Phys. Rev. Lett. (1977); A. J. Buras et al., Nuc. Phys. B131, 308 (1977); A. J. Buras and K. J. F. Gaemers, CERN preprint TH 2322 (1977); O. Nachtmann in Proc. of 1977 Int. Symp. on Lepton and Photon Interactions at High Energy (DESY, Hamburg, 1977).
16. G. J. Feldman and M. L. Perl, Phys. Reports 19C, 234 (1975), Eq. 5.20.
17. G. Wolf, these proceedings.
18. G. Hanson, these proceedings and SLAC-PUB-2118 (1978).
19. G. J. Feldman and M. L. Perl, Phys. Reports 33C, 286 (1977), Sec. 2.
20. Y. Sacquin, these proceedings.
21. (a) I. Cohen et al., CLNS Preprint CLNS-378 (1977); (b) J. M. Scarr et al., DESY Preprint DESY-77/77 (1977).
22. For a more quantitative review see A. Seiden, T. L. Schalk and J. F. Martin, SLAC-PUB-2107 (1978), submitted to Phys. Rev. D.
23. R. Brandelik et al., Phys. Lett. 67B, 358 (1977).
24. For a review see Ref. 3 of this paper.
25. J. Bürger, these proceedings.
26. G. Grindhammer, these proceedings.
27. A. Diament-Berger, these proceedings.
28. R. Brandelik et al., Phys. Lett. 73B, 109 (1975).
29. J. Kirkby et al., to be published.
30. M. L. Perl in Proc. of 1977 Int. Symp. on Lepton and Photon Interactions at High Energy (DESY, Hamburg, 1977).
31. R. Palmer, these proceedings.
32. A. N. Cnops et al., Phys. Rev. Lett. 40, 144 (1978).
33. M. J. Murtagh in Proc. of 1977 Int. Symp. on Photon and Lepton Interactions at High Energy (DESY, Hamburg, 1977).
34. F. J. Heile et al., SLAC-PUB-2059 (1977), to be published in Nuc. Phys.
35. For a discussion of other assignments for ν_τ see S. P. Rosen, Phys. Rev. Lett. 40, 1057 (1978).

36. R. Devenish, paper presented at the Washington, D.C. meeting of the American Physical Society (April, 1978).
37. M. L. Perl et al., Phys. Lett. 70B, 487 (1977).
38. G. Feldman in Proc. of Int. Conf. on Neutrino Physics-Neutrinos 1978 (Purdue, 1978), to be published.
39. G. Alexander et al., Phys. Lett. 73B, 99 (1978).
40. J. Jaros et al., Phys. Rev. Lett. 40, 1120 (1978).
41. Y. S. Tsai, SLAC-PUB-2105; Phys. Rev. (to be published).
42. G. Feldman in Proc. of Summer Inst. on Particle Physics-1977 (SLAC Report 204).
43. J. M. Feller et al., Phys. Rev. Lett. 40, 274 (1978); J. M. Feller et al., LBL Preprint LBL-7523 (1978), submitted to Phys. Rev. Lett.
44. W. Bacino et al., Phys. Rev. Lett. 40, 671 (1978).
45. R. Brandelik et al., Phys. Lett. 70B, 132 (1977).
46. D. Lüke, SLAC-PUB-2086 (1978), to be published in Proc. of 1977 Meeting of Division of Particles and Fields of American Physical Society (Argonne, 1977).
47. M. Piccolo et al., Phys. Rev. Lett. 39, 1503 (1977).
48. F. Richard, these proceedings.
49. B. Barish et al., CIT preprint CALT 68-655 (1978).
50. F. Jacquet; these proceedings.
51. P. Aliban et al., Phys. Lett. 74B, 134 (1978).
52. K. L. Wernhard, these proceedings.
53. P. C. Bosetti et al., Phys. Lett. 74B, 143 (1978).
54. P. Bloch, these proceedings.
55. T. Hansl et al., Phys. Lett. 74B, 139 (1978).
56. K. Schultze, talk given at Stanford Linear Accelerator Center, May 1978.
57. D. Cline in Proc. of 1977 Int. Symp. on Lepton and Photon Interactions at High Energy (DESY, Hamburg, 1977).
58. B. C. Barish et al., Phys. Rev. Lett. 38, 577 (1977).
59. A. Benvenuti et al., Phys. Rev. Lett. 38, 1110 (1977), 40, 432, 488 (1978).
60. K. Kleinknecht, these proceedings.
61. J. Smith, these proceedings.
62. V. Barger et al., Preprint COO-881-32 (1978).
63. D. D. Reeder in Proc. of 1977 Int. Symp. on Lepton and Photon Interactions at High Energy (DESY, Hamburg, 1977).
64. T. Y. Ling, these proceedings.
65. If the explanation is correct, then associated charm production will be a major contribution to the trimuon event ratio, contrary to the discussion in Sec. 5A.a.
66. M. Holder et al., Phys. Lett. 73B, 105 (1978).
67. M. J. Labatti, these proceedings.
68. R. J. Loveless et al., Preprint COO-088-29 (1978).
69. F. Laplanche, these proceedings.
70. M. Spinetti, these proceedings.
71. See papers by F. Laplanche and by C. Bemporad in Proc. of 1977 Int. Symp. on Lepton and Photon Physics at High Energy (DESY, Hamburg, 1977).

MORIOND PROCEEDINGS

N° 1	First Rencontre de Moriond	: 2 vol (1966)
N° 2	Second Rencontre de Moriond	: 2 vol (1967)
N° 3	Third Rencontre de Moriond	: 2 vol (1968)
N° 4	Fourth Rencontre de Moriond	: 1 vol (1969)
N° 5	Fifth Rencontre de Moriond	: 1 vol (1970)
N° 6	Electromagnetic and Weak Interactions	: (1971)
N° 7	High-Energy Phenomenology	: (1971)
N° 8	Two Body Collisions	: (1972)
N° 9	Multiparticle phenomene and inclusive reactions	: (1972)
N° 10	Electromagnetic and Weak Interactions	: (1973)
N° 11	The Pomeron	: (1973)
N° 12	High energy hadronic interactions	: (1974)
N° 13	High energy leptonic interactions	: (1974)
N° 14	Phenomenology of hadronic Structure	: (1975)
N° 15	Charm, Color and the J	: (1975)
N° 16	New fields in hadronic physics	: (1976)
N° 17	Weak Interactions and neutrino physics	: (1976)
N° 18	Storage Ring Physics	: (1976)
N° 19	Leptons and Multileptons	(1977)
N° 20	Deep Scattering and Hadronic Structure	(1977)
N° 21	Color Symmetry and Quark Confinement	(1977)
N° 22	**Phenomenology of Quantum Chromodynamics**	**(1978)**
N° 23	**Gauge Theories and Leptons**	**(1978)**

14 PHENOMENOLOGY OF HADRONIC STRUCTURE

CONTENTS

First Session

15 CHARM, COLOR AND THE Ψ

CONTENTS

16 NEW FIELDS IN HADRONIC PHYSICS

CONTENTS

17 WEAK INTERACTIONS AND NEUTRINO PHYSICS

CONTENTS

18 STORAGE RING PHYSICS

CONTENTS

19 LEPTONS AND MULTILEPTONS

CONTENTS

20 DEEP SCATTERING AND HADRONIC STRUCTURE

CONTENTS

21 COLOR SYMMETRY AND QUARK CONFINEMENT

This is a book with chapters based on talks given at the XIIth Annual Rencontre de Moriond (April 1977) plus an added pedagogical introduction. The book is intended to be useful for learning about Color Symmetry, how to work with it, and how it can be tested experimentally.

CONTENTS

22 PHENOMENOLOGY OF QUANTUM CHROMODYNAMICS

CONTENTS

23 GAUGE THEORIES AND LEPTONS

CONTENTS